ION CHANNELS AND TRANSPORTERS IN EPILEPSY: FROM GENES AND MECHANISMS TO DISEASE-TARGETED THERAPIES

EDITED BY: Jing Peng, Tobias Stauber, Weiping Liao, Yuwu Jiang and Yongguo Yu

PUBLISHED IN: Frontiers in Molecular Neuroscience

frontiers Research Topics

ISSN 1664-8714
ISBN 978-2-83250-407-9
DOI 10.3389/978-2-83250-407-9

About Frontiers

Frontiers is more than just an open-access publisher of scholarly articles: it is a pioneering approach to the world of academia, radically improving the way scholarly research is managed. The grand vision of Frontiers is a world where all people have an equal opportunity to seek, share and generate knowledge. Frontiers provides immediate and permanent online open access to all its publications, but this alone is not enough to realize our grand goals.

Frontiers Journal Series

The Frontiers Journal Series is a multi-tier and interdisciplinary set of open-access, online journals, promising a paradigm shift from the current review, selection and dissemination processes in academic publishing. All Frontiers journals are driven by researchers for researchers; therefore, they constitute a service to the scholarly community. At the same time, the Frontiers Journal Series operates on a revolutionary invention, the tiered publishing system, initially addressing specific communities of scholars, and gradually climbing up to broader public understanding, thus serving the interests of the lay society, too.

Dedication to Quality

Each Frontiers article is a landmark of the highest quality, thanks to genuinely collaborative interactions between authors and review editors, who include some of the world's best academicians. Research must be certified by peers before entering a stream of knowledge that may eventually reach the public - and shape society; therefore, Frontiers only applies the most rigorous and unbiased reviews.
Frontiers revolutionizes research publishing by freely delivering the most outstanding research, evaluated with no bias from both the academic and social point of view. By applying the most advanced information technologies, Frontiers is catapulting scholarly publishing into a new generation.

What are Frontiers Research Topics?

Frontiers Research Topics are very popular trademarks of the Frontiers Journals Series: they are collections of at least ten articles, all centered on a particular subject. With their unique mix of varied contributions from Original Research to Review Articles, Frontiers Research Topics unify the most influential researchers, the latest key findings and historical advances in a hot research area! Find out more on how to host your own Frontiers Research Topic or contribute to one as an author by contacting the Frontiers Editorial Office: frontiersin.org/about/contact

ION CHANNELS AND TRANSPORTERS IN EPILEPSY: FROM GENES AND MECHANISMS TO DISEASE-TARGETED THERAPIES

Topic Editors:
Jing Peng, Central South University, China
Tobias Stauber, Medical School Hamburg, Germany
Weiping Liao, Second Affiliated Hospital of Guangzhou Medical University, China
Yuwu Jiang, Peking University, China
Yongguo Yu, Shanghai Jiao Tong University, China

Citation: Peng, J., Stauber, T., Liao, W., Jiang, Y., Yu, Y., eds. (2022). Ion Channels and Transporters in Epilepsy: From Genes and Mechanisms to Disease-Targeted Therapies. Lausanne: Frontiers Media SA. doi: 10.3389/978-2-83250-407-9

Table of Contents

frontiers | Frontiers in Molecular Neuroscience

TYPE Editorial
PUBLISHED 21 September 2022
DOI 10.3389/fnmol.2022.1011843

OPEN ACCESS

EDITED AND REVIEWED BY
Detlev Boison,
Rutgers, The State University of New Jersey, United States

*CORRESPONDENCE
Jing Peng
pengjing4346@163.com

SPECIALTY SECTION
This article was submitted to Brain Disease Mechanisms, a section of the journal Frontiers in Molecular Neuroscience

RECEIVED 04 August 2022
ACCEPTED 17 August 2022
PUBLISHED 21 September 2022

CITATION
He H, Stauber T, Liao W, Jiang Y, Yu Y and Peng J (2022) Editorial: Ion channels and transporters in epilepsy: From genes and mechanisms to disease-targeted therapies. *Front. Mol. Neurosci.* 15:1011843. doi: 10.3389/fnmol.2022.1011843

Editorial: Ion channels and transporters in epilepsy: From genes and mechanisms to disease-targeted therapies

Hailan He[1,2], Tobias Stauber[3], Weiping Liao[4], Yuwu Jiang[5], Yongguo Yu[6] and Jing Peng[1,2]*

[1]Department of Pediatrics, Xiangya Hospital, Central South University, Changsha, China, [2]Clinical Research Center for Children Neurodevelopmental Disabilities of Hunan Province, Changsha, China, [3]Department of Human Medicine and Institute for Molecular Medicine, MSH Medical School Hamburg, Hamburg, Germany, [4]Department of Neurology, Second Affiliated Hospital of Guangzhou Medical University, Guangzhou, China, [5]Department of Pediatrics, Peking University First Hospital, Beijing, China, [6]Xinhua Hospital, School of Medicine, Shanghai Jiao Tong University, Shanghai, China

KEYWORDS

ion channels, ion transporters, gene, neuronal excitability, epilepsy

Editorial on the Research Topic
Ion channels and transporters in epilepsy: From genes and mechanisms to disease-targeted therapies

Epilepsy is a common, serious neurological disease with affecting more than 50 million people in the world (Singh and Sander, 2020). Neuronal excitability is determined by the flux of ions through ion channels and transporters, and dysfunction of ion homeostasis has been implicated in human epilepsy (Graves, 2006; Wei et al., 2017; Oyrer et al., 2018). The complex pathogenesis of epilepsy is caused by the imbalance of excitation and inhibition of the central nervous system, which is closely related to ion channel and transporters abnormalities (Mizielinska, 2007). Therefore, understanding the role of ion channels and transporter in epilepsy might not only contribute to clarify the mechanism of epileptogenesis but also provide potential targets for the precise treatment of epilepsy. Within this context, we launched our Research Topic on April 23th, 2021, and invited researchers to address *Ion channels and transporters in epilepsy: From genes and mechanisms to disease-targeted therapies*. Despite all the hardships, and uncertainty caused by the COVID-19 pandemic, we have received diverse and insightful manuscripts. In a cohort of 221 pediatric epilepsy, Jiang et al. described that genetic testing may help identify the molecular etiology of early onset epilepsy and developmental delay/intellectual disability and further aid to choose the appropriate treatment strategy for patients. Liu X.-R. et al. studied the role of *GRIN2A* gene in idiopathic generalized epilepsies and the potential underlying mechanism for phenotypic variation. Their results suggested a relationship between the severity of gain-of-function effects of GluN2A and the severity of the phenotypes as well as a link between the location of the variations in the different domains of the GluN2A protein and the epileptic

phenotypes. Kessi et al. reviewed the contribution of hyperpolarization-activated cyclic nucleotide-gated (HCN) channelopathies in different epileptic syndromes. They update knowledge about the human genetic changes, genotype–phenotype correlations, the available animal models, and the drugs available for each subtype of channel in the HCN family. Xie et al. identified five HCN1 channel variants in five patients with epilepsy, four of which were novel. They further demonstrated that these mutations affect the biophysical properties of HCN1 channels and neuronal excitability *in vitro* experiments. Yang M. et al. showed an increased expression of Beclin1 upon epileptic activity in human and mouse brain. The authors also showed haploinsufficiency of *Beclin1* results in decreased seizure susceptibility accompanied by decreased frequency and amplitude in miniature excitatory synaptic currents and decreased number of dendritic spines in hippocampal neurons in *Beclin1*$^{+/-}$ mice. Xiao et al. reported 30 unrelated patients with novel variants in the *KCNQ2* gene, including 19 single nucleotide variations and 11 copy number variants who experienced seizures or neurological development delay. Their study expands the genotypic and phenotypic spectrum of *KCNQ2*-related disorder. Yang et al. described the phenotypes of *GABRG2*-related epilepsy were ranged from mild febrile seizures to severe epileptic encephalopathies. Seizure outcome was favorable in most patients with *GABRG2* variants, and most patients benefited from treatment with valproate and/or levetiracetam. Zeng et al. analyzed the phenotypic spectrum, treatment and prognosis of 72 Chinese epilepsy children with *SCN2A* variants. The epilepsy phenotypes of these patients with *SCN2A* variants were variable, ranging from febrile seizures (plus), benign epilepsy to epileptic encephalopathy, and 79.1% patients had developmental delay. Of the patients with *SCN2A* variants, 22.6% had achieved seizure control with valproate, 28.9% with oxcarbazepine, while 6 patients had seizure worsening by oxcarbazepine. Weng et al. presented recent evidence of iPSC analysis of certain ion channel mutations found in humans with epilepsy and genes related to mTOR signaling. Recent years, there has been a great increase in the use of human iPSC models of genetic epilepsy syndromes, so this review is a timely contribution. Chen et al. described detailed genotype-phenotype information for a group of 41 patients with pathogenic *SCN1A* variants. The authors classified these 41 epilepsy patients into two groups, Dravet syndrome and non-Dravet syndrome, and retrospectively compared the phenotypic differences between the two groups. Ma et al. reported 22 epileptic patients with *SCN1A* variants, including 12 novel variants. Interestingly, two patients in their cohort displayed rare phenotypes, benign epilepsy with centrotemporal spikes and atypical childhood epilepsy with centrotemporal spikes. Therefore, studies of both Chen et al. and Ma et al. expand the genotypes and phenotypes of *SCN1A*-related epilepsy. Almog et al. studied the electrophysiological characterization of inhibitory and pyramidal neurons in CA1 hippocampal region of *Scn1a*A$^{1783V/+}$ knock-in mouse model of Dravet syndrome. Their data reveal synaptic and excitability alterations in both CA1 excitatory neurons and CA1 stratum-oriens interneurons in *Scn1a*$^{A1783V/+}$ mice, supporting global homeostatic changes within the CA1 microcircuit that may partially compensate for the Dravet syndrome-related interneurons hypoexcitability. Guzman et al. studied the functional characterization of *CLCN4* variants associated with X-linked intellectual disability and epilepsy. Their results showed these mutations led to a variety of changes in ClC-4 function, ranging from gain/loss of function and impaired heterodimerization with ClC-3 to subtle impairments in transport functions. These findings provide insights into understanding the linkage between *CLCN4* mutations and their associated neurological phenotypes. Liu X. et al. investigated the mechanism that underlie a protective role of neural precursor cell expressed developmentally down-regulated gene 4-like (NEDD4-2) against the endoplasmic reticulum (ER) stress and seizure susceptibility with the RER1 as a possible mediator. The authors found that Nedd4-2 haploinsufficiency in mice impairs the ubiquitination of Rer1 and increases the susceptibility to ER stress and seizures. Their study enriches our knowledge on the underlying mechanism of seizure contributing to ER stress.

Taken together, a total of fourteen articles were published under this collection, which have improved our understanding about the molecular basis underlying genetic epilepsy caused by mutations in ion channels and transporters, as well as related clinical problems. We hope that all the selected clinical and basic studies published in this Research Topic have provided insights on the link between ion channels, ion transporters and epilepsy, with promising outcomes and future perspectives. However, deciphering the mechanisms and understanding the role of the ion channels and transporters in epilepsy is a long way to go.

Author contributions

All authors listed have made a substantial, direct, and intellectual contribution to the work and approved it for publication.

Funding

This study was supported by the National Natural Science Foundation of China (Nos. 81771409 and 82071462).

Acknowledgments

We deeply thank all the authors who proposed their work, all the researchers who reviewed the submissions to this Research Topic, and to the people in

Frontiers in Molecular Neuroscience for proofreading the editorial manuscript.

Conflict of interest

The authors declare that the research was conducted in the absence of any commercial or financial relationships that could be construed as a potential conflict of interest.

Publisher's note

References

Graves, T. D. (2006). Ion channels and epilepsy. *QJM* 99, 201–17. doi: 10.1093/qjmed/hcl021

Mizielinska, S. M. (2007). Ion channels in epilepsy. *Biochem. Soc. Trans*. 35, 1077–9. doi: 10.1042/BST0351077

Oyrer, J., Maljevic, S., Scheffer, I. E., Berkovic, S. F., Petrou, S., Reid, C. A., et al. (2018). Ion channels in genetic epilepsy: from genes and mechanisms to disease-targeted therapies. *Pharmacol. Rev*. 70, 142–73. doi: 10.1124/pr.117.014456

Singh, G., and Sander, J. W. (2020). The global burden of epilepsy report: implications for low- and middle-income countries. *Epilepsy Behav*. 105, 106949. doi: 10.1016/j.yebeh.2020.106949

Wei, F., Yan, L. M., Su, T., He, N., Lin, Z. J., Wang, J., et al. (2017). Ion channel genes and epilepsy: functional alteration, pathogenic potential, and mechanism of epilepsy. *Neurosci. Bull*. 33, 455–77. doi: 10.1007/s12264-017-0134-1

frontiers in Molecular Neuroscience

ORIGINAL RESEARCH
published: 19 August 2021
doi: 10.3389/fnmol.2021.699574

Application of Trio-Whole Exome Sequencing in Genetic Diagnosis and Therapy in Chinese Children With Epilepsy

*Tiejia Jiang[1], Jia Gao[1], Lihua Jiang[1], Lu Xu[1], Congying Zhao[1], Xiaojun Su[1], Yaping Shen[1], Weiyue Gu[2], Xiaohong Kong[2], Ying Yang[2] and Feng Gao[1]**

[1] Department of Neurology, The Children's Hospital, Zhejiang University School of Medicine, National Clinical Research Center for Child Health, Hangzhou, China, [2] Beijing Chigene Translational Medical Research Center Co., Ltd., Beijing, China

Epilepsy is one of the most common neurological disorders in pediatric patients with other underlying neurological defects. Identifying the underlying etiology is crucial for better management of the disorder. We performed trio-whole exome sequencing in 221 pediatric patients with epilepsy. Probands were divided into seizures with developmental delay/intellectual disability (DD/ID) and seizures without DD/ID groups. Pathogenic (P) or likely pathogenic (LP) variants were identified in 71/110 (64.5%) patients in the seizures with DD/ID group and 21/111 (18.9%) patients in the seizures without DD/ID group ($P < 0.001$). Eighty-seven distinct P/LP single nucleotide variants (SNVs)/insertion deletions (Indels) were detected, with 55.2% (48/87) of them being novel. All aneuploidy and P/LP copy number variants (CNVs) larger than 100 Kb were identifiable by both whole-exome sequencing and copy number variation sequencing (CNVseq) in 123 of individuals (41 pedigrees). Ten of P/LP CNVs in nine patients and one aneuploidy variant in one patient (Patient #56, #47, XXY) were identified by CNVseq. Herein, we identified seven genes (*NCL*, *SEPHS2*, *PA2G4*, *SLC35G2*, *MYO1C*, *GPR158*, and *POU3F1*) with *de novo* variants but unknown pathogenicity that were not previously associated with epilepsy. Potential effective treatment options were available for 32 patients with a P/LP variant, based on the molecular diagnosis. Genetic testing may help identify the molecular etiology of early onset epilepsy and DD/ID and further aid to choose the appropriate treatment strategy for patients.

Keywords: epilepsy, seizure, whole-exome sequencing, copy number variation sequencing, genetic diagnosis

OPEN ACCESS

Edited by:
Jing Peng,
Central South University, China

Reviewed by:
Zhixian Yang,
Peking University First Hospital, China
Marco Venturin,
University of Milan, Italy

****Correspondence:***
Feng Gao
epilepsy@zju.edu.cn

Specialty section:
This article was submitted to Brain Disease Mechanisms, a section of the journal Frontiers in Molecular Neuroscience

Received: *23 April 2021*
Accepted: *30 July 2021*
Published: *19 August 2021*

Citation:
Jiang T, Gao J, Jiang L, Xu L, Zhao C, Su X, Shen Y, Gu W, Kong X, Yang Y and Gao F (2021) Application of Trio-Whole Exome Sequencing in Genetic Diagnosis and Therapy in Chinese Children With Epilepsy. Front. Mol. Neurosci. 14:699574. doi: 10.3389/fnmol.2021.699574

INTRODUCTION

Epilepsy is one of the most common neurological disorders with 50–100 million affected, and 2–4 million new cases diagnosed each year worldwide (Pitkänen et al., 2016). Epilepsy is a chronic disorder characterized by recurrent spontaneous seizures, and often begins in childhood. Repeated and refractory seizures cause decreased social participation, long-term cognitive impairment, and significantly lower quality of life (Nickels et al., 2016). A genetic basis for some forms of epilepsy was confirmed via gene mapping in families, and the specific mutations associated with epilepsy

syndromes were identified in the 1990's (Annegers et al., 1982; Scheffer and Berkovic, 1997; Myers and Mefford, 2015).

The genetic etiology of epilepsy may be monogenic, resulting from single-gene mutations. Mutations or variants in multiple genes are also important to cause epilepsy (Møller et al., 2015). Currently, epilepsy genetics can be broadly characterized into two categories: (i) genes and loci associated with primary epilepsy; and (ii) genes associated with neurological disorders where epilepsy may be one of the symptoms (Poduri and Lowenstein, 2011). High throughput sequencing technologies have contributed to explore novel epilepsy genes. To date, numerous pathogenic variants in several genes have been associated with epilepsy and seizures (Yang et al., 2019).

The development of next-generation sequencing have greatly increased our knowledge on the genetic changes occurring across the entire human genome, allowing for the rapid and efficient discovery of genes involved in many diseases. Whole-exome sequencing (WES) is a powerful tool for detecting variants, especially the single nucleotide variants (SNVs) and the small insertions and deletions (InDels). WES is intensively being applied to clinical practice due to its low cost, high diagnostic yields, and excellent advantages regarding the analysis of novel genes and their subsequent investigation.

Diagnostic genetic tests for these complex conditions are becoming increasingly important (Berg et al., 2019) as their clinical heterogeneity and molecular complexity pose a great challenge for their clinical diagnosis and subsequent treatment. In this study, we retrospectively analyzed the diagnostic yields of trio-WES in 221 pediatric patients with epilepsy of unclear etiology and explored novel possible pathogenic genes. We aimed to explore the P/LP variants in family and specifically focus on patients with developmental delay (DD)/intellectual disability (ID) or without DD/ID. Meanwhile, we also wanted to explore the treatment strategies based on molecular diagnosis. More importantly, analysis of novel epilepsy candidate genes was performed when no pathogenic mutations were clearly identified in the characterized genetic diseases. We identified several novel genes variations such as SCN1A, MECP2, and KCNT1, which were confined as pathogenic or likely pathogenic variants of epilepsy. Herein, our results suggest that the application of WES would benefit for defining epilepsy genetic factors and treatment strategies in the clinic.

MATERIALS AND METHODS

Study Design and Sample Collection

The outline of the study design is illustrated in **Figure 1**. The inclusion criteria were: (1) occurrence of seizures or epilepsy before the age of 16 years-old, (2) epileptic syndromes/epileptic encephalopathy with unknown etiology, and (3) severe seizures in neonates or generalized epilepsy or intractable epilepsy in infancy with generalized tonic–clonic seizures. Patients would be excluded if the seizures were caused by non-genetic factors such as cerebral trauma, cerebral tumor, cerebral infection, cerebrovascular disorders, or diagnosed metabolic disorders. All patients underwent electroencephalogram (EEG) and magnetic resonance imaging. Epilepsy diagnoses and classifications were made by a pediatric neurologist following the criteria published by the International League Against Epilepsy. The phenotypic features of eligible patients were assessed by clinicians during the reviews of the medical records and classified according to the Human Phenotype Ontology (HPO) terms. Clinical information of the family members was obtained through face-to-face inquiries by investigators. Biological parentage was confirmed using the genomic data as described previously (Manichaikul et al., 2010).

Patients with developmental delay (DD)/intellectual disability (ID) were diagnosed by the pediatric neurologists according to the Diagnostic and Statistical Manual of Mental Disorders, Fifth Edition (DSM-5). The developmental profile of patients <36 months of age was assessed via clinical observation, the Ages and Stages Questionnaires, Third Edition (ASD-3), and the Gesell Developmental Observation-Revised (GDO-R) assessment. The Wechsler Intelligence Scale, clinical observation, and Peabody picture vocabulary tests were used for patients aged from 3 to 10 years. ID was assessed by an IQ under 70 using the Wechsler Preschool and Primary Scale of Intelligence-Fourth Edition (WPPSI-IV) for patients between the ages of 4 and 6 years, and the Wechsler Intelligence Scale for Children-Fourth Edition (WISC-IV) for patients aged over 7 years old.

Whole-Exome Sequencing (WES)

Whole-exome sequencing and bioinformatics analyses were performed following the previously proposed guidelines (MacArthur et al., 2014; Richards et al., 2015). In brief, peripheral venous blood (2∼4 mL) was collected from the patients and their family members. The genomic DNA was extracted using the Blood genome column medium extraction kit following the manufacturer's instructions (Kangweishiji, China). Using genomic DNA, the exonic regions and flanking splice junctions of the genome were captured using the xGen Exome Research Panel v1.0 (IDT, Coralville, IA, United States). Finally, the libraries were sequenced on an Illumina NovaSeq 6000 series sequencer with the following parameters: PE150, minimum of 11.6 million reads. The sequencing was performed by the Beijing Chigene Translational Medicine Research Center Co., Ltd., Beijing, China.

Raw data were processed using the *fastp* tool to remove the adapters and filter out the low-quality reads. The paired-end reads were performed using a Burrows-Wheeler Aligner (BWA) against the Ensembl GRCh37/hg19 human reference genome (Li and Durbin, 2010). Both SNVs and small InDels were called using the Genomic Analysis Toolkit (GATK) software (version 4.1.7) (McKenna et al., 2010). The copy number variant (CNV) calling was based on the ExomeDepth algorithm. The total read count of the sample mapped to each exon in the same batch as described previously (Plagnol et al., 2012).

Variants were annotated using an online system, developed by Chigene which contains 35 public databases, while our in-house database contains WES data from 69015 individuals (**Supplementary Table 1**). Candidate SNVs/small InDels were confirmed by Sanger sequencing. A small CNV (<10 kb) would

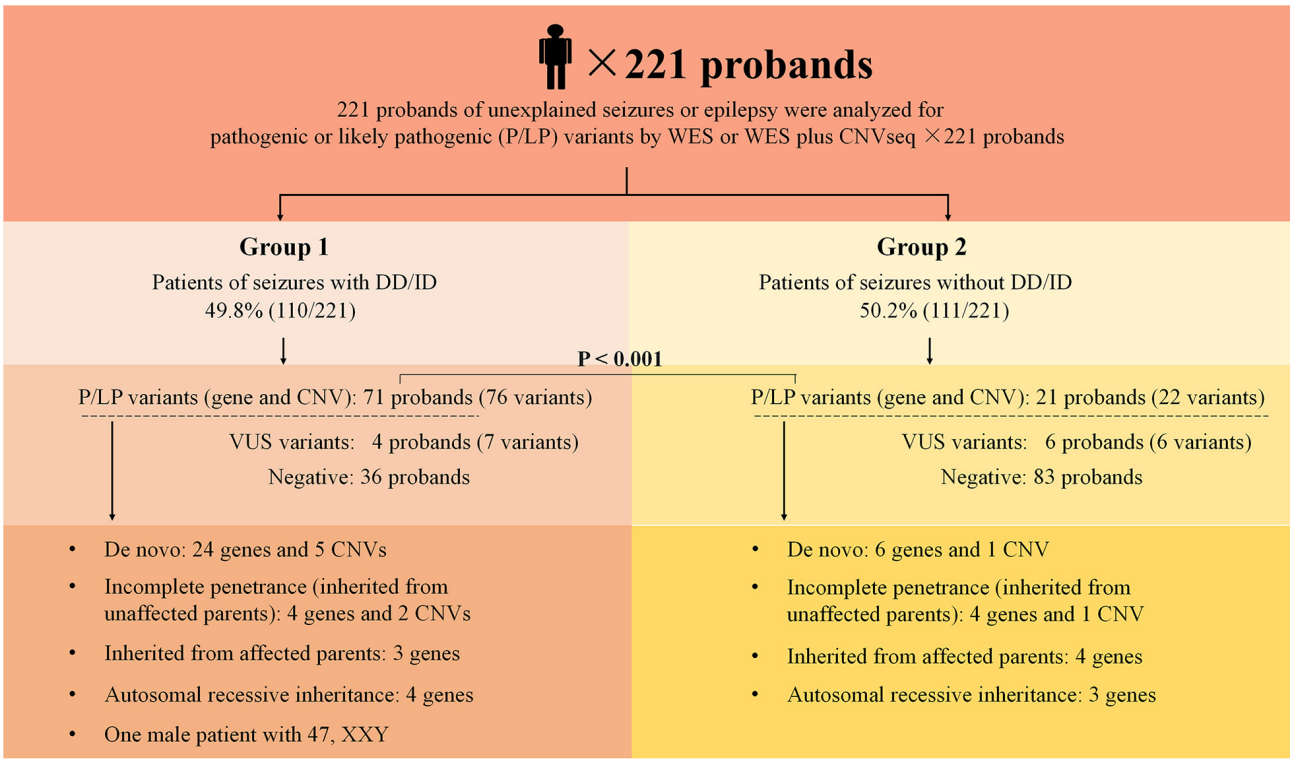

FIGURE 1 | Schematic summarizing the 221 probands from non-consanguineous pedigree. Two groups were considered in this study: epilepsy with DD/ID and epilepsy without DD/ID. Pathogenic or likely pathogenic variants were categorized as: *De novo*, incomplete penetrance, inherited from affected parents, autosomal recessive inheritance. DD, developmental delay; ID, intellectual disability; P, pathogenic; LP, likely pathogenic; VUS, variant uncertain significance; CNV, copy number variant; CNVseq, CNV sequencing; WES, whole-exome sequencing.

be considered if the phenotype was highly related to the candidate gene located in this CNV region; these were confirmed by quantitative polymerase chain reaction (qPCR). We classified the candidate variants according to the American College of Medical Genetics and Genomics (Richards et al., 2015) and Sequence Variant Interpretation Working Group international guidelines (SVI WG)[1].

Copy Number Variation Sequencing (CNVseq)

Copy number Variation Sequencing (CNVseq) was performed as previously described (Gao et al., 2019). Briefly, the genomic DNA was fragmented by sonication (Covaris, United States) into 200–300 bp fragments and checked using agarose gel electrophoresis. After genomic library preparation, DNA samples were subsequently sequenced on an Illumina NovaSeq 6000 series sequencer (Illumina, San Diego, CA, United States). Raw image files were processed using BclToFastq (Illumina) for the base calling and raw data generation. The reads were then mapped to the GRCh37/hg19 human reference genome using the BWA software (Li and Durbin, 2010). Variant calling for CNVs ≥100 kb was performed using an in-house pipeline, and the candidate CNVs were filtered and detected using public CNV databases (Decipher, ClinVar, OMIM, DGV, and ClinGen). The pathogenicity of CNVs was classified according to the American College of Medical Genetics and Genomics guidelines (Riggs et al., 2020).

Identification of Candidate Pathogenic *de novo* Variants

Variants (SNVs and InDels in coding region; canonical ± 1 or 2 splice sites) were considered to be candidate pathogenic *de novo* if they met the following criteria: (1) in patients with normal parental phenotype; (2) genotype call ratio > 0.3 and supporting read depth > 20; (3) minor allele frequency (MAF) < 0.0001 as reported in the Genome Aggregation Database (gnomAD); (4) Pathogenic variants were in the Ensembl canonical transcript.

Statistical Analysis

Categorical data are expressed in percentage and the comparisons between the groups were analyzed using the Pearson's Chi-square test or a two-tailed Fisher's exact test (for $N < 40$), in which a P-value smaller than 0.05 was considered to be statistically significant. We performed statistical analyses using SPSS software, version 25.0 (SPSS Inc., Chicago, IL, United States).

[1]https://www.clinicalgenome.org/working-groups/sequence-variant-interpretation/

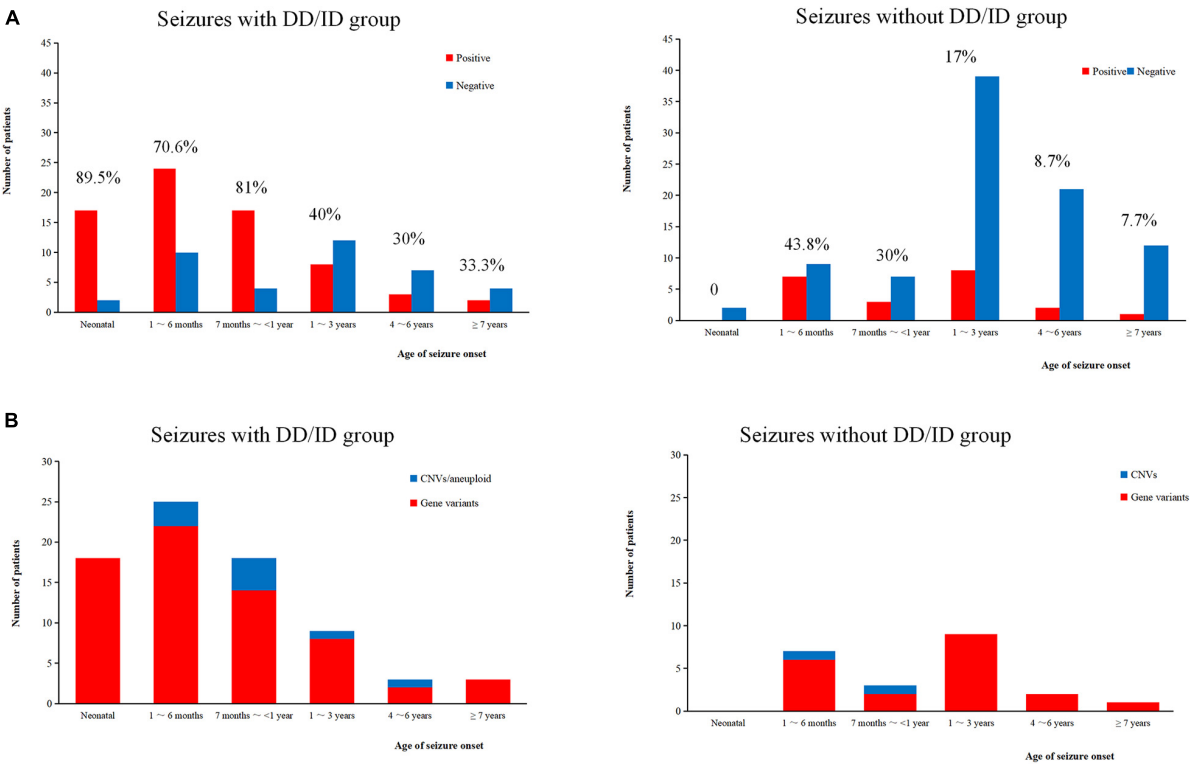

FIGURE 2 | Molecular diagnosis yield in different ages. **(A)** The molecular diagnosis yield in the groups of epilepsy with DD/ID and without DD/ID during different ages of seizure onset. **(B)** The individuals containing gene variants in the groups of epilepsy with DD/ID and without DD/ID during different ages of seizure onset. The percentage in the diagram represents the diagnosis positive rate = (P + LP)/all individuals in this age.

RESULTS

Participant Demographics and Phenotypes

Two hundred and twenty one of unrelated patients (96 females and 125 males) and their families were recruited from our hospital between January 2016 and November 2019. Patients were from non-consanguineous families in Southeast China. The age of seizure onset ranged from 1 day after birth to 15-years old. Sixty-six of the patients had family history of seizures. Patients were divided into two groups: the seizures with DD/ID group and the seizures without DD/ID group (**Figure 1**). Clinical information of the patients was summarized in **Supplementary Tables 2**, **3**.

Molecular Diagnosis Yields

We conducted WES to detect the epilepsy-associated gene variants. Pathogenic (P) or likely pathogenic (LP) variants were identified in 92 patients (92/221 = 41.6%), consisting of 87 distinct gene-level variants in eighty-two patients, 10 CNVs in nine patients, and one male patients with 47, XXY. These mutations were found in 71 patients in the group of seizures with DD/ID (71/110 = 64.5%) and 21 patients in the group of seizures without DD/ID group (21/111 = 18.9%), respectively (**Figure 2A**). The patients in the group of seizures with DD/ID had more P/LP mutations than those in the group of seizures without DD/ID ($P < 0.001$) (**Figure 2B**). Interestingly, the patients with seizures in DD/ID group under 1 year-old showed more P/LP variants than those of other groups. P/LP gene variants were identified in sixty patients under 1 year-old and 86.7% of the patients belong to DD/ID group. Intriguingly, 47 *de novo* variants and 29 novel variants were identified in 62 variants in the patients under 1-year-old (**Table 1**). Moreover, the number of *de novo* gene variants in patients with DD/ID was more than that of patients without DD/ID (**Table 2**). In addition, we also identified 13 variants of uncertain significance (VUS) in 4.5% (10/221) of the patients (**Supplementary Table 3**).

Gene Variants

To better understand the epilepsy-associated gene variants, we categorized the gene variants as *de novo*, incomplete penetrance, inherited from affected parents, and autosomal recessive (AR) variants. We found 58 *de novo* gene variants and 48 novel variants (**Table 3**, **Figure 3A**, and **Supplementary Table 2**). Thirty-two genes were associated with DD/ID group. *SCN1A* was most frequently involved, followed by *KCNQ2* and *TSC2*. *PRRT2* was most frequently involved in the group of seizures without DD/ID (**Figure 3B**).

It is interesting to explore the novel gene variants in the 129 epilepsy patients without P/LP variants. So we re-analyzed the data and selected 16 novel candidate genes from 14

TABLE 1 | Number of patients with P/LP gene variants.

	Patients with P/LP variants	Patients with P/LP of seizure onset <1 year variants
Total	92	68
With DD/ID	71	58
Without DD/ID	21	10
Gene variations		
Individuals containing gene variations	82	60
Total gene variants	87	62
No. of *de novo* variants	58	47
No. of Novel variants	48	29
Patients of CNVs/Aneuploid	10	8
No. of variants	11	9
No. of *de novo* variants	8	7

TABLE 2 | Number of *de novo* and novel gene variants in the patient under 1 year-old.

	With DD/ID	Without DD/ID	Total
De novo variants	43	4	47
Novel variants	26	3	29

individuals (**Figure 3C** and **Supplementary Table 4**); however, nine of the genes contain several *de novo* variants in the in-house control database, suggesting that these nine genes cannot be evaluated as the *de novo* genes associated with epilepsy. *De novo* variants in the other seven genes (*NCL*, *SEPHS2*, *PA2G4*, *SLC35G2*, *MYO1C*, *GPR158*, and *POU3F1*) were not found in the in-house control database. In addition, we found that *GPR158* and *POU3F1* are highly expressed in the nervous system according to the Genotype-Tissue Expression (GTEx) database[2]. It suggests that these seven genes may be related to epilepsy, while the functions of them need to be further confirmed.

Moreover, we also acquired seven variants from affected parent families, including *TSC1*, *PRRT2*, *TSC1*, *PROKR2*, *RYR2*, *GABRA1*, and *KCNMA1* genes (**Figure 3D**). Interestingly, a *de novo* variant, *SCN2A* c.668G>A was detected in patient #68 with epileptic encephalitis. Her brother also had *SCN2A* c.668G>A variant and showed hand clenching accompanied by slight shaking and up rolling of eyeballs. Then, we conducted ultra-deep sequencing (average deep: 20000×) and detected the *SCN2A*: c.668G>A variant in father's oral formulas, urine and seminal fluid. The results showed that the mosaicism percentage of oral formulas, urine and seminal fluid were 13.14, 12.7, and 23.26%, respectively. We confirmed that SCN2A c.668G>A variant was paternal germ line mosaicism (**Figure 3D** and **Supplementary Table 2**).

[2]https://www.gtexportal.org/home/

TABLE 3 | Forty-eight novel pathogenic or likely pathogenic variants.

Gene	Gene NM#	Variants of nucleic acid	Variants of protein	het/hom
ALDH7A1	NM_001182	exon 12	/	het
AP4M1	NM_004722	c.1264C>T	p.R422X	het
ARID1B	NM_020732	c.1910_c.1911 delGG	p.R637Ifs*15	het
ATM	NM_000051	c.7878_c.7882del TTATA	p.A2626Afs*28	het
DEPDC5	NM_001242896	c.562+1G>T	/	het
	NM_001242896	c.2731G>T	p.E911X	het
	NM_001242896	c.484-1_c.485delGGT	p.V162Gfs*18	het
DLG3	NM_021120	c.1861C>T	p.R621W	het
EEF1A2	NM_001958	c.289G>A	p.D97N	het
GABRA1	NM_001127644	c.466T>C	p.Y156H	het
GABRB2	NM_021911	c.946G>A	p.V316I	het
	NM_021911	c.486G>T	p.M162I	het
GRIN2A	NM_001134407	c.1965delA	p.Q655Qfs*8	het
	NM_001134407	c.2389delinsCAG	p.T797Qfs*12	het
KCNMA1	NM_001271520	c.391_c.392ins GGCGGC	p.L131delinsRRL	het
KCNQ2	NM_004518	c.836G>T	p.G279V	het
	NM_172107	c.485A>G	p.K162R	het
	NM_172107	c.504_c.505delCT	p.F168Lfs*4	het
MBD5	NM_018328	c.1628C>T	p.T543I	het
NPRL2	NM_006545	c.673C>T	p.Q225X	het
PCDH19	NM_001105243	c.497dupA	p.Y166X	het
	NM_001184880	c.470A>G	p.D157G	het
PLA2G6	NM_003560	c.127C>T	p.Q43X	hom
PRRT2	NM_001256443	c.489delG	p.Q163Qfs*13	het
RAI1	NM_030665	c.3301C>T	p.P1101S	het
	NM_030665	c.5254_c.5266 delGGGAAGCC CCCCA	p.G1752Gfs*94	het
RYR2	NM_001035	c.14767A>T	p.M4923L	het
SCN1A	NM_001202435	c.724C>T	p.Q242X	het
	NM_001165963	c.2791C>T	p.R931C	het
	NM_001202435	c.603-2A>T	/	het
	NM_001202435	c.4476+3_c.4476 +8 delAAGTAT	/	het
	NM_001165963	c.632delA	p.N211Mfs*5	het
	NM_001202435	c.479C>A	p.T160N	het
	NM_001202435	exon:26-27	/	het
SCN2A	NM_021007	c.4959G>C	p.L1653F	het
	NM_021007	c.4823-2A>C	NA	het
SLC13A5	NM_177550	c.202C>T	p.P68S	het
	NM_177550	c.429_c.437 delGCCGTGGTT	p.A143_A146 delinsA	het
SLC6A1	NM_003042	c.1367G>A	p.S456N	het
	NM_003042	c.1348_c.1349de lTT	p.F450Xfs*1	het
SPTAN1	NM_001130438	c.1595A>G	p.K532R	het
	NM_001130438	c.6614_c.66 16delAGG	p.Q2205_E2206 delinsQ	het
STXBP1	NM_003165	c.814delG	p.G272Gfs*5	het
	NM_003165	c.990dupG	p.L331Afs*21	het
	NM_003165	c.1A>T	p.M1L	het
TDP2	NM_016614	c.650delG	p.G217Efs*7	hom
TSC1	NM_000368	c.2041+2T>G	/	het
TSC2	NM_000548	c.3023_c.3038del TGGCCCAGG CTGACGA	p.V1008Vfs*3	het

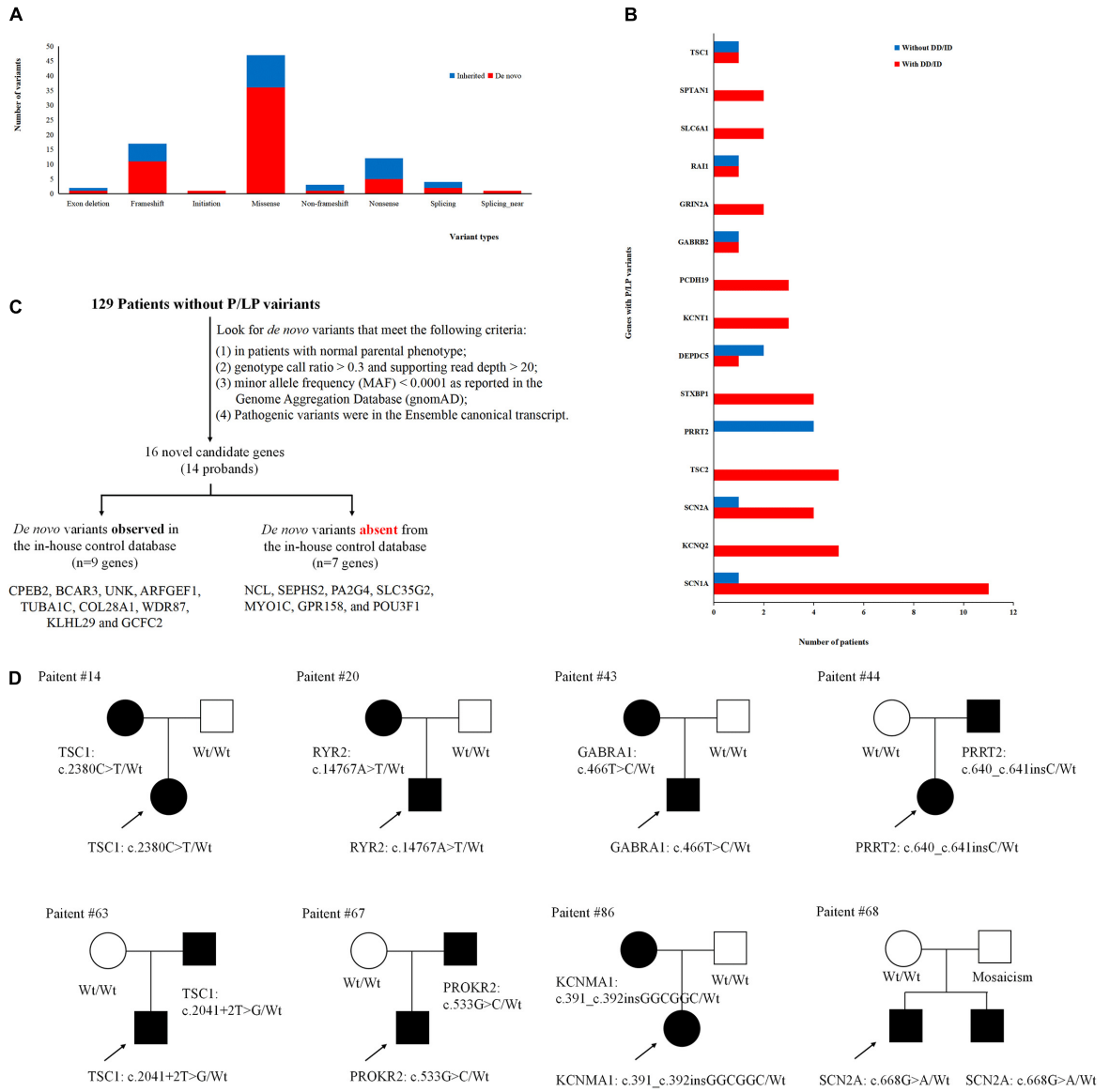

FIGURE 3 | Gene variants analysis. **(A)** The number of different variant types observed in patients. **(B)** Identification procedure of candidate pathogenic *de novo* variants. **(C)** Distribution of recurrent (≥2 patients) genes with pathogenic or likely pathogenic variants in the groups of epilepsy with DD/ID and without DD/ID. **(D)** The diagram of epilepsy pedigrees. ○ represents female; □ represents male; ● and ■ represents affected individuals; arrow represents probands; wt represents wild type.

CNVs by WES and CNVseq

In addition, we investigated CNVs in 123 of individuals (41 pedigrees). All aneuploidy and P/LP CNVs (>100 kb in size) were identifiable by WES and CNVseq (**Figures 1**, **4**). Ten P/LP CNVs in nine patients and one aneuploidy variant in one patient (Patient #56, #47, XXY) were identified by CNVseq. Three CNVs were located in chromosome 16 and belong to 16p11.2 deletion syndrome. Two CNVs were duplications and eight CNVs were deletions, ranging from 411 to 12 Mb (**Table 4** and **Supplementary Tables 5**, **6**). Patient #73 carried two *de novo* CNVs, which manifests as developmental delay and seizures. One of the CNVs was a deletion and located in Chr4, including *ZNF141*, *PIGG*, *PDE6B*, and *CPLX1* genes; another CNV was a duplication variant and located in Chr15, involving *MEF2A*, *ADAMTS17*, *CERS3*, *LINS*, *ALDH1A3*, and *CHSY1* genes. It was demonstrated that *CPLX1* gene functional aberration caused severe infantile myoclonic epilepsy and ID (Redler et al., 2017).

Therapeutic Implications

There were specific therapeutic recommendations for 10 genes with P/LP variants in the current cohort, including *ALDH7A1* (n = 1), *DEPDC5* (n = 3), *GRIN2A* (n = 2), *KCNQ2* (n = 5), *SCN1A* (n = 12), *SCN2A* (n = 5), *SLC2A1* (n = 1), *SLC6A1* (n = 2), *TSC1* (n = 2), and *TSC2* (n = 5). In this study, 32 patients

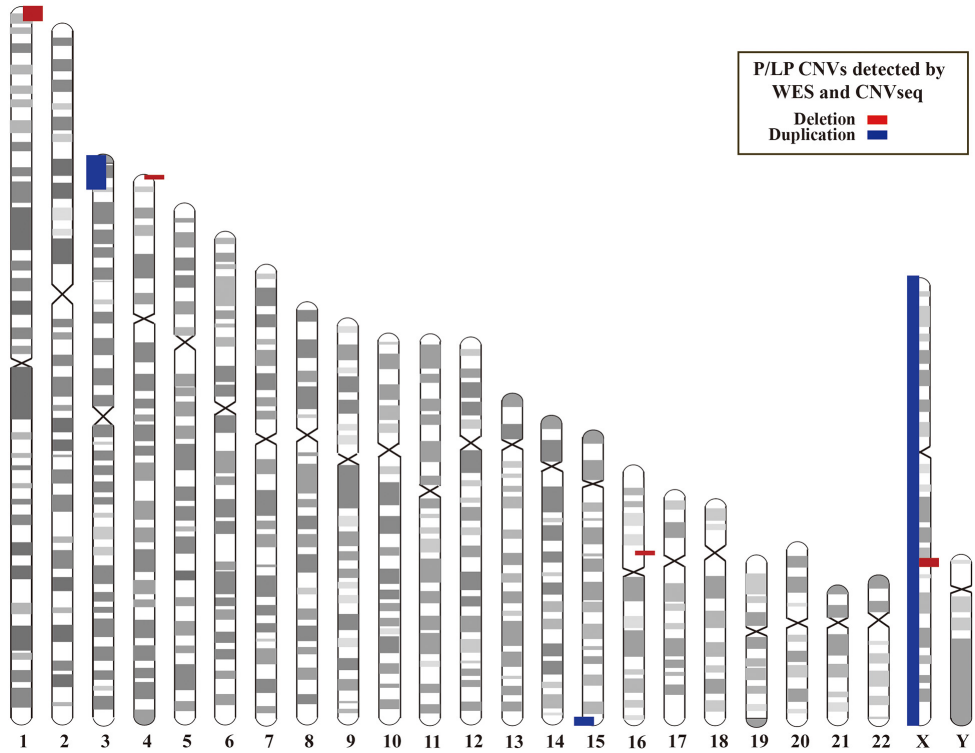

FIGURE 4 | Locations of P/LP CNVs identified by WES and/or CNVseq. CNV, copy number variant; CNVseq, CNV sequencing; WES, whole-exome sequencing.

were applicable drug selection based on molecular diagnosis. For example, the patient #24 was a 13 years-old female with mild ID. Prior to the genetic testing referral, she kept monthly seizures despite treatment with sodium valproate, levetiracetam, and lamotrigine. Genetic test revealed a missense variant in *SLC2A1* (c.997C>T, p.R333W), which cause the GLUT1 deficiency syndrome. Then a ketogenic diet was initiated based on the genetic results. Surprisingly, the patient kept seizure-free developmental improvement (cognitive and behavioral) after treatment. She has subsequently been tapered off all of the anti-epileptic drugs. For patients with the *SCN1A* gene mutations, a combination of VPA and TMP improved the seizures effectively and the whole treatment process should not use sodium channel blockers. In addition, vigabatrin treatment decreased the seizure frequency and improved EEG in four of patients with *TSC1* or *TSC2* gene mutations. Oxcarbazepine was effective for five of patients with *KCNQ2* gene mutations (**Table 5**).

DISCUSSION

Genetic factors were estimated to play a role in 70∼80% of epilepsy cases, especially in children and neonates (Hildebrand et al., 2013). Several studies have focused on the application of next-generation sequencing as a diagnostic tool for epilepsy (Veeramah et al., 2013; Dyment et al., 2015; Parrini et al., 2017). Recent cohort studies suggested that the diagnostic yield of WES varies from 23 to 42% in patients with epilepsy (Helbig et al., 2016; McTague et al., 2016; Costain et al., 2019; Snoeijen-Schouwenaars et al., 2019; Yang et al., 2019; Johannesen et al., 2020; Rochtus et al., 2020). In these studies, the phenotypes of patients varied widely, the inclusion and exclusion criteria of patients were also not consistent, and the pathogenic genes/pathways might be different. In the present study, the overall diagnostic yield was 41.6%. Further, we also found the diagnostic yield of the seizures with the DD/ID group to be higher than that in previous studies, especially in seizure onset under 1-year-old (∼78.4%) (Trump et al., 2016; Yang et al., 2019). It may be attributed to the following reasons. Firstly, our study analyzed SNVs, InDels, and CNVs, which can lead to a higher diagnostic yield. Secondly, the non-randomized selection/hospital-enrichment of the patients may lead to sampling bias. Pediatricians were likely to have subjective preference in the selection of patients with DD/ID for clinical genetic testing as it is easier to discover disease-related P/LP variants. Thirdly, for some patients in the seizures without DD/ID group, the patients under 4 years old might develop to ID later.

In the present study, thirteen of the patients carried P/LP variants that are inherited from unaffected parents (**Supplementary Table 2**), 53.8% (7/13) of them had autism spectrum disorder (ASD)/DD/ID (**Figure 1**). The unaffected phenotype of carriers was likely due to the incomplete penetrance, which was previously reported for the six genes: *DEPDC5*, *SCN1A*, *PCDH19*, *PRRT2*, *GRIN2A*, and *NPRL2*; 16p11.2 deletion and 16p12.1 microdeletion syndrome

TABLE 4 | Pathogenic/likely pathogenic CNVs identified by WES and CNVseq in forty-one pedigrees.

Patient ID	ASD	DD/ID	Position (hg19)	Size	Type	Inheritance	Associated Genetic Syndrome (OMIM disease ID)	Interpretation
26	N	N	chr4:76393-1613145	1.5M	deletion	*De novo*	/	LP
41	N	P	chr3:60001-12282678	12M	duplication	*De novo*	/	P
48	N	P	chr1:10001-4651608	4.6M	deletion	*De novo*	1p36 deletion syndrome (OMIM:#607872)	P
73	N	P	chr4:53382-964860	911Kb	deletion	*De novo*	/	LP
	/	/	chr15:100214597-102284775	2M	duplication	*De novo*	/	LP
76	N	P	chrX:96603114-99663595	3M	deletion	*De novo*	/	P
81	P	P	chr16:29468170-30301199	833Kb	deletion	*De novo*	16p11.2 deletion syndrome (OMIM:#611913)	LP
58	N	P	chr16:29594293-30171789	577Kb	deletion	paternal	16p11.2 deletion syndrome (OMIM:#611913)	LP
78	N	N	chr16:29571179-30189789	618Kb	deletion	paternal	16p11.2 deletion syndrome (OMIM:#611913)	LP
87	N	P	chr16:21964744-22376335	411Kb	deletion	paternal	16p12.1 deletion syndrome (OMIM:#136570)	LP

suggested that other modifier gene(s), as well as epigenetic or environmental factors, modulate the phenotype (Weiss et al., 2008; Girirajan et al., 2010; Dimova et al., 2012; Heron et al., 2012; Ishida et al., 2013; Lesca et al., 2013; Meng et al., 2015; Ricos et al., 2016). For example, the penetrance of *DEPDC5* variants with different forms of focal epilepsy was incomplete, varying from 50 to 82% (Ishida et al., 2013; Ricos et al., 2016). In this study, the *DEPDC5* gene variants were null variants (c.562+1G>T, c.2731G>T, c.484-1_c.485delGGT) carried by three patients with focal epilepsy (Patient #10, #46, and #84). Only patient #10 had epilepsy with DD. Actually the patient #10 carried two *DEPDC5* variants, c.562+1G>T and c.2507A>G (p.Y836C), the latter was inherited from his asymptomatic father. We can't confirm the *DEPDC5* gene with an AR inheritance in our local database. So this bi-allelic defect may exacerbate the clinical symptoms and further studies are required to confirm the functions.

Some studies defined that therapeutic outcomes of epilepsy were mostly based on the effect of protein function, clinical observation, and literature reports (Schoonjans et al., 2017; Yang et al., 2019; Johannesen et al., 2020). Herein, we reported the choices of therapeutic intervention in 32 of patients were affected based on the genetic diagnosis and the symptoms of some patients were improved effectively (**Table 5**). As some types of epilepsies responded to particular antiepileptic medications, personalized therapeutic strategies will be the best choice of epilepsy therapy. The top three most frequently mutated genes were the same as reported in this cohorts, including *SCN1A*, *KCNQ2*, and *TSC2* (Yang et al., 2019). In addition, we also found that *PRRT2* heterogeneous variant was the most frequent mutated gene in the group of seizures without DD/ID. Moreover, we detected three cases with 16p11.2 deletion (includes *PRRT2* gene). Two of the patients (#58 and #81) were with DD/ID and one patient (#78) hasn't shown DD/ID (<4 years-old). Our results are consistent with the previous reported (Ebrahimi-Fakhari et al., 1993; Termsarasab et al., 2014). Ebrahimi-Fakhari et al. (1993) reported that the patients with *PRRT2* heterogenous variants commonly exhibited epilepsy and paroxysmal movement disorders (PRRT2-associated paroxysmal movement disorders, RRT2-PxMD) without intellectual delay. While the individuals with 16p11.2 deletion, or with rare bi-allelic *PRRT2* pathogenic variants exhibited DD/ID or ASD. Meanwhile, we identified seven genes with *de novo* variants in pathogenically uncertain patients, which included the previously reported *GPR158* (OMIM: 614573) gene. *GPR158* gene is related to seizures (Elmariah et al., 2014) and highly expressed in the nervous system. It may be a promising epilepsy candidate gene. The function of the other six genes (*NCL*, *SEPHS2*, *PA2G4*, *SLC35G2*, *MYO1C*, and *POU3F1*) is currently unknown in the nervous system and the gene variations were observed in only one individual. The functions of these genes need to be further confirmed. Briefly, WES could help physicians identify epilepsy-associated genes in early onset patients and further provide effective treatment in clinic and improve patients' life quality.

In fact, this study still had several limitations. Firstly, our data revealed several *de novo* SNVs/InDels; however, mosaicism was not confirmed. Secondly, we didn't identify the plausible causal mutations in more than half of the patients. It indicates that these patients may not be an aggregate of simple Mendelian disorders and therefore require further powerful tools to evaluate the disease elucidation. Thirdly, in our study, although we identified seven potential candidate genes related to epilepsy disease, there is currently not enough evidence to support their pathogenicity. Therefore, a more comprehensive testing tool and further genetic studies with larger cohorts are required to fully elucidate the underlying etiology. Meanwhile, functional tests are urgent for assessing the epilepsy-associated genes.

In conclusion, our study demonstrates that the simultaneous analysis of SNVs, InDels, and CNVs based on NGS data

TABLE 5 | Treatment strategies of 32 cases of patients based on WES diagnosis.

Patient ID	Age of seizure onset	Diagnosis	Treatment Impact	All Treatment	Prognosis	Gene	Variants of nucleic acid	Variants of protein
6	1 year 1 month	FE	Treated with VB6	VPA, VB6	No seizures in the last years	*ALDH7A1*	c.1061A>G	p.Y354C
						ALDH7A1	exon 12	/
10	1 month 4 days	FE	Treated with KD, improved in seizure frequency	OXC, TPM, VPA, LEV, LTG, KD	4 seizures in the last years	*DEPDC5*	c.562+1G>T	/
19	3 years 2 months	EE (EAS)	Treated with ACTH and LEV, decreased epileptic discharges during sleep	VPA, ACTH, LEV	5 seizures in the last years	*GRIN2A*	c.1965delA	p.Q655Qfs*8
77	3 years 10 months	EE (EAS)	Treated with LEV, decreased epileptic discharges during sleep	VPA, LEV	No seizures in the last years	*GRIN2A*	c.2389delinsCAG	p.T797Qfs*12
23	7 days	EE (OS)	Treated with OXC, improved the seizure frequency	VPA, TMP, OXC	1 seizures in the last years	*KCNQ2*	c.587C>T	p.A196V
34	1 day	EE (OS)	Treated with OXC, no change in seizure frequency	NZP, LEV, OXC	1–3 seizures per month	*KCNQ2*	c.836G>T	p.G279V
40	2 day	EE (OS)	Treated with OXC, improved the seizure frequency	PB, OXC, TMP, OXC	No seizures in the last 5 months	*KCNQ2*	c.881C>T	p.A294V
80	3 days	EE	Treated with OXC, improved the seizure frequency	TMP, OXC	No seizures in the last 3 months	*KCNQ2*	c.485A>G	p.K162R
89	9 days	EE	Treated with OXC, improved the seizure frequency	VPA, TMP, OXC	Seizures almost every months	*KCNQ2*	c.504_c.505delCT	p.F168Lfs*4
5	7 months	EE (DS or DS-like)	Avoiding sodium channel blockers and Change from LEV to VPA, TMP	LEV, CZP, VPA, TPM	Seizures 1–2 times a year, mostly heat-related	*SCN1A*	c.724C>T	p.Q242X
7	7 months	EE (DS or DS-like)	Avoiding sodium channel blockers and started Valproic acid early	VPA, TPM	Seizures 1–2 times a year, mostly heat-related	*SCN1A*	c.1198A>C	p.M400L
33	7 months	EE (DS or DS-like)	Avoiding sodium channel blockers and Change from LEV to VPA, TMP	LEV, TMP, VPA	4 seizures in the last years, heat-related	*SCN1A*	c.603-2A > T	/
35	7 months	EE (DS or DS-like)	Avoiding sodium channel blockers and unnecessary medical investigations	VPA, TMP	3 seizures in the last years, heat-related	*SCN1A*	c.4476+3_c.4476+8 delAAGTAT	/
38	1 months 25 days	EE	Change from OXC to VPA, improved the seizure frequency	OXC, VPA	No seizures in the last 3 months	*SCN1A*	c.677C>T	p.T226M
39	5 months	EE (DS or DS-like)	Avoiding sodium channel blockers	CZP, TMP, LEV	5 seizures in the last years, heat-related	*SCN1A*	c.632delA	p.N211Mfs*5
42	8 months	GE	Avoiding sodium channel blockers and started Valproic acid early	VPA, LEV	No seizures in the last 3 months	*SCN1A*	c.695G>T	p.G232V
53	8 months	EE (DS or DS-like)	Avoiding sodium channel blockers	VPA, LEV	4 seizures in the last years, heat-related	*SCN1A*	c.2134C>T	p.R712X
65	5 months	EE (DS or DS-like)	Avoiding sodium channel blockers and started Valproic acid early	VPA, LEV	No seizures in the last 3 months	*SCN1A*	c.5339T>G	p.M1780R

(Continued)

TABLE 5 | Continued

Patient ID	Age of seizure onset	Diagnosis	Treatment Impact	All Treatment	Prognosis	Gene	Variants of nucleic acid	Variants of protein
72	5 months	EE (DS or DS-like)	Change from OXC to VPA, improved the seizure frequency	OXC, VPA	4 seizures in the last years, mostly heat-related	*SCN1A*	c.479C>A	p.T160N
92	8 months	EE	Avoiding sodium channel blockers and started Valproic acid early	VPA, TMP	2 seizures in the last years, heat-related	*SCN1A*	exon:26-27	/
30	19 days	EE (OS)	Treated with LCS, no improvement in seizure frequency	VPA, NZP, TMP, LCS	Seizures almost every month	*SCN2A*	c.4959G>C	p.L1653F
52	1 years 9 months	FE	Treated with LCS, improved the seizure frequency	OXC, LCS	No seizures in the last years	*SCN2A*	c.4823-2A>C	NA
54	1 days	EE	Treated with LCS, improved the seizure frequency	OXC, TMP, LCS	Seizures almost every weeks	*SCN2A*	c.640T>C	p.S214P
24	5 months	EE, GULT1-DS	Treatment with KD, seizure-free and significant improvement in development, and significant progress in cognitive and behavioral development	VPA, LEV, LTG, KD	No seizures in the last 3 years	*SLC2A1*	c.997C>T	p.R333W
61	4 years	EE (DOOSE)	Treated with KD, improved the seizure frequency	LEV, NZP, KD	No seizures in the last years	*SLC6A1*	c.1348_c.1349delTT	p.F450Xfs*1
14	11 months	EE, TSC	Influenced choice of future treatment	VPA, CZP, TMP, LEV	3 seizures in the last years	*TSC1*	c.2380C>T	p.Q794X
63	1 years 3 months	FE, TSC	Influenced choice of future treatment	CBZ	No seizures in the last 3 months	*TSC1*	c.2041+2T>G	/
3	9 months	FE, TSC	Treated with VGB and Rapamycin, improved the seizure frequency and EEG	VPA, VGB, Rapamycin	3–5 seizures per week	*TSC2*	c.3023_c.3038del TGGCCCAGG CTGACGA	p.V1008Vfs*3
9	1 years	FE, TSC	Influenced choice of future treatment	VPA, TMP	No seizures in the last years	*TSC2*	c.4925G>A	p.G1642D
16	7 months	EE (West), TCS	Treated with VGB, improved the seizure frequency and EEG	ACTH, Prednisone, VPA, TMP, VGB	5 seizures in the last years	*TSC2*	c.3608C>G	p.T1203R
70	5 months	FE, TSC	Treated with VGB, improved the seizure frequency and EEG	ACTH, Prednisone, VPA, LCS, VGB	Seizures almost every days	*TSC2*	c.4868C>T	p.T1623I
83	11 months	EE (WEST)	Treated with VGB and LEV, improved the seizure frequency and EEG	Prednisone, VPA, VGB, LEV	Seizures almost every weeks	*TSC2*	c.1831C>T	p.R611W

can provide a high diagnostic yield for epilepsy, especially for patients with DD/ID, age of seizure onset under 1-year-old. We further demonstrate the potential of genetic diagnosis impacts on choosing the optimal treatment strategy for these patients.

DATA AVAILABILITY STATEMENT

The original contributions presented in the study are included in the article. Data on patients cannot be made fully accessible in accordance with local research ethics protocols. Further inquiries can be directed to the corresponding author/s.

ETHICS STATEMENT

The studies involving human participants were reviewed and approved by the Ethics Committee of the Children's Hospital, Zhejiang University School of Medicine. Written informed consent to participate in this study was provided by the participants' legal guardian/next of kin.

AUTHOR CONTRIBUTIONS

TJ, JG, LJ, and FG designed the data collection instruments, collected the data, and carried out the initial analyses. TJ,

YS, YY, and FG reviewed and revised the manuscript. LX, CZ, XS, WG, and XK conceptualized the study and coordinated and supervised data collection. All authors approved the final manuscript as submitted and agreed to be accountable for all aspects of the work.

FUNDING

This work is supported by the Key Research and Development Program of Zhejiang Province, Grant/Award Number: 2020C03038; the National Natural Science Foundation of China Project, Grant/Award Number: U1909209; and the Natural Science Foundation of Zhejiang Province, Grant/Award Number: LBY21H090002.

ACKNOWLEDGMENTS

We thank the patients and their families for participating in our research. We also thank the many physicians and families for referring patients.

SUPPLEMENTARY MATERIAL

The Supplementary Material for this article can be found online at: https://www.frontiersin.org/articles/10.3389/fnmol.2021.699574/full#supplementary-material

Supplementary Table 1 | The information of the public databases used in Chigene database.

Supplementary Table 2 | Clinical and molecular features of positive patients with positive genetic diagnosis. M, male; F, female; Y, year(s); M, month(s); D, day(s). Diagnosis: BFIS, benign familial infantile seizures; CCHD, critical congenital heart disease; CPVT, catecholaminergic polymorphic ventricular tachycardia; DOOSE, Doose Syndrome; DS or DS-like, Dravet syndrome or Dravet syndrome-like; EAS, epilepsy-aphasia spectrum; EE, epileptic encephalopathy; FE, focal epilepsy; FFEVF, familial focal epilepsy with variable foci; GE, generalized epilepsy; GEFS+, genetic epilepsy with febrile seizures plus; GULT1-DS, glucose transporter type 1 deficiency syndrome; IT, immune thrombocytopenia; LGS, Lennox-Gastaut Syndrome; MMPSI, malignant migrating partial seizures of infancy; OS, Ohtahara syndrome; PKD, paroxysmal kinesigenic dyskinesia; RTT, Rett syndrome; TSC, tuberous sclerosis; WEST, West syndrome. FOS, focal onset; FS, febrile seizures; GOS, generalized onset; DD, Developmental delay: ASD, autism spectrum disorder. Treatment: ACTH, adrenocorticotropic hormone; CBZ, carbamazepine; CLB, clobazam; CZP, clonazepam; KD, ketogenic diet; LCS, lacosamide; LCT, L-carnitine; LEV, levetiracetam; LTG, lamotrigine; NZP, nitrazepam; OXC, oxcarbazepine; PA, prednisone acetate; PB, phenobarbitone; RPM, rapamycin; TPM, topiramate; VB6, vitamin B6; VGB, vigabatrin; VPA, valproate. AR, autosomal recessive; AD, autosomal dominant; XL, X-linked; XLD, X-linked dominant; XLR, X-linked recessive; P, positive; N, negative; nd, not determined.

Supplementary Table 3 | Clinical and molecular features of patients with variants of uncertain significance (VUS) identify in the cohort. M, male; F, female; Y, year(s); M, month(s); D, day(s); AR, autosomal recessive; AD, autosomal dominant; P, positive; N, negative; nd, not determined.

Supplementary Table 4 | Clinical and molecular features of patients with *de novo* variants identified in the negative cohort. M, male; F, female; Y, year(s); M, month(s); D, day(s); AR, autosomal recessive; AD, autosomal dominant; XLD, X-linked dominant; XLR, X-linked recessive.

Supplementary Table 5 | Sequencing data quality of whole-exome sequencing and CNVseq for the patients and their parents. CNVseq, copy number variant sequencing.

Supplementary Table 6 | Pathogenic/likely pathogenic CNVs identified by WES and CNVseq in the cohort. M, male; F, female.

REFERENCES

Annegers, J. F., Hauser, W. A., Anderson, V. E., and Kurland, L. T. (1982). The risks of seizure disorders among relatives of patients with childhood onset epilepsy. *Neurology* 32, 174–179. doi: 10.1212/wnl.32.2.174

Berg, A. T., Wusthoff, C., Shellhaas, R. A., Loddenkemper, T., Grinspan, Z. M., Saneto, R. P., et al. (2019). Immediate outcomes in early life epilepsy: A contemporary account. *Epilepsy Behav.* 97, 44–50. doi: 10.1016/j.yebeh.2019.05.011

Costain, G., Cordeiro, D., Matviychuk, D., and Mercimek-Andrews, S. (2019). Clinical application of targeted next-generation sequencing panels and whole exome sequencing in childhood epilepsy. *Neuroscience* 418, 291–310. doi: 10.1016/j.neuroscience.2019.08.016

Dimova, P. S., Kirov, A., Todorova, A., Todorov, T., and Mitev, V. (2012). A novel PCDH19 mutation inherited from an unaffected mother. *Pediatr. Neurol.* 46, 397–400. doi: 10.1016/j.pediatrneurol.2012.03.004

Dyment, D. A., Tetreault, M., Beaulieu, C. L., Hartley, T., Ferreira, P., Chardon, J. W., et al. (2015). Whole-exome sequencing broadens the phenotypic spectrum of rare pediatric epilepsy: a retrospective study. *Clin. Genet.* 88, 34–40. doi: 10.1111/cge.12464

Ebrahimi-Fakhari, D., Moufawad El Achkar, C., and Klein, C. (1993). "PRRT2-associated paroxysmal movement disorders," in *GeneReviews(®), © 1993-2021, University of Washington, Seattle*, eds M. P. Adam, H. H. Ardinger, and R. A. Pagon (Seattle, WA: University of Washington).

Elmariah, H., Garrett, M. E., Soldano, K. L., Ataga, K. I., Eckman, J. R., Telen, M. J., et al. (2014). Genes associated with survival in adult sickle cell disease. *Blood* 124:2719.

Gao, C., Wang, X., Mei, S., Li, D., Duan, J., Zhang, P., et al. (2019). Diagnostic yields of trio-WES accompanied by CNVseq for rare neurodevelopmental disorders. *Front. Genet.* 10:485. doi: 10.3389/fgene.2019.00485

Girirajan, S., Rosenfeld, J. A., Cooper, G. M., Antonacci, F., Siswara, P., Itsara, A., et al. (2010). A recurrent 16p12.1 microdeletion supports a two-hit model for severe developmental delay. *Nat. Genet.* 42, 203–209. doi: 10.1038/ng.534

Helbig, K. L., Farwell Hagman, K. D., Shinde, D. N., Mroske, C., Powis, Z., Li, S., et al. (2016). Diagnostic exome sequencing provides a molecular diagnosis for a significant proportion of patients with epilepsy. *Genet. Med.* 18, 898–905. doi: 10.1038/gim.2015.186

Heron, S. E., Grinton, B. E., Kivity, S., Afawi, Z., Zuberi, S. M., Hughes, J. N., et al. (2012). PRRT2 mutations cause benign familial infantile epilepsy and infantile convulsions with choreoathetosis syndrome. *Am. J. Hum. Genet.* 90, 152–160. doi: 10.1016/j.ajhg.2011.12.003

Hildebrand, M. S., Dahl, H. H., Damiano, J. A., Smith, R. J., Scheffer, I. E., and Berkovic, S. F. (2013). Recent advances in the molecular genetics of epilepsy. *J. Med. Genet.* 50, 271–279. doi: 10.1136/jmedgenet-2012-101448

Ishida, S., Picard, F., Rudolf, G., Noé, E., Achaz, G., Thomas, P., et al. (2013). Mutations of DEPDC5 cause autosomal dominant focal epilepsies. *Nat. Genet.* 45, 552–555. doi: 10.1038/ng.2601

Johannesen, K. M., Nikanorova, N., Marjanovic, D., Pavbro, A., Larsen, L. H. G., Rubboli, G., et al. (2020). Utility of genetic testing for therapeutic decision-making in adults with epilepsy. *Epilepsia* 61, 1234–1239. doi: 10.1111/epi.16533

Lesca, G., Rudolf, G., Bruneau, N., Lozovaya, N., Labalme, A., Boutry-Kryza, N., et al. (2013). GRIN2A mutations in acquired epileptic aphasia and related childhood focal epilepsies and encephalopathies with speech and language dysfunction. *Nat. Genet.* 45, 1061–1066. doi: 10.1038/ng.2726

Li, H., and Durbin, R. (2010). Fast and accurate long-read alignment with Burrows-Wheeler transform. *Bioinformatics* 26, 589–595. doi: 10.1093/bioinformatics/btp698

MacArthur, D. G., Manolio, T. A., Dimmock, D. P., Rehm, H. L., Shendure, J., Abecasis, G. R., et al. (2014). Guidelines for investigating causality of

sequence variants in human disease. *Nature* 508, 469–476. doi: 10.1038/nature13127

Manichaikul, A., Mychaleckyj, J. C., Rich, S. S., Daly, K., Sale, M., and Chen, W.-M. (2010). Robust relationship inference in genome-wide association studies. *Bioinformatics* 26, 2867–2873. doi: 10.1093/bioinformatics/btq559

McKenna, A., Hanna, M., Banks, E., Sivachenko, A., Cibulskis, K., Kernytsky, A., et al. (2010). The genome analysis toolkit: a MapReduce framework for analyzing next-generation DNA sequencing data. *Genome Res.* 20, 1297–1303. doi: 10.1101/gr.107524.110

McTague, A., Howell, K. B., Cross, J. H., Kurian, M. A., and Scheffer, I. E. (2016). The genetic landscape of the epileptic encephalopathies of infancy and childhood. *Lancet Neurol.* 15, 304–316. doi: 10.1016/s1474-4422(15)00250-1

Meng, H., Xu, H. Q., Yu, L., Lin, G. W., He, N., Su, T., et al. (2015). The SCN1A mutation database: updating information and analysis of the relationships among genotype, functional alteration, and phenotype. *Hum. Mutat.* 36, 573–580. doi: 10.1002/humu.22782

Møller, R. S., Dahl, H. A., and Helbig, I. (2015). The contribution of next generation sequencing to epilepsy genetics. *Expert Rev. Mol. Diagnost.* 15, 1531–1538. doi: 10.1586/14737159.2015.1113132

Myers, C. T., and Mefford, H. C. (2015). Advancing epilepsy genetics in the genomic era. *Genome Med.* 7:91. doi: 10.1186/s13073-015-0214-7

Nickels, K. C., Zaccariello, M. J., Hamiwka, L. D., and Wirrell, E. C. (2016). Cognitive and neurodevelopmental comorbidities in paediatric epilepsy. *Nat. Rev. Neurol.* 12, 465–476. doi: 10.1038/nrneurol.2016.98

Parrini, E., Marini, C., Mei, D., Galuppi, A., Cellini, E., Pucatti, D., et al. (2017). Diagnostic targeted resequencing in 349 patients with drug-resistant pediatric epilepsies identifies causative mutations in 30 different genes. *Hum. Mutat.* 38, 216–225. doi: 10.1002/humu.23149

Pitkänen, A., Löscher, W., Vezzani, A., Becker, A. J., Simonato, M., Lukasiuk, K., et al. (2016). Advances in the development of biomarkers for epilepsy. *Lancet Neurol.* 15, 843–856. doi: 10.1016/s1474-4422(16)00112-5

Plagnol, V., Curtis, J., Epstein, M., Mok, K. Y., Stebbings, E., Grigoriadou, S., et al. (2012). A robust model for read count data in exome sequencing experiments and implications for copy number variant calling. *Bioinformatics* 28, 2747–2754. doi: 10.1093/bioinformatics/bts526

Poduri, A., and Lowenstein, D. (2011). Epilepsy genetics–past, present, and future. *Curr. Opin. Genet. Dev.* 21, 325–332. doi: 10.1016/j.gde.2011.01.005

Redler, S., Strom, T. M., Wieland, T., Cremer, K., Engels, H., Distelmaier, F., et al. (2017). Variants in CPLX1 in two families with autosomal-recessive severe infantile myoclonic epilepsy and ID. *Eur. J. Hum. Genet.* 25, 889–893. doi: 10.1038/ejhg.2017.52

Richards, S., Aziz, N., Bale, S., Bick, D., Das, S., Gastier-Foster, J., et al. (2015). Standards and guidelines for the interpretation of sequence variants: a joint consensus recommendation of the American College of Medical Genetics and Genomics and the Association for Molecular Pathology. *Genet. Med.* 17, 405–424. doi: 10.1038/gim.2015.30

Ricos, M. G., Hodgson, B. L., Pippucci, T., Saidin, A., Ong, Y. S., Heron, S. E., et al. (2016). Mutations in the mammalian target of rapamycin pathway regulators NPRL2 and NPRL3 cause focal epilepsy. *Ann. Neurol.* 79, 120–131. doi: 10.1002/ana.24547

Riggs, E. R., Andersen, E. F., Cherry, A. M., Kantarci, S., Kearney, H., Patel, A., et al. (2020). Technical standards for the interpretation and reporting of constitutional copy-number variants: a joint consensus recommendation of the American College of Medical Genetics and Genomics (ACMG) and the Clinical Genome Resource (ClinGen). *Genet. Med.* 22, 245–257. doi: 10.1038/s41436-019-0686-8

Rochtus, A., Olson, H. E., Smith, L., Keith, L. G., El Achkar, C., Taylor, A., et al. (2020). Genetic diagnoses in epilepsy: the impact of dynamic exome analysis in a pediatric cohort. *Epilepsia* 61, 249–258. doi: 10.1111/epi.16427

Scheffer, I. E., and Berkovic, S. F. (1997). Generalized epilepsy with febrile seizures plus. A genetic disorder with heterogeneous clinical phenotypes. *Brain* 120(Pt 3), 479–490. doi: 10.1093/brain/120.3.479

Schoonjans, A., Paelinck, B. P., Marchau, F., Gunning, B., Gammaitoni, A., Galer, B. S., et al. (2017). Low-dose fenfluramine significantly reduces seizure frequency in Dravet syndrome: a prospective study of a new cohort of patients. *Eur. J. Neurol.* 24, 309–314. doi: 10.1111/ene.13195

Snoeijen-Schouwenaars, F. M., van Ool, J. S., Verhoeven, J. S., van Mierlo, P., Braakman, H. M. H., Smeets, E. E., et al. (2019). Diagnostic exome sequencing in 100 consecutive patients with both epilepsy and intellectual disability. *Epilepsia* 60, 155–164. doi: 10.1111/epi.14618

Termsarasab, P., Yang, A. C., Reiner, J., Mei, H., Scott, S. A., and Frucht, S. J. (2014). Paroxysmal kinesigenic dyskinesia caused by 16p11.2 microdeletion. *Tremor Other Hyperkinet. Mov.* 4:274.

Trump, N., McTague, A., Brittain, H., Papandreou, A., Meyer, E., Ngoh, A., et al. (2016). Improving diagnosis and broadening the phenotypes in early-onset seizure and severe developmental delay disorders through gene panel analysis. *J. Med. Genet.* 53, 310–317. doi: 10.1136/jmedgenet-2015-103263

Veeramah, K. R., Johnstone, L., Karafet, T. M., Wolf, D., Sprissler, R., Salogiannis, J., et al. (2013). Exome sequencing reveals new causal mutations in children with epileptic encephalopathies. *Epilepsia* 54, 1270–1281. doi: 10.1111/epi.12201

Weiss, L. A., Shen, Y., Korn, J. M., Arking, D. E., Miller, D. T., Fossdal, R., et al. (2008). Association between microdeletion and microduplication at 16p11.2 and autism. *N. Engl. J. Med.* 358, 667–675. doi: 10.1056/NEJMoa075974

Yang, L., Kong, Y., Dong, X., Hu, L., Lin, Y., Chen, X., et al. (2019). Clinical and genetic spectrum of a large cohort of children with epilepsy in China. *Genet. Med.* 21, 564–571. doi: 10.1038/s41436-018-0091-8

Conflict of Interest: WG, XK, YY was employed by company Beijing Chigene Translational Medical Research Center Co., Ltd.

The remaining authors declare that the research was conducted in the absence of any commercial or financial relationships that could be construed as a potential conflict of interest.

Publisher's Note: All claims expressed in this article are solely those of the authors and do not necessarily represent those of their affiliated organizations, or those of the publisher, the editors and the reviewers. Any product that may be evaluated in this article, or claim that may be made by its manufacturer, is not guaranteed or endorsed by the publisher.

frontiers in Molecular Neuroscience

ORIGINAL RESEARCH
published: 14 October 2021
doi: 10.3389/fnmol.2021.720984

GRIN2A Variants Associated With Idiopathic Generalized Epilepsies

Xiao-Rong Liu[1†‡], Xing-Xing Xu[2‡], Si-Mei Lin[1], Cui-Ying Fan[3], Ting-Ting Ye[1], Bin Tang[1], Yi-Wu Shi[1], Tao Su[1], Bing-Mei Li[1], Yong-Hong Yi[1], Jian-Hong Luo[3†] and Wei-Ping Liao[1*†] for the China Epilepsy Gene 1.0 Project*

[1] Key Laboratory of Neurogenetics and Channelopathies of Guangdong Province and the Ministry of Education of China, Institute of Neuroscience and Department of Neurology of the Second Affiliated Hospital of Guangzhou Medical University, Guangzhou, China, [2] Department of Physiology, Wenzhou Medical University, Wenzhou, China, [3] NHC and CAMS Key Laboratory of Medical Neurobiology, MOE Frontier Science Center for Brain Research and Brain-Machine Integration, School of Brain Science and Brain Medicine, Zhejiang University School of Medicine, Hangzhou, China

OPEN ACCESS

Edited by:
Nobuyuki Takei,
Niigata University, Japan

Reviewed by:
Hiroki Kitaura,
Niigata University, Japan
Pierre Szepetowski,
INSERM U901 Institut de Neurobiologie de la Méditerranée, France

***Correspondence:**
Wei-Ping Liao
wpliao@vip.tom.com
Jian-Hong Luo
luojianhong@zju.edu.cn

†ORCID:
Xiao-Rong Liu
orcid.org/0000-0002-7769-9564
Wei-Ping Liao
orcid.org/0000-0001-9929-9185
Jian-Hong Luo
orcid.org/0000-0001-7832-496X

‡These authors have contributed equally to this work

Specialty section:
This article was submitted to Brain Disease Mechanisms, a section of the journal Frontiers in Molecular Neuroscience

Received: 05 June 2021
Accepted: 30 August 2021
Published: 14 October 2021

Citation:
Liu X-R, Xu X-X, Lin S-M, Fan C-Y, Ye T-T, Tang B, Shi Y-W, Su T, Li B-M, Yi Y-H, Luo J-H and Liao W-P (2021) GRIN2A Variants Associated With Idiopathic Generalized Epilepsies. Front. Mol. Neurosci. 14:720984. doi: 10.3389/fnmol.2021.720984

Objective: The objective of this study is to explore the role of *GRIN2A* gene in idiopathic generalized epilepsies and the potential underlying mechanism for phenotypic variation.

Methods: Whole-exome sequencing was performed in a cohort of 88 patients with idiopathic generalized epilepsies. Electro-physiological alterations of the recombinant *N*-methyl-D-aspartate receptors (NMDARs) containing GluN2A mutants were examined using two-electrode voltage-clamp recordings. The alterations of protein expression were detected by immunofluorescence staining and biotinylation. Previous studies reported that epilepsy related *GRIN2A* missense mutations were reviewed. The correlation among phenotypes, functional alterations, and molecular locations was analyzed.

Results: Three novel heterozygous missense *GRIN2A* mutations (c.1770A > C/p.K590N, c.2636A > G/p.K879R, and c.3199C > T/p.R1067W) were identified in three unrelated cases. Electrophysiological analysis demonstrated R1067W significantly increased the current density of GluN1/GluN2A NMDARs. Immunofluorescence staining indicated GluN2A mutants had abundant distribution in the membrane and cytoplasm. Western blotting showed the ratios of surface and total expression of the three GluN2A-mutants were significantly increased comparing to the wild type. Further analysis on the reported missense mutations demonstrated that mutations with severe gain-of-function were associated with epileptic encephalopathy, while mutations with mild gain of function were associated with mild phenotypes, suggesting a quantitative correlation between gain-of-function and phenotypic severity. The mutations located around transmembrane domains were more frequently associated with severe phenotypes and absence seizure-related mutations were mostly located in carboxyl-terminal domain, suggesting molecular sub-regional effects.

Significance: This study revealed *GRIN2A* gene was potentially a candidate pathogenic gene of idiopathic generalized epilepsies. The functional quantitative correlation and the molecular sub-regional implication of mutations helped in explaining the relatively mild clinical phenotypes and incomplete penetrance associated with *GRIN2A* variants.

Keywords: *GRIN2A* gene, *N*-methyl-D-aspartate receptors, gain of function, sub-regional effect, idiopathic generalized epilepsy

INTRODUCTION

Idiopathic generalized epilepsies (IGEs) (G40.3 in ICD-10 2016, WHO), also known as genetic generalized epilepsies (GGE, OMIM# 600669), are a group of self-limited epileptic syndromes characterized by recurring generalized seizures without any underlying anatomic or neurological abnormality (Berrin et al., 2015; Scheffer et al., 2017; Collaborative, 2019). Idiopathic generalized epilepsies include juvenile myoclonic epilepsy (JME), juvenile absence epilepsy (JAE), childhood absence epilepsy (CAE), and epilepsy with generalized tonic-clonic seizures alone (EGTCS) (Engel and International League Against Epilepsy [ILAE], 2001). Generally, IGEs were regarded as a group of genetically determined disorders (Mullen and Berkovic, 2018). Monogenic abnormalities only account for 2–8% of IGEs (Weber and Lerche, 2008; Prasad et al., 2013). Exome-based genetic screening studies have demonstrated that over twenty genes were associated with IGEs, such as *CACNA1H*, *CACNB4*, *CASR*, *CHD4*, *CLCN2*, *EFHC1*, *GABRD*, *GABRA1*, *GABRG2*, *GABRB3*, *HCN2*, *KCC2*, *KCNMA1*, *RORB*, *SCN1A*, *SLC12A5*, *SLC2A1*, *RYR2*, and *THBS1* (DiFrancesco et al., 2011; Striano et al., 2012; Kahle et al., 2014; Rudolf et al., 2016; Santolini et al., 2017; Wang et al., 2017; Abou El Ella et al., 2018; Li et al., 2018; Yap and Smyth, 2019; Chan et al., 2020; Liu et al., 2021). Recent studies also identified several copy number variants associated with IGEs, such as duplication at 8q21.13-q22.2 and microdeletions at 1q21.1, 15q11.2, 15q13.3, and 16p13.11 (de Kovel et al., 2010; Kirov et al., 2013; Møller et al., 2013; Jähn et al., 2014; Rezazadeh et al., 2017). Clinically, genetic etiologies in majority of the cases with IGEs remain unknown. On the other hand, although IGEs were generally considered as genetic epileptic syndromes, big pedigrees of IGEs were rare. Variants with incomplete penetrance in IGEs-associated genes are common.

GRIN2A gene (OMIM* 138253), encoding GluN2A subunit of *N*-methyl-D-aspartate receptors (NMDARs), is comprehensively expressed in human cerebral cortex since embryonic period[1] and plays a critical role in excitatory synaptic transmission, plasticity and excitotoxicity in the mammalian central nervous system (Bar-Shira et al., 2015; Bagasrawala et al., 2017). Previously, *GRIN2A* mutations were found to be mainly associated with idiopathic focal epilepsy with incomplete penetrance (Carvill et al., 2013; Lemke et al., 2013; Lesca et al., 2013) and occasionally with epileptic encephalopathy (EE) (Venkateswaran et al., 2014; Yuan et al., 2014). So far, no *GRIN2A* mutation has been identified in patients with IGEs.

In the present study, trio-based whole-exome sequencing was performed in a cohort of patients with IGEs. Three novel missense mutations in *GRIN2A* gene were identified. Further studies showed that the missense mutations led to gain of function of NMDARs and/or increased membrane protein expression. To understand the underlying molecular mechanism for phenotypic variation, the correlations between the functional alterations and phenotypic severity, and the sub-regional effect of missense mutations were analyzed.

Abbreviations: NMDAR, *N*-methyl-D-aspartate receptor; ATD, amino-terminal domain; LBD, ligand-binding domain; TMD, transmembrane domains; CTD, carboxyl-terminal domain; LOF, loss of function; GOF, gain of function; GTCS, generalized tonic-clonic seizure; IGE, idiopathic generalized epilepsy; JME, juvenile myoclonic epilepsy; JAE, juvenile absence epilepsy; CAE, childhood absence epilepsy; EGTCS, epilepsy with generalized tonic-clonic seizures alone; BECTS, benign epilepsy with centro-temporal spikes; LKS, Landau-Kleffner syndrome; CSWSS, continuous spikes and waves during slow sleep; EE, epileptic encephalopathy.

[1]https://www.proteinatlas.org/ENSG00000183454-GRIN2A/tissue

MATERIALS AND METHODS

Subjects

A total of 88 patients with IGEs, including 47 patients with JME, 15 with JAE, 12 with CAE, and 14 with EGTCS, were recruited in Epilepsy Center of the Second Affiliated Hospital of Guangzhou Medical University from February 2013 to December 2018. Patients with IGEs were diagnosed according to the classification of epilepsy and epileptic syndromes by International League Against Epilepsy (Commission on Classification and Terminology of the International League Against Epilepsy, 1989; Engel and International League Against Epilepsy [ILAE], 2001; Helbig, 2015; Scheffer et al., 2017). The collected clinical data included semiology and evolution of the disorders, family history, and the data of treatment. The patients with abnormalities of general and/or neurological examinations were excluded. Video-electroencephalogram (EEG) monitoring recordings that included hyperventilation, intermittent photic stimulation, and sleep recordings were obtained to confirm the diagnosis of IGEs. The patients were included if they had at least one subtype of generalized seizures (including primarily generalized tonic-clonic seizure, myoclonic, and absence seizure) but no partial seizure. Their electroencephalogram (EEG) was characterized by generalized discharges of 3–6 Hz or faster on normal background. Brain magnetic resonances, cognitive and behavioral evaluation, and neurometabolic testing were performed to exclude symptomatic epilepsy. The patients have no or little cognitive impairment and neurodevelopmental comorbidities were included (Helbig, 2015).

The studies adhered to the guidelines of the International Committee of Medical Journal Editors with regard to patient consent for research or participation and received approval from the Ethics Committee of the Second Affiliated Hospital of Guangzhou Medical University (2021-hs-06).

Trio-Based Whole-Exome Sequencing and Mutation Analysis

Blood samples of the probands and their biological parents were collected. Genomic DNA was extracted. Trio Whole Exome Sequencing (Trio-WES) was conducted as previously reported (Wang et al., 2018). Population-based filtration removed common variants presenting a minor allele frequency $\geq$ 0.005 in genome aggregation database (gnomAD). The potential disease-causing mutations were screened under five models, namely, epilepsy-associated gene model, dominant or *de novo* model, autosomal recessive inheritance model, X-linked model, and co-segregation analysis model. The candidate variants were validated by Sanger sequencing. Conservation of mutated positions was evaluated using sequence alignment of different

species. All *GRIN2A* mutations were annotated based on the transcript NM_000833.4.

To evaluate the damaging effect of *GRIN2A* mutations, protein modeling was performed using Iterative Threading ASSEmbly Refinement (I-TASSER) software (Yang and Zhang, 2015; Zhang et al., 2017). The confidence of each modeling was quantitatively measured by C-score of -1.72. The three-dimensional structures were shown using PyMOL 1.7.

cDNA Construction, Cell Culture, and Transfection

Rat GluN2A-K590, GluN2A-K879, and GluN2A-R1067 cDNA mutants were generated from the plasmid pcDNA3.1$^+$-GluN2A by the site-directed mutagenesis kit, KOD-Plus-Neo (KOD-401, TOYOBO). As described in a previous study (Luo et al., 2002), the N-terminal GFP-tagged versions (GFP-GluN2A-K590N, GFP-GluN2A-K879R, and GFP-GluN2A-R1067W) were constructed using the GFP-GluN2A plasmid as a template. All these expression constructs were verified by DNA sequencing. Human embryonic kidney (HEK) 293 and 293T cells were grown in Dulbecco's modified eagle medium (11995065, Gibco), supplemented with 10% fetal bovine serum (10099141, Gibco) and 1% penicillin and streptomycin (10378016, Gibco) in a humidified atmosphere of 5% CO_2 at 37°C. Appropriate plasmids (2–4 μg per 35-mm dish) were transfected into the cells using the Lipofectamine 2000 Reagent (11668019, Invitrogen), according to the instructions of the manufacturer. To avoid NMDARs-mediated toxicity, 200 μM D, L-2-amino-5-phosphonovaleric acid (A8054, Sigma, United States) and 1 mM kynurenic acid (K3375, Sigma) were added to the culture medium. All experiments were performed in accordance with United Kingdom Animal Scientific Procedures Act (1986) following local ethical review (2021-hs-06).

Whole-Cell Recordings and Immunofluorescence Analysis

Whole-cell current recordings were performed as previously described (the details listed in **Supplementary Data 1**) (Xu et al., 2018). Surface immunofluorescence staining has been described previously (Luo et al., 2002). Twenty-four hours after GluN1-1a/GFP-GluN2A or GluN1-1a/GFP-GluN2A-mutant cDNAs transfection, HEK293 cells were rinsed once with PBS, incubated with rabbit anti-GFP antibody (Chemicon) for 7 min subsequently. After rinsing three times, cells were incubated with secondary antibody (A11010, Invitrogen) for another 7 min. Cells were immediately fixed with 4% paraformaldehyde for 10 min following three washes. Images were acquired with a fluorescence microscope (BX51, Olympus) and analyzed using the MetaMorph image analysis software (Universal Imaging, West Chester, PA, United States). Red signal outlined around the transfected HEK 293 cells represented surface expression, and green signal represented intracellular expression.

Cell Surface Biotinylation

HEK293T cells were incubated for 48 h after transfection and collected for extraction of total and surface protein. For total protein, cells were extracted using lysis buffer (FNN0021, Thermo Fisher Scientific), containing 1% phenylmethylsulfonyl fluoride and protease inhibitor cocktail (87786, Thermo Fisher Scientific). For surface protein, cells were permeabilized with permeabilization buffer (87786, Thermo Fisher Scientific, United States) supplemented with protease inhibitor cocktail (87786, Thermo Fisher Scientific). Surface protein was solubilized with solubilization buffer including protease inhibitor cocktail. The concentration of protein was measured using Bicinchoninic Acid (BCA) Protein Assay (23225, Thermo Fisher Scientific, United States). Equivalent amounts of the protein (200 μg for surface protein and 100 μg for total protein) was resolved over 7.5% sodium dodecyl sulfate-polyacrylamide gel electrophoresis, and transferred to polyvinylidene difluoride membrane (0.2 μm, 1620177, BIO-RAD, United States). The membranes were blocked within 5% non-fat milk for 2 h at room temperature and then incubated, respectively, with anti-GluN2A (1:4,000, ab124913, Abcam, United Kingdom), anti-β-actin (1:4,000, Proteintech, China), and anti-ATP1A1 (1:20,000, 14418-1-AP, Proteintech, China) antibodies at 4°C overnight. After washing the membranes in the mixture of tris-buffered saline and Tween 20 three times, the membranes were incubated with corresponding secondary antibodies for 2 h. Blots were representative of five independent experiments with similar results. Positive signals were analyzed by using ImageJ (National Institutes of Health, Bethesda, DC, United States).

Analysis of Effect of *GRIN2A* Mutation and Phenotypic Variation

In an attempt to investigate the mechanism for phenotypic variation, epilepsy-related *GRIN2A* missense mutations and their corresponding phenotypes were systematically retrieved from the PubMed database using "*GRIN2A*" and "epilepsy" as search terms until December 2019. All *GRIN2A* mutations were annotated based on the transcript NM_000833.4. The functional alterations of the missense mutations were reviewed based on the results coming from two electrode voltage clamp recordings. The severity of functional changes was ranked based on the results of glutamate potency and response to Mg^{2+} block, and simultaneously referred to other electrophysiological evaluation indicators, such as current density, glycine potency, and protein expression, etc. The severity was classified into (1) severe functional alteration that was of equal to or more than five-fold increase or decrease of the glutamate potency and/or Mg^{2+} block or other minor functional changes, (2) intermediate functional alteration that was of more than two-fold and less than five-fold increase or decrease of the glutamate potency and/or Mg^{2+} block, and (3) mild functional alteration that was defined as less than or equal to two-fold increase or decrease of the glutamate potency and/or Mg^{2+} block in the mutations comparing to the wild type.

The phenotypes were divided into (1) severe phenotype, i.e., EE, (2) intermediate phenotype, including atypical benign partial epilepsy, Landau-Kleffner syndrome (LKS), continuous spikes and waves during slow sleep (CSWSS), myoclonic-astatic

epilepsy, and focal epilepsy, and (3) mild phenotype that included benign epilepsy with centro-temporal spikes (BECTS) and IGEs.

Statistical Analysis

All data values were expressed as mean ± SEM derived from at least three separate transfections. Graphpad Prism software and Statistical Package for the Social Sciences (SPSS) software were used for statistical analysis. The frequencies of *GRIN2A* variants in the cohort of IGEs and those in the general population were compared by two-sided Fisher's exact test. Whole-cell current density and surface expression levels between wild-type and mutant receptors were compared by unpaired *t*-test. EC_{50} values between wild-type and mutant receptors (K590N, K879R, and R1067W) were compared by one-way ANOVA with Bonferroni *post hoc* multiple comparison test. The proportions of severe and mild phenotypes in different domains were compared by Pearson's chi-square test. A P value of < 0.05 was considered to be statistically significant.

RESULTS

Identification of *GRIN2A* Mutations

Three novel inherited heterozygous missense *GRIN2A* mutations were identified in two unrelated sporadic cases and one family with IGEs (**Figures 1A,B**). Mutation c.1770A > C/p.K590N was identified in a case with JME, mutation c.2636A > G/p.K879R in a case with JAE, and mutation c.3199C > T/p.R1067W in two individuals in a family with CAE and unclassified IGE, respectively (**Table 1**). Mutations K590N and K879R presented at a minor allele frequency of 0.00002849 and 0.0002 in general population in gnomAD database, respectively, while mutation R1067W was not observed in gnomAD database. A statistical analysis showed that the frequency of the *GRIN2A* variants in the present cohort of IGEs was significantly higher than that in the general population or East-Asian population (in gnomAD) (3/176 vs. 67/282366 in general population, $p = 0.000002$, and 3/176 vs. 67/19946 in East-Asian population, $p = 0.003625$; **Table 2**). Mutations K590N, K879R, and R1067W were predicted to be damaging or probably damaging by 6, 14, and 18 out of the 25 *in silico* prediction tools, respectively (**Supplementary Data 2**). The amino acid sequence alignments showed that residues K590, K879, and R1067 were highly conserved across vertebrates (**Figure 1C**), indicating an important role of these residues in NMDARs functions. All cases had no other pathogenic or likely pathogenic mutations in genes known to be associated with seizure disorders.

The mutation K590N was located in the intracellular domain and close to M2 domain, while the mutations K879R and R1067W were located in the carboxyl-terminal domain (CTD) (**Figures 2A,B**). The alterations of hydrogen bonds caused by the missense variants were further analyzed by protein modeling using Iterative Threading ASSEmbly Refinement (I-TASSER). Originally, residue K590 formed a hydrogen bond with residue L588. When lysine was replaced by asparagine at residue 590, the hydrogen bond was destroyed (**Figure 2C**). Residue K879 formed hydrogen bonds with residues H875, E877, K881, and S882, respectively. When lysine was replaced by arginine, the hydrogen bonds between residues E877 and K881 were broken, and the hydrogen bonds between H875 and S882 were preserved (**Figure 2C**). Residue R1067 formed two hydrogen bonds with N1076, and one hydrogen bond with T1064 and T1069 each. When arginine was replaced by tryptophan, the hydrogen bonds between N1076 and T1064 were destroyed, and only the hydrogen bond with T1069 were preserved (**Figure 2C**). The evidences indicated the mutations may alter the protein local conformation.

Clinical Features of the Patients With *GRIN2A* Mutations

All affected cases showed childhood or adolescence-onset generalized epilepsy. Their clinical features were summarized in **Table 1**.

The patient with mutation K590N was a 20-year-old female with no family history of epilepsy and febrile seizures. She had the first generalized tonic-clonic seizure (GTCS) at the age of 11 years old. Thereafter, she had clusters of myoclonic jerks approximately 2–3 times per week. The video-EEG monitoring obtained at the age of 14 years old demonstrated intermittent high voltage 3–5 Hz generalized spike and polyspike-and-waves (**Figure 3A**). She was diagnosed as JME with myoclonic seizures and GTCSs, and was seizure free on lamotrigine 75 mg/day at 15 years old. The EEG obtained at the age of 15 years old showed that the epileptiform discharges dramatically decreased.

The patient with mutation K879R was a 27-year-old male with negative family history of epilepsy and febrile seizures. He had frequent absence seizures and one GTCS at the age of 13 years. The Video-EEG monitoring recorded frequently regular high voltage generalized 3 Hz spike-and-waves (**Figure 3B-1**) and occasionally bilateral frontal synchronous spike-and-waves (**Figure 3B-2**). He was diagnosed as JAE with typical absence seizures and GTCS. He was seizure free at 22 years old with the combination of valproate acid 500 mg/day, lamotrigine 200 mg/day, and levetiracetam 625 mg/day. The EEG returned to normal by 25 years old.

The family with mutation R1067W had two affected individuals. The proband was a 10-year-old girl, who was found to have repeated daily episodes of staring spells for about 10 s at 5 years old. The EEG obtained at 5 years old showed intermittent high voltage generalized 3 Hz spike-and-waves (**Figure 3C-1**) and bilateral independent centro-temporal spike-and-waves (**Figure 3C-2**). Frequent episodes of typical absence seizures were recorded. She was on valproate 18 mg/kg/day and seizure free for 5 years. The EEG obtained at 10 years old still showed epileptic discharges in left or right centro-temporal regions, but no focal seizure was found. The other patient was the proband's cousin, an 8-year-old boy, appearing daily myoclonic and atonic seizures since he was 3 years old. He had mild speech delay, cognitive disabilities, and autistic tendencies. The EEG obtained at 3 years old showed high voltage irregular 2.5–3.5 Hz generalized polyspike-and-wave discharges (**Figure 3D**) and focal discharges in bilateral fronto-centro regions. He was diagnosed as unclassified IGE and was seizure free with the combination

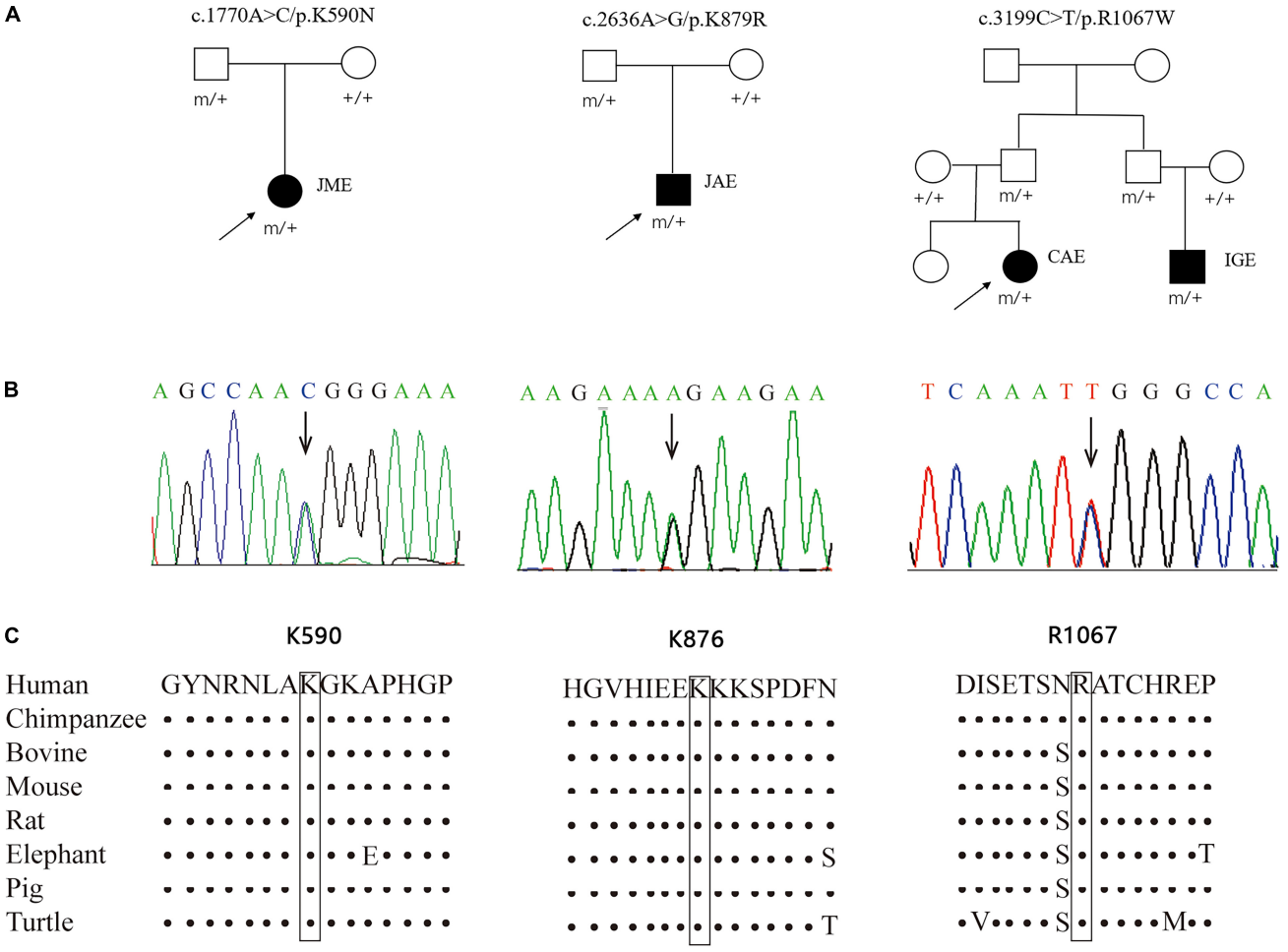

FIGURE 1 | Genetic data about *GRIN2A* mutations. **(A)** Pedigrees of the three cases with *GRIN2A* mutations and their corresponding phenotypes. **(B)** DNA sequence chromatogram of the *GRIN2A* mutations. Arrows indicate the positions of the mutations. **(C)** The amino acid sequence alignment of the three mutations shows that residues K590, K879, and R1067 were highly conserved across vertebrates. JME, juvenile myoclonic epilepsy; JAE, juvenile absence epilepsy; CAE, childhood absence epilepsy; IGE, idiopathic generalized epilepsy.

of valproate (25 mg/kg/day) and lamotrigine (3.5 mg/kg/day) by the age of six.

Biophysiological Features of GluN2A-Mutants

To examine the functional changes of NMDARs caused by the mutants, electrophysiological experiments were conducted. As shown in **Figures 4A,B**, the average current density of GluN1/GluN2A-K590N NMDARs was similar to GluN1/GluN2A-WT NMDARs (143.1 ± 12.19 pA/pF, n = 13 vs. 138.1 ± 12.75 pA/pF, n = 15; $p > 0.05$). The average current density of GluN1/GluN2A-K879R NMDARs was slightly increased but not statistically significant from that of GluN1/GluN2A-WT NMDARs (143.4 ± 10.85 pA/pF, n = 12 vs. 130.9 ± 19.51 pA/pF, n = 10; $p > 0.05$; **Figures 4A,C**). However, the current density of GluN1/GluN2A-R1067W NMDARs was 31% higher than that of the wild type (185.6 ± 15.59 pA/pF, n = 13 vs. 141.6 ± 12.32 pA/pF, n = 12; $p < 0.05$; **Figures 4A,D**), suggesting a gain-of-function effect for GluN1/GluN2A-R1067W NMDARs.

To test whether the mutants change glutamate sensitivity of NMDARs, glutamate concentration-response assessments were performed. None of these mutants was revealed alteration in glutamate potency of NMDARs. The half-maximally effective concentration (EC50) was similar between GluN1/GluN2A-WT and mutant NMDARs (n = 6, $p > 0.05$; **Figure 4E**).

Immunofluorescence staining was performed to analyze the effect of mutants on cellular distribution of NMDARs. As shown in **Figure 5A**, all NMDARs with GluN2A mutants had abundant distribution in the membrane and cytoplasm as that of GluN1/GluN2A WT NMDARs. Biotinylation was conducted to assess the protein expression level. Compared to the wild type, both the total and surface expression levels of GluN2A-mutants NMDARs were significantly increased (**Figures 5B,C**; $p < 0.01$), and the ratios of surface and total expression of GluN2A-mutants were also higher than that of wild type ($p < 0.05$).

TABLE 1 | Clinical manifestations of the cases with *GRIN2A* mutations.

	Case 1	Case 2	Case 3-1	Case 3-2
Mutation	c.1770A>C/p.K590N	c.2636A>G/p.K879R	c.3199C>T/p.R1067W	c.3199C>T/p.R1067W
Phenotype	JME	JAE	CAE	MAE
Gender	Female	Male	Female	Male
Age (year)	20	27	10	8
Age of onset (year)	11	13	5	3
Seizure types	Myoclonic, GTCS	Absence, GTCS	Absence, GTCS	Myoclonic, atonic
Intelligence and development	Normal	Normal	Normal	Mild language and cognitive disabilities, autistic tendency
EEG findings	3-5 Hz generalized spike-waves and polyspike-waves	3 Hz generalized spike-waves and bi-frontal spike-waves	3 Hz generalized spike-waves and bi-centrotemporal spike-waves	2.5-3.5Hz generalized spike-waves and bi-frontocentral spike-waves
Brain MRI	Normal	Normal	Normal	Normal
Treatment	LTG	VPA, LTG	VPA	VPA, LTG
Prognosis	Seizure free	Seizure free	Seizure free	Seizure free
MAF in ExAC	0.00002849	0.0002	-	-

JME, juvenile myoclonic epilepsy; JAE, juvenile absence epilepsy; CAE, childhood absence epilepsy; MAE, myoclonic-astatic epilepsy; GTCS, generalized tonic-clonic seizure; LTG, lamogrigine; VPA, valproic acid.

TABLE 2 | Gene-based burden analysis for *GRIN2A* mutations identified in this study.

	Allele count/number in this study	Allele count/number in gnomAD-all populations	Allele count/number in gnomAD-East Asian populations	Allele count/number in controls of gnomAD-all populations	Allele count/number in controls of gnomAD-East Asian populations
Identified *GRIN2A* mutations					
Chr16: 9927969: c.1770A>C/p.K590N	1/176 (0.00568)	10/282366 (0.00003542)	10/19950 (0.0005013)	6/120276 (0.00004989)	6/9960 (0.0006024)
Chr16: 9858765: c.2636A>G/p.K879R	1/176 (0.00568)	57/282532 (0.0002017)	57/19946 (0.002858)	27/120275 (0.0002245)	27/9956 (0.002712)
Chr16:9858202: c.3199C>T/p.R1067W	1/176 (0.00568)	–/–	–/–	–/–	–/–
Total	3/176 (0.01705)	67/282366 (0.00002373)	67/19946 (0.003359)	33/120275 (0.00002743)	33/9956 (0.003315)
***p* value**		0.000002	0.003625	0.000003	0.003766
OR (95% CI)		45.877–482.033	3.230–33.947	38.700–427.351	3.193-35.272

p values and odds ratio were estimated with 2-sided Fisher's exact test.
CI, confidence interval; gnomAD, Genome Aggregation Database; OR, odd ratio.

Effect of *GRIN2A* Mutation and Phenotypic Variation

In order to understand the mechanism underlying phenotypic variations, all reported epilepsy-related *GRIN2A* missense mutations and their functional alterations were reviewed (**Supplementary Data 3**).

To date, 71 epilepsy-related missense mutations were reported. Electrophysiological tests were performed in 35 mutations previously (Endele et al., 2010; de Ligt et al., 2012; Carvill et al., 2013; DeVries and Patel, 2013; Lemke et al., 2013; Lesca et al., 2013; Conroy et al., 2014; Venkateswaran et al., 2014; Yuan et al., 2014; Fainberg et al., 2016; Retterer et al., 2016; Serraz et al., 2016; Singh et al., 2016; Swanger et al., 2016; Monies et al., 2017; von Stulpnagel et al., 2017; Dazzo et al., 2018; Hesse et al., 2018; Lindy et al., 2018; Lionel et al., 2018; Miao et al., 2018; Xu et al., 2018; Yang et al., 2018; Snoeijen-Schouwenaars et al., 2019; Strehlow et al., 2019). Among the 35 tested mutations, 10 mutations were demonstrated to cause gain of function (GOF), 16 mutations led to loss of function (LOF), and 9 mutations had no detectable electrophysiological changes in the aspects investigated.

Since the consequence of the mutations in the present study was GOF of NMDARs featured by increased current density and surface expression of protein, the correlation between GOF and phenotypic severity was analyzed. The detailed electrophysiological alterations and phenotypes were listed in **Table 3** (Endele et al., 2010; Lemke et al., 2013; Yuan et al., 2014; Swanger et al., 2016; Chen et al., 2017; Ogden et al., 2017; Xu et al., 2018; Marwick et al., 2019a; Bertocchi et al., 2021). Three mutations (P552R, M817V, and L812M) significantly increased glutamate potency and glycine potency by over five-fold, and one mutation (N615K) led to a complete loss of

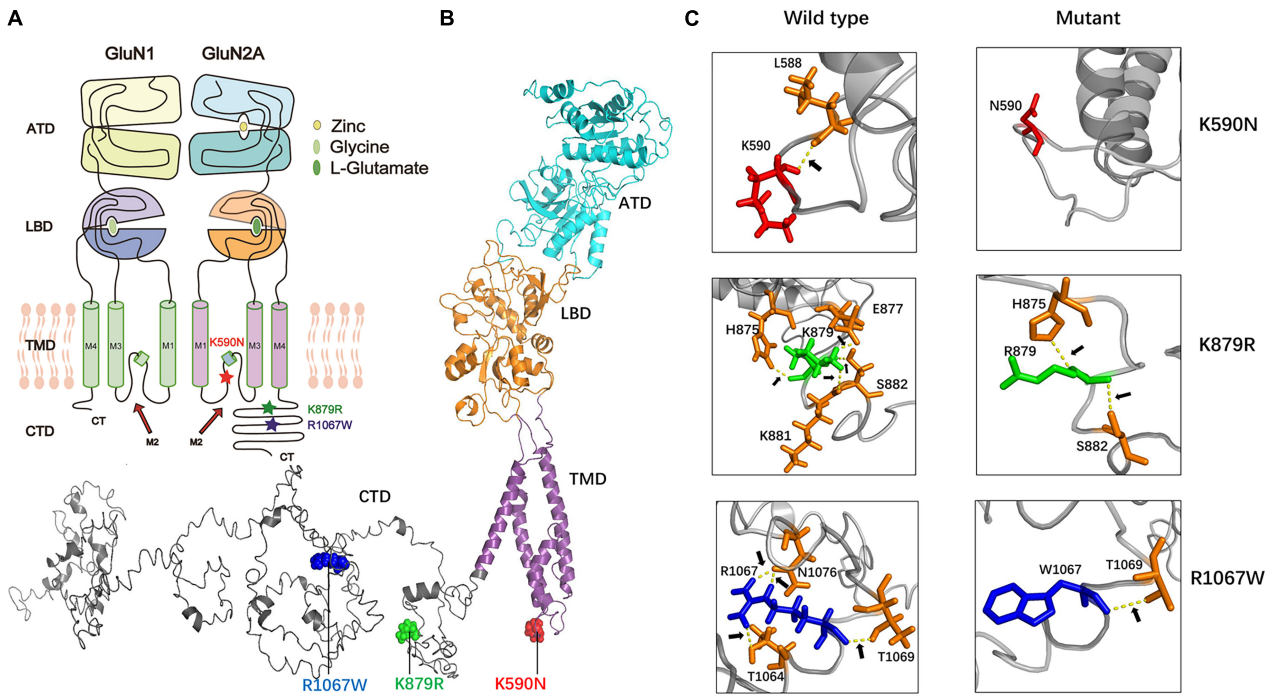

FIGURE 2 | The alterations of hydrogen bonds with surrounding amino acids. **(A)** The locations of missense mutations in topological structure of GluN1/GluN2A. Residue K590N in GluN2A lies within the channel pore of the NMDAR, while residues K879R and R1067W lie in carboxyl-terminal domain. Mutation K590N was colored in red, mutation K876R was colored in green, and mutation R1067W was colored in blue. **(B)** Schematic illustration of the location of mutations in the three-dimensional structure of GluN2A. **(C)** Alterations of hydrogen bonds with surrounding amino acids. In wild type, residue K590 forms one hydrogen bond with L588. In the mutant, this hydrogen bond was destroyed. In wild type, residue K879 forms hydrogen bonds with H875, E877, K881, and S882 while in the mutant, the hydrogen bonds with E877 and K881 were destroyed. In wild type, residue R1067 forms hydrogen bonds with T1064, T1069, and N1076 while in the mutant, only hydrogen bond with T1069 was kept.

Mg^{2+} blocker. The GOF of the four mutations were classified as severe, and the associated phenotypes were severe epilepsies, including two cases with early-onset epileptic encephalopathy and two with refractory epilepsy with severe developmental delay. Two mutations presented intermediate GOF. Mutation V452M caused 3.4-fold increase of glutamate potency and was associated with early infantile epileptic encephalopathy. Mutation K669N caused 3.1-fold increase of glutamate potency and was associated with intermediate phenotype CSWSS. Four mutations (N447K, V506A, P699S, and A243V) caused mild GOF, all of which were associated with mild phenotypes, including three cases with BECTS and one with unclassified epilepsy with incomplete penetrance. Three mutations identified in the study caused mild GOF or increased the expression of membrane protein, all of which were all associated with IGEs, which was classified as mild phenotype. This evidence indicated a quantitative correlation between the degree of GOF and the severity phenotype.

In previous studies, sixteen mutations were presented as LOF. Specifically, seven mutations were classified as severe featured by over five-fold decreased glutamate potency or complete trafficking defect (**Supplementary Data 4**; Swanger et al., 2016; Addis et al., 2017; Gao et al., 2017; Ogden et al., 2017; Strehlow et al., 2019), of which mutation V685G was associated with EE and the rest were associated with intermediate phenotypes. Four mutations were classified as intermediate LOF, and all associated with intermediate phenotypes. The remaining five mutations were ranked as mild LOF, of which three mutations (A727T, V734L, and R370W) were associated with BECTS. Thus, there was a tendency of correlation between the degree of LOF and phenotype severity. However, no definite conclusion could be drawn because majority of mutations with LOF were associated with intermediate phenotypes.

Nine mutations presented no detectable nor statistically significant alterations in the electrophysiological aspects examined (**Supplementary Data 2**).

There was no difference in phenotypic spectrum between the mutants with GOF and those with LOF. Electrophysiological alteration appeared not to be the only explanation for phenotypic variation. The previous study indicated that the molecular sub-regional location of mutations was associated with the damaging effects and, subsequently, the phenotypic severity (Tang et al., 2019). The relationship between the molecular sub-regional location of *GRIN2A* mutations and the severity of phenotype was therefore analyzed.

The epilepsy-related missense mutations were scattered over all domains of GluN2A except M1 helix (**Figure 6A**). The mutations located around the transmembrane domains (TMD) were more frequently associated with EE than those in amino- terminal domain (ATD) and ligand-binding domain (LBD) (**Figure 6B**), suggesting a

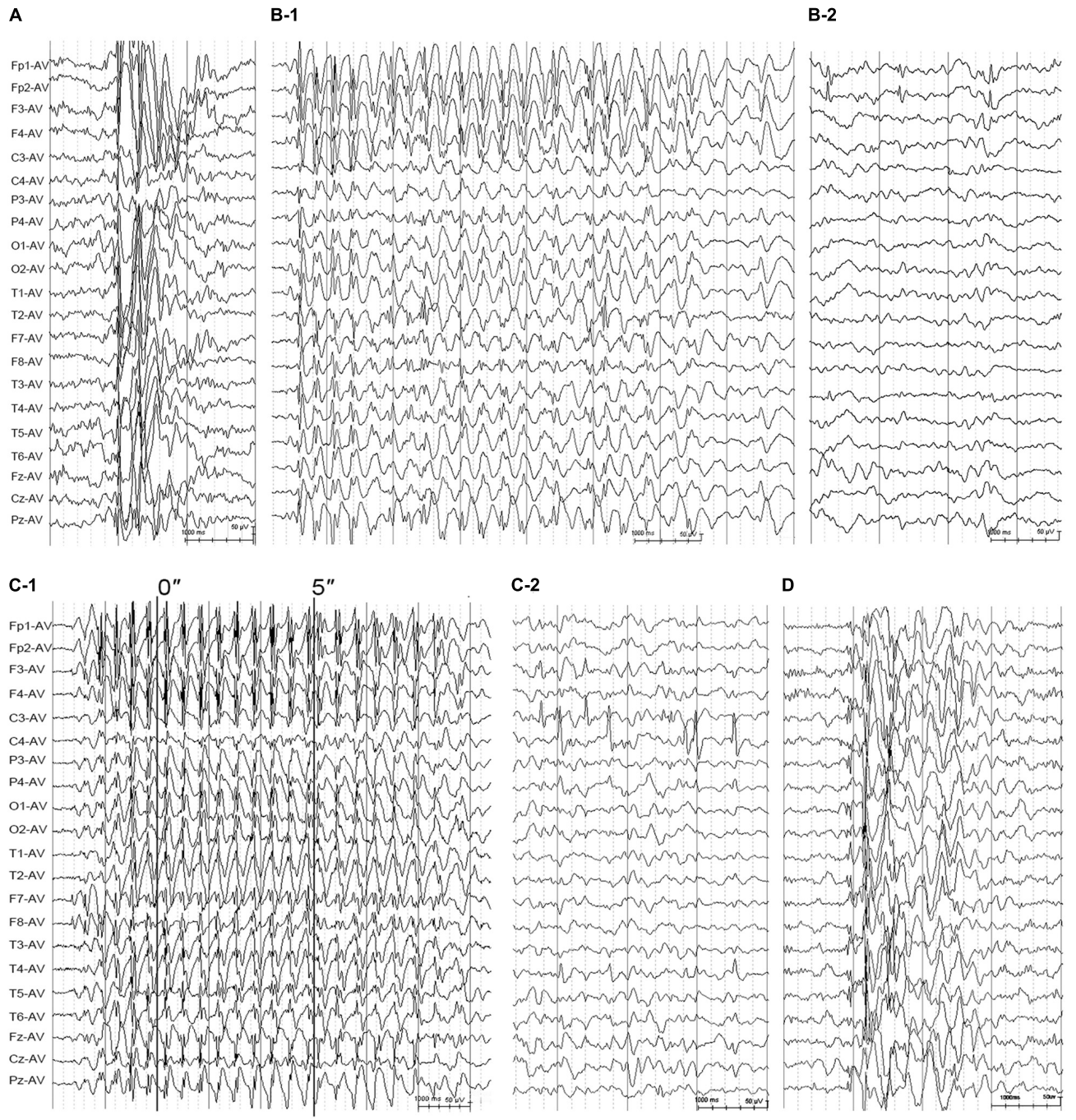

FIGURE 3 | Electroencephalogram changes in the cases with idiopathic generalized epilepsy with *GRIN2A* mutations. **(A)** Interictal EEG for the patient with juvenile myoclonic epilepsy with mutation K590N obtained at the age of 14 years showed high-voltage generalized 3.5 Hz polyspike-and-waves. **(B)** Interictal EEG for the case with juvenile absence epilepsy with mutation K879R obtained at the age of 13 years showed 3–3.5 Hz spike- and -waves **(B-1)** and interictal bilateral frontal focal spikes **(B-2)**. **(C)** EEG for the patient with CAE with mutation R1067W obtained at the age of 5 years. The ictal EEG showed regular high voltage 3–3.5 Hz spike- and -waves with typical absence seizure **(C-1)**. The interictal EEG showed bilateral centro-temporal spikes during sleep **(C-2)**. **(D)** The interictal EEG of the patient with unclassified IGE with mutation R1067W obtained at the age of 3 years showed irregular spike-and-waves. EEG, electroencephalogram.

molecular sub-regional effect. Previously, four patients with missense mutations had absence seizures, although they were diagnosed as LKS, CSWSS, and EE, respectively (Lemke et al., 2013; Lesca et al., 2013). Three of the four mutations were located in CTD. In this study, absence seizure-related mutations were also located in CTD. These data suggested a potential association between absence seizures and CTD.

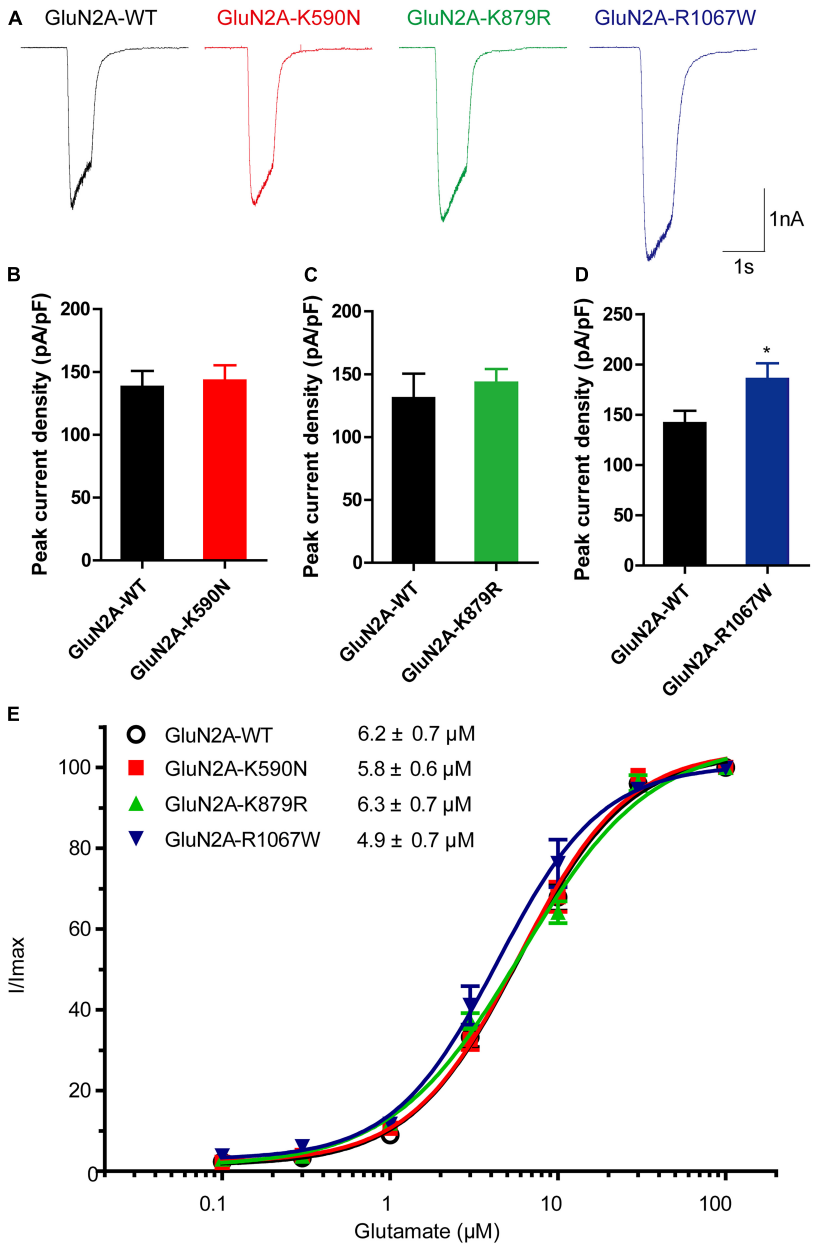

FIGURE 4 | Electrophysiological functional alterations of GluN2A-mutant NMDARs. **(A)** Representative current traces of GluN1/GluN2A-WT, GluN2A-K590N, GluN2A-K879R, and GluN2A-R1067W NMDARs evoked by 20 μM glycine and 100 μM glutamate (current scale bar, 1 nA; time scale bar, 2 s). **(B)** Quantitative analysis of whole-cell current density of GluN2A-WT (n = 15) and GluN2A-K590N (n = 13) NMDARs (Student's t-test, $p > 0.05$). **(C)** Quantitative analysis of whole-cell current density GluN2A-WT (n = 10) and GluN2A-K879R (n = 12) NMDARs (Student's t-test, $p > 0.05$). **(D)** Quantitative analysis of whole-cell current density of GluN2A-WT (n = 12) and GluN2A-R1067W (n = 13) NMDARs (Student's t-test, $^*p < 0.05$). **(E)** Glutamate concentration-response curves of GluN1/GluN2A-WT (black open circles, n = 6), GluN2A-K590N (red squares, n = 6), GluN2A-K879R (green triangles, n = 6), and GluN2A-R1067W (blue triangles, n = 6) NMDARs (One-way ANOVA with Bonferroni *post hoc* multiple comparison test, $p > 0.05$). NMDAR, *N*-methyl-D-aspartate receptors.

DISCUSSION

The *GRIN2A* gene has been demonstrated to be associated with idiopathic focal epilepsy and EE. In the present study, three novel missense *GRIN2A* mutations were identified in unrelated cases with IGEs. These mutations presented significantly higher frequency in the case cohort than in general populations. Experimental studies demonstrated that these mutations caused mild GOF of NMDARs or expression alterations of GluN2A. Further analysis showed that the phenotypic severity was correlated with the degree of GOF and sub-regional locations. This study suggested that *GRIN2A* gene was potentially a candidate pathogenic gene of IGEs and would help understand the pathogenesis of IGEs.

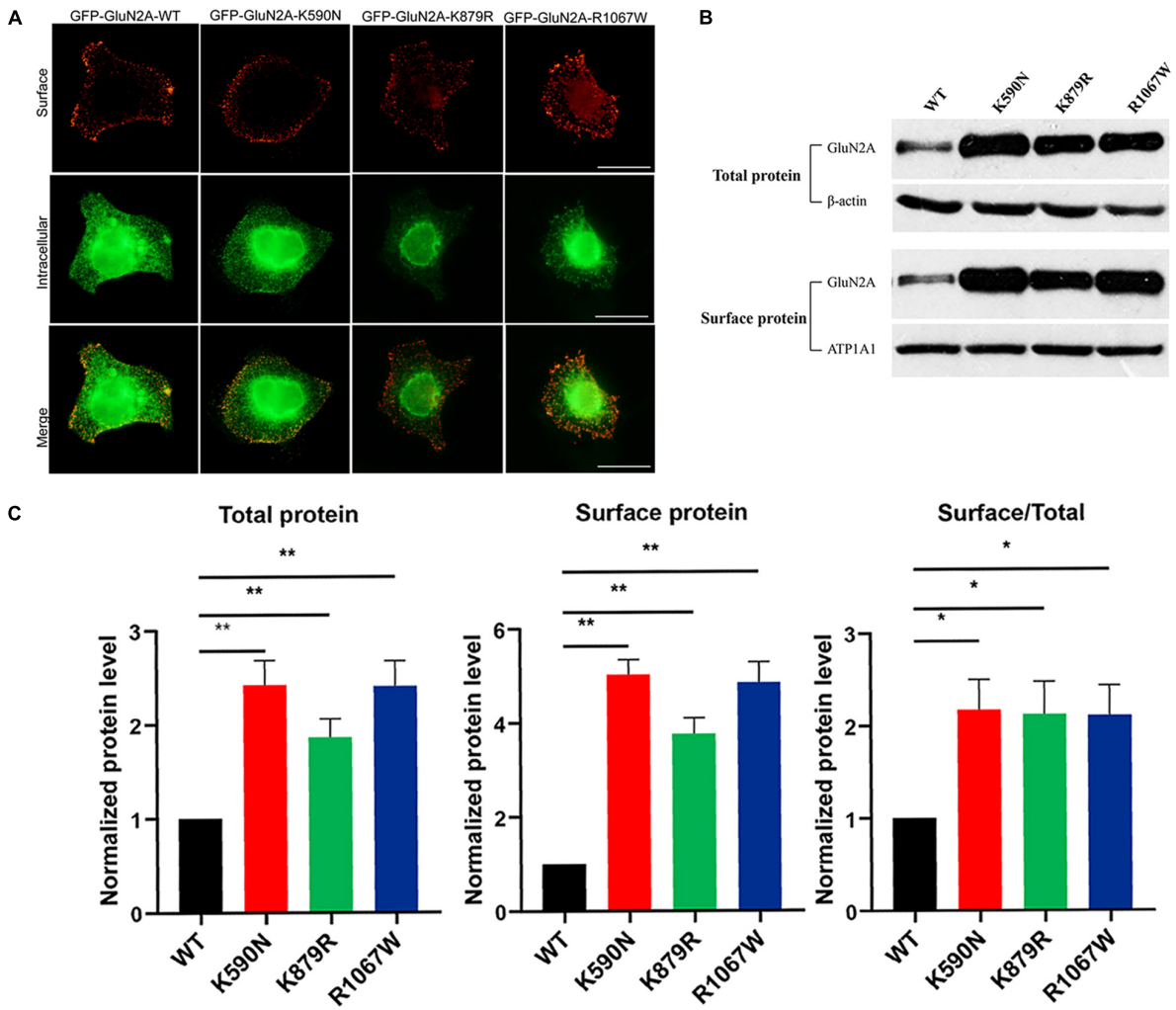

FIGURE 5 | Surface and total expression of GluN2A-WT and GluN2A-mutant NMDARs detected by immunofluorescence staining and biotinylation. **(A)** Surface (red, upper row) and intracellular (green, lower row) expression of GluN1/GluN2A-WT or mutant NMDARs in HEK 293 cells. **(B)** Western blot detected the total and surface protein expression of GluN2A-WT, GluN2A-K590N, GluN2A-K879R, and GluN2A-R1067W NMDARs. **(C)** Quantitative analysis of the total and surface expression of GluN2A-WT and GluN2A-mutants NMDARs and their corresponding ratio of the surface/total expression as shown in panel **(B)** ($n = 5$. One-way ANOVA with Bonferroni *post hoc* multiple comparison test, $^{*}P < 0.05$; $^{**}P < 0.01$). NMDAR, *N*-methyl-D-aspartate receptors.

The gene *GRIN2A* encodes GluN2A, a subunit of NMDARs, which are excitatory glutamate-gated channels with high Ca^{2+} permeability. *GRIN2A* is broadly expressed in multiple regions of the brain, including the cortex, cerebellum, and hippocampus since the embryonic period and is gradually increased during human development (Bar-Shira et al., 2015; Bagasrawala et al., 2017). A similar expression pattern was observed in rats (Sheng et al., 1994; Goebel and Poosch, 1999). GluN2A is critical for the formation and maturation of excitatory synapses and neuronal circuits (Swanger et al., 2016). To date, more than 140 *GRIN2A* mutations have been identified in focal epilepsy with or without speech disorders and EE. In the present study, three missense *GRIN2A* mutations were identified in the patients with IGEs. These mutations presented no or low allele frequencies in the gnomAD database and statistically higher frequency in the cohort of IGEs than in the populations of gnomAD. Experimental studies revealed increased current density in mutant NMDARs with R1067W and increased membrane protein expression in the three mutants. Considering that NMDARs generally mediate excitatory neurotransmission and are critical for the regulation of neuronal excitability in the brain, it potentially explains the association between *GRIN2A* variants and epilepsy. This study provided an insight into the underlying mechanism for the pathogenesis of IGEs.

Previously, 10 *GRIN2A* mutations with epilepsy were identified as GOF through two-electrode voltage clamp recordings (Endele et al., 2010; Lemke et al., 2013; Yuan et al., 2014; Swanger et al., 2016; Chen et al., 2017; Ogden et al., 2017; Xu et al., 2018). Further analysis in the study revealed that the severe GOF were associated with EE, while the mild GOF were mainly associated with mild phenotypes, specifically, BECTS or IGEs, indicating a quantitative correlation

TABLE 3 | Electrophysiological alterations featured by gain of function in *GRIN2A* mutations.

No.	Mutation	Glutamate potency	Glycine potency	Current density	Mg^{2+} block	Ca^{2+} permeability	Zn^{2+} inhibition	Proton Sensitivity	Membrane expression	Function summary	Epileptic phenotypes	References
1	c.1655C>G/p.P552R	↑↑↑(10-fold)	↑↑↑(20-fold)	+/−	NA	NA	NA	NA	NA	Severe GOF	Epilepsy & severe DD	Ogden et al., 2017
2	c.2449A>G/p.M817V	↑↑↑(9.5-fold)	↑↑↑(7.3-fold)	+/−	↓↓(3.33-fold)	NA	↓	↓	NA	Severe GOF	Refractory epilepsy & severe DD	Chen et al., 2017
3	c.2434C>A/p.L812M	↑↑↑(8-fold)	↑↑↑(8-fold)	+/−	↓(2-fold)	+/−	↓↓↓(loss)	↓	NA	Severe GOF	EOEE	Yuan et al., 2014
4	c.1845C>A/p.N615K	+/−	+/−	NA	↓↓↓(loss)	↓↓(2.88-fold)	NA	NA	NA	Severe GOF	EOEE	Endele et al., 2010; Marwick et al., 2019a; Bertocchi et al., 2021
5	c.1354G>A/p.V452M	↑↑(3.4-fold)	+/−	+/−	NA	NA	NA	NA	+/−	Intermediate GOF	EIEE	Swanger et al., 2016
6	c.2007G>T/p.K669N	↑↑(3.1-fold)	+/−	+/−	NA	NA	NA	NA	+/−	Intermediate GOF	CSWSS	Swanger et al., 2016
7	c.1341T>A/p.N447K	↑(2-fold)	NA	↑(1.2-fold)	↓(1.71-fold)	↑	↑	↑	+/−	Mild GOF	BECTS	Xu et al., 2018
8	c.1517T>C/p.V506A	↑(1.7-fold)	+/−	+/−	NA	NA	NA	NA	↑	Mild GOF	Unclassified Epilepsy, incomplete penetrance	Swanger et al., 2016
9	c.2095C>T/p.P699S	↑(1.6-fold)	+/−	+/−	NA	NA	NA	NA	↓	Mild GOF	BECTS	Swanger et al., 2016
10	c.728C>T/p.A243V	+/−	+/−	+/−	NA	NA	↓	+/−	+/−	Mild GOF	BECTS	Lemke et al., 2013
11	c.3199C>T/p.R1067W	+/−	NA	↑(1.3-fold)	NA	NA	NA	NA	↑↑	Mild GOF	CAE/MAE	This study
12	c.2636A>G/p.K879R	+/−	NA	+/−	NA	NA	NA	NA	↑↑	Mild GOF	JAE	This study
13	c.1770A>C/p.K590N	+/−	NA	+/−	NA	NA	NA	NA	↑↑	Mild GOF	JME	This study

↑↑/ ↓↓↓: more than 5-fold increase/decrease compare to the wild type; ↑↑/↓↓: increase/decrease 2-5-fold compare to the wild type; ↑/↓: less or equal to 2- old increase/decrease compare to the wild type; +/−: no statistically significant difference between the mutant and the wild-type.

BECTS, benign epilepsy with centro-temporal spikes; DD, developmental delay; EOEE, early onset epileptic encephalopathy; EIEE, early infantile epileptic encephalopathy; CSWSS, continuous spike and waves during sleep; JME, juvenile myoclonic epilepsy; JAE, juvenile absence epilepsy; CAE, childhood absence epilepsy; MAE, myoclonic-astatic epilepsy; NA, not available.

between functional alteration and phenotypic severity. In the present study, mutation R1067W had no allele frequency in the general population, caused more severe functional changes, and was predicted to be damaging by more *in silico* tools than mutations K590N and K879R. Clinically, mutation R1067W was associated with relatively more severe phenotypes, i.e., unclassified IGE with earlier onset, more frequent seizures, poorer response to AEDS, more than one individual affected, and potentially intellectual and developmental impairments. These findings provided additional pieces of evidence on quantitative correlation between functional alteration and phenotypic severity, potentially explaining the mild clinical manifestation, and incomplete penetrance.

In previous studies, incomplete penetrance and intra or inter-familial phenotypic variability of *GRIN2A* mutations were commonly observed in the families with idiopathic focal epilepsy (Lemke et al., 2013; Lesca et al., 2013). The phenomenon was also observed in the present study. The underlying mechanism remains undetermined. The numerous genomic variations in each individual and environmental factors might modify the phenotype. Generally, the variants with strong pathogenicity usually produce a relatively accordant phenotype, such as the variants in genes related to epileptic encephalopathy. In contrast, the variants with less pathogenicity tend to present phenotypic variation and incomplete penetrance and be associated with the mild functional alteration. In this study, the mutations K590N and K879R presented low frequency in control populations and lead to milder alterations of GluN2A expression, which might be one of the explanations for incomplete penetrance and intra or inter-familial phenotypic variability. It is possible that the *GRIN2A* variants with the mild impact played a risk, rather than a causal role in IGE, and were associated with only increased susceptibility to epilepsy.

Generally, the electrophysiological properties of channels are directly related to neuronal excitability, which determines the susceptibility of epilepsy. However, mutations with electrophysiological LOF of NMDARs have been identified previously (Swanger et al., 2016; Addis et al., 2017; Gao et al., 2017; Ogden et al., 2017; Strehlow et al., 2019). Truncating mutations and gross deletions of *GRIN2A* gene were also reported (Endele et al., 2010; Lesca et al., 2013). In animal models, homozygotes of targeted null *GRIN2A* exhibited jumpiness, increased locomotor activity, and loss of analgesic tolerance after repeated morphine doses (Sakimura et al., 1995; Kadotani et al., 1996). In *Grin2a* knockout mice, spontaneous epileptiform discharges were detected (Salmi et al., 2018, 2019). These clues indicated that loss of GluN2A protein was associated with increased neuronal excitability. Therefore, LOF of *GRIN2A* was potentially pathogenic for epilepsy. The analysis revealed a tendency of quantitative correlation between the degree of LOF and phenotypic severity. However, a conclusion cannot be drawn for LOF at present due to the data limitation. Additionally, several mutations had no detectable electrophysiological alterations. The pathogenic mechanism for these mutations was unknown. Electrophysiological alterations of NMDARs appeared to be not the only explanation of epileptogenesis. *GRIN2A* is broadly expressed in the human brain since the

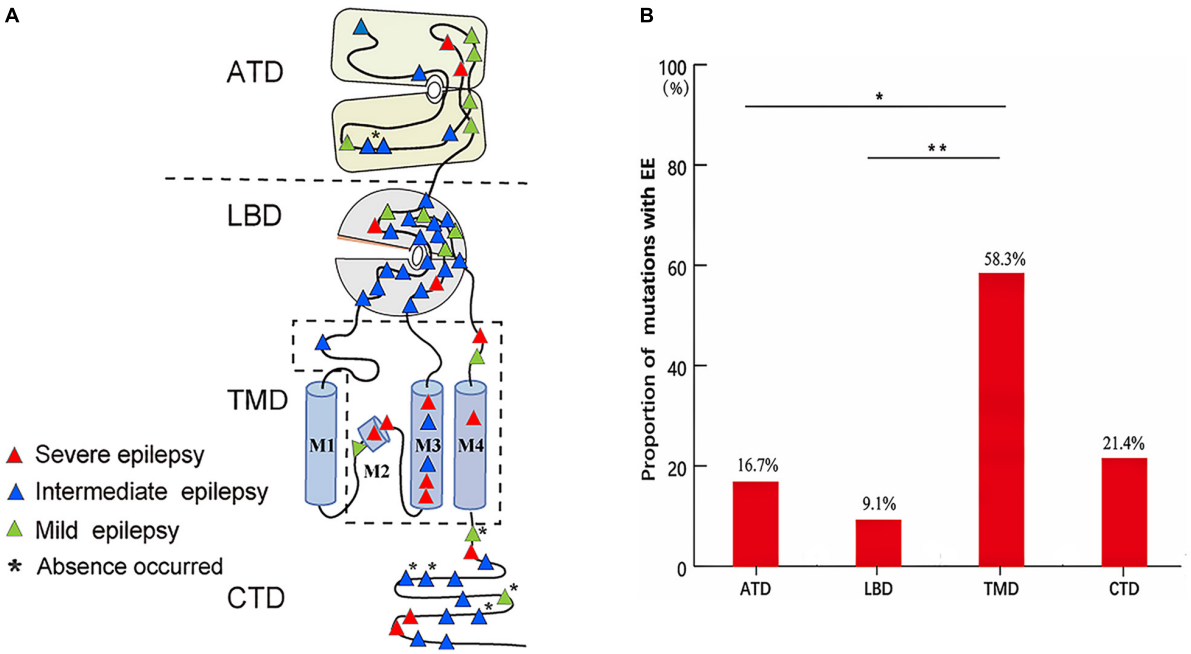

FIGURE 6 | The locations and corresponding phenotypes of epilepsy-related missense *GRIN2A* mutations. **(A)** Topological distribution of the *GRIN2A* missense mutations with different phenotypes. **(B)** The proportion of *GRIN2A* mutations with EE in different molecular regions. The proportion of missense mutations with EE around TMD was significantly higher than that in ATD and LBD (Pearson's chi-square test, $*p < 0.05$; $**p < 0.01$). ATD, amino terminal domain; LBD, ligand-binding domain; TMD, transmembrane domains; M1, M3, and M4, transmembrane domains; M2, re-entrant pore loop; CTD, carboxyl-terminal domain; EE, epileptic encephalopathy.

embryonic period, indicating *GRIN2A* potentially plays a role in neurodevelopment. Clinically, patients with *GRIN2A* mutations had variable neurodevelopmental abnormalities. It is, therefore, possible that *GRIN2A* mutations will cause neurodevelopmental abnormalities and subsequently secondary epilepsy, for which the underlying mechanism warrants further studies.

A recent study showed that molecular sub-regional locations of mutations were associated with the pathogenicity (Tang et al., 2019). Previous studies showed that the locations of missense mutations affected the severity of developmental phenotypes. The missense mutations in transmembrane and linker domains were associated with severe developmental delay (Strehlow et al., 2019). The present study revealed that the severity of epileptic phenotypes was also associated with the locations of missense mutations. Particularly, the missense mutations in TMD of GluN2A were more frequently associated with more severe phenotypes of epilepsy, whereas the mutations in ATD and LBD were more frequently associated with milder epilepsies. Additionally, five of the six absence associated mutations were located in CTD. These findings suggest the phenotypes were affected by a molecular sub-regional effect of *GRIN2A* mutations.

In the present study, two variants K879R and R1067W were located in C-terminal. C-terminal is less conservative in evolution with divergence among different species (Hedegaard et al., 2012). However, K879 and R1067 and their interacting residues were conservative residues (**Figures 1C**, **2C**). Variant R1067W had no allele frequency in controls of general population, and led to functional alterations of NMDARs. In previous studies, thirteen C-term variants with no or low allele frequency in general population were reported in the patients with epilepsy, even in the patients with epileptic encephalopathy. Functional studies had been performed in two C-term variants previously (Addis et al., 2017; Mota Vieira et al., 2020). The variant of GluN2A-N976S had no detectable electrophysiological alteration, while GluN2A-S1459G was proved to reduce spontaneous miniature excitatory synaptic current (mEPSC) frequency, decrease NMDAR surface expression, disrupt NMDAR interactions, and reduce synaptic function (Mota Vieira et al., 2020). It was suggested that the pathogenicity of C-term variants was variable and some of variants were potentially pathogenic, for which further experimental investigations were needed.

Clinically, features of BECTS and IGEs might consecutively or contemporarily coexist in the same patients (Esmail et al., 2016; Verrotti et al., 2017). In the present study, focal discharges were also observed in the patients with JAE and CAE (**Figure 3**). Both BECTS and IGEs were associated with *GRIN2A* mutations, which were potentially the common genetic basis of the two phenotypes. However, the absence-associated mutations were mainly located in CTD, while BECTS-associated mutations did not appear in this region. The difference in the distribution of mutations would potentially explain the phenotypic variation, for which the underlying mechanisms warrants further investigation.

This study has several limitations. More cases with IGEs are required to confirm the association between *GRIN2A* variants and IGEs. Further studies should be performed to elucidate

the mechanism underlying the pathogenesis of IGEs. Recently, increasing evidence showed that triheteromers (GluN1/2A/2B) were prominent in the alterations of electrophysiological functions as compared with diheteromers (GluN1/2A) (Marwick et al., 2019b), which is potentially an alternative approach to determine the electrophysiological functional alterations of *GRIN2A* variants.

In conclusion, the present study revealed *GRIN2A* gene was potentially a candidate pathogenic gene of IGEs. The molecular sub-regional effects of missense mutations and the quantitative correlation between the degree of GOF and the phenotypic severity provided evidence to explain the relatively mild clinical phenotypes and incomplete penetrance of *GRIN2A* variants, which would help understand the underlying mechanisms of phenotypic variation.

DATA AVAILABILITY STATEMENT

The datasets presented in this study can be found in online repositories. The names of the repository/repositories and accession number(s) can be found in the article/ **Supplementary Material**.

ETHICS STATEMENT

The studies involving human participants were reviewed and approved by the Ethics Committee of the Second Affiliated Hospital of Guangzhou Medical University (2021-hs-06). Written informed consent to participate in this study was provided by the participants' legal guardian/next of kin.

AUTHOR CONTRIBUTIONS

X-RL, J-HL, and W-PL designed and conceptualized the study, analyzed and interpreted the data, and drafted and revised the manuscript. J-HL and W-PL had full access to all of the data in the study and take responsibility for the integrity of the data and the accuracy of the data analysis. X-RL, B-ML, and Y-HY contributed to the clinical data collection. X-RL, X-XX, S-ML, and C-YF contributed to the electrophysiological and protein expression analysis. X-RL, T-TY, BT, Y-WS, and TS contributed to *in silico* analysis and the statistical analysis. All authors collected the data and revised and contributed to wrote the manuscript.

FUNDING

This work was funded by grants from the National Natural Science Foundation of China (Grant Nos. 81871015, 81671162, 81821091, 3192010300, and 31871418), Natural Science Foundation of Guangdong Province (2020A1515010108), China Association Against Epilepsy-UCB Pharma Ltd. Joint Science Research Foundation (Grant No. 2018024), Science and Technology Project of Guangzhou (Grant No. 201904020028), the Key-Area Research and Development Program of Guangdong Province (2019B030335001), and Science and Technology Project of Guangdong Province (Grant Nos. 2017B090904036 and 2017B030314159).

ACKNOWLEDGMENTS

The authors are deeply grateful to the patients and clinicians who participated in this study.

SUPPLEMENTARY MATERIAL

The Supplementary Material for this article can be found online at: https://www.frontiersin.org/articles/10.3389/fnmol.2021.720984/full#supplementary-material

REFERENCES

Abou El Ella, S. S., Tawfik, M. A., Abo El Fotoh, W. M. M., and Soliman, O. A. M. (2018). The genetic variant "C588T" of GABARG2 is linked to childhood idiopathic generalized epilepsy and resistance to antiepileptic drugs. *Seizure* 60, 39–43. doi: 10.1016/j.seizure.2018.06.004

Addis, L., Virdee, J. K., Vidler, L. R., Collier, D. A., Pal, D. K., and Ursu, D. (2017). Epilepsy-associated GRIN2A mutations reduce NMDA receptor trafficking and agonist potency - molecular profiling and functional rescue. *Sci. Rep.* 7:66. doi: 10.1038/s41598-017-00115-w

Bagasrawala, I., Memi, F., Radonjic, N. V., and Zecevic, N. (2017). N-Methyl d-Aspartate receptor expression patterns in the human fetal cerebral cortex. *Cereb. Cortex* 27, 5041–5053. doi: 10.1093/cercor/bhw289

Bar-Shira, O., Maor, R., and Chechik, G. (2015). Gene expression switching of receptor subunits in human brain development. *PLoS Comput. Biol.* 11:e1004559. doi: 10.1371/journal.pcbi.1004559

Berrin, T., Hikmet, Y., Gulsen, V., Ferda, B., Erdal, B., and Ece, O. (2015). No relation between EFHC2 gene polymorphism and Idiopathic generalized epilepsy. *Afr. Health Sci.* 15, 1204–1210. doi: 10.4314/ahs.v15i4.20

Bertocchi, I., Eltokhi, A., Rozov, A., Chi, V. N., Jensen, V., Bus, T., et al. (2021). Voltage-independent GluN2A-type NMDA receptor Ca(2+) signaling promotes audiogenic seizures, attentional and cognitive deficits in mice. *Commun. Biol.* 4:59. doi: 10.1038/s42003-020-01538-4

Carvill, G. L., Regan, B. M., Yendle, S. C., O'Roak, B. J., Lozovaya, N., Bruneau, N., et al. (2013). GRIN2A mutations cause epilepsy-aphasia spectrum disorders. *Nat. Genet.* 45, 1073–1076. doi: 10.1038/ng.2727

Chan, C. K., Low, J. S., Lim, K. S., Low, S. K., Tan, C. T., and Ng, C. C. (2020). Whole exome sequencing identifies a novel SCN1A mutation in genetic (idiopathic) generalized epilepsy and juvenile myoclonic epilepsy subtypes. *Neurol. Sci.* 41, 591–598. doi: 10.1007/s10072-019-04122-9

Chen, W., Tankovic, A., Burger, P. B., Kusumoto, H., Traynelis, S. F., and Yuan, H. (2017). Functional evaluation of a de novo GRIN2A mutation identified in a patient with profound global developmental delay and refractory epilepsy. *Mol. Pharmacol.* 91, 317–330. doi: 10.1124/mol.116.106781

Collaborative, E. (2019). Ultra-Rare genetic variation in the epilepsies: a whole-exome sequencing study of 17,606 individuals. *Am. J. Hum. Genet.* 105, 267–282. doi: 10.1016/j.ajhg.2019.05.020

Commission on Classification and Terminology of the International League Against Epilepsy (1989). Proposal for revised classification of epilepsies and epileptic syndromes. Commission on classification and terminology of the

international league against epilepsy. *Epilepsia* 30, 389–399. doi: 10.1111/j.1528-1157.1989.tb05316.x

Conroy, J., McGettigan, P. A., McCreary, D., Shah, N., Collins, K., Parry-Fielder, B., et al. (2014). Towards the identification of a genetic basis for Landau-Kleffner syndrome. *Epilepsia* 55, 858–865. doi: 10.1111/epi.12645

Dazzo, E., Rehberg, K., Michelucci, R., Passarelli, D., Boniver, C., Dri, V. V., et al. (2018). Mutations in MICAL-1 cause autosomal dominant lateral temporal epilepsy. *Ann. Neurol.* 83, 483–493. doi: 10.1002/aan.25167

de Kovel, C. G., Trucks, H., Helbig, I., Mefford, H. C., Baker, C., Leu, C., et al. (2010). Recurrent microdeletions at 15q11.2 and 16p13.11 predispose to idiopathic generalized epilepsies. *Brain* 133, 23–32. doi: 10.1093/brain/awp262

de Ligt, J., Willemsen, M. H., van Bon, B. W., Kleefstra, T., Yntema, H. G., Kroes, T., et al. (2012). Diagnostic exome sequencing in persons with severe intellectual disability. *N. Engl. J. Med.* 367, 1921–1929. doi: 10.1056/NEJMoa1206524

DeVries, S. P., and Patel, A. D. (2013). Two patients with a GRIN2A mutation and childhood-onset epilepsy. *Pediatr. Neurol.* 49, 482–485. doi: 10.1016/j.pediatrneurol.2013.08.023

DiFrancesco, J. C., Barbuti, A., Milanesi, R., Coco, S., Bucchi, A., Bottelli, G., et al. (2011). Recessive loss-of-function mutation in the pacemaker HCN2 channel causing increased neuronal excitability in a patient with idiopathic generalized epilepsy. *J. Neurosci.* 31, 17327–17337. doi: 10.1523/jneurosci.3727-11.2011

Endele, S., Rosenberger, G., Geider, K., Popp, B., Tamer, C., Stefanova, I., et al. (2010). Mutations in GRIN2A and GRIN2B encoding regulatory subunits of NMDA receptors cause variable neurodevelopmental phenotypes. *Nat. Genet.* 42, 1021–1026. doi: 10.1038/ng.677

Engel, J. Jr., and International League Against Epilepsy [ILAE] (2001). A proposed diagnostic scheme for people with epileptic seizures and with epilepsy: report of the ILAE Task Force on Classification and Terminology. *Epilepsia* 42, 796–803. doi: 10.1046/j.1528-1157.2001.10401.x

Esmail, E. H., Nawito, A. M., Labib, D. M., and Basheer, M. A. (2016). Focal interictal epileptiform discharges in idiopathic generalized epilepsy. *Neurol. Sci.* 37, 1071–1077. doi: 10.1007/s10072-016-2538-5

Fainberg, N., Harper, A., Tchapyjnikov, D., and Mikati, M. A. (2016). Response to immunotherapy in a patient with Landau-Kleffner syndrome and GRIN2A mutation. *Epileptic. Disord.* 18, 97–100. doi: 10.1684/epd.2016.0791

Gao, K., Tankovic, A., Zhang, Y., Kusumoto, H., Zhang, J., Chen, W., et al. (2017). A de novo loss-of-function GRIN2A mutation associated with childhood focal epilepsy and acquired epileptic aphasia. *PLoS One* 12:e0170818. doi: 10.1371/journal.pone.0170818

Goebel, D. J., and Poosch, M. S. (1999). NMDA receptor subunit gene expression in the rat brain: a quantitative analysis of endogenous mRNA levels of NR1Com, NR2A, NR2B, NR2C, NR2D and NR3A. *Brain Res. Mol. Brain Res.* 69, 164–170. doi: 10.1016/s0169-328x(99)00100-x

Hedegaard, M., Hansen, K. B., Andersen, K. T., Bräuner-Osborne, H., and Traynelis, S. F. (2012). Molecular pharmacology of human NMDA receptors. *Neurochem. Int.* 61, 601–609. doi: 10.1016/j.neuint.2011.11.016

Helbig, I. (2015). Genetic causes of generalized epilepsies. *Semin. Neurol.* 35, 288–292. doi: 10.1055/s-0035-1552922

Hesse, A. N., Bevilacqua, J., Shankar, K., and Reddi, H. V. (2018). Retrospective genotype-phenotype analysis in a 305 patient cohort referred for testing of a targeted epilepsy panel. *Epilepsy Res.* 144, 53–61. doi: 10.1016/j.eplepsyres.2018.05.004

Jähn, J. A., von Spiczak, S., Muhle, H., Obermeier, T., Franke, A., Mefford, H. C., et al. (2014). Iterative phenotyping of 15q11.2, 15q13.3 and 16p13.11 microdeletion carriers in pediatric epilepsies. *Epilepsy Res.* 108, 109–116. doi: 10.1016/j.eplepsyres.2013.10.001

Kadotani, H., Hirano, T., Masugi, M., Nakamura, K., Nakao, K., Katsuki, M., et al. (1996). Motor discoordination results from combined gene disruption of the NMDA receptor NR2A and NR2C subunits, but not from single disruption of the NR2A or NR2C subunit. *J. Neurosci.* 16, 7859–7867.

Kahle, K. T., Merner, N. D., Friedel, P., Silayeva, L., Liang, B., Khanna, A., et al. (2014). Genetically encoded impairment of neuronal KCC2 cotransporter function in human idiopathic generalized epilepsy. *EMBO Rep.* 15, 766–774. doi: 10.15252/embr.201438840

Kirov, A., Dimova, P., Todorova, A., Mefford, H., Todorov, T., Saraylieva, G., et al. (2013). 15q13.3 microdeletions in a prospectively recruited cohort of patients with idiopathic generalized epilepsy in Bulgaria. *Epilepsy Res.* 104, 241–245. doi: 10.1016/j.eplepsyres.2012.10.013

Lemke, J. R., Lal, D., Reinthaler, E. M., Steiner, I., Nothnagel, M., Alber, M., et al. (2013). Mutations in GRIN2A cause idiopathic focal epilepsy with rolandic spikes. *Nat. Genet.* 45, 1067–1072. doi: 10.1038/ng.2728

Lesca, G., Rudolf, G., Bruneau, N., Lozovaya, N., Labalme, A., Boutry-Kryza, N., et al. (2013). GRIN2A mutations in acquired epileptic aphasia and related childhood focal epilepsies and encephalopathies with speech and language dysfunction. *Nat. Genet.* 45, 1061–1066. doi: 10.1038/ng.2726

Li, M., Maljevic, S., Phillips, A. M., Petrovski, S., Hildebrand, M. S., Burgess, R., et al. (2018). Gain-of-function HCN2 variants in genetic epilepsy. *Hum. Mutat.* 39, 202–209. doi: 10.1002/humu.23357

Lindy, A. S., Stosser, M. B., Butler, E., Downtain-Pickersgill, C., Shanmugham, A., Retterer, K., et al. (2018). Diagnostic outcomes for genetic testing of 70 genes in 8565 patients with epilepsy and neurodevelopmental disorders. *Epilepsia* 59, 1062–1071. doi: 10.1111/epi.14074

Lionel, A. C., Costain, G., Monfared, N., Walker, S., Reuter, M. S., Hosseini, S. M., et al. (2018). Improved diagnostic yield compared with targeted gene sequencing panels suggests a role for whole-genome sequencing as a first-tier genetic test. *Genet. Med.* 20, 435–443. doi: 10.1038/gim.2017.119

Liu, X. R., Ye, T. T., Zhang, W. J., Guo, X., Wang, J., Huang, S. P., et al. (2021). CHD4 variants are associated with childhood idiopathic epilepsy with sinus arrhythmia. *CNS Neurosci. Ther. [Online ahead of print]* doi: 10.1111/cns.13692

Luo, J. H., Fu, Z. Y., Losi, G., Kim, B. G., Prybylowski, K., Vissel, B., et al. (2002). Functional expression of distinct NMDA channel subunits tagged with green fluorescent protein in hippocampal neurons in culture. *Neuropharmacology* 42, 306–318. doi: 10.1016/s0028-3908(01)00188-5

Marwick, K. F. M., Skehel, P. A., Hardingham, G. E., and Wyllie, D. J. A. (2019a). The human NMDA receptor GluN2A(N615K) variant influences channel blocker potency. *Pharmacol. Res. Perspect.* 7:e00495. doi: 10.1002/prp2.495

Marwick, K. F. M., Hansen, K. B., Skehel, P. A., Hardingham, G. E., and Wyllie, D. J. A. (2019b). Functional assessment of triheteromeric NMDA receptors containing a human variant associated with epilepsy. *J. Physiol.* 597, 1691–1704. doi: 10.1113/JP277292

Miao, P., Feng, J., Guo, Y., Wang, J., Xu, X., Wang, Y., et al. (2018). Genotype and phenotype analysis using an epilepsy-associated gene panel in Chinese pediatric epilepsy patients. *Clin. Genet.* 94, 512–520. doi: 10.1111/cge.13441

Møller, R. S., Weber, Y. G., Klitten, L. L., Trucks, H., Muhle, H., Kunz, W. S., et al. (2013). Exon-disrupting deletions of NRXN1 in idiopathic generalized epilepsy. *Epilepsia* 54, 256–264. doi: 10.1111/epi.12078

Monies, D., Abouelhoda, M., AlSayed, M., Alhassnan, Z., Alotaibi, M., Kayyali, H., et al. (2017). The landscape of genetic diseases in Saudi Arabia based on the first 1000 diagnostic panels and exomes. *Hum. Genet.* 136, 921–939. doi: 10.1007/s00439-017-1821-8

Mota Vieira, M., Nguyen, T. A., Wu, K., Badger, J. D. 2nd., Collins, B. M., Anggono, V., et al. (2020). An Epilepsy-Associated GRIN2A rare variant disrupts CaMKIIalpha phosphorylation of GluN2A and NMDA receptor trafficking. *Cell. Rep.* 32:108104. doi: 10.1016/j.celrep.2020.108104

Mullen, S. A., and Berkovic, S. F. (2018). Genetic generalized epilepsies. *Epilepsia* 59, 1148–1153. doi: 10.1111/epi.14042

Ogden, K. K., Chen, W., Swanger, S. A., McDaniel, M. J., Fan, L. Z., Hu, C., et al. (2017). Molecular mechanism of disease-associated mutations in the Pre-M1 Helix of NMDA receptors and potential rescue pharmacology. *PLoS Genet.* 13:e1006536. doi: 10.1371/journal.pgen.1006536

Prasad, D. K., Satyanarayana, U., and Munshi, A. (2013). Genetics of idiopathic generalized epilepsy: an overview. *Neurol. Ind.* 61, 572–577. doi: 10.4103/0028-3886.125240

Retterer, K., Juusola, J., Cho, M. T., Vitazka, P., Millan, F., Gibellini, F., et al. (2016). Clinical application of whole-exome sequencing across clinical indications. *Genet. Med.* 18, 696–704. doi: 10.1038/gim.2015.148

Rezazadeh, A., Borlot, F., Faghfoury, H., and Andrade, D. M. (2017). Genetic generalized epilepsy in three siblings with 8q21.13-q22.2 duplication. *Seizure* 48, 57–61. doi: 10.1016/j.seizure.2017.04.004

Rudolf, G., Lesca, G., Mehrjouy, M. M., Labalme, A., Salmi, M., Bache, I., et al. (2016). Loss of function of the retinoid-related nuclear receptor (RORB) gene and epilepsy. *Eur. J. Hum. Genet.* 24, 1761–1770. doi: 10.1038/ejhg.2016.80

Sakimura, K., Kutsuwada, T., Ito, I., Manabe, T., Takayama, C., Kushiya, E., et al. (1995). Reduced Hippocampal LTP and spatial learning in mice lacking NMDA receptor epsilon 1 subunit. *Nature* 373, 151–155.

Salmi, M., Bolbos, R., Bauer, S., Minlebaev, M., Burnashev, N., and Szepetowski, P. (2018). Transient microstructural brain anomalies and epileptiform discharges in mice defective for epilepsy and language-related NMDA receptor subunit gene Grin2a. *Epilepsia* 59, 1919–1930. doi: 10.1111/epi.14543

Salmi, M., Del Gallo, F., Minlebaev, M., Zakharov, A., Pauly, V., Perron, P., et al. (2019). Impaired vocal communication, sleep-related discharges, and transient alteration of slow-wave sleep in developing mice lacking the GluN2A subunit of N-methyl-d-aspartate receptors. *Epilepsia* 60, 1424–1437. doi: 10.1111/epi.16060

Santolini, I., Celli, R., Cannella, M., Imbriglio, T., Guiducci, M., Parisi, P., et al. (2017). Alterations in the α(2) δ ligand, thrombospondin-1, in a rat model of spontaneous absence epilepsy and in patients with idiopathic/genetic generalized epilepsies. *Epilepsia* 58, 1993–2001. doi: 10.1111/epi.13898

Scheffer, I. E., Berkovic, S., Capovilla, G., Connolly, M. B., French, J., Guilhoto, L., et al. (2017). ILAE classification of the epilepsies: position paper of the ILAE Commission for Classification and Terminology. *Epilepsia* 58, 512–521. doi: 10.1111/epi.13709

Serraz, B., Grand, T., and Paoletti, P. (2016). Altered zinc sensitivity of NMDA receptors harboring clinically-relevant mutations. *Neuropharmacology* 109, 196–204. doi: 10.1016/j.neuropharm.2016.06.008

Sheng, M., Cummings, J., Roldan, L. A., Jan, Y. N., and Jan, L. Y. (1994). Changing subunit composition of heteromeric NMDA receptors during development of rat cortex. *Nature* 368, 144–147. doi: 10.1038/368144a0

Singh, D., Lau, M., Ayers, T., Singh, Y., Akingbola, O., Barbiero, L., et al. (2016). De novo heterogeneous mutations in SCN2A and GRIN2A genes and seizures with ictal vocalizations. *Clin. Pediatr.* 55, 867–870. doi: 10.1177/0009922815601060

Snoeijen-Schouwenaars, F. M., van Ool, J. S., Verhoeven, J. S., van Mierlo, P., Braakman, H. M. H., Smeets, E. E., et al. (2019). Diagnostic exome sequencing in 100 consecutive patients with both epilepsy and intellectual disability. *Epilepsia* 60, 155–164. doi: 10.1111/epi.14618

Strehlow, V., Heyne, H. O., Vlaskamp, D. R. M., Marwick, K. F. M., Rudolf, G., de Bellescize, J., et al. (2019). GRIN2A-related disorders: genotype and functional consequence predict phenotype. *Brain* 142, 80–92. doi: 10.1093/brain/awy304

Striano, P., Weber, Y. G., Toliat, M. R., Schubert, J., Leu, C., Chaimana, R., et al. (2012). GLUT1 mutations are a rare cause of familial idiopathic generalized epilepsy. *Neurology* 78, 557–562. doi: 10.1212/WNL.0b013e318247ff54

Swanger, S. A., Chen, W., Wells, G., Burger, P. B., Tankovic, A., Bhattacharya, S., et al. (2016). Mechanistic insight into NMDA receptor dysregulation by rare variants in the GluN2A and GluN2B agonist binding domains. *Am. J. Hum. Genet.* 99, 1261–1280. doi: 10.1016/j.ajhg.2016.10.002

Tang, B., Li, B., Gao, L. D., He, N., Liu, X. R., Long, Y. S., et al. (2019). Optimization of in silico tools for predicting genetic variants: individualizing for genes with molecular sub-regional stratification. *Brief Bioinform.* 21, 1776–1786. doi: 10.1093/bib/bbz115

Venkateswaran, S., Myers, K. A., Smith, A. C., Beaulieu, C. L., Schwartzentruber, J. A., Consortium, F. C., et al. (2014). Whole-exome sequencing in an individual with severe global developmental delay and intractable epilepsy identifies a novel, de novo GRIN2A mutation. *Epilepsia* 55, e75–e79. doi: 10.1111/epi.12663

Verrotti, A., Casciato, S., Spalice, A., Carotenuto, M., Striano, P., Parisi, P., et al. (2017). Coexistence of childhood absence epilepsy and benign epilepsy with centrotemporal spikes: a case series. *Eur. J. Paediatr. Neurol.* 21, 570–575. doi: 10.1016/j.ejpn.2017.02.002

von Stulpnagel, C., Ensslen, M., Moller, R. S., Pal, D. K., Masnada, S., Veggiotti, P., et al. (2017). Epilepsy in patients with GRIN2A alterations: genetics, neurodevelopment, epileptic phenotype and response to anticonvulsive drugs. *Eur. J. Paediatr. Neurol.* 21, 530–541. doi: 10.1016/j.ejpn.2017.01.001

Wang, J., Lin, Z. J., Liu, L., Xu, H. Q., Shi, Y. W., Yi, Y. H., et al. (2017). Epilepsy-associated genes. *Seizure* 44, 11–20. doi: 10.1016/j.seizure.2016.11.030

Wang, Y., Yu, H., Chen, Y., Li, G., Lei, Y., and Zhao, J. (2018). Derivation of induced pluripotent stem cells TUSMi006 from an 87-year old Chinese Han Alzheimer's disease patient carrying GRINB and SORL1 mutations. *Stem. Cell Res.* 31, 127–130. doi: 10.1016/j.scr.2018.07.018

Weber, Y. G., and Lerche, H. (2008). Genetic mechanisms in idiopathic epilepsies. *Dev. Med. Child. Neurol.* 50, 648–654. doi: 10.1111/j.1469-8749.2008.03058.x

Xu, X. X., Liu, X. R., Fan, C. Y., Lai, J. X., Shi, Y. W., Yang, W., et al. (2018). Functional investigation of a GRIN2A variant associated with rolandic epilepsy. *Neurosci. Bull.* 34, 237–246. doi: 10.1007/s12264-017-0182-6

Yang, J., and Zhang, Y. (2015). I-TASSER server: new development for protein structure and function predictions. *Nucleic Acids Res.* 43, W174–W181. doi: 10.1093/nar/gkv342

Yang, X., Qian, P., Xu, X., Liu, X., Wu, X., Zhang, Y., et al. (2018). GRIN2A mutations in epilepsy-aphasia spectrum disorders. *Brain Dev.* 40, 205–210. doi: 10.1016/j.braindev.2017.09.007

Yap, S. M., and Smyth, S. (2019). Ryanodine receptor 2 (RYR2) mutation: a potentially novel neurocardiac calcium channelopathy manifesting as primary generalised epilepsy. *Seizure* 67, 11–14. doi: 10.1016/j.seizure.2019.02.017

Yuan, H., Hansen, K. B., Zhang, J., Pierson, T. M., Markello, T. C., Fajardo, K. V., et al. (2014). Functional analysis of a de novo GRIN2A missense mutation associated with early-onset epileptic encephalopathy. *Nat. Commun.* 5:3251. doi: 10.1038/ncomms4251

Zhang, C., Freddolino, P. L., and Zhang, Y. (2017). COFACTOR: improved protein function prediction by combining structure, sequence and protein-protein interaction information. *Nucleic Acids Res.* 45, W291–W299. doi: 10.1093/nar/gkx366

Conflict of Interest: The authors declare that the research was conducted in the absence of any commercial or financial relationships that could be construed as a potential conflict of interest.

Publisher's Note: All claims expressed in this article are solely those of the authors and do not necessarily represent those of their affiliated organizations, or those of the publisher, the editors and the reviewers. Any product that may be evaluated in this article, or claim that may be made by its manufacturer, is not guaranteed or endorsed by the publisher.

frontiers in Molecular Neuroscience

REVIEW
published: 10 March 2022
doi: 10.3389/fnmol.2022.810081

Modeling Epilepsy Using Human Induced Pluripotent Stem Cells-Derived Neuronal Cultures Carrying Mutations in Ion Channels and the Mechanistic Target of Rapamycin Pathway

Octavia Yifang Weng[1,2,3], *Yun Li*[1,4]* *and Lu-Yang Wang*[2,3]*

[1] Program in Developmental and Stem Cell Biology, Sick Kids Research Institutes, Toronto, ON, Canada, [2] Program in Neuroscience and Mental Health, Sick Kids Research Institutes, Toronto, ON, Canada, [3] Department of Physiology, University of Toronto, Toronto, ON, Canada, [4] Department of Molecular Genetics, University of Toronto, Toronto, ON, Canada

OPEN ACCESS

Edited by:
Jing Peng,
Xiangya Hospital, Central South University, China

Reviewed by:
Karl Daniel Murray,
University of California, Davis, United States
Eric Levine,
University of Connecticut, United States

***Correspondence:**
Yun Li
yun.li@sickkids.ca
Lu-Yang Wang
luyang.wang@utoronto.ca

Specialty section:
This article was submitted to Brain Disease Mechanisms, a section of the journal Frontiers in Molecular Neuroscience

Received: 06 November 2021
Accepted: 02 February 2022
Published: 10 March 2022

Citation:
Weng OY, Li Y and Wang L-Y (2022) Modeling Epilepsy Using Human Induced Pluripotent Stem Cells-Derived Neuronal Cultures Carrying Mutations in Ion Channels and the Mechanistic Target of Rapamycin Pathway. Front. Mol. Neurosci. 15:810081. doi: 10.3389/fnmol.2022.810081

Epilepsy is a neurological disorder that affects over 65 million people globally. It is characterized by periods of seizure activity of the brain as a result of excitation and inhibition (E/I) imbalance, which is regarded as the core underpinning of epileptic activity. Both gain- and loss-of-function (GOF and LOF) mutations of ion channels, synaptic proteins and signaling molecules along the mechanistic target of rapamycin (mTOR) pathway have been linked to this imbalance. The pathogenesis of epilepsy often has its roots in the early stage of brain development. It remains a major challenge to extrapolate the findings from many animal models carrying these GOF or LOF mutations to the understanding of disease mechanisms in the developing human brain. Recent advent of the human pluripotent stem cells (hPSCs) technology opens up a new avenue to recapitulate patient conditions and to identify druggable molecular targets. In the following review, we discuss the progress, challenges and prospects of employing hPSCs-derived neural cultures to study epilepsy. We propose a tentative working model to conceptualize the possible impact of these GOF and LOF mutations in ion channels and mTOR signaling molecules on the morphological and functional remodeling of intrinsic excitability, synaptic transmission and circuits, ultimately E/I imbalance and behavioral phenotypes in epilepsy.

Keywords: epilepsy, iPSC, ion channel, mTOR signaling, homeostasis

Seizure is the result of a temporary disruption in neuronal activity due to excessive synchrony of neurons. Epilepsy is a chronic condition during which recurrent periods of seizures take place and is sometimes accompanied by comorbidities such as developmental and intellectual delay, depression, anxiety, heart disease, and others. Epilepsy is diagnosed based on the abnormal electrical activity

and brain structure underlying the hypersynchrony in neurons. Neuroimaging techniques such as electroencephalogram (EEG), magnetic resonance imaging (MRI), positron emission tomography (PET), and single-photon emission computerized tomography (SPECT) have all been used for diagnosis. Currently, epilepsy is categorized into four types, including generalized epilepsy, focal epilepsy, generalized and focal epilepsy, and unknown epilepsy. In generalized epilepsy, seizures start on both sides of the brain, leading to absence epilepsy with little to no movement or tonic-clonic epilepsy with stiffening or jerking movements. Myoclonic epilepsy involves local or global muscles contraction whilst atonic epilepsy is associated with a sudden loss of consciousness, both of which have been observed in generalized epilepsy. In contrast, seizures in focal epilepsy start at a confined region in the brain, and the patient symptoms usually depend on the region affected. In this type of epilepsy, patients can be awake or unconscious (Stafstrom and Carmant, 2015). The third type involves the combination of focal and generalized epilepsy, where the seizures can start either locally or globally in the patients. When the clinical diagnosis fails to ascribe symptoms to focal or generalized epilepsy, the patient is assigned to the last category, unknown epilepsy.

Genetic mutations, *de novo* or inherited, play a major role in the pathogenesis of epilepsy. Among various forms of epilepsy, mutations in ion channels and mTOR signaling molecules lead to converging epileptic types, ranging from focal to generalized epilepsy (Mulley et al., 2003; Perucca, 2018; Proietti Onori et al., 2021). Many of the genetic mutations underlying channelopathies directly affect the intrinsic excitability of neurons and/or synaptic transmission (Mulley et al., 2003; Lascano et al., 2016; Bartolini et al., 2020), while other mutations along the mTOR signaling pathway can indirectly affect the level and activity of ion channels that determine neuronal firing rate, patterns and network activity (Cho, 2011). Epilepsy can be caused by structural changes in the brain, which could be congenital or acquired later in life through external means such as brain trauma or stroke, and epilepsy itself can also promote aberrant neuronal growth known as sprouting (Scharfman, 2007; Cho, 2011). Other factors such as changes in the metabolic and immune environment in the brain may increase the propensity of epilepsy (Patel, 2018; Xu et al., 2018). In this review, we will focus on epilepsy primarily stemming from genetic mutations.

Epileptic pathogenesis has been linked to excitatory/inhibitory (E/I) imbalance, where the excitatory and inhibitory input ratio is pathologically altered. E/I balance can be defined as a singular entity at a global circuit level, where it has been shown to affect brain states, such as an increase in inhibition ratio in awake over the anesthetized state (Haider et al., 2013). At a single neuron level, E/I balance can be shaped by intrinsic neuronal excitability from various ion channels and the interplay of excitatory and inhibitory synaptic inputs, typically glutamatergic or GABAergic signals, defining wiring and firing property in normal development. In epilepsy, changes in ion channels, synaptic inputs, and morphology such as activity-induced neuronal sprouting lead to misfiring and miswiring in a vicious cycle, underlying a progressively hypersynchronous brain circuit (Cavarsan et al., 2018). While disruption of short-term E/I balance can lead to hyperexcitation underlying seizure activity, the chronic nature of epilepsy development may need cooperative changes to remodel the homeostatic setpoint which is influenced by many factors. For example, mitochondrial dihydroorotate dehydrogenase (DHODH) (Styr et al., 2019; Ruggiero et al., 2021) has been shown to be one of the key determinants of the homeostatic setpoint as inhibition of DHODH can reduce firing rate setpoint and the susceptibility to seizures.

Rodent models have been widely used to study epilepsy. Conventional models include audiogenic seizure susceptible DBA/2 mouse or genetic *absence* epilepsy rat from Strasbourg (GAERS), in which many antiepileptic drugs (AEDs) were developed (Löscher, 2017). More recently, genetically engineered animal models have been developed by introducing patient mutations into animals to mimic the human disease conditions (Hirose et al., 2020). These studies have built an essential groundwork for the understanding of epilepsy mechanisms and the exploration of therapeutic solutions. Some animal models recapitulate seizure activity well, such as those with SCN1A mutation for Dravet syndrome (Ogiwara et al., 2007). However, other mouse models, such as those with disease-relevant KCNQ2 mutations, were unable to reproduce the spontaneous seizure phenotypes seen in human patients (Ihara et al., 2016; Hirose et al., 2020). In addition, AEDs that are effective in animal models often fail to do so in human patients, suggesting that species difference may be an important factor that influences the effectiveness of treatment, especially for patients with intractable epilepsy (Löscher and Schmidt, 2011). These challenges highlight the pressing need to build a continuum of models from laboratory animals to human subjects.

Since the introduction of induced pluripotent stem cells (iPSCs) in 2007 (Takahashi and Yamanaka, 2006; Takahashi et al., 2007), the generation and the biobanking of patient-specific pluripotent stem cell lines have opened up a new avenue to study human diseases. It is now possible to gain mechanistic understandings of the genesis and pathologies associated with epilepsy, and to investigate suitable treatment options for individual patients. Combined with an ongoing revolution in the gene editing field, such as the CRISPR/Cas9 technology, human *in vitro* model systems represent an unprecedented opportunity to capture the clinical conditions and further apprehend the underpinnings of a variety of other genetic disorders including epilepsy. With the insights from previous animal models and the rapid technological developments in stem cells and genetic engineering, we now have scalable tools to study the spatiotemporal nature of epileptic pathogenesis. Specifically, by mapping out where aberrant activity initiates, how the original epileptic loci recruit neighboring neurons and the temporal stage at which such phenotypes appear, we will gain in-depth knowledge into epilepsy pathogenesis and identify new molecular substrates for potential therapeutics. This review will examine recent advancements in human *in vitro* studies on epilepsy caused by different genetic mutations, followed by prospective discussions on the key issues that can further advance the mechanistic understanding of epilepsy.

MODELING CHANNELOPATHY IN EPILEPSY WITH HUMAN *IN VITRO* SYSTEM

Channelopathy accounts for the majority of genetic mutations associated with epilepsy. The most common ion channel mutated in epilepsy include voltage-gated sodium, potassium, calcium channels, ligand-gated glutamatergic and GABAergic receptors (Oyrer et al., 2018). Although various ion channels mutations reported from clinical data have been studied in animal models, only a few have been studied using the human *in vitro* systems.

Voltage-Gated Sodium Channels

Voltage-gated sodium channels (Nav) play an essential role in the depolarizing phase of the action potential (or spike), promoting spike firings. In the mature central nervous system of mammals, Nav1.1, Nav1.2, and Nav1.6 (encoded by SCN1A, SCN2A, and SCN8A, respectively) are the most abundant. While all three are linked to epilepsy, only Nav1.1 has been extensively studied in the human *in vitro* system. Nav1.1 is located on the axon initiation site (AIS) of neurons and contributes to the initiation and propagation of action potentials as well as their excitability (Child and Benarroch, 2014). Using epilepsy patient iPSCs-derived inhibitory neurons, it has been shown that neurons carrying a loss-of-function (LOF) SCN1A mutation (S1328P) displayed a reduction in Na^+ current amplitude (Sun et al., 2016) (**Table 1**). SCN1A (c.4261G>T/c.3576_3580del TCAAA) mutated neurons exhibited decreased Na^+ current density (Kim et al., 2018), with SCN1A (c. 4261G > T) showing more reduction in Na^+ current compared to SCN1A (c.3576_3580del TCAAA). The differences in biophysical properties from these mutations also matched with the symptom severity in the patients whose iPSCs were generated from. Interestingly, the changes in electrical activity were mainly observed with inhibitory neurons but not excitatory neurons (Sun et al., 2016). In contrast, a gain-of-function (GOF) effect from SCN1A (F1415I) or SCN1A (Q1923R) in excitatory neurons with hyperexcitability has also been reported (Jiao et al., 2013). This discrepancy led to a series of follow-up studies clarifying the role of Nav1.1 mutation in inhibitory neurons and excitatory neurons. One possible explanation was that the mutations and the genetic background of the patient in the studies were different. To rule out the interference of the genetic background, genetically engineered isogenic control and mutant cells carrying patient-specific mutation SCN1A (Q1923R) were generated (Liu et al., 2016). Mutant inhibitory neurons displayed a decrease in Na^+ current density, leading to reduced amplitude and number of action potential in response to the same magnitude of current injections. In addition, frequency and amplitude of spontaneous inhibitory postsynaptic currents (sIPSCs) in the inhibitory neurons decreased, indicating that lowered excitability in these neurons likely attenuates inhibitory output onto other cells to elevate E/I ratio. Furthermore, both inhibitory and excitatory neurons derived from patient cells or CRISPR/Cas9 engineered iPSCs carrying the same patient mutation SCN1A (K1270T) confirmed convergent phenotypes in inhibitory neurons, including decreased action potential frequency, amplitude, and Na^+ current density. In contrast, decreased Na^+ current density was reported in excitatory neurons, paradoxically, with an increase in firing frequency. The heightened frequency may result from the mutation and lead to a broader voltage range for sodium channel openings (Xie et al., 2020). These findings demonstrate the importance of LOF mutations in inhibitory neurons, but do not rule out the possibility of GOF mutations with a different genetic background targeting excitatory neurons as previously reported. Future experiments on co-culture of both excitatory and inhibitory neurons to directly measure E/I ratio with the same genetic background is clearly needed to draw a firm conclusion on the roles of SCN1A LOF and GOF mutations in epilepsy. Although the literature has largely focused on SCN1A, cell lines derived from epilepsy patients with SCN2A and SCN8A LOF mutations have been developed for future studies (Tidball et al., 2017).

Potassium Channels

Potassium channels comprise the largest group of ion channels. Voltage-gated potassium channels (Kv) allow selective efflux of potassium ions, regulating neuronal spike waveform and firing patterns by repolarizing and hyperpolarizing membrane potentials to prevent hyperactivity and aberrant firings. Numerous mutations have been linked to epilepsy, but only a few, such as Kv7.2 and KNa1.1, have been modeled in the human *in vitro* system. A study investigated KCNQ2, encoding Kv7.2 mediating a current called M-current, which lowers the excitability of neurons and limits repetitive firings. The authors observed that KCNQ2 LOF mutation (c.1742G > A) led to faster action potential repolarization and shorter spike width (Simkin and Kiskinis, 2018). With a loss of Kv7.2 activity, the mutant neurons showed higher spontaneous firing frequency and burst activity than the control as revealed by a multi-electrode array (MEA) assay. This showed that LOF mutation of KCNQ2 in excitatory neurons led to an increased excitability. Several studies have established cell lines from patients with KCNA2 LOF mutations as the tools for future studies (Schwarz et al., 2018, 2019; Uysal et al., 2019). In addition, a GOF mutation in KCNT1, encoding for a sodium-activated potassium channel KNa1.1, has been reported in patients with focal epilepsy. Patient-derived neurons with KCNT1 (P924L) mutation showed hyperexcitability with narrower spike width, higher spontaneous firing rate burst activity and synchronized discharge of the network, though it is unknown if excitatory or inhibitory or both neurons express KCNT1 mutation (Quraishi et al., 2019).

Epilepsy is a multicomponent disease, in which genetic mutations of many types of ion channels from human patients have been implicated. These include hyperpolarization-activated cyclic nucleotide-gated (HCN) channels and calcium channels, which have not yet been modeled using the human *in vitro* model. E/I balance and maintenance of the neuronal network are critically dependent on ion channels. Channelopathies result in dysregulated intrinsic excitability of excitatory and/or inhibitory neurons and their outputs, and consequentially an E/I imbalance, as exemplified by either higher excitability (e.g., LOF mutation in KCNQ2 or GOF mutation in KCNT1) or lowered inhibition (e.g.,

TABLE 1 | Summary of human iPSC-derived cultures on epilepsy related to ion channels and mTOR pathway mutations.

Gene	Epileptic syndrome	Morphological and electrical characterizations	Model
Ion channel			
SCN1A	Dravet's syndrome	Increased excitability and Na^+ current in excitatory neurons	Patient (F1415I/Q1923R) iPSCs derived excitatory neurons (Jiao et al., 2013)
SCN1A	Dravet's syndrome	Decreased Na^+ current and AP in inhibitory neurons, but not in excitatory neurons	Patient (S1328P) iPSCs derived inhibitory and excitatory neurons (Sun et al., 2016)
SCN1A	Dravet's syndrome	Decreased Na^+ current density and lowered AP amplitude and number in current clamp; lower frequency and amplitude of sIPSCs in inhibitory neurons	Patient (Q1923R) iPSCs derived inhibitory neurons (Liu et al., 2016)
SCN1A	Dravet's syndrome	Decreased number of AP and Na^+ current density in derived GABAergic neurons	Patient (c.4261G > T/c.3576_3580del TCAAA) iPSCs derived inhibitory neurons (Kim et al., 2018)
SCN1A	Dravet's syndrome	Decreased AP frequency, amplitude, and Na^+ current density in inhibitory neurons; decreased Na^+ current density but increased firing frequency in excitatory neurons	Patient (K1270T) iPSCs or CRISPR/Cas9 engineered iPSCs carrying patient mutations derived inhibitory or excitatory neurons (Xie et al., 2020)
KCNQ2	Neonatal epileptic encephalopathy	Increased bursting firing with faster AP repolarization and shorter AP half width	Patient (c.1742G > A) iPSCs derived excitatory neurons (Simkin and Kiskinis, 2018)
KCNT1	Malignant migrating partial seizures of infancy	Shorter AP, increased KNa^+ current, increased afterhyperpolarization amplitude	Patient (P924L) iPSCs derived neurons (mixture of glutamatergic and GABAergic neurons) (Quraishi et al., 2019)
mTOR pathway			
TSC1/2	Tuberous sclerosis	Increased proliferation rate in neural stem cells	Patient (c.1444-2A > C) iPSCs derived neural stem cells (Li et al., 2017)
TSC1/2	Tuberous sclerosis	Enlarged soma size and altered neurite length; elevated network activity, with increased synchrony and mean firing rate	Patient (c.5238_5255del) iPSCs derived neurons (Winden et al., 2019)
TSC1/2	Tuberous sclerosis	Increased frequency of calcium influx and spontaneous spikes	Patient (c.2249G > A/c.1563dupA) iPSCs derived neurons (Nadadhur et al., 2019)
TSC1/2	Tuberous sclerosis	Reduced firing frequency and mEPSCs frequency	Patient iPSCs (Chr16:2088303-2088320_del 18bp/Chr16:2088299-2088306_del8bp) derived cerebellar Purkinje neurons (Sundberg et al., 2018)
TSC1/2	Tuberous sclerosis	Increased soma size and dendritic arborization; lower input resistance, decreased mEPSCs and sEPSCs frequency	Zinc-finger nuclease-mediated targeted gene targeting exon 11 of TSC2 gene in hESCs cell line differentiated into neurons (Costa et al., 2016)
DEPDC5	Familial focal epilepsy	Enlarged soma size; altered mTOR signaling rescued by rapamycin	Patient (c.2620C > T; p.R874*/c.59-493_146 + 710; p.D20Afs*25) iPSCs derived neurons (Klofas et al., 2020)
CDKL5	CDKL5 deficiency disorder	Reduced proliferation rate and increased death in neural progenitor cells; increased dendritic length, higher complexity, and increased hyperexcitability with more number of evoked AP, elevated sEPSC frequency and increased firing rate and synchrony in neurons	Patient (R59X/R550X/S855X/R59X/p.D135_F154del/ Xp22.13del) iPSCs derived neural progenitor cells and neurons (Negraes et al., 2021)
UBE3A	Angelman syndrome	Fewer Ca^{2+} transients, decreased AP amplitude, AP threshold, and elevated AP width at later development time point (week 20 and later); reduced frequency of spontaneous currents when induced for LTP	CRISPR/Cas9 edited iPSCs-derived neurons to knockout UBE3A with non-homologous end joining or knockdown UBE3A with antisense oligonucleotides (Fink et al., 2017)
UBE3A	15q11-q13 duplication syndrome	Increased number of dendritic protrusions, heightened excitatory synaptic current frequency and amplitude, lowered inhibitory synaptic currency and amplitude. Disrupted ion channel (KCNQ2) function, impaired activity dependent plasticity, and synaptic scaling	15q11-13 patient iPSCs-derived neurons (Fink et al., 2021)
MECP2	Rett syndrome	Enlarged soma size and increased dendritic branching; reduced protein synthesis and translation	TALEN edited hESCs-derived neurons targeting third exon of MECP2 gene (Li et al., 2013)

LOF mutation in SCN1A). In this regard, *in vitro* human models such as patient-derived neurons, mutations in ion channels, complemented with CRISPR/Cas9 technology, have provided important mechanistic insights into how ion channelopathy, especially in sodium and potassium channels, could affect action potential waveform and firing patterns of the neurons, contributing to E/I imbalance underlying epileptic activity.

HUMAN *IN VITRO* MODEL RECAPITULATING EPILEPSY CAUSED BY THE MECHANISTIC TARGET OF RAPAMYCIN PATHWAY MUTATIONS

Another cluster of genes often found mutated in epilepsy patients are those encoding components of the mTOR pathway, an essential regulator of cell metabolism and physiology. Upon binding of growth factors, phosphoinositide-3-kinase (PI3K) is activated, which converts phosphatidylinositol (4,5)-bisphosphate (PIP2) to phosphatidylinositol (3,4,5)-triphosphate (PIP3). PIP3 serves as a docking site for AKT, a serine/threonine kinase. When phosphorylated, AKT is released into the cytoplasm and inhibits the tuberous sclerosis protein complex (TSC), which acts as an inhibitor for mTOR thereby controlling cell proliferation, cell growth, and cell survival. Previous clinical and *in vitro* studies have revealed the importance of the mTOR pathway in epileptic pathogenesis, where mutations of key signaling molecules along the mTOR pathway were associated with brain malformations and seizures activity, including but not limited to PTEN, PI3K, AKT3, TSC1/2, DEPDC5, and mTOR (Griffith and Wong, 2018).

Tuberous Sclerosis Complex

Previous studies have targeted tuberous sclerosis complex (TSC1 and TSC2) to model tuberous sclerosis, a multi-organ disorder characterized by the growth of non-cancerous tumors. TSC1/2 serves as a direct inhibitor of mTORC1, and the loss of TSC1/2 leads to hyperactivation of this pathway, affecting various downstream signaling cascades. Although non-cancerous growing mass is the most common presenting symptom in tuberous sclerosis, 80–90% of patients develop epilepsy along the course of the disease (Thiele, 2004). Animal models with TSC1 mutation revealed neurological deficits such as changes in myelination, enlarged neurons, and development of epilepsy (Meikle et al., 2007; Zeng et al., 2008). Mice with TSC2 inactivation mutation also exhibited neurological deficits, including megacephaly and epilepsy (Zeng et al., 2011). Although TSC1/2 has been studied in mouse models, its role in human neurons has only been investigated recently using human *in vitro* models. Human tuberous sclerosis patient-derived neuroepithelial cells carrying TSC2 mutations displayed increased proliferation rate (Li et al., 2017), and mutant cortical neurons developed enlarged soma and altered neurite length (Winden et al., 2019). Functional analysis revealed an overall hyperexcitability coinciding with increased frequency of calcium oscillations and spontaneous spikes (Nadadhur et al., 2019). These patient-derived cortical neurons formed a network with elevated activity, shown by increased firing rate and synchrony (Winden et al., 2019). In contrast, a different study reported lower input resistance, decreased frequency in miniature and spontaneous excitatory postsynaptic currents (mEPSCs and sEPSCs) in neurons derived from ESCs carrying TSC2 mutations (Costa et al., 2016). In addition, human iPSCs-derived cerebellar Purkinje neurons with TSC1/2 mutation showed reduced firing frequency upon current injection and reduced mEPSCs frequency (Sundberg et al., 2018). These inconsistent results of firing frequency from cortical neurons with TSC2 mutation could be due to the interference from the patient genetic background. Alternatively, as Purkinje neurons project to GABAergic outputs, reduced excitatory synaptic activity to these neurons can be transformed to the disinhibition of downstream neurons, leading to hyperexcitable networks underlying epilepsy.

DEP Domain-Containing Protein 5

DEP domain-containing protein 5 (DEPDC5) encodes a protein within the GATOR1 complex that negatively regulates the mTOR pathway, and its mutation is commonly found in patients with familial focal epilepsy. As germline homozygous DEPDC5 knockout is embryonic lethal, animal studies used conditional knockout targeting specific brain regions or heterozygous DEPDC5 mutants and reported cell morphological change and seizure activity (Yuskaitis et al., 2018). Similarly, human neural progenitor cells (NPCs) with heterozygous LOF DEPDC5 mutation from epilepsy patients iPSCs displayed elevated mTOR signaling reflected by S6 phosphorylation and larger soma size, which were reversed by rapamycin treatment. Mutant neurons also showed elevated responses to amino acids deprivation which is regulated by the mTOR signaling pathway (Klofas et al., 2020). However, it remains unknown whether and how DEPDC5 mutation impacts firing and wiring that account for the pathologic defects in epilepsy.

Cyclin-Dependent Kinase-Like 5, Ubiquitin-Protein Ligase E3A, and Methyl CpG Binding Protein

While TSC1/2 and DEPDC5 directly regulate the mTOR pathway, other neurodevelopmental disorder genes such as cyclin-dependent kinase-like 5 (CDKL5), ubiquitin-protein ligase E3A (UBE3A), and methyl CpG binding protein (MECP2) are also known to affect or be affected by the mTOR signaling. Although the exact mechanisms of how these genes are linked to the mTOR signaling are yet to be clarified, patients with CDKL5, UBE3A, and MECP2 mutations often develop epilepsy and display altered mTOR activity (Sun et al., 2018; Negraes et al., 2021). CDKL5 is a gene causally linked to CDKL5 deficiency disorder (CDD), where patients develop intellectual delay and epilepsy. CDKL5 was previously found to alter the expression of components of the mTOR signaling and other synaptic elements in mice, possibly leading to changes in neuronal circuitry and excitability (Schroeder et al., 2019). CDKL5 mutant mouse model has been established, although some human patients' phenotypes were not captured in the mice

model, including the lack of spontaneous seizures in young mice (Negraes et al., 2021). By deriving iPSCs from CDD patient fibroblasts, and then differentiating them into neural precursors, the authors observed reduced proliferation and increased cell death. Neurons derived from CDD patient iPSCs displayed altered morphology and electrical activity. Specifically, neurons with CDKL5 LOF mutation showed increased dendritic length and higher complexity when compared to control neurons. In addition, CDD neurons exhibited hyperexcitability, characterized by an increased number of evoked action potentials and elevated frequency of sEPSCs. The authors also reported an upregulation in the co-association between synaptic proteins in CDD neurons, including mGluR5 and Homer, and GluR1 and GluR2 (Negraes et al., 2021). The alterations in glutamate receptor composition can largely affect synaptic strength of excitatory inputs in these neurons. Interestingly, this observation of hyperexcitability was accompanied by decreased Synapsin 1 and PSD95 density. The CDD neurons also showed increased phosphorylation of molecules in the mTOR pathway, including RPTOR and LARP1, and less responsive feedback to the removal of amino acids, which is regulated by the mTOR pathway. CDD cerebral organoids generated from mutant cells revealed convergent findings as those observed in the monolayer neuronal culture, including aberrant electrical activity, increase in mean firing rate and synchrony consistent with epileptic phenotypes.

Another neurodevelopment disorder related to epilepsy is Angelman syndrome (AS), caused by mutations in the UBE3A gene. Patients with AS usually display intellectual disability, developmental delays and seizures. The link between mTOR and AS was minimally examined in human neurons, although a mouse study revealed that the mTOR complexes played a critical role in AS, where the UBE3A mutant mice displayed increased TSC2 inhibition and hyperactivated mTOR signaling, resulting in motor dysfunction. The effect was rescued by rapamycin treatment (Sun et al., 2015). The link between UBE3A and epilepsy or alteration in the mTOR pathway has not been extensively studied in human *in vitro* models until recently. UBE3A mutant human neurons, generated by CRISPR-mediated knockout or antisense oligonucleotide-mediated knockdown, showed a more depolarized resting membrane potential (Fink et al., 2017). These human AS neurons also contained a lower proportion of cells with mature spike waveform and firing patterns. Action potential threshold and amplitude were reduced while the spike width was broadened. Fewer calcium transients were observed at later development time points (week 20). In contrast to the control neurons with the frequency of sEPSCs being readily upregulated by the stimulation paradigm for long-term potentiation, AS neurons were irresponsive to the same stimulation. Another recent study investigated 15q11-q13 duplication syndrome, a neurodevelopmental disorder related to epilepsy. UBE3A resides within the duplicated region and is thought to contribute to disease pathology. This study found that 15q11-q13 duplication human neurons had overall heightened neuronal excitability and excitatory neurotransmission but reduced inhibitory neurotransmission, tipping the E/I balance. Similar to findings in the AS study, activity-dependent plasticity was absent in the 15q11-q13 duplication neurons (Fink et al., 2021). Together these findings demonstrate disrupted electrophysiological properties and plasticity primarily in excitatory neurons carrying UBE3A patient mutations.

MECP2, a global transcriptional repressor, has a vital role in regulating gene expression and chromatin stability. Patients with mutations in MECP2 develop Rett syndrome, a neurodevelopmental disorder characterized by intellectual delays, progressive loss of motor skills and speech, and seizures. Clinical data has suggested a link between MECP2 and mTOR, as elevated mTOR phosphorylation and increased P70S6K has been reported in Rett syndrome patient brains (Olson et al., 2018). Human cortical neurons derived from gene-edited, isogenic MECP2 mutant human embryonic stem cells (hESCs) developed smaller soma, less complex dendritic arborization, and reduced electric activity. These changes were found to coincide with impaired protein synthesis and reduced mTOR pathway activity. Both morphological phenotypes and protein synthesis defects in the mutant neurons were rescued with genetic activation of the mTOR pathway (Li et al., 2013), highlighting the possible role of the mTOR pathway in Rett Syndrome.

HOMEOSTASIS AND GENETIC EPILEPSY

Synaptic Homeostasis in Neuronal Circuit

The term homeostasis was first coined in 1865 by Claude Bernard as "the stability of the internal environment." In general, homeostasis involves maintaining the balance of a physiological state or the biological systems through self-regulating mechanisms. In the field of neuroscience, homeostasis has important implications for maintaining normal brain development and function. The brain circuits are formed by different cells connecting to each other, and synaptic communication between them is highly dynamic and activity-dependent. At the individual neuron level, the overall output (i.e., firing rate) of any given neuron is tightly regulated by internal feedback loops to regulate its intrinsic excitability (e.g., voltage-gated ion channels) and by external inputs (e.g., glutamatergic and GABAergic) from other cells in the network to achieve equilibrium (or setpoint). The maintenance of the synaptic balance at a specific setpoint between neurons can be described as synaptic homeostasis, where the excitation of the cells is counteracted by inhibition in brain circuits.

Previous studies have identified that the hippocampus homeostatic setpoint is regulated by DHODH (Styr et al., 2019; Ruggiero et al., 2021), an enzyme residing in the inner membrane of mitochondria and facilitating the electron transfer from dihydroorotate to ubiquinone. Specifically, DHODH inhibition reduced the firing rate in hippocampal neuronal culture measured by MEA plate, which stayed at a reduced rate days after inhibition, resetting a homeostatic setpoint for the neurons. The studies implicated a metabolic substrate

underlying the firing setpoint, providing an explanation for the chronic development of epilepsy. Although the relation between mitochondria and the mTOR pathway in the brain remains unclear, studies have revealed that rapamycin treatment inhibiting the mTOR pathway led to changes in mitochondrial protein phosphorylation in human T lymphocyte cells (Betz and Hall, 2013). These studies allude a critical role of mitochondria in homeostasis, which could be modulated by mTOR activity.

Synaptic Homeostasis in Genetic Epilepsy

In normal development, homeostasis is maintained at a setpoint value, while in the case of epilepsy, homeostatic plasticity is disrupted with an elevated setpoint of global excitation over inhibition due to maladaptive changes, such as mutations of signaling molecules along the mTOR pathway or ion channels underlying intrinsic excitability or synaptic proteins. As discussed above, changes of ion channels in excitatory neurons, such as LOF in KCNQ2 or GOF in KCNT1, can lead to an increase in intrinsic excitability and excessive firing from the neurons. Other ion channel mutations, such as SCN1A in the inhibitory neurons, can lead to decreased excitability, allowing disinhibition of the excitatory neurons. Components along the mTOR pathway have also been shown to be a hotspot for epilepsy, reflected by its mutation displaying not only a higher firing rate, but also changes in morphology. Although often overlooked under the context of electrical activity, morphological alteration such as sprouting is closely linked to hyperconnectivity and, in turn, disrupted electrical activity in the brain circuit can lead to epilepsy. While the changes in intrinsic excitability, synaptic activity, and morphology may be parallel and converging, there is no direct evidence with human *in vitro* studies that explicitly parse out primary, secondary and/or compensatory effects. This presents a major challenge for the field to test. It is conceivable that morphological and electrical analysis can be done in a time series experiment to temporally map the changes in intrinsic excitability, synaptic activity, and morphology. Experiments blocking one process or another at different time points with pharmacological blockers or genetic perturbations will help clarify their intricate relationships and reciprocal dependence.

Both ion channel and the mTOR pathway mutations are tightly related with synaptic dynamics and epileptic activity, and these two groups of mutations might be associated with each other. While one paper has discovered ion channel deficit (KCNQ2) in UBE3A human *in vitro* model, the underlying connection between the ion channel and the mTOR pathway has rarely been explored in the human *in vitro* model, it has been examined in mouse podocytes, where mTOR was found to regulate intrinsic excitability by increasing calcium-activated potassium channels (BK channels) expression and BK channel conductance was decreased when the pathway was inhibited by AKT inhibitor (Wang et al., 2019). Interestingly, the mTOR pathway can also directly regulate ion channels and synaptic proteins. For example, NMDAR recruits PTEN onto postsynaptic density and decreases AMPAR mediated responses (Jurado et al., 2010). In addition, PTEN knockdown in iPSC-derived motor neurons has been shown to alter the properties of AMPARs directly, such as their expression level and activity reflecting synaptic strength and transmission (Yang et al., 2014). Ion channels and the mTOR pathway can both regulate synaptic plasticity, remodeling the dynamics between individual synapses and the setpoint of neurons and networks. In other studies using mice and rat models (Niere and Raab-Graham, 2017), mTOR inactivation elevated Kv1.1 and Kv1.2 expression and regulated NMDAR activity, which controlled Ca^{2+} influx into the cell to alter mTOR activity. This self-regulated feedback loop maintains cellular excitability by balancing the changes in ion channels and mTOR activity, likely through excitation-transcription coupling. More importantly, a study directly examined the link between ion channel and mTOR pathway under the context of epilepsy (Nguyen and Anderson, 2018). In PTEN KO mice, hippocampal Kv1.1 protein expression was increased, and inhibition of mTOR with rapamycin normalized the aberrant expression. In light of these results, where mTOR has a significant effect on the protein synthesis for Kv1.1, it is possible that mTOR can also alter the translation and activity of a variety of ion channels in the neurons, and thus regulating excitability in the neuronal network. Clarifying the type of neurons associated with Kv1.1 reduction and their impact on the E/I dynamics will unravel its relation to epilepsy in the PTEN KO mice.

To conceptualize the findings from both human *in vitro* system and rodent models in which the roles of the mTOR pathway in regulating ion channels and synaptic receptors are evidently established, we propose a hypothetical working model that dysregulation of mTOR signaling may underlie the inability for neurons to adjust the setpoint in their intrinsic excitability and synaptic inputs, both of which converge to an E/I imbalance in the network, leading to seizure activity (**Figure 1**). Furthermore, cells with mTOR mutations have also shown morphological changes, including enlarged soma and increased dendritic spine density, contributing to hyperfiring and hyperwiring in epilepsy. To maintain a functional neural circuit under the dynamic changes to perturbations, the presence of negative feedback to maintain homeostasis is extremely crucial. Under the normal condition, a neuronal network renders a typical firing rate which is maintained at a particular setpoint for homeostasis, possibly facilitated by a metabolic regulator mitochondrial DHODH and its inhibition. When perturbation in the electrical activity (e.g., sudden hyperexcitation or hypersynchrony) is present, the neuronal circuit can sense the change and efficiently make adjustments to return to the original setpoint. In epilepsy, mutations in the mTOR pathway may reset not only cellular excitability and seizures, but also dysregulate mitochondrial function and morphological sprouting, precluding perturbation-induced readjustment of the setpoint from transforming a highly synchronized and excited state back to the norm. Therefore, the mTOR pathway may play an indispensable role in reciprocally coupling of excitation, transcription and translation of key substrates that are important for self-facilitated homeostasis and E/I balance. Mutations along the mTOR pathway converge to changes in intrinsic neuronal excitability and synaptic inputs, aggravating the hypersynchrony in the network and leading to epilepsy.

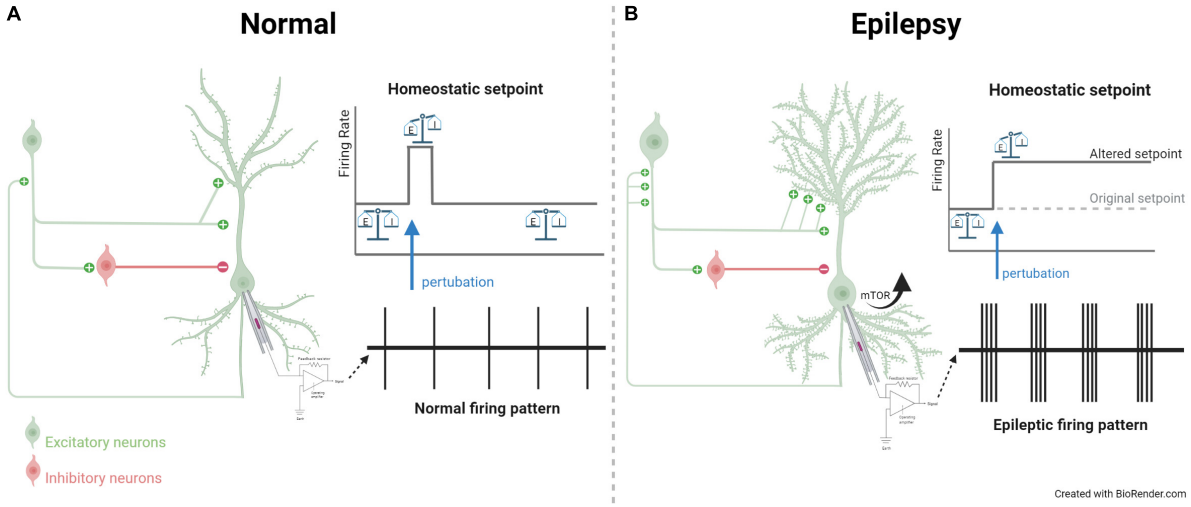

FIGURE 1 | Hypothetical working model contrasting a microcircuit in normal and epileptic brain. **(A)** In normal condition, excitatory and inhibitory inputs synapsing onto a neuron with a balanced E/I ratio and firing pattern. Upon perturbation, homeostatic setpoint resets the electrical activity back to baseline. **(B)** In epilepsy, channelopathy or mTOR signaling mutations can lead to changes in intrinsic excitability and synaptic strength of inputs. These changes lead to E/I imbalance and result in characteristic epileptic electrical activity, as indicated by the firing pattern recorded from extracellular recording. Alterations in mTOR pathway also result in morphological changes, including enlarged soma and increased sprouting, further aggravating an imbalanced neuronal circuit. During such a perturbation, the homeostatic setpoint is altered in epilepsy and the electrical activity is unable to return to the baseline setpoint. The figure is created with Biorender with publication license.

CONCLUDING REMARKS AND FUTURE DIRECTION

Previous animal models have provided important insights into epilepsy, but our lack of understanding in species differences limits our comprehension of epileptogenesis in human brains and the development of effective treatments for patients. In this review, we summarize a series of studies of ion channels in epilepsy using human pluripotent stem cells derived *in vitro* culture, including voltage-gated sodium and potassium channels. Many other ion channels, such as calcium channels and HCN channels, that have been investigated in animal models are yet to be studied in human *in vitro* culture. In addition, synaptic receptors that are important for synaptic plasticity, such as NMDAR and GABAergic receptors, that are implicated in patients and studied in animal models (Oyrer et al., 2018), await systematic studies in human *in vitro* systems. Finally, components along the mTOR pathway, including PTEN, PI3K, AKT that are all reported in epilepsy patients remain underexplored in the context of epilepsy with PSC-derived systems. Many of the studies have used relatively simplified neuronal cultures. As these models serve as a reductionist approach to study epilepsy, it is also essential to acknowledge the crucial roles of interactive dynamics in neurons and neuronal networks. Homeostasis probably requires a highly complex circuit model with excitatory principal neurons and inhibitory interneurons and other cell types including astrocytes, oligodendrocytes and microglia. To achieve this, co-cultures of mixed cell types or brain organoids can be employed to develop a more physiologically relevant network. Other models such as the xenografted mouse model carrying specific human patient cells should be used to provide a native host for these induced neurons to form complex circuits reminiscent of epileptic loci *in vivo*. In doing so, one can address the possibility how mutant neurons prime the seizure and epilepsy with EEG correlate and behavioral outcomes as objective readouts. As proposed in our hypothetical working model, we suggest that the mTOR activity affects ion channels, synaptic plasticity and hyperwiring, which underlies E/I imbalance and permanently altered homeostatic set point, preventing the electrical activity from being renormalized after perturbation. The dynamic interactions between the mTOR pathway, ion channels, and synaptic plasticity have hardly been investigated using human *in vitro* systems, which undoubtedly will offer efficient platforms for us to scrutinize complex brain networks and gain unprecedented insights into homeostatic alterations in epileptogenesis for developing therapies.

AUTHOR CONTRIBUTIONS

OW, YL, and L-YW contributed to conception and design of the study. OW wrote the first draft of the manuscript. All authors contributed to manuscript revision, read, and approved the submitted version.

FUNDING

This work was supported by the Canadian Institutes of Health Research (PJT-156034 and PJT-156439), the Natural Science and Engineering Research Council (RGPIN-2017-06665), the Canada Research Chairs Program, the Simons Foundation, Can-GARD, Epilepsy Canada, and Ontario Graduate Scholarships.

REFERENCES

Bartolini, E., Campostrini, R., Kiferle, L., Pradella, S., Rosati, E., Chinthapalli, K., et al. (2020). Epilepsy and brain channelopathies from infancy to adulthood. *Neurol. Sci.* 41, 749–761. doi: 10.1007/s10072-019-04190-x

Betz, C., and Hall, M. N. (2013). Where is mTOR and what is it doing there? *J. Cell Biol.* 203, 563–574. doi: 10.1083/jcb.201306041

Cavarsan, C. F., Malheiros, J., Hamani, C., Najm, I., and Covolan, L. (2018). Is mossy fiber sprouting a potential therapeutic target for epilepsy? *Front. Neurol.* 9:1023. doi: 10.3389/fneur.2018.01023

Child, N. D., and Benarroch, E. E. (2014). Differential distribution of voltage-gated ion channels in cortical neurons: implications for epilepsy. *Neurology* 82, 989–999. doi: 10.1212/WNL.0000000000000228

Cho, C.-H. (2011). Frontier of epilepsy research - mTOR signaling pathway. *Exp. Mol. Med.* 43, 231–274. doi: 10.3858/emm.2011.43.5.032

Costa, V., Aigner, S., Vukcevic, M., Sauter, E., Behr, K., Ebeling, M., et al. (2016). mTORC1 inhibition corrects neurodevelopmental and synaptic alterations in a human stem cell model of tuberous sclerosis. *Cell Rep.* 15, 86–95. doi: 10.1016/j.celrep.2016.02.090

Fink, J. J., Robinson, T. M., Germain, N. D., Sirois, C. L., Bolduc, K. A., Ward, A. J., et al. (2017). Disrupted neuronal maturation in Angelman syndrome-derived induced pluripotent stem cells. *Nat. Commun.* 8:15038. doi: 10.1038/ncomms15038

Fink, J. J., Schreiner, J. D., Bloom, J. E., James, J., Baker, D. S., Robinson, T. M., et al. (2021). Hyperexcitable phenotypes in induced pluripotent stem cell–derived neurons from patients with 15q11-q13 duplication syndrome, a genetic form of autism. *Biol. Psychiatry* 90, 756–765. doi: 10.1016/j.biopsych.2021.07.018

Griffith, J. L., and Wong, M. (2018). The mTOR pathway in treatment of epilepsy: a clinical update. *Future Neurol.* 13, 49–58. doi: 10.2217/fnl-2018-0001

Haider, B., Häusser, M., and Carandini, M. (2013). Inhibition dominates sensory responses in awake cortex. *Nature* 493, 97–100. doi: 10.1038/nature11665

Hirose, S., Tanaka, Y., Shibata, M., Kimura, Y., Ishikawa, M., Higurashi, N., et al. (2020). Application of induced pluripotent stem cells in epilepsy. *Mol. Cell. Neurosci.* 108:103535. doi: 10.1016/j.mcn.2020.103535

Ihara, Y., Tomonoh, Y., Deshimaru, M., Zhang, B., Uchida, T., Ishii, A., et al. (2016). Retigabine, a Kv7.2/Kv7.3-channel opener, attenuates drug-induced seizures in knock-in mice harboring Kcnq2 mutations. *PLoS One* 11:e0150095. doi: 10.1371/journal.pone.0150095

Jiao, J., Yang, Y., Shi, Y., Chen, J., Gao, R., Fan, Y., et al. (2013). Modeling Dravet syndrome using induced pluripotent stem cells (iPSCs) and directly converted neurons. *Hum. Mol. Genet.* 22, 4241–4252. doi: 10.1093/hmg/ddt275

Jurado, S., Benoist, M., Lario, A., Knafo, S., Petrok, C. N., and Esteban, J. A. (2010). PTEN is recruited to the postsynaptic terminal for NMDA receptor-dependent long-term depression. *EMBO J.* 29, 2827–2840. doi: 10.1038/emboj.2010.160

Kim, H. W., Quan, Z., Kim, Y.-B., Cheong, E., Kim, H. D., Cho, M., et al. (2018). Differential effects on sodium current impairments by distinct SCN1A mutations in GABAergic neurons derived from Dravet syndrome patients. *Brain Dev.* 40, 287–298. doi: 10.1016/j.braindev.2017.12.002

Klofas, L. K., Short, B. P., Snow, J. P., Sinnaeve, J., Rushing, G. V., Westlake, G., et al. (2020). DEPDC5 haploinsufficiency drives increased mTORC1 signaling and abnormal morphology in human iPSC-derived cortical neurons. *Neurobiol. Dis.* 143:104975. doi: 10.1016/j.nbd.2020.104975

Lascano, A. M., Korff, C. M., and Picard, F. (2016). Seizures and epilepsies due to channelopathies and neurotransmitter receptor dysfunction: a parallel between genetic and immune aspects. *Mol. Syndromol.* 7, 197–209. doi: 10.1159/000447707

Li, Y., Cao, J., Chen, M., Li, J., Sun, Y., Zhang, Y., et al. (2017). Abnormal neural progenitor cells differentiated from induced pluripotent stem cells partially mimicked development of TSC2 neurological abnormalities. *Stem Cell Rep.* 8, 883–893. doi: 10.1016/j.stemcr.2017.02.020

Li, Y., Wang, H., Muffat, J., Cheng, A. W., Orlando, D. A., Lovén, J., et al. (2013). Global transcriptional and translational repression in human-embryonic-stem-cell-derived Rett syndrome neurons. *Cell Stem Cell* 13, 446–458. doi: 10.1016/j.stem.2013.09.001

Liu, J., Gao, C., Chen, W., Ma, W., Li, X., Shi, Y., et al. (2016). CRISPR/Cas9 facilitates investigation of neural circuit disease using human iPSCs: mechanism of epilepsy caused by an SCN1A loss-of-function mutation. *Transl. Psychiatry* 6:e703. doi: 10.1038/tp.2015.203

Löscher, W. (2017). Animal models of seizures and epilepsy: past, present, and future role for the discovery of antiseizure drugs. *Neurochem. Res.* 42, 1873–1888. doi: 10.1007/s11064-017-2222-z

Löscher, W., and Schmidt, D. (2011). Modern antiepileptic drug development has failed to deliver: ways out of the current dilemma. *Epilepsia* 52, 657–678. doi: 10.1111/j.1528-1167.2011.03024.x

Meikle, L., Talos, D. M., Onda, H., Pollizzi, K., Rotenberg, A., Sahin, M., et al. (2007). A mouse model of tuberous sclerosis: neuronal loss of tsc1 causes dysplastic and ectopic neurons, reduced myelination, seizure activity, and limited survival. *J. Neurosci.* 27, 5546–5558. doi: 10.1523/JNEUROSCI.5540-06.2007

Mulley, J. C., Scheffer, I. E., Petrou, S., and Berkovic, S. F. (2003). Channelopathies as a genetic cause of epilepsy. *Curr. Opin. Neurol.* 16, 171–176. doi: 10.1097/01.wco.0000063767.15877.c7

Nadadhur, A. G., Alsaqati, M., Gasparotto, L., Cornelissen-Steijger, P., van Hugte, E., Dooves, S., et al. (2019). Neuron-glia interactions increase neuronal phenotypes in tuberous sclerosis complex patient iPSC-derived models. *Stem Cell Rep.* 12, 42–56. doi: 10.1016/j.stemcr.2018.11.019

Negraes, P. D., Trujillo, C. A., Yu, N.-K., Wu, W., Yao, H., Liang, N., et al. (2021). Altered network and rescue of human neurons derived from individuals with early-onset genetic epilepsy. *Mol. Psychiatry* 26, 7047–7068. doi: 10.1038/s41380-021-01104-2

Nguyen, L. H., and Anderson, A. E. (2018). mTOR-dependent alterations of Kv1.1 subunit expression in the neuronal subset-specific Pten knockout mouse model of cortical dysplasia with epilepsy. *Sci. Rep.* 8:3568. doi: 10.1038/s41598-018-21656-8

Niere, F., and Raab-Graham, K. F. (2017). mTORC1 is a local, postsynaptic voltage sensor regulated by positive and negative feedback pathways. *Front. Cell. Neurosci.* 11:152. doi: 10.3389/fncel.2017.00152

Ogiwara, I., Miyamoto, H., Morita, N., Atapour, N., Mazaki, E., Inoue, I., et al. (2007). Nav1.1 localizes to axons of parvalbumin-positive inhibitory interneurons: a circuit basis for epileptic seizures in mice carrying an scn1a gene mutation. *J. Neurosci.* 27, 5903–5914. doi: 10.1523/JNEUROSCI.5270-06.2007

Olson, C. O., Pejhan, S., Kroft, D., Sheikholeslami, K., Fuss, D., Buist, M., et al. (2018). MECP2 mutation interrupts nucleolin-mTOR-P70S6K signaling in rett syndrome patients. *Front. Genet.* 9:635. doi: 10.3389/fgene.2018.00635

Oyrer, J., Maljevic, S., Scheffer, I. E., Berkovic, S. F., Petrou, S., and Reid, C. A. (2018). Ion channels in genetic epilepsy: from genes and mechanisms to disease-targeted therapies. *Pharmacol. Rev.* 70, 142–173. doi: 10.1124/pr.117.014456

Patel, M. (2018). A metabolic paradigm for epilepsy. *Epilepsy Curr.* 18, 318–322. doi: 10.5698/1535-7597.18.5.318

Perucca, P. (2018). Genetics of focal epilepsies: What do we know and where are we heading? *Epilepsy Curr.* 18, 356–362. doi: 10.5698/1535-7597.18.6.356

Proietti Onori, M., Koene, L. M. C., Schäfer, C. B., Nellist, M., de Brito van Velze, M., Gao, Z., et al. (2021). RHEB/mTOR hyperactivity causes cortical malformations and epileptic seizures through increased axonal connectivity. *PLoS Biol.* 19:e3001279. doi: 10.1371/journal.pbio.3001279

Quraishi, I. H., Stern, S., Mangan, K. P., Zhang, Y., Ali, S. R., Mercier, M. R., et al. (2019). An epilepsy-associated KCNT1 mutation enhances excitability of human iPSC-derived neurons by increasing slack KNa currents. *J. Neurosci. Off. J. Soc. Neurosci.* 39, 7438–7449. doi: 10.1523/JNEUROSCI.1628-18.2019

Ruggiero, A., Katsenelson, M., and Slutsky, I. (2021). Mitochondria: new players in homeostatic regulation of firing rate set points. *Trends Neurosci.* 44, 605–618. doi: 10.1016/j.tins.2021.03.002

Scharfman, H. E. (2007). The neurobiology of epilepsy. *Curr. Neurol. Neurosci. Rep.* 7, 348–354.

Schroeder, E., Yuan, L., Seong, E., Ligon, C., DeKorver, N., Gurumurthy, C. B., et al. (2019). Neuron-type specific loss of CDKL5 leads to alterations in mTOR signaling and synaptic markers. *Mol. Neurobiol.* 56, 4151–4162. doi: 10.1007/s12035-018-1346-8

Schwarz, N., Uysal, B., Rosa, F., Löffler, H., Mau-Holzmann, U. A., Liebau, S., et al. (2018). Generation of an induced pluripotent stem cell (iPSC) line from a patient with developmental and epileptic encephalopathy carrying a KCNA2 (p.Leu328Val) mutation. *Stem Cell Res.* 33, 6–9. doi: 10.1016/j.scr.2018.08.019

Schwarz, N., Uysal, B., Rosa, F., Löffler, H., Mau-Holzmann, U. A., Liebau, S., et al. (2019). Establishment of a human induced pluripotent stem cell (iPSC) line (HIHDNEi002-A) from a patient with developmental and epileptic

encephalopathy carrying a KCNA2 (p.Arg297Gln) mutation. *Stem Cell Res.* 37:101445. doi: 10.1016/j.scr.2019.101445

Simkin, D., and Kiskinis, E. (2018). Modeling pediatric epilepsy through iPSC-based technologies. *Epilepsy Curr.* 18, 240–245. doi: 10.5698/1535-7597.18.4.240

Stafstrom, C. E., and Carmant, L. (2015). Seizures and epilepsy: an overview for neuroscientists. *Cold Spring Harb. Perspect. Med.* 5:a022426. doi: 10.1101/cshperspect.a022426

Styr, B., Gonen, N., Zarhin, D., Ruggiero, A., Atsmon, R., Gazit, N., et al. (2019). Mitochondrial regulation of the hippocampal firing rate set point and seizure susceptibility. *Neuron* 102, 1009–1024.e8. doi: 10.1016/j.neuron.2019.03.045

Sun, J., Liu, Y., Jia, Y., Hao, X., Lin, W. J., Tran, J., et al. (2018). UBE3A-mediated p18/LAMTOR1 ubiquitination and degradation regulate mTORC1 activity and synaptic plasticity. *Elife* 7:e37993. doi: 10.7554/eLife.37993

Sun, J., Liu, Y., Moreno, S., Baudry, M., and Bi, X. (2015). Imbalanced mechanistic target of rapamycin C1 and C2 activity in the cerebellum of angelman syndrome mice impairs motor function. *J. Neurosci.* 35, 4706–4718. doi: 10.1523/JNEUROSCI.4276-14.2015

Sun, Y., Paşca, S. P., Portmann, T., Goold, C., Worringer, K. A., Guan, W., et al. (2016). A deleterious Nav1.1 mutation selectively impairs telencephalic inhibitory neurons derived from Dravet Syndrome patients. *Elife* 5:e13073. doi: 10.7554/eLife.13073

Sundberg, M., Tochitsky, I., Buchholz, D. E., Winden, K., Kujala, V., Kapur, K., et al. (2018). Purkinje cells derived from TSC patients display hypoexcitability and synaptic deficits associated with reduced FMRP levels and reversed by rapamycin. *Mol. Psychiatry* 23, 2167–2183. doi: 10.1038/s41380-018-0018-4

Takahashi, K., Tanabe, K., Ohnuki, M., Narita, M., Ichisaka, T., Tomoda, K., et al. (2007). Induction of pluripotent stem cells from adult human fibroblasts by defined factors. *Cell* 131, 861–872. doi: 10.1016/j.cell.2007.11.019

Takahashi, K., and Yamanaka, S. (2006). Induction of pluripotent stem cells from mouse embryonic and adult fibroblast cultures by defined factors. *Cell* 126, 663–676. doi: 10.1016/j.cell.2006.07.024

Thiele, E. A. (2004). Managing epilepsy in tuberous sclerosis complex. *J. Child Neurol.* 19, 680–686. doi: 10.1177/08830738040190090801

Tidball, A. M., Dang, L. T., Glenn, T. W., Kilbane, E. G., Klarr, D. J., Margolis, J. L., et al. (2017). Rapid generation of human genetic loss-of-function iPSC Lines by simultaneous reprogramming and gene editing. *Stem Cell Rep.* 9, 725–731. doi: 10.1016/j.stemcr.2017.07.003

Uysal, B., Löffler, H., Rosa, F., Lerche, H., and Schwarz, N. (2019). Generation of an induced pluripotent stem cell (iPSC) line (HIHDNEi003-A) from a patient with developmental and epileptic encephalopathy carrying a KCNA2 (p.Thr374Ala) mutation. *Stem Cell Res.* 40:101543. doi: 10.1016/j.scr.2019.101543

Wang, Y., Tao, J., Wang, M., Yang, L., Ning, F., Xin, H., et al. (2019). Mechanism of regulation of big-conductance Ca2+-activated K+ channels by mTOR complex 2 in podocytes. *Front. Physiol.* 10:167. doi: 10.3389/fphys.2019.00167

Winden, K. D., Sundberg, M., Yang, C., Wafa, S. M. A., Dwyer, S., Chen, P.-F., et al. (2019). Biallelic mutations in TSC2 lead to abnormalities associated with cortical tubers in human iPSC-derived neurons. *J. Neurosci.* 39, 9294–9305. doi: 10.1523/JNEUROSCI.0642-19.2019

Xie, Y., Ng, N. N., Safrina, O. S., Ramos, C. M., Ess, K. C., Schwartz, P. H., et al. (2020). Comparisons of dual isogenic human iPSC pairs identify functional alterations directly caused by an epilepsy associated SCN1A mutation. *Neurobiol. Dis.* 134:104627. doi: 10.1016/j.nbd.2019.104627

Xu, D., Robinson, A. P., Ishii, T., Duncan, D. S., Alden, T. D., Goings, G. E., et al. (2018). Peripherally derived T regulatory and γδ T cells have opposing roles in the pathogenesis of intractable pediatric epilepsy. *J. Exp. Med.* 215, 1169–1186. doi: 10.1084/jem.20171285

Yang, D.-J., Wang, X.-L., Ismail, A., Ashman, C. J., Valori, C. F., Wang, G., et al. (2014). PTEN regulates AMPA receptor-mediated cell viability in iPS-derived motor neurons. *Cell Death Dis.* 5:e1096. doi: 10.1038/cddis.2014.55

Yuskaitis, C. J., Jones, B. M., Wolfson, R. L., Super, C. E., Dhamne, S. C., Rotenberg, A., et al. (2018). A mouse model of DEPDC5-related epilepsy: neuronal loss of Depdc5 causes dysplastic and ectopic neurons, increased mTOR signaling, and seizure susceptibility. *Neurobiol. Dis.* 111, 91–101. doi: 10.1016/j.nbd.2017.12.010

Zeng, L.-H., Rensing, N. R., Zhang, B., Gutmann, D. H., Gambello, M. J., and Wong, M. (2011). Tsc2 gene inactivation causes a more severe epilepsy phenotype than Tsc1 inactivation in a mouse model of tuberous sclerosis complex. *Hum. Mol. Genet.* 20, 445–454. doi: 10.1093/hmg/ddq491

Zeng, L.-H., Xu, L., Gutmann, D. H., and Wong, M. (2008). Rapamycin prevents epilepsy in a mouse model of tuberous sclerosis complex. *Ann. Neurol.* 63, 444–453. doi: 10.1002/ana.21331

Conflict of Interest: The authors declare that the research was conducted in the absence of any commercial or financial relationships that could be construed as a potential conflict of interest.

Publisher's Note: All claims expressed in this article are solely those of the authors and do not necessarily represent those of their affiliated organizations, or those of the publisher, the editors and the reviewers. Any product that may be evaluated in this article, or claim that may be made by its manufacturer, is not guaranteed or endorsed by the publisher.

frontiers in Molecular Neuroscience

ORIGINAL RESEARCH
published: 14 March 2022
doi: 10.3389/fnmol.2022.809163

Phenotypic Spectrum and Prognosis of Epilepsy Patients With *GABRG2* Variants

*Ying Yang[1], Xueyang Niu[1], Miaomiao Cheng[1], Qi Zeng[2], Jie Deng[3], Xiaojuan Tian[3], Yi Wang[4], Jing Yu[5], Wenli Shi[6], Wenjuan Wu[7], Jiehui Ma[8], Yufen Li[9], Xiaoling Yang[1], Xiaoli Zhang[10], Tianming Jia[10], Zhixian Yang[1], Jianxiang Liao[2], Yan Sun[5], Hong Zheng[6], Suzhen Sun[7], Dan Sun[8], Yuwu Jiang[1] and Yuehua Zhang[1]**

[1] Department of Pediatrics, Peking University First Hospital, Beijing, China, [2] Department of Neurology, Shenzhen Children's Hospital, Shenzhen, China, [3] Department of Neurology, Beijing Children's Hospital, Capital Medical University, Beijing, China, [4] Department of Neurology, National Children's Medical Center, Children's Hospital of Fudan University, Shanghai, China, [5] Department of Neurology, Children's Hospital of Xinjiang Uygur Autonomous Region, Xinjiang Hospital of Beijing Children's Hospital, Ürümqi, China, [6] Department of Pediatrics, The First Affiliated Hospital of Henan University of Chinese Medicine, Zhengzhou, China, [7] Department of Neurology, Hebei Children's Hospital, Shijiazhuang, China, [8] Department of Neurology, Wuhan Children's Hospital, Tongji Medical College, Huazhong University of Science and Technology, Wuhan, China, [9] Department of Pediatrics, Linyi People's Hospital, Linyi, China, [10] Department of Pediatrics, The Third Affiliated Hospital of Zhengzhou University, Zhengzhou, China

OPEN ACCESS

Edited by:
Andrei Surguchov, University of Kansas Medical Center, United States

Reviewed by:
Irina G. Sourgoutcheva, University of Kansas Medical Center, United States
Charlotte Dravet, Scientific Institute for Research, Hospitalization and Healthcare (IRCCS), Italy
Svetlana Gataullina, Hôpital Antoine-Béclère, France

***Correspondence:**
Yuehua Zhang
zhangyhdr@126.com

Specialty section:
This article was submitted to Brain Disease Mechanisms, a section of the journal Frontiers in Molecular Neuroscience

Received: *04 November 2021*
Accepted: *28 January 2022*
Published: *14 March 2022*

Citation:
Yang Y, Niu X, Cheng M, Zeng Q, Deng J, Tian X, Wang Y, Yu J, Shi W, Wu W, Ma J, Li Y, Yang X, Zhang X, Jia T, Yang Z, Liao J, Sun Y, Zheng H, Sun S, Sun D, Jiang Y and Zhang Y (2022) Phenotypic Spectrum and Prognosis of Epilepsy Patients With GABRG2 Variants. Front. Mol. Neurosci. 15:809163. doi: 10.3389/fnmol.2022.809163

Objective: This study aimed to obtain a comprehensive understanding of the genetic and phenotypic aspects of *GABRG2*-related epilepsy and its prognosis and to explore the potential prospects for personalized medicine.

Methods: Through a multicenter collaboration in China, we analyzed the genotype-phenotype correlation and antiseizure medication (ASM) of patients with *GABRG2*-related epilepsy. The three-dimensional protein structure of the *GABRG2* variant was modeled to predict the effect of *GABRG2* missense variants using PyMOL 2.3 software.

Results: In 35 patients with *GABRG2* variants, 22 variants were *de novo*, and 18 variants were novel. The seizure onset age was ranged from 2 days after birth to 34 months (median age: 9 months). The seizure onset age was less than 1 year old in 22 patients (22/35, 62.9%). Seizure types included focal seizures (68.6%), generalized tonic-clonic seizures (60%), myoclonic seizures (14.3%), and absence seizures (11.4%). Other clinical features included fever-sensitive seizures (91.4%), cluster seizures (57.1%), and developmental delay (45.7%). Neuroimaging was abnormal in 2 patients, including dysplasia of the frontotemporal cortex and delayed myelination of white matter. Twelve patients were diagnosed with febrile seizures plus, eleven with epilepsy and developmental delay, two with Dravet syndrome, two with developmental and epileptic encephalopathy, two with focal epilepsy, two with febrile seizures, and four with unclassified epilepsy. The proportions of patients with missense variants in the extracellular region and the transmembrane region exhibiting developmental delay were 40% and 63.2%, respectively. The last follow-up age ranged from 11 months to 17 years. Seizures were controlled in 71.4% of patients, and 92% of their seizures were controlled by valproate and/or levetiracetam.

Conclusion: The clinical features of *GABRG2*-related epilepsy included seizure onset, usually in infancy, and seizures were fever-sensitive. More than half of the patients had cluster seizures. Phenotypes of *GABRG2*-related epilepsy were ranged from mild febrile seizures to severe epileptic encephalopathies. Most patients with *GABRG2* variants who experienced seizures had a good prognosis. Valproate and levetiracetam were effective treatments for most patients.

Keywords: GABRG2, epilepsy, infancy, fever-sensitive, prognosis

INTRODUCTION

Epilepsy is characterized by an enduring predisposition to generate epileptic seizures. Numerous genetic defects underlying different forms of epilepsy have been identified with most of these genes encoding ion channel proteins (Surguchov et al., 2017). *GABRG2* (OMIM:137164) resides on chromosome 5q34 and is a member of the gamma-aminobutyric acid-A ($GABA_A$) receptor gene family of heteromeric pentameric ligand-gated ion channels. $GABA_A$ receptor subunits contains a extracellular N-terminus, four transmembrane domains, a small extracellular loop between the second and third transmembrane domains and a larger intracellular loop between the third and the fourth transmembrane domains (**Figure 1**). The first variant in *GABRG2* (p.R43Q) was reported to be related to genetic epilepsy with febrile seizures (GEFS+) in 2001 in an Australian family (Wallace et al., 2001). In the same year, Baulac et al. (2001) identified a *GABRG2* heterozygous missense variant (K328M) in a 3-generation French family with variable seizure phenotypes and most consistent with GEFS+. With the broad application of next-generation sequencing (NGS) in patients with epilepsy, pathogenic variants of *GABRG2* related to developmental and epileptic encephalopathy 74 (DEE74, OMIM:618396) were reported. To our knowledge, no detailed descriptions of the phenotypic spectrum of patients with epilepsy carrying *GABRG2* variants are available. Therefore, this study aimed to determine the phenotypic spectrum of epilepsy patients carrying *GABRG2* variants and the prognosis of patients in a Chinese cohort from multicenter.

MATERIALS AND METHODS

Participants

Genetic testing was conducted in all patients diagnosed with epilepsy without acquired factors (e.g., perinatal brain injury, traumatic brain injury, and central nervous system infections). Thirty-five patients with epilepsy and *GABRG2* variants who attended the Pediatric Department of Peking University First Hospital from January 2008 to August 2021 were included in this study, including 22 males and 13 females. Clinical information about the age at seizure onset, seizure frequency, seizure types, developmental milestones, neurological status, family history, the results of accessory examinations including electroencephalogram (EEG) and brain magnetic resonance imaging (MRI), and treatment were collected in the clinic. Brain MRI and video EEG were reviewed by neuroradiologists and neurophysiologists, respectively. All patients identified with *GABRG2* variants were followed in outpatient settings or by telephone at least every 3 months.

The Ethics Committee of Peking University First Hospital and the institutional review boards of collaborating groups approved the project (approval number 2012[453]). Written informed consent was obtained from the parents of all patients. The study was performed in accordance with the ethical standards established in the 1964 Declaration of Helsinki and its later amendments.

Genetic Analysis

GABRG2 variations (NM_000816, GRCh37/hg19) were determined using targeted next-generation sequencing of epilepsy (epilepsy gene panel) or whole-exome sequencing. Synonymous variants and single nucleotide polymorphisms with minor allele frequencies greater than 5% were removed[1]. Functional consequences were predicted by Mutation Taster[2], Polyphen-2[3], and PROVEAN[4]. The pathogenicity of variants was evaluated according to the American College of Medical Genetics and Genomics (ACMG) guidelines (Richards et al., 2015). Sanger sequencing was used to verify variations and identify the inheritance of variants.

Structural Modeling

Three-dimensional protein structure were modeled to predict the effect of *GABRG2* missense variants using PyMOL 2.3 software, and the pathogenicity of candidate variants was evaluated.

RESULTS

Genetic Analysis

Our cohort of 35 patients carried 24 unique *GABRG2* variants, including 27 missense variants, 5 splicing variants, 1 nonsense variant, 1 frameshift variant, and 1 small deletion variant (**Table 1** and **Supplementary Table 1**). Eighteen variants were novel (p.T90M, p.W121C, p.R125P, p.R125C, p.N140S, p.N167K, p.P205H, c.631 + 4A > G, c.631 + 5G > T, c.922 + 1G > T, p.A303T, p.S306F, p.T310I, p.T317I, c.1128 + 5G > A, p.C382Sfs*57, c.1249-7C > T, and exon1-11 deletion). Six

[1]https://gnomad.broadinstitute.org

[2]https://www.mutationtaster.org/

[3]http://genetics.bwh.harvard.edu/pph2/

[4]http://provean.jcvi.org/protein_batch_submit.php?species=human

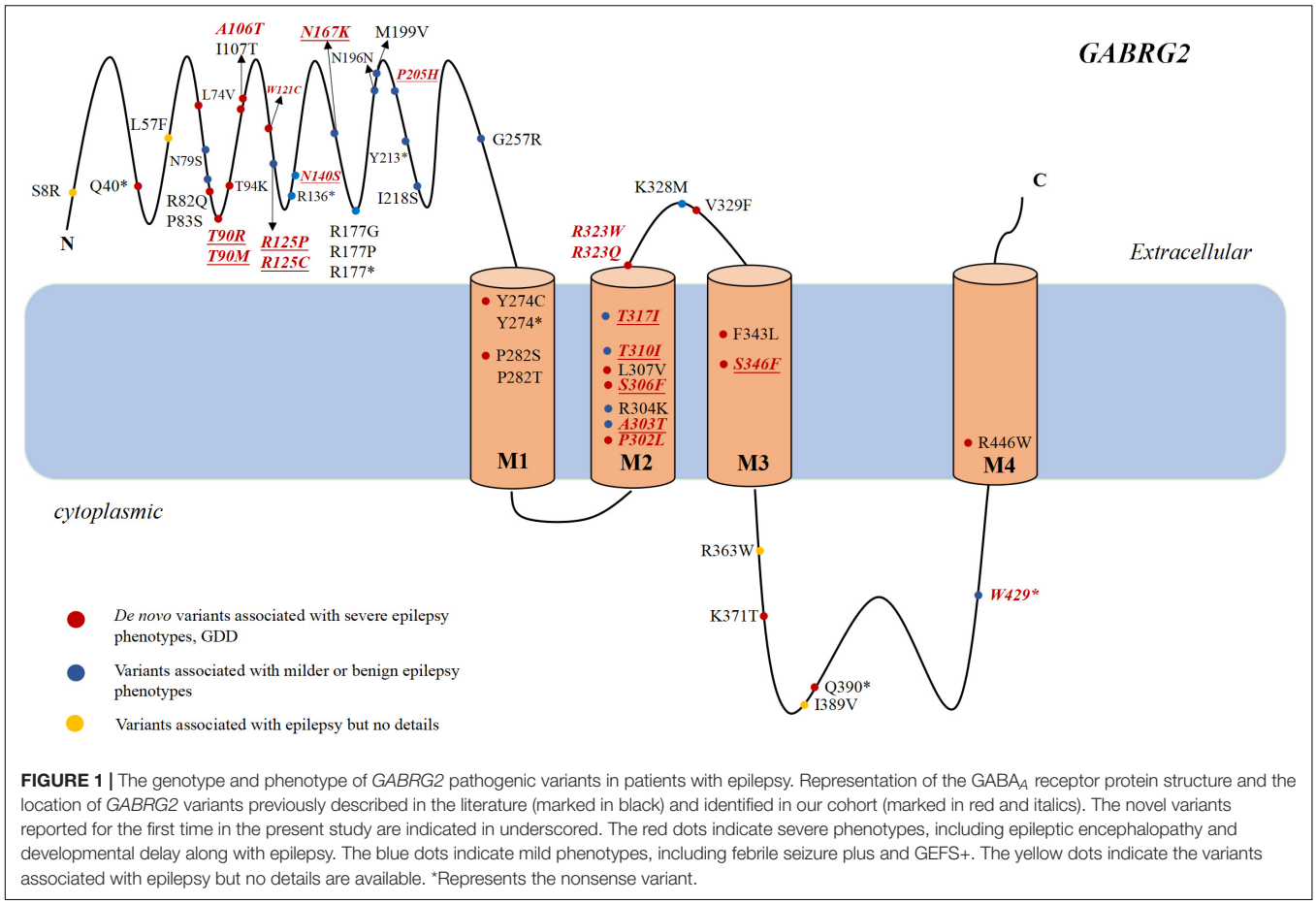

FIGURE 1 | The genotype and phenotype of *GABRG2* pathogenic variants in patients with epilepsy. Representation of the $GABA_A$ receptor protein structure and the location of *GABRG2* variants previously described in the literature (marked in black) and identified in our cohort (marked in red and italics). The novel variants reported for the first time in the present study are indicated in underscored. The red dots indicate severe phenotypes, including epileptic encephalopathy and developmental delay along with epilepsy. The blue dots indicate mild phenotypes, including febrile seizure plus and GEFS+. The yellow dots indicate the variants associated with epilepsy but no details are available. *Represents the nonsense variant.

variants (p.T90R, p.A106T, p.P302L, p.R323W, p.R323Q and p.W429X) have been previously reported (Sun et al., 2008; Shen et al., 2017; Zou et al., 2017; Hernandez et al., 2021). Variants T310I, A106T, and R323W recurred twice, and R323Q recurred nine times, respectively. Twenty-two patients carried *de novo* variants and 13 patients had inherited variants. None of these variants were found in the Genome Aggregation Database.

Seizure Types

In 35 children with epilepsy carrying *GABRG2* variants, the seizure onset age ranged from 2 days to 34 months of age (median age: 9 months). The seizure onset age was less than 1 year old in 22 patients (22/35, 62.9%). Seizure types were predominantly focal seizures (24/35, 68.6%). Other seizure types included generalized tonic-clonic seizures (21/35, 60%), myoclonic seizures (5/35, 14.3%), and absence seizures (4/35, 11.4%). A striking feature was the occurrence of fever-sensitive seizures in 32/35 (91.4%) patients. Notably, 57.1% (20/35) patients had a cluster of seizures.

Neurodevelopment and Additional Comorbidities

In our cohort, 15 patients (42.8%, 15/35) experienced developmental delays. Two patients (patients 3, and 4) were unable to raise their heads at the age of 1 year. One patient (patient 29) walked after the age of 2 years. Five patients (patients 1, 14, 18, 24, and 25) walked at approximately the age of 18 months but had poor motor coordination. Patient 1 expressed herself in simple language with no more than four words at the age of 16 years. Patient 13 had a mild speech impediment, and he spoke disfluently at 6 years of age. Patient 14 also had learning difficulties. Eight patients had a mild intellectual disability (patients 5, 16, 20, 21, 23, 26, 27, and 28), and some of them had learning difficulties in school (patients 16, 21, 23, and 27). Microcephaly was observed in 1 patient (patient 3). One patient (patient 18) was diagnosed with attention deficit and hyperactivity disorder (ADHD). Twenty patients showed normal psychomotor development at the last follow-up.

Video Electroencephalogram and Brain Imaging

Thirty-five patients underwent video EEG monitoring for 4–24 h (**Table 1**). The EEG exhibited diffuse slow background activity in 5 patients. Interictal epileptiform discharges were captured in 24 patients, including multifocal spike-slow waves in 5 patients and focal spike-slow waves in 10 patients. Generalized spike-wave or polyspike wave discharges were observed in 9 patients. Seizures were observed in 7 (20%, 7/35) patients, consisting of

TABLE 1 | The phenotype and genotype of 35 patients with *GABRG2* variants in our cohort.

#	Gender	variants	Inheritance	Family history: Y or N	Seizure-onset age	Seizure types	Seizures fever sensitivity: Y or N	Cluster seizures: Y or N	Developmental	EEG	Brain MRI	Other clinical findings	Diagnosis	AEDs	Seizure-off age	Age at last follow-up
1	F	c.269C > G/p.T90R	*De novo*	N	7 months	FS, GTCS, AS, focal SE	Y	Y	delay	MF	Normal (15 years 8 months)	NS	Dravet syndrome	LEV	15 years 9 months	17 years
2	F	c.269C > T/p.T90M	Maternal	Y	1 year 4 months	FS	Y	N	normal	normal	Normal (5 years 8 months)	NS	Focal epilepsy	VPA; LEV; LTG	8 years	9 years 10 months
3	M	c.316G > A/p.A106T	*De novo*	N	40 days	FS	N	N	delay	GFW	Dysplasia of the frontal and temporal cortex, delayed myelination (1y)	Microcephaly	DEE	VPA; OXC	1 year	3 years 8 months
4	M	c.316G > A/p.A106T	*De novo*	N	2 days	FS, GTCS SE	N	Y	delay	FSS	normal (6 months)	NS	DEE	TPM; LEV	5 month	1 year 11 months
5	M	c.363G > C/p.W121C	*De novo*	N	9 months	GTCS	Y	N	delay	normal	normal (9 months)	NS	Epilepsy and developmental delay	VPA	1 year 2 months	3 years 7 months
6	M	c.374G > C/p.R125P	Maternal	Y	9 months	GTCS, FS	Y	Y	normal	normal	NA	NS	FS +	VPA	2 years 10 months	3 years 10 months
7	F	c.373C > T/p.R125C	Maternal	Y	2 years 1 month	FS	Y	N	normal	FSS	normal (5 years 9 months)	NS	FS +	VPA	5 years 11 months	8 years
8	M	c.419A > G/p.N140S	Maternal	Y	1 year 6 months	GTCS	Y	Y	normal	NA	normal	NS	FS	LEV	3 years 3 months	5 years 7 months
9	M	c.501C > A/p.N167K	*De novo*	N	7 months	GTCS	Y	Y	normal	GSW	NA	NS	FS +	VPA	1 year 9 months	3 years 4 months
10	F	c.614C > A/p.P205H	*De novo*	N	9 months	GTCS	Y	Y	normal	GSW, FSS, DS	Normal (9 months)	NS	FS	LEV	Ongoing	11 months
11	M	c.631 + 4A > G	Maternal	Y	9 months	GTCS	Y	N	normal	normal	normal	NS	FS +	LEV	2 years 3 months	3 years 1 month
12	M	c.631 + 5G > T	Paternal	Y	9 months	GTCS, FS	Y	Y	normal	normal	Normal (2 years)	NS	FS +	VPA; OXC	Ongoing	2 years 2 months
13	M	c.922 + 1G > T	Maternal	Y	2 years	FS	Y	N	normal	FSS	NA	NS	FS +	LEV	3 years	4 years 9 months
14	M	c.905C > T/p.P302L	*De novo*	N	7 months	GTCS, FS, AS, MS, GTCS SE	Y	Y	delay	GSW, MF	normal (10 years)	NS	Dravet syndrome	VPA; *OXC*; CLB	Ongoing	12 years
15	M	c.907G > A/p.A303T	*De novo*	N	2 years	GTCS	Y	N	normal	MF, GSW	normal	NS	Epilepsy	VPA	13 years 8 months	14 years 10 months
16	F	c.917C > T/p.S306F	*De novo*	N	1 year 8 months	FS	N	Y	delay	DS	normal	NS	Epilepsy and developmental delay	NA	Ongoing	9 years
17	M	c.929C > T/p.T310I	*De novo*	N	6 months	FS	Y	Y	normal	GSW	Normal (1 year)	NS	Focal epilepsy	VPA; LEV	4 years 11 months	6 years 7 months
18	F	c.929C > T/p.T310I	*De novo*	N	8 months	GTCS, MS	Y	Y	normal	FSS	Normal (1 year)	ADHD	Epilepsy	VPA; LEV	2 years 2 months	12 years
19	M	c.950C > T/p.T317I	*De novo*	N	8 months	FS	Y	Y	normal	Normal	Normal (1 year 4 months)	NS	FS +	VPA	5 years 4 months	6 years 8 months
20	F	c.967C > T/p.R323W	Maternal	Y	9 months	FS, SE	Y	N	delay	GSW	normal	NS	Epilepsy and developmental delay	VPA	Ongoing	1 year 3 months

(Continued)

TABLE 1 | (Continued)

#	Gender	variants	Inheritance	Family history: Y or N	Seizure-onset age	Seizure types	Seizures fever sensitivity: Y or N	Cluster seizures: Y or N	Developmental	EEG	Brain MRI	Other clinical findings	Diagnosis	AEDs	Seizure-off age	Age at last follow-up
21	M	c.967C > T/p.R323W	*De novo*	N	8 months	GTCS, FS	Y	N	delay	Normal	normal	NS	Epilepsy and developmental delay	LEV; CZP; VPA	Ongoing	9 years
22	M	c.968G > A/p.R323Q	Paternal	Y	1 year 3 months	GTCS	Y	N	normal	Normal	normal	NS	FS +	LEV	2 years 3 months	4 years
23	M	c.968G > A/p.R323Q	*De novo*	N	10 months	MS, AS	Y	N	delay	GSW, DS, MF	normal	NS	Epilepsy and developmental delay	VPA; LEV; PER	4 years 4 months	7 years
24	M	c.968G > A/p.R323Q	*De novo*	N	8 months	FS	Y	N	delay	NA	NA	NS	Epilepsy and developmental delay	VPA; LEV	6 years 6 months	8 years
25	M	c.968G > A/p.R323Q	*De novo*	N	8 months	FS	Y	Y	delay	FSS	Dysplasia of the frontal and temporal cortex, delayed myelination (1 year 6 months)	NS	Epilepsy and developmental delay	VPA	1 year	4 years
26	F	c.968G > A/p.R323Q	*De novo*	N	1 year 1 month	GTCS, MS, FS	Y	Y	delay	GSW	normal	NS	Epilepsy and developmental delay	VPA; LEV	2 years 3 months	3 years 3 months
27	F	c.968G > A/p.R323Q	*De novo*	N	1 year 1 month	GTCS, FS	Y	N	delay	Normal	Normal (6 years)	NS	Epilepsy and developmental delay	VPA; LEV	6 years	8 years
28	F	c.968G > A/p.R323Q	*De novo*	N	6 months	FS	Y	Y	delay	FSS	Normal (9 months)	NS	Epilepsy and developmental delay	VPA; LEV	1 year 7 months	4 years
29	F	c.968G > A/p.R323Q	*De novo*	N	11 months	GTCS, FS	Y	Y	delay	DS, MF	Normal (1 year)	NS	Epilepsy and developmental delay	PER; VPA; CZP; *LTG;* OXC	Ongoing	1 year 3 months
30	M	c.968G > A/p.R323Q	*De novo*	N	10 months	GTCS, FS, AS	Y	Y	normal	FSS	Normal (3 years)	NS	Epilepsy	VPA; LEV	Ongoing	3 years 6 months
31	F	c.1128 + 5G > A	*De novo*	N	2 years 3 months	MS, GTCS	Y	Y	normal	GSW	Normal (2 years 6 months)	NS	Epilepsy	VPA; LEV	Ongoing	2 years 10 months
32	F	c.1140_1143del/ p.C382Sfs*57	Maternal	Y	2 years 10 months	GTCS	Y	N	normal	Normal	Normal (3 years)	NS	FS +	VPA	3 years	4 years 4 months
33	M	c.1249-7C > T	Maternal	Y	1 year 6 months	FS	Y	Y	normal	DS, FSS	Normal (3 years)	NS	FS +	VPA; *TPM; CZP; NZP*	3 years 3 months	5 years 10 months
34	M	c.1287G > A/p.W429X	Maternal	Y	1 year 3 months	FS	Y	Y	normal	Normal	Normal	NS	FS +	VPA	6 years 6 months	14 years
35	M	exon 1-11 deletion	Maternal	Y	9 months	GTCS	Y	N	normal	FSS	Normal (1 year 6 months)	NS	FS +	VPA; LEV	Ongoing	2 years 2 months

F, female; M, male; AS, absence seizure; C, clonic seizure; DEE, developmental and epileptic encephalopathy; FS, focal seizure; GTCS, generalized tonic-clonic seizure; MS, myoclonic seizure; SE, status epilepticus; T, tonic seizure; TC, tonic-clonic seizure; NA, not applicable; NS, no specific. EEG, electroencephalography; DS, diffuse slowing; FSS, focal spike slow waves; MF, multifocal; GSW, generalized spike wave; GFW, generalized fast wave; MRI, magnetic resonance imaging; ASD autistic spectrum disorder; AED, anti-epileptic therapy; LEV, levetiracetam; VPA, valproic acid; TPM, topiramate; CLB, clobazam; VGB, vigabatrin; DZP, diazepam; PB, phenobarbital; PER, Perampanel; CZP, clonazepam; KD, ketogenic diet; OXC, oxcarbazepine. Underlining indicates treatment with clinical response (decreased seizure frequency or severity), and italics indicates a negative response (aggravation of seizure frequency and/or severity).

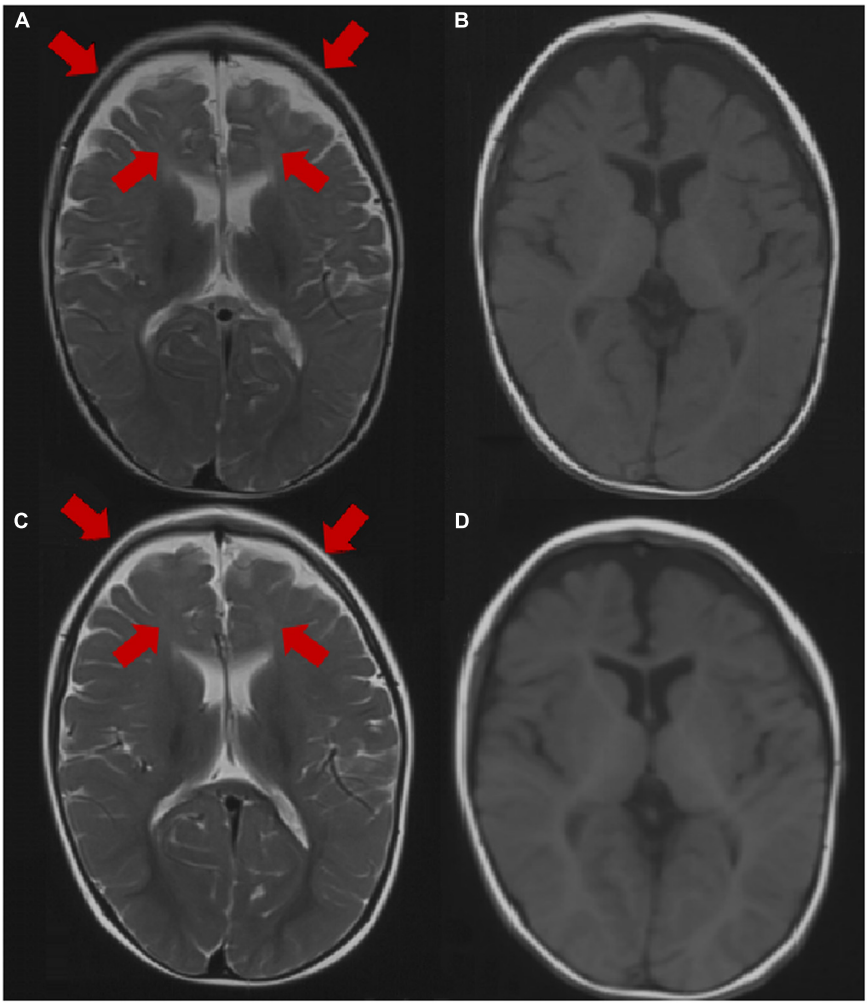

FIGURE 2 | Brain MRI image of patient 3 at the age of 1 year. **(A,B)** Axial images (T1WI and T2WI) showing dysplasia of the frontal and temporal cortex and delayed myelination. Brain MRI image of patient 3 at the age of 2 years. **(C,D)** Axial images (T1WI, T2WI) showing dysplasia of the frontal cortex and delayed myelination. The arrow points to the lesion.

focal seizures in 3, absence seizures in 3, and myoclonic seizures in one patient. Eleven patients had a normal EEG.

Brain MRI was abnormal in 2 patients (2/31, 6.5%), including dysplasia of the frontotemporal cortex and delayed myelination of white matter in 2 patients (patient 3 and patient 25). The brain MRI of 29 patients was normal at the last follow-up. The brain MRI results of patient 3 are shown in **Figure 2**.

Diagnosis of the Phenotype

Twelve of 35 patients were diagnosed with FS+. Eleven patients were diagnosed with developmental delays and epilepsy, and their seizure onset ages ranged from 6 to 20 months. Two patients were diagnosed with Dravet syndrome. They had various seizure types including focal seizures, GTCS, myoclonic seizures, atypical absence seizures, and seizures with fever-sensitivity. Two patients (patients 3 and 4) were diagnosed with DEE, and their seizure onset ages were 2 days and 40 days. Two patients (patients 2 and 17) were diagnosed with focal epilepsy. Two patients (patients 8 and 10) had FS, one of whom inherited the variant from his mother (patient 8), and his mother had FS in childhood. Four patients (patients 15, 18, 30, and 31) were diagnosed with unclassified epilepsy.

Structural Alterations in the *GABRG2* Protein and Genotype-Phenotype Correlation of *GABRG2* Variants

All *GABRG2* variants, including those in reported and our cohort, were analyzed to explore the mechanism underlying genotype-phenotype correlations. To date, 58 patients with 40 different variants have been reported, including 25 missense, 2 splicing, and 13 destructive variants (7 frameshift, 5 nonsense variants, and 1 small deletion variant). Their clinical characteristics are listed in **Table 2**. In our cohort of 35 patients, 23 unique variants were identified, including 16 missense variants, 4 splicing variants, 1 nonsense variant, 1 frameshift variant, and 1 small

TABLE 2 | The genotype and phenotype of 58 patients reported in literature with *GABRG2* variants related to epilepsy.

	Cases	Variants	Seizure onset age	Seizure types	Seizures fever sensitivity: Y or N	EEG	Brain MRI	Developmental	Diagnosis	Other clinical findings
Kang et al., 2019	2	*Inheritance* p.S8R (×2)	22 months 68 months	FS FS	N Y	Not reported	Not reported	Not reported	Genetic epilepsy	Not reported
Huang et al., 2012	1	*de novo* p.Q40X	Not reported	Not reported	NA	Not reported	Not reported	Not reported	Dravet syndrome	Not reported
Ishii et al., 2014	2	*Paternal* p.Q40X (×2)	2 months	Not reported	Y	Not reported	Not reported	Not reported	Dravet syndrome (×2)	Not reported
Shi et al., 2010	1	*de novo* p.N79S	15 years	GTCS	Y	Not reported	Not reported	normal	epilepsy	Not reported
Wallace et al., 2001	1	*de novo* p.R82Q	13 months	Not reported	Not reported	GSS, SW	Not reported	Not reported	GEFS+	Not reported
Stosser et al., 2018	1	*de novo* p.T94K	Not reported	Not reported	Not reported	Not reported	Not reported	Not reported	Epilepsy related neurodevelopmental disorders	Not reported
Lachance-Touchette et al., 2011	1	*de novo* p.P83S	5 months	GTCS	Y	GSS, SW	Not reported	normal	Genetic epilepsy	Not reported
Komulainen-Ebrahim et al., 2019	3	*de novo* p.P282T p.S306F *Paternal* p.P83S	 4 years 2 days 9 months	 Ats, GTCS, MS Hemi clonic GTCS, AS	Not reported	 GSS, SW, FS FS	 Cerebral cortical dysplasia Not reported normal	 GDD GDD GDD	 LGS-like EIMFS LGS	Nystagmus, feeding problems, hypotonia, movement disorders Feeding problems, hypotonia NA
Ma et al., 2019	1	*de novo* p.R136*	Neonatal	GTCS, MS, FS	Not reported	SB	Not reported	GDD	Ohtahara syndrome	Not reported
Johnston et al., 2014	1	*Inheritance* p.R136*	24 months	Not reported	Y	Not reported	Not reported	normal	GEFS +	Not reported
Shen et al., 2017	8	*de novo* p.A106T (×2) p.I107T p.P282S p.R323Q (×2) p.R323W p.F343L	 1 day/3 months 1.5 months 1 year 10 months/ 1 year 11 months 1 year	 GTCS, TS/TS, GTCS, Ats TS, ES GTCS, AS FS, GTCS, MS, AS/FS, MS, Ats, AAS GTCS, AS TS	Not reported	 Normal/DS, MF DS, FSS GSS, MF GSS/GSS GSS DS, FSS	 Delayed myelination of white matter/ ventricular enlargement Normal Normal Normal/normal Normal thin corpus callosum	GDD (×8)	EE (×8)	nystagmus, hypotonia/ hypotonia, nystagmus, movement disorders hypotonia, nystagmus, hand stereotype, chorea hypotonia normal/ hypotonia, mild ataxia normal hypotonia
Zou et al., 2017	5	*De novo* p.A106T p.A106T p.A106T p.A106T p.A106T	 4 months 3 months 6 weeks 1 day 2 day	 GTCS FS FS, GTCS FS, GTCS, MS FS, GTCS, MS	Not reported	 GSS, SW SW PSW FSS SW	 Normal Enlargement of lateral ventricle and dysplasia of frontotemporal region Normal Normal Normal	GDD (×5)	EOEE (×5)	Ataxia, movement disorders, Visual impairment Ataxia, visual impairment Hypotonia Hypotonia, stereotype Ataxia, visual impairment, nystagmus
Yamamoto et al., 2019	1	*De novo* p.A106T	4 months	ES	Not reported	PSW, MF	Not reported	GDD	EOEE	Dystonia, nystagmus
Epi4K consortium and Epilepsy Phenome/Genome Project, 2017	1	*Inheritance* p.R177P	Not reported	Not reported	Not reported	Not reported	Not reported	normal	Genetic epilepsy	Not reported
Salam et al., 2012	1	*unknown* p.N196N	Not reported	Not reported	Y	normal	Not reported	normal	FS	Not reported

Continued

TABLE 2 | (Continued)

	Cases	Variants	Seizure onset age	Seizure types	Seizures fever sensitivity: Y or N	EEG	Brain MRI	Developmental	Diagnosis	Other clinical findings
Parrini et al., 2017	1	*De novo* p.Y274C	3 years	GTCS, MS, AtS	Not reported	Not reported	Not reported	delay	EMAS	Not reported
Perucca et al., 2017	1	*Maternal* p.I218S	18 months	AS, GTCS	Not reported	GSS	normal	normal	CAE	Not reported
Boillot et al., 2015	5	*Inheritance* p.E402fs*3 p.R196* p.V462fs*33 p.P59fs*12 p.M199V	24 months 20 months 14 months Not reported 6 months	FS Not reported Not reported GTCS GTCS, AS	Y	FSS NA NA NA NA	normal Not reported Not reported Not reported Not reported	normal	GEFS+	Not reported
May et al., 2018	3	*unknown* p.Y213* c.452_ 455delTCTT c.769-2T > G	Not reported	Not reported	Not reported	Not reported	Not reported	Not reported	Genetic epilepsy	Not reported
Peng et al., 2019	1	*De novo* p.R323W	Not reported	Not reported	Y	Not reported	Not reported	Not reported	Dravet syndrome	Not reported
Baulac et al., 2001	1	*Inheritance* p.K328M	Not reported	Not reported	Y	Not reported	Not reported	Not reported	GEFS +	Not reported
Reinthaler et al., 2015	5	*Inheritance* c.769-2T > G(×2) p.G257R p.R232Q p.I389V	Not reported	Not reported	Not reported	Not reported	Not reported	Not reported	BECT (×5)	Not reported
Hernandez et al., 2017	1	*De novo* p.P302L	1 year	FS, GTCS, AtS, MS	Y	normal	Not reported	delay	Dravet syndrome	NA
Carvill et al., 2013	1	*De novo* p.R323Q	8 months	FS, AS, AtS, MS, GTCS	Not reported	normal	Not reported	normal	EMAS	Not reported
Angione et al., 2019	4	*Paternal* p.R363Q p.K374del *Unknown* c.770-1G > A p. K371T	3 years 2 years 20 months 3 years	GTCS, AtS, TS, MS, AAS GTCS, AS MS, AS, GTCS GTCS, AS, MS, AtS	Not reported	DS, GSS, SW, MF GSS, DS, SW GSS, SW GSS	normal (×4)	GDD GDD normal normal	LGS EMAS EMAS EMAS	ASD NA NA NA
Cogliati et al., 2019	1	*De novo* c.937_938delinsGG	Not reported	Not reported	Not reported	Not reported	Not reported	GDD	Rett syndrome	Ataxia, hand stereotype
Della Mina et al., 2015	1	*Paternal* c.351dupT	1 year	GTCS	Y	Not reported	Not reported	normal	GEFS +	Not reported
Tian et al., 2013	1	*Inheritance* c.1329delC	Not reported	Not reported	Y	Not reported	Not reported	Not reported	GEFS +	Not reported
Harkin et al., 2002	1	*Inheritance* p.Q390*	3 months	FS, GTCS, MS, AtS, SE	Y	GSS, SW	normal	delay	GEFS+	photosensitivity
Kananura et al., 2002	1	*Inheritance* c.769-2T > G	4 years	AS	Not reported	Not reported	Not reported	normal	CAE	Not reported

*AAS, atypical absence seizure; ADHD, attention deficit and hyperactivity disorder; AS, absence seizure; ASD, autistic spectrum disorder; AtS, atonic seizure; CAE, childhood absence epilepsy; CS, clonic seizure; DS, diffuse slow waves; EMIFS, epilepsy of infancy with migrating focal seizures; EOEE, early-onset epileptic encephalopathy; GDD, global developmental delay; GSS, generalized seizures discharge; LGS, Lennox-Gastaut syndrome; EE, epileptic encephalopathy; EMAS, epilepsy with myoclonic atonic seizure; ES, epileptic spasms; FS, focal seizure; FSS, focal seizure discharge; FTS, focal tonic seizure; GTCS, generalized tonic-clonic seizure; SE, status epilepticus; MA, myoclonic atonic seizure; TS, tonic seizure; MS, myoclonic seizure; MF, multifocal; EEG, electroencephalography; SB, Suppression-burst; PSW, poly-spike wave; SW, spike wave; NA, not applicable. *Represents the nonsense variant.*

deletion variant. Overall, including our data and those from the literature, we reviewed data from 63 distinct variants identified in 93 unrelated patients (**Figure 1** and **Tables 1**, **2**). The variants included 41 missense variants (41/63, 65.1%), eight frameshift variants (8/63, 12.7%), six nonsense variants (6/63, 9.5%), six splicing variants (6/63, 9.5%), and two small deletion variants (2/63, 3.2%).

Most variants (42/63, 66.7%) were located in the extracellular region and transmembrane region of the protein. Two were located at amino acid position 323 (p.R323Q and p.R323W), representing a potential variant hotspot. The p.R323Q variant was detected in 11 patients (patients 22–30, Carvill et al., 2013; Shen et al., 2017), whereas the p.R323W variant was found in 3 patients (patients 20–21, Peng et al., 2019). In the literature, the phenotypes of some patients with epilepsy carrying *GABRG2* variants were not described in detail; therefore, we were only able to analyze the genotype and phenotype correlations in our cohort. In our cohort, seven recurrent variants are located in the transmembrane region of the channel, including p.P302L, p.A303T, p.T310I, p.T317I, p.R323Q, p.R323W, and p.S346F (**Figure 1**). Six of them (p.P302L, p.A303T, p.T310I, p.T317I, p.R323Q, and p.R323W) are located in the M2 domain. The p.S346F variant was located in the M3 region. Nine variants were located toward the extracellular region, including p.T90R, p.T90M, p.A106T, p.W121C, p.R125P, p.R125C, p.N140S, p.N167K, and p.P205H. The p.R429X variant is located in the inner part of the cytoplasmic domain. The proportions of patients with variants in the extracellular region and in the transmembrane region who experienced developmental delay were 40% (4/10) and 63.2% (12/19), respectively.

Patient 3 and patient 4 carried the same *GABRG2* variant (p.A106T) that was located in the extracellular region. Both patients presented with DEE. However, a patient with the R125P variant near the A106T variant was diagnosed with FS+. The R323Q and R323W variants (potential variant hotspots) are located in the transmembrane region. The molecular effect of the missense variants was further analyzed by protein modeling using PyMOL 2.3. Residue A106 originally formed one hydrogen bond with V104. When alanine 106 was replaced by threonine, the hydrogen bonds with I107 and S325 were reestablished. Residue R125 originally formed three hydrogen bonds with D123, two with L81, and one each with Y77 and D78. When arginine 125 was replaced with proline acid, the hydrogen bonds with Y77, D78, L81 and D123 were all destroyed. Residue R323 originally formed one hydrogen bond with residues P327, V329 and D336. In contrast, when arginine 323 was replaced by tryptophan, the hydrogen bonds with residues P327, V329 and D336 were all destroyed, and only one hydrogen bond was retained with L326. Additionally, when arginine 323 was replaced by glutamine, the hydrogen bonds with residues P327, and V329 were destroyed, and only one hydrogen bond was retained with D336 (**Figure 3**).

Treatment and Follow-up

Treatment information was available for 35 patients. The final follow-up age ranged from 11 months to 17 years old. At the last follow-up, 25 patients (71.4%, 25/35) were seizure-free for 1 year to 7.5 years. Effective ASMs in terms of seizure freedom included valproate monotherapy ($n = 9$), levetiracetam monotherapy ($n = 6$), perampanel monotherapy ($n = 1$), valproate and levetiracetam combination therapy ($n = 5$), multitherapy (valproate, topiramate and perampanel combination therapy, $n = 1$), and biotherapy other than valproate combine with levetiracetam in 5 patients (patients 2, 3, 4, 12, and 33).

Ten patients still had seizures. One patient (patient 14) was diagnosed with Dravet syndrome. During the last follow-up visit, he still had frequent eyelid myoclonic seizures at the age of 10 years and 6 months. He showed no response to three different ASMs (valproate, levetiracetam, and clobazam). One patient (patient 29) with intractable epilepsy and developmental delay tried three ASMs (valproate, lamotrigine, and oxcarbazepine), but she still experienced cluster focal seizures. When she was treated with perampanel, and the seizure frequency was markedly reduced. Her afebrile seizures were controlled, but she still experienced fever-induced seizures. Patient 16 did not use ASMs due to poor parental compliance, and the seizures were not controlled. For the 7 other patients, the follow-up was too short to evaluate the effect of medication.

DISCUSSION

Pathogenic *GABRG2* variants have been reported in patients with epilepsy, developmental delays and behavioral disorders. The phenotypic spectrum of *GABRG2* variants extends to the pharmacoresistant epilepsies, including Dravet syndrome and developmental epileptic encephalopathies (DEEs) (Harkin et al., 2002; Shen et al., 2017; Oyrer et al., 2018). Recently, *GABRG2* was included in DEE74 (OMIM: 618396). The pathogenic variants in *GABRG2* (p.Q40X) were first reported in a patient with Dravet syndrome in Kanaumi et al. (2004). In 2013, Carvill (Carvill et al., 2013) reported a male patient with epilepsy presenting myoclonic-atonic seizures (EMAS) who carried a *GABRG2* variant (p.R323Q) and experienced multiple seizure types, including GTCS, absence seizures, atonic seizures, myoclonic seizures, and tonic-clonic seizures. Additionally, Zou et al. (2017) identified 5 patients with seizures carrying the same *GABRG2 de novo* variants (p.A106T) associated with DEE. To date, *GABRG2* variants have been reported in 58 patients who presented with epilepsy in multiple epilepsy centers (**Table 2**). However, the largest number of patients evaluated in a single study was only 8. To date, systematic research on the phenotypic spectrum and prognosis of *GABRG2* variants related to epilepsy is lacking. Here, we identified 31 novel and 4 previously reported *GABRG2* variants in patients with epilepsy (Sun et al., 2008; Shen et al., 2017; Zou et al., 2017). The phenotypic spectrum and prognosis of patients with *GABRG2*-related epilepsy were further studied.

Among the 35 patients with *GABRG2* variants in our cohort, the seizure onset age in 62.9% of patients (22/35) was during the 1st year of life, and the seizure onset ages of the remaining patients ranged from 1 year and 1 month to 2 years and 10 months. In previous reports, the seizure onset age ranged from birth to 15 years (median age: 1 year) (**Table 2**). This observation indicated that the seizure onset age of *GABRG2*-related epilepsy

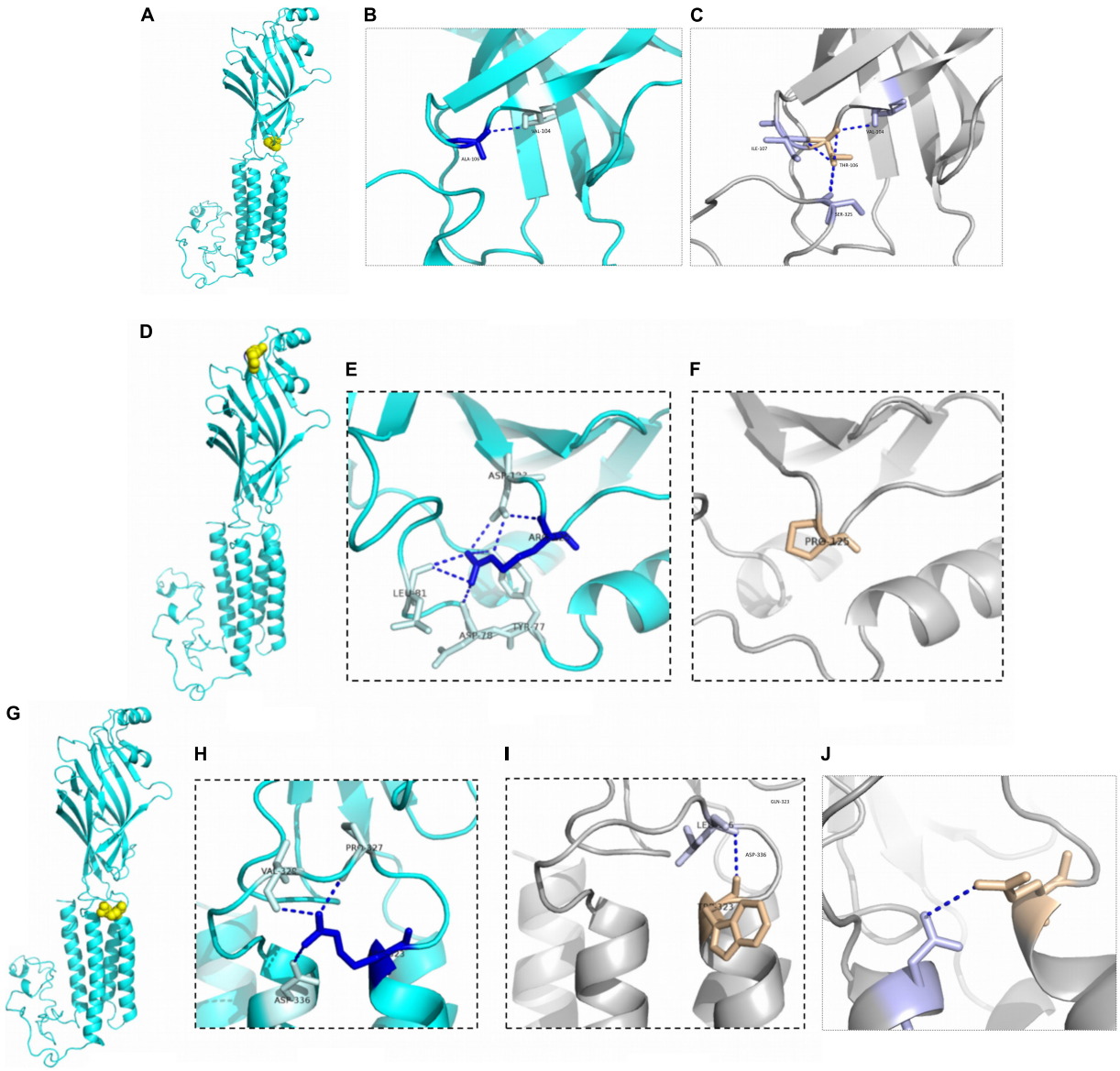

FIGURE 3 | Structural modeling of *GABRG2* variants (A106T, R125P, R323W, and R323Q). **(A)** The position of the 106th amino acid in the subunit (yellow). **(B)** Wild-type 106A forms ionic bonds with surrounding amino acid residues. **(C)** The number of ionic bonds between variant 125T amino acid residues and surrounding amino acid residues is increased. **(D)** The position of the 125th amino acid in the subunit (yellow). **(E)** Wild-type 125R forms ionic bonds with surrounding amino acid residues. **(F)** The number of ionic bonds between variant 125P amino acid residues and surrounding amino acid residues is reduced. **(G)** The position of the 323rd amino acid in the subunit (yellow). **(H)** Wild-type 323R forms ionic bonds with surrounding amino acid residues. **(I)** Change in forces between variant 323W amino acid residues and adjacent α helix. **(J)** Change in forces between variant 323Q amino acid residues.

occurred mainly before 1 year of age. In our cohort, we identified several key phenotypic features as part of the *GABRG2*-related disease spectrum; 91.4% of patients had fever-sensitive seizures, 68.6% of patients had focal seizures, and most of the patients (71.4%) were seizure-free after ASMs treatment.

Seizures with fever sensitivity have been reported in some patients; however, the percentage of patients presenting this feature had not been delineated. In previous reports, 47.4% (18/38) of patients with *GABRG2* variants experienced seizures associated with fever-sensitivity (**Table 2**). Fever sensitivity was not reported in the remaining patients. Boillot et al. (2015) reported 5 families with inherited *GABRG2* variants who had febrile seizures and temporal lobe epilepsy. One patient (p.P302L) who experienced febrile seizures, multiple seizure types, and early psychomotor and language developmental delay was diagnosed with Dravet syndrome (Hernandez et al., 2017).

We observed developmental delay in 42.8% (15/35) of patients with *GABRG2* variants, while 66.7% (24/36) of the previously published patients (available data) had developmental delay (**Table 2**). Most of the patients in our study were still

young, and the proportion of patients with developmental delay should be further studied in a large cohort. However, Komulainen-Ebrahim et al. (2019) reported 3 patients with *GABRG2* variants presenting with global developmental delay. Eight patients with *de novo GABRG2* variants associated with epileptic encephalopathies were reported by Shen et al. (2017). In our cohort, the clinical phenotypes of patients with normal development were mostly diagnosed with FS and FS+. The patients with developmental delay mostly had an early seizure onset, and multiple seizure types, some of which were diagnosed with developmental and epileptic encephalopathy.

In our study, no specific EEG pattern in the seizure evolution was observed in the patients with *GABRG2* variants. Interictal EEG performed in patients with epileptic encephalopathy patients, showed epileptiform discharges, including focal and multifocal spike waves, generalized spike waves and polyspike waves. Of the 58 patients reported previously, 51.7% of patients (30/58) were monitored for epileptiform discharges in interictal EEG. One patient with variant p. R136* presented a suppression burst pattern on interictal EEG (Ma et al., 2019). In our cohort, 33.3% (11/33) of patients had a normal EEG, which may be related to the benign phenotype of most children. However, only 13.3% (4/30) of patients had a normal EEG in the published cohort, and the difference may be related to the patients recruited from different research centers; the number of patients must be further expanded for an in-depth analysis. Brain MRI of patients with *GABRG2* variants was usually normal. In our cohort, the brain MRI of 2 patients (patients 3 and 25) was abnormal. These two patients had severe developmental delays. Their phenotypes included DEE, developmental delay and epilepsy. In the published studies, only 22.7% (5/22) of patients had an abnormal MRI: delayed myelination of white matter in one, ventricular enlargement in one, thin corpus callosum in one, and all with epileptic encephalopathy (Shen et al., 2017); enlargement of lateral ventricles and dysplasia of the frontotemporal region in one patient with early-onset epileptic encephalopathy (Zou et al., 2017); and cerebral cortical dysplasia in one patient with an LGS-like syndrome (Komulainen-Ebrahim et al., 2019). All these five patients had a global developmental delay.

Several studies have documented the phenotypic heterogeneity of *GABRG2*-related epilepsy. Of the 58 patients with *GABRG2* variants reported previously, the epilepsy phenotypes were varied (**Table 2**). The phenotypic spectrum observed for *GABRG2* variants, ranging from febrile seizures to epileptic encephalopathy, is similar to those of the other $GABA_A$ receptor genes *GABRA1*, *GABRB2*, and *GABRB3* (Johannesen et al., 2016; Moller et al., 2017; Yang et al., 2020, 2021). However, the prognosis of patients with *GABRG2*-related epilepsy is better than that of patients carrying variants in the other three genes. In our cohort, 57.1% (20/35) of patients presented with milder phenotypes, including febrile seizures, febrile seizures plus, focal epilepsy and unclassified epilepsy with normal development. Additionally, 38.1% (16/42) of patients manifested milder phenotypes than those in the previously published cohort (**Table 2**).

The mechanism of the phenotypic variation caused by $GABA_A$ receptor family genes is unclear. From the perspective of biological functions, the γ2 subunit (gene *GABRG2*) plays a critical role in $GABA_A$ receptor trafficking and localization at the postsynapse and yields benzodiazepine-sensitive and Zn^{2+}-insensitive $GABA_A$ receptors (Alldred et al., 2005; Kang and Macdonald, 2016). *GABRG2* functions as a part of $GABA_A$ receptor complexes, potentially explaining the variability of the clinical phenotypes. Further analysis showed that the *GABRG2* missense variants associated with severe epilepsy phenotypes were mainly clustered in the transmembrane region from the M1 region to the M3 domain. However, the variants located in the extracellular region were associated with phenotypes ranging from mild to severe. Moreover, few variants were located in the cytoplasmic region.

Bioinformatics analysis supported the deleterious effects of the p.R125P and p.R323W variants. The number of ion bonds between amino acid residues decreased in p.R125P according to the structural modeling. These changes may partially be responsible for the instability of protein structure. Arginine is an amino acid that increases the stability of proteins to a certain extent, and the variant at this site may reduce the stability of proteins (Cai et al., 2018). In our cohort, patient 6 with the R125P variant manifested febrile seizures plus. Nine patients were detected with the p.R323Q variant of *GABRG2*. Two patients were detected with the p.R323W variant of *GABRG2*. However, their phenotypes were different. The p.R323W and p.R323Q variants were located in the transmembrane domain. According to cryo-EM, the transmembrane domain is composed of a five-fold symmetric of the α-helix structure (Laverty et al., 2019). Both the R323W and R323Q variants change the ionic bonds with the adjacent α-helix according to structural modeling. Structural studies have shown that the transmembrane domain of the GABA receptor has larger flexibility (Zhu et al., 2018), and the variant in the adjacent α-helix also presents local flexibility in the transmembrane domain in some aspects. This genetic study may provide potential prospects for personalized medicine. The precise mechanism of *GABRG2*-related epilepsy is complex and requires further study in the future. The lack of functional studies limits our understanding of the impact of variants on proteins (loss or gain function).

Valproate and levetiracetam treatment might be suitable for patients harboring *GABRG2* variants. In this study, eight patients were effectively treated with valproate and levetiracetam. Previously, few reports described the effect of ASMs on patients with *GABRG2* variants. Zou reported that seizures were effectively controlled in two patients with *GABRG2* variant (A106T)- related epileptic encephalopathies after treatment with oxcarbazepine (Zou et al., 2017). In our cohort, patient 3 achieved seizure control after receiving treatment with oxcarbazepine. However, oxcarbazepine was ineffective in two patients. One patient with intractable epilepsy had a reduction in seizures after receiving perampanel treatment. Perampanel, is a novel non-competitive α-amino-3-hydroxyl-5-methyl-4-isoxazole-propionate (AMPA) receptor antagonist. An imbalance between glutamate and gamma-aminobutyric acid neurotransmitter systems may lead to hyperexcitability (Engelborghs et al., 2000). However, due to the limited number of patients with follow-up data, further studies are needed in the future. In our previous study of other types of $GABA_A$ receptor-related epilepsy, we found that patients with *GABRB2*

and *GABRB3* variant-related epilepsy patients also had a good response to valproate and levetiracetam (Yang et al., 2020, 2021). The heterogeneity of the clinical presentations related to the *GABRG2* variants makes early diagnosis difficult, and the lack of explanation for this heterogeneity does not currently allow personalized treatment.

DATA AVAILABILITY STATEMENT

The original contributions presented in the study are included in the article/**Supplementary Files**, further inquiries can be directed to the corresponding author/s.

ETHICS STATEMENT

The studies involving human participants were reviewed and approved by the Ethics Committee of Peking University First Hospital. Written informed consent to participate in this study was provided by the participants' legal guardian/next of kin. Written informed consent was obtained from the individual(s), and minor(s)' legal guardian/next of kin, for the publication of any potentially identifiable images or data included in this article.

AUTHOR CONTRIBUTIONS

YY wrote the article under the supervision of YZ. XN, MC, QZ, JD, XT, YW, JY, WS, WW, JM, YL, XY, XZ, TJ, ZY, JL, YS, HZ, SS, DS, and YJ had collected relevant patient information. All authors read and approved the final manuscript.

FUNDING

This study was supported in part by the National Natural Science Foundation of China (82071451), and Key Research Project of the Ministry of Science and Technology of China (Grant numbers: 2016YFC0904400 and 2016YFC0904401).

ACKNOWLEDGMENTS

We would like to extend our deep appreciation to the patients and their families who participated in this study. We would also like to thank team of staff who assisted with data collection. We would also like to thank Jintong Jia from the Singleron Biotechnologies, Ltd., for assisting with structural modeling using PyMOL2.3. We would also like to thank Dr. Xiaodong Wang from the Cipher Gene, Ltd., for assisting with manuscript editing.

SUPPLEMENTARY MATERIAL

The Supplementary Material for this article can be found online at: https://www.frontiersin.org/articles/10.3389/fnmol.2022.809163/full#supplementary-material

REFERENCES

Alldred, M. J., Mulder-Rosi, J., Lingenfelter, S. E., Chen, G., and Luscher, B. (2005). Distinct gamma2 subunit domains mediate clustering and synaptic function of postsynaptic GABAA receptors and gephyrin. *J. Neurosci.* 25, 594–603. doi: 10.1523/JNEUROSCI.4011-04.2005

Angione, K., Eschbach, K., Smith, G., Joshi, C., and Demarest, S. (2019). Genetic testing in a cohort of patients with potential epilepsy with myoclonic-atonic seizures. *Epilepsy Res.* 150, 70–77. doi: 10.1016/j.eplepsyres.2019.01.008

Baulac, S., Huberfeld, G., Gourfinkel-An, I., Mitropoulou, G., Beranger, A., Prud'homme, J. F., et al. (2001). First genetic evidence of GABA(A) receptor dysfunction in epilepsy: a mutation in the gamma2-subunit gene. *Nat. Genet.* 28, 46–48. doi: 10.1038/88254

Boillot, M., Morin-Brureau, M., Picard, F., Weckhuysen, S., Lambrecq, V., Minetti, C., et al. (2015). Novel GABRG2 mutations cause familial febrile seizures. *Neurol. Genet* 1:e35. doi: 10.1212/NXG.0000000000000035

Cai, X., Jiang, H., Zhang, T., Jiang, B., Mu, W., and Miao, M. (2018). Thermostability and Specific-Activity Enhancement of an Arginine Deiminase from Enterococcus faecalis SK23.001 *via* Semirational Design for l-Citrulline Production. *J. Agric. Food Chem.* 66, 8841–8850. doi: 10.1021/acs.jafc.8b02858

Carvill, G. L., Heavin, S. B., Yendle, S. C., McMahon, J. M., O'Roak, B. J., Cook, J., et al. (2013). Targeted resequencing in epileptic encephalopathies identifies de novo mutations in CHD2 and SYNGAP1. *Nat. Genet.* 45, 825–830. doi: 10.1038/ng.2646

Cogliati, F., Giorgini, V., Masciadri, M., Bonati, M. T., Marchi, M., Cracco, I., et al. (2019). Pathogenic Variants in STXBP1 and in Genes for GABAa Receptor Subunities Cause Atypical Rett/Rett-like Phenotypes. *Int. J. Mol. Sci.* 20:3621. doi: 10.3390/ijms20153621

Della Mina, E., Ciccone, R., Brustia, F., Bayindir, B., Limongelli, I., Vetro, A., et al. (2015). Improving molecular diagnosis in epilepsy by a dedicated high-throughput sequencing platform. *Eur. J. Hum. Genet.* 23, 354–362. doi: 10.1038/ejhg.2014.92

Engelborghs, S., D'Hooge, R., and De Deyn, P. P. (2000). Pathophysiology of epilepsy. *Acta Neurol. Belg.* 100, 201–213.

Epi4K consortium, and Epilepsy Phenome/Genome Project (2017). Ultra-rare genetic variation in common epilepsies: a case-control sequencing study. *Lancet Neurol.* 16, 135–143. doi: 10.1016/S1474-4422(16)30359-3

Harkin, L. A., Bowser, D. N., Dibbens, L. M., Singh, R., Phillips, F., Wallace, R. H., et al. (2002). Truncation of the GABA(A)-receptor gamma2 subunit in a family with generalized epilepsy with febrile seizures plus. *Am. J. Hum. Genet.* 70, 530–536. doi: 10.1086/338710

Hernandez, C. C., Kong, W., Hu, N., Zhang, Y., Shen, W., Jackson, L., et al. (2017). Altered Channel Conductance States and Gating of GABAA Receptors by a Pore Mutation Linked to Dravet Syndrome. *eNeuro* 4:ENEURO.251–ENEURO.216. doi: 10.1523/ENEURO.0251-16.2017

Hernandez, C. C., Tian, X., Hu, N., Shen, W., Catron, M. A., Yang, Y., et al. (2021). Dravet syndrome-associated mutations in GABRA1, GABRB2 and GABRG2 define the genetic landscape of defects of GABAA receptors. *Brain Commun.* 3:fcab033. doi: 10.1093/braincomms/fcab033

Huang, X., Tian, M., Hernandez, C. C., Hu, N., and Macdonald, R. L. (2012). The GABRG2 nonsense mutation, Q40X, associated with Dravet syndrome activated NMD and generated a truncated subunit that was partially rescued by aminoglycoside-induced stop codon read-through. *Neurobiol. Dis.* 48, 115–123. doi: 10.1016/j.nbd.2012.06.013

Ishii, A., Kanaumi, T., Sohda, M., Misumi, Y., Zhang, B., Kakinuma, N., et al. (2014). Association of nonsense mutation in GABRG2 with abnormal trafficking of GABAA receptors in severe epilepsy. *Epilepsy Res.* 108, 420–432. doi: 10.1016/j.eplepsyres.2013.12.005

Johannesen, K., Marini, C., Pfeffer, S., Moller, R. S., Dorn, T., Niturad, C. E., et al. (2016). Phenotypic spectrum of GABRA1: from generalized epilepsies to severe epileptic encephalopathies. *Neurology* 87, 1140–1151. doi: 10.1212/WNL.0000000000003087

Johnston, A. J., Kang, J. Q., Shen, W., Pickrell, W. O., Cushion, T. D., Davies, J. S., et al. (2014). A novel GABRG2 mutation, p.R136*, in a family with GEFS+

and extended phenotypes. *Neurobiol. Dis.* 64, 131–141. doi: 10.1016/j.nbd.2013.12.013

Kananura, C., Haug, K., Sander, T., Runge, U., Gu, W., Hallmann, K., et al. (2002). A splice-site mutation in GABRG2 associated with childhood absence epilepsy and febrile convulsions. *Arch. Neurol.* 59, 1137–1141. doi: 10.1001/archneur.59.7.1137

Kanaumi, T. F. G., Ueno, S., Ishii, A., Haga, Y., Hamachi, A., Yonetani, M., et al. (2004). Possible pathogenesis of severe myoclonic epilepsy in infancy: a novel nonsense mutation of GABRG2 leading to aggregation of GABAA receptors in neurons. *Neurol. Asia* 9:151.

Kang, J. Q., and Macdonald, R. L. (2016). Molecular Pathogenic Basis for GABRG2 Mutations Associated With a Spectrum of Epilepsy Syndromes, From Generalized Absence Epilepsy to Dravet Syndrome. *JAMA Neurol.* 73, 1009–1016. doi: 10.1001/jamaneurol.2016.0449

Kang, K. W., Kim, W., Cho, Y. W., Lee, S. K., Jung, K. Y., Shin, W., et al. (2019). Genetic characteristics of non-familial epilepsy. *PeerJ* 7:e8278. doi: 10.7717/peerj.8278

Komulainen-Ebrahim, J., Schreiber, J. M., Kangas, S. M., Pylkas, K., Suo-Palosaari, M., Rahikkala, E., et al. (2019). Novel variants and phenotypes widen the phenotypic spectrum of GABRG2-related disorders. *Seizure* 69, 99–104. doi: 10.1016/j.seizure.2019.03.010

Lachance-Touchette, P., Brown, P., Meloche, C., Kinirons, P., Lapointe, L., Lacasse, H., et al. (2011). Novel alpha1 and gamma2 GABAA receptor subunit mutations in families with idiopathic generalized epilepsy. *Eur. J. Neurosci.* 34, 237–249. doi: 10.1111/j.1460-9568.2011.07767.x

Laverty, D., Desai, R., Uchanski, T., Masiulis, S., Stec, W. J., Malinauskas, T., et al. (2019). Cryo-EM structure of the human alpha 1 beta 3 gamma 2 GABA(A) receptor in a lipid bilayer. *Nature* 565, 516–520. doi: 10.1038/s41586-018-0833-4

Ma, X., Yang, F., and Hua, Z. (2019). Genetic diagnosis of neonatal-onset seizures. *Genes Dis.* 6, 441–447. doi: 10.1016/j.gendis.2019.02.002

May, P., Girard, S., Harrer, M., Bobbili, D. R., Schubert, J., Wolking, S., et al. (2018). Rare coding variants in genes encoding GABA(A) receptors in genetic generalised epilepsies: an exome-based case-control study. *Lancet Neurol.* 17, 699–708. doi: 10.1016/S1474-4422(18)30215-1

Moller, R. S., Wuttke, T. V., Helbig, I., Marini, C., Johannesen, K. M., Brilstra, E. H., et al. (2017). Mutations in GABRB3: from febrile seizures to epileptic encephalopathies. *Neurology* 88, 483–492. doi: 10.1212/WNL.0000000000003565

Oyrer, J., Maljevic, S., Scheffer, I. E., Berkovic, S. F., Petrou, S., and Reid, C. A. (2018). Ion Channels in Genetic Epilepsy: from Genes and Mechanisms to Disease-Targeted Therapies. *Pharmacol. Rev.* 70, 142–173. doi: 10.1124/pr.117.014456

Parrini, E., Marini, C., Mei, D., Galuppi, A., Cellini, E., Pucatti, D., et al. (2017). Diagnostic Targeted Resequencing in 349 Patients with Drug-Resistant Pediatric Epilepsies Identifies Causative Mutations in 30 Different Genes. *Hum. Mutat.* 38, 216–225. doi: 10.1002/humu.23149

Peng, J., Pang, N., Wang, Y., Wang, X. L., Chen, J., Xiong, J., et al. (2019). Next-generation sequencing improves treatment efficacy and reduces hospitalization in children with drug-resistant epilepsy. *CNS Neurosci. Ther.* 25, 14–20. doi: 10.1111/cns.12869

Perucca, P., Scheffer, I. E., Harvey, A. S., James, P. A., Lunke, S., Thorne, N., et al. (2017). Real-world utility of whole exome sequencing with targeted gene analysis for focal epilepsy. *Epilepsy Res.* 131, 1–8. doi: 10.1016/j.eplepsyres.2017.02.001

Reinthaler, E. M., Dejanovic, B., Lal, D., Semtner, M., Merkler, Y., Reinhold, A., et al. (2015). Rare variants in gamma-aminobutyric acid type A receptor genes in rolandic epilepsy and related syndromes. *Ann. Neurol.* 77, 972–986. doi: 10.1002/ana.24395

Richards, S., Aziz, N., Bale, S., Bick, D., Das, S., Gastier-Foster, J., et al. (2015). Standards and guidelines for the interpretation of sequence variants: a joint consensus recommendation of the American College of Medical Genetics and Genomics and the Association for Molecular Pathology. *Genet Med.* 17, 405–424. doi: 10.1038/gim.2015.30

Salam, S. M., Rahman, H. M., and Karam, R. A. (2012). GABRG2 gene polymorphisms in Egyptian children with simple febrile seizures. *Indian J. Pediatr.* 79, 1514–1516. doi: 10.1007/s12098-011-0564-0

Shen, D., Hernandez, C. C., Shen, W., Hu, N., Poduri, A., Shiedley, B., et al. (2017). De novo GABRG2 mutations associated with epileptic encephalopathies. *Brain* 140, 49–67. doi: 10.1093/brain/aww272

Shi, X., Huang, M. C., Ishii, A., Yoshida, S., Okada, M., Morita, K., et al. (2010). Mutational analysis of GABRG2 in a Japanese cohort with childhood epilepsies. *J. Hum. Genet.* 55, 375–378. doi: 10.1038/jhg.2010.47

Stosser, M. B., Lindy, A. S., Butler, E., Retterer, K., Piccirillo-Stosser, C. M., Richard, G., et al. (2018). High frequency of mosaic pathogenic variants in genes causing epilepsy-related neurodevelopmental disorders. *Genet. Med.* 20, 403–410. doi: 10.1038/gim.2017.114

Sun, H. H., Zhang, Y. H., Liang, J. M., Liu, X. Y., Ma, X. W., Wu, H. S., et al. (2008). SCN1A, SCN1B, and GABRG2 gene mutation analysis in Chinese families with generalized epilepsy with febrile seizures plus. *J. Hum. Genet.* 53, 769–774. doi: 10.1007/s10038-008-0306-y

Surguchov, A., Surgucheva, I., Sharma, M., Sharma, R., and Singh, V. (2017). Pore-Forming Proteins as Mediators of Novel Epigenetic Mechanism of Epilepsy. *Front. Neurol.* 8:3. doi: 10.3389/fneur.2017.00003

Tian, M., Mei, D., Freri, E., Hernandez, C. C., Granata, T., Shen, W., et al. (2013). Impaired surface alphabetagamma GABA(A) receptor expression in familial epilepsy due to a GABRG2 frameshift mutation. *Neurobiol. Dis.* 50, 135–141. doi: 10.1016/j.nbd.2012.10.008

Wallace, R. H., Marini, C., Petrou, S., Harkin, L. A., Bowser, D. N., Panchal, R. G., et al. (2001). Mutant GABA(A) receptor gamma2-subunit in childhood absence epilepsy and febrile seizures. *Nat. Genet.* 28, 49–52. doi: 10.1038/88259

Yamamoto, T., Imaizumi, T., Yamamoto-Shimojima, K., Lu, Y., Yanagishita, T., Shimada, S., et al. (2019). Genomic backgrounds of Japanese patients with undiagnosed neurodevelopmental disorders. *Brain Dev.* 41, 776–782. doi: 10.1016/j.braindev.2019.05.007

Yang, Y., Xiangwei, W., Zhang, X., Xiao, J., Chen, J., Yang, X., et al. (2020). Phenotypic spectrum of patients with GABRB2 variants: from mild febrile seizures to severe epileptic encephalopathy. *Dev. Med. Child Neurol.* 62, 1213–1220. doi: 10.1111/dmcn.14614

Yang, Y., Zeng, Q., Cheng, M., Niu, X., Xiangwei, W., Gong, P., et al. (2021). GABRB3-related epilepsy: novel variants, clinical features and therapeutic implications. *J. Neurol.* [Online ahead of print] doi: 10.1007/s00415-021-10834-w

Zhu, S., Noviello, C. M., Teng, J., Walsh, R. M. Jr., Kim, J. J., and Hibbs, R. E. (2018). Structure of a human synaptic GABAA receptor. *Nature* 559, 67–72. doi: 10.1038/s41586-018-0255-3

Zou, F. G., McWalter, K., Schmidt, L., Decker, A., Picker, J. D., Lincoln, S., et al. (2017). Expanding the phenotypic spectrum of GABRG2 variants: a recurrent GABRG2 missense variant associated with a severe phenotype. *J. Neurogenet.* 31, 30–36. doi: 10.1080/01677063.2017.1315417

Conflict of Interest: The authors declare that the research was conducted in the absence of any commercial or financial relationships that could be construed as a potential conflict of interest.

frontiers in Molecular Neuroscience

ORIGINAL RESEARCH
published: 16 March 2022
doi: 10.3389/fnmol.2022.823640

Functional Investigation of a Neuronal Microcircuit in the CA1 Area of the Hippocampus Reveals Synaptic Dysfunction in Dravet Syndrome Mice

*Yael Almog[1,2], Anat Mavashov[1,3], Marina Brusel[1] and Moran Rubinstein[1,2,3]**

[1] Goldschleger Eye Research Institute, Sackler Faculty of Medicine, Tel Aviv University, Tel Aviv, Israel, [2] The Department of Human Molecular Genetics and Biochemistry, Sackler Faculty of Medicine, Tel Aviv University, Tel Aviv, Israel, [3] Sagol School of Neuroscience, Tel Aviv University, Tel Aviv, Israel

OPEN ACCESS

Edited by:
Tobias Stauber, Medical School Hamburg, Germany

Reviewed by:
Massimo Mantegazza, UMR 7275 Institut de Pharmacologie Moléculaire et Cellulaire (IPMC), France
Gabriele Lignani, University College London, United Kingdom

***Correspondence:**
Moran Rubinstein
moranrub@tauex.tau.ac.il

Specialty section:
This article was submitted to Brain Disease Mechanisms, a section of the journal Frontiers in Molecular Neuroscience

Received: *27 November 2021*
Accepted: *21 February 2022*
Published: *16 March 2022*

Citation:
Almog Y, Mavashov A, Brusel M and Rubinstein M (2022) Functional Investigation of a Neuronal Microcircuit in the CA1 Area of the Hippocampus Reveals Synaptic Dysfunction in Dravet Syndrome Mice. Front. Mol. Neurosci. 15:823640. doi: 10.3389/fnmol.2022.823640

Dravet syndrome is severe childhood-onset epilepsy, caused by loss of function mutations in the *SCN1A* gene, encoding for the voltage-gated sodium channel $Na_V1.1$. The leading hypothesis is that Dravet is caused by selective reduction in the excitability of inhibitory neurons, due to hampered activity of $Na_V1.1$ channels in these cells. However, these initial neuronal changes can lead to further network alterations. Here, focusing on the CA1 microcircuit in hippocampal brain slices of Dravet syndrome (DS, *Scn1a*$^{A1783V/WT}$) and wild-type (WT) mice, we examined the functional response to the application of Hm1a, a specific $Na_V1.1$ activator, in CA1 stratum-oriens (SO) interneurons and CA1 pyramidal excitatory neurons. DS SO interneurons demonstrated reduced firing and depolarized threshold for action potential (AP), indicating impaired activity. Nevertheless, Hm1a induced a similar AP threshold hyperpolarization in WT and DS interneurons. Conversely, a smaller effect of Hm1a was observed in CA1 pyramidal neurons of DS mice. In these excitatory cells, Hm1a application resulted in WT-specific AP threshold hyperpolarization and increased firing probability, with no effect on DS neurons. Additionally, when the firing of SO interneurons was triggered by CA3 stimulation and relayed via activation of CA1 excitatory neurons, the firing probability was similar in WT and DS interneurons, also featuring a comparable increase in the firing probability following Hm1a application. Interestingly, a similar functional response to Hm1a was observed in a second DS mouse model, harboring the nonsense *Scn1a*^{R613X} mutation. Furthermore, we show homeostatic synaptic alterations in both CA1 pyramidal neurons and SO interneurons, consistent with reduced excitation and inhibition onto CA1 pyramidal neurons and increased release probability in the CA1-SO synapse. Together, these results suggest global neuronal alterations within the CA1 microcircuit extending beyond the direct impact of $Na_V1.1$ dysfunction.

Keywords: Dravet syndrome, CA1 microcircuit, Nav1.1 voltage gated sodium channel, stratum-oriens, pyramidal neurons, Hm1a

INTRODUCTION

Dravet syndrome (Dravet) is a developmental epileptic encephalopathy (DEE) of early childhood with an ominous course. Children develop normally during the first year of life, but subsequently exhibit febrile seizures that progress to prolonged spontaneous seizures, frequent episodes of status epilepticus, global developmental delay, and a high risk of sudden death (Dravet, 2011; Dravet and Oguni, 2013). The underlying genetic cause of Dravet, in ∼90% of the patients, is heterozygous loss of function mutations in the *SCN1A* gene, encoding for the alpha subunit of the voltage-gated sodium channel (Na_V), $Na_V1.1$ (Claes et al., 2001). $Na_V1.1$ channels are crucial for neuronal excitability, contributing to the initiation and propagation of action potentials as well as amplification of synaptic depolarizations (Catterall et al., 2010). According to the prevailing hypothesis, the severity of *SCN1A*-related epileptic phenotypes correlates with the level of $Na_V1.1$ loss of function. While haploinsufficiency in $Na_V1.1$ activity results in Dravet, milder *SCN1A* mutations lead to less severe and treatable epilepsies, such as Generalized Epilepsy with Febrile Seizures Plus (GEFS+) and benign febrile seizures (Catterall et al., 2010; Nissenkorn et al., 2019).

Dravet mouse models (DS) are among the most accurate animal model representations of any human disease. Like Dravet patients, DS mice are mostly asymptomatic until their fourth week of life [postnatal day (P) 20–27], when they start experiencing seizures and profound premature mortality (Yu et al., 2006; Ogiwara et al., 2007, 2013; Cheah et al., 2012; Miller et al., 2014; Tsai et al., 2015; Mantegazza and Broccoli, 2019; Ricobaraza et al., 2019; Dyment et al., 2020; Fadila et al., 2020; Almog et al., 2021).

Studies of DS models that focused on recordings of single cortical or hippocampal neurons, in response to depolarizing current injections directly into the soma, demonstrated hypo-excitation of multiple types of inhibitory neurons, indicating that disinhibition serves as the root cause of Dravet (Yu et al., 2006; Kalume et al., 2007; Ogiwara et al., 2007; Mistry et al., 2014; Tai et al., 2014; Rubinstein et al., 2015b; De Stasi et al., 2016; Favero et al., 2018; Richards et al., 2018; Goff and Goldberg, 2019; Kuo et al., 2019; Dyment et al., 2020; Almog et al., 2021). Nevertheless, other studies proposed that the neuronal mechanism of Dravet is more complex. Specifically, changes in the activity of excitatory neurons, revealing reduced or enhanced activity, were reported (Ogiwara et al., 2013; Mistry et al., 2014; Salgueiro-Pereira et al., 2019; Almog et al., 2021; Studtmann et al., 2021). Moreover, the examination of spontaneous neuronal activity *in vivo* did not provide evidence for the predicted disinhibition (De Stasi et al., 2016; Tran et al., 2020). However, reduced inhibition can trigger multiple additional homeostatic network changes to stabilize neuronal firing (Antoine et al., 2019).

Dysfunction of the hippocampal CA1 microcircuit was implicated before in Dravet (Liautard et al., 2013; Rubinstein et al., 2015b; Cheah et al., 2019; Stein et al., 2019; Almog et al., 2021). In this circuit, inputs from CA3 Schaffer collaterals (SC) activate CA1 pyramidal neurons. Next, recurrent collaterals of CA1 pyramidal cells activate stratum-oriens (SO)-residing horizontal interneurons, which in turn provide strong feedback inhibition to the same CA1 excitatory neurons (**Figure 1A**). This results in the modulation of the final output to extra-hippocampal regions (Müller and Remy, 2014).

Using acute brain slices from WT and DS mice, we studied the neuronal changes in both excitatory and inhibitory neurons within this microcircuit, focusing on the severe stage of epilepsy (P20–25). Previously, we demonstrated that CA1 SO interneurons are hypo-excitable in Dravet (Rubinstein et al., 2015b; Almog et al., 2021). However, the direct contribution of $Na_V1.1$ loss of function to this phenotype was not tested. Moreover, alterations in synaptic communication within this circuit were not examined. The functional contribution of $Na_V1.1$ was evaluated by measuring the functional response to the $Na_V1.1$ activator, Hm1a (Osteen et al., 2016; Richards et al., 2018). Surprisingly, Hm1a had a similar effect on SO interneurons from WT and DS mice. Conversely, Hm1a had a smaller functional effect on DS CA1 pyramidal neurons. Additionally, to test the activity of the CA1 microcircuit, we examined the response of SO interneurons to SC stimulation, demonstrating similar firing probability in WT and DS, along with homeostatic synaptic changes within this circuit. Together, our results reveal multiple DS-related neuronal alterations, indicating that Dravet pathophysiology is highly complex, involving synaptic and neuronal function variations occurring concomitantly in excitatory and inhibitory neurons of the CA1 microcircuit.

MATERIALS AND METHODS

Mice

All animal experiments were in accordance with the Animal Care and Use Committee (IACUC) of Tel Aviv University. Mice were group-housed in a standard animal facility at the Goldschleger Eye Institute at a constant (22°C) temperature, on a 12-h light/dark cycle, with *ad libitum* access to food and water.

Dravet syndrome mice harboring the heterozygous global $Scn1a^{A1783V/WT}$ mutation were generated as reported before (Almog et al., 2021); briefly, males carrying the conditional floxed stop $Scn1a^{A1783Vfl}$ allele [B6(Cg)-Scn1atm1.1Dsf/J; strain 026133; The Jackson Laboratory, Bar Harbor, ME, United States] were crossed with CMV-Cre females [B6·C-Tg(CMV-Cre)1Cgn/J; strain 006054; The Jackson Laboratory, Bar Harbor, ME, United States]. Both lines were maintained on the pure C57BL/6J genetic background. Both males and females, at similar proportions, were used for the electrophysiological recordings. DS $Scn1a^{A1783V/WT}$ mice experience spontaneous convulsive seizures starting at P19, and all the mice experience such spontaneous seizures at the severe stage of the disease (Fadila et al., 2020; Almog et al., 2021). While the mice used for this study were not placed under video surveillance from P19 until the recording day, they displayed a characteristic DS behavior, including apparent hyperactivity and increased anxiety, and were easily distinguished from their WT littermates in their home cage. Based on these phenotypes, we speculate that these mice have

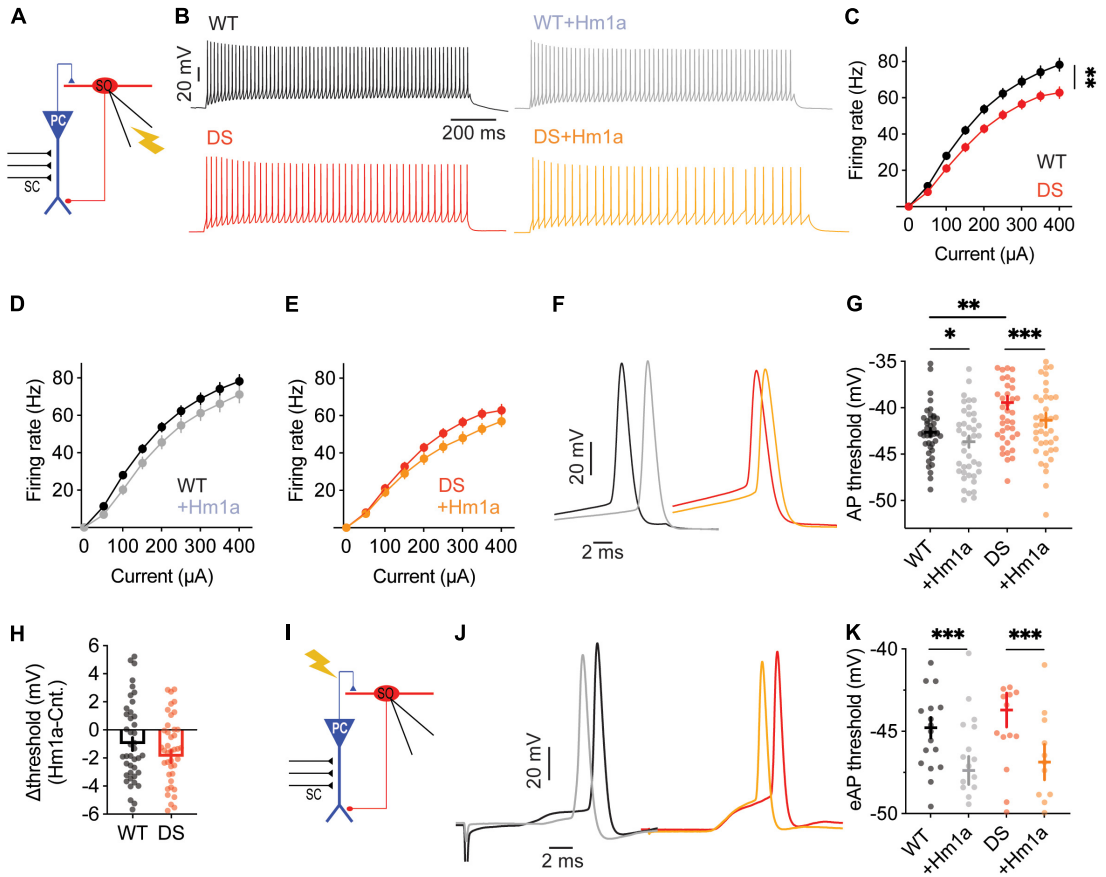

FIGURE 1 | Stratum-oriens interneurons from WT and DS *Scn1a*$^{A1783V/WT}$ mice respond similarly to Hm1a. **(A)** Illustration of the recording configuration. Firing properties of SO interneurons (red) were measured in response to current injection through the patch pipette **(B–H)**. **(B)** Representative traces of whole-cell current clamp recordings from WT and DS SO interneurons in response to current injection of +150 pA, before and after Hm1a application. **(C)** Firing frequency in response to depolarizing current injection at the indicated intensities in WT and DS. Statistical analysis utilized Mixed Model Repeated Measures ANOVA. **(D,E)** The effect of Hm1a on firing frequencies, in response to current injection through the whole-cell patch electrode in WT **(D)** and DS **(E)** mice. Statistical analysis utilized Two Way Repeated Measures ANOVA; **(D)** $p = 0.36$ for Hm1a treatment, $p = 0.96$ for current × treatment; **(E)** $p = 0.37$ for Hm1a treatment, $p = 0.44$ for current × treatment. **(F)** Representative WT and DS APs at rheobase, before and after Hm1a application. **(G)** The effect of Hm1a on AP threshold at rheobase current. Statistical analysis utilized Two Way Repeated Measures ANOVA. The markings on the graph depict the results of Bonferroni *post hoc* analysis: $p = 0.001$ (**) for genotype; $p < 0.001$ (***) for Hm1a treatment; $p = 0.23$ for the interaction. **(H)** The difference in AP threshold. The data in **(C–H)** included WT: $n = 42$ cells from 17 mice; DS: $n = 43$ cells from 14 mice. **(I)** Illustration of the recording configuration. Synaptic activation of SO interneurons (red) was triggered by antidromic activation of CA1 pyramidal neurons via stimulation of the alveus.**(J)** Representative traces of eAPs before and after Hm1a application. **(K)** The difference in eAP threshold. Statistical analysis utilized Two Way Repeated Measures ANOVA. The markings on the graph depict the results of Bonferroni *post hoc* analysis: $p = 0.18$ for genotype; $p < 0.001$ (***) for Hm1a treatment; $p = 0.28$ for the interaction. WT: $n = 18$ cells from 5 mice; DS: $n = 15$ cells from 4 mice.

experienced spontaneous convulsive seizures. Nevertheless, the genotype was still confirmed by genotyping after the experiment.

Dravet syndrome mice harboring the heterozygous nonsense *Scn1a*$^{R613X/WT}$ (129S1/SvImJ-Scn1aem1Dsf/J; strain 034129, The Jackson Laboratory, Bar Harbor, ME, United States), were generated by crossing DS *Scn1a*$^{R613X/WT}$ on the pure 129S1/SvImJ background with WT C57BL/6J mice (strain 000664), to generate mice on the mixed 50:50 129S1/SvImJ:C57BL/6J background. Both males and females were used for real-time PCR and electrophysiological recordings. While some mice were observed to have spontaneous seizures, they could not be distinguished from their WT littermates without genotyping.

Brain Slice Electrophysiology

Hippocampal slices (300–400 μm thick) were prepared from WT or DS mice aged P20-25 as described previously (Rubinstein et al., 2015b; Almog et al., 2021), with minor modifications. Briefly, mice were decapitated under isoflurane anesthesia. The brain was quickly removed and placed into ice-cold slicing solution containing 75 mM sucrose, 87 mM NaCl, 25 mM $NaHCO_3$, 25 mM D-glucose, 2.5 mM KCl, 1.25 mM NaH_2PO_4, 0.5 mM $CaCl_2$ and 7 mM $MgCl_2$. Slicing was performed using a Leica VT1200S vibratome (Leica Biosystems, Wetzlar, Germany). Parasagittal slices were used for whole-cell recordings of horizontal SO interneurons to better preserve the synaptic connections. The brain was cut midline and

the hemispheres were glued on their callosal side onto a slope of 45°, forming longitudinal sagittal slices. To record CA1 pyramidal cells, the brain was glued on its ventral side, without any tilt, and horizontal slices were taken. Slices were transferred to a storage chamber with fresh artificial cerebrospinal fluid (ACSF) containing 125 mM NaCl, 3 mM KCl, 2 mM $MgCl_2$, 2 mM $CaCl_2$, 1.25 mM NaH_2PO_4, 26 mM $NaHCO_3$, and 10 mM D-glucose, and incubated for 45 min at 37°C, followed by a 30 min recovery at room temperature. All solutions were saturated with 95% O_2 and 5% CO_2. The cells were visualized under oblique illumination with near-infrared LED and an upright microscope (SOM; Sutter Instrument, Novato, CA, United States). Horizontal SO interneurons were identified based on their horizontal fusiform somata and characteristic electrophysiological properties (Tricoire et al., 2011). Their characteristic morphology was also verified using biocytin (0.2%). Pyramidal cells were identified based on their location, morphology, and electrophysiological properties. $Na_V1.1$ functional contribution was examined by application of 50 nM Hm1a (Alomone Labs, Jerusalem, Israel, Catalog #STH-601). Control experiments with vehicle, instead of Hm1a, confirmed the lack of effect on AP threshold (–46.2 ± 0.6 vs. –46.8 ± 0.4, $p = 0.66$), or firing probability (0.5 ± 0.1 vs. 0.6 ± 0.2, $p = 0.5$, $n = 3$).

Recordings were obtained using a Multiclamp 700B amplifier (Molecular Devices, San Jose, CA, United States) and Clampex 10.7 software (Molecular Devices, San Jose, CA, United States). For whole-cell current clamp recordings and measurements of paired pulse ratio (PPR), the patch pipette was filled with an internal solution containing: 145 mM K-Gluconate, 2 mM $MgCl_2$, 0.5 mM EGTA, 2 mM ATP-Tris, 0.2 mM Na_2-GTP and 10 mM HEPES, pH 7.2. To measure evoked EPSCs and IPSCs, we used an internal solution containing: 140 mM Cs-methanesulfonate, 5 mM CsCl, 2 mM $MgCl_2$, 2 mM 2 ATP-Tris, 0.2 mM Na_2-GTP, 10 mM HEPES and 5 mM QX-314. When filled with an intracellular solution, the patch electrode resistance ranged from 4 to 7 MΩ. Access resistance was monitored continuously for each cell. Only cells with access resistance lower than 30 MΩ, that were stable through the recording (changing by less than 20%) were included. The resting membrane potential was set to –60 mV by injection of no more than 50 pA, ranging from –50 to +50 pA. Bridge balance and pipette capacitance neutralization, based on the amplifier circuit, were applied to all current clamp recordings.

We used different paradigm for current clamp recordings, as illustrated in the Figures. Firing rates were determined by injection of 1 s long depolarizing current through the patch pipette. AP threshold was measured by injection of 10 ms long depolarizing current at rheobase, as we did before (Almog et al., 2021). To record synaptic evoked AP (eAP) from SO interneurons we stimulated the alveus; to evoke firing of pyramidal neurons, we stimulated the SC, as we did before (Almog et al., 2021). The stimulation strength was set to produce firing probability of 50% (i.e., 5 APs out of 10 stimuli at 1 Hz). Cells that produced 4 to 6 APs were used for analysis. For simultaneous field potential and whole-cell recordings (**Figures 3–5**), the stimulating electrode was put on the SC, the field electrode (1–2 MΩ, filled with ACSF) was placed on the stratum radiatum, 200–600 μm from the stimulating electrode; while patching the horizontal SO interneuron. The slopes of evoked extracellular field EPSPs (fEPSPs) were measured by calculating the linear regression of the initial part (20–80%) of the rising phase. The firing probability was calculated as the number of eAPs out of these 10 stimulations. For each cell, we recorded the response to different stimulus intensities. First, we determined the stimulation that produced firing of 50%, i.e., 5 APs out of 10 stimuli (1X). Next, we repeated the recording with half of the intensity (0.5X), as well as higher intensity (1.5X). We than repeated this recording after the addition of Hm1a (50 nM), without altering the stimulation strength, to look for changes in the firing probability. This stage was followed by the readjustment of the stimulation strength to reproduce a firing probability of 50%, which was used for measurements of the eAP threshold. The slice was changed following Hm1a application (to avoid any chances for partial wash off) and the perfusion pipes and chamber were washed thoroughly, for least 10 min, with ACSF prior to placing the next slice.

Paired-pulse ratio experiments were recorded in voltage clamp mode at a holding potential of –60 mV with an inter-stimulus interval (ISI) of 50 ms (**Figures 6B–D**, **7B–D**). For EPSP measurements, we first determined the stimulation intensity that produced firing probability of 50%, then reset the intensity to half of that, and measured subthreshold responses to a train of stimulations given at 30 Hz. Neurons that fired eAP within this train of stimuli were excluded from the analysis (**Figures 6E–G**, **7E–G**). Recordings of evoked EPSCs and IPSCs and excitation-inhibition balance were performed as described before (Antoine et al., 2019), with some adaptations. Briefly, membrane voltage was held at –60 or 0 mV for EPSC or IPSC recordings, respectively. The minimal response in **Figures 6H–J**, **7H–J** was defined experimentally, as the stimulation intensity that produced a measurable current response in the recorded postsynaptic cell (1xEθ). As such, 1xEθ responses had a similar amplitude in both WT and DS. Next, EPSCs and IPSCs were measured in response to stronger stimuli (1.25–2.5xEθ). As the inhibitory neurons are not stimulated directly, IPSCs are the result of feed-forward and feedback inhibition.

Data were analyzed using Clampfit 10.7 (Molecular Devices), Igor Pro (WaveMetrics, Lake Oswego, OR, United States) and GraphPad Prism (GraphPad Software, La Jolla, CA, United States). AP threshold was defined as the voltage at which the first derivative of the AP waveform (dV/dt) reached 10 mV/ms.

Real-Time PCR

Total RNA was extracted from the hippocampi of WT and DS *Scn1a*$^{R613X/WT}$ mice at P20–25, using Purelink RNA mini kit according to the manufacturer's instructions. cDNA was synthesized from 500 ng RNA using Maxima H Minus cDNA synthesis kit (Thermo Fisher Scientific, Life Technologies, Carlsbad, CA, United States). Real-time PCR reactions were performed in triplicates in a final volume of 10 μl with 5 ng of RNA as template, with TaqMan gene expression assays: *Scn1a* (Mm00450580_m1) and *Tfrc*

(Mm00441941_m1) as endogenous control, on StepOnePlus real-time PCR system (Applied Biosystems, Thermo Fisher Scientific, Life Technologies, Carlsbad, CA, United States). Efficiency of 100%, dynamic range, and lack of genomic DNA amplification were verified. The relative expression was calculated as $2^{-\Delta\Delta CT}$.

Experimental Design and Statistical Analysis

Statistical analysis was performed using GraphPad Prism 9.2 (GraphPad Software, La Jolla, CA, United States). Two Way Repeated Measures ANOVA with Bonferroni *post hoc* analysis was used when multiple measurements were obtained from the same cell. Mixed Model Repeated Measures ANOVA was used to compare between firing rates in response to injection of 1 s long depolarizing current, and the excitation-inhibition balance. The Mann–Whitney test was used to compare two groups. The Correlations between fiber volley and fEPSP utilized linear regression analysis followed by statistical comparison of the slopes. The specific statistic comparison for each panel is indicated in the Figure legend. We defined $p < 0.05$ as statistically significant and marked $^{*}p < 0.05$, $^{**}p < 0.01$, $^{***}p < 0.001$.

RESULTS

Similar Response of Wild-Type and Dravet Syndrome *Scn1a*$^{A1783V/WT}$ Stratum-Oriens Interneurons to Hm1a

Previous studies demonstrated a reduction of ∼50% in sodium currents of DS interneurons (Yu et al., 2006; Kalume et al., 2007; Mistry et al., 2014; Rubinstein et al., 2015b), as well as hypo-excitability of multiple types of GABAergic neurons. Similarly, the Dravet causing *Scn1a*^{A1783V} mutation was demonstrated to cause loss of function of $Na_V1.1$ (Layer et al., 2021), as well as reduced firing and increased threshold for action potentials (APs) of inhibitory neurons (Kuo et al., 2019; Almog et al., 2021; Layer et al., 2021). These data indicate that reduced activity of $Na_V1.1$ in inhibitory neurons is the cause for their reduced excitability. To directly test that here, we examined the change in the activity of SO interneurons before and after the application of Hm1a, a specific $Na_V1.1$ activator. Hm1a inhibits the inactivation of $Na_V1.1$, with a reduced effect on $Na_V1.3$ and low impact on $Na_V1.2$ and $Na_V1.6$ (Osteen et al., 2016; Richards et al., 2018). We hypothesized a smaller effect of Hm1a on SO interneurons from DS mice, in accordance with $Na_V1.1$ haploinsufficiency.

First, we confirmed that DS *Scn1a*$^{A1783V/WT}$ SO interneurons were hypo-excitable (**Figures 1B,C**), similar to previous data (Rubinstein et al., 2015b; Almog et al., 2021). Moreover, an examination of the threshold for AP demonstrated a more depolarized threshold voltage in DS (**Figure 1G**), in accordance with reduced firing of these SO interneurons. Next, we examined the effect of the application of Hm1a, at 50 nM, a concentration that was previously found to enhance the firing of fast spiking interneurons in DS mice (Richards et al., 2018; Goff and Goldberg, 2019; Chever et al., 2021). The application of Hm1a had no significant effect on the firing rates of WT and DS (**Figures 1D,E**). While this was somewhat unexpected, lack of effect on the firing frequency was reported before by Richards et al. (2018), who reported that Hm1a did not increase the firing rates of non-collapsing WT CA1 GABAergic interneurons. Nevertheless, Hm1a hyperpolarized the AP threshold in both WT and DS *Scn1a*$^{A1783V/WT}$ (**Figures 1F,G**). Intriguingly, the extent of this Hm1a-induced threshold shift showed a slightly smaller effect in WT, resulting in the dissipation of the difference between the threshold levels of WT and DS following Hm1a application (**Figures 1F–H**).

Under physiological synaptic activation, excitatory inputs are received by the dendrites, integrated and transferred through the cell soma to the axon initial segment (AIS) (Stuart and Spruston, 2015). Conversely, injection of prolonged depolarizing current, close to the AIS, bypasses this natural path, resulting in direct AIS depolarization, that may lead to misinterpretation of the data. Therefore, to test the effect of Hm1a following synaptically evoked firing, we stimulated the axons of CA1 pyramidal neurons, located in the alveus, while recording the postsynaptic response of SO interneurons under whole-cell current clamp (**Figure 1I**). The stimulation strength was set to produce firing probability of 50%, representing the middle of their dynamic range of response, resulting in 5 synaptically evoked APs (eAPs) out of 10 stimuli that were given at 1 Hz, as we did before (Rubinstein et al., 2015b; Almog et al., 2021). However, the effect of Hm1a was similar in both genotypes, again, with hyperpolarization of the threshold by ∼3 mV (**Figures 1J,K**). Together, these data show that while SO interneurons are hypo-excitable in DS *Scn1a*$^{A1783V/WT}$, demonstrated by reduced firing and increased threshold, the functional change in response to Hm1a is comparable between WT and DS.

CA1 Pyramidal Neurons From Dravet Syndrome *Scn1a*$^{A1783V/WT}$ Mice Demonstrate Reduced Response to Hm1a

While $Na_V1.1$ channels were shown to be expressed in pyramidal excitatory neurons (Westenbroek et al., 1989; Yu et al., 2006; Cembrowski et al., 2016) and several studies demonstrated their structural and functional changes in DS (Mistry et al., 2014; Tsai et al., 2015; Salgueiro-Pereira et al., 2019; Almog et al., 2021), others reported unaltered excitability of these cells (Yu et al., 2006; Rubinstein et al., 2015b; De Stasi et al., 2016; Favero et al., 2018). Here we tested the functional response of CA1 pyramidal cells to Hm1a.

When firing was evoked by direct injections of depolarizing current through the patch pipette, the application of Hm1a had no significant effect on the firing rate in either WT or DS *Scn1a*$^{A1783V/WT}$ (**Figures 2A–D**). However, the application of Hm1a resulted in AP threshold hyperpolarization, that was comparable in both genotypes (**Figures 2E,F**). Next, to examine the effect of Hm1a on synaptically evoked firing and eAP threshold, the stimulating electrode was placed on CA3 SC, and the stimulation intensity was set to produce firing probability of 50% in the recorded postsynaptic CA1

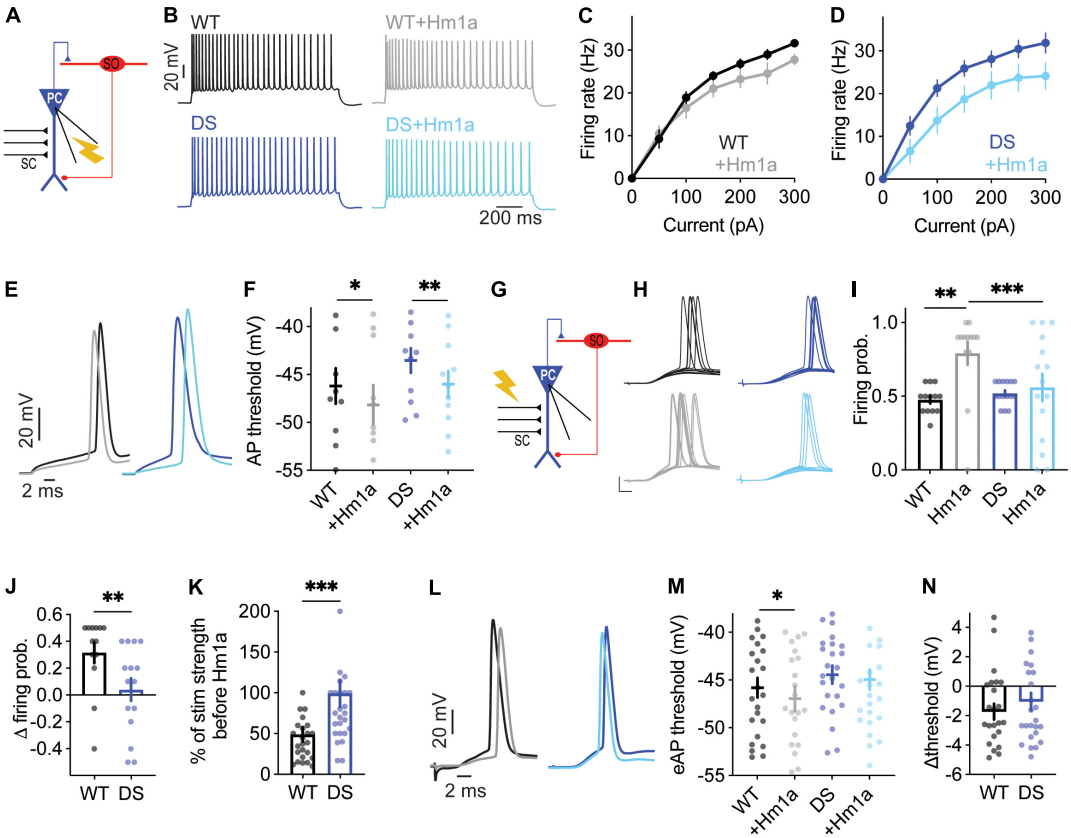

FIGURE 2 | Reduced evoked synaptic response of DS *Scn1a*$^{A1783V/WT}$ CA1 pyramidal neurons to Hm1a application. **(A)** Illustration of the recording configuration. Neuronal firing of CA1 pyramidal neurons (blue) was evoked by injection of depolarizing current through the patch pipette. **(B)** Representative traces of whole-cell current clamp recordings from CA1 pyramidal neurons in response to current injection of +150 pA, before and after Hm1a application. **(C,D)** The effect of Hm1a on firing in response to current injection through the whole-cell patch electrode in WT **(C)** and DS **(D)** CA1 pyramidal neurons. Statistical analysis utilized Mixed Model Analysis of Variance; **(C)** $p = 0.08$ for Hm1a treatment, $p = 0.06$ for current × treatment; **(D)** $p = 0.07$ for Hm1a treatment, $p = 0.09$ for current × treatment. **(E)** Representative WT and DS APs at rheobase, before and after Hm1a application. **(F)** The effect of Hm1a on AP threshold at rheobase current. Statistical analysis utilized Two Way Repeated Measures ANOVA. The markings on the graph depict the results of Bonferroni *post hoc* analysis: $p = 0.30$ for genotype; $p < 0.001$ (***) for Hm1a treatment, and $p = 0.58$ for the interaction. The data in **(C–F)** included: WT: $n = 11$ cells from 4 mice; DS: $n = 16$ cells from 3 mice. **(G)** Schematic illustration of the SC stimulation and whole-cell recording of a CA1 pyramidal neuron. **(H)** Representative traces of WT and DS CA1 pyramidal neurons in response to a train of 10 stimuli at 1 Hz, delivered to the SC, with or without Hm1a. Scale bar = 20 mV, 5 ms. **(I,J)** The effect of Hm1a on the firing probability of WT and DS CA1 pyramidal neurons **(I)**, and the difference in firing probability calculated for each cell **(J)**. Statistical analysis for the data presented in **I** utilized Two Way Repeated Measures ANOVA. The markings depict the results of Bonferroni *post hoc* analysis: $p = 0.036$ (*) for genotype; $p = 0.070$ for Hm1a treatment; $p = 0.002$ (**) for the interaction. The Mann–Whitney test was used to analyze the data in **(J)**. **(K)** The effect of Hm1a on the stimulation intensity required to produce 50% firing probability. Statistical analysis utilized the Mann–Whitney test. **(L–N)** Representative traces of eAPs before and after Hm1a application **(L)**, the overall effect of Hm1a on the eAP threshold **(M)**, and the difference in eAP threshold **(N)**. Statistical analysis utilized Two Way Repeated Measures ANOVA. The markings depict the results of Bonferroni *post hoc* analysis: $p = 0.3$ for genotype; $p = 0.019$ (*) for Hm1a treatment; $p = 0.19$ for the interaction. The data in **(I–N)** included WT: $n = 25$ cells from 9 mice; DS: $n = 27$ cells from 8 mice.

excitatory cell (**Figure 2G**). Under this experimental paradigm, the application of Hm1a increased the firing probability of WT CA1 pyramidal neurons (**Figures 2H–J**). Next, in the presence of Hm1a, we readjusted the stimulation strength to reproduce a firing probability of 50%. In WT CA1 pyramidal neurons, this required about half of the original stimulation strength, in accordance with the initial increased firing probability (**Figure 2K**). In addition, Hm1a application caused a small, but significant, hyperpolarization of the threshold for eAP (**Figures 2L–N**). Conversely, Hm1a had no significant effect on the firing probability or eAP threshold in CA1 pyramidal neurons of DS *Scn1a*$^{A1783V/WT}$ mice (**Figures 2H–N**). Together, these data demonstrated reduced response of CA1 pyramidal neurons in DS mice to Hm1a.

Dravet Syndrome *Scn1a*$^{A1783V/WT}$ Mice Feature Reduced Synaptic Activation of CA1 Pyramidal Neurons and Preserved Firing of Stratum-Oriens Interneurons

With the differential effect of Hm1a on excitatory and inhibitory neurons, we set to simultaneously probe the activity of excitatory and inhibitory neurons within the CA1 microcircuit. We stimulated the CA3 SC while monitoring synaptic responses

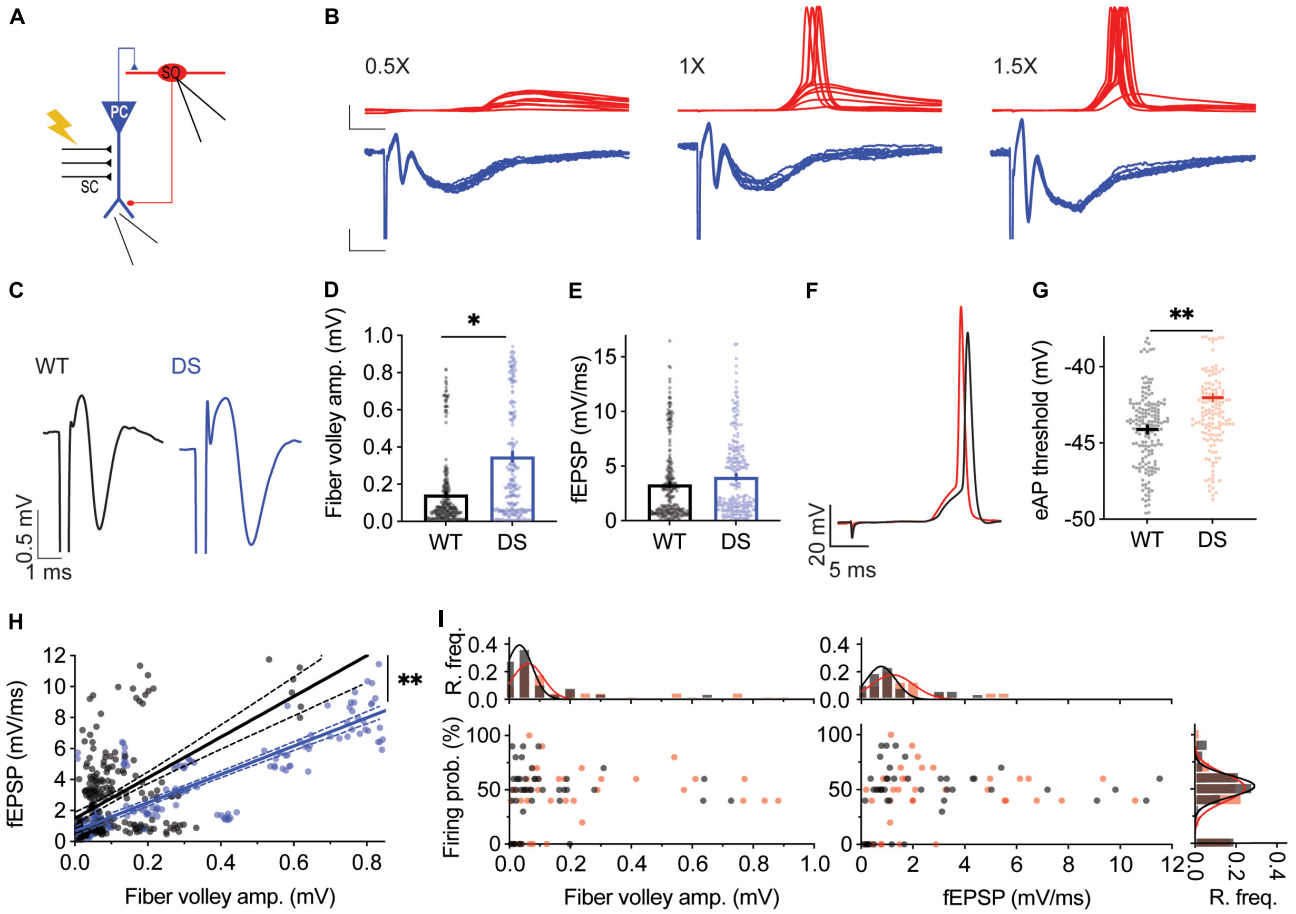

FIGURE 3 | Preserved firing of DS *Scn1a*$^{A1783V/WT}$ SO interneurons in response to CA3 stimulation. **(A)** Illustration of the experimental setup. The stimulating electrode was placed on the CA3, with extracellular field potentials recorded from CA1 pyramidal neurons (blue), concomitantly with whole-cell recordings of a SO interneuron (red). **(B)** Representative traces of field potential of CA1 pyramidal neurons (blue) and whole-cell recording of a SO interneuron (red) at different stimulation intensities. Left: low stimulation intensity (0.5X) that produced subthreshold responses in the recorded SO interneuron. Middle: intermediate stimulation intensity (1X) that produced firing probability of 50%, i.e., 5 AP and 5 EPSPs out of 10 stimulations at 1 Hz. Right: stronger stimulation intensity (1.5X), that produced firing probability of 90% in the recorded SO interneuron. Scale bar: top: 20 mV, 5 ms; bottom: 0.2 mV, 5 ms. **(C)** Representative traces of WT (black) and DS (blue) field potentials. **(D,E)** Average fiber volley amplitudes **(D)** and fEPSP **(E)** in recordings at which the firing probability of SO interneurons was 50% (1X). Statistical analysis utilized Mixed Model Analysis of Variance. **(F)** Representative traces of WT (black) and DS (red) synaptically evoked APs (eAPs) recorded from SO interneuron. **(G)** Average eAP threshold of WT and DS SO interneurons. Statistical analysis utilized Mixed Model Analysis of Variance. **(H)** Linear regression analysis of fEPSP slope vs. fiber volley amplitude. The solid lines represent the linear fit, and the dashed lines depict the 95% confidence interval. The fitted equation was $Y = 13.14*X + 1.4$ for WT ($R^2 = 0.33$) and $Y = 9.14*X + 0.67$ in DS ($R^2 = 0.72$). The statistical difference between the slopes is presented ($p = 0.0052$). We repeated this analysis by fitting a non-linear exponential model to the data. The goodness of the fit was: WT: $R^2 = 0.33$, DS: $R^2 = 0.77$, and the statistical difference between the curves was $p < 0.001$. **(I)** SO interneurons firing probability vs. fiber volley amplitude or fEPSP. R.freq: the relative frequency histograms and Gaussian fit (solid line) of fiber volley amplitude, fEPSP or SO firing probability in WT and DS. WT: 28 cells from 11 mice; DS: 23 cells from 7 mice.

of CA1 pyramidal neurons using extracellular field-potential measurements, concomitantly with whole-cell recordings of SO interneurons (**Figure 3A**). This experimental paradigm enables the measurements of fiber volley amplitudes, reporting the level of CA3 stimulation, the field excitatory post-synaptic potential (fEPSP) initial slope, corresponding mostly to the synaptic responses of CA1 pyramidal neurons (Hawkins et al., 2016), and SO responses under whole-cell current clamp. For each SO cell, the CA3 SC were stimulated at different amplitudes (1X, 0.5X, and 1.5X) (**Figure 3B**). 1X stimulation was defined as the stimulation intensity that resulted in a firing probability of 50% in the recorded SO interneuron. Next, for the same cell, the stimulation intensity was reduced by half (0.5X) or increased by half (1.5X), to cover a wide dynamic range of responses. Low stimulation intensities of CA3 SC (0.5X) induced field responses in CA1 pyramidal neurons, with almost no eAPs in the recorded SO interneuron (**Figure 3B**, left). Conversely, stronger suprathreshold stimulation (1.5X) resulted in CA1 depolarization, followed by high firing probability of SO interneurons (**Figure 3B**, right). Focusing on stimulation intensities yielding a 50% SO firing probability (1X), larger fiber volley amplitudes, with similar fEPSP slopes were measured in DS *Scn1a*$^{A1783V/WT}$ (**Figures 3C–E**). These results indicate that stronger SC stimulation is needed to produce comparable

synaptic responses in DS CA1 pyramidal neurons. Analyses of the threshold for eAP of SO interneurons, using this experimental paradigm, demonstrated a more depolarized voltage in DS *Scn1a*$^{A1783V/WT}$ (**Figures 3F,G**), in agreement with reduced excitability of these interneurons (**Figures 1C,G**). Analysis of the relationship between fiber volley amplitude and fEPSP, across the full range of responses (0.5X, 1X, 1.5X), revealed that for the same fiber volley amplitude, lower fEPSP was measured in DS *Scn1a*$^{A1783V/WT}$ (**Figure 3H**). Together, these recordings suggest that in DS the CA3-CA1 synaptic strength is weaker, and the excitability of SO interneurons is reduced. Based on these measurements, we expected an additive reduction in the firing probability of SO interneurons, following SC stimulation. However, surprisingly, the firing probability of SO interneurons, along the range of fiber volley amplitudes or CA1 fEPSP tested, was similar between WT and DS (**Figure 3I**) indicating a preserved activity of SO interneurons under these conditions, in response to a low frequency (1 Hz) stimulation.

The effect of Hm1a using this recording configuration was also tested (**Figure 4A**). Analysis of the extracellular field recordings of CA1 excitatory neurons demonstrated that Hm1a application did not change the fiber volley, but the fEPSP was increased in WT CA1 (**Figures 4B–D**). Conversely, in recordings of DS *Scn1a*$^{A1783V/WT}$ CA1, Hm1a did not affect the fiber volley or fEPSP slope (**Figures 4B–D**). Thus, Hm1a-induced enhancement of synaptic responses in CA1 pyramidal neurons was not observed in DS *Scn1a*$^{A1783V/WT}$.

Given that Hm1a did not increase the firing probability or the fEPSP of CA1 pyramidal cells from DS mice (**Figures 2G–I**, **4D**), we expected an overall smaller increase in the firing probability of SO *Scn1a*$^{A1783V/WT}$ interneurons, when their firing was initiated

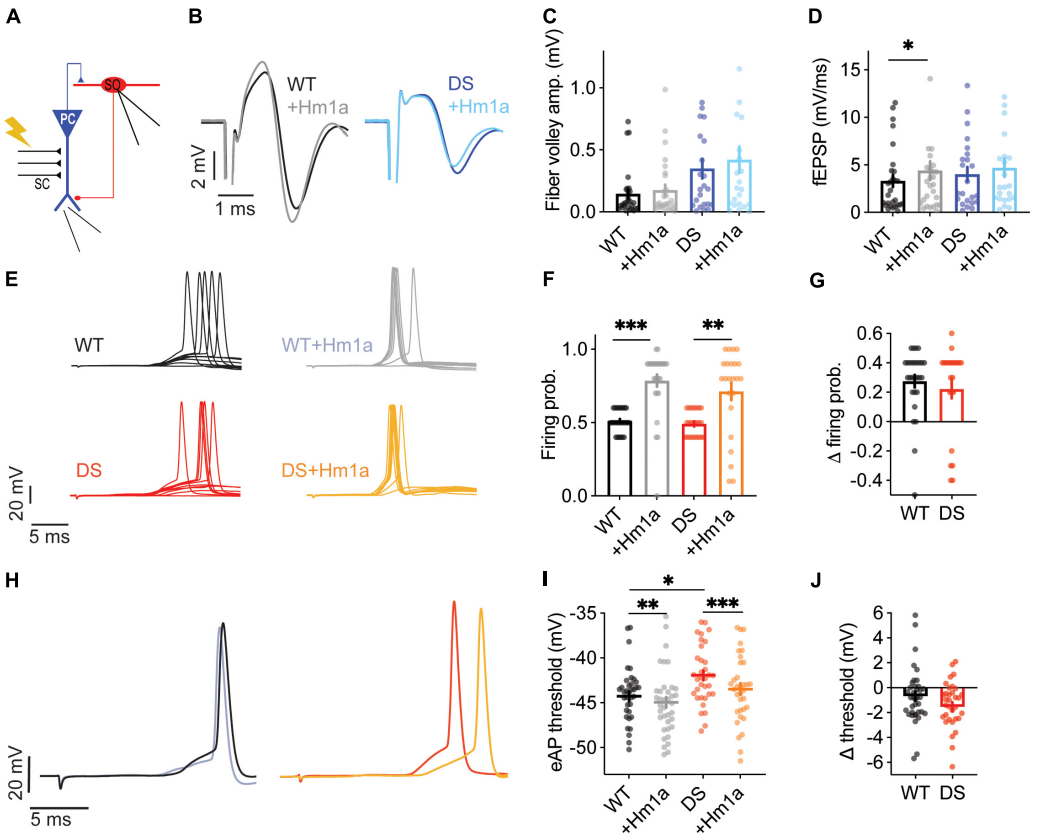

FIGURE 4 | Hm1a increased the firing of DS *Scn1a*$^{A1783V/WT}$ SO interneurons following SC stimulation. **(A)** Illustration of the experimental setup. **(B)** Representative traces of WT (black or gray) and DS (dark or pale blue) field potentials before and after Hm1a application. **(C,D)** Average fiber volley amplitudes **(C)** and fEPSP **(D)** before and after Hm1a application. Statistical analysis utilized Two Way Repeated Measures ANOVA. The markings depict the results of Bonferroni *post hoc* analysis. In **(C)** $p = 0.02$ (*) for genotype; $p = 0.02$ (*) for Hm1a treatment; $p = 0.33$ for the interaction. For **(D)** $p = 0.66$ for genotype; $p = 0.01$ (*) for Hm1a treatment; $p = 0.54$ for the interaction. The stimulation intensities in these experiments were 328 ± 84.6 mA in WT and 1045 ± 259.5 mA in DS ($p = 0.002$, Mann–Whitney test). **(E)** Representative traces of WT and DS SO interneurons in response to a train of 10 stimuli at 1 Hz, delivered to the SC, with or without Hm1a. **(F,G)** The effect of Hm1a on the firing probability of WT and DS SO interneurons **(F)**, and the difference in firing probability calculated for each cell **(G)**. Firing probability was calculated as the number of eAPs divided by 10 (stimuli). Statistical analysis for the data presented in F utilized Two Way Repeated Measures ANOVA. The markings depict the results of Bonferroni *post hoc* analysis: $p = 0.22$ for genotype; $p < 0.0001$ (***) for Hm1a treatment; $p = 0.47$ for the interaction. **(H)** Representative traces of eAPs before and after Hm1a application. **(I)** The effect of Hm1a on the eAP threshold. Statistical analysis utilized Two Way Repeated Measures ANOVA. The markings depict the results of Bonferroni *post hoc* analysis: $p = 0.02$ (*) for genotype; $p < 0.0001$ (***) for Hm1a treatment; $p = 0.18$ for the interaction. **(J)** The difference in eAP threshold. WT: $n = 28$ cells from 11 mice; DS: $n = 23$ cells from 7 mice.

by stimulation of the CA3 SC and relayed by CA1 activation (**Figure 4A**). However, Hm1a increased the firing probability of SO interneurons in WT and DS *Scn1a*$^{A1783V/WT}$ by ∼30% (**Figures 4E–G**). Interestingly, Hm1a also affected the spike timing in DS, causing slight delay, that was only observed in DS SO interneurons (WT: 18.45 ± 0.48 ms, vs. 18.99 ± 0.4 ms after Hm1a, Bonferroni *post hoc* analysis $p = 0.15$; DS: 15.58 ± 0.6 ms vs. 16.86 ± 0.6 ms after Hm1a, $p = 0.006$).

Moreover, despite the more depolarized eAP threshold in DS (**Figures 3F,G**), Hm1a similarly hyperpolarized the eAP threshold in WT and DS (**Figures 4H–J**). Thus, interestingly, despite the lower contribution of Hm1a-sensitive channels to CA1 field response and pyramidal neurons firing in DS *Scn1a*$^{A1783V/WT}$, enhancement of the firing probability of SO interneurons was preserved, suggesting a possible compensatory mechanism within the CA1 microcircuit.

Hm1a Increases the Firing Probability of Stratum-Oriens Interneurons From Dravet Syndrome Mice Harboring the Nonsense *Scn1a*$^{R613X/WT}$ Mutation

As the preserved Hm1a effect in DS *Scn1a*$^{A1783V/WT}$ was surprising, we repeated these experiments in another DS model, harboring the heterozygous nonsense *Scn1a*$^{R613X/WT}$ mutation. Notably, these mice were kept on a mixed 129S1/SvImJ:C57BL/6J genetic background and therefore displayed milder epileptic phenotypes compared to DS *Scn1a*$^{A1783V/WT}$ on the pure

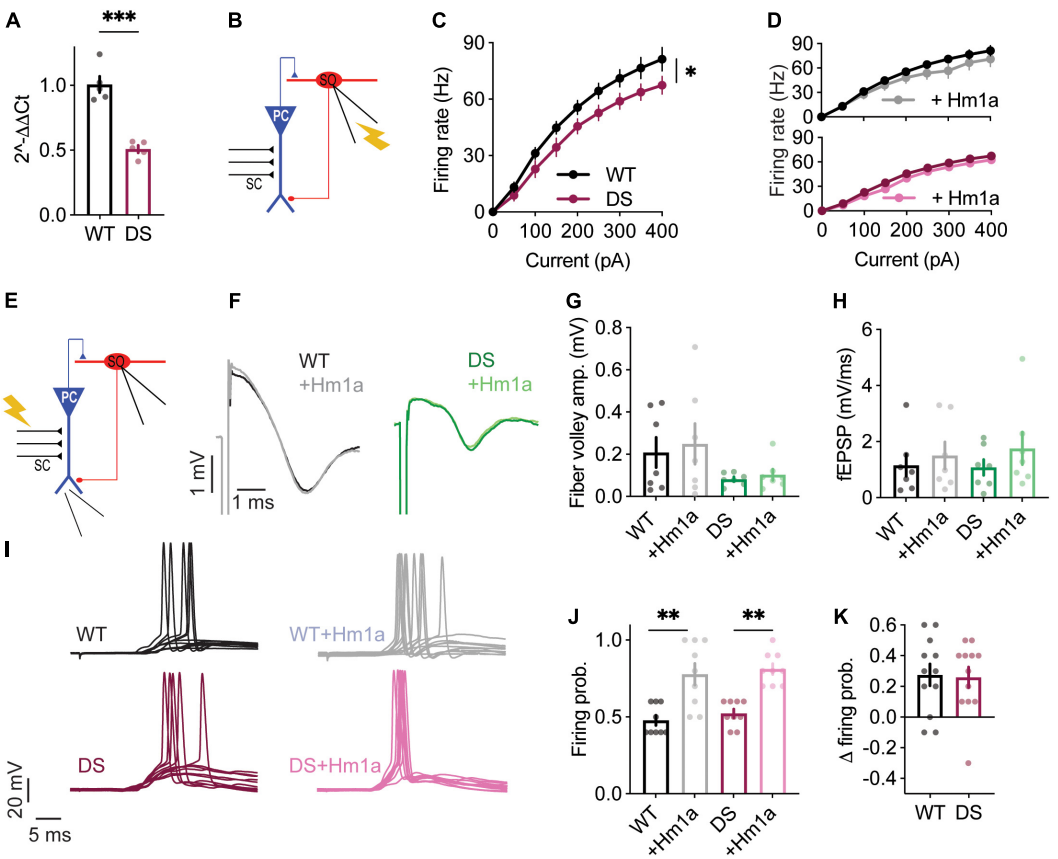

FIGURE 5 | Hm1a increased the firing of DS *Scn1a*$^{R613X/WT}$ SO interneurons following SC stimulation. **(A)** Quantitative real-time PCR analysis of hippocampal *Scn1a* mRNA expression, $n = 5$ in each genotype. Statistical analysis utilized unpaired *t*-test. **(B)** Illustration of the experimental setup used for **(C,D)**. **(C)** Firing frequency in response to depolarizing current injection at the indicated intensities in WT and DS. **(D)** The effect of Hm1a on firing frequencies, in response to current injection through the whole-cell patch electrode in WT and DS mice. Statistical analysis in panels **(C,D)** utilized Mixed Model Repeated Measures ANOVA. **(E)** Illustration of the experimental setup used for **(F–K)**. **(F)** Representative traces of WT (black or gray) and DS (green or pale green) field potentials before and after Hm1a application. **(G,H)** Average fiber volley amplitudes **(G)** and fEPSP **(H)** before and after Hm1a application. Statistical analysis utilized Two Way Repeated Measures ANOVA with Bonferroni *post hoc* analysis. In **(G)** $p = 0.12$ for genotype; $p = 0.35$ for Hm1a treatment; $p = 0.76$ for the interaction. For **(H)** $p = 0.88$ for genotype; $p = 0.06$ for Hm1a treatment; $p = 0.51$ for the interaction. The stimulation intensities in these experiments were 394 ± 68.7 mA in WT and 160 ± 48 mA in DS ($p = 0.014$, Mann–Whitney test). **(I)** Representative traces of WT and DS SO interneurons in response to a train of 10 stimuli at 1 Hz, delivered to the SC, with or without Hm1a. **(J,K)** The effect of Hm1a on the firing probability of WT and DS SO interneurons **(J)**, and the difference in firing probability calculated for each cell **(K)**. Firing probability was calculated as the number of eAPs divided by 10 (stimuli). Statistical analysis utilized Two Way Repeated Measures ANOVA. The markings depict the results of Bonferroni *post hoc* analysis: $p = 0.28$ for genotype; $p < 0.0001$ (***) for Hm1a treatment; $p = 0.91$ for the interaction. In these experiments Hm1a had a tendency towards hyperpolarization of the eAP threshold (WT: –46.19 ± 1 vs. –47.6 ± 1.4 after Hm1a; DS: –43.65 ± 1 vs. –46.1 ± 2.6 after Hm1a). WT: $n = 9$ cells from 4 mice; DS: $n = 10$ cells from 4 mice.

C57BL/6J background (Yu et al., 2006; Miller et al., 2014; Mistry et al., 2014; Rubinstein et al., 2015b).

Quantitative real-time PCR analysis confirmed the expected reduction in *Scn1a* mRNA expression in the hippocampus (**Figure 5A**), as well as reduced firing rates of SO interneurons from *Scn1a*$^{R613X/WT}$ DS mice in response to prolonged injection of depolarizing current (**Figures 5B,C**). Similar to our data with DS *Scn1a*$^{A1783V/WT}$, Hm1a did not affect the firing rates of *Scn1a*$^{R613X/WT}$ SO interneurons following prolonged current injections (**Figure 5D**).

Next, we tested the effect of Hm1a following stimulation of the CA3 SC, with concomitant CA1 field potential recordings and whole cell recordings of SO interneurons (**Figure 5E**). In these DS mice, Hm1a had no effect on synaptic responses of CA1 excitatory neurons (**Figures 5F–H**), and a tendency toward hyperpolarization of the eAP threshold, but with no statistical effect, in either genotype (WT: −46.19 ± 1 vs. −47.6 ± 1.4 after Hm1a; DS: −43.65 ± 1 vs. −46.1 ± 2.6 after Hm1a). Nevertheless, Hm1a application significantly increased the firing probability of SO interneurons in both WT and DS *Scn1a*$^{R613X/WT}$ by ∼30% (**Figures 5I–K**), resembling the increase we observed in DS *Scn1a*$^{A1783V/WT}$ (**Figures 4E–G**).

Genetic background greatly affects the severity of the epileptic phenotypes and the function of excitatory and inhibitory neurons (Mistry et al., 2014; Rubinstein et al., 2015b). Therefore, while additional studies are needed for thorough characterization of the epileptic phenotypes of DS *Scn1a*$^{R613X/WT}$, variations in the extent of Hm1a effect on CA1 field response and eAP threshold may be related to the mixed 129S1/SvImJ:C57BL/6J background of these mice. Nevertheless, these data demonstrate that the application of Hm1a comparably increases the firing of SO interneurons from WT mice as well as DS mice harboring the nonsense *Scn1a*^{R613X} or missense *Scn1a*^{A1783V} mutation.

Reduced Excitation and Inhibition Onto CA1 Pyramidal Neurons of Dravet Syndrome *Scn1a*$^{A1783V/WT}$ Mice

Higher fiber volley amplitudes were observed in DS *Scn1a*$^{A1783V/WT}$, while the fEPSP was similar in both genotypes (**Figures 3C–E,H**). These properties may result from alterations in excitatory synaptic transmission within the CA3-CA1 axis by reduced neurotransmitter release from CA3 terminals, inhibited CA1 pyramidal neurons postsynaptic response, or changes in the ratio between excitation and inhibition. To further examine the properties of CA3 release, we used the paired pulse ratio (PPR) protocol (Zucker and Regehr, 2002). For each postsynaptic CA1 neuron, we first measured the stimulation strength needed to produce firing probability of 50% (1X, under current clamp), and used half of this stimulation (0.5X) to record the PPR responses. The EPSCs and PPR were similar between WT and DS mice, suggesting similar presynaptic properties (**Figures 6A–D**). Next, to examine the processing of synaptic excitation by CA1 neurons, we switched to current-clamp mode and measured the change in voltage in response to SC stimulation at 30 Hz. These recordings also demonstrated comparable postsynaptic CA1 responses, with an overall similar depolarization with each stimulus in both WT and DS neurons (**Figures 6E–G**), suggesting similar processing of excitatory inputs.

In addition, we examined the properties of EPSCs and inhibitory post-synaptic currents (IPSCs), and the balance between them. In this protocol, we measured the minimal stimulation required to evoke a measurable response (1xEθ, EPSCs or IPSCs), followed by increasing the stimulation intensity up to 2.5-fold of the initial minimal intensity (1–2.5×Eθ). Notably, in this protocol stimulation intensity is normalized to the minimal response, in contrast to the measurements of PPR or synaptic depolarization, in which the stimulation was stronger and normalized to suprathreshold stimulation, leading to the firing probability of 50%. Therefore, these different stimulation regimens enable to examine a wide spectrum of synaptic stimulations. As expected, the amplitude of the minimal response was similar between DS *Scn1a*$^{A1783V/WT}$ and WT. Conversely, with increasing stimulation strength, the EPSCs and IPSCs amplitudes were lower in DS (**Figures 6H–J**), indicating reduced synaptic conductance in DS. The ratio between excitation and inhibition was shown to be increased in DS (Han et al., 2012; Rubinstein et al., 2015a). In accordance, the calculation of the ratio between excitatory and inhibitory currents (E/I balance), demonstrated enhanced excitation in DS, indicating that despite an overall reduction in synaptic conductances, the inhibition was further reduced (**Figure 6K**). Together, our data demonstrate reduced synaptic currents in the CA3-CA1 synapse. While reduced synaptic excitation correlates with larger fiber volley amplitudes measured in DS *Scn1a*$^{A1783V/WT}$ CA1 neurons (**Figures 3C–E,H**), increased E/I balance is in line with previous studies of DS mice (Mantegazza and Broccoli, 2019).

Reduced Facilitation in the CA1-SO Synapse in Dravet Syndrome *Scn1a*$^{A1783V/WT}$ Mice

Similar firing of WT and DS SO interneurons, under CA3 stimulation, may also stem from altered synaptic communication in the CA1-SO axis, such as changes in release probability, processing of synaptic depolarization or E/I balance. First, we examined the PPR of the CA1-SO synapse. The stimulation strength was set to 0.5X, as we did in the CA3-CA1 analysis. Examination of the PPR demonstrated greater facilitation in WT compared to DS *Scn1a*$^{A1783V/WT}$ SO interneurons, indicating higher release probability in the first pulse in DS (**Figures 7A–D**). Next, we tested the postsynaptic SO interneurons depolarization in response to a train of alveus stimulations, at 30 Hz. These recordings showed an incremental and persistent depolarization increase with each stimulation in WT (**Figures 7E–G**). Conversely, in DS *Scn1a*$^{A1783V/WT}$, an increase in the depolarization was evident only following the first stimulus, with subsequent trains resulting in no significant increments (**Figures 7E–G**). These data are consistent with higher initial release probability in the first stimulation in DS with reduced facilitation in subsequent stimulations. Additionally, we measured the amplitudes of evoked EPSCs and IPSCs and E/I balance. In contrast to the changes observed in CA1 pyramidal neurons, SO interneurons demonstrated no difference between

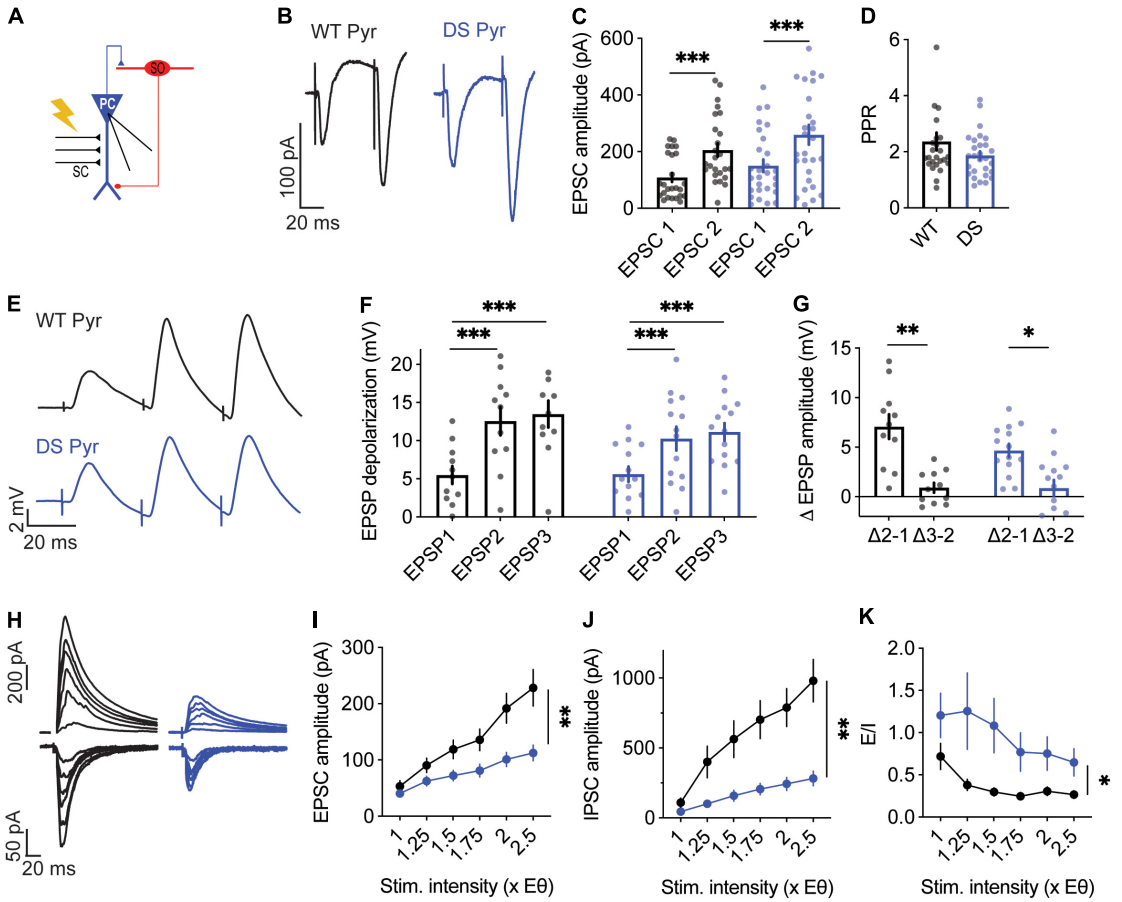

FIGURE 6 | Altered excitatory and inhibitory synaptic currents in DS *Scn1a*$^{A1783V/WT}$ CA1 pyramidal neurons. **(A)** Illustration of the stimulation setup. The stimulating electrode was placed on the CA3 SC while the CA1 pyramidal neurons were measured using whole-cell patch clamp. **(B)** Representative traces of WT (black) and DS (blue) paired-pulse responses. **(C)** Average EPSC amplitudes of the 1st and 2nd stimuli that were given within 50 ms. Statistical analysis utilized Two Way repeated measures ANOVA. The markings depict the results of Bonferroni *post hoc* analysis: $p = 0.167$ for genotype; $p < 0.0001$ (***) for the EPSC number; and $p = 0.62$ for the interaction. **(D)** Paired-pulse ratio (EPSP2/EPSP1). Statistical analysis utilized the Mann–Whitney test. WT: $n = 13$ cells from 4 mice, DS: $n = 13$ cells from 3 mice. **(E)** Representative EPSPs in WT and DS CA1 pyramidal neurons in response to a train of stimuli at 30 Hz. **(F)** EPSP amplitude at each of the three stimuli. Statistical analysis utilized Two Way Repeated Measures ANOVA. The markings depict the results of Bonferroni *post hoc* analysis: $p = 0.43$ for genotype; $p < 0.001$ (***) for the EPSP number; $p = 0.07$ for the interaction. **(G)** The added depolarization of each EPSP. Statistical analysis utilized Two Way Repeated Measures ANOVA. The markings depict the results of Bonferroni *post hoc* analysis: $p = 0.052$ for genotype; $p < 0.001$ (***) for the EPSP number; $p = 0.25$ for the interaction. WT: $n = 13$ cells from 4 mice; DS: $n = 13$ cells from 3 mice. **(H–J)** Representative traces **(H)**, average EPSCs **(I)** and IPSCs **(J)** evoked by SC stimulation at different stimulation intensities from WT and DS mice. EPSCs were measured at a holding potential –60 mV, and IPSCs were measured at 0 mV. Statistical analysis utilized Two Way Repeated Measures ANOVA. For the EPSCs: $p = 0.009$ (**) for genotype; $p < 0.001$ (***) for the interaction; for the IPSCs: $p = 0.001$ (**) for genotype; $p < 0.001$ (***) for the interaction. **(K)** E/I ratio. Statistical analysis utilized Mixed Model Repeated Measures ANOVA: $p = 0.01$ (*) for genotype; $p = 0.001$ (**) for the stimulation intensity; $p = 0.3$ for the interaction. WT: $n = 15$ cells from 3 mice; DS: $n = 13$ cells from 3 mice.

WT and DS *Scn1a*$^{A1783V/WT}$ (**Figures 7H–K**). Together, lower PPR and synaptic depolarization in DS suggest higher release probability of CA1 pyramidal neurons. These properties may be related to the ability of SO interneurons to preserve their firing within the CA1 microcircuit, despite their reduced excitability.

DISCUSSION

The prevailing hypothesis for Dravet syndrome neuropathology suggests that its root cause lies with loss of function of $Na_V1.1$, leading to dysfunction of multiple types of inhibitory neurons (Mantegazza and Broccoli, 2019). However, spontaneous firing rates of interneurons *in vivo* were not reduced (De Stasi et al., 2016; Tran et al., 2020). Moreover, in brain slices reduced inhibition was not observed in older mice, indicating homeostatic neuronal changes (Favero et al., 2018). Unexpectedly, while characterizing the functional effect in response to the application of Hm1a, we saw that despite hypo-excitability of DS *Scn1a*$^{A1783V/WT}$ and *Scn1a*$^{R613X/WT}$ SO interneurons, their response to Hm1a was preserved. Moreover, using synaptically evoked activity measurements in the hippocampal CA1 microcircuit, we demonstrate DS-related neuronal changes consistent with synaptic alterations in both

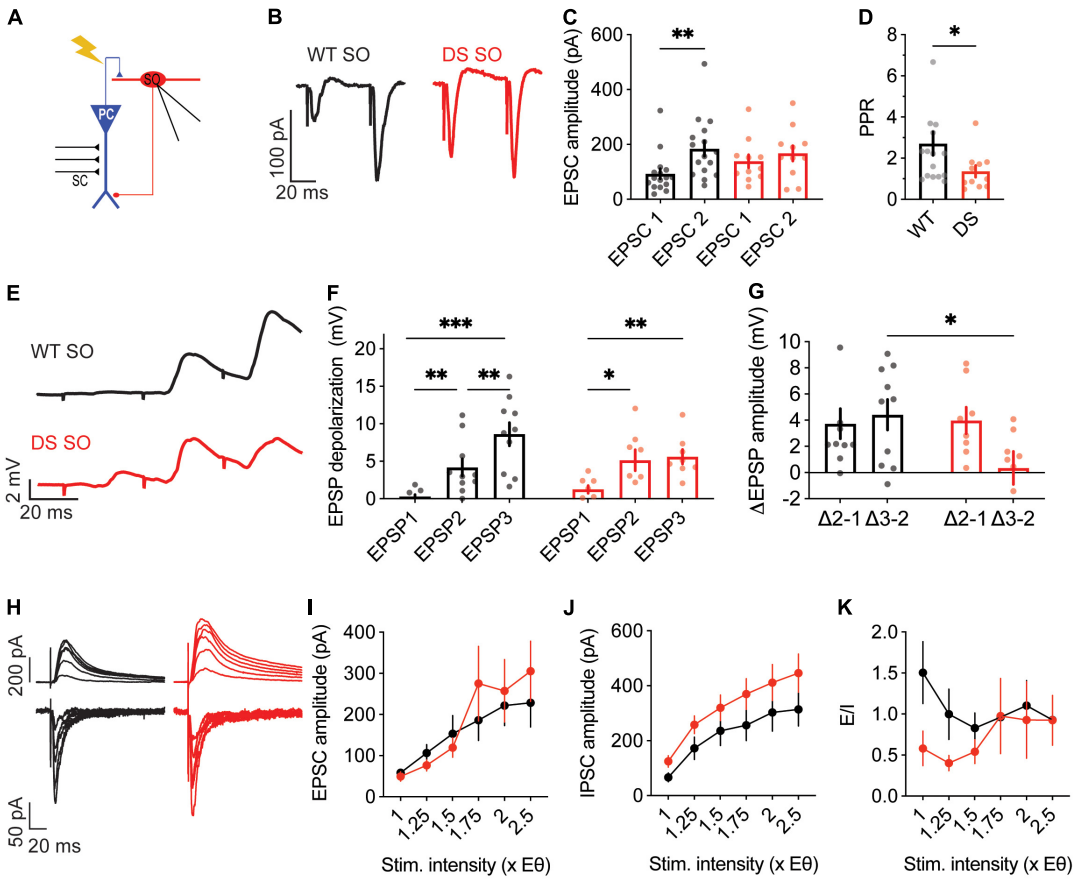

FIGURE 7 | Reduced paired pulse facilitation, with normal excitatory and inhibitory synaptic currents, in DS *Scn1a*$^{A1783V/WT}$ SO interneurons. **(A)** Illustration of the experimental setup. Synaptic activation of SO interneurons was triggered by stimulation of the alveus. **(B)** Representative traces of WT (black) and DS (red) paired-pulse responses. **(C)** Average EPSC amplitudes of the 1st and 2nd stimuli that were given within 50 ms. Statistical analysis utilized Two Way Repeated Measures ANOVA. The markings depict the results of Bonferroni *post hoc* analysis: $p = 0.62$ for genotype, $p = 0.01$ (*) for the EPSC number, $p = 0.16$ for the interaction. **(D)** Paired-pulse ratio (EPSP2/EPSP1). Statistical analysis utilized the Mann–Whitney test. WT: $n = 17$ cells from 5 mice; DS: $n = 11$ cells from 4 mice. **(E)** Representative EPSPs in WT and DS SO interneurons in response to a train of stimuli at 30 Hz. **(F)** EPSP amplitude at each of the three stimuli. Statistical analysis utilized Two Way Repeated Measures ANOVA. The markings depict the results of Bonferroni *post hoc* analysis: $p = 0.75$ for genotype; $p < 0.001$ (***) for the EPSP number, $p = 0.052$ for the interaction. **(G)** The added depolarization of each EPSPs. Statistical analysis utilized Two Way Repeated Measures ANOVA. The markings depict the results of Bonferroni *post hoc* analysis: $p = 0.07$ for genotype; $p = 0.28$ for the EPSP added depolarization; $p = 0.12$ for the interaction. WT: $n = 10$ cells from 6 mice; DS: $n = 9$ cell from 5 mice. **(H–J)** Representative traces **(H)** and average EPSCs **(I)** and IPSCs **(J)** evoked by alveus stimulation at different stimulation intensities from WT and DS mice. EPSCs were measured at a holding potential –60 mV, and IPSCs were measured at 0 mV. Statistical analysis utilized Two Way Repeated Measures ANOVA. For the EPSCs: $p = 0.7$ for genotype; $p = 0.4$ for the interaction; for the IPSCs: $p = 0.15$ for genotype; $p = 0.68$ for the interaction. **(K)** E/I ratio. Statistical analysis utilized Mixed Model Repeated Measures ANOVA: $p = 0.1$ for genotype; $p = 0.3$ for the stimulation intensity; $p = 0.51$ for the interaction. WT: $n = 12$ cells from 3 mice; DS: $n = 11$ cells from 3 mice.

CA1 pyramidal neurons and SO interneurons. Together, these results suggest neuronal alterations within the CA1 circuit, that may not be limited to loss of function of $Na_V1.1$.

The Interplay Between Stratum-Oriens Interneurons Hypo-Excitability and $Na_V1.1$ Function in Dravet Syndrome

Similar to previous studies (Catterall, 2018), we also observed reduced excitability of SO interneurons in DS *Scn1a*$^{A1783V/WT}$, with elevated threshold for AP (**Figures 1G**, **3F,G**) and reduced firing in response to prolonged current injections (**Figures 1B,C**). Mechanistically, hypo-excitability of inhibitory neurons in DS was assumed to be related to reduced function of $Na_V1.1$, because of the Dravet associated *Scn1a* haploinsufficiency. However, if indeed interneurons in DS mice have reduced activity of $Na_V1.1$ channels, their response to Hm1a application is expected to be smaller. Surprisingly, WT and DS *Scn1a*$^{A1783V/WT}$ had comparable response to Hm1a, with hyperpolarization of the threshold for APs (**Figures 1**, **4**), and an increase in their firing probability (**Figures 4E–G**). Moreover, while before the application of Hm1a there was a statistical difference between WT and DS, the effect of Hm1a on the threshold for AP was slightly larger in DS *Scn1a*$^{A1783V/WT}$, causing these differences to dissipate in its presence (**Figures 1G,H**, **4I,J**). Hence, despite the DS associated *Scn1a* loss of function mutation, and the

characteristic DS-associated interneurons hypo-excitability, there is a similar functional expression of Hm1a-sensitive sodium channels in both genotypes.

One possible explanation for these unexpected results is that the model used here, harboring the A1783V missense mutation in the *Scn1a* gene, causes Dravet by a different mechanism, that does not involve reduced activity of $Na_V1.1$. We deem this possibility less likely because: (i) similar preserved Hm1a effect on firing probability was observed in DS mice harboring the $Scn1a^{R613X}$ nonsense mutation, despite reduction in the mRNA levels of *Scn1a* (**Figure 5**); (ii) the phenotypes of these DS $Scn1a^{A1783V/WT}$ mice are the same as those of other models of DS that are based on truncation mutations of the *Scn1a* gene, including the presentation of Dravet associated epileptic and non-epileptic comorbidities, as well as the time course of the disease (Ricobaraza et al., 2019; Fadila et al., 2020; Almog et al., 2021; Miljanovic et al., 2021; Pernici et al., 2021); (iii) the $SCN1A^{A1783V}$ confers loss of function of $Na_V1.1$ channels via a right shift of the voltage dependency of activation, as well as left shift of the slow inactivation, resulting in *SCN1A* haploinsufficiency (Layer et al., 2021); (iv) similar to other DS mouse models, $Scn1a^{A1783V/WT}$ mice feature reduced excitability of multiple types of inhibitory neurons (Kuo et al., 2019; Almog et al., 2021; Layer et al., 2021); (v) the deficits we observed in the activity of SO interneurons were almost identical to those found in another DS model, harboring a truncation mutation in the *Scn1a* gene (Rubinstein et al., 2015b; Almog et al., 2021).

In accordance with our data, Richards et al. (2018) reported that Hm1a had an effect on interneurons from DS mice harboring the $Scn1a^{R1407X}$ truncation mutation, but not in WT mice. These DS mice were shown to express lower levels of $Na_V1.1$ (Ogiwara et al., 2007), and are therefore expected to have a smaller response to Hm1a application. Nevertheless, focusing on CA1 stratum radiatum interneurons, Richards et al. (2018) demonstrated that although Hm1a did not affect the firing rates or peak amplitude of AP in WT neurons, it rescued the AP firing deficit and prevented the attenuated spike height accommodation in DS $Scn1a^{R1407X}$. Thus, these data from DS $Scn1a^{R1407X}$ mice further support our conclusion that despite interneuron hypo-excitability in DS, the response to Hm1a is not reduced. Interestingly, studies that utilized measurements of sodium currents in dissociated neurons or nucleated patches also reported similar sodium current densities in WT and DS neurons at this age group (at seizure onset) (Hedrich et al., 2014; Rubinstein et al., 2015b). Of note, other studies that examined the functional effect of Hm1a did not provide a direct comparison between the genotypes and reported on either DS (Goff and Goldberg, 2019; Mattis et al., 2021) or WT (Chever et al., 2021) interneurons.

Another possible explanation for the lack of differences in the Hm1a impact on WT and DS SO interneurons, is that different Hm1a-sensitive sodium channel(s) repertoire is expressed in each genotype. Moreover, while Hm1a is relatively selective for $Na_V1.1$, at 50 nM there might be some modulation of additional Na_V channels (Osteen et al., 2016; Richards et al., 2018; Chever et al., 2021). One candidate is $Na_V1.3$, which also displays a relatively high affinity to Hm1a (Osteen et al., 2016; Richards et al., 2018), and was suggested to be upregulated in DS mice (Yu et al., 2006). Therefore, it is possible that the upregulation of $Na_V1.3$ in DS masks the loss of function of $Na_V1.1$, mediating the response to Hm1a. Hippocampal single cells RNA-seq data of juvenile mice (P26–35) showed that the predominate Na_V channel in SO interneurons is *Scn1a*, with an expression of ∼180 Fragments Per Kilobase Million (FPKM), in contrast to *Scn2a* (∼80 FPKM), *Scn3a* (∼8 FPKM), and *Scn8a* (∼40 FPKM) (Cembrowski et al., 2016). Thus, with these expression levels, $Na_V1.3$ should be significantly upregulated to mediate comparable responses to Hm1a. However, while immunohistological analysis indicated a dramatic increase in $Na_V1.3$ expression (Yu et al., 2006), RNA-seq and proteomic analysis of hippocampi from DS mice did not show substantial upregulation of any Na_V subtype, including $Na_V1.3$ (Hawkins et al., 2019; Miljanovic et al., 2021).

In addition to its effect on voltage gated sodium channels, Hm1a can also inhibit voltage gated potassium channels. However, the affinity to potassium channels was reported to be lower, with ∼20% inhibition of $K_V2.1$ and $K_V2.2$ at 100 nM (Escoubas et al., 2002), and ∼40% inhibition of K_V4 channels (Escoubas et al., 2002) and ∼10% inhibition of $K_V11.1$ (hERG) (Richards et al., 2018) by 300 nM. Thus, at 50 nM, the Hm1a concentration used here, this toxin is expected to be relatively selective for sodium channels. Nevertheless, as these specificity and affinity studies were performed in expression systems, and these parameters may differ in brain slices, we cannot exclude the possible contribution of weak inhibition of potassium channels to the observed preservation of the Hm1a response in DS interneurons.

Furthermore, as our results are based on stimulations at low frequency (1 Hz), it remains to be determined if stimulation at higher frequencies can expose additional neuronal alterations in DS that can be directly correlated with loss of function of $Na_V1.1$.

Together, we demonstrate that the functional effect of Hm1a was preserved in two DS models, harboring a missense or a nonsense mutation in the *Scn1a* gene, despite reduced excitability of SO interneurons. Based on these observations, we propose that during epileptogenesis, genetic *Scn1a* mutations, that cause reduced activity of $Na_V1.1$, trigger additional complex neuronal changes that eventually lead to the apparent and unexpected, preserved functional response to Hm1a. Indeed, DS-related dysregulations of voltage-gated potassium and calcium channels were reported before (Goff and Goldberg, 2019; Ritter-Makinson et al., 2019; Miljanovic et al., 2021), indicating the involvement of multiple ion channels in Dravet pathophysiology.

CA1 Pyramidal Neurons of Dravet Syndrome $Scn1a^{A1783V/WT}$ Mice Demonstrate Reduced Effect of Hm1a

The role of excitatory neurons in DS pathophysiology is debated. While the firing of these neurons in brain slices is mostly unaltered in DS (Yu et al., 2006; Tai et al., 2014; Rubinstein et al., 2015b; De Stasi et al., 2016), others have reported changes in firing or dendritic arborization (Mistry et al., 2014; Tsai et al., 2015; Salgueiro-Pereira et al., 2019; Almog et al., 2021). Similar to previous reports (Richards et al., 2018; Chever et al., 2021),

our data also demonstrate that, when firing was evoked by direct injection of depolarizing currents through the patch pipette, Hm1a application did not affect the firing rates of CA1 excitatory neurons (**Figures 2A–D**). In contrast, diverse effects of Hm1a were observed in response to synaptic stimulation, in which excitatory inputs are received and processed by the dendrites. Interestingly, when the firing was evoked by stimulation of the SC, Hm1a application increased the firing probability of CA1 pyramidal neurons (**Figures 2H–K**), reduced the threshold voltage for eAP (**Figures 2L,M**) and augmented the CA1 fEPSP in WT neurons (**Figures 4B–D**). These Hm1a induced changes indicate the contribution of $Na_V1.1$ channels to the amplification of synaptic inputs in CA1 pyramidal neurons (Stuart and Sakmann, 1995; Fricker and Miles, 2000; González-Burgos and Barrionuevo, 2001). Contrariwise, these Hm1a effects were absent in DS mice (**Figures 2H–M**, **4B–D**), indicating reduced functional expression of dendritic Hm1a-sensitive sodium channels in DS mice.

The RNA-seq data of WT juvenile mice indicated abundant expression of $Na_V1.2$ and $Na_V1.6$ in these neurons (*Scn2a*: ∼120 FPKM; *Scn8a*: ∼90 FPKM), low expression of $Na_V1.3$ (*Scn3a*: ∼11 FPKM), and intermediate expression of $Na_V1.1$ (*Scn1a*: ∼40 FPKM, 4.5-fold lower compared to their expression in SO interneurons) (Cembrowski et al., 2016). While $Na_V1.6$ and $Na_V1.2$ are the predominant sodium channels found in the AIS (Hu et al., 2009; Lorincz and Nusser, 2010; Katz et al., 2018), and $Na_V1.2$ are the primary dendritic sodium channels (Spratt et al., 2021), the spatial expression of $Na_V1.1$ in these cells remains poorly defined, with evidence supporting somato-dendritic expression (Westenbroek et al., 1989; Yu et al., 2006). Since Hm1a shows some activity also toward $Na_V1.2$ channels (Chever et al., 2021), and due to the high dendritic expression of these channels in CA1 pyramidal neurons (Cembrowski et al., 2016), we cannot exclude the possibility that the reduced effect of Hm1a in DS *Scn1a*$^{A1783V/WT}$ is governed by alterations in the functional expression of $Na_V1.1$ and $Na_V1.2$ (**Figures 2**, **4A–D**). Nevertheless, while reduced activity of $Na_V1.1$ can be directly linked to the DS-associated *Scn1a*^{A1783V} mutation, the molecular mechanisms that may lead to DS-related reduction in the expression levels of $Na_V1.2$ remain to be determined. Together, these data indicate that excitatory neurons of DS *Scn1a*$^{A1783V/WT}$ mice display divergent expression of Hm1a-sensitive channels, highlighting alterations in Na_V functions in these cells.

Preserved Firing Probability of Stratum-Oriens Interneurons Within the CA1 Microcircuit

Dravet syndrome associated seizures and age-dependent homeostatic changes, extending beyond the loss of function of $Na_V1.1$, were reported before. These included developmental changes and correction of the hypo-excitability of cortical inhibitory neurons (Favero et al., 2018), age-dependent changes in the activity of hippocampal inhibitory and excitatory neurons (Almog et al., 2021), seizure-induced hyper-excitability of dentate gyrus granule cells (Salgueiro-Pereira et al., 2019), as well as maturation related changes in field potential paired-pulse facilitation (Liautard et al., 2013).

Our data add additional findings that indicate reduced synaptic strength between CA3 and CA1 (**Figures 3C–E,H**). Specifically, we observed that increased fiber volley amplitudes were needed to produce comparable fEPSP (**Figures 3C–E,H**). Moreover, we show reduced synaptic conductances in CA1 pyramidal neurons from DS mice (**Figures 6H–J**). While $Na_V1.1$ haploinsufficiency may contribute to reduced boosting of incoming EPSPs (Stuart and Sakmann, 1995; Fricker and Miles, 2000; González-Burgos and Barrionuevo, 2001; Carter et al., 2012), reduced excitatory and inhibitory conductances are probably related to reduced connectivity or lower expression of synaptic receptors. Interestingly, a recent comparative proteomic analysis of hippocampal cells from DS mice demonstrated wide expressional changes, with variations in multiple types of proteins involved in excitatory and inhibitory synaptic transmissions, including lower levels of glutamate and GABA receptors (Miljanovic et al., 2021). Moreover, reduced synaptic conductances were reported in multiple mouse models of autism, and were suggested to be related to homeostatic synaptic changes (Antoine et al., 2019).

Based on these deficits in the CA3-CA1 synapse and SO excitability, we hypothesized an additive reduction in the firing probability of SO interneurons in response to SC stimulation. Nevertheless, surprisingly, the firing probability of SO interneurons was unaltered in DS *Scn1a*$^{A1783V/WT}$, along a range of CA3 stimulation intensities (**Figures 3I,J**). This preserved firing may be related to synaptic changes that we observed in the CA1-SO synapse, including lower PPR, indicating higher initial release probability from CA1 terminals, as well as the lack of change in the synaptic conductances onto the SO interneurons (**Figure 7**).

Despite these unexpected data, reduced inhibition in DS was demonstrated to be related to the pathophysiology, and was also demonstrated here (**Figures 1**, **3–6**). Indeed, selective genetic perturbation of the *Scn1a* gene in interneurons was sufficient to recapitulate key pathophysiological features of Dravet in mice (Cheah et al., 2012; Ogiwara et al., 2013; Rubinstein et al., 2015a; Tatsukawa et al., 2018; Kuo et al., 2019). Moreover, the overall frequency of inhibitory inputs onto CA1 neurons was shown to be reduced in DS (Han et al., 2012; Liautard et al., 2013; Almog et al., 2021). Furthermore, our data also demonstrate increased E/I balance within the CA1 microcircuit (**Figure 6K**). Nevertheless, rather than reduced firing probability, disinhibition may be related to a reduction in synaptic inhibitory connections onto pyramidal neurons, reduced number of interneurons (Dyment et al., 2020), reduced expression of $GABA_AR$ (Miljanovic et al., 2021), or alterations in the reversal potential of $GABA_AR$ (Yuan et al., 2019). Moreover, it is possible that SO interneurons can preserve normal firing when stimulated at 1 Hz but would fail at high frequencies. Indeed, several studies demonstrated that DS interneurons can preserve firing at low frequencies (Yu et al., 2006; Hedrich et al., 2014; Favero et al., 2018; Lemaire et al., 2021). Furthermore, while we focused on the activity of SO interneurons (**Figure 3**), reduced firing of parvalbumin (PV) positive interneurons governs the observed deficits in the E/I balance. Over 80% of SO interneurons are somatostatin (SST)

positive O-LM cells (Tricoire et al., 2011; Winterer et al., 2019; Almog et al., 2021). Studies of conditional mice with selective deletion of the *Scn1a* gene in PV or SST interneurons showed that loss of function of *Scn1a* in PV neurons results in more severe phenotypes compared to selective deletion in SST neurons (Rubinstein et al., 2015a; Tatsukawa et al., 2018). However, deletion in both types of interneurons had a more profound effect (Rubinstein et al., 2015a). Thus, while DS epilepsy involves inhibitory neuron dysfunctions, the neuronal mechanism may be more complex than reduced firing probability.

CONCLUSION

In conclusion, our data reveal synaptic and excitability alterations in both CA1 excitatory neurons and CA1 SO interneurons in DS mice, supporting global homeostatic changes within the CA1 microcircuit that may partially compensate for the DS-related interneurons hypo-excitability.

DATA AVAILABILITY STATEMENT

The raw data supporting the conclusions of this article will be made available by the authors, without undue reservation.

ETHICS STATEMENT

The animal study was reviewed and approved by the Animal Care and Use Committee (IACUC) of Tel Aviv University.

AUTHOR CONTRIBUTIONS

YA and MR conceived and designed the experiments, analyzed the data, and wrote the manuscript. YA, AM, and MB performed the experiments. All authors contributed to the article and approved the submitted version.

FUNDING

This study was supported by the Israel Science Foundation (grant 1454/17, MR). Support also came from ERA-NET E-Rare (grant CureDravet, MR), the National Institute for Psychobiology in Israel (MR), Fritz Thyssen Stiftung (grant 1659 10.17.1.023MN, MR), Fundación Síndrome de Dravet (Dravet Syndrome Foundation Spain, MR), Dravet Syndrome Foundation (MR), and the Claire and Amedee Maratier Institute for the Study of Blindness and Visual Disorders, Sackler Faculty of Medicine, Tel-Aviv University (MR). Support for open access publication was provided by Fundación Síndrome de Dravet (Dravet Syndrome Foundation Spain, grant number FSD-OASP-XI-IV).

ACKNOWLEDGMENTS

This work was performed in partial fulfillment of the requirements for a Ph.D. degree of YA, Sackler Faculty of Medicine, Tel Aviv University, Israel. We thank Haitin Y. and Giladi M. for helpful discussions and critical reading of the manuscript.

SUPPLEMENTARY MATERIAL

The Supplementary Material for this article can be found online at: https://www.frontiersin.org/articles/10.3389/fnmol.2022.823640/full#supplementary-material

REFERENCES

Almog, Y., Fadila, S., Brusel, M., Mavashov, A., Anderson, K., and Rubinstein, M. (2021). Developmental alterations in firing properties of hippocampal CA1 inhibitory and excitatory neurons in a mouse model of Dravet syndrome. *Neurobiol. Dis.* 148:105209. doi: 10.1016/j.nbd.2020.105209

Antoine, M. W., Langberg, T., Schnepel, P., and Feldman, D. E. (2019). Increased excitation-inhibition ratio stabilizes synapse and circuit excitability in four autism mouse models. *Neuron* 101, 648.e4–661.e4. doi: 10.1016/j.neuron.2018.12.026

Carter, B. C., Giessel, A. J., Sabatini, B. L., and Bean, B. P. (2012). Transient sodium current at subthreshold voltages: activation by EPSP waveforms. *Neuron* 75, 1081–1093. doi: 10.1016/j.neuron.2012.08.033

Catterall, W. A. (2018). Dravet syndrome: a sodium channel interneuronopathy. *Curr. Opin. Physiol.* 2, 42–50. doi: 10.1016/j.cophys.2017.12.007

Catterall, W. A., Kalume, F., and Oakley, J. C. (2010). $Na_V1.1$ channels and epilepsy. *J. Physiol.* 588, 1849–1859. doi: 10.1113/jphysiol.2010.187484

Cembrowski, M. S., Wang, L., Sugino, K., Shields, B. C., and Spruston, N. (2016). Hipposeq: a comprehensive RNA-seq database of gene expression in hippocampal principal neurons. *Elife* 5:e14997. doi: 10.7554/eLife.14997

Cheah, C. S., Lundstrom, B. N., Catteral, W. A., and Oakley, J. C. (2019). Impairment of sharp-wave ripples in a murine model of Dravet syndrome. *J. Neurosci.* 39, 9251–9260. doi: 10.1523/JNEUROSCI.0890-19.2019

Cheah, C. S., Yu, F. H., Westenbroek, R. E., Kalume, F. K., Oakley, J. C., Potter, G. B., et al. (2012). Specific deletion of $Na_V1.1$ sodium channels in inhibitory interneurons causes seizures and premature death in a mouse model of Dravet syndrome. *Proc. Natl. Acad. Sci.* 109, 14646–14651. doi: 10.1073/pnas.1211591109

Chever, O., Zerimech, S., Scalmani, P., Lemaire, L., Pizzamiglio, L., Loucif, A., et al. (2021). Initiation of migraine-related cortical spreading depolarization by hyperactivity of GABAergic neurons and $Na_V1.1$ channels. *J. Clin. Invest.* 131:e142203. doi: 10.1172/jci142203

Claes, L., Del-Favero, J., Ceulemans, B., Lagae, L., Van Broeckhoven, C., and De Jonghe, P. (2001). De novo mutations in the sodium-channel gene *SCN1A* cause severe myoclonic epilepsy of infancy. *Am. J. Hum. Genet.* 68, 1327–1332. doi: 10.1086/320609

De Stasi, A. M., Farisello, P., Marcon, I., Cavallari, S., Forli, A., Vecchia, D., et al. (2016). Unaltered network activity and interneuronal firing during spontaneous cortical dynamics *in vivo* in a mouse model of severe myoclonic epilepsy of infancy. *Cereb. Cortex* 26, 1778–1794. doi: 10.1093/cercor/bhw002

Dravet, C. (2011). The core Dravet syndrome phenotype. *Epilepsia* 52, 3–9. doi: 10.1111/j.1528-1167.2011.02994.x

Dravet, C., and Oguni, H. (2013). Dravet syndrome (severe myoclonic epilepsy in infancy). *Handb. Clin. Neurol.* 111, 627–633. doi: 10.1016/B978-0-444-52891-9.00065-8

Dyment, D. A., Schock, S. C., Deloughery, K., Tran, M. H., Ure, K., Nutter, L. M. J., et al. (2020). Electrophysiological alterations of pyramidal cells and interneurons of the CA1 region of the hippocampus in a novel mouse model of Dravet syndrome. *Genetics* 215, 1055–1066. doi: 10.1534/genetics.120.303399

Escoubas, P., Diochot, S., Célérier, M. L., Nakajima, T., and Lazdunski, M. (2002). Novel Tarantula toxins for subtypes of voltage-dependent potassium channels in the Kv2 and Kv4 subfamilies. *Mol. Pharmacol.* 62, 48–57. doi: 10.1124/MOL.62.1.48

Fadila, S., Quinn, S., Turchetti Maia, A., Yakubovich, D., Ovadia, M., Anderson, K. L., et al. (2020). Convulsive seizures and some behavioral comorbidities are uncoupled in the *Scn1a*^{A1783V} Dravet syndrome mouse model. *Epilepsia* 61, 2289–2300. doi: 10.1111/epi.16662

Favero, M., Sotuyo, N. P., Lopez, E., Kearney, J. A., and Goldberg, E. M. (2018). A transient developmental window of fast-spiking interneuron dysfunction in a mouse model of dravet syndrome. *J. Neurosci.* 38, 7912–7927. doi: 10.1523/JNEUROSCI.0193-18.2018

Fricker, D., and Miles, R. (2000). EPSP amplification and the precision of spike timing in hippocampal neurons. *Neuron* 28, 559–569. doi: 10.1016/S0896-6273(00)00133-1

Goff, K. M., and Goldberg, E. M. (2019). Vasoactive intestinal peptide-expressing interneurons are impaired in a mouse model of Dravet syndrome. *Elife* 8:e46846. doi: 10.7554/eLife.46846

González-Burgos, G., and Barrionuevo, G. (2001). Voltage-gated sodium channels shape subthreshold EPSPs in layer 5 pyramidal neurons from rat prefrontal cortex. *J. Neurophysiol.* 86, 1671–1684. doi: 10.1152/jn.2001.86.4.1671

Han, S., Tai, C., Westenbroek, R. E., Yu, F. H., Cheah, C. S., Potter, G. B., et al. (2012). Autistic-like behaviour in *Scn1a*$^{+/-}$ mice and rescue by enhanced GABA-mediated neurotransmission. *Nature* 489, 385–390. doi: 10.1038/nature11356

Hawkins, K. E., Gavin, C. F., and Sweatt, D. (2016). *Long-Term Potentiation: A Candidate Cellular Mechanism for Information Storage in the CNS, in The Curated Reference Collection in Neuroscience and Biobehavioral Psychology*. Cambridge, MA: Academic Press, 33–64. doi: 10.1016/B978-0-12-809324-5.21103-6

Hawkins, N. A., Calhoun, J. D., Huffman, A. M., and Kearney, J. A. (2019). Gene expression profiling in a mouse model of Dravet syndrome. *Exp. Neurol.* 311, 247–256. doi: 10.1016/j.expneurol.2018.10.010

Hedrich, U. B. S., Liautard, C., Kirschenbaum, D., Pofahl, M., Lavigne, J., Liu, Y., et al. (2014). Impaired action potential initiation in GABAergic interneurons causes hyperexcitable networks in an epileptic mouse model carrying a human $Na_V1.1$ mutation. *J. Neurosci.* 34, 14874–14889. doi: 10.1523/JNEUROSCI.0721-14.2014

Hu, W., Tian, C., Li, T., Yang, M., Hou, H., and Shu, Y. (2009). Distinct contributions of $Na_V1.6$ and $Na_V1.2$ in action potential initiation and backpropagation. *Nat. Neurosci.* 12, 996–1002. doi: 10.1038/nn.2359

Kalume, F., Yu, F. H., Westenbroek, R. E., Scheuer, T., and Catterall, W. A. (2007). Reduced sodium current in Purkinje neurons from $Na_V1.1$ mutant mice: implications for ataxia in severe myoclonic epilepsy in infancy. *J. Neurosci.* 27, 11065–11074. doi: 10.1523/jneurosci.2162-07.2007

Katz, E., Stoler, O., Scheller, A., Khrapunsky, Y., Goebbels, S., Kirchhoff, F., et al. (2018). Role of sodium channel subtype in action potential generation by neocortical pyramidal neurons. *Proc. Natl. Acad. Sci. U.S.A.* 115, E7184–E7192. doi: 10.1073/pnas.1720493115

Kuo, F.-S., Cleary, C. M., LoTurco, J. J. L., Chen, X., and Mulkey, D. K. (2019). Disordered breathing in a mouse model of Dravet syndrome. *Elife* 8:e43387. doi: 10.7554/eLife.43387

Layer, N., Sonnenberg, L., Pardo González, E., Benda, J., Hedrich, U. B. S., Lerche, H., et al. (2021). Dravet variant *SCN1A*^{A1783V} impairs interneuron firing predominantly by altered channel activation. *Front. Cell. Neurosci.* 15:754530. doi: 10.3389/fncel.2021.754530

Lemaire, L., Desroches, M., Krupa, M., Pizzamiglio, L., Scalmani, P., and Mantegazza, M. (2021). Modeling $Na_V1.1$/*SCN1A* sodium channel mutations in a microcircuit with realistic ion concentration dynamics suggests differential GABAergic mechanisms leading to hyperexcitability in epilepsy and hemiplegic migraine. *PLoS Comput. Biol.* 17:e1009239. doi: 10.1371/JOURNAL.PCBI.1009239

Liautard, C., Scalmani, P., Carriero, G., De Curtis, M., Franceschetti, S., and Mantegazza, M. (2013). Hippocampal hyperexcitability and specific epileptiform activity in a mouse model of Dravet syndrome. *Epilepsia* 54, 1251–1261. doi: 10.1111/epi.12213

Lorincz, A., and Nusser, Z. (2010). Molecular identity of dendritic voltage-gated sodium channels. *Science* 328, 906–909. doi: 10.1126/science.1187958

Mantegazza, M., and Broccoli, V. (2019). *SCN1A* / $Na_V1.1$ channelopathies: mechanisms in expression systems, animal models, and human iPSC models. *Epilepsia* 60, S25–S38. doi: 10.1111/epi.14700

Mattis, J., Somarowthu, A., Goff, K. M., Yom, J., Sotuyo, N. P., McGarry, L. M., et al. (2021). Corticohippocampal circuit dysfunction in a mouse model of Dravet syndrome. *bioRxiv* [Preprint]. doi: 10.1101/2021.05.01.442271

Miljanovic, N., Hauck, S. M., van Dijk, R. M., Di Liberto, V., Rezaei, A., and Potschka, H. (2021). Proteomic signature of the Dravet syndrome in the genetic *Scn1a*^{A1783V} mouse model. *Neurobiol. Dis.* 157:105423. doi: 10.1016/j.nbd.2021.105423

Miller, A. R., Hawkins, N. A., McCollom, C. E., and Kearney, J. A. (2014). Mapping genetic modifiers of survival in a mouse model of Dravet syndrome. *Genes Brain Behav.* 13, 163–172. doi: 10.1111/gbb.12099

Mistry, A. M., Thompson, C. H., Miller, A. R., Vanoye, C. G., George, A. L., and Kearney, J. A. (2014). Strain- and age-dependent hippocampal neuron sodium currents correlate with epilepsy severity in Dravet syndrome mice. *Neurobiol. Dis.* 65, 1–11. doi: 10.1016/j.nbd.2014.01.006

Müller, C., and Remy, S. (2014). Dendritic inhibition mediated by O-LM and bistratified interneurons in the hippocampus. *Front. Synaptic Neurosci.* 6:23. doi: 10.3389/fnsyn.2014.00023

Nissenkorn, A., Almog, Y., Adler, I., Safrin, M., Brusel, M., Marom, M., et al. (2019). *In vivo*, *in vitro* and *in silico* correlations of four de novo *SCN1A* missense mutations. *PLoS One* 14:e0211901. doi: 10.1371/journal.pone.0211901

Ogiwara, I., Iwasato, T., Miyamoto, H., Iwata, R., Yamagata, T., Mazaki, E., et al. (2013). $Na_V1.1$ haploinsufficiency in excitatory neurons ameliorates seizure-associated sudden death in a mouse model of dravet syndrome. *Hum. Mol. Genet.* 22, 4784–4804. doi: 10.1093/hmg/ddt331

Ogiwara, I., Miyamoto, H., Morita, N., Atapour, N., Mazaki, E., Inoue, I., et al. (2007). $Na_V1.1$ localizes to axons of parvalbumin-positive inhibitory interneurons: a circuit basis for epileptic seizures in mice carrying an *Scn1a* gene mutation. *J. Neurosci.* 27, 5903–5914. doi: 10.1523/JNEUROSCI.5270-06.2007

Osteen, J. D., Herzig, V., Gilchrist, J., Emrick, J. J., Zhang, C., Wang, X., et al. (2016). Selective spider toxins reveal a role for the $Na_V1.1$ channel in mechanical pain. *Nature* 534, 494–499. doi: 10.1038/nature17976

Pernici, C. D., Mensah, J. A., Dahle, E. J., Johnson, K. J., Handy, L., Buxton, L., et al. (2021). Development of an antiseizure drug screening platform for Dravet syndrome at the NINDS contract site for the epilepsy therapy screening program. *Epilepsia* 62, 1665–1676. doi: 10.1111/epi.16925

Richards, K. L., Milligan, C. J., Richardson, R. J., Jancovski, N., Grunnet, M., Jacobson, L. H., et al. (2018). Selective $Na_V1.1$ activation rescues Dravet syndrome mice from seizures and premature death. *Proc. Natl. Acad. Sci. U.S.A.* 115, E8077–E8085. doi: 10.1073/pnas.1804764115

Ricobaraza, A., Mora-Jimenez, L., Puerta, E., Sanchez-Carpintero, R., Mingorance, A., Artieda, J., et al. (2019). Epilepsy and neuropsychiatric comorbidities in mice carrying a recurrent Dravet syndrome *SCN1A* missense mutation. *Sci. Rep.* 9:14172. doi: 10.1038/s41598-019-50627-w

Ritter-Makinson, S., Clemente-Perez, A., Higashikubo, B., Cho, F. S., Holden, S. S., Bennett, E., et al. (2019). Augmented reticular thalamic bursting and seizures in *Scn1a*-Dravet syndrome. *Cell Rep.* 26, 54.e6–64.e6. doi: 10.1016/j.celrep.2018.12.018

Rubinstein, M., Han, S., Tai, C., Westenbroek, R. E., Hunker, A., Scheuer, T., et al. (2015a). Dissecting the phenotypes of Dravet syndrome by gene deletion. *Brain* 138, 2219–2233. doi: 10.1093/brain/awv142

Rubinstein, M., Westenbroek, R. E., Yu, F. H., Jones, C. J., Scheuer, T., and Catterall, W. A. (2015b). Genetic background modulates impaired excitability of inhibitory neurons in a mouse model of Dravet syndrome. *Neurobiol. Dis.* 73, 106–117. doi: 10.1016/j.nbd.2014.09.017

Salgueiro-Pereira, A. R., Duprat, F., Pousinha, P. A., Loucif, A., Douchamps, V., Regondi, C., et al. (2019). A two-hit story: seizures and genetic mutation interaction sets phenotype severity in *SCN1A* epilepsies. *Neurobiol. Dis.* 125, 31–44. doi: 10.1016/J.NBD.2019.01.006

Spratt, P. W. E., Alexander, R. P. D., Ben-Shalom, R., Sahagun, A., Kyoung, H., Keeshen, C. M., et al. (2021). Paradoxical hyperexcitability from $Na_V1.2$ sodium

channel loss in neocortical pyramidal cells. *Cell Rep.* 36:109483. doi: 10.1016/j.celrep.2021.109483

Stein, R. E., Kaplan, J. S., Li, J., and Catterall, W. A. (2019). Hippocampal deletion of $Na_V1.1$ channels in mice causes thermal seizures and cognitive deficit characteristic of Dravet Syndrome. *Proc. Natl. Acad. Sci.* 116, 16571–16576. doi: 10.1073/pnas.1906833116

Stuart, G. J., and Spruston, N. (2015). Dendritic integration: 60 years of progress. *Nat. Neurosci.* 18, 1713–1721. doi: 10.1038/nn.4157

Stuart, G., and Sakmann, B. (1995). Amplification of EPSPs by axosomatic sodium channels in neocortical pyramidal neurons. *Neuron* 15, 1065–1076. doi: 10.1016/0896-6273(95)90095-0

Studtmann, C., Ladislav, M., Topolski, M. A., Safari, M., and Swanger, S. A. (2021). Synaptic and intrinsic mechanisms impair reticular thalamus and thalamocortical neuron function in a Dravet syndrome mouse model. *bioRxiv* [Preprint]. doi: 10.1101/2021.09.03.458635

Tai, C., Abe, Y., Westenbroek, R. E., Scheuer, T., and Catterall, W. A. (2014). Impaired excitability of somatostatin- and parvalbumin-expressing cortical interneurons in a mouse model of Dravet syndrome. *Proc. Natl. Acad. Sci.* 111, E3139–E3148. doi: 10.1073/pnas.1411131111

Tatsukawa, T., Ogiwara, I., Mazaki, E., Shimohata, A., and Yamakawa, K. (2018). Impairments in social novelty recognition and spatial memory in mice with conditional deletion of *Scn1a* in parvalbumin-expressing cells. *Neurobiol. Dis.* 112, 24–34. doi: 10.1016/j.nbd.2018.01.009

Tran, C. H., Vaiana, M., Nakuci, J., Somarowthu, A., Goff, K. M., Goldstein, N., et al. (2020). Interneuron desynchronization precedes seizures in a mouse model of Dravet syndrome. *J. Neurosci.* 40, 2764–2775. doi: 10.1523/JNEUROSCI.2370-19.2020

Tricoire, L., Pelkey, K. A., Erkkila, B. E., Jeffries, B. W., Yuan, X., and McBain, C. J. (2011). A blueprint for the spatiotemporal origins of mouse hippocampal interneuron diversity. *J. Neurosci.* 31, 10948–10970. doi: 10.1523/JNEUROSCI.0323-11.2011

Tsai, M. S., Lee, M. L., Chang, C. Y., Fan, H. H., Yu, I. S., Chen, Y. T., et al. (2015). Functional and structural deficits of the dentate gyrus network coincide with emerging spontaneous seizures in an *Scn1a* mutant dravet syndrome model during development. *Neurobiol. Dis.* 77, 35–48. doi: 10.1016/j.nbd.2015.02.010

Westenbroek, R. E., Merrick, D. K., and Catterall, W. A. (1989). Differential subcellular localization of the RI and RII Na+ channel subtypes in central neurons. *Neuron* 3, 695–704. doi: 10.1016/0896-6273(89)90238-9

Winterer, J., Lukacsovich, D., Que, L., Sartori, A. M., Luo, W., and Földy, C. (2019). Single-cell RNA-Seq characterization of anatomically identified OLM interneurons in different transgenic mouse lines. *Eur. J. Neurosci.* 50, 3750–3771. doi: 10.1111/ejn.14549

Yu, F. H., Mantegazza, M., Westenbroek, R. E., Robbins, C. A., Kalume, F., Burton, K. A., et al. (2006). Reduced sodium current in GABAergic interneurons in a mouse model of severe myoclonic epilepsy in infancy. *Nat. Neurosci.* 9, 1142–1149. doi: 10.1038/nn1754

Yuan, Y., O'Malley, H. A., Smaldino, M. A., Bouza, A. A., Hull, J. M., and Isom, L. L. (2019). Delayed maturation of GABAergic signaling in the *Scn1a* and *Scn1b* mouse models of Dravet Syndrome. *Sci. Rep.* 9:6210. doi: 10.1038/s41598-019-42191-0

Zucker, R. S., and Regehr, W. G. (2002). Short-term synaptic plasticity. *Annu. Rev. Physiol.* 64, 355–405. doi: 10.1146/annurev.physiol.64.092501.114547

Conflict of Interest: The authors declare that the research was conducted in the absence of any commercial or financial relationships that could be construed as a potential conflict of interest.

Publisher's Note: All claims expressed in this article are solely those of the authors and do not necessarily represent those of their affiliated organizations, or those of the publisher, the editors and the reviewers. Any product that may be evaluated in this article, or claim that may be made by its manufacturer, is not guaranteed or endorsed by the publisher.

frontiers in Molecular Neuroscience

ORIGINAL RESEARCH
published: 30 March 2022
doi: 10.3389/fnmol.2022.809951

SCN2A-Related Epilepsy: The Phenotypic Spectrum, Treatment and Prognosis

Qi Zeng[1,2†], Ying Yang[1†], Jing Duan[2], Xueyang Niu[1], Yi Chen[1], Dan Wang[1], Jing Zhang[1], Jiaoyang Chen[1], Xiaoling Yang[1], Jinliang Li[1], Zhixian Yang[1], Yuwu Jiang[1], Jianxiang Liao[2] and Yuehua Zhang[1]**

[1] Department of Pediatrics, Peking University First Hospital, Beijing, China, [2] Department of Neurology, Shenzhen Children's Hospital, Shenzhen, China

OPEN ACCESS

Edited by:
Massimo Mantegazza, UMR 7275 Institut de Pharmacologie Moléculaire et Cellulaire (IPMC), France

Reviewed by:
Edward Haig Beamer, Nottingham Trent University, United Kingdom
Dinesh Upadhya, Manipal Academy of Higher Education, India

***Correspondence:**
Jianxiang Liao
liaojianxiang@vip.sina.com
Yuehua Zhang
zhangyhdr@126.com

[†] These authors have contributed equally to this work

Specialty section:
This article was submitted to Brain Disease Mechanisms, a section of the journal Frontiers in Molecular Neuroscience

Received: 05 November 2021
Accepted: 14 February 2022
Published: 30 March 2022

Citation:
Zeng Q, Yang Y, Duan J, Niu X, Chen Y, Wang D, Zhang J, Chen J, Yang X, Li J, Yang Z, Jiang Y, Liao J and Zhang Y (2022) SCN2A-Related Epilepsy: The Phenotypic Spectrum, Treatment and Prognosis. Front. Mol. Neurosci. 15:809951. doi: 10.3389/fnmol.2022.809951

Objective: The aim of this study was to analyze the phenotypic spectrum, treatment, and prognosis of 72 Chinese children with *SCN2A* variants.

Methods: The *SCN2A* variants were detected by next-generation sequencing. All patients were followed up at a pediatric neurology clinic in our hospital or by telephone.

Results: In 72 patients with *SCN2A* variants, the seizure onset age ranged from the first day of life to 2 years and 6 months. The epilepsy phenotypes included febrile seizures (plus) (n = 2), benign (familial) infantile epilepsy (n = 9), benign familial neonatal-infantile epilepsy (n = 3), benign neonatal epilepsy (n = 1), West syndrome (n = 16), Ohtahara syndrome (n = 15), epilepsy of infancy with migrating focal seizures (n = 2), Dravet syndrome (n = 1), early infantile epileptic encephalopathy (n = 15), and unclassifiable developmental and epileptic encephalopathy (n = 8). Approximately 79.2% (57/72) patients had varying degrees of developmental delay. All patients had abnormal MRI findings with developmental delay. 91.7% (55/60) patients with *de novo SCN2A* variants had development delay, while only 16.7% (2/12) patients with inherited *SCN2A* variants had abnormal development. 83.9% (26/31) *SCN2A* variants that were located in transmembrane regions of the protein were detected in patients with development delay. Approximately 69.2% (9/13) *SCN2A* variants detected in patients with normal development were located in the non-transmembrane regions. Approximately 54.2% (39/72) patients were seizure-free at a median age of 8 months. Oxcarbazepine has been used by 38 patients, and seizure-free was observed in 11 of them (11/38, 28.9%), while 6 patients had seizure worsening by oxcarbazepine. All 3 patients used oxcarbazepine and with seizure onset age $>$ 1 year presented seizure exacerbation after taking oxcarbazepine. Valproate has been used by 53 patients, seizure-free was observed in 22.6% (12/53) of them.

Conclusion: The phenotypic spectrum of *SCN2A*-related epilepsy was broad, ranging from benign epilepsy in neonate and infancy to severe epileptic encephalopathy. Oxcarbazepine and valproate were the most effective drugs in epilepsy patients with

SCN2A variants. Sodium channel blockers often worsen seizures in patients with seizure onset beyond 1 year of age. Abnormal brain MRI findings and *de novo* variations were often related to poor prognosis. Most *SCN2A* variants located in transmembrane regions were related to patients with developmental delay.

Keywords: epilepsy, *SCN2A* gene, variant, phenotype, treatment

INTRODUCTION

The etiology of epilepsy is a major determinant of clinical course and prognosis. Six etiologic groups of epilepsy include structural, metabolic, genetic, infectious, and immune, as well as an unknown group (Scheffer et al., 2017). As genetic testing is broadly used in pediatric neurology, more than half of epilepsy children are thought to have a genetic cause (Reif et al., 2017). At present, voltage-gated sodium channel genes such as *SCN1A*, *SCN2A*, *SCN3A*, and *SCN8A* were reported to be causative genes of epilepsy (Ademuwagun et al., 2021), among them *SCN2A* has been reported to be the second most common, next only to *SCN1A*, the first reported causative gene for epilepsy (Heyne et al., 2019). Epilepsy caused by *SCN2A* variants mostly starts in early childhood and has a wide phenotypic spectrum, ranging from self-limited epilepsy with a favorable outcome to developmental and epileptic encephalopathy, and most of them respond well to sodium channel blockers (SCBs) (Grinton et al., 2015; Trump et al., 2016; Dilena et al., 2017; Flor-Hirsch et al., 2018; Kim et al., 2020; Melikishvili et al., 2020; Miao et al., 2020; Penkl et al., 2021). China has a large population and a large number of epilepsy children. However, the epilepsy phenotypes and prognosis caused by *SCN2A* variation in Chinese children have not yet been studied in a large sample. In this study, the phenotypic spectrum, treatment, and prognosis of epilepsy children with *SCN2A* variants were studied in a Chinese cohort from two pediatric clinical centers.

MATERIALS AND METHODS

Participants

In this study, epilepsy children who were suspected of genetic etiology and identified with *SCN2A* variants by next-generation sequencing were enrolled in Peking University First Hospital and Shenzhen Children's hospital from September 2006 to January 2021. All epilepsy patients fulfilled the following criteria: (1) no identifiable immediate or remote cause and (2) no metabolic or mitochondrial disorders. Clinical information includes the age of seizure onset, seizure types, developmental milestones, neurologic status, electroencephalogram (EEG), brain MRI, and treatment data of the patients and their relatives were collected using a pre-test questionnaire completed by the recruiting clinician by telephone or from medical records. Patients were followed up at a pediatric neurology clinic at our hospital or by telephone. The effect of anti-seizure medication (ASM) therapy were retrospectively assessed and classified according to the judgment of the treating physicians into seizure freedom, seizure reduction (reduction in seizure frequency $>$ 50%), no effect or seizure worsening. This study was approved by the Ethics Committee of Peking University First Hospital and Shenzhen Children's hospital, respectively. The written informed consent for the analysis and publication of clinical and genetic details was obtained from the patients or their parents.

Genetic Analysis

Blood samples were obtained from these probands and their family members when possible. Genomic DNA was extracted from peripheral blood by a standard method. All patients were screened for pathogenic variants either through a custom-designed gene panel in which candidate genes associated with epilepsy including *SCN2A* was selected as the genes of interest or by whole-exome sequencing. The potential pathogenic variations suggested by the targeted next-generation sequencing were validated using Sanger sequencing.

RESULTS

SCN2A Variants

A total of 72 unrelated epilepsy patients with heterozygous *SCN2A* variants were collected. Among them, patients 1–8 have been reported in a previous study of benign familial epilepsy (Zeng et al., 2018). Fifty-nine *SCN2A* variants were identified, including 54 missense variants (91.5%, 54/59), 2 frameshift variants, 2 in-frame deletion variants, and 1 non-sense variant. A total of 22 *SCN2A* variants were novel. The *SCN2A* variants were scattered in different regions of the gene, and there were no obvious hot spot variants (see **Figure 1**). V261M, R853Q, H1853R, E999K, E1211K, R1319Q, A1500T, R1629H, and P1658S were recurrent variants, each was identified in two or three patients (see **Table 1**). A total of 12 (12/72, 16.7%) patients had inherited variants, and the other 60 (60/72, 83.3%) patients had *de novo* variants. All 12 patients with inherited variants had a family history of epilepsy or febrile seizures. All of the affected parents had heterozygous variants as their children, except the mother of patient 48. She carries the same *SCN2A* variant with a ratio of about 21.5% in the peripheral blood by next-generation sequencing.

Clinical Phenotypes of Patients With *SCN2A* Variants

Among 72 patients with *SCN2A* variants, 50 are men, 22 are women. The seizure onset age was ranged from the first day of life to 2 years and 6 months. A total of 36 patients had seizure onset in neonates (50.0%, 36/72). A total of 18 patients had seizure onset between 1 and 6 months of age (25.0%, 18/72).

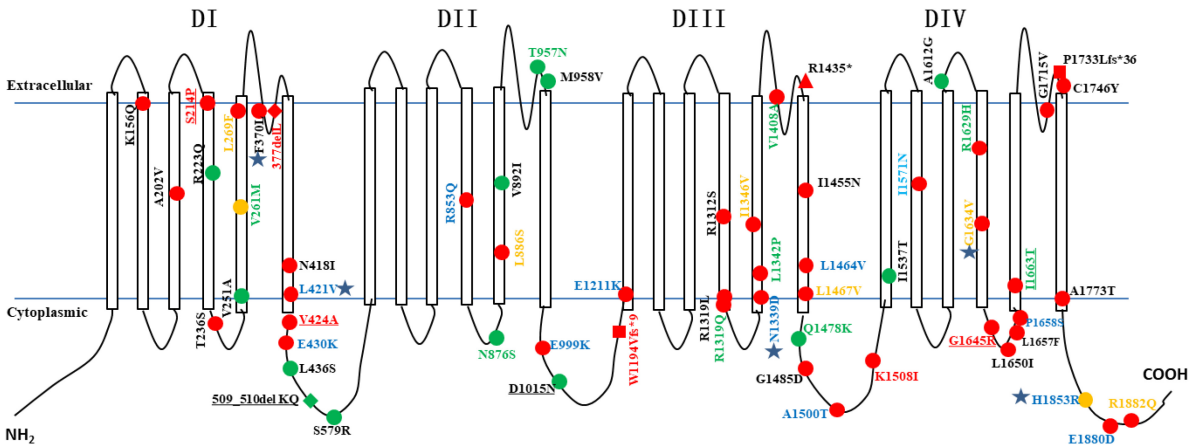

FIGURE 1 | The developmental outcome and treatment effects to oxcarbazepine of epilepsy patients with *SCN2A* variants. A total of 59 *SCN2A* variants was included. The shapes of variation sites represent different variation types (circle = missense variation; triangle = nonsense variation; square = frameshift variation; rhombu = in-frame deletion variation). The colors of the shape represent different developmental outcome (red = developmental delay; green = normal development; orange = both patients with normal development and developmental delay were observed). The colors of the variants represent the treatment effects of oxcarbazepine (green = seizure freedom; blue = seizure reduction; orange = no effect; red = seizure worsening; black = never used). The variation underlined indicates fever-sensitivity. Pentagons indicate one patient with the variants died.

A total of 11 patients had seizure onset between 7 month and 1 year of age (15.3%, 11/72). Seizure onset age was beyond 1 year in 7 patients (9.7%, 7/72). The seizure onset age of 5 patients with non-missense variants was between 11 months to 2 years and 6 months.

Focal seizures were observed in 65 patients(90.3%, 65/72), epileptic spasms in 38(52.8%, 38/72), tonic spasms in 15, myoclonic seizures in 5, tonic seizures in 4, generalized tonic-clonic seizures in 4, absence seizures in 3, and atonic seizures in 1, respectively. A total of 41 (41/72, 56.9%) patients presented 2 or more seizure types. Seizures manifested fever-sensitivity in 6 (8.3%, 6/72) patients (patient 9, 10, 20, 25, 50, and 55).

A total of 72 patients with *SCN2A* variants underwent video EEG. Interictal EEG abnormalities were heterogeneous, such as focal or multifocal epileptic discharges in 45 patients, hypsarrhythmia in 30, burst suppression in 18, and generalized discharges in 13, respectively. A total of 10 patients had normal interictal EEG. Seizures were recorded in 48 patients, such as focal seizures in 34 patients, epileptic spasms in 31, tonic spasms in 4, myoclonic seizures in 5, tonic seizures in 4, and absence seizures in 3, respectively.

Brain MRI was performed in all 72 patients with *SCN2A* variants, which revealed abnormalities in 29 (29/72, 40.3%) patients. The abnormalities included dysplasia of frontal or frontotemporal lobes in 16, enlargement of the unilateral or bilateral lateral ventricle in 13, agenesis of the corpus callosum in 12, delayed white matter myelination in 8, and hippocampal atrophy in 2 patients, respectively (see **Figure 2**). The other 43 probands had normal brain MRI.

Among 72 patients with *SCN2A* variants, 57 patients (57/72, 79.2%) had varying degrees of developmental delay, and the other 15 patients had normal development. The 28 of 57 (28/57, 49.1%) patients with developmental delay cannot control head at last follow-up (median age: 2 years and 7 months; range: 3 months to 8 years and 2 months). All patients had epileptic spasms, burst suppression and hypsarrhythmia, abnormal MRI findings had developmental delay. Autism spectrum disorder (ASD) was diagnosed in 3 patients. All affected parents of the proband had normal development.

In 72 patients, the phenotypes were diagnosed febrile seizures (plus) ($n = 2$), benign (familial) infantile epilepsy ($n = 9$), benign familial neonatal-infantile epilepsy ($n = 3$), benign neonatal epilepsy ($n = 1$), West syndrome ($n = 16$), Ohtahara syndrome ($n = 15$), epilepsy of infancy with migrating focal seizures (EIMFS) ($n = 2$), Dravet syndrome ($n = 1$), early infantile epileptic encephalopathy (EIEE) ($n = 15$), and unclassifiable developmental and epileptic encephalopathy (DEE) ($n = 8$) (**Figure 3**). A total of 16 (16/72, 22.2%) patients were initially diagnosed with West syndrome. A total of 15 patients (15/72, 20.8%) were diagnosed with Ohtahara syndrome at first, but 12 (12/15, 80%) of them evolved into West syndrome afterward. Both Patient 9 and Patient 10 were probands of generalized epilepsy with febrile seizures plus (GEFS+) families. Several paternal family members of Patient 9 had histories of febrile seizures in childhood. The Patient 10 was detected with maternal *SCN2A* variation I1663T which was inherited from his grandmother. His mother had 2 febrile seizures in early childhood. However, his maternal grandmother had no history of seizures. The Patient 48 was diagnosed with intractable West syndrome, recurrent *SCN2A* variation R853Q was detected. His mosaic mother had several seizures before 1 year of age. Her seizures were self-limited without using any ASM therapy.

Genotype–Phenotype Correlation

Of the 59 *SCN2A* variants, 31 were located in transmembrane regions, while the other 28 were in non-transmembrane regions. Carriers of 2 recurrent variants (R1319Q and V261M) included both patients with normal development (Patient 57 and Patient

TABLE 1 | The genetic testing results and clinical features of 72 patients with *SCN2A* variants.

Patient	Gender	Variation	Reported/ novel	Inheritance	Seizure onset age	Age at last follow-up	EEG features	Seizure types	MRI	Psychomotor development	Phenotype	Age at seizure free	Seizure free therapy	Other conditions
1	Male	c.2627A > G(p.N876S)	Reported	Maternal	2 months	5 years 6 months	Normal	FS	Normal	Normal	BFNIE	4 months	OXC	
2	Female	c.2674G > A(p.V892I)	Reported	Maternal	2 male	6 years 11 months	FS	FS	Normal	Normal	BFNIE	6 months	LEV, TPM	
3	Female	c.2872A > G(p.M958V)	Reported	Paternal	3 months	6 years 1 months	FD	FS	Normal	Normal	BFNIE	4 months	VPA	
4	Male	c.668G > A(p.R223Q)	Reported	Paternal	4 months	11 years	Normal	FS	Normal	Normal	BFIE	7 months	VPA	
5	Male	c.752T > C(p.V251A)	Reported	Maternal	3 months	9 years	FD	FS	Normal	Normal	BFIE	4 months	PB	
6	Male	c.1307T > C(p.L436S)	Reported	Maternal	3 months	10 years	Normal	FS	Normal	Normal	BFIE	8 months	VPA	
7	Female	c.1737C > G(p.S579R)	Reported	Paternal	1 year 2 months	6 years 2 months	Normal	FS	Normal	Normal	BFIE	1 year 3 months	Self-limited	
8	Male	c.4835C > G(p.A1612G)	Reported	Maternal	3 months	8 years 10 months	Normal	FS	Normal	Normal	BFIE	4 months	Self-limited	
9	Male	c.1523_1528 delAGAAAC (p.509_510del KQ)	Novel	Paternal	11 months	10 years	GD	GTCS, AtS	Normal	Normal	FSP	2 years	VPA	Fever sensetivity
10	Male	c.4988T > C(p.I1663T)	Novel	Maternal	6 months	7 years	GD, FD, MS	GTCS, MS, FS	Normal	Delay, walk at 3 years 6 months, speak at 1 year 3 months	DS	5 years	VPA, CLZ, OXC	Fever sensetivity
11	Male	c.1108T > C(p.F370L)	Novel	*De novo*	8 days	2 years 7 months	BS, FS, SS	TSS, SS, FS	Normal	Delay, cannot control head and speak	OS	8 months	VGB, TPM	Died at 2 years 7 months
12	Male	c.781G > A(p.V261M)	Reported	*De novo*	4 days	5 years	MD, FS	SS, FS	Normal	Delay, head control at 2 years 6 months, sit alone at 4 years	EIEE	8 months	VPA, TPM	
13	Female	c.466A > C(p.K156Q)	Novel	*De novo*	3 days	1 year 4 months	GD, TS	TS	DWMM	Delay, cannot control head and speak	EIEE	Non-remission		
14	Female	c.1261T > G(p.L421V)	Reported	*De novo*	10 days	4 years 3 months	BS, HPS, TSS, FS, SS	TSS, SS, FS	ACC, DWMM, DFTL, ELV	Delay, cannot control head and speak	OS → WS	Non-remission		Died at 4 years 3 months
15	Male	c.5558A > G(p.H1853R)	Reported	*De novo*	2 days	2 years 9 months	BS, HPS, FS, SS	TSS, SS, FS	Normal	Delay, cannot control head and speak	OS → WS	8 months	TPM	Died at 2 years 9 months
16	Male	c.4223T > C(p.V1408A)	Reported	*De novo*	2 days	8 years 1 months	FD	FS	Normal	Delay, walk at 1 year 8 months, normal speech	EIEE	5 months	OXC, LEV	
17	Male	c.2995G > A(p.E999K)	Reported	*De novo*	2 days	3 years 10 months	HPS, MD	SS, FS	Normal	Delay, cannot control head and speak	WS	3 months	VPA, LEV, TPM	
18	Male	c.4364T > A(p.I1455N)	Reported	*De novo*	2 days	7 years	HPS, FS, SS	SS, FS	Normal	Delay, cannot control head and speak	WS	2 years 5 months	TPM, VPA	
19	Male	c.4454G > A(p.G1485D)	Novel	*De novo*	3 months	7 years 6 months	Normal	FS	Normal	Delay, walk at 1 years 4 months, poor school performance	EIEE	2 years	VPA	
20	Male	c.1271T > C(p.V424A)	Reported	*De novo*	1 days	8 years 2 months	GD, FS	FS, GTCS	DFTL, ELV	Delay, cannot control head and speak	EIEE	Non-remission		Fever sensetivity
21	Female	c.5144G > T(p.G1715V)	Reported	*De novo*	8 months	8 years 3 months	HPS, FD, MD, AS	SS, AS	Normal	Delay, walk at 2 years 1 months, can only speak a few words	WS	3 years 1 months	VPA, LTG	

(Continued)

TABLE 1 | (Continued)

Patient	Gender	Variation	Reported/ novel	Inheritance	Seizure onset age	Age at last follow-up	EEG features	Seizure types	MRI	Psychomotor development	Phenotype	Age at seizure free	Seizure free therapy	Other conditions
22	Male	c.3631G > A(p E1211K)	Reported	*De novo*	4 months	6 years 11 months	HPS, FD, SS, FS	SS, FS	ELV	Delay, control head at 1 years 4 months, cannot sit alone and speak	WS	Non-remission		
23	Male	c.4498G > A(p.A1500T)	Reported	*De novo*	2 days	1 years 6 months	HPS, FD, SS, FS	SS, FS, TSS	Normal	Delay, cannot control head and speak	WS	Non-remission		
24	Male	c.5196delC (p.P1733Lfs*36)	Novel	*De novo*	11 months	5 years	HPS, SS	SS	DFTL	Delay, cannot control head and speak	WS	Non-remission		
25	Male	c.4933G > A(p.G1645R)	Novel	*De novo*	2 years	5 years 11 months	GD	GTCS, FS	Normal	Delay, poor speech and school performance	DEE	5 years 4 months	LEV, VPA	Fever sensetivity
26	Female	c.4399C > G(p.L1467V)	Novel	*De novo*	10 months	6 years 7 months	FD	FS	ELV	Delay before seizure onset, cannot walk and speak	DEE	1 years 11 months	VPA, LEV, TPM	
27	Male	c.1128_1130de lCTT(p.377del L)	Novel	*De novo*	2 years 3 months	6 years 4 months	FD	FS	Normal	Delay before seizure onset, walk at 1 years 6 months, cannot speak	DEE	2 years 10 months	VPA, LEV	
28	Male	c.4303C > T(p.R1435*)	Reported	*De novo*	2 years 6 months	7 years 3 months	FD	FS	Normal	Delay before seizure onset, walk at 2 years,cannot speak	DEE	3 years 4 months	VPA, LEV, TPM	ASD
29	Female	c.4015A > G(p.N1339D)	Reported	*De novo*	14 days	2 years 8 months	BS, HPS, FS, SS, MS	TSS, FS, MS	ELV, ACC, DFTL	Delay, cannot control head and speak	OS → WS	Non-remission		Died at 2 years 8 months
30	Male	c.781G > A(p.V261M)	Reported	*De novo*	3 days	4 years 1 months	MD, FS	FS	Normal	Delay, walk at 1 year 2 months, slightly poor language performance	EIEE	Non-remission		
31	Male	c.5558A > G(p.H1853R)	Reported	*De novo*	2 days	5 years 8 months	FD, FS	FS	Normal	Delay, walk at 1 year 6 months, poor language performance	EIEE	1 month	PB	
32	Male	c.605C > T(p.A202V)	Reported	*De novo*	3 days	6 years 2 months	MD, FS	FS	Normal	Delay, walk at 1 year 2 months, slightly poor language performance	EIEE	3 months	PB	
33	Male	c.5317G > A(p.A1773T)	Reported	*De novo*	8 months	13 years	HPS, GD, FD, SS, MS, AS	FS, SS, MS, AS	Normal	Delay, walk at 4 years, cannot speak	WS	Non-remission		
34	Male	c.3631G > A(p.E1211K)	Reported	*De novo*	1 year	5 years	HPS, MD, SS	SS	DFL, ELV	Delay before seizure onset, walk at 4 years 8 months, cannot speak	WS	Non-remission		ASD
35	Male	c.3956G > T(p.R1319L)	Reported	*De novo*	2 days	6 years 1 month	MD, FD, FS, SS, AS	FS, SS, AS	Normal	Delay, walk with help at 6 years, cannot speak	EIEE	Non-remission		
36	Male	c.4712T > C(p.I1571T)	Reported	*De novo*	2 days	1 year 3 months	BS, HPS, MD, FS, SS	TSS, FS, S	Normal	Delay, cannot control head and speak	OS → WS	Non-remission		
37	Female	c.4523A > T(p.K1508I)	Novel	*De novo*	1 day	2 years 9 months	BS, HPS, MD, FS, SS, TS	TS, SS, FS	DFTL, DWMM	Delay, cannot control head and speak	OS → WS	Non-remission		
38	Female	c.4498G > A(p.A1500T	Reported	*De novo*	2 days	3 years 9 months	BS, HPS, FD, FS, SS	TSS, SS, FS	Normal	Delay, cannot control head and speak	OS → WS	Non-remission		
39	Male	c.4025T > C(p.L1342P)	Reported	*De novo*	6 months	4 years 5 months	HPS, MD	SS	ACC, DWMM, ELV	Delay, cannot control head and speak	WS	1 year 6 months	VPA, OXC	
40	Male	c.4036A > G(p.I1346V)	Reported	*De novo*	1 days	3 years 11 months	BS, HPS, FS, SS, TSS	FS, SS, TSS	ACC, DFTL	Delay, cannot control head and speak	OS → WS	Non-remission		

(Continued)

TABLE 1 | (Continued)

Patient	Gender	Variation	Reported/ novel	Inheritance	Seizure onset age	Age at last follow-up	EEG features	Seizure types	MRI	Psychomotor development	Phenotype	Age at seizure free	Seizure free therapy	Other conditions
41	Male	c.807G > T(p.L269F)	Novel	*De novo*	1 days	2 year 5 months	HPS, MD, FS, SS	FS, SS	DFTL	Delay, cannot control head and speak	WS	3 months	LEV	
42	Male	c.4972C > T(p.P1658S)	Reported	*De novo*	1 days	3 years 3 months	MD, FD	FS	DFTL, HA	Delay, cannot control head and speak	EIEE	Non-remission		
43	Male	c.4948C > A(p.L1650I)	Novel	*De novo*	2 days	1 year	BS, HPS, FS, SS	FS, SS, TSS	Normal	Delay, cannot control head and speak	OS → WS	Non-remission		
44	Male	c.5237G > A(p.C1746Y)	Novel	*De novo*	1 year 3 months	6 years 9 months	GD, MD, FD, SS	FS, SS	ELV	Delay before seizure onset, cannot walk and speak	EIEE	1 year 10 months	LEV, VPA, TPM	
45	Female	c.2657T > C(p.L886S)	Reported	*De novo*	1 days	5 years 1 months	BS, FD, FS	TSS, FS	DWMM	Delay, cannot control head and speak	OS	Non-remission		
46	Female	c.4432C > A(p.Q1478K)	Novel	*De novo*	1 month (30 days)	3 years 3 months	FS	FS	Normal	Normal	BIE	3 months	OXC	
47	Female	c.3579_3580 delCT > (p.W1194Vfs*9)	Reported	*De novo*	1 year 5 months	5 year	GD, MD, FD, SS	SS	HA	Delay before seizure onset, cannot walk and speak	DEE	Non-remission		
48	Female	c.2558G > A(p.R853Q)	Reported	Maternal	10 months	1 year 2 months	HPS, GD, MD, FS	FS, SS	DFTL,ACC	Delay before seizure onset, cannot sit and speak	WS	Non-remission		
49	Male	c.781G > A(p.V261M)	Reported	*De novo*	2 days	2 years 3 months	Normal	FS	Normal	Normal	BNE	3 months	OXC	
50	Male	c.640T > C(p.S214P)	Reported	*De novo*	2 months	2 years 11 months	HPS, FD, SS	FS, SS	ACC	Delay, cannot control head and speak	WS	Non-remission		Fever sensetivity
51	Female	c.3936G > T(p.R1312S)	Novel	*De novo*	4 months	1 year 6 months	MD, FS, SS	FS, SS	DFTL	Delay before seizure onset, cannot control head and speak	DEE	Non-remission		
52	Male	c.5558A > G(p.H1853R)	Reported	*De novo*	9 days	1 year 8 months	BS, HPS, FD, FS, SS, TSS	TSS, SS, FS	ACC, DWMM, ELV	Delay, cannot control head and speak	OS → WS	Non-remission		
53	Male	c.5640A > C(p.E1880D)	Novel	*De novo*	1 days	1 year 4 months	HPS, ED, MD, SS, MS, TS	TS, FS, SS, MS	DFTL	Delay, cannot control head and speak	WS	Non-remission		
54	Female	c.1253A > T(p.N418I)	Novel	*De novo*	1 year 5 months	2 years 3 months	MD, SS, MS	FS, MS, SS	Normal	Delay before seizure onset, cannot walk and speak	DEE	Non-remission		
55	Female	c.3043G > A(p.D1015N)	Reported	*De novo*	1 year	13 years	Normal	FS	Normal	Normal	FSs	11 years	VPA	Fever sensetivity
56	Female	c.4886G > A(p.R1629H)	Reported	*De novo*	1 days	5 years 2 months	BS, MD	TSS, FS	Normal	Delay, walk at 2 years, can speak only a few words	OS	4 m	OXC, KD	
57	Male	c.3956G > A(p.R1319Q)	Reported	*De novo*	4 months	2 years 2 months	MD, FS	FS	Normal	Normal	BIE	5 months	OXC	
58	Male	c.2558G > A(p.R853Q)	Reported	*De novo*	11 months	1 years	HPS, FD, SS	SS, FS	ELV, DFTL	Delay before seizure onset, 6 months control head	WS	Non-remission		
59	Male	c.4886G > A(p.R1629H)	Reported	*De novo*	4 days	5 years 11 months	BS, MD, FD	FS	Normal	Delay, slightly poor language performance	EIEE	1 month	OXC	
60	Female	c.4972C > T(p.P1658S)	Reported	*De novo*	2 months	7 years 2 months	FD	FS	Normal	Delay, walk at 2 years 8 months, speak at 9 months	EIEE	Non-remission		
61	Male	c.3956G > A(p.R1319Q)	Reported	*De novo*	2 months	6 years 3 months	FD, FS	FS	DFL	Delay, normal motor development, cannot speak	DEE	5 months	OXC	ASD
62	Male	c.2870C > A(p.T957N)	Novel	*De novo*	2 days	4 years 4 months	FD	FS	Normal	Normal	BIE	3 months	OXC	
63	Male	c.2558G > A(p.R853Q)	Reported	*De novo*	8 months	1 year 4 months	HPS	FS, SS	ACC	Delay, cannot control head and speak	WS	Non-remission		
64	Male	c.2995G > A(p.E999K)	Reported	*De novo*	1 day	1 year 3 months	BS, HPS, MFS, SS	FS, SS	Normal	Delay, cannot control head and speak	EIMFS	1 year	CBZ	

(Continued)

TABLE 1 | (Continued)

Patient	Gender	Variation	Reported/ novel	Inheritance	Seizure onset age	Age at last follow-up	EEG features	Seizure types	MRI	Psychomotor development	Phenotype	Age at seizure free	Seizure free therapy	Other conditions
65	Male	c.4901G > T(p.G1634V)	Reported	*De novo*	1 days	3 months	BS, MFS, SE	FS, SS	ACC, ELV	Delay, cannot control head	EIMFS	Non-remission		Died at 3 months
66	Female	c.3631G > A(p.E1211K)	Reported	*De novo*	10 months	4 years 2 months	HPS, FD, SS, NCSE	FS, SS	Normal	Delay before seizure onset, cannot walk and speak	WS	2 years 2 months	VPA	
67	Female	c.4969C > T(p.L1657F)	Novel	*De novo*	6 days	2 years 8 months	HPS, GD, MD, FD, SS, FS	FS, SS	ACC, ELV, DFTL	Delay, cannot control head and speak	EIEE	Non-remission		
68	Male	c.4391C > T(p.T1464I)	Novel	*De novo*	2 days	2 years 2 months	FS, GD, MD, TS	FS, SS, TS	DWMM	Delay, control head at 2 years, cannot sit and speak	EIEE	1 year 3 months	VGB, PRP	
69	Female	c.1288G > A(p.E430K)	Novel	*De novo*	8 days	1 year 8 months	BS, HPS, MD, FS, SS	FS, SS, TSS	ACC,DWMM, DFTL,ELV	Delay, cannot control head and speak	OS → WS	Non-remission		
70	Male	c.707C > G(p.T236S)	Reported	*De novo*	20 days	6 months	BS, HPS, FS, TSS, SS	FS, SS, TSS	ACC	Delay, cannot control head and speak	OS → WS	Non-remission		
71	Male	c.5645G > A(p.R1882Q)	Reported	*De novo*	2 days	9 months	BS, HPS, GD, FS, SE, SS	FS, TSS	Normal	Delay, cannot control head and speak	OS → WS	Non-remission		
72	Male	c.4610T > C(p.I1537T)	Novel	Paternal	3 months	1 year 6 months	MD	FS	Normal	Normal	BFIE	4 months	LEV	

MS, myoclonic seizure; FS, focal seizure; GTCS, generalized tonic clonic seizure; AtS, atonic seizure; SS, spasm; TSS, tonic spasm seizure; TS, tonic seizure; AS, absence seizure; FD, focal discharges; MD, multifocal discharges; BS, burst suppression; GD, generalized discharges; HPS, hypsarrhythmia; SE, status epilepticus; NCSE, nonconvulsive status epilepticus; DWMM, delayed white matter myelination; ELV, Enlargement of lateral ventricles; ACC, agenesis of corpus callosum; DFTL, dysplasia of frontotemporal lobes; DFL, dysplasia of frontal lobes; HA, hippocampal atrophy; BFNIE, benign familial neonatal-infantile epilepsy; BNE, benign neonatal epilepsy; BIE, benign infantile epilepsy; WS, West syndrome; EIEE, early infantile epileptic encephalopathy; OS, Ohtahara syndrome; DEE, developmental and epileptic encephalopathy. EIMFS, epilepsy of infancy with migrating focal seizures; FSs, febrile seizures; FSP, febrile seizures plus; DS, Dravet syndrome; KD, ketogenic diet; OXC, oxcarbazepine; LEV, levetiracetam; TPM, topiramate; VPA, valproate; PB, phenobarbital; CLZ, clonazepam; LTG, lamotrigine; KD, ketogenic diet; CBZ, carbamazepine; PRP, perampanel; VGB, vigabatrin; ASD, autistic spectrum disorder.

49) and patients with developmental delay (Patient 61, Patient 12, and Patient 30). A total of 13 variants were only detected in patients with normal development, 9 (9/13, 69.2%) of them were located in non-transmembrane regions, and the remaining 4 were located in transmembrane regions which accounting for 12.9% (4/31) of all transmembrane region variations. A total of 44 variants were only detected in patients with developmental delay, 26 (26/44, 59.1%) were located in transmembrane regions, accounting for 83.9% (26/31) of transmembrane region variants, and 18 were located in non-transmembrane regions (see **Figure 1**). The 10 of 12 (83.3%) patients with inherited *SCN2A* variants had normal intelligence; however, the other 2 (2/12, 16.7%) patients had a developmental delay (Patient 10 and 48). Among 60 patients with *de novo SCN2A* variants, 55 had development delay (91.7%, 55/60), and the remaining 5 patients had normal development.

Seizure Treatment and Prognosis

At the last follow-up (median age: 4 years and 4 months; range: 3 months to 13 years), 39 (54.2%, 39/72) patients were seizure-free at a median age of 8 months (range: 1 month to 5 years 4 months of age), the remaining 33 patients still had refractory seizures (median age: 2 years 8 months; range: 3 months to 13 years). Among 39 patients with seizure freedom, 2 patients who were diagnosed with benign familial infantile epilepsy did not use any ASM therapy, 21 (21/39, 53.8%) patients used monotherapy, 11 used two-drug treatment, and 5 used polytherapy. All 33 patients with uncontrolled seizures have tried at least 2 ASM therapies. All 15 patients had normal development were seizure-free. Of the 29 children with abnormal brain MRI, 23 (23/29, 79.3%) patients still had seizures at the last follow-up, and only 6 had seizure freedom.

At least one patient in the study experienced seizure control after treatment with SCBs such as oxcarbazepine, carbamazepine, lamotrigine, and other ASM therapy like valproate, topiramate, levetiracetam, phenobarbital, ACTH, vigabatrin, and perampanel. The effect of these ASM therapies is shown in **Figure 4**. No patient experienced seizure control after using phenytoin, zonisamide, lacosamide, clonazepam, nitrazepam, clobazam, cannabidiol, ketogenic diet, and vagus nerve stimulation.

Oxcarbazepine has been used in 38 patients, seizure freedom, seizure reduction, no effect, and seizure worsening were observed in 11 (11/38, 28.9%), 15 (15/38, 39.5%), 6 (6/38, 15.8%), and 6 (6/38, 15.8%) patients, respectively. Among those 38 patients, 35 patients had seizure onset age < 3 months, 6 patients had seizure onset age between 4 months and 1 year of age, and the other 3 patients had seizure onset age > 1 year. For 29 patients with seizure onset age < 3 months, seizure freedom, seizure reduction, no effect, and seizure worsening were observed in 8 (8/29, 27.6%), 13 (13/29, 44.8%), 5 (5/29, 17.2%), and 3 (3/29, 10.3%) patients (patients 20, 25, and 37), respectively. For 6 patients with seizure onset age between 4 months and 1 year of age, seizure freedom, seizure reduction, and no effect were observed in 3, 2, and 1 patient, respectively, no patients experienced seizure worsening. All 3 patients with seizure onset age > 1 year had seizure exacerbation caused by oxcarbazepine (Patients 27, 47, and 50).

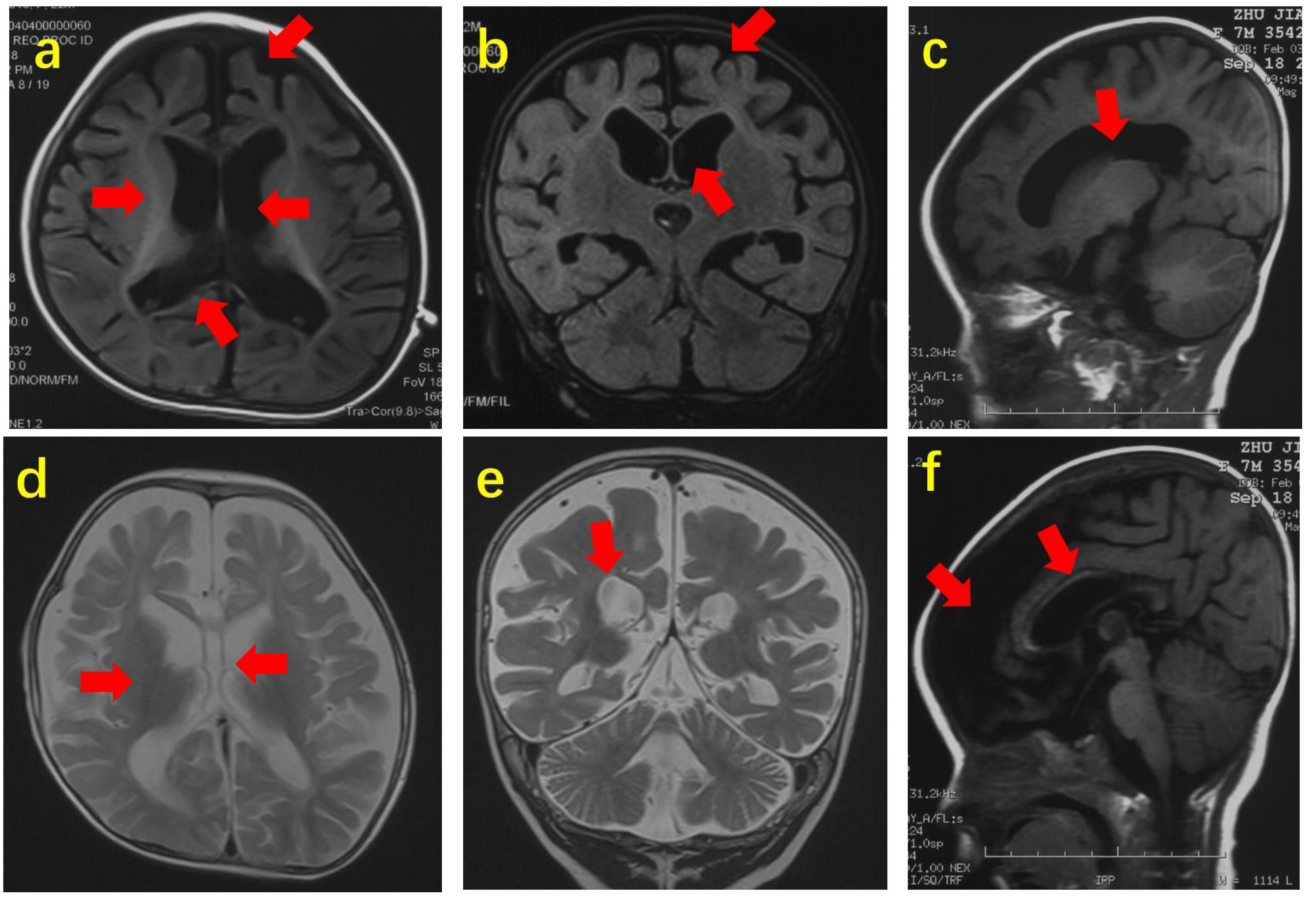

FIGURE 2 | Abnormal brain MRI of 3 patients with *SCN2A* variants. Brain MRI of Patient 14 at the age of 22 months. **(a,b)**. Axial and coronal images (T1WI) showing agenesis of corpus callosum, delayed white matter myelination, dysplasia of frontotemporal lobes and enlargement of lateral ventricles. Brain MRI of Patient 29 at the age of 7 months. **(c,f)** Sagittal images (T1WI) showing enlargement of lateral ventricles, agenesis of corpus callosum and dysplasia of frontotemporal lobes. Brain MRI of Patient 39 at the age of 12 months. **(d,e)** Axial and coronal images (T2WI) showing agenesis of corpus callosum, delayed white matter myelination and enlargement of lateral ventricles. The arrow points to the lesion.

The Patient 10 was diagnosed with Dravet syndrome and his seizure was controlled after the addition of oxcarbazepine at the age of 5 years old and had no relapse for nearly 2 years. The effects of oxcarbazepine in patients with different *SCN2A* variants have been presented in **Figure 1**. Carbamazepine has been used in 11 patients, seizure freedom, seizure reduction, no effect, and seizure worsening were observed in 1 (1/11, 9.1%), 6 (6/11, 54.5%), 3 (3/11, 27.3%), and 1 (1/11, 9.1%) patients, respectively. Lamotrigine has been used in 9 patients, seizure freedom, seizure reduction, no effect, and seizure worsening were observed in 1 (1/9, 11.1%), 2(2/9, 22.2%), 4(4/9, 44.4%), and 2 (2/9, 22.2%) patients, respectively.

Valproate has been used in 53 patients with *SCN2A* variants, seizure freedom, seizure reduction, no effect, and seizure worsening were observed in 12 (12/53, 22.6%), 21 (21/53, 39.6%), 18 (18/53, 34.0%), and 2 (2/53, 3.8%) patients, respectively. Seizures were controlled by topiramate, levetiracetam, and phenobarbital in 4 (4/46, 8.7%), 3 (3/45, 6.7%), and 3 (3/29, 10.3%) patients, respectively. One patient was seizure free after taking ACTH, vigabatrin, and perampanel, respectively. No patient had seizure exacerbation caused by levetiracetam, vigabatrin, and perampanel. Seizure worsening caused by ACTH was observed in 5 (5/16, 31.3%) patients.

Five (5/72, 6.9%) patients died at the age of 3 months to 4 years and 3 months (Patients 11, 14, 15, 29, and 65). All those 5 patients started seizures in neonate. Four patients were initially diagnosed with Ohtahara syndrome, and the other patient diagnosed with EIMFS. Three of them (Patients 14, 29, and 65) manifested intractable seizures with no effect to multiple ASM therapies. The causes of those 3 patients were unknown. Both Patients 11 and 15 were seizure free at the age of 8 months, and suffered possible sudden unexpected death in epilepsy (SUDEP).

DISCUSSION

SCN2A gene is located on chromosome 2q24.3. The gene which contains 26 exons encodes the α2 subunit of the voltage-gated sodium channel (Nav1.2). Nav1.2 is mainly expressed in the initial part of excitatory neuron axons and unmyelinated axons.

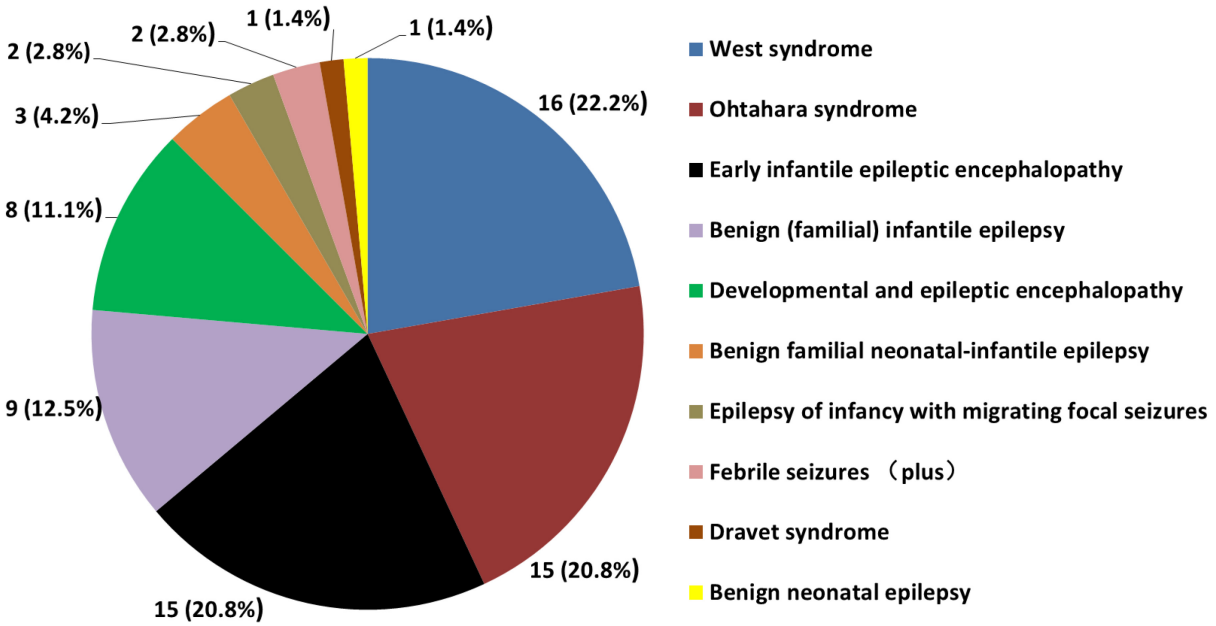

FIGURE 3 | Distribution of 72 Chinese epilepsy patients with *SCN2A* variants according to phenotypes [*n* (%)].

The protein is widely distributed in the cortex, hippocampus, striatum, and midbrain. Variations in *SCN2A* gene are associated with a spectrum of neurodevelopmental and epileptic disorders, such as epilepsy, intellectual disability, ASD, schizophrenia, and periodic ataxia, presenting an autosomal dominant inheritance (Carroll et al., 2016; Yokoi et al., 2018; Long et al., 2019; Schwarz et al., 2019; Suddaby et al., 2019; Epifanio et al., 2021). In recent years, a lot of *SCN2A* variants have been reported. The variation types include missense variation, in-frame deletion or insertion variation, non-sense variation, frameshift variation, and splice site variation. It has been reported that missense variation was the most common variation type of *SCN2A* variants (Wolff et al., 2017). In this study, we have found 59 *SCN2A* variants in 72 Chinese epilepsy patients, and 22 of them are novel variants. The *SCN2A* variants detected in our study show no hotspot and more than 90% of the variants are missense variants. Other variation types such as in-frame deletion or insertion variant, non-sense variant, and frameshift variant were also presented in our study, but the percentage is small. In our cohort, more than 80% of patients had *de novo SCN2A* variants.

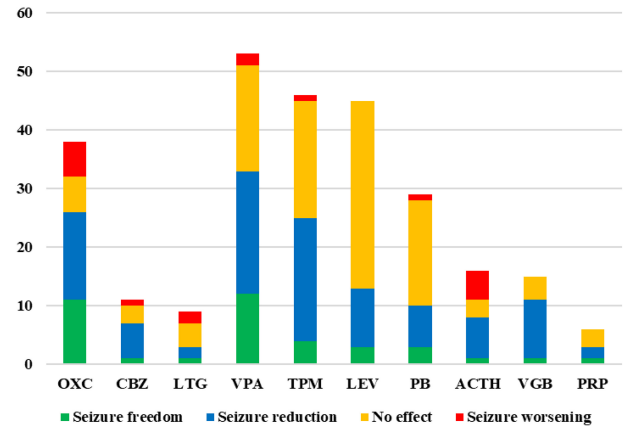

FIGURE 4 | Treatment effects of anti-seizure medication (ASM) therapies in epilepsy patients with *SCN2A* variants. Number of treated patients and their seizure outcome (green = seizure freedom; blue = seizure reduction; orange = no effect; red = seizure worsening) that have been treated with different ASM therapies. Only effects of ASM therapies that at least one patient achieved seizure free are shown. OXC, oxcarbazepine; CBZ, carbamazepine; LTG, lamotrigine; VPA, valproate; TPM, topiramate; LEV, levetiracetam; PB, phenobarbital; VGB, vigabatrin; PRP, perampanel.

Sugawara et al. (2001) firstly reported *SCN2A* missense variant R187W in a Japanese family with GEFS+. The affected patients in this family showed febrile seizures and focal epilepsy. Heron et al. (2002) reported that *SCN2A* gene was the major causative gene of benign familial neonatal-infantile epilepsy. At first, some researchers believed that missense variations tend to result in benign epilepsy, whereas truncation variations lead to severe and intractable epilepsy (Yamakawa, 2006). With the wide application of next-generation sequencing in clinical practice, *SCN2A* variants have been reported in severe early onset epileptic encephalopathy and most of them were *de novo* variants.

Most patients with *SCN2A* variants start seizures in early childhood. Wolff et al. (2017) reported that about half of patients with *SCN2A* variants had seizure onset in the neonate. In our study, half of the patients started seizures during the neonatal period. Nearly 80% of patients started seizures within 6 months of age. It suggests that seizures caused by *SCN2A* variants tend to start in early infancy. The seizure types of patients with *SCN2A* variants are varied. In our cohort, the most common

seizure types were focal seizures and epileptic spasms, observed in about 90% and 50% of patients, respectively. Other seizure types, such as tonic spasm, myoclonic seizures, atonic seizures, tonic seizures, clonic seizures, generalized tonic-clonic seizures, and absence seizures were also observed in some patients. Those seizure types were relatively rare but all of them have been reported in the literature. In our study, the abnormal interictal EEG of epilepsy patients with *SCN2A* variants such as focal or multifocal epileptic discharges, hypsarrhythmia, burst suppression, and generalized discharges. About 40% of patients in this study had brain MRI abnormalities, such as dysplasia of the frontal or frontotemporal lobes, enlargement of unilateral or bilateral lateral ventricle, agenesis of the corpus callosum, delayed white matter myelination, and hippocampal atrophy. The dysplasia of frontal or frontotemporal lobes is a common defect in our patients with brain MRI abnormalities. The abnormal neuroimages mainly indicated cerebral dysplasia. Nearly 80% of patients had developmental delays, and about half of them cannot control their heads at a median age of 2 years and 7 months.

Wolff et al. (2017) reported 66 families or sporadic cases with *SCN2A* variants which were collected by a multicenter study that participated by 74 clinical or research institutions. The phenotypes reported in the multicenter study included benign (familial) neonatal/infantile epilepsy, Ohtahara syndrome, EIMFS, encephalopathy with early infantile-onset epilepsy, West syndrome, myoclonic-atonic epilepsy, Lennox–Gastaut syndrome, epileptic encephalopathy with infantile/childhood-onset epilepsy, intellectual disability, and/or autism without epilepsy. Most of the patients were diagnosed with epilepsy. In this study, we analyzed the epilepsy phenotypes of patients with *SCN2A* variants. The oldest child in our group at the last follow-up was 13 years old. Some of the patients in this study were diagnosed with epilepsy at our clinical center at an early stage of life and were confirmed with *SCN2A* variants in recent years. The common epilepsy phenotypes of patients with *SCN2A* variants include benign epilepsy in the first year of life, Ohtahara syndrome, West syndrome, and EIEE. Those epilepsy phenotypes account for more than 80% of this cohort. Most of the patients who were initially diagnosed with Ohtahara syndrome evolved into infantile spasms. Other rare epilepsy phenotypes include febrile seizures (plus), EIMFS, and Dravet syndrome in our study. Wolff et al. (2017) did not report any patient with Dravet syndrome, febrile seizures, or febrile seizures plus. In addition, only 6 patients (8.3%, 6/72) in our study had fever-sensitive seizures, indicating that fever sensitivity is a rare feature of epilepsy patients with *SCN2A* variants. All those 8 patients diagnosed with unclassifiable DEE had a developmental delay before seizure onset and developmental regression after seizure onset and cannot be diagnosed with any known epilepsy syndrome. In this study, some patients with developmental delay showed little improvement after seizure control, which further suggests that the variation itself has a significant impact on brain development. The mother of Patient 48 carried a mosaic *SCN2A* variant R853Q with a ratio of about 20% in the peripheral blood. R853Q is a recurrent variation that has been reported repeatedly in the literature (Ganguly et al., 2021). Both the Patient 48 and two other patients with the same variant in our study, as well as patients with the same variant reported in the literature, were diagnosed with West syndrome. However, the mother of Patient 48 had self-limited seizures before 1 year of age and normal development. It indicates that the phenotype severity caused by *SCN2A* variants is related to the dose of variation.

At the last follow-up, about half of the patients (54.2%, 39/72) were seizure-free at the median age of 8 months. Few of them were self-limited. Liao et al. (2010) found that *SCN2A* had high expression in the initial segment of the axon of hippocampal neuron of a mouse during 5–15 days after birth, and the function was gradually replaced by the protein encoded by *SCN8A*. It speculated that this may be the reason why benign epilepsy due to *SCN2A* variants could be self-limited with age. About half of the patients with seizure control were treated with monotherapy, while the rest were treated with 2 or 3 drugs. The seizures were not controlled in nearly half of the patients, and the median age of these patients at the last follow-up was 2 years and 8 months, with the oldest being 13 years. All those patients presented with refractory epilepsy. Seizures were not controlled in all patients with brain MRI abnormalities in this study.

It has been suggested that SCBs are effective drugs in the treatment of epilepsy of patients with *SCN2A* variation (Reif et al., 2017). More than half of the patients in our study had used SCBs. Probably because it comes in liquid form, oxcarbazepine was the most commonly used SCBs in our cohort which has been used in 39 patients. Although oxcarbazepine was indeed the most effective ASM therapy in our study, the rate of seizure control was still less than 30%. It has been reported (Wolff et al., 2017) that, patients with seizure onset age less than 3 months always carry *SCN2A* variants that cause the gain of function and SCBs were often effective for seizures. However, those patients had a seizure onset age later than 3 months, *SCN2A* variation often causes loss of function and SCBs worsen the seizure. Brunklaus et al. (2020) also reported that individuals with gain-of-function *SCN2A*/3A/8A most frequently present with early-onset epilepsy (<3 months), and have a good response to SCBs, which is not completely consistent with our results. In this study, about 27% of patients with seizure onset age <3 months had seizures controlled by oxcarbazepine, but another 3 patients had seizure exacerbation. Half of the patients with onset age from 4 months to 1 year had seizure control after administration of oxcarbazepine and no patient presented seizure exacerbation. All 3 patients with onset age > 1 year had seizure exacerbation due to oxcarbazepine. *SCN2A* gain-of-function has recently been recognized as a cause of early infantile-onset epileptic encephalopathies, whereas loss-of-function *SCN2A* variations often cause ASD or intellectual disability with later-onset mild epilepsy or without epilepsy (Yamakawa, 2006; Ben-Shalom et al., 2017; Wolff et al., 2017). Based on the results of our study and those in the literature, SCBs are not recommended for patients with seizure onset age > 1 year, while SCBs can be tried for patients with seizure onset age < 1 year, but the possibility of seizure exacerbation still needs to be warned. Phenotypes caused by *SCN2A* variation are associated with underlying functional changes caused by the variants. Although the rate of seizure control was low, in this study, seizure control was observed in one patient by carbamazepine and lamotrigine, respectively. Since a few cases of

Dravet syndrome caused by *SCN2A* variants has been reported (Wang et al., 2012), the effect of SCBs for those patients has not been reported. In our study, Patient 10 was diagnosed with Dravet syndrome, he was seizure free after adding oxcarbazepine at the age of 5 years old, suggesting that Dravet syndrome is caused by *SCN2A* variant. It is different from that Dravet syndrome caused by *SCN1A* variation is mostly not responsive to or might even be exacerbated by SCBs. Although *SCN2A* and *SCN1A* are both sodium channel genes, the underlying pathogenesis of Dravet syndrome caused by *SCN2A* variation may be different from that of *SCN1A*.

Besides of SCBs, valproate was also the effective ASM therapy in this study, with a seizure control rate of about 22%, slightly lower than oxcarbazepine. In addition, the proportion of exacerbations caused by valproate was lower than that caused by oxcarbazepine. In this study, a large number of patients had used topiramate, levetiracetam, and phenobarbital, and seizure control was achieved in some patients by each of those drugs, although the rates of seizure control were relatively low. In addition, although there were fewer patients who had used ACTH, vigabatrin, and perampanel, there was one case of seizure control for each drug, respectively. ACTH is the preferred drug for the treatment of West syndrome, but nearly one-third of the patients in this study experienced increased seizure frequency after the use of ACTH. The specific mechanism of exacerbation of seizures needs to be further studied. No seizure exacerbation occurred after taking levetiracetam, perampanel, or vigabatrin.

In this study, 5 children died, accounting for about 7% (5/72) of the cases in this group. All 5 patients started seizures during the neonatal period and were diagnosed with severe epileptic syndromes such as Ohtahara syndrome or EIMFS. Two of the patients were seizure-free and the possible cause of death was SUDEP, while the other 3 patients still had frequent seizures and the exact cause of death was unknown. The underlying pathophysiology of SUDEP remains unclear. SUDEP cannot be predicted in advance, because the complete underlying pathophysiology of the phenomenon is likely multifactorial and prognostic biomarkers were still not found (Goldman et al., 2016; Sahly et al., 2022). Our study indicates that frequent seizures and *SCN2A* variations themselves may be important factors leading to death in these patients.

Phenotypes caused by *SCN2A* variants are heterogeneous. It has been reported that phenotypic variability from benign infantile epilepsy to Ohtahara syndrome was observed in 3 affected individuals of a family with *SCN2A* variation (Syrbe et al., 2016). In our study, both benign epilepsy with normal development and epileptic encephalopathy with developmental delay were observed in unrelated patients carrying variants R1319Q and V261M. This was also confirmed by the different phenotypes in the family of Patient 48, ranging from normal to Dravet syndrome in the carriers of the same *SCN2A* variant.

More than 80% of patients with inherited *SCN2A* variants had a benign outcome in our study. However, more than 90% of patients with *de novo SCN2A* variants showed developmental delay, which was identical to the reported studies (Wolff et al., 2017). In this study, the seizure onset age of patients with non-missense *SCN2A* variants was late, and the seizure onset age was after 11 months, which was consistent with the literature reports (Lauxmann et al., 2018). It may be most non-missense variations will lead to loss-of-function, and the early manifestations of such functional changes are mostly developmental delay or autism, while epilepsy often begins in late infancy or early childhood (Begemann et al., 2019). The number of *SCN2A* variants located in transmembrane regions was similar to that in non-transmembrane regions in our study. Only 13 *SCN2A* variants merely in patients with normal development, and about 70% of them were located in non-transmembrane regions. However, more than 80% of variants located in transmembrane regions were related to patients with developmental delay. This may be due to *SCN2A* variants in transmembrane regions having a greater effect on protein function than those in non-transmembrane regions.

SCN2A is a common causative gene of genetic epilepsy in children. Patients with *SCN2A de novo* variation usually have a poor prognosis lacking precise treatment. In this study, epilepsy patients with *SCN2A* variants from 2 pediatric clinical centers in China were studied. Multi-center, large-sample, and prospective studies are needed to further analyze the genotype–phenotype correlations of *SCN2A*-related epilepsy for precise medicine.

DATA AVAILABILITY STATEMENT

The data presented in this study are available through Clinvar (http://www.clinvar.com/), with the following accession numbers SCV002099454 – SCV002099517. Further inquiry can be directed to the corresponding author.

ETHICS STATEMENT

The studies involving human participants were reviewed and approved by Peking University First Hospital and Shenzhen Children's hospital. Written informed consent to participate in this study was provided by the participants' legal guardian/next of kin.

AUTHOR CONTRIBUTIONS

YZ and JXL contributed to the design and implementation of the research. ZY and YJ were involved in supervised the work. JD and QZ were responsible for assessing the pathogenicity of variants. XN, YC, DW, JZ, JC, XY, and JLL were responsible for follow-up of the patients. QZ and YY contributed to the analysis of the results and to the writing of the manuscript. All authors contributed to the article and approved the submitted version.

FUNDING

This work was supported by the Key Research Project of the Ministry of Science and Technology of China (Grant Nos. 2016YFC0904400 and 2016YFC0904401) and Sanming Project of Medicine in Shenzhen (Grant No. SZSM201812005).

REFERENCES

Ademuwagun, I. A., Rotimi, S. O., Syrbe, S., Ajamma, Y. U., and Adebiyi, E. (2021). Voltage Gated Sodium Channel Genes in Epilepsy: mutations, Functional Studies, and Treatment Dimensions. *Front. Neurol.* 12:600050. doi: 10.3389/fneur.2021.600050

Begemann, A., Acuña, M. A., Zweier, M., Vincent, M., Steindl, K., Bachmann-Gagescu, R., et al. (2019). Further corroboration of distinct functional features in *SCN2A* variants causing intellectual disability or epileptic phenotypes. *Mol. Med.* 25:6. doi: 10.1186/s10020-019-0073-6

Ben-Shalom, R., Keeshen, C. M., Berrios, K. N., An, J. Y., Sanders, S. J., and Bender, K. J. (2017). Opposing effects on Nav1.2 function underlie differences between *SCN2A* variants observed in individuals with autism spectrum disorder or infantile seizures. *Biol. Psychiatry* 82, 224–232. doi: 10.1016/j.biopsych.2017.01.009

Brunklaus, A., Du, J., Steckler, F., Ghanty, I. I., Johannesen, K. M., Fenger, C. D., et al. (2020). Biological concepts in human sodium channel epilepsies and their relevance in clinical practice. *Epilepsia* 61, 387–399. doi: 10.1111/epi.16438

Carroll, L. S., Woolf, R., Ibrahim, Y., Williams, H. J., Dwyer, S., Walters, J., et al. (2016). Mutation screening of *SCN2A* in schizophrenia and identification of a novel loss-of-function mutation. *Psychiatr. Genet.* 26, 60–65. doi: 10.1097/YPG.0000000000000110

Dilena, R., Striano, P., Gennaro, E., Bassi, L., Olivotto, S., Tadini, L., et al. (2017). Efficacy of sodium channel blockers in *SCN2A* early infantile epileptic encephalopathy. *Brain Dev.* 39, 345–348. doi: 10.1016/j.braindev.2016.10.015

Epifanio, R., Giorda, R., Merlano, M. C., Zanotta, N., Romaniello, R., Marelli, S., et al. (2021). *SCN2A* Pathogenic Variants and Epilepsy: heterogeneous Clinical, Genetic and Diagnostic Features. *Brain Sci.* 12:18. doi: 10.3390/brainsci12010018

Flor-Hirsch, H., Heyman, E., Livneh, A., Reish, O., Watemberg, N., Litmanovits, I., et al. (2018). Lacosamide for *SCN2A*-related intractable neonatal and infantile seizures. *Epileptic Disord.* 20, 440–446. doi: 10.1684/epd.2018.1001

Ganguly, S., Thompson, C. H., and George, A. L. Jr. (2021). Enhanced slow inactivation contributes to dysfunction of a recurrent *SCN2A* mutation associated with developmental and epileptic encephalopathy. *J. Physiol.* 599, 4375–4388. doi: 10.1113/JP281834

Goldman, A. M., Behr, E. R., Semsarian, C., Bagnall, R. D., Sisodiya, S., and Cooper, P. N. (2016). Sudden unexpected death in epilepsy genetics: molecular diagnostics and prevention. *Epilepsia* 57, 17–25. doi: 10.1111/epi.13232

Grinton, B. E., Heron, S. E., Pelekanos, J. T., Zuberi, S. M., Kivity, S., Afawi, Z., et al. (2015). Familial neonatal seizures in 36 families: clinical and genetic features correlate with outcome. *Epilepsia* 56, 1071–1080. doi: 10.1111/epi.13020

Heron, S. E., Crossland, K. M., Andermann, E., Phillips, H. A., Hall, A. J., Bleasel, A., et al. (2002). Sodium-channel defects in benign familial neonatal-infantile seizures. *Lancet* 360, 851–852. doi: 10.1016/S0140-6736(02)09968-3

Heyne, H. O., Artomov, M., Battke, F., Bianchini, C., Smith, D. R., Liebmann, N., et al. (2019). Targeted gene sequencing in 6994 individuals with neurodevelopmental disorder with epilepsy. *Genet. Med.* 21, 2496–2503. doi: 10.1038/s41436-019-0531-0

Kim, H. J., Yang, D., Kim, S. H., Kim, B., Kim, H. D., Lee, J. S., et al. (2020). The phenotype and treatment of *SCN2A*-related developmental and epileptic encephalopathy. *Epileptic Disord.* 22, 563–570. doi: 10.1684/epd.2020.1199

Lauxmann, S., Verbeek, N. E., Liu, Y., Zaichuk, M., Müller, S., Lemke, J. R., et al. (2018). Relationship of electrophysiological dysfunction and clinical severity in *SCN2A*-related epilepsies. *Hum. Mutat.* 39, 1942–1956. doi: 10.1002/humu.23619

Liao, Y., Deprez, L., Maljevic, S., Pitsch, J., Claes, L., Hristova, D., et al. (2010). Molecular correlates of age-dependent seizures in an inherited neonatal-infantile epilepsy. *Brain* 133, 1403–1414. doi: 10.1093/brain/awq057

Long, S., Zhou, H., Li, S., Wang, T., Ma, Y., Li, C., et al. (2019). The Clinical and Genetic Features of Co-occurring Epilepsy and Autism Spectrum Disorder in Chinese Children. *Front. Neurol.* 10:505. doi: 10.3389/fneur.2019.00505

Melikishvili, G., Dulac, O., and Gataullina, S. (2020). Neonatal *SCN2A* encephalopathy: a peculiar recognizable electroclinical sequence. *Epilepsy Behav.* 111:107187. doi: 10.1016/j.yebeh.2020.107187

Miao, P., Tang, S., Ye, J., Wang, J., Lou, Y., Zhang, B., et al. (2020). Electrophysiological features: the next precise step for *SCN2A* developmental epileptic encephalopathy. *Mol. Genet. Genom. Med.* 8:e1250. doi: 10.1002/mgg3.1250

Penkl, A., Reunert, J., Debus, O. M., Homann, A., Och, U., Rust, S., et al. (2021). A mutation in the neonatal isoform of *SCN2A* causes neonatal-onset epilepsy. *Am. J. Med. Genet. A.* 188, 941-947. doi: 10.1002/ajmg.a.62581

Reif, P. S., Tsai, M. H., Helbig, I., Rosenow, F., and Klein, K. M. (2017). Precision medicine in genetic epilepsies: break of dawn? *Expert Rev. Neurother.* 17, 381–392. doi: 10.1080/14737175.2017.1253476

Sahly, A. N., Shevell, M., Sadleir, L. G., and Myers, K. A. (2022). SUDEP risk and autonomic dysfunction in genetic epilepsies. *Auton. Neurosci.* 237:102907. doi: 10.1016/j.autneu.2021.102907

Scheffer, I. E., Berkovic, S., Capovilla, G., Connolly, M. B., French, J., Guilhoto, L., et al. (2017). ILAE classification of the epilepsies: position paper of the ILAE Commission for Classification and Terminology. *Epilepsia* 58, 512–521. doi: 10.1111/epi.13709

Schwarz, N., Bast, T., Gaily, E., Golla, G., Gorman, K. M., Griffiths, L. R., et al. (2019). Clinical and genetic spectrum of *SCN2A*-associated episodic ataxia *SCN2A*. *Eur. J. Paediatr. Neurol.* 23, 438–447. doi: 10.1016/j.ejpn.2019.03.001

Suddaby, J. S., Silver, J., and So, J. (2019). Understanding the schizophrenia phenotype in the first patient with the full *SCN2A* phenotypic spectrum. *Psychiatr. Genet.* 29, 91–94. doi: 10.1097/YPG.0000000000000219

Sugawara, T., Tsurubuchi, Y., Agarwala, K. L., Ito, M., Fukuma, G., Mazaki-Miyazaki, E., et al. (2001). A missense variant of the Na+ channel alpha II subunit gene Na(v)1.2 in a patient with febrile and afebrile seizures causes channel dysfunction. *Proc. Natl. Acad. Sci. U.S.A.* 98, 6384–6389. doi: 10.1073/pnas.111065098

Syrbe, S., Zhorov, B. S., Bertsche, A., Bernhard, M. K., Hornemann, F., Mütze, U., et al. (2016). Phenotypic Variability from Benign Infantile Epilepsy to Ohtahara Syndrome Associated with a Novel Mutation in *SCN2A*. *Mol. Syndromol.* 7, 182–188. doi: 10.1159/000447526

Trump, N., McTague, A., Brittain, H., Papandreou, A., Meyer, E., Ngoh, A., et al. (2016). Improving diagnosis and broadening the phenotypes in early-onset seizure and severe developmental delay disorders through gene panel analysis. *J. Med. Genet.* 53, 310–317. doi: 10.1136/jmedgenet-2015-103263

Wang, J. W., Shi, X. Y., Kurahashi, H., Hwang, S. K., Ishii, A., Higurashi, N., et al. (2012). Prevalence of SCN1A mutations in children with suspected Dravet syndrome and intractable childhood epilepsy. *Epilepsy Res.* 102, 195–200. doi: 10.1016/j.eplepsyres.2012.06.006

Wolff, M., Johannesen, K. M., Hedrich, U. B. S., Masnada, S., Rubboli, G., Gardella, E., et al. (2017). Genetic and phenotypic heterogeneity suggest therapeutic implications in *SCN2A*-related disorders. *Brain* 140, 1316–1336. doi: 10.1093/brain/awx054

Yamakawa, K. (2006). Na channel gene mutations in epilepsy–the functional consequences. *Rev. Epilepsy Res.* 70, S218–S222. doi: 10.1016/j.eplepsyres.2005.11.025

Yokoi, T., Enomoto, Y., Tsurusaki, Y., Naruto, T., and Kurosawa, K. (2018). Nonsyndromic intellectual disability with novel heterozygous *SCN2A* mutation and epilepsy. *Hum. Genome Var.* 5:20. doi: 10.1038/s41439-018-0019-5

Zeng, Q., Yang, X., Zhang, J., Liu, A., Yang, Z., Liu, X., et al. (2018). Genetic analysis of benign familial epilepsies in the first year of life in a Chinese cohort. *J. Hum. Genet.* 63, 9–18. doi: 10.1038/s10038-017-0359-x

Conflict of Interest: The authors declare that the research was conducted in the absence of any commercial or financial relationships that could be construed as a potential conflict of interest.

Publisher's Note: All claims expressed in this article are solely those of the authors and do not necessarily represent those of their affiliated organizations, or those of the publisher, the editors and the reviewers. Any product that may be evaluated in this article, or claim that may be made by its manufacturer, is not guaranteed or endorsed by the publisher.

frontiers | Frontiers in Molecular Neuroscience

ORIGINAL RESEARCH
published: 26 April 2022
doi: 10.3389/fnmol.2022.809810

Clinical Study of 30 Novel *KCNQ2* Variants/Deletions in *KCNQ2*-Related Disorders

Tiantian Xiao[1†], Xiang Chen[1†], Yan Xu[2], Huiyao Chen[3], Xinran Dong[3], Lin Yang[4], Bingbing Wu[3], Liping Chen[5], Long Li[6], Deyi Zhuang[7], Dongmei Chen[8], Yuanfeng Zhou[2], Huijun Wang[3*] and Wenhao Zhou[1,3]*

[1] Department of Neonatology, National Children's Medical Center, Children's Hospital of Fudan University, Shanghai, China, [2] Division of Neurology, National Children's Medical Center, Children's Hospital of Fudan University, Shanghai, China, [3] Center for Molecular Medicine, National Children's Medical Center, Children's Hospital of Fudan University, Shanghai, China, [4] Department of Endocrinology and Inherited Metabolic Diseases, National Children's Medical Center, Children's Hospital of Fudan University, Shanghai, China, [5] Jiangxi Provincial Children's Hospital, Nanchang, China, [6] Department of Neonatology, People's Hospital of Xinjiang Uygur Autonomous Region, Urumqi, China, [7] Xiamen Children's Hospital, Xiamen, China, [8] Quanzhou Women and Children's Hospital, Quanzhou, China

OPEN ACCESS

Edited by:
Jing Peng,
Central South University, China

Reviewed by:
Weiping Liao,
Second Affiliated Hospital of Guangzhou Medical University, China
Fei Yin,
Xiangyang Central Hospital, China

***Correspondence:**
Yuanfeng Zhou
yuanfengzhou99@163.com
Huijun Wang
huijunwang@fudan.edu.cn

[†]These authors have contributed equally to this work

Specialty section:
This article was submitted to Brain Disease Mechanisms, a section of the journal Frontiers in Molecular Neuroscience

Received: *05 November 2021*
Accepted: *02 March 2022*
Published: *26 April 2022*

Citation:
Xiao T, Chen X, Xu Y, Chen H, Dong X, Yang L, Wu B, Chen L, Li L, Zhuang D, Chen D, Zhou Y, Wang H and Zhou W (2022) Clinical Study of 30 Novel KCNQ2 Variants/Deletions in KCNQ2-Related Disorders. Front. Mol. Neurosci. 15:809810. doi: 10.3389/fnmol.2022.809810

Background: *KCNQ2*-related disorder is typically characterized as neonatal onset seizure and epileptic encephalopathy. The relationship between its phenotype and genotype is still elusive. This study aims to provide clinical features, management, and prognosis of patients with novel candidate variants of the *KCNQ2* gene.

Methods: We enrolled patients with novel variants in the *KCNQ2* gene from the China Neonatal Genomes Project between January 2018 and January 2021. All patients underwent next-generation sequencing tests and genetic data were analyzed by an in-house pipeline. The pathogenicity of variants was classified according to the guideline of the American College of Medical Genetics. Each case was evaluated by two geneticists back to back. Patients' information was acquired from clinical records.

Results: A total of 30 unrelated patients with novel variants in the *KCNQ2* gene were identified, including 19 patients with single-nucleotide variants (SNVs) and 11 patients with copy number variants (CNVs). For the 19 SNVs, 12 missense variants and 7 truncating variants were identified. Of them, 36.8% (7/19) of the *KCNQ2* variants were located in C-terminal regions, 15.7% (3/19) in segment S2, and 15.7% (3/19) in segment S4. Among them, 18 of 19 patients experienced seizures in the early neonatal period. However, one patient presented neurodevelopmental delay (NDD) as initial phenotype when he was 2 months old, and he had severe NDD when he was 3 years old. This patient did not present seizure but had abnormal electrographic background activity and brain imaging. Moreover, for the 11 patients with CNVs, 20q13.3 deletions involving *EEF1A2*, *KCNQ2*, and *CHRNA4* genes were detected. All of them presented neonatal-onset seizures, responded to antiepileptic drugs, and had normal neurological development.

Conclusion: In this study, patients with novel *KCNQ2* variants have variable phenotypes, whereas patients with 20q13.3 deletion involving *EEF1A2*, *KCNQ2*, and *CHRNA4* genes tend to have normal neurological development.

Keywords: *KCNQ2*, Kv7.2, newborn, epilepsy, epileptic encephalopathy

INTRODUCTIONS

KCNQ2 encodes the Kv7.2 subunit of potassium channels. It is located in the neuronal axon initial segment, which plays a critical role in spike initiation (Pan et al., 2006). In the *Kcnq2*-conditional knock-out mice model, the pyramidal neurons located in layer 2/3 (L2/3) were hyperactivated (Niday et al., 2017). Therefore, the *KCNQ2* gene is essential for the regulation of neuronal excitability. In human beings, pathogenic variants in the *KCNQ2* gene could cause benign neonatal seizures and epileptic encephalopathy. Seizure onset usually occurs in the neonatal period. The clinical features of *KCNQ2*-related disorders have a large spectrum of phenotypes, ranging from *KCNQ2*-related benign familial neonatal epilepsy (*KCNQ2*-BFNE) to *KCNQ2*-related neonatal epileptic encephalopathy (*KCNQ2*-NEE) (Numis et al., 2014). Other rare phenotypes, including myokymia, benign familial infantile seizures (BFIS), and infantile spasms, have also been reported in *KCNQ2*-related disorders. The studies reveal that the electroencephalogram (EEG) is characterized as burst-suppression and multifocal epileptic activity (Kato et al., 2013; Lee et al., 2021). Most patients do not present structural abnormality in brain imaging. However, some studies reveal that patients can have thin corpus callosum and abnormal signals in globus pallidus in magnetic resonance imaging (MRI) (Weckhuysen et al., 2012). Regarding management, the response to antiepileptic drugs (AED) also varies (Kuersten et al., 2020). Moreover, the prognostic spectrum is broad in *KCNQ2*-related disorders. Phenotype severity could range from seizure freedom spontaneously to mental developmental delay (Dalen Meurs-van der Schoor et al., 2014). With heterogeneous clinical features, treatment responses, and prognosis, researchers tried to investigate the relationship between the genotype and the phenotype. However, the clear correlation is unknown. In this study, we aim to explore novel candidate variants of *KCNQ2* and provide the related clinical features, AED, and prognosis as well. This information can provide evidence on clinical management in patients with suspected *KCNQ2*-related disorders.

METHODS

Study Population

In this retrospective study, from January 2018 to January 2021, we enrolled patients with novel pathogenic or likely pathogenic variants of *KCNQ2* or copy number variants (CNVs) covering the *KCNQ2* gene from the China Neonatal Genomes Project (CNGP). All variants were classified according to the guideline of the American College of Medical Genetics (Richards et al., 2015) (**Supplementary Table S1**). These variants were checked in the Epilepsy Gene project (updated in July 2014; http://www.wzgenomics.cn/EpilepsyGene/), the RIKEE project (updated in December 2015; https://www.rikee.org/), ClinVar (https://www.ncbi.nlm.nih.gov/clinvar/), the Human Gene Mutation Database (HGMD, updated in November 2021, http://www.hgmd.cf.ac.uk).

Clinical data were extracted from medical records, including clinical features, MRI, or EEG findings, and follow-up information in the clinic. The last follow-up was performed by phone call if possible. The study was conducted following the Declaration of Helsinki (as revised in 2013). The Children's Hospital of Fudan University ethics committee approved this study since the study began (No. 2020-227). Pretest counseling was performed by physicians and geneticists. Informed consent was obtained from the patients' parents.

Next-Generation Sequencing and Sanger Confirmation

Sequences were generated using the Agilent ClearSeq Inherited Disease Kit, Illumina Cluster, and SBS Kit and performed on an Illumina HiSeq 2000/2500 platform. The detected variants were confirmed using polymerase chain reaction (PCR) and PCR-amplified DNA products, which were subjected to direct automated sequencing (3500XL Genetic Analyzer, Applied Biosystems). *De novo* variants were confirmed by parental evaluation *via* Sanger sequencing. We performed HMZDelFinder (Gambin et al., 2017) and CANOES (Backenroth et al., 2014) for the CNV detection. Each case was evaluated by two geneticists back to back. The annotation and filtrations of both SNVs and CNVs have been described in a published work (Dong et al., 2020).

RESULTS

Genetic Analysis of Novel Variants of *KCNQ2* Gene

From January 2018 to June 2021, we identified 30 patients with pathogenic variations in the *KCNQ2* gene by the in-house pipeline, including 19 single-nucleotide variants (SNVs) and 11 CNVs. Among the 19 SNVs, one was classified as pathogenic variant, and 18 were likely pathogenic variants (**Supplementary Table S1**). These variants had not been reported with the detailed clinical phenotypes in the public database. Among them, 12 missense variants, four frameshift variants, two stop-gained variants, and one splicing variant were identified (**Figure 1**). Nine variants were confirmed as *de novo* variants by Sanger sequencing their parents (**Table 1**). We identified patient 8 with the variant of c.1623_1631+5del of the *KCNQ2* gene. His father carried a 24% mosaic in his blood, without a seizure history or any neurological phenotype.

For the 19 variants, 36.8% (7/19) of the *KCNQ2* variants were located in C-terminal regions, 15.7% (3/19) in segment S2, and 15.7% (3/19) in segment S4. The variant of c.171_172delinsAA located in the N-terminal region, two variants (exon4:c.562C>A and exon4:c.584C>G) in the extracellular region, three variants (exon3:c.394G>A, exon2:c.385C>G, and exon2:c.367delG) in segment S2, two variants (exon4:c. 533C>T and exon4:c.553G>A) in segment S3, three variants (exon4:c.617T>G, exon4:c.650C>T; and exon4:c.650C>T) in segment S4, one variant (exon4:c.668C>T) in cytoplasmic domain between segment S4 and segment S5, and seven variants (exon13:c.1420G>T, exon14:c.1623_1631+5del, exon8:c.1045A>C, exon10c.1154dupA, exon15:c.1663T>A,

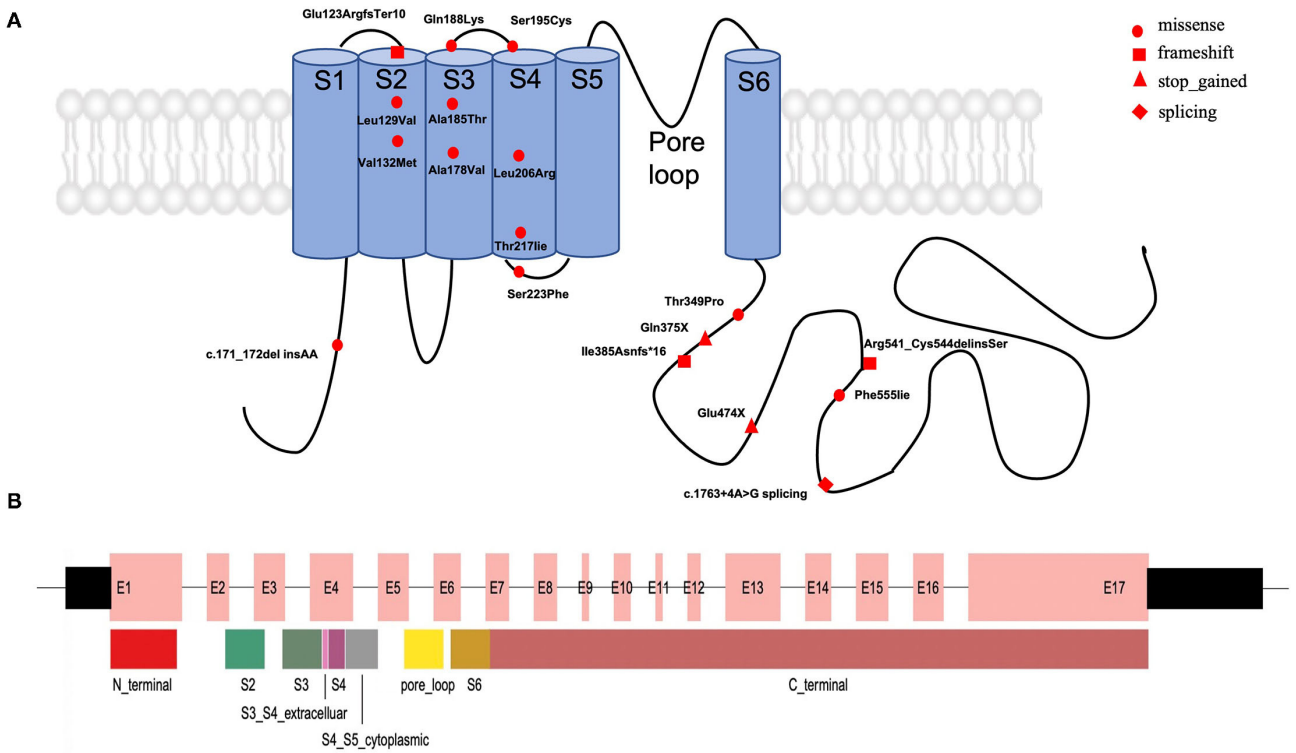

FIGURE 1 | The distribution of the 19 novel variations in the *KCNQ2* gene. **(A)** Approximate locations of the 19 novel *KCNQ2* variants. KCNQ2 protein has six transmembrane domains (blue). The fourth segment acts as the voltage sensor, and the loop between the fifth and sixth domains forms the ion pore in the Kv7.2 potassium channel. **(B)** The distribution of exons and protein domain in the *KCNQ2* gene. The wide box represents the coding region in the 17 exons. S1: segment S1, S2: segment S2, S3: segment S3, S4: segment S4, S5: segment S5, S6: segment S6, S3_S4_extracelluar: the extracellular region between segment S3 and segment S4; S4_S5_cytoplasmic: the cytoplasmic region between segment S4 and segment S5; pore_loop: the loop between the fifth and sixth domains forms the ion pore in a K7.2 potassium channel.

exon9:c.1123C>T, and exon15:c.1763+4A>G) in C-terminal region (**Figure 1**).

We also detected 11 patients with 20q13.3 deletion. The size of deletion ranges from 59 kb to 1.8 Mb. In this region, three genes including *KCNQ2*, *EEF1A2*, and *CHRNA4* were related to dominant epileptic encephalopathy, and *KCNQ2* is the key gene. Seven patients had a continuous deletion of *EEF1A2*, *KCNQ2*, and *CHRNA4* genes; three had a deletion of *CHRNA4* and *KCNQ2* genes; one had a deletion of *KCNQ2* and *EEF1A2* genes.

Clinical Features of Patients With *KCNQ2* Variants

Seizures are the dominant and initial features (29/30, 96.7%) in this cohort (**Tables 1**, **2**). The onset time of seizures ranged from 8 h of life to 15 days of life. The most common EEG finding is spike-and-slow wave and multifocal spikes with mild-to-severe abnormality of EEG background activity. Eight patients had positive MRI findings, showing abnormal signal in the left basal ganglia (patient 3), hypoplasia of the brain (patient 10), delayed myelination (patient 17), left ventricle enlargement (patient 20 and patient 21), an abnormal signal in the right frontal lobe (patient 24), and dilation of bilateral ventricles (patient 27 and patient 28). All patients with 20q13.3 deletion presented tonic seizures or tonic-clonic seizures during the neonatal period. Moreover, there were no significant different motor manifestations or imaging findings between the groups with SNVs and CNVs in the neonatal period.

Among them, we found a male term patient (patient 10) presented with motor developmental delay as the initial phenotype when he was 2 months old. He was born uneventfully. He was diagnosed with pneumonia after birth and admitted to the neonatal department. He presented poor head control at 2 months of age, and he was referred to a local children's hospital. He could sit unsupported until 10 months old and was diagnosed with motor developmental delay. Cranial MRI showed a reduced number of sulci, wide gyri, and delayed myelination. The EEG finding is abnormal. As the EEG was performed after the onset of motor developmental delay disorder, whether the EEG was positive at the early stage was not available. The seizure and tremor phenotype of this patient is negative (information from his mother).

Clinical Management and Prognosis of Patients With *KCNQ2* Variants

The overall prognosis was favorable for the patients with follow-up in the clinic. Among the 19 patients with SNVs, nine

TABLE 1 | Novel variants in *KCNQ2* gene identified in 19 neonates with *KCNQ2*-related disorders.

Patient	Sex	Exon: variant/variation type/domain	Inheritance	Initial phenotypes/age at seizures onset	EEG reports/MRI presentations during neonatal period	Treatment received/response to treatment/age at last follow-up/prognosis
1	F	exon4:c.533C>T: (p.Ala178Val)/ Missense/Segment S3	*De novo*	Generalized tonic-clonic convulsion/3 d	Normal MRI	PB, OXC, LEV, perampanel/ No/9 years/Drug-resistant epilepsy and NDD
2	M	exon3:c.394G>A (p.Val132Met)/Missense/Segment S2	NA	Generalized tonic-clonic convulsion and cyanosis. Several time per day/1 d	NA	Lost follow-up
3	M	exon4:c.617T>G (p.Leu206Arg)/Missense/Segment S4	De novo	Eye deviation to one side and generalized tonic with cyanosis. 1–2 times per day/12 d	Spike-and-slow wave and multifocal spikes with moderate abnormality of EEG background activity/ Abnormal signal in the left basal ganglia, indicating focal leukomalacia and subdural hemorrhage/	PB, TPM, LEV/Yes, seizure-free since 15 MOL/2 years/ Normal ND
4	M	exon4:c.553G>A (p.Ala185Thr)/Missense/Segment S3	De novo	Eye fixation and generalized tonic extension with cyanosis. 3–5 times per day/4 d	Spike-and-slow wave and multifocal spikes with mild abnormality of EEG background activity. Asymmetric/ Normal MRI	PB, LEV/Yes, seizure-free since 8 MOL/8 months/Normal ND
5	M	exon13:c.1420G>T (p.Glu474X)/ Stop_gain/C-terminal region	NA	Eye blinking with generalized clonic components. Several times per day/2 d	NA/Normal MRI	PB/Yes, seizure-free since 12 MOL/3 years/Normal ND
6*	M	exon2:c.385C>G (p.Leu129Val)/ Missense/Segment S2	*De novo*	Seizures with cyanosis. 3 times/1 d/	Multifocal spikes in frontal and Rolandic areas with mild abnormality of EEG background activity/ Normal MRI	Lost follow-up
7*	M	exon2:c.367delG (p.Glu123ArgfsTer10)/ Frameshift/Segment S2	NA	Seizures since neonatal period. Daily/4 d	Normal EEG background activity/ Normal MRI	Lost follow-up
8*	M	exon14:c.1623_1631+5del (p.Arg541_Cys544delinsSer)/Frameshift/C-terminal region	Paternal (mosaic)	Generalized tonic extension with cyanosis and apnea. 3 times before admission/1 d	NA	Lost follow-up
9	M	exon4:c.668C>T (p.Ser223Phe)/Missense/C-terminal region	NA	Preterm infant. Eye fixation and generalized clonic components with cyanosis. 1–2 times per day/9 d	Spike-and-slow wave and multifocal spikes with moderate abnormality of EEG background activity/ Normal MRI	Lost follow-up
10	M	exon1:c.171_172del insAA/ Frameshift/N-terminal region	De novo	Poor head control at 2 months of age, but no seizures movements were observed.	Abnormal EEG background activity/Reduced number of sulci, wide gyri, and delayed myelination	3 years/NDD
11	F	exon4:c.562C>A (p.Gln188Lys)/ Missense/Extracellular	NA	Eye fixation and generalized clonic components with cyanosis/15 d	Spike-and-slow wave and multifocal spikes with severe abnormality of EEG background activity	PB, OXC/Yes, seizure-free since 4 MOL/2.5 years/ Normal ND
12	M	exon8:c.1045A>C (p.Thr349Pro)/Missense/C-terminal region	NA	Generalized clonic components with cyanosis. Severe time per day/3d	Abnormality of EEG background activity/Normal MRI	PB, VitB6/Yes/Lost follow-up

(Continued)

TABLE 1 | Continued

Patient	Sex	Exon: variant/variation type/domain	Inheritance	Initial phenotypes/age at seizures onset	EEG reports/MRI presentations during neonatal period	Treatment received/response to treatment/age at last follow-up/prognosis
13	M	exon10:c.1154dupA (p.Ile385Asnfs*16)/Frameshift/C-terminal region	*De novo*	Eye fixation or deviation to one side, generalized tonic-clonic convulsion with cyanosis. Several times per day/2 d	SB with severe abnormality of EEG background activity	PB, VitB6/ Lost follow-up
14	M	exon15:c.1663T>A (p.Phe555lie)/Missense/C-terminal region	*De novo*	Seizures since neonatal period. Daily/3d	Multifocal spikes with an abnormality of EEG background activity/Normal MRI	PB, LEV, VPA/Yes/ Lost follow-up
15	M	exon9:c.1123C>T (p.Gln375X)/ Stop_gained/C-terminal region	NA	Seizures since neonatal period. More than 10 times per day/4d	Multifocal spikes with abnormality of EEG background activity/ Normal MRI	VPA/ Yes/ 1 year/ Normal ND
16*	M	exon15:c.1763+4A>G/ splicing/C-terminal region	NA	Generalized tonic-clonic convulsion with cyanosis. 4 times before admission/8 h	Normal EEG background activity/ Normal MRI	PB, TPM/Yes/Lost follow-up
17	F	exon4:c.650C>T (p.Thr217lie)/ Missense/Segment S4	*De novo*	Eye deviation to one side, generalized clonic components with bradycardia and cyanosis/10 d	Normal EEG background/ Delayed myelination and subarachnoid hemorrhage	PB/Yes/Lost follow-up
18	M	exon4: c.584C>G (p.Ser195Cys)/ Missense/Extracellular	*De novo*	Cyanosis with generalized tonic extension. Several times per day/2 d	Spike-and-slow wave and multifocal spikes with moderate abnormality of EEG background activity	PB, VitB6/presented seizure with PB and vitB6 during hospitalization and lost follow-up.
19	M	exon4:c.650C>T (p.Thr217lie)/ Missense/Segment S4	NA	Generalized tonic extension/1 d	NA	Lost follow-up

MOL, months of life; ND, neurological development; NDD, neurodevelopmental delay; PB, phenobarbital; TPM, topiramate; LEV, Levetiracetam; VPA, valproic acid; OXC, Oxcarbazepine.
SB, suppression-burst pattern; CPAP, Continuous Positive Airway Pressure; NA, not available.
** These neonates had a family history. Patient 6: his mother had seizures in childhood. Patient 7: his father was diagnosed with schizophrenia and his mother had an intellectual disability. Patient 8: his sister was diagnosed with epilepsy managed by an antiepileptic drug. She has been seizure-free since 4 months old. Patient 16: his brother and mother were diagnosed with epilepsy. His brother was managed by antiepileptic drug and seizure-free since one-year-old. His mother's aunt was diagnosed with epilepsy and her son and daughter also.*

TABLE 2 | Novel deletion in *KCNQ2* gene identified in 11 neonates with *KCNQ2*-related disorders.

Patient	Sex	Chromosome: position (start-end); size (covered genes)	Initial phenotypes/age at seizures onset	EEG reports/MRI presentations during neonatal period	Treatment received/response to treatment/age at last follow-up/prognosis
20*	M	Chr20: 61944468-62104030; 159 kb (*CHRNA4, KCNQ2*)	Upper limb tonic extension/3 d	Moderate abnormality of EEG background activity/ Left ventricle enlargement	PB/Yes. Seizure free since 9 MOL/ 16 m/Normal ND
21	F	Chr20: 62069977-62129187; 59 kb (*KCNQ2, EEF1A2*)	Apnea/2 d	NA/ Left ventricle enlargement	PB/Yes. No seizure after discharging home/2 y/Normal ND
22*	M	Chr20: 61974574-62129187; 154 kb (*CHRNA4, KCNQ2, EEF1A2*)	Upper limb tonic extension with lower limb tonic extension. Three times before admission/2 d	Normal EEG/ Normal MRI	PB/Yes. No seizure after discharging home/2 y/Normal ND
23	M	Chr20:61974574-62129187; 154 kb (*CHRNA4, KCNQ2, EEF1A2*)	Apnea assisted by CPAP, followed by generalized tonic extension. Several times per day/3 d	Spike-and-slow wave and multifocal spikes with mild abnormality of EEG background activity/ Normal MRI	PB, LEV/No/5 m/Drug-resistant epilepsy but Normal ND
24	M	Chr20: 61974574-62078190; 103 kb (*CHRNA4, KCNQ2, EEF1A2*)	Eye deviation to one side, generalized clonic components with cyanosis and tachycardia. Daily/2 d	Spike-and-slow wave and multifocal spikes with moderate abnormality of EEG background activity/ Subdural hemorrhage, and focal injury of the right frontal lobe	PB/Yes. Seizure-free since 3 MOL/ 14 m/Normal ND
25*	F	Chr20: 61986847-62055559; 68 kb (*CHRNA4, KCNQ2*)	Eye fixation and generalized clonic components/3 d	Spike-and-slow wave and multifocal spikes with abnormality of EEG background activity	Lost follow-up
26	F	Chr20: 61041481-62680992; 1.6 Mb (*EEF1A2, KCNQ2, CHRNA4*)	Generalized clonic components/2 d	NA/NA	PB/Yes. Lost follow-up
27	F	Chr20:61273854-62907579; 1.6 Mb (*EEF1A2, KCNQ2, CHRNA4*)	Eye fixation and generalized tonic extension with bradycardia and cyanosis. Daily/2 d	Spike-and-slow wave and multifocal spikes with severe abnormality of EEG background activity. Asymmetric/ Dilation of the bilateral ventricles	PB, LEV/Yes. Seizure-free since 3 MOL/ 4m/Normal ND
28	F	Chr20: 61038552-62907579; 1.8Mb (*EEF1A2, KCNQ2, CHRNA4*)	Eye deviation to one side, generalized tonic extension with cyanosis. Several times before admission/3 d	Moderate abnormality of EEG background activity/ Dilation of bilateral ventricles, multiple ependymomas in the bilateral ventricles	PB, OXC/Yes. Seizure-free since 9 MOL/ 9 m/Normal ND
29*	F	Chr20: 61986847-62224435; 68kb (*CHRNA4, KCNQ2*)	Generalized tonic extension with cyanosis. 3-4 times per day/8d	Normal EEG/ Normal MRI	PB/Yes. No seizure after discharging home/10 m/Normal ND
30*	F	Chr20: 61826780-2660844; 834kb (*EEF1A2, KCNQ2, CHRNA4*)	Eye deviation to one side, generalized tonic extension with cyanosis. 3–4 times per day/3 d	Spike-and-slow wave and multifocal spikes with moderate abnormality of EEG background activity	PB, TPM/Yes. Seizure-free since 3 MOL 4 m/Normal ND

MOL, months of life; ND, neurological development; NDD, neurodevelopmental delay; PB, phenobarbital; TPM, topiramate; LEV, Levetiracetam; VPA, valproic acid; OXC, Oxcarbazepine. SB, suppression-burst pattern; CPAP, Continuous Positive Airway Pressure; NA, not available.

** These neonates had a family history. Patient 20: both his mother and aunt presented seizures, but were improved without medication. Patient 25: both her father and grandmother presented seizures in their childhood. Patient 29: her brother presented seizures after birth and was resolved. Patient 30: her mother presented seizures in childhood.*

patients were responsive to AED and seizure-free by 2 years old, one patient (patient 1, segment S3, p.Ala178Val) had drug-resistant epilepsy, one patient (patient 10) did not present seizure, and eight patients lost follow-up. Among the 9 patients who were seizure-free, the regions where the variants were located included two segment S4 regions (patient 3, p.Leu206Arg; patient 17, p.Thr217Iie), 1 segment S3 (patient 4, p.Ala185Thr), one extracellular region (patient 11, p.Gln188Lys), and 5 C-terminal regions (patient 5, p.Glu474X; patient 12, p.Thr349Pro; patient 14, p.Phe555Iie; patient 15, p.Gln375X; and patient 16, exon15:c.1763+4A>G). Regarding the prognosis, two patients (patient 1 and patient 10) presented neurodevelopmental delay (NDD), nine patients had normal neurological development, and eight patients lost follow-up.

Among the 11 patients with 20q13.3 deletion, nine patients were responsive to AED, and eight of them were seizure-free by 2 years old. The remaining two patients, one (patient 23) had drug-resistant epilepsy, and one (patient 25) lost follow-up. Regarding the prognosis, one (patient 25) had NDD. Different from the variable outcomes of patients with SNVs, all patients with 20q13.3 deletions with available information had normal neurological development.

DISCUSSION

We report 30 unrelated patients with novel variants in the *KCNQ2* gene, including 19 SNVs and 11 CNVs. For SNVs, missense was the most common mutation type (63.2%, 12/19), and 36.8% (7/19) of the *KCNQ2* variants were located in C-terminal regions in our cohort. Mosaic parents in *the KCNQ2* gene were reported in the literature, the mosaic state of asymptomatic parents is from 5% to 28% (Milh et al., 2015). One father with 30% mosaicism had a neurological phenotype (Weckhuysen et al., 2012). This information may indicate that mosaicism could not be ignored in epileptic encephalopathy. Furthermore, parental carrier testing should be considered regarding suffering. The next baby may still have a chance to inherit the pathogenic variant and will be affected.

In our study, all but one patient (patient 10 with the variant of c.171_172delinsAA) presented seizures in the neonatal period. Patient 10 presented motor developmental delay as an initial clinical feature. Ten EEG findings showed multifocal epileptiform with an abnormality of background activity. However, the clear phenotype–genotype correlation is unknown (Malerba et al., 2020). Previous studies indicated that *KCNQ2* missense variants were associated with severe epilepsy phenotype and poor neurological outcomes because of dominant-negative effects (Orhan et al., 2014), whereas truncating variants were likely to be *KCNQ2*-BFNE (Soldovieri et al., 2007). Research suggested that the phenotype of patients was not only related to the mutation type but also associated with the affected regions of *KCNQ2* (Goto et al., 2019). For example, missense variants in segment S6 and its nearby regions are likely to result in poor neurological outcomes (Goto et al., 2019). However, in our study, patient 1 with missense variant located in segment S3 had NDD, but patient 4 also with missense variant located in segment S3 had normal neurological development (aged 8 months old). Other patients with missense variants located in segment S4 also had normal neurological development. Therefore, the characteristics of pathogenic variants are still difficult to be linked to their clinical characteristics.

Consistent with previous studies, the patients who were responsive to AED could have variants located in segment S2 (Soldovieri et al., 2019), pore-loop domain (Weckhuysen et al., 2012; Pisano et al., 2015; Gomis-Perez et al., 2019), segment S4 (Weckhuysen et al., 2012; Pisano et al., 2015), segment S6 (Abidi et al., 2015; Pisano et al., 2015), C-terminal region (Weckhuysen et al., 2012; Pisano et al., 2015; Lee et al., 2017; Gomis-Perez et al., 2019), and extracellular region (Weckhuysen et al., 2012). Moreover, one patient (patient 4) with a variant located in segment S3 was responsive to AED and was seizure-free since he was 8 months old.

Neurodevelopmental delay often onset after seizure in *KCNQ2*-related disorders. In this study, we reported one patient had NDD as the initial phenotype. Then, the EEG was abnormal. No tremor or seizure was observed in this patient. This patient carried a *de novo* frameshift variant (c.171_172delinsAA). This variant was ranked as a likely pathogenic variant (**Supplementary Table S1**). Apart from NDD, the *KCNQ2* gene is also related to autism (Millichap et al., 2016; Long et al., 2019). This study is reported in patients and was proved by the animal model (Kim et al., 2020). Therefore, the *KCNQ2* gene may also be the candidate gene in patients with social behavior abnormalities in clinical genetic counseling.

The 20q13.3 microdeletion syndrome is characterized as seizure, brain abnormalities, NDD, and psychological problems (Pascual et al., 2013). There are variable phenotypes of 20q13.33 deletion (Kurahashi et al., 2009; Traylor et al., 2010; Mefford et al., 2012). The severe neurological phenotypes include learning disability, hyperlaxity, and strabismus (Béna et al., 2007). In this study, we reported a mild phenotype in 11 patients with 20q13.3 deletion involving *EEF1A2*, *KCNQ2* and *CHRNA4* genes. These clinical features are similar to BFNE caused by *KCNQ2* variations and are different from those of autosomal-dominant nocturnal frontal lobe epilepsy (ADNFLE) caused by *CHRNA4* variations (Steinlein et al., 1995) and developmental and epileptic encephalopathy 33 (DEE33) caused by *EEF1A2* variations (Carvill et al., 2020). Moreover, the dosage sensitivity curations of the above three genes in the ClinGen (https://search.clinicalgenome.org/kb/gene-dosage?page=1&size=25&search=) suggested that *KCNQ2* gene had sufficient evidence for haploinsufficiency and was ranked as the top 1 causative gene based on gnomAD pLI score and gnomAD predicted loss-of-function, whereas the other two genes were not yet evaluated. Therefore, the *KCNQ2* gene is considered the causative gene of the patients with 20q13.3 deletions in our study.

Consistent with a previous study (Okumura et al., 2015), 20q13.3 deletions are restricted to just *KCNQ2* and *CHRNA4* genes are likely to result in *KCNQ2*-BFNE, and one case with 20q13.3 deletion involving *EEF1A2*, *KCNQ2*, and *CHRNA4* had normal psychomotor development (Okumura et al., 2015). However, the studies indicated that patients with NDD had a larger deletion of the *KCNQ2* gene (Kurahashi et al., 2009; Traylor et al., 2010; Mefford et al., 2012; Pascual et al., 2013; Okumura et al., 2015). Patient 27 and patient 28 had a large deletion (>1 Mb). They were seizure-free and had normal neurological development. However, both of them were <1 year old at the last visit. Therefore, long-term follow-up will be necessary to determine precise phenotypes. These patients had a milder phenotype than some patients with one single-nucleotide *KCNQ2* pathogenic variant. The underlying reason is elusive and needs to be investigated.

Our study has limitations. The follow-up information was absent in some patients because patients did not present for follow-up in the clinic consistently. Therefore, we cannot diagnose the *KCNQ2*-BFNE or *KCNQ2*-NEE in some patients according to the current information. The EEG and MRI findings

were not available because some patients were enrolled from other hospitals, and they could not perform EEG or MRI. Third, our study ended in January 2021. Some patients were <1 year old. Therefore, it will be essential to follow these families up to assess neurological development.

CONCLUSION

In conclusion, we reported 30 unrelated patients with novel variations in the *KCNQ2* gene, including SNVs and CNVs. The clinical features and prognosis are heterogeneous in patients with SNVs. However, patients with 20q13.3 deletions restricted to *KCNQ2, CHRNA4,* and *EEF1A2* genes have similar to the phenotypes of BFNE. These findings could assist clinicians in diagnosing and predicting the prognosis of *KCNQ2*-related disorders.

DATA AVAILABILITY STATEMENT

The datasets presented in this study can be found in online repositories. The names of the repository/repositories and accession number(s) can be found in the article/**Supplementary Material**.

ETHICS STATEMENT

The studies involving human participants were reviewed and approved by Children's Hospital of Fudan University. Written informed consent to participate in this study was provided by the participants' legal guardian/next of kin. Written informed consent was obtained from the individual(s), and minor(s)' legal guardian/next of kin, for the publication of any potentially identifiable images or data included in this article.

AUTHOR CONTRIBUTIONS

TX, XC, YZ, HW, and WZ: conception and design. HW and WZ: administrative support. TX, XC, YX, LY, BW, LC, LL, DZ, and DC: provision of study materials or patients. TX, XC, HC, XD, and HW: collection and assembly of data. XC, XD, and LY: data analysis and interpretation. All authors: manuscript writing and final approval of manuscript.

FUNDING

The work was funded by the Clinical Research Plan of SHDC (No. SHDC2020CR4085).

ACKNOWLEDGMENTS

The authors sincerely thank all the family members for their participation in this study.

SUPPLEMENTARY MATERIAL

The Supplementary Material for this article can be found online at: https://www.frontiersin.org/articles/10.3389/fnmol.2022.809810/full#supplementary-material

REFERENCES

Abidi, A., Devaux, J. J., Molinari, F., Alcaraz, G., Michon, F. X., Sutera-Sardo, J., et al. (2015). A recurrent KCNQ2 pore mutation causing early onset epileptic encephalopathy has a moderate effect on M current but alters subcellular localization of Kv7 channels. *Neurobiol Dis.* 80, 80–92. doi: 10.1016/j.nbd.2015.04.017

Backenroth, D., Homsy, J., Murillo, L. R., Glessner, J., Lin, E., Brueckner, M., et al. (2014). CANOES: detecting rare copy number variants from whole exome sequencing data. *Nucleic Acids Res.* 42, e97. doi: 10.1093/nar/gku345

Béna, F., Bottani, A., Marcelli, F., Sizonenko, L. D., Conrad, B., and Dahoun, S. (2007). A de novo 1.1-1.6 Mb subtelomeric deletion of chromosome 20q13.33 in a patient with learning difficulties but without obvious dysmorphic features. *Am. J. Med. Genet. A.* 143a, 1894–1899. doi: 10.1002/ajmg.a.31789

Carvill, G. L., Helbig, K. L., Myers, C. T., Scala, M., Huether, R., Lewis, S., et al. (2020). Damaging de novo missense variants in EEF1A2 lead to a developmental and degenerative epileptic-dyskinetic encephalopathy. *Hum Mutat* 41, 1263–1279. doi: 10.1002/humu.24015

Dalen Meurs-van der Schoor, C., van Weissenbruch, M., van Kempen, M., Bugiani, M., Aronica, E., Ronner, H., et al. (2014). Severe Neonatal Epileptic Encephalopathy and KCNQ2 Mutation: Neuropathological Substrate? *Front Pediatr* 2, 136. doi: 10.3389/fped.2014.00136

Dong, X., Liu, B., Yang, L., Wang, H., Wu, B., Liu, R., et al. (2020). Clinical exome sequencing as the first-tier test for diagnosing developmental disorders covering both CNV and SNV: a Chinese cohort. *J. Med. Genet.* 57, 558–566. doi: 10.1136/jmedgenet-2019-106377

Gambin, T., Akdemir, Z. C., Yuan, B., Gu, S., Chiang, T., Carvalho, C. M. B., et al. (2017). Homozygous and hemizygous CNV detection from exome sequencing data in a Mendelian disease cohort. *Nucleic Acids Res.* 45, 1633–1648. doi: 10.1093/nar/gkw1237

Gomis-Perez, C., Urrutia, J., Marce-Grau, A., Malo, C., Lopez-Laso, E., Felipe-Rucian, A., et al. (2019). Homomeric Kv7.2 current suppression is a common feature in KCNQ2 epileptic encephalopathy. *Epilepsia.* 60, 139–148. doi: 10.1111/epi.14609

Goto, A., Ishii, A., Shibata, M., Ihara, Y., Cooper, E. C., and Hirose, S. (2019). Characteristics of KCNQ2 variants causing either benign neonatal epilepsy or developmental and epileptic encephalopathy. *Epilepsia.* 60, 1870–1880. doi: 10.1111/epi.16314

Kato, M., Yamagata, T., Kubota, M., Arai, H., Yamashita, S., Nakagawa, T., et al. (2013). Clinical spectrum of early onset epileptic encephalopathies caused by KCNQ2 mutation. *Epilepsia.* 54, 1282–1287. doi: 10.1111/epi.12200

Kim, E. C., Patel, J., Zhang, J., Soh, H., Rhodes, J. S., Tzingounis, A. V., et al. (2020). Heterozygous loss of epilepsy gene KCNQ2 alters social, repetitive and exploratory behaviors. *Genes. Brain Behav.* 19, e12599. doi: 10.1111/gbb.12599

Kuersten, M., Tacke, M., Gerstl, L., Hoelz, H., Stülpnagel, C. V., and Borggraefe, I. (2020). Antiepileptic therapy approaches in KCNQ2 related epilepsy: A systematic review. *Eur. J. Med Genet.* 63, 103628. doi: 10.1016/j.ejmg.2019.02.001

Kurahashi, H., Wang, J. W., Ishii, A., Kojima, T., Wakai, S., Kizawa, T., et al. (2009). Deletions involving both KCNQ2 and CHRNA4 present with benign familial neonatal seizures. *Neurology.* 73, 1214–1217. doi: 10.1212/WNL.0b013e3181bc0158

Lee, I. C., Chang, M. Y., Liang, J. S., and Chang, T. M. (2021). Ictal and interictal electroencephalographic findings can contribute to early diagnosis and prompt treatment in KCNQ2-associated epileptic encephalopathy. *J. Formos Med. Assoc. 120(1 Pt* 3), 744–754. doi: 10.1016/j.jfma.2020.08.014

Lee, I. C., Yang, J. J., Liang, J. S., Chang, T. M., and Li, S. Y. (2017). KCNQ2-Associated Neonatal Epilepsy: Phenotype Might Correlate With Genotype. *J. Child Neurol.* 32, 704–711. doi: 10.1177/0883073817701873

Long, S., Zhou, H., Li, S., Wang, T., Ma, Y., Li, C., et al. (2019). The Clinical and Genetic Features of Co-occurring Epilepsy and Autism Spectrum Disorder in Chinese Children. *Front Neurol* 10, 505. doi: 10.3389/fneur.2019.00505

Malerba, F., Alberini, G., Balagura, G., Marchese, F., Amadori, E., Riva, A., et al. (2020). Genotype-phenotype correlations in patients with de novo KCNQ2 pathogenic variants. *Neurol Genet.* 6, e528. doi: 10.1212/NXG.0000000000000528

Mefford, H. C., Cook, J., and Gospe, S. M. Jr. (2012). Epilepsy due to 20q13.33 subtelomere deletion masquerading as pyridoxine-dependent epilepsy. *Am. J. Med Genet. A*. 158A, 3190–3195. doi: 10.1002/ajmg.a.35633

Milh, M., Lacoste, C., Cacciagli, P., Abidi, A., Sutera-Sardo, J., Tzelepis, I., et al. (2015). Variable clinical expression in patients with mosaicism for KCNQ2 mutations. *Am. J. Med. Genet. A* 167A, 2314–2318. doi: 10.1002/ajmg.a.37152

Millichap, J. J., Park, K. L., Tsuchida, T., Ben-Zeev, B., Carmant, L., Flamini, R., et al. (2016). KCNQ2 encephalopathy: Features, mutational hot spots, and ezogabine treatment of 11 patients. *Neurol. Genet.* 2, e96. doi: 10.1212/NXG.0000000000000096

Niday, Z., Hawkins, V. E., Soh, H., Mulkey, D. K., and Tzingounis, A. V. (2017). Epilepsy-Associated KCNQ2 Channels Regulate Multiple Intrinsic Properties of Layer 2/3 Pyramidal Neurons. *J. Neurosci.* 37, 576–586. doi: 10.1523/JNEUROSCI.1425-16.2016

Numis, A. L., Angriman, M., Sullivan, J. E., Lewis, A. J., Striano, P., Nabbout, R., et al. (2014). KCNQ2 encephalopathy: delineation of the electroclinical phenotype and treatment response. *Neurology.* 82, 368–370. doi: 10.1212/WNL.0000000000000060

Okumura, A., Atsushi, I., Shimojima, K., Kurahashi, H., and Yoshitomi, S., Imai, K., et al. (2015). Phenotypes of children with 20q13.3 microdeletion affecting KCNQ2 and CHRNA4. *Epileptic Disord.* 17, 165–171. doi: 10.1684/epd.2015.0746

Orhan, G., Bock, M., Schepers, D., Ilina, E. I., Reichel, S. N., Loffler, H., et al. (2014). Dominant-negative effects of KCNQ2 mutations are associated with epileptic encephalopathy. *Ann. Neurol.* 75, 382–394. doi: 10.1002/ana.24080

Pan, Z., Kao, T., Horvath, Z., Lemos, J., Sul, J. Y., Cranstoun, S. D., et al. (2006). A common ankyrin-G-based mechanism retains KCNQ and NaV channels at electrically active domains of the axon. *J. Neurosc.i* 26, 2599–2613. doi: 10.1523/JNEUROSCI.4314-05.2006

Pascual, F. T., Wierenga, K. J., and Ng, Y. T. (2013). Contiguous deletion of KCNQ2 and CHRNA4 may cause a different disorder from benign familial neonatal seizures. *Epilepsy Behav. Case Rep.* 1, 35–38. doi: 10.1016/j.ebcr.2013.01.004

Pisano, T., Numis, A. L., Heavin, S. B., Weckhuysen, S., Angriman, M., Suls, A., et al. (2015). Early and effective treatment of KCNQ2 encephalopathy. *Epilepsia.* 56, 685–691. doi: 10.1111/epi.12984

Richards, S., Aziz, N., Bale, S., Bick, D., Das, S., Gastier-Foster, J., et al. (2015). Standards and guidelines for the interpretation of sequence variants: a joint consensus recommendation of the American College of Medical Genetics and Genomics and the Association for Molecular Pathology. *Genet. Med.* 17, 405–424. doi: 10.1038/gim.2015.30

Soldovieri, M. V., Ambrosino, P., Mosca, I., Miceli, F., Franco, C., Canzoniero, L. M. T., et al. (2019). Epileptic encephalopathy in a patient with a novel variant In The Kv7.2 S2 transmembrane segment: clinical, genetic, and functional features. *Int. J. Mol. Sci.* 20. doi: 10.3390/ijms20143382

Soldovieri, M. V., Miceli, F., Bellini, G., Coppola, G., Pascotto, A., and Taglialatela, M. (2007). Correlating the clinical and genetic features of benign familial neonatal seizures (BFNS) with the functional consequences of underlying mutations. *Channels (Austin).* 1, 228–233. doi: 10.4161/chan.4823

Steinlein, O. K., Mulley, J. C., Propping, P., Wallace, R. H., Phillips, H. A., Sutherland, G. R., et al. (1995). A missense mutation in the neuronal nicotinic acetylcholine receptor alpha 4 subunit is associated with autosomal dominant nocturnal frontal lobe epilepsy. *Nat. Genet.* 11, 201–203. doi: 10.1038/ng1095-201

Traylor, R. N., Bruno, D. L., Burgess, T., Wildin, R., Spencer, A., Ganesamoorthy, D., et al. (2010). A genotype-first approach for the molecular and clinical characterization of uncommon de novo microdeletion of 20q13.33. *PLoS ONE.* 5, e12462. doi: 10.1371/journal.pone.0012462

Weckhuysen, S., Mandelstam, S., Suls, A., Audenaert, D., Deconinck, T., Claes, L. R., et al. (2012). KCNQ2 encephalopathy: emerging phenotype of a neonatal epileptic encephalopathy. *Ann. Neurol.* 71, 15–25. doi: 10.1002/ana.22644

Conflict of Interest: The authors declare that the research was conducted in the absence of any commercial or financial relationships that could be construed as a potential conflict of interest.

Publisher's Note: All claims expressed in this article are solely those of the authors and do not necessarily represent those of their affiliated organizations, or those of the publisher, the editors and the reviewers. Any product that may be evaluated in this article, or claim that may be made by its manufacturer, is not guaranteed or endorsed by the publisher.

frontiers | Frontiers in Molecular Neuroscience

ORIGINAL RESEARCH
published: 28 April 2022
doi: 10.3389/fnmol.2022.821012

Phenotypic and Genotypic Characteristics of *SCN1A* Associated Seizure Diseases

Chunhong Chen, Fang Fang, Xu Wang, Junlan Lv, Xiaohui Wang and Hong Jin*

Department of Neurology, National Center for Children's Health, Beijing Children's Hospital, Capital Medical University, Beijing, China

Although *SCN1A* variants result in a wide range of phenotypes, genotype-phenotype associations are not well established. We aimed to explore the phenotypic characteristics of *SCN1A* associated seizure diseases and establish genotype-phenotype correlations. We retrospectively analyzed clinical data and results of genetic testing in 41 patients carrying *SCN1A* variants. Patients were divided into two groups based on their clinical manifestations: the Dravet Syndrome (DS) and non-DS groups. In the DS group, the age of seizure onset was significantly earlier and ranged from 3 to 11 months, with a median age of 6 months, than in the non-DS group, where it ranged from 7 months to 2 years, with a median age of 10 and a half months. In DS group, onset of seizures in 11 patients was febrile, in seven was afebrile, in two was febrile/afebrile and one patient developed fever post seizure. In the non-DS group, onset in all patients was febrile. While in the DS group, three patients had unilateral clonic seizures at onset, and the rest had generalized or secondary generalized seizures at onset, while in the non-DS group, all patients had generalized or secondary generalized seizures without unilateral clonic seizures. The duration of seizure in the DS group was significantly longer and ranged from 2 to 70 min (median, 20 min), than in the non-DS group where it ranged from 1 to 30 min (median, 5 min). Thirty-one patients harbored *de novo* variants, and nine patients had inherited variants. Localization of missense variants in the voltage sensor region (S4) or pore-forming region (S5–S6) was seen in seven of the 11 patients in the DS group and seven of the 17 patients in the non-DS group. The phenotypes of *SCN1A*-related seizure disease were diverse and spread over a continuous spectrum from mild to severe. The phenotypes demonstrate commonalities and individualistic differences and are not solely determined by variant location or type, but also due to functional changes, genetic modifiers as well as other known and unknown factors.

Keywords: epilepsy, sodium channel, *SCN1A*, genetic, generalized epilepsy with febrile seizures plus, severe myoclonic epilepsy of infancy, dravet syndrome

OPEN ACCESS

Edited by:
Yuwu Jiang,
Peking University First Hospital, China

Reviewed by:
Lori L. Isom,
University of Michigan, United States
Atsushi Ishii,
Fukuoka Sanno Hospital, Japan

****Correspondence:***
Chunhong Chen
sjkbch@sina.com

Specialty section:
This article was submitted to Brain Disease Mechanisms, a section of the journal Frontiers in Molecular Neuroscience

Received: *23 November 2021*
Accepted: *09 March 2022*
Published: *28 April 2022*

Citation:
Chen C, Fang F, Wang X, Lv J, Wang X and Jin H (2022) Phenotypic and Genotypic Characteristics of SCN1A Associated Seizure Diseases. Front. Mol. Neurosci. 15:821012. doi: 10.3389/fnmol.2022.821012

INTRODUCTION

Since the first discovery of *SCN1A* gene associated with epilepsy in 2000 (Escayg et al., 2000), *SCN1A* has remained the most common and important epilepsy pathogenic gene. The gene is located on chromosome $2q^{24.3}$ and encodes the alpha 1 subunit of the voltage-gated sodium channel Nav1.1, a 2,000 amino acid protein and exhibits dominant interneuron-specific expression. *SCN1A* variants lead to dysfunction of the sodium channel which initiates and propagates neuronal

action potentials, thereby causing epilepsy (Stafstrom, 2009). It has an autosomal dominant mode of inheritance with incomplete penetrance. Its pathogenic variants cause a wide range of phenotypes, ranging from the mildest simple febrile seizures (FS) to severe myoclonic epilepsy in infancy (SMEI), or early onset developmental and epileptic encephalopathies (Scheffer and Nabbout, 2019). Although the various phenotypes have distinct characteristics, they often have similar presentations at onset, such as early stage febrile convulsions, thereby making it difficult to predict phenotype development. To date, 2,127 pathogenic variants of the *SCN1A* have been reported and documented in the Human Gene Mutation Database. However, genotype-phenotype correlation of these seizure disorders is still unclear. This study retrospectively documented the clinical phenotype and genotype data of 41 patients with *SCN1A* variants, to explore genotype-phenotypic associations. The results can be used to define the phenotypic spectrum as well as provide a scientific basis for precision-based clinical treatment and genetic counseling for *SCN1A*-related seizure disorders.

MATERIALS AND METHODS

Study Design and Sample Collection

From March 2015 to June 2021, a total of 41 patients with *SCN1A* variants who presented with convulsions at the Department of Neurology, Beijing Children's Hospital Affiliated to Capital Medical University, China were recruited. The clinical data of these patients and their family members, including sex, age, age of seizure onset, clinical manifestations, seizure evolution, birth history, growth and development history, family history, cranial imaging, electroencephalogram (EEG), and other laboratory examinations, as well as clinical diagnosis, treatment, and follow-up were collected and summarized.

Based on the clinical manifestations, the 41 patients were divided into two groups. In the first, the Dravet syndrome (DS) group, included patients with severe myoclonic epilepsy in infancy (SMEI) and severe myoclonic epilepsy in infancy borderline (SMEB), that also covered intractable childhood epilepsy with generalized tonic-clonic seizures (ICEGTC) (Fujiwara et al., 2003). The second group contained patients of non-Dravet syndrome (non-DS), including genetic epilepsy with febrile seizures plus ($GEFS^+$), febrile seizures (FS), febrile seizures plus (FS^+), and epilepsy not classified as a specific epileptic syndrome. The diagnosis of the patients was made after meeting the specific diagnostic criteria of febrile seizures, epilepsy, and epilepsy syndrome (Commission on Classification and Terminology of the International League Against Epilepsy, 1989).

This study was a retrospective cohort study. The research scheme was approved by the medical ethics committee of Beijing Children's Hospital Affiliated to Capital Medical University.

Diagnostic Criteria

Severe myoclonic epilepsy in infancy (SMEI) typically presents with prolonged febrile and afebrile seizures in infants without impaired physical or neurologic development prior to onset. Myoclonic, focal, atypical absence, and atonic seizures present between the ages of 1 and 4 years, This form of epilepsy is usually intractable, and affected children develop epileptic encephalopathy with cognitive, behavioral, and motor impairment. The patient often has a family history of epilepsy or febrile seizures. Severe myoclonic epilepsy in infancy borderline (SMEB) refers to patients who lack several of the key features of SMEI, such as myoclonic seizure or generalized spike-wave discharges in EEG, or exhibit cognitive function impairment to a lesser degree (Scheffer et al., 2009; Guerrini and Oguni, 2011; Wirrell et al., 2017).

Febrile seizures (FS) refer to generalized tonic-clonic seizures (GTCS) with fever that occur between 6 months and 6 years. Febrile seizures that occur outside the normal age limits of classical FS (6 months to 6 years), or afebrile generalized tonic-clonic seizures occur as well as febrile convulsive seizures are referred to as febrile seizures plus (FS^+). Genetic epilepsy with febrile seizures plus ($GEFS^+$) is characterized by a wide phenotypic spectrum, including febrile seizures (FS), FS plus (FS^+), and FS along with other minor seizure types, although it is considered a familial epilepsy syndrome, but it does not always occur in a familial context, patients with $GEFS^+$ phenotypes may have *de novo* variants (Myers et al., 2017; Zhang et al., 2017).

Statistical Analysis

Data analysis was performed using SPSS version 25.0. Measurement data were expressed as the median while the enumeration data were expressed as the number of cases. For measurement data that presented a normal distribution, a *t*-test was used, else the Mann-Whitney was used for analysis. Enumeration data were analyzed using the chi-square test. Differences were considered statistically significant at $p < 0.05$.

RESULTS

Clinical Features of Patients

The clinical information of the 41 patients (26 males and 15 females) with the *SCN1A* variants they harbored is summarized in **Tables 1**, **2**. Of the 41 patients, 21 were classified as DS group (five of SMEI and 16 of SMEB) and 20 patients were non-DS group (four of epilepsy not conforming to definite epilepsy syndrome, 11 of $GEFS^+$, four of FS, and one of FS^+).

In the DS group, the age of seizure onset ranged from 3 to 11 months, with a median age of 6 months. Of these, 52.4% (11/21) had seizure onset before 6 months of age, and 47.6% (10/21) had seizure onset between 7 months and 1 year of age. In the non-DS group, the age of seizure onset ranged from 7 months to 2 years, with a median age of ten and a half months. Of these, 65% (13/20) had seizure onset between 7 months and 1 year, and 35% (7/20) had seizure onset beyond 1 year of age. The age of seizure onset in the DS group was therefore significantly earlier than that in the non-DS group ($p < 0.01$, **Supplementary File 1**). Seizure onset patterns differed considerably between the two groups. The patients in the DS group had varied seizure onset patterns since 11 (52.4%) presented with febrile seizure, seven (33.3%) with afebrile seizure and one of them with seizure that occurred

TABLE 1 | Clinical features of patients with SCN1A variant.

Patient No.	Sex	Age at seizure onset	Age at last follow-up	Seizure type	Seizure onset pattern	Seizure evolution	Seizure duration (common/max)	Seizure frequency during 24 h	Birth history	Development history	Family history	EEG (first visit)	Brain MRI	Diagnosis (group)	Medication trials	Seizure condition
1	F	7 m	6 y 6 m	GCS, MS	FS	FS/aFS	1-2 mi n/20 min	1	Normal	Mild retardation	no	Normal	Normal	SMEI (DS)	VPA	seldom
2	M	4 m	5 y	GTCS, AS, FOS	aFS	FS/aFS	20–30 min/30 min	1	Normal	Retardation	no	Abnormal (epileptiform discharges in posterior)	Abnormal (subarachnoid space widening)	SMEI (DS)	VPA LEV CLB KD	Intermittent
3	F	3 m	5 y 4 m	UCS	aFS	FS/aFS	<1 min/20 min	1	Normal	Mild retardation	no	Normal	Abnormal (subarachnoid space widening)	SMEB (DS)	VPA LEV TPM KD	Intermittent
4	F	6 m	4 y	UCS	aFS	aFS (fever after seizure)	2-3 min/30 min	1	Normal	Normal	no	Normal	Normal	SMEB (DS)	LEV VPA	intermittent
5	M	5.7 m	3 y 1 m	GCS	FS	FS/aFS	2–15 min/70 min	1	Normal	Normal	no	Normal	Normal	SMEB (DS)	VPA	intermittent
6	F	6 m	2 y 11 m	sGCS, GCS	FS	FS/aFS	1-2 min/20 min	2	Normal	Normal	no	Normal	Normal	SMEB (DS)	LEV VPA	intermittent
7	M	4 m	3 y 3 m	sGCS	FS/aFS	FS/aFS (seizure during bathing)	10 min/60 min	1	Normal	Mild retardation	Yes/mother	Normal	Abnormal (subarachnoid space widening)	SMEB (DS)	VPA LEV TPM	Intermittent
8	F	4 m	1 y 5 m	sGCS, GCS	aFS (fever after seizure)	FS/aFS	3–5 min/40 min	1	Normal	Retardation	no	Normal	Normal	SMEB (DS)	VPA LEV	Intermittent
9	F	5 m	8 y 1 m	GTCS, FOS	aFS	FS/ aFS	1–5 min	1	Normal	Retardation	no	Normal	Normal	SMEB (DS)	VPA	Intermittent
10	M	3 m	1 y 6 m	sGCS, MS	aFS	FS/aFS	3–5 mi n/30 min	1	Normal	Normal	no	Abnormal (generalized epilepstiform discharges)	Abnormal (subarachnoid space widening)	SMEI (DS)	LEV TPM	Intermittent
11	M	12 m	6 y	GTCS, FOS	FS	aFS	3-4min/6 min	1	Normal	Normal	Yes/mother, father	Abnormal (epilepstiform discharges in left posterior region)	Normal	GEFS$^+$(non-DS)	LEV	Loss
12	M	10 m	3 y 11 m	GCS	FS	FS/aFS	1-2 min/10 min	2	Normal	Normal	no	Normal	Normal	GEFS$^+$(non-DS)	VPA	Loss
13	M	10 m	6 y 6 m	GCS, FOS	FS	aFS	10 min/20 min	1	Normal	Language retardation	yes/father	Abnormal (epilepstiform discharges in left frontal and central region)	Normal	GEFS$^+$ (non-DS)	LEV	No seizure
14	F	10 m	4 y	GCS, FOS	FS	aFS	1-2 min/2 min	2	Normal	Normal	Yes/mother, grandmother	Abnormal (generalized epilepstiform discharges)	Normal	GEFS$^+$ (non-DS)	NO	Loss
15	F	10 m	6 y 1 m	GCS, FOS	FS	aFS	2-3 min/6 min	1	Normal	Normal	no	Not available	Normal	SMEB (DS)	LEV VPA TPM NZP	No seizure
16	F	5 m	9 y	GCS, FOS	aFS (seizure during bathing)	FS/aFS	1-2 min/2 min	2	Abnormal (post mature delivery postnatal mild hypoxia)	Retardation	no	Normal	Abnormal (poor myelination of periventricular white matter)	SMEB (DS)	LEV VPA TPM NZP	Intermittent
17	M	8 m	7 y 6 m	GTCS	FS	FS/aFS	2-3 min/3 min	5	Abnormal (postnatal mild hypoxia)	Mild retardation	no	Normal	Normal	SMEB (DS)	VPA TPM	Intermittent
18	F	11 m	3 y 5 m	GTCS, aAS	FS/aFS	FS/aFS	4-5 min/5 min	1	Normal	Mild retardation	no	Normal	Abnormal (right hippocampal signal increased slightly)	SMEI (DS)	VPA LEV TPM	intermittent
19	M	10 m	2 y 6 m	GTCS, MS, FOS	FS	FS/aFS	1-2 min/2 min	3	Normal	Mild retardation	no	Abnormal (generalized epilepstiform discharges)	Abnormal (slightly enlarged lateral ventricles)	SMEI (DS)	VPA	seldom
20	M	12 m	4 y 7 m	GTCS	FS	FS/aFS	3-5 min/5 min	1	Normal	Normal	Yes/father, aunt, brother	Abnormal (epileptiform discharges in Rolandic region)	Normal	GEFS$^+$ (non-DS)	LEV VPA	No seizure
21	M	7 m	4 y 3 m	GTCS	FS	FS/aFS (seizure during bathing)	3 min/30 min	1	Normal	Mild retardation	no	Normal	Normal	EP (non-DS)	LEV	seldom
22	F	8 m	2 y	GTCS	FS	FS/aFS	5 min/5 min	3	Normal	Normal	no	Boundary (rare spikes infrontal and central regions)	Normal	EP (non-DS)	VPA	intermittent
23	M	9 m	3 y 6 m	GTCS, FOS	FS	aFS	1-2 min/30 min	1	Normal	Normal	Yes/grandfather, sister	Abnormal (small spike in central region)	Normal	GEFS$^+$ (non-DS)	VPA LEV	intermittent
24	M	10 m	2 y 10 m	GTCS	FS	aFS(fever after seizure)	1-2 min/5 min	1	Normal	Normal	no	Normal	Normal	EP (non-DS)	No drug	No seizure
25	F	6 m	12 y 11 m	GTCS, FOS	FS	aFS	1-2 min/6 min	3	Normal	Retardation	no	Not available	Normal	SMEB (DS)	VPA LEV	intermittent

(Continued)

TABLE 1 | (Continued)

Patient No.	Sex	Age at seizure onset	Age at last follow-up	Seizure type	Seizure onset pattern	Seizure evolution	Seizure duration (common/max)	Seizure frequency during 24 h	Birth history	Development history	Family history	EEG (first visit)	Brain MRI	Diagnosis (group)	Medication trials	Seizure condition
26	F	1 y 2 m	5 y	GTCS, FOS	FS	aFS	5-6 min/15 min	1	Normal	Normal	Yes/mother	Abnormal (epilepstiform discharges in posterior region)	Normal	$GEFS^+$ (non-DS)	VPA	intermittent
27	M	8 m	7 y 2 m	GTCS	FS	aFS	1-2 min/2 min	1	Normal	Normal	no	Normal	Normal	$GEFS^+$ (non-DS)	NO	seldom
28	M	11 m	8 y	GTCS	FS	FS/aFS	2-5 min/5 min	1	Normal	Normal	Yes/father	Normal	Normal	$GEFS^+$ (non-DS)	VPA LEV	Loss
29	F	7 m	6 y 4 m	GTCS, FOS	aFS	aFS (seizure usually during infection)	1-2 min/10 min	1	Normal	Normal	no	Normal	Normal	SMEB (DS)	VPA LEV TPM	intermittent
30	F	2 y	4 y 8 m	GTCS, FOS	FS	aFS (fever after seizure)	5-6 min/10 min	1	Normal	Normal	Yes/mother	Abnormal (epileptiform discharges in right frontal, central and temporal regions)	Normal	$GEFS^+$ (non-DS)	VPA	Loss
31	M	9 m	2 y 11 m	GCS, aAS	FS	aFS	1-3 min/10 min	1	Normal	Normal	no	Normal	Normal	SMEB (DS)	VPA	intermittent
32	M	1 y 1 m	2 y 7 m	GTCS, FOS	FS	aFS	1-2 min/2 min	1	Normal	Normal	no	Boundary (rare spikes in frontal and central regions)	Abnormal (slightly enlarged lateral ventricles	EP (non-DS)	NO	seldom
33	M	1 y 7 m	8 y	GTCS, FOS	FS	aFS	1 min/1 min	1	Normal	Normal	Yes/father sister	Abnormal (epileptiform discharges in frontal region)	Abnormal (poor myelination of periventricular white matter)	$GEFS^+$ (non-DS)	LEV	No seizure
34	M	7 m	10 y 11 m	GTCS, FOS	FS	aFS	1 min/20 min	1	Normal	Mild retardation	Yes/mother	Normal	Normal	SMEB (DS)	VPA LEV	seldom
35	M	10 m	3 y 9 m	GTCS	FS	FS/aFS	1-2 min/30 min	3	Normal	Normal	no	Abnormal (rare epileptiform discharges)	Normal	SMEB (DS)	VPA	seldom
36	M	7 m	4 y 3 m	GTCS, FOS	FS	FS/aFS	2 min/40 min	1	Normal	Mild retardation	Yes/brother	Abnormal (epileptiform discharges in left frontal region)	Normal	SMEB (DS)	VPA LEV TPM NZP	seldom
37	M	10 m	8 y 8 m	GTCS	FS	FS	5 min/5 min	1	Normal	Normal	no	Normal	Normal	FS (non-DS)	NO	No seizure
38	M	2 y	9 y 2 m	GCS	FS	FS	3-5 min/5 min	2	Normal	Normal	no	Not available	Normal	FS^+ (non-DS)	NO	No seizure
39	M	1 y 5 m	7 y 5 m	GTCS, FOS	FS	FS	2-3 min/3 min	2	Normal	Language retardation	Yes/mother	Not available	Normal	FS (non-DS)	NO	No seizure
40	M	8 m	4 y 8 m	GTCS	FS	FS	1 min/1 min	2	Normal	Normal	no	Normal	Normal	FS (non-DS)	NO	No seizure
41	M	1 y 6 m	5 y	GTCS	FS	FS	1-2 min/2 min	2	Normal	Normal	Yes/brother	Abnormal (epileptiform discharges in posterior)	Normal	FS (non-DS)	NO	No seizure

AS, absence seizure; aAS, atypical absence seizure; MS, myoclonic seizures; GTCS, generalized tonic–clonic seizure; GCS, generalized clonic seizure; sGCS, secondary generalized clonic seizure; UCS, unilateral clonic seizure; FOS, focal seizure; SMEI, severe myoclonic epilepsy in infancy; SMEB, severe myoclonic epilepsy in infancy borderline; $GEFS^+$, genetic epilepsy with febrile seizures plus; FS, febrile seizures; aFS, afebrile seizures; FS^+, febrile seizures plus; EP, epilepsy; LEV, levetiracetam; TPM, topiramate; VPA, valproate; NZP, nitrazepam; CLB, chlorbazam; KD, ketogenic diet; EEG, electroencephalography; MRI, magnetic resonance imaging.

TABLE 2 | Summary of 41 patients' clinical data.

	DS group	non-DS group
Sex		
Male	10	16
Female	11	4
Age at seizure onset (months)		
≤6 m	11	0
7–12 m	10	11
≥12 m	0	9
Mode of onset		
Onset with febrile seizure	11	20
Onset with afebrile seizue	7	0
Onset with febrile/afebrile seizure	2	0
Onset with fever after seizure	1	0
Age at first afebrile seizure (months) among onset with febrile seizure		
≤12 m	2	0
12–36 m	7	6
≥36 m	2	7
Not available	0	2
Mode of seizure evolution		
Evolution to afebrile seizure	5	8
Evolution to febrile/afebrile seizure	15	4
Evolution to fever after seizure	1	3
No seizure	0	4
Still febrile seizure	0	1
Types of seizure		
Focal	3	0
Focal and secondary generalized	9	9
Generalized	6	11
Focal, generalized and other	3	0
Duration of seizure		
<5 min	3	6
≥5 min <10 min	4	8
≥10 min <30 min	6	4
≥30 min	8	2
Seizure frequency during one day		
1	15	13
2	2	6
>2	4	1
Birth history		
Normal	19	20
Abnormal	2	0
Family history		
Yes	3	11
No	18	9
Developmental delay		
Yes	13	3
No	8	17
EEG at initial visit		
Abnormal	5	9
Normal	14	7
Boundary	0	2
No exam	2	2
Brain MRI/CT		
Nonspecific abnormal	7	2
Normal	14	18
Treatment		
Single AEDs	6	8
Two AEDs	7	3
Three or more AEDs	8	0
No treatment	0	9
Loss follow-up	0	5
Seizure outcome		
Still seizure	20	6
No seizure	1	9
Loss follow-up	0	5

during bathing, two (9.5%) with febrile or afebrile seizure, and one (4.8%) with fever after seizure. However, all 20 patients in the non-DS group presented with febrile seizures as their seizure onset pattern. Further, in the DS group, among the 11 patients with febrile seizure onset, two patients evolved to afebrile seizure before the age of 1 year, seven between 1 and 3 years of age, and only two patients after the age of 3 years. In contrast, of the 20 patients in the non-DS group with febrile seizure onset, six patients progressed to afebrile seizure between 1 and 3 years of age, seven after 3 years of age, and none before 1 year of age. It can therefore be inferred that patients in DS group evolve to afebrile seizure earlier than those in non-DS group, however, there was no significant difference in the age of occurrence of the first afebrile seizure between the two groups ($p > 0.05$, **Supplementary File 2**).

In the DS group, five patients were afebrile at the time of seizure and one developed fever post seizure. The remaining 15 patients later developed febrile or afebrile seizure. Of these, seizures were triggered in four patients by elevated ambient temperature, such as during bathing or vigorous exercise. In the non-DS group, eight patients developed afebrile seizures, one of which occurred during bathing, four presented with febrile or afebrile seizure, three developed fever post seizure, four patients had no recurrence at the time of follow-up, and one patient still experienced febrile seizures. Thus, 58.5% (24/41) of the patients experienced seizures associated with fever or a hot environment with disease progression. This was markedly obvious in the DS group.

The following distribution of type of seizure was seen in the 41 patients included in this study. In the DS group, nine (42.9%) patients presented with generalized or secondary generalized clonic or tonic-clonic seizure, six (28.6%) with generalized clonic or tonic-clonic seizures, three (14.3%) with unilateral clonic seizures, and three (14.3%) with multiple seizures, such as unilateral clonic seizure or generalized tonic-clonic or clonic seizure, myoclonic seizure, and atypical absence seizure. In the non-DS group, nine (45%) patients presented with generalized or secondary generalized tonic-clonic or clonic seizures, and 11 (55%) with generalized tonic-clonic or clonic seizures.

The maximum duration of seizure in the DS group ranged from 2 to 70 min with a median of 20 min, while in the non-DS group it ranged from 1 to 30 min, with a median of 5 min. The duration of seizure was longer than 30 min in eight (38.1%) patients, 10–30 min in six (28.6%) patients, 5–10 min in four (19%) patients, and less than 5 min in three (14.3%) patients in the DS group. In the non-DS group, six (30%) patients had seizure episodes of less than 5 min, eight (40%) patients of 5–10 min, four (20%) patients of 10–30 min, and two (10%) patients of more than 30 min. Seizure duration was therefore significantly longer in the DS group than in the non-DS group ($p < 0.05$, **Supplementary File 3**). The two groups did not show a significant difference ($p > 0.05$, **Supplementary File 4**) with respect to frequency of seizure occurrence during a 24 h period, with 15 patients in DS group and 13 patients in non-DS group presenting with a frequency of one seizure, while two patients in DS group and six patients in non-DS group had two seizures, and four patients in DS group and one patient in non-DS group had more than two seizures.

Among the 41 patients, all except for two patients with mild hypoxia at birth had normal antenatal history. Thirteen patients in the DS group and three in the non-DS group had varying degrees of cognitive and motor development retardation. A positive family history of epilepsy or febrile seizures was recorded in 3 and 11 patients in the DS group and non-DS group, respectively.

Brain MRI of nine patients (seven in the DS group and two in the non-DS group) showed non-specific abnormalities, including four patients in DS group showed subarachnoid space widening, one patient in DS group and one patient in non-DS group showed poor myelination of periventricular white matter, one patient in DS group showed marginally higher hippocampal signal, and one in DS group and one in non-DS group showed slightly enlarged lateral ventricles. At least one electroencephalography (EEG) examination was performed on 37 patients. At the first visit, but not necessarily early in the course of the disease, EEG abnormalities including focal and generalized epileptiform discharges were seen in 14 patients (five in the DS group and nine in the non-DS group). Another two patients in the non-DS group had borderline abnormal changes and the remaining 21 patients (14 in the DS group and seven in the non-DS group) had normal EEG. In the DS group, the EEG of 14 patients were normal, of which eight patients were examined EEG before the age of 1 year at the initial stage of seizure onset, six patients were examined between 1 and 2 years old. The EEG results of remaining two patients in the DS group were unknown, which were not provided by their parents at the first visit, and the other two patients in non-DS group were diagnosed with FS and FS^+, respectively without examination of EEG.

All patients were followed up with outpatient services or telephonic consultations. In the DS group, the age at last follow-up ranged from 1 year and 5 months to 12 years and 11 months, with a median of 4 years and 3 months. In the non-DS group, it ranged from 2 to 10 years and 11 months, with a median of 5 years. There was no significant difference in age at last follow-up between the two groups ($p > 0.05$, **Supplementary File 5**). At the time of follow up, 26 patients, including 20 (20/21, 95.2%) patients in the DS group and six (6/20, 30%) patients in the non-DS group continued to experience seizures. Another 10 patients, nine (9/20, 45%) patients in the non-DS group and one (1/21, 4.8%) patient in the DS group no longer suffer from seizures at present, and the remaining five were lost to follow-up. In the DS group, eight (8/21, 38.1%) patients were treated with more than three antiepileptic drugs, seven (7/21, 33.3%) with two antiepileptic drugs, and six (6/21, 28.6%) with only one antiepileptic drug. By the time of follow-up, only one patient in the DS group had not experienced seizures for 8 months after treatment with four antiepileptic drugs. In the non-DS group, eight (8/20, 40%) patients were not prescribed drugs and advised to prevent hyperthermia alongside temporary administration of sedatives to prevent convulsions during fever, six of whom experienced no seizures, and two experienced seldom seizures. The remaining two patients, one of whom no longer has seizures, and the other who rarely experience seizures, were prescribed two antiepileptic drugs. Another five patients had one antiepileptic drug, two of whom experienced no seizures, and three experienced intermittent seizures.

Genetic Characteristic of *SCN1A* Variants Identified in This Study

Details of the identified *SCN1A* variants are summarized in **Tables 3**, **4**. Among the 41 patients, 31(75.6%) had *de novo* variants, including 20 patients in the DS group and 11 in the non-DS group. Inherited variants were seen in nine (22%) patients, including one patient in the DS group and eight in the non-DS group, all of whom reported a family history of febrile seizure or epilepsy. Among the patients with *de novo* variants, four (two in the DS group and two in the non-DS group) had a positive family history of febrile seizures despite not having inherited a pathogenic variant. Additionally, the origin of the variant identified in a single patient could not be verified due to unavailability of the father's blood sample.

The distribution of variant type in the DS group included nonsense variants in five patients, frameshift variants in four, a splice site variant in one, and missense variants in the remaining eleven. Missense variants were found in 17 patients, and the remaining three had a deletion, a partial deletion of *SCN1A* exon 20–29, and a $2q^{24.3}$ deletion each in the non-DS group.

A wide distribution of the 39 *SCN1A* point variants identified across all domains of the sodium channels were observed (**Figure 1**). Of these, 10 mapped to the sodium channel pore-forming region (S5–S6), six to the voltage sensor region (S4), eight to the linker regions, and the remaining 15 were scattered evenly throughout the sodium channels Nav1.1 (**Figure 2**). Among the eleven missense variants in the DS group, three were located in the S4 region, four in the S5–S6 region, and the rest were evenly distributed. Of the 10 termination variants, including nonsense, frameshift, and splice site variants, five were located in the linker region, and the rest were distributed evenly (**Figure 3**). In the non-DS group, 17 patients harbored missense variants, of which five were located in the S5–S6 region, two in the S4 region, and the remaining were evenly distributed (**Figure 4**).

TABLE 3 | Genetic characteristic of 41 *SCN1A* variants identified in this study.

No./Phenotype	Exon	cDNA*	Variant	Location in protein	Mutation type	Transmission	Reported mutation (references) (previous diagnosis)
1/SMEI	4	c.563A > C	p.D188A	DIS2-DIS3	Missense	De novo	No
2/SMEI	26	c.4571delC	p.P1524Lfs*15	DIIIS6-DIVS1	Frameshift	De novo	No
3/SMEB	26	c.5035delC	p.L1679X	DIVS5	Nonsense	De novo	No
4/SMEB	16	c.3111dupC	p.F1038Lfs*3	DIIS6-DIIIS1	Frameshift	De novo	No
5/SMEB	26	c.4439G > T	p.G1480V	DIIIS6-DIVS1	Missense	De novo	Yes (Harkin et al., 2007) MAE
6/SMEB	4	c.272T > C	p.I91T	$H3N^{+}$-DI	Missense	De novo	Yes (Sun et al., 2008) SMEI
7/SMEB	13	c.1837C > T	p.R613X	DIS6-DIIS1	Nonsense	Maternal	Yes (Kearney et al., 2006) SMEI
8/SMEB	25	c.4301G > A	p.W1434X	DIIIS5-DIIIS6	Nonsense	De novo	Yes (Zucca et al., 2008) SMEI
9/SMEB	19	c.3759dupA	p.Y1254Ifs*3	DIIIS2	Frameshift	De novo	No
10/SMEI	23	c.3981delA	p.L1327Ffs*7	DIIIS4	Frameshift	De novo	No
11/$GEFS^{+}$	1	c.1852C > T	p.R618C	DIS6-DIIS1	Missense	Maternal	Yes (Brunklaus et al., 2015) $GEFS^{+}$ SMEI
12/$GEFS^{+}$	15	c.2732_2733delinsAA	p.L911Q	DIIS5-DIIS6	Missense	De novo	No
13/$GEFS^{+}$	21	c.4112G > C	p.G1371A	DIIIS5-DIIIS6	Missense	De novo	No
14/$GEFS^{+}$	2	c.364A > G	p.I122V	$H3N^{+}$-DI	Missense	Maternal	Yes (Till et al., 2020) SMBI
15/SMEB	18	c.2791C > T	p.R931C	DIIS5-DIIS6	Missense	De novo	Yes (Ohmori et al., 2002) SMEI
16/SMEB	28	c.4762T > C	p.C1588R	DIVS2	Missense	De novo	Yes (Marini et al., 2007) SMEI
17/SMEB	18	c.2946+2T > C	(splicing)	DIIS6	Splice site	De novo	No
18/SMEI	12	c.2134C > T	p.R712X	DIS6-DIIS1	Nonsense	De novo	Yes (Sugawara et al., 2002) SMEI
19/SMEI	15	c.2134C > T	p.R712X	DIS6-DIIS1	Nonsense	De novo	Yes (Sugawara et al., 2002) SMEI
20/$GEFS^{+}$	28	c.4741A > G	p.I1581V	DIVS2	Missense	Paternal	No
21/EP	6	c.706A > T	p.I236F	DIS4-DIS5	Missense	De novo	No
22/EP	20-29del				Partial exon deletion	De novo	No
23/$GEFS^{+}$	28	c.5218G > T	p.D1740Y	DIVS5-DIVS6	Missense	Paternal	No
24/EP	2q24.3del				2q24.3 deletion	De novo	No
25/SMEB	9	c.825T > G	p.N275K	DIS5-DIS6	Missense	De novo	No
26/$GEFS^{+}$	7	c.493T > C	p.Y165H	DIS2	Missense	Maternal	Yes (Fernández-Marmiesse et al., 2019) SMBI
27/$GEFS^{+}$	19	c.3867_3869delCTT	p.1289delF	DIIIS3	Deletion	De novo	Yes (Ohmori et al., 2006) SMBI
28/$GEFS^{+}$	14	c.2576G > A	p.R859H	DIIS4	Missense	De novo	Yes (Volkers et al., 2011) $GEFS^{+}$
29/SMEB	5	c.680T > G	p.I227S	DIS4	Missense	De novo	Yes (Nabbout et al., 2003) SMEI
30/$GEFS^{+}$	26	c.5770C > G	p.R1924G	DIVS6-CO2-	Missense	Maternal	No
31/SMEB	24	c.4049T > C	p.V1350A	DIIIS4	Missense	De novo	No
32/EP	18	c.2735T > C	p.F912S	DIIS5-DIIS6	Missense	De novo	No
33/$GEFS^{+}$	6	c.G709C	p.V237L	DIS4-DIS5	Missense	Paternal	No
34/SMEB	21	c.4168G > A	p.V1390M	DIIIS5-DIIIS6	Missense	De novo	Yes (Rilstone et al., 2012) SMEI
35/SMEB	17	c.2585G > T	p.R862L	DIIS4	Missense	De novo	No
36/SMEB	28	c.5108A > C	p.D1703A	DIVS5-DIVS6	Missense	De novo	No
37/FS	18	c.3643G > T	p.V1215F	DIIS6-DIIIS1	Missense	De novo	No
38/FS^{+}	20	c.3973A > G	p.R1325G	DIIIS4	Missense	De novo	No
39/FS	29	c.5389G > T	p.A1797S	DIV-CO2	Missense	Unknown	No
40/FS	26	c.5078C > A	p.A1693D	DIVS5-DIVS6	Missense	De novo	No
41/FS	28	c.4787G > A	p.R1596H	DIVS2-DIVS3	Missense	Paternal	Yes (Zuberi et al., 2011) $GEFS^{+}$

*DIS1, domain 1 segment 1; SMEI, severe myoclonic epilepsy in infancy; SMEB, severe myoclonic epilepsy in infancy borderline; $GEFS^{+}$, genetic epilepsy with febrile seizures plus; EP, epilepsy not classified as a specific epileptic syndrome; FS^{+}, febrile seizures plus; FS, febrile seizures. *Coding DNA reference sequence NM_001165963 does not contain intron sequences.*

TABLE 4 | Summary of 41 patients' genetic data.

ITEM\case	DS group	Non-DS group	Total
	21	20	41
Genetic variation	1	8	9
De novo	20	11	31
Unknown	0	1	1
Missense mutation	11	17	28
Nonsense mutation	5	0	5
Frameshift	4	0	4
Splice site	1	0	1
Deletion mutation	0	1	1
Partial deletion of SCN1A exon	0	1	1
$2q^{24.3}$ deletion	0	1	1

DISCUSSION

The *SCN1A* gene was first associated with genetic (formerly generalized) epilepsy with febrile seizures plus (GEFS+) (Escayg et al., 2000). Subsequently, it was discovered that the vast majority of patients with Dravet syndrome harbored *SCN1A* variants with an increasing number of *SCN1A* variants being reported. To date, the clinical spectrum of epilepsies related to *SCN1A* variants encompass various phenotypes, the most common being SMEI and SMEB, and a small proportion being $GEFS^+$, including FS and FS^+. Other phenotypes included epilepsies not classified as a definite epileptic syndrome and rare early onset developmental and epileptic encephalopathy (Sadleir et al., 2017).

Although the 41 patients in our study presented with the same complaint of intermittent convulsions with or without fever in the early stage of the disease, other clinical manifestations were not similar. Age of seizure onset in the DS group was significantly earlier than that of the non-DS group, since all the patients were below 1 year of age, and most were symptomatic before 6 months of age. The pattern of onset in the DS group was either febrile or afebrile seizures, or an alternate occurrence of the two. In the non-DS group the only pattern of onset was febrile seizures. Patients in the DS group initially showed unilateral clonic seizure or secondary generalized clonic or tonic-clonic seizures, or generalized clonic or tonic-clonic seizures. However, those in the non-DS group showed generalized or secondary generalized clonic or tonic-clonic seizures without unilateral clonic seizures. Longer duration of seizures as well as a greater tendency to be prone to status epilepticus was reported from patients in the DS group than those in the non-DS group. The vast majority of patients in the DS group experienced seizures with a frequency of one every 24 h, however, some in the non-DS group experienced more than two seizures in the same time period and demonstrated some clustered features. While there was no significant difference between the two groups, the age of first afebrile seizure in patients with febrile seizure at onset was slightly earlier in the DS group than in the non-DS group. To summarize, the clinical manifestations of both groups are specific and vary in terms of severity and complexity.

In spite of phenotypic differences, several core features remained consistent. Seizure-related fever was observed in 34 patients (83%) at onset, and the remaining seven patients with

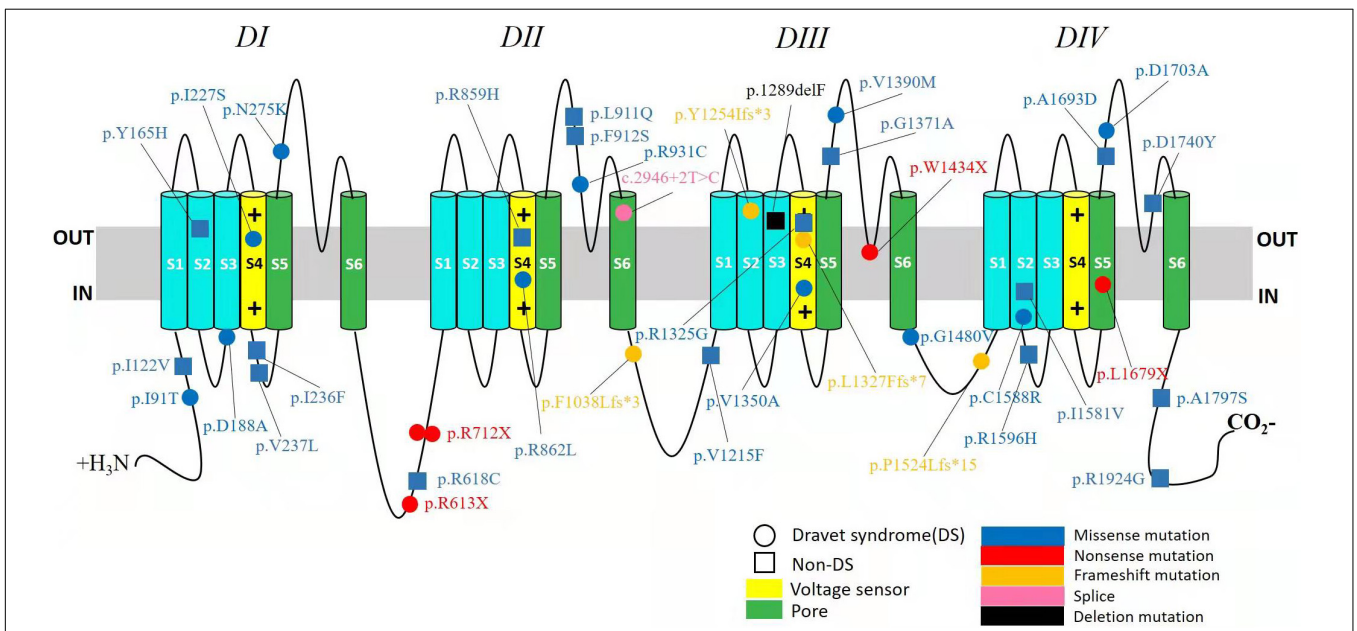

FIGURE 1 | Structure of the human Nav1.1 channel and the location of *SCN1A* variants identified in this study. Nav1.1 channels α subunit consist of four homologous domains (DI–DIV), each with six transmembrane segments (S1–S6). The fourth segment (S4) of each domain functions as a voltage sensor. The S5 and S6 segments of each domain make up the pore of the channel, and the connecting loop between S5 and S6 is the pore loop. The identified variants in DS group were depicted with circle and in non-DS group with square. Missense variants are shown in blue. Nonsense variants are shown in red. Frameshift variants are shown in orange. Splice site variant is shown in pink and deletion variant in black.

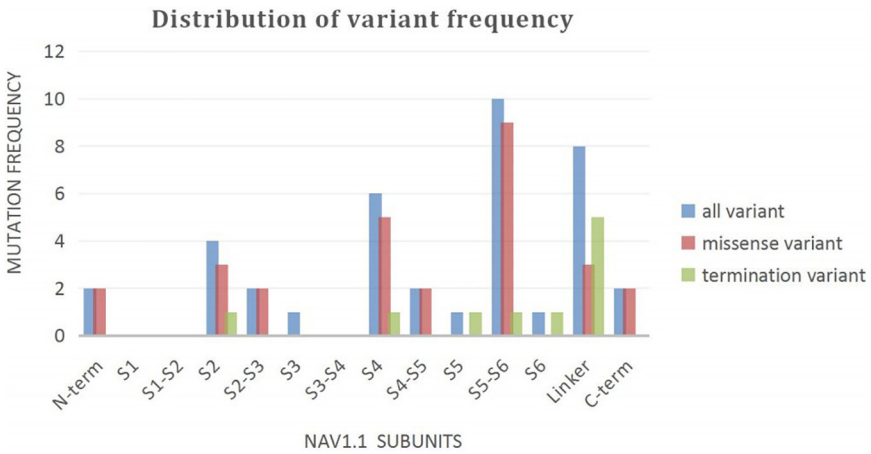

FIGURE 2 | Distribution of variant frequency of 39 patients with point variant in our study.

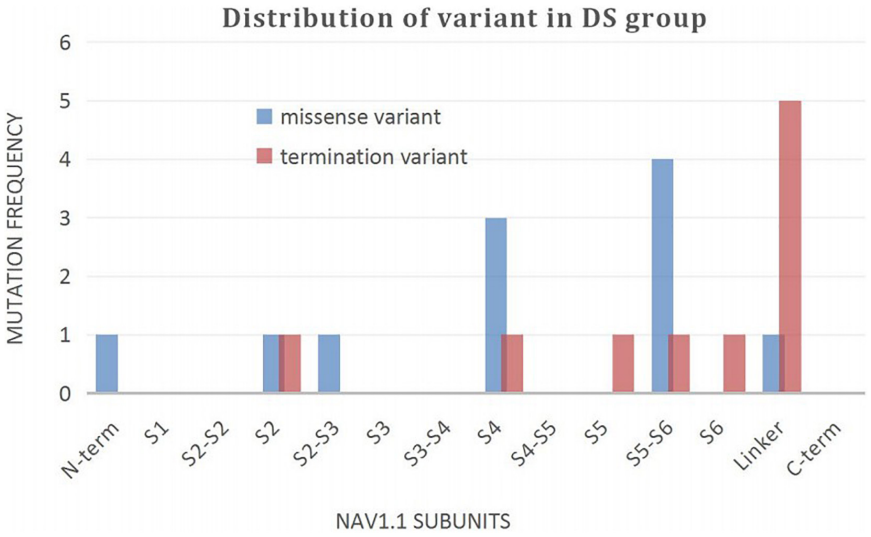

FIGURE 3 | Distribution of variant in DS group.

afebrile onset of seizure eventually developed febrile seizures in the course of the disease. In addition, 32 patients (78%) experienced seizure durations of more than 5 min, and 20 patients (50%) had prolonged seizures that lasted longer than 10 min, especially in the DS group. Consequently, in concordance with previous findings, fever-related and/or prolonged seizures are prominent phenotypes associated with *SCN1A* variants (Guerrini and Oguni, 2011).

The phenotype of *SCN1A* variant is a continuous disease spectrum ranging from the mild self-limited and drug-reactive diseases, such as GEFS$^+$, FS, and FS$^+$ to the severe drug-refractory developmental epileptic encephalopathies (DEE), including DS and other rare phenotypes such as myoclonic-atonic epilepsy (MAE), epilepsy of infancy with migrating focal seizures (EIMFS), and early onset *SCN1A*- related DEE, which have been reported in rare cases (Wallace et al., 2001; Carranza Rojo et al., 2011; Freilich et al., 2011). With the wide application of gene sequencing technology, some focal epilepsies have been found to be associated with *SCN1A* variants (McDonald et al., 2017; Bisulli et al., 2019). Thus, the phenotypes of *SCN1A* variants possess significant heterogeneity. Many of the differences between DS and non-DS are a function of the definitions of the disease. They have common genetic etiology and are a continuous entity of a disease with a wide range of seizure types and severities. Sometimes, it is very hard to separate adjacent phenotypes with a line.

As many as 2,127 diverse variations in the *SCN1A* have been reported that map to almost every domain of the voltage-gated sodium channel alpha 1 subunit protein, resulting in a large assortment of potential alterations in channel function. Phenotypic variations as the consequence of *SCN1A* variations depend on a variety of factors including position, type, and the

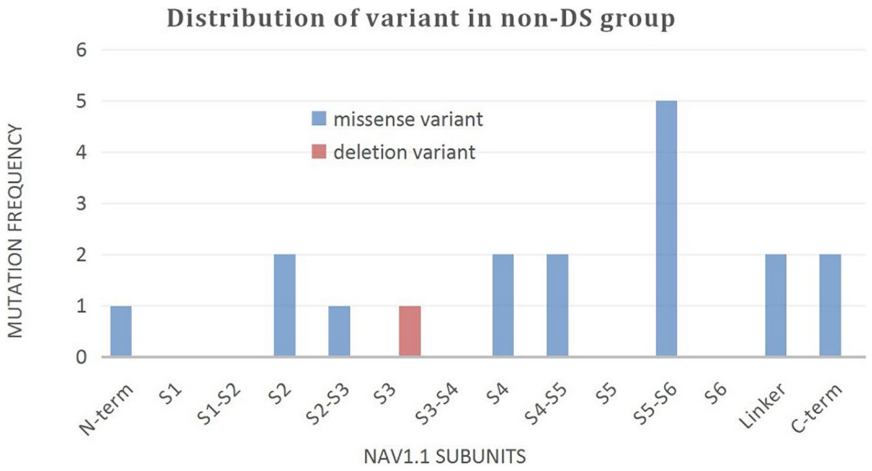

FIGURE 4 | Distribution of variant in non-DS group.

category of functional change induced by variants, as well as the role of other modifier genes and environmental effects (Meng et al., 2015; Fang et al., 2019). The main etiology of *SCN1A* associated epileptic phenotypes is closely related to its functional changes. The functional researches of *SCN1A* variants have confirmed that loss-of-function leading to haploinsufficiency is the main effect of both Dravet syndrome and GEFS$^+$, although for some variants, mixed loss- and gain-of-function effects and for few variants a net gain-of-function have been observed (Mantegazza and Broccoli, 2019). Recent study has investigated that *SCN1A* T226M variant presents gain-of-function in early infantile development and epileptic encephalopathy which is far more severe than typical Dravet syndrome (Berecki et al., 2019). Previous studies have demonstrated the correlation of clinical severity with variant type, with missense changes resulting in milder and truncations causing severe epilepsy (Kanai et al., 2004; Stafstrom, 2009). So, genotypes determine phenotypes, the relationship appears unexpected complexity involving numerous known and unknown factors related to intrinsically complex pathophysiologic responses as well as environmental factors, which yet remain to be fully disentangled.

In our study, 10 patients in the DS group carried protein termination variants, including five nonsense, four frameshift, and one splice site variant. Termination of protein translation resulting in a short truncated protein is predicted to cause complete loss of sodium channel function and a consequent severe phenotype. The remaining eleven patients harbored missense variants, of which seven were located within functionally important domains including the sodium channel ion pore and voltage sensor regions and still had seizures up to the last follow-up, only one patient treated with four kinds of antiepileptic drugs without seizures for 8 months. Our results are consistent with those of previous studies (Ceulemans et al., 2004; Kanai et al., 2004; Zuberi et al., 2011) and demonstrate a correlation between genotype (such as the nature and location of variants) and phenotype. Of the variants associated with severe phenotypes, truncation variants are often evenly distributed in the sodium channels, while missense variants are mostly concentrated around voltage sensors and channel pores (Zuberi et al., 2011). Our results demonstrate a higher distribution of termination variants in the linker region. Given that this is a novel finding, it will be interesting to validate it in a large sample size study. About truncation variants, another situation requires attention. It is identified that few DS patients are caused by poison exons that are naturally occurring and highly conserved exons, these poison exons contain a premature termination codon, alternative splicing of such an exon is predicted to lead to nonsense mediated decay, decreasing the amount of protein produced (Carvill and Mefford, 2020; Aziz et al., 2021). Therefore, the results of nonsense mediated decay are similar to those of truncation variants.

Among the 17 patients with missense variants in the non-DS group, seven carried variants that were located within the sodium channel ion pore and voltage sensor regions. Except two patients lost to follow-up, only two patients with the phenotypes of GEFS$^+$ and epilepsy not classified as a specific epileptic syndrome continued to experience intermittent seizures, the other three patients, including one case of GEFS$^+$, FS and FS$^+$, respectively, fared better with stoppage of seizure episodes. We were therefore able to conclude that variant location in a functionally important domain of the sodium channel need not necessarily translate into a serious phenotype. The reason why certain missense variations are linked to severe phenotypes, while others are not, is not well elucidated. Similarly, in the DS group, two patients with identical genotypes carrying the same nonsense variants had significantly different phenotypes, one with mild epilepsy and the other suffering from severe disease. This strongly suggests the influence of other factors including modifier genes, environmental effects, and brain development in determining the phenotypic expression of the disease (Stafstrom, 2009; Parihar and Ganesh, 2013). Genetic modifiers are genes distinct from the primary mutation that modulate the severity of the disease phenotype (Kearney, 2011). The studies identified several genetic modifiers such as *Hlf*, the gene encoding hepatic leukemia factor, *Cacna1g*, the gene

encoding Cav3.1 and *Gabra2*, the gene encoding the $GABA_A$ receptor α2 subunit that influence the phenotypes and severity of *Scn1a*$^{+/-}$ mouse model of Dravet syndrome (Hawkins and Kearney, 2016; Calhoun et al., 2017; Hawkins et al., 2021). In addition, it is also reported that variants in *Scn2a, Kcnq2*, and *Scn8a* can dramatically influence the phenotype of mice carrying the *Scn1a*-R1648H mutation (Hawkins et al., 2011). The ability to study the complex genetic interactions in model organisms contributes to our understanding of the genetic factors that influence neurological disease and suggest candidate genes for follow-up study in human patients.

With the researches of the pathogenic mechanism of *SCN1A*-related epilepsy, especially the functional changes and genetic modifiers, there are some novel therapeutic approaches that target seizure control through genetic modulation have emerged. Due to *SCN1A* haploinsufficiency of most DS patients, the first precision therapy was antisense oligonucleotides (ASO) which can restore functional *SCN1A* mRNA and NaV1.1 levels. It was developed using Targeted Augmentation of Nuclear Gene Output (TANGO) technology (Lim et al., 2020). Another gene therapy focuses on adeno-associated virus (AAV)-delivered gene modulation. For example, an adeno-associated virus serotype 9 (AAV9) vector-based, GABAergic neuron-selective, which can upregulate endogenous *SCN1A* gene expression to prevent GABAergic neurons disinhibition (Isom and Knupp, 2021). The treatments of genetic epilepsy will no longer be solely symptomatic to control seizures, but will be transformed into genomics-driven personalized therapy for underlying molecular defects or its consequences.

Our findings should be interpreted in the context of certain limitations. This retrospective study only includes patients who came to our hospital for diagnosis and treatment, which may result in some bias. Additionally, our sample size is small and follow-up duration was short. These limitations can be overcome by further long term follow up studies in large cohorts. Our findings will help to further understand the clinical characteristic significance of *SCN1A* variants. The phenotypes of *SCN1A* associated seizure disorder are significantly heterogeneous over a continuous spectrum from mild to severe with both commonness and individuality. The effect of variants on phenotype is not completely determined by location and type, but also due to functional changes, genetic modifiers as well as other known and unknown factors, therefore genotype-phenotype predictions cannot be easily made. Evaluation of patients in the early stage of disease, with respect to clinical manifestations and *SCN1A* variant features is crucial to assess disease progression for early identification of patients who may benefit most from precise medical intervention.

DATA AVAILABILITY STATEMENT

The original contributions presented in the study are included in the article/**Supplementary Material**, further inquiries can be directed to the corresponding author/s.

ETHICS STATEMENT

The studies involving human participants were reviewed and approved by the medical ethics committee of Beijing Children's Hospital Affiliated to Capital Medical University. Written informed consent to participate in this study was provided by the participants' legal guardian/next of kin. Written informed consent was obtained from the minor(s)' legal guardian/next of kin for the publication of any potentially identifiable images or data included in this article.

AUTHOR CONTRIBUTIONS

CC conceptualized and designed the study, drafted the initial manuscript, and reviewed and revised the manuscript. CC, FF, XW, JL, XHW, and HJ collected data and carried out the initial analyses. All authors approved the final manuscript as submitted and agreed to be accountable for all aspects of the work.

ACKNOWLEDGMENTS

We thank the patients and their families for their cooperation in this study. We would like to thank Mr. Kangkang Peng for helping to complete figures and tables as well as some statistical calculations. We would also like to thank Editage (www.editage.com) for English language editing.

SUPPLEMENTARY MATERIAL

The Supplementary Material for this article can be found online at: https://www.frontiersin.org/articles/10.3389/fnmol.2022.821012/full#supplementary-material

REFERENCES

Aziz, M. C., Schneider, P. N., and Carvill, G. L. (2021). Targeting poison exons to treat developmental and epileptic encephalopathy. *Dev. Neurosci.* 43, 241–246. doi: 10.1159/000516143

Berecki, G., Bryson, A., Terhag, J., Maljevic, S., Gazina, E. V., Hill, S. L., et al. (2019). SCN1A gain of function in early infantile encephalopathy. *Ann. Neurol.* 85, 514–525. doi: 10.1002/ana.25438

Bisulli, F., Licchetta, L., Baldassari, S., Muccioli, L., Marconi, C., Cantalupo, G., et al. (2019). SCN1A mutations in focal epilepsy with auditory features: widening the spectrum of GEFS plus. *Epileptic Disord.* 21, 185–191. doi: 10.1684/epd.2019.1046

Brunklaus, A., Ellis, R., Stewart, H., Aylett, S., Reavey, E., Jefferson, R., et al. (2015). Homozygous mutations in the SCN1A gene associated with genetic epilepsy with febrile seizures plus and Dravet syndrome in 2 families. *Eur. J. Paediat. Neurol.* 19, 484–488. doi: 10.1016/j.ejpn.2015.02.001

Calhoun, J. D., Hawkins, N. A., Zachwieja, N. J., and Kearney, J. A. (2017). Cacna1g is a genetic modifier of epilepsy in a mouse model of Dravet syndrome. *Epilepsia* 58, e111–e115. doi: 10.1111/epi.13811

Carranza Rojo, D., Hamiwka, L., McMahon, J. M., Dibbens, L. M., Arsov, T., Suls, A., et al. (2011). De novo SCN1A mutations in migrating partial seizures of infancy. *Neurology* 77, 380–383. doi: 10.1212/WNL.0b013e318227046d

Carvill, G. L., and Mefford, H. C. (2020). Poison exons in neurodevelopment and disease. *Curr. Opin. Genet. Dev.* 65, 98–102. doi: 10.1016/j.gde.2020.05.030

Ceulemans, B. P., Claes, L. R., and Lagae, L. G. (2004). Clinical correlations of mutations in the SCN1A gene: from febrile seizures to severe myoclonic epilepsy in infancy. *Pediatr. Neurol.* 30, 236–243. doi: 10.1016/j.pediatrneurol.2003.10.012

Commission on Classification and Terminology of the International League Against Epilepsy (1989). Commission on classification and terminology of the international league against epilepsy. Proposal for revised classification of epilepsies and epileptic syndromes. *Epilepsia* 30, 389–399. doi: 10.1111/j.1528-1157.1989.tb05316

Escayg, A., MacDonald, B. T., Meisler, M. H., Baulac, S., Huberfeld, G., An-Gourfinkel, I., et al. (2000). Mutations of SCN1A, encoding a neuronal sodium channel, in two families with GEFS+2. *Nat. Genet.* 24, 343–345. doi: 10.1038/74159

Fang, Z. X., Hong, S. Q., Li, T. S., Wang, J., Xie, L. L., Han, W., et al. (2019). Genetic and phenotypic characteristics of SCN1A-related epilepsy in Chinese children. *NeuroReport* 30, 671–680. doi: 10.1097/WNR.0000000000001259

Fernández-Marmiesse, A., Roca, I., Díaz-Flores, F., Cantarín, V., Pérez-Poyato, M. S., Fontalba, A., et al. (2019). Rare variants in 48 genes account for 42% of cases of epilepsy with or without neurodevelopmental delay in 246 pediatric patients. *Front. Neurosci.* 13:1135. doi: 10.3389/fnins.2019.01135

Freilich, E. R., Jones, J. M., Gaillard, W. D., Conry, J. A., Tsuchida, T. N., Reyes, C., et al. (2011). Novel SCN1A mutation in a proband with malignant migrating partial seizures of infancy. *Arch. Neurol.* 68, 665–671. doi: 10.1001/archneurol.2011.98

Fujiwara, T., Sugawara, T., Mazaki-Miyazaki, E., Takahashi, Y., Fukushima, K., Watanabe, M., et al. (2003). Mutations of sodium channel alpha subunit type 1 (SCN1A) in intractable childhood epilepsies with frequent generalized tonic-clonic seizures. *Brain* 126, 531–546. doi: 10.1093/brain/awg053

Guerrini, R., and Oguni, H. (2011). Borderline Dravet syndrome: a useful diagnostic category? *Epilepsia* 52(Suppl. 2), 10–12. doi: 10.1111/j.1528-1167.2011.02995.x

Harkin, L. A., McMahon, J. M., Iona, X., Dibbens, L., Pelekanos, J. T., Zuberi, S. M., et al. (2007). The spectrum of SCN1A-related infantile epileptic encephalopathies. *Brain* 130, 843–852. doi: 10.1093/brain/awm002

Hawkins, N. A., Martin, M. S., Frankel, W. N., Kearney, J. A., and Escayg, A. (2011). Neuronal voltage-gated ion channels are genetic modifiers of generalized epilepsy with febrile seizures plus. *Neurobiol. Dis.* 41, 655–660. doi: 10.1016/j.nbd.2010.11.016

Hawkins, N. A., Nomura, T., Duarte, S., Barse, L., Williams, R. W., Homanics, G. E., et al. (2021). Gabra2 is a genetic modifier of Dravet syndrome in mice. *Mamm. Genome* 32, 350–363. doi: 10.1007/s00335-021-09877-1

Hawkins, N. A., and Kearney, J. A. (2016). Hlf is a genetic modifier of epilepsy caused by voltage-gated sodium channel mutations. *Epilepsy Res.* 119, 20–23. doi: 10.1016/j.eplepsyres.2015.11.016

Isom, L. L., and Knupp, K. G. (2021). Dravet syndrome: novel approaches for the most common genetic epilepsy. *Neurotherapeutics* 18, 1524–1534. doi: 10.1007/s13311-021-01095-6

Kanai, K., Hirose, S., Oguni, H., Fukuma, G., Shirasaka, Y., Miyajima, T., et al. (2004). Effect of localization of missense mutations in SCN1A on epilepsy phenotype severity. *Neurology* 63, 329–334. doi: 10.1212/01.wnl.0000129829.31179.5b

Kearney, J. A. (2011). Genetic modifiers of neurological disease. *Curr. Opin. Genet. Dev.* 21, 349–353. doi: 10.1016/j.gde.2010.12.007

Kearney, J. A., Wiste, A. K., Stephani, U., Trudeau, M. M., Siegel, A., RamachandranNair, R., et al. (2006). Recurrent *de novo* mutations of SCN1A in severe myoclonic epilepsy of infancy. *Pediat. Neurol.* 34, 116–120. doi: 10.1016/j.pediatrneurol.2005.07.009

Lim, K. H., Han, Z., Jeon, H. Y., Kach, J., Jing, E., Weyn-Vanhentenryck, S., et al. (2020). Antisense oligonucleotide modulation of non-productive alternative splicing upregulates gene expression. *Nat. Commun.* 11:3501. doi: 10.1038/s41467-020-17093-9

Mantegazza, M., and Broccoli, V. (2019). SCN1A/Na_V1.1 channelopathies: mechanisms in expression systems, animal models, and human iPSC models. *Epilepsia* 60(Suppl. 3), S25–S38. doi: 10.1111/epi.14700

Marini, C., Mei, D., Temudo, T., Ferrari, A. R., Buti, D., Dravet, C., et al. (2007). Idiopathic epilepsies with seizures precipitated by fever and SCN1A abnormalities. *Epilepsia* 48, 1678–1685. doi: 10.1111/j.1528-1167.2007.01122.x

McDonald, C. L., Saneto, R. P., Carmant, L., and Sotero de Menezes, M. A. (2017). Focal seizures in patients with SCN1A mutations. *J. Child Neurol.* 32, 170–176. doi: 10.1177/0883073816672379

Meng, H., Xu, H. Q., Yu, L., Lin, G. W., He, N., Su, T., et al. (2015). The SCN1A mutation database: updating information and analysis of the relationships among genotype, functional alteration and phenotype. *Hum. Mutat.* 36, 573–580. doi: 10.1002/humu.22782

Myers, K. A., Burgess, R., Afawi, Z., Damiano, J. A., Berkovic, S. F., Hildebrand, M. S., et al. (2017). De novo SCN1A pathogenic variants in the GEFS+ spectrum: not always a familial syndrome. *Epilepsia* 58, e26–e30. doi: 10.1111/epi.13649

Nabbout, R., Gennaro, E., Bernardina, B. D., Dulac, O., Madia, F., Bertini, E., et al. (2003). Spectrum of SCN1A mutations in severe myoclonic epilepsy of infancy. *Neurology* 60, 1961–1967. doi: 10.1212/01.wnl.0000069463.41870.2f

Ohmori, I., Kahlig, K. M., Rhodes, T. H., Wang, D. W., and George, A. L. (2006). Nonfunctional SCN1A is common in severe myoclonic epilepsy of infancy. *Epilepsia* 47, 1636–1642. doi: 10.1111/j.1528-1167.2006.00643.x

Ohmori, I., Ouchida, M., Ohtsuka, Y., Oka, E., and Shimizu, K. (2002). Significant correlation of the SCN1A mutations and severe myoclonic epilepsy in infancy. *Biochem. Biophys. Res. Commun.* 295, 17–23. doi: 10.1016/s0006-291x(02)00617-4

Parihar, R., and Ganesh, S. (2013). The SCN1A gene variants and epileptic encephalopathies. *J. Hum. Genet.* 58, 573–580. doi: 10.1038/jhg.2013.77

Rilstone, J. J., Coelho, F. M., Minassian, B. A., and Andrade, D. M. (2012). Dravet syndrome: seizure control and gait in adults with different SCN1A mutations. *Epilepsia* 53, 1421–1428. doi: 10.1111/j.1528-1167.2012.03583.x

Sadleir, L. G., Mountier, E. I., Gill, D., Davis, S., Joshi, C., DeVile, C., et al. (2017). Not all SCN1A epileptic encephalopathies are Dravet syndrome: early profound Thr226Met phenotype. *Neurology* 89, 1035–1042. doi: 10.1212/WNL.0000000000004331

Scheffer, I. E., and Nabbout, R. (2019). SCN1A-related phenotypes: epilepsy and beyond. *Epilepsia* 60 (Suppl. 3), S17–S24. doi: 10.1111/epi.16386

Scheffer, I. E., Zhang, Y. H., Jansen, F. E., and Dibbens, L. (2009). Dravet syndrome or genetic (generalized) epilepsy with febrile seizures plus? *Brain Dev.* 31, 394–400. doi: 10.1016/j.braindev.2009.01.001

Stafstrom, C. E. (2009). Severe epilepsy syndromes of early childhood: the link between genetics and pathophysiology with a focus on SCN1A mutations. *J. Child Neurol.* 24(Suppl. 8), 15S–23S. doi: 10.1177/0883073809338152

Sugawara, T., Mazaki-Miyazaki, E., Fukushima, K., Shimomura, J., Fujiwara, T., Hamano, S., et al. (2002). Frequent mutations of SCN1A in severe myoclonic epilepsy in infancy. *Neurology* 58, 1122–1124. doi: 10.1212/wnl.58.7.1122

Sun, H. H., Zhang, Y. H., Liang, J. M., Liu, X. Y., Ma, X. W., and Qin, J. (2008). Seven novel SCN1A mutations in Chinese patients with severe myoclonic epilepsy of infancy. *Epilepsia* 49, 1104–1107. doi: 10.1111/j.1528-1167.2008.01549_2.x

Till, A., Zima, J., Fekete, A., Bene, J., Czakó, M., Szabó, A., et al. (2020). Mutation spectrum of the SCN1A gene in a Hungarian population with epilepsy. *Seizure* 74, 8–13. doi: 10.1016/j.seizure.2019.10.019

Volkers, L., Kahlig, K. M., Verbeek, N. E., Das, J. H. G., Kempen, M. J. A., Stroink, H., et al. (2011). Nav 1.1 dysfunction in genetic epilepsy with febrile seizures-plus or Dravet syndrome. *Eur. J. Neurosci.* 34, 1268–1275. doi: 10.1111/j.1460-9568.2011.07826.x

Wallace, R. H., Scheffer, I. E., Barnett, S., Richards, M., Dibbens, L., Desai, R. R., et al. (2001). Neuronal sodium-channel alpha1-subunit mutations in generalized epilepsy with febrile seizures plus. *Am. J. Hum. Genet.* 68, 859–865. doi: 10.1086/319516

Wirrell, E. C., Laux, L., Donner, E., Jette, N., Knupp, K., Meskis, M. A., et al. (2017). Optimizing the diagnosis and management of Dravet syndrome: recommendations from a North American consensus panel. *Pediatr. Neurol.* 68, 18–34. doi: 10.1016/j.pediatrneurol.2017.01.025

Zhang, Y. H., Burgess, R., Malone, J. P., Glubb, G. C., Helbig, K. L., Vadlamudi, L., et al. (2017). Genetic epilepsy with febrile seizures plus: refining

the spectrum. *Neurology* 89, 1210–1219. doi: 10.1212/WNL.0000000000004384

Zuberi, S. M., Brunklaus, A., Birch, R., Reavey, E., Duncan, J., and Forbes, G. H. (2011). Genotype phenotype associations in SCN1A-related epilepsies. *Neurology* 76, 594–600. doi: 10.1212/WNL.0b013e31820c309b

Zucca, C., Redaelli, F., Epifanio, R., Zanotta, N., Romeo, A., Lodi, M., et al. (2008). Cryptogenic epileptic syndromes related to SCN1A: twelve novel mutations identified. *Arch. Neurol.* 65, 489–498. doi: 10.1001/archneur.65.4.489

Conflict of Interest: The authors declare that the research was conducted in the absence of any commercial or financial relationships that could be construed as a potential conflict of interest.

Publisher's Note: All claims expressed in this article are solely those of the authors and do not necessarily represent those of their affiliated organizations, or those of the publisher, the editors and the reviewers. Any product that may be evaluated in this article, or claim that may be made by its manufacturer, is not guaranteed or endorsed by the publisher.

frontiers | Frontiers in Molecular Neuroscience

SYSTEMATIC REVIEW
published: 19 May 2022
doi: 10.3389/fnmol.2022.807202

The Contribution of HCN Channelopathies in Different Epileptic Syndromes, Mechanisms, Modulators, and Potential Treatment Targets: A Systematic Review

Miriam Kessi[1,2,3], *Jing Peng*[1,2], *Haolin Duan*[1,2], *Hailan He*[1,2], *Baiyu Chen*[1,2], *Juan Xiong*[1,2], *Ying Wang*[1,2], *Lifen Yang*[1,2], *Guoli Wang*[1,2], *Karlmax Kiprotich*[4], *Olumuyiwa A. Bamgbade*[5], *Fang He*[1,2] *and Fei Yin*[1,2]*

[1] Department of Pediatrics, Xiangya Hospital, Central South University, Changsha, China, [2] Hunan Intellectual and Developmental Disabilities Research Center, Changsha, China, [3] Department of Pediatrics, Kilimanjaro Christian Medical University College, Moshi, Tanzania, [4] Department of Epidemiology and Medical Statistics, School of Public Health, Moi University, Eldoret, Kenya, [5] Department of Anesthesiology and Pharmacology, University of British Columbia, Vancouver, BC, Canada

OPEN ACCESS

Edited by:
Heinz Krestel,
Bern University Hospital, Switzerland

Reviewed by:
Gerald Seifert,
University Hospital Bonn, Germany
Ilaria Rivolta,
University of Milano-Bicocca, Italy

***Correspondence:**
Fei Yin
yf2323@hotmail.com

Specialty section:
This article was submitted to Brain Disease Mechanisms, a section of the journal Frontiers in Molecular Neuroscience

Received: 01 November 2021
Accepted: 06 April 2022
Published: 19 May 2022

Citation:
Kessi M, Peng J, Duan H, He H, Chen B, Xiong J, Wang Y, Yang L, Wang G, Kiprotich K, Bamgbade OA, He F and Yin F (2022) The Contribution of HCN Channelopathies in Different Epileptic Syndromes, Mechanisms, Modulators, and Potential Treatment Targets: A Systematic Review. Front. Mol. Neurosci. 15:807202. doi: 10.3389/fnmol.2022.807202

Background: Hyperpolarization-activated cyclic nucleotide-gated (HCN) current reduces dendritic summation, suppresses dendritic calcium spikes, and enables inhibitory GABA-mediated postsynaptic potentials, thereby suppressing epilepsy. However, it is unclear whether increased HCN current can produce epilepsy. We hypothesized that gain-of-function (GOF) and loss-of-function (LOF) variants of HCN channel genes may cause epilepsy.

Objectives: This systematic review aims to summarize the role of HCN channelopathies in epilepsy, update genetic findings in patients, create genotype–phenotype correlations, and discuss animal models, GOF and LOF mechanisms, and potential treatment targets.

Methods: The review was conducted in accordance with the Preferred Reporting Items for Systematic Reviews and Meta-Analyses statement, for all years until August 2021.

Results: We identified pathogenic variants of *HCN1* ($n = 24$), *HCN2* ($n = 8$), *HCN3* ($n = 2$), and *HCN4* ($n = 6$) that were associated with epilepsy in 74 cases (43 *HCN1*, 20 *HCN2*, 2 *HCN3*, and 9 *HCN4*). Epilepsy was associated with GOF and LOF variants, and the mechanisms were indeterminate. Less than half of the cases became seizure-free and some developed drug-resistant epilepsy. Of the 74 cases, 12 (16.2%) died, comprising *HCN1* ($n = 4$), *HCN2* ($n = 2$), *HCN3* ($n = 2$), and *HCN4* ($n = 4$). Of the deceased cases, 10 (83%) had a sudden unexpected death in epilepsy (SUDEP) and 2 (16.7%) due to cardiopulmonary failure. SUDEP affected more adults ($n = 10$) than children ($n = 2$). *HCN1* variants p.M234R, p.C329S, p.V414M, p.M153I, and p.M305L, as well as *HCN2* variants p.S632W and delPPP (p.719–721), were associated with different phenotypes. *HCN1* p.L157V and *HCN4* p.R550C were associated with genetic generalized epilepsy. There are several HCN animal models, pharmacological targets, and modulators, but precise drugs have not been developed. Currently, there are no HCN channel openers.

Conclusion: We recommend clinicians to include *HCN* genes in epilepsy gene panels. Researchers should explore the possible underlying mechanisms for GOF and LOF variants by identifying the specific neuronal subtypes and neuroanatomical locations of each identified pathogenic variant. Researchers should identify specific HCN channel openers and blockers with high binding affinity. Such information will give clarity to the involvement of HCN channelopathies in epilepsy and provide the opportunity to develop targeted treatments.

Keywords: HCN channelopathies, epilepsy, acquired channelopathy, neuro-inflammation, SUDEP

INTRODUCTION

Epilepsy is a common neurological disorder with a lifetime prevalence of 7.60 per 1,000 persons (Fiest et al., 2017). The types with the highest prevalence are epilepsy of unknown cause and generalized seizures (Fiest et al., 2017). It is estimated that there are 50 million people with epilepsy globally, of whom 125,000 die annually and 13 million develop disabilities (Singh and Sander, 2020). Sudden unexpected death in epilepsy (SUDEP) is a cause of death with an estimated incidence of 1 case per 10,000 patient-years for newly diagnosed epilepsy, 1–2 cases per 1,000 patient-years for chronic epilepsy, and 2–10 cases per 1,000 patient-years for drug-resistant epilepsy (Shankar et al., 2017). The causes of SUDEP are not clear, but most cases present with postictal cardiorespiratory dysfunction, and the commonest risk factor is a previous history of generalized tonic–clonic seizures (Shankar et al., 2017). With advanced genomic sequencing methods, new channel genes that are related to epilepsy have been discovered, including calcium (Noebels, 2012; Kessi et al., 2021), potassium (Brenner and Wilcox, 2012; Kessi et al., 2020a), and HCN (hyperpolarization-activated, cyclic nucleotide-gated) channels.

Hyperpolarization-activated cyclic nucleotide-gated channels are the types of non-selective cation channels which are mainly found in the neurons and heart. They can alter the intrinsic and synaptic excitability of principal neurons and GABAergic interneurons (Albertson et al., 2013; Zhao et al., 2016; Bohannon and Hablitz, 2018). Hippocampal excitatory neurons and hippocampal somatostatin-expressing interneurons express HCN channels commonly in the soma and dendrites, whereas parvalbumin-positive interneurons (GABAergic interneurons) express HCN channels solely in axons and nerve terminals (Roth and Hu, 2020; Speigel et al., 2022). HCN channels belong to a six transmembrane-ion channel family and are activated by membrane hyperpolarization (Benarroch, 2013). They conduct mixed cation, sodium, and potassium ion currents. They may form channels in a homomeric or heteromeric manner (Benarroch, 2013). HCN channels have a highly efficient cyclic nucleotide-binding domain (CNBD) at the C terminus (intrinsic regulatory site), which confers an isoform-specific sensitivity to cyclic AMP (cAMP) (Biel et al., 2009; Rivolta et al., 2020). HCN channels are enhanced by the direct binding of cAMP (Herrmann et al., 2007). HCN2 and HCN4 isoforms are most sensitive to cAMP, followed by HCN1, but HCN3 is not sensitive (Santoro and Shah, 2020). CNBD has an inhibitory effect on HCN channel gating (Tsay et al., 2007). Minor differences in the energies of the closed and open states of HCN channels result from different interactions between the voltage sensor and the pore; this explains why they are only activated during hyperpolarization (Ramentol et al., 2020). They produce currents that are termed as "If" in the heart and "Ih" in the brain (Benarroch, 2013). The currents are produced by 4 subtypes, namely, HCN1–4; each subtype is made up of four polymers consisting of six transmembrane domains, namely, S1-6, and intracellular amino and carboxyl termini (Sartiani et al., 2017). There is a pore-forming region between S5 and S6; S4 forms a voltage sensor (Sartiani et al., 2017). HCN channels have some intracellular auxiliary interacting proteins, including tetratricopeptide repeat-containing Rab8b-interacting protein (TRIP8b), His321, S4-S5 linker, pH sensitivity region, C-linker (subunit–subunit interactions), and Tyr476 (Src phosphorylation site) and extracellular auxiliary interacting proteins, including N-glycosylation site (Rivolta et al., 2020).

HCN channels, can regulate neuronal excitability. Therefore, any dysregulation of these channels can play a role in epileptogenesis. HCN channels are more expressed in the dendrites and are important for dendritic integration or regulation of synaptic currents, by changing the membrane resistance (Lewis et al., 2010; Noam et al., 2011). Ih-mediated depolarization inhibits calcium influx in T-type calcium channels, thereby interfering with synaptic release in the axon terminals of layer 3 entorhinal cortex neurons (Huang et al., 2011). Ih currents also exist in presynaptic membranes, but their role in the human brain is not clear (Noam et al., 2011). Dendritic Ih current also modulates the conduction of ions in other channels, including voltage-gated calcium channels (T-type and N-type) and rectifier M-type potassium channels (Tsay et al., 2007; George et al., 2009). It is known that Ih current can reduce dendritic summation, suppress dendritic calcium spikes, and enhance inhibitory GABAA-mediated postsynaptic potentials in pyramidal neurons (Noam et al., 2011), thereby preventing the occurrence of epilepsy. Despite the fact that loss-of-function (LOF) variants can eliminate dendritic attenuation in pyramidal neurons and contribute to hyperexcitability, it is generally known that epilepsies are more likely to result from a loss of the inhibitory component than from a gain of the excitatory component. It is unclear whether epilepsy can occur due to gain of the excitatory component, and if so, the specific neuroanatomical location of the gain-of-function (GOF) variants

and distribution patterns (soma, dendrites, axons, or nerve terminals) are yet to be unveiled. We hypothesized that both GOF and LOF variants of HCN channel genes in different neurons can cause epilepsy, and that acquired HCN channelopathy can play a role in the pathogenesis of other epileptic syndromes.

This article provides a comprehensive review of the role of HCN channelopathies in different epileptic syndromes. It updates relevant information regarding human genetic changes, genotype–phenotype correlations, animal models, GOF or LOF mechanisms, and potential treatment targets. It highlights the implications of HCN channelopathies in other epilepsy syndromes, such as temporal lobe epilepsy, febrile seizures, Rett syndrome, absence seizures, malformation of cortical development, and febrile infection-related epilepsy syndrome (FIRES). The article discusses the role of HCN channelopathies in the occurrence of SUDEP.

METHODS

Literature Search and Selection

The systematic review was conducted in accordance with the Preferred Reporting Items for Systematic Reviews and Meta-Analyses (PRISMA) statement (Moher et al., 2009). A thorough literature search was performed in PubMed and EMBASE, covering all the years until August 2021. A hand-search of the reference lists of published articles was also performed. Only the papers published in English were included. The search terms included the combination of the HCN channel and epilepsy or seizures or convulsions (**Data Sheet 1**). A librarian was consulted for the creation of search strategies. The two independent reviewers searched the articles to select the papers that meet the selection requirements.

The articles selected were cohort studies, case–control studies, cross-sectional studies, case series, and case reports. The review included published studies regarding epilepsy, HCN channel gene mutations, HCN channels related to auxiliary subunits, animal models, cell line model modulators, and treatments. The review also included articles that are related to HCN channelopathies with other epileptic syndromes, such as temporal lobe epilepsy, febrile seizures, Rett syndrome, absence seizures, and malformation of cortical development. The review excluded articles about epileptic cases that were associated with other types of channelopathies (sodium, potassium, calcium, and chloride) or other gene mutations. It also excluded abstracts, reviews, patents, book chapters, and conference papers.

Data Extraction

The two independent reviewers scrutinized the article titles and abstracts and then read the full texts of the articles that met the inclusion criteria. The accuracy of the extracted information was guaranteed through team discussion and agreement. The major outcome measures of this review included the demographics of epileptic cases that are associated with HCN channelopathies (sex, age at seizure onset), initial seizure semiology, seizure types during the disease course, epileptic syndrome or phenotype, the presence or absence of status epilepticus, other clinical features or organ disorders, nucleotide or protein change, mode of inheritance, altered protein function (GOF or LOF), brain imaging results, electroencephalography findings, therapies used, prognosis, and the corresponding references. All identified HCN epilepsy-associated genes were further studied in OMIM, PubMed, and ClinVar databases to identify their function, expression, animal and cell model study outcomes, available treatments, pharmacological targets, and possible mechanisms of epilepsy.

Data Analysis

The data were entered, processed, and analzsed using IBM® SPSS® Statistics 22 (IBM Corp, Armonk, NY). Data are summarized and presented as the mean age of onset, sex, seizure semiology, seizure outcome, disease course, therapies, and other outcome measures.

RESULTS

The initial literature search yielded 468 articles. Following the elimination of duplicates and articles that lacked full texts and/or were non-English, 199 remained eligible. All full texts were read and screened for eligibility. The articles that met all the inclusion criteria were 119, of which 14 were clinical studies and the remaining 105 involved animal studies, cell model studies, regulators, and pharmacology studies. The flowchart can be found in **Supplementary Material**.

HCN Channelopathies Associated With Epilepsy and Their Functional Properties

There were several genetic mutations in 4 *HCN* genes that were related to epilepsy in 74 cases, comprising *HCN1* (43 cases), *HCN2* (20 cases), *HCN3* (2 cases), and *HCN4* (9 cases) **Supplementary Table S1** in Supplementary Material. Both GOF and LOF variants were found in *HCN1* and *HCN2* genes (**Figures 1**, **2**), with unknown functional effects for the *HCN3* gene (**Figure 3**), and only LOF variants were reported in *HCN4* genes (**Figure 4**). For the *HCN1* gene, 37.2% (16) of the 43 cases were diagnosed with either febrile seizures, or febrile seizure plus or genetic generalized epilepsy with febrile seizure plus, 23.3% (10) were diagnosed with genetic or idiopathic generalized epilepsy, 16.3% (7) were diagnosed with early infantile epileptic encephalopathy (EIEE), 11.6% (5) were diagnosed with febrile EIEE, and 11.6% (5) presented with unclassified epileptic syndromes (**Figure 5**). Interestingly, some of the *HCN1* variants are related to different epileptic syndromes: p.M234R is associated with both typical and atypical febrile seizures, p.C329S and p.V414M are related to both febrile seizures and genetic/idiopathic generalized epilepsy, and p.M153I and p.M305L are each related to both EIEE and unclassified epilepsy which occurs in infants (**Figure 6**). Among 20 cases carrying *HCN2* gene pathogenic variants, 45% (9) were diagnosed with either febrile seizures, or febrile seizure plus or genetic generalized epilepsy with febrile seizure plus, 45% (9) were diagnosed with genetic or idiopathic generalized epilepsy, and 10% (2) presented with unclassed epileptic syndromes (**Figure 7**). Noteworthy, p.S632W and delPPP (p.719–721) are each related to both febrile seizures and genetic or idiopathic

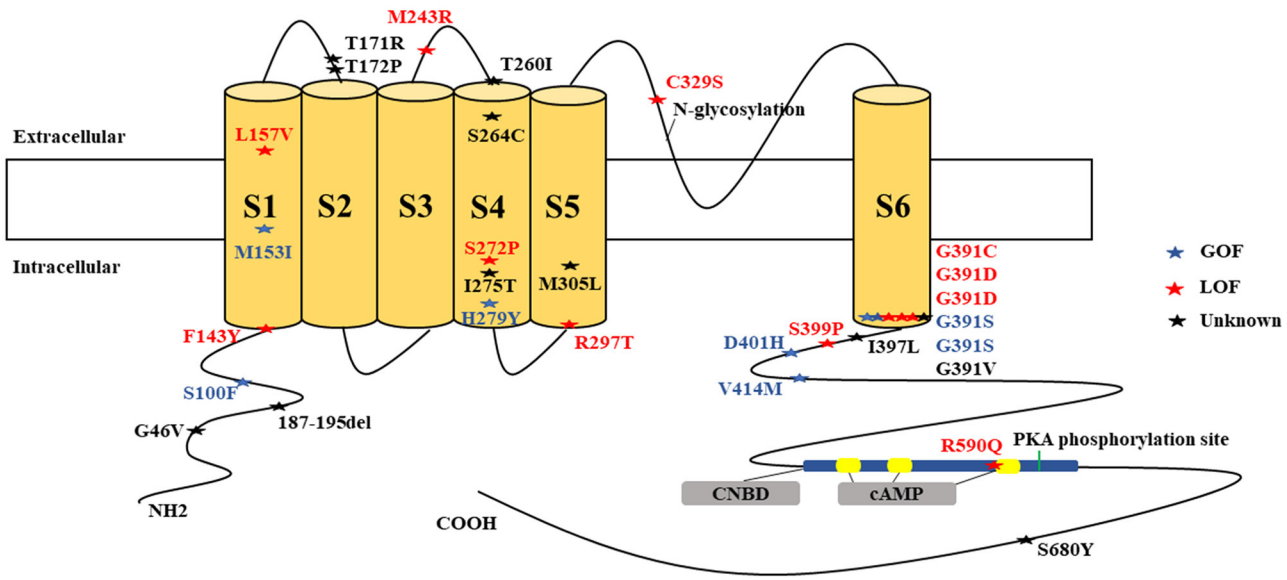

FIGURE 1 | Schematic presentation of the HCN1 channel with 6 transmembrane domains (S1–S6), the locations of the pathogenic variants related to epilepsy and the altered protein functions. Most of mutations are located in S6, the intracellular linker between S6 and CNBD as well as in N-terminal. Notably, variants related to both epilepsy and SUDEP (p.G391D, p.G46V, and 187-195del) are located both in the N- and C-terminals and there is a hotspot in residue G391. Variants in blue correspond to gain-of-function (GOF) effects, variants in red correspond to loss-of-function (LOF) effects, and variants in black stand for the variants with unknown or clear effects.

generalized epilepsy (**Figure 8**). All carriers of the *HCN3* gene variants had unclassified or unknown epileptic syndrome (**Figure 9**), and the locations of the variants are shown in **Figure 10**. For the *HCN4* gene, 56% (5) of the 9 cases were diagnosed with genetic or idiopathic generalized epilepsy whereas 44% (4) had unclassified or unknown epileptic syndrome (**Figure 11**). The locations of the *HCN4* gene variants that are related to unclassified or unknown epileptic syndrome are shown in **Figure 12**.

Of those 74 cases, 12 (16.2%) died, comprising *HCN1* (n = 4), *HCN2* (n = 2), *HCN3* (n = 2), and *HCN4* (n = 4). A number of ten cases (83%) died due to SUDEP and 2 (16.7%) died due to cardiopulmonary failure. A number of one case died at the age of 14 months, one case died at the age of 15 months, one case died at the age of 23 years, and the rest died at the mean age of 40 years. **Table 1** provides a summary of the general information of the HCN1–4 channelopathies in relation to epilepsy. **Table 2** summarizes the overview of HCN channel subunits, modulators, and pharmacology. **Table 3** summarizes the *HCN* genes that are associated with epilepsy and are available in animal models. The detailed results and discussion can be found in the sections below.

HCN1

HCN1 encodes for the hyperpolarization-activated cyclic nucleotide-gated potassium channel 1 (HCN1). HCN1 protein is expressed in the hippocampus (Lee et al., 2019), cerebral cortex (Shah, 2014; Zhou et al., 2019b), cerebellum (Luján et al., 2005), thalamus (Kanyshkova et al., 2012), amygdala (Knoll et al., 2016), and entorhinal cortex (Nolan et al., 2007). In the brain, they are further spread in layer 5 of neocortical neurons, CA1 and CA3 hippocampal regions, molecular cell layer of the cerebellum (Gravante et al., 2004), superficial layers (II/III) of the pyramidal neurons (Santoro and Shah, 2020), and parvalbumin-positive interneurons (Notomi and Shigemoto, 2004). In the cerebral cortex, HCN1 channels are primarily located on pyramidal cell dendrites and at lower concentrations in the soma of pyramidal neurons where they regulate spike firing and synaptic potential integration by influencing the membrane resistance and resting membrane potential (Shah, 2014). HCN1 current does modulate excitatory and inhibitory postsynaptic potentials in the cerebral cortex and hippocampal neurons and regulates the tonic firing of cerebellar neurons (Rivolta et al., 2020). Besides, HCN1 channels are expressed in astrocytes (Honsa et al., 2014) and microglia (Vay et al., 2020). *HCN1* pathogenic variants are related to several types of epileptic syndromes (**Figure 5**). More than half of the cases do present with intellectual disability (ID) or global developmental delay (GDD). Some cases may manifest additional clinical features, such as behavioral disturbances, autistic features, polyphagia, motor delay, attention-deficit hyperactivity disorder (ADHD), truncal ataxia, language delay, and microcephaly. Both GOF and LOF variants are implicated in *HCN1* (**Figure 1**). It is a major concern that 4 *HCN1* cases died (**Table 1**). Most of the mutations are located in S6, N-terminal, and the intracellular linker between S6 and CNBD. Notably, variants that are related to SUDEP are located both in the N- and C-terminals, and there are hotspots in residue G391 (**Figure 1**).

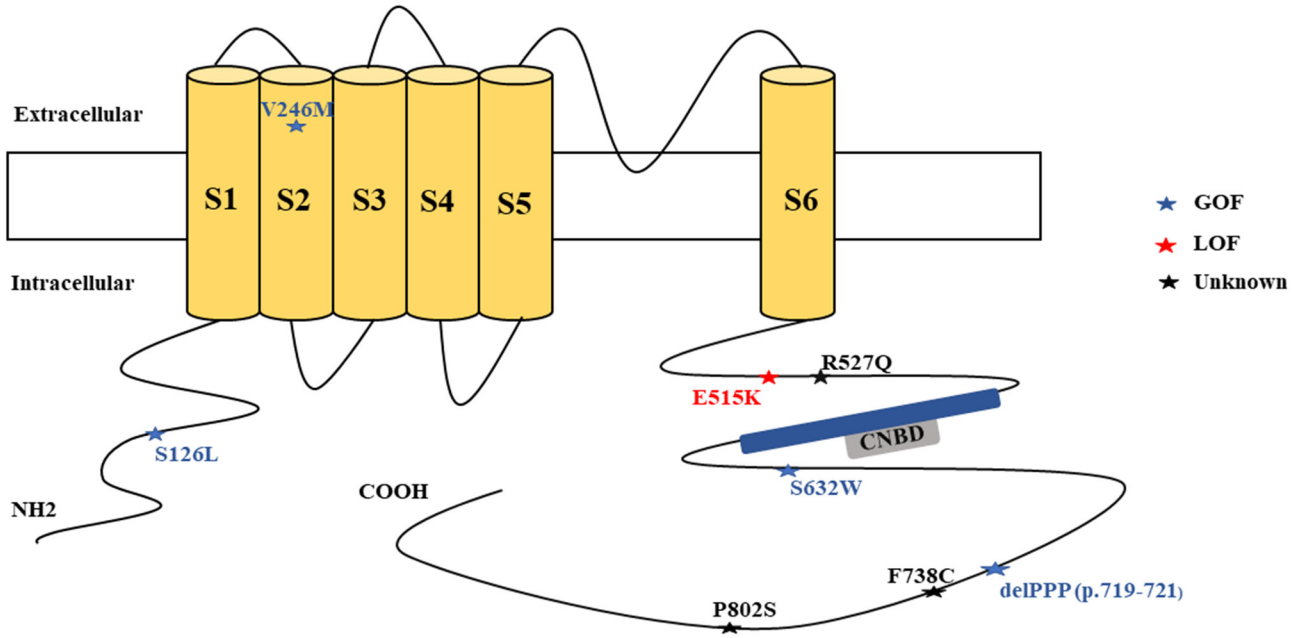

FIGURE 2 | Schematic presentation of the HCN2 channel with 6 transmembrane domains (S1–S6), the locations of the pathogenic variants related to epilepsy, and the altered protein functions. Most of the mutations are located in the intracellular linker before and after the CNBD region. Notably, variants related to both epilepsy and SUDEP are located in C-terminal (p.F738C and p.P802S). Variants in blue correspond to gain-of-function (GOF) effects, variants in red correspond to loss-of-function (LOF) effects, and variants in black stand for the variants with unknown or clear effects.

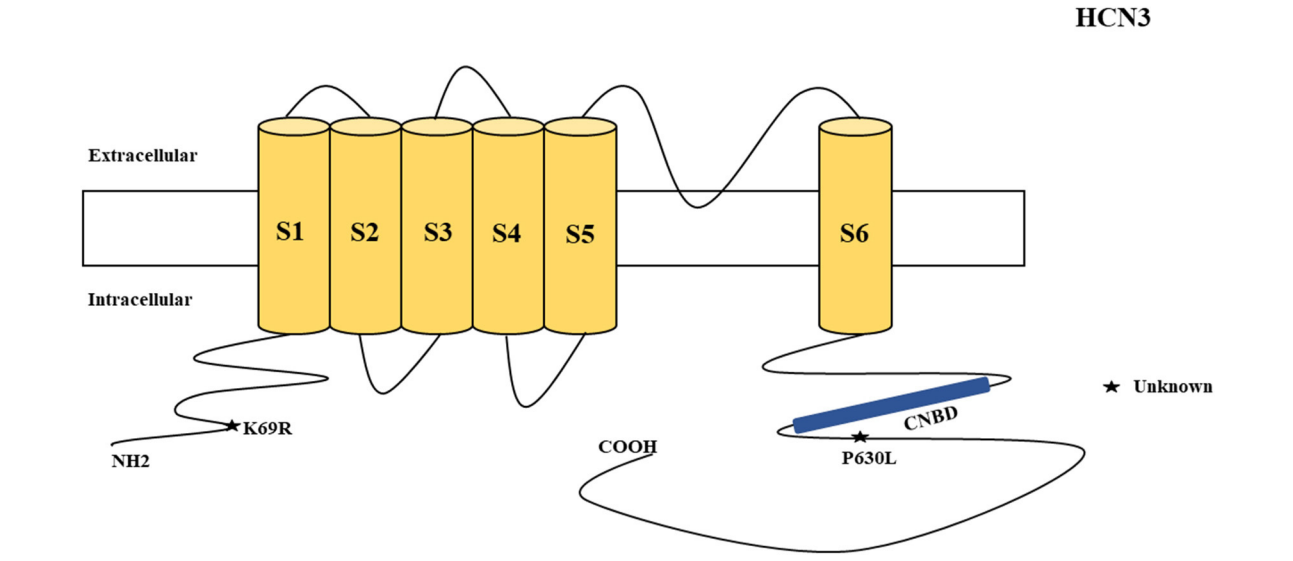

FIGURE 3 | Schematic presentation of the HCN3 channel with 6 transmembrane domains (S1–S6) and the locations of the pathogenic variants related to epilepsy. Variants in black have unknown functional effects and both of them are related to both epilepsy and SUDEP.

Epilepsies are more likely to result from a loss of the inhibitory component than from a gain of the excitatory component. Therefore, it is expected that only LOF mutations (loss of the inhibitory component in interneurons) can result in epilepsy. Interestingly, GOF variants can also produce epilepsy, and this suggests the existence of other unknown mechanisms. We

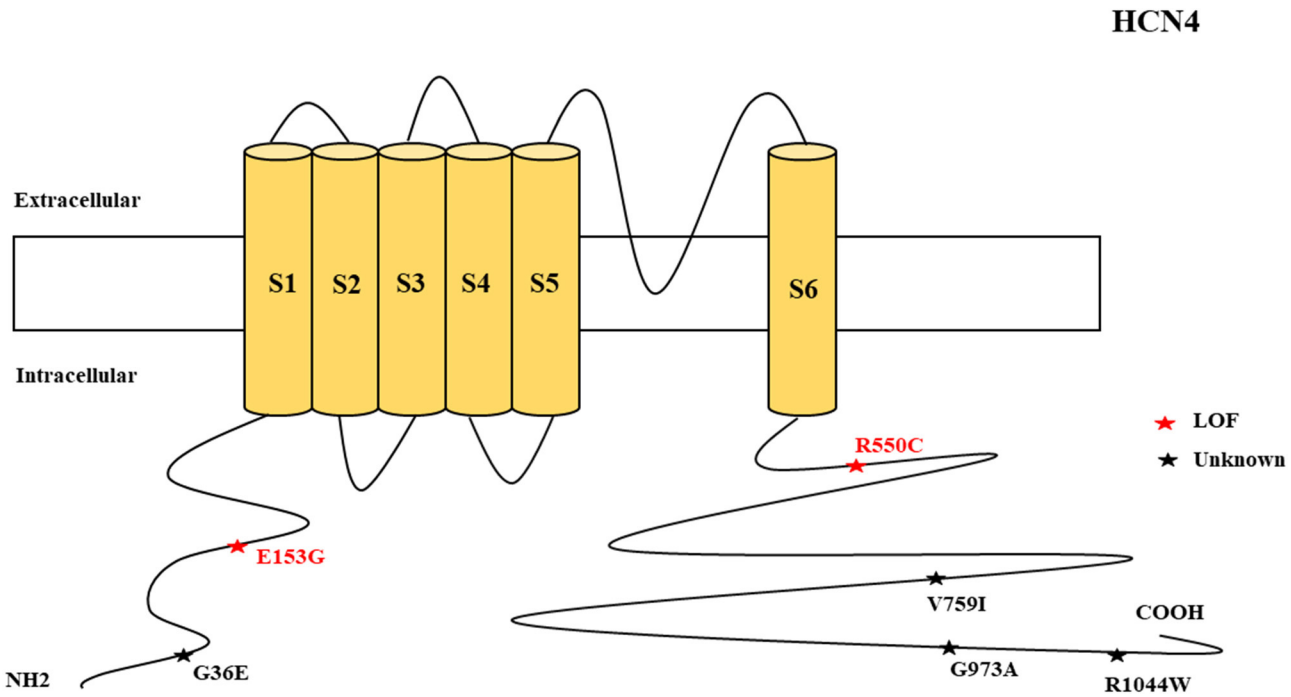

FIGURE 4 | Schematic presentation of the HCN4 channel with 6 transmembrane domains (S1–S6), the locations of the pathogenic variants related to epilepsy, and the altered protein functions. Most of the mutations are located in C-terminal, including those related to both epilepsy and SUDEP (p.G36E, p.V759I, p.G973R, and p.R1044W). Variants in blue correspond to gain-of-function (GOF) effects, variants in red correspond to loss-of-function (LOF) effects, and variants in black stand for the variants with unknown or clear effects.

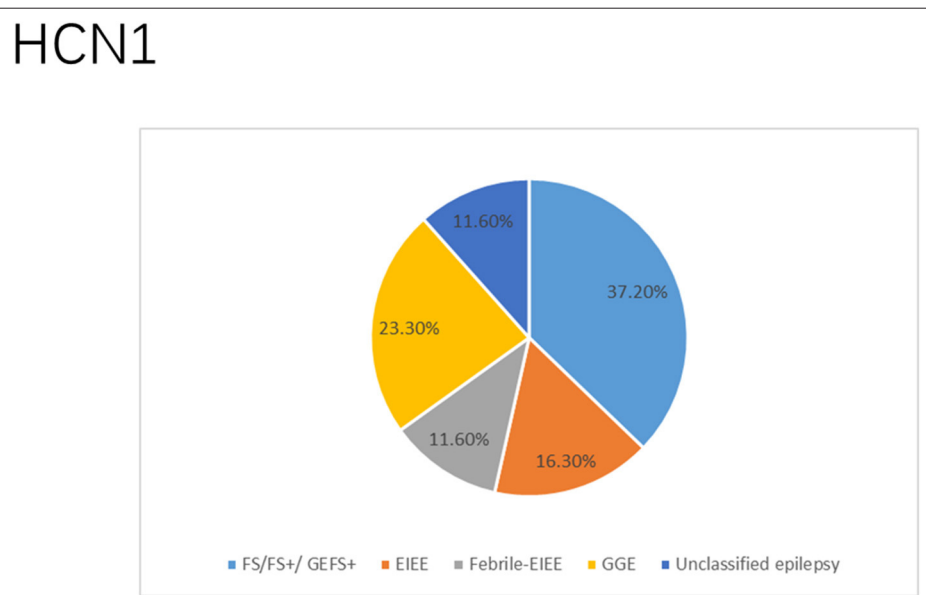

FIGURE 5 | Clinical phenotypes related to *HCN1* variants. Most cases presented with febrile seizures (FS), or febrile seizure plus (FS+) or genetic generalized epilepsy with febrile seizure plus (GEFS+) followed by genetic or idiopathic generalized epilepsy (GGE), early infantile epileptic encephalopathy (EIEE), febrile EIEE, and few had unclassed epileptic syndromes (including those who died due to SUDEP and those reported to have unclassified epilepsy infantile).

hypothesize that the neuroanatomical localization of the HCN pathogenic variants either on principal or pyramidal neurons or on inhibitory interneurons along with their distribution patterns either in the dendrites, axons, or soma can possibly explain the underlying mechanisms for epilepsy for both GOF and LOF variants. Unfortunately, most of the functional studies performed

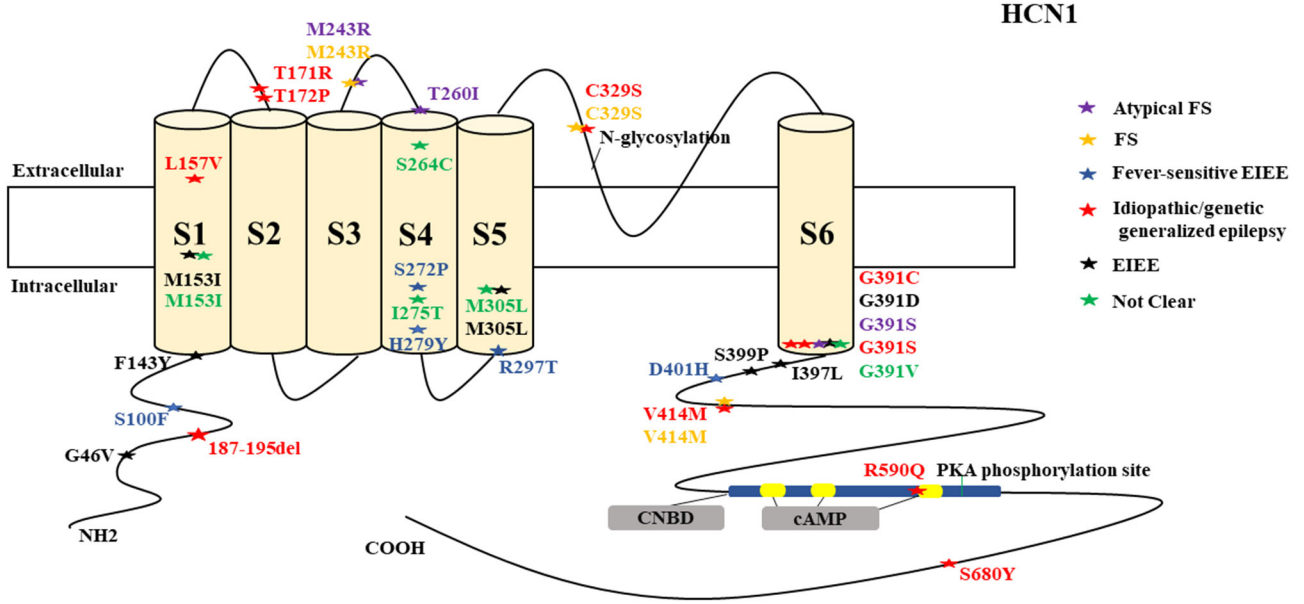

FIGURE 6 | Schematic representation of *HCN1* variants related to different clinical epileptic phenotypes. Some of the variants are related to different epileptic syndromes: p.M234R is associated with both typical and atypical febrile seizures, p.C329S and p.V414M are each related to both febrile seizures and genetic or idiopathic generalized epilepsy, p.M153I and p.M305L are each related to both EIEE and unclassified epilepsy which occurs in infants. Atypical febrile seizures group includes cases with febrile seizure plus and genetic generalized epilepsy with febrile seizure plus. FS stands for febrile seizures and EIEE for early infantile epileptic encephalopathy.

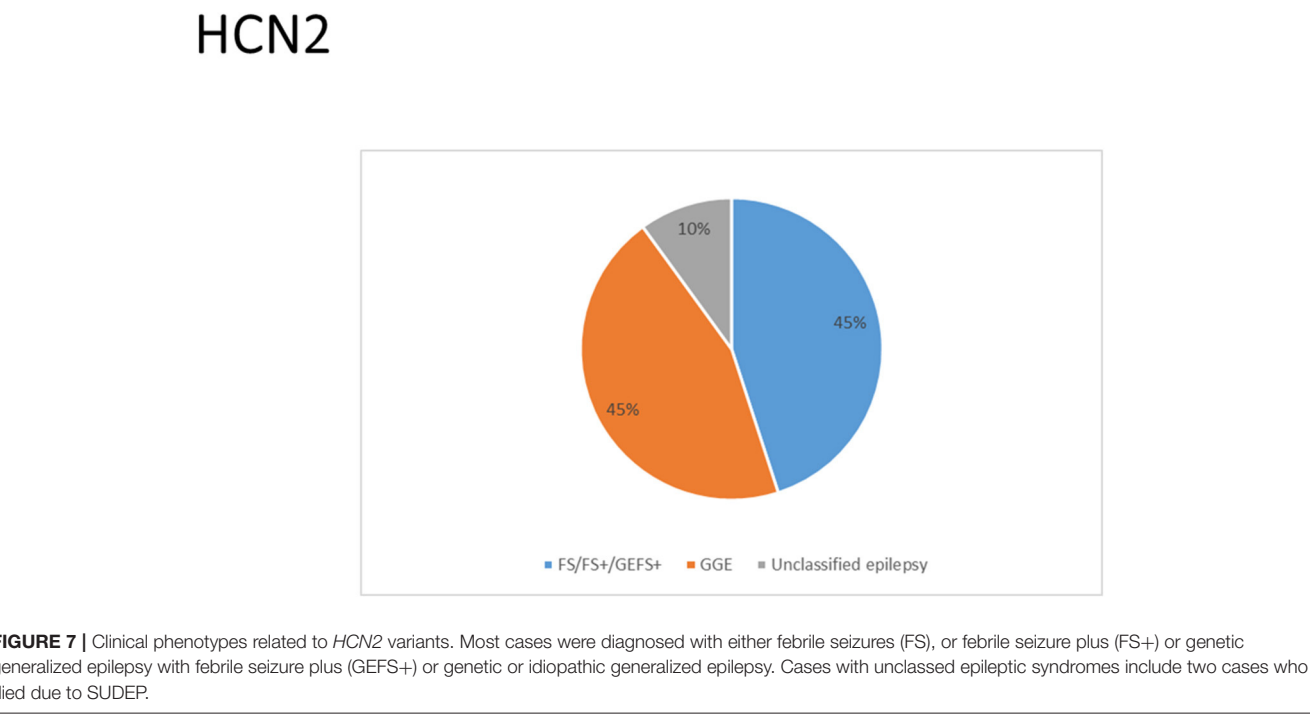

FIGURE 7 | Clinical phenotypes related to *HCN2* variants. Most cases were diagnosed with either febrile seizures (FS), or febrile seizure plus (FS+) or genetic generalized epilepsy with febrile seizure plus (GEFS+) or genetic or idiopathic generalized epilepsy. Cases with unclassed epileptic syndromes include two cases who died due to SUDEP.

for the reported variants were limited to the electrophysiological studies, and only a few were done to explore the neuroanatomical localization in different neuronal subtypes not to mention the distribution patterns.

Fever-sensitive EIEE can be caused by both GOF (p.S100F, p.D401H, and p.H279Y) and LOF (p.S272P, and p.R297T) HCN1 pathogenic variants, and the outcome is poor (Nava et al., 2014). A number of two cases from different studies with

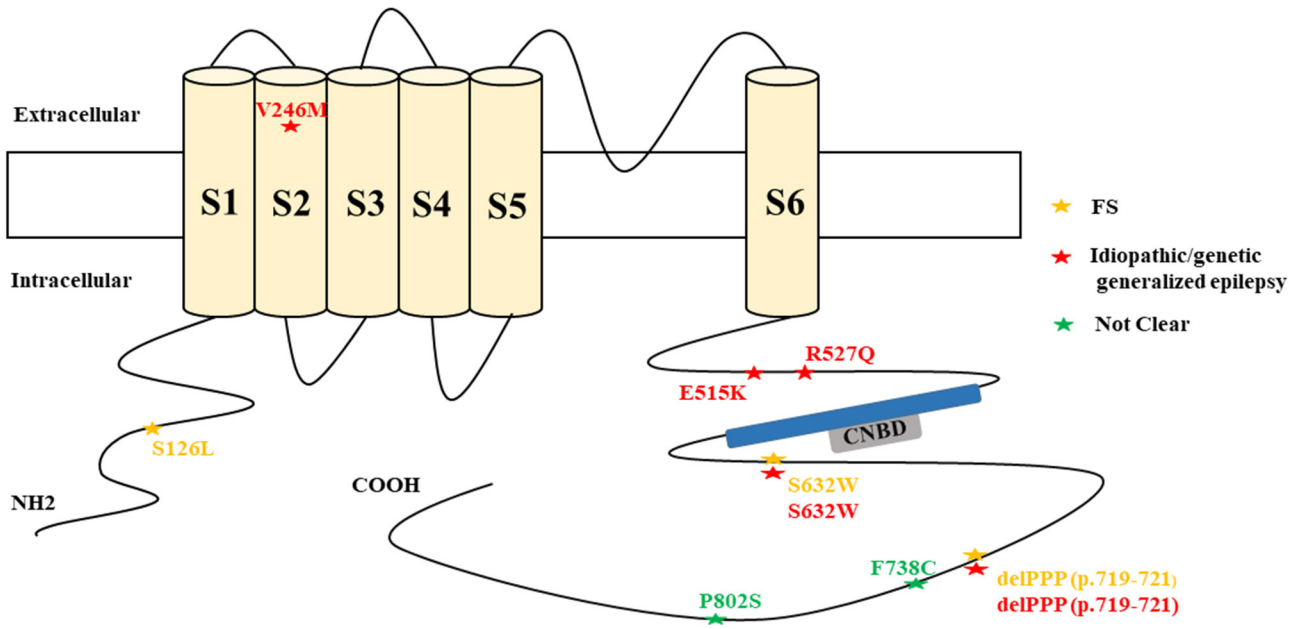

FIGURE 8 | Schematic representation of *HCN2* variants related to different clinical epileptic phenotypes. The p.S632W and delPPP (p. 719–721) are individually related to both febrile seizures and genetic or idiopathic generalized epilepsy. FS stands for febrile seizures and EIEE for early infantile epileptic encephalopathy.

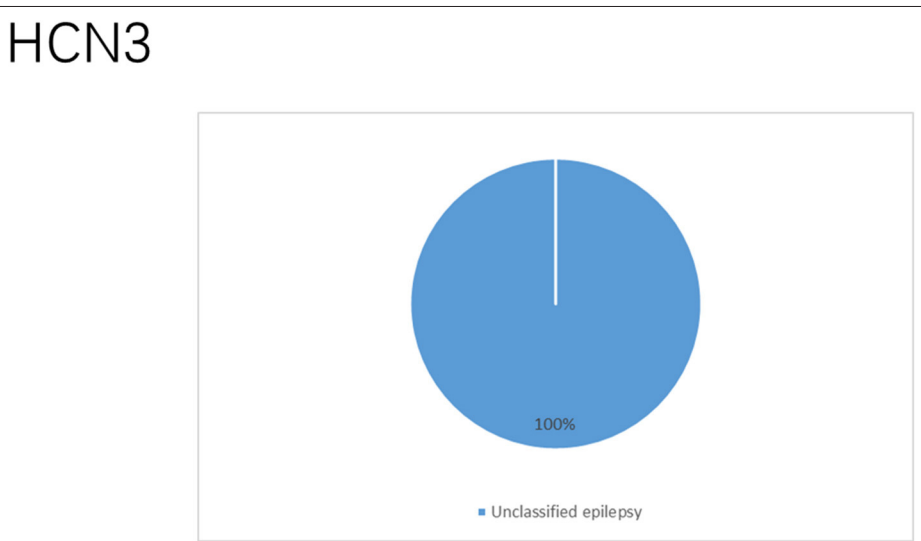

FIGURE 9 | Clinical phenotypes related to *HCN3* variants. All reported cases had unclassified or unknown epileptic syndromes. These are the two cases who died due to SUDEP.

the same pathogenic variant (p.L157V) with LOF (dominant-negative effect) effect on the electrophysiological studies carried out on Chinese hamster ovary (CHO) cells and neonatal rat cortical neurons, presented with the same clinical phenotype of genetic generalized epilepsy, although the outcome was unclear for one case (Bonzanni et al., 2018; DiFrancesco et al., 2019). The LOF effect of p.L157V on neonatal rat cortical neurons increased neuronal excitability and discharge activity, hypothetically related to epileptogenesis. The effect of this mutation on cortical neurons seems to be similar to pyramidal neurons; however, further experiments are needed to know whether the loss of Ih current for this particular

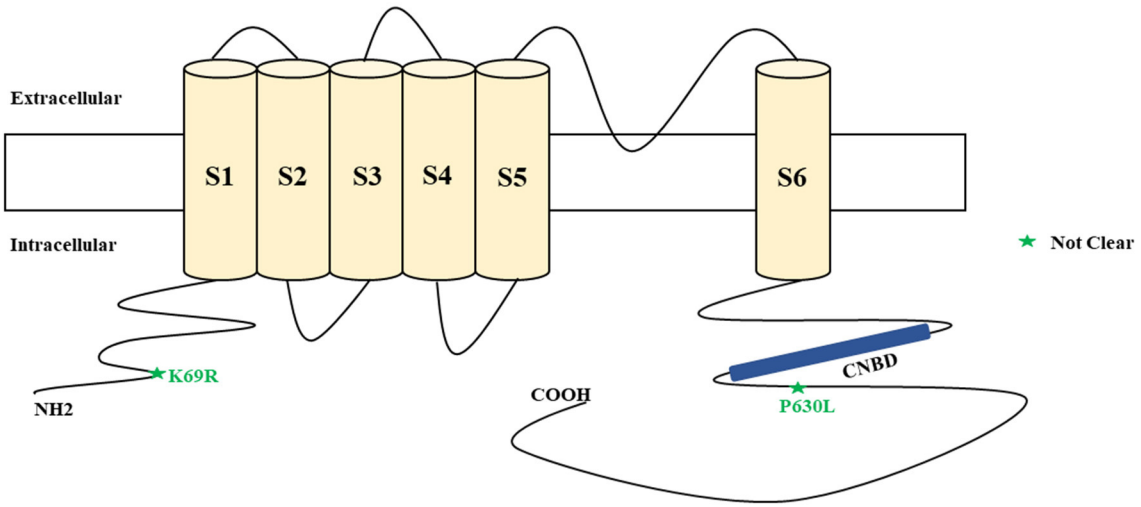

FIGURE 10 | Schematic representation of *HCN3* variants which relate to unclassified or unknown epileptic syndromes.

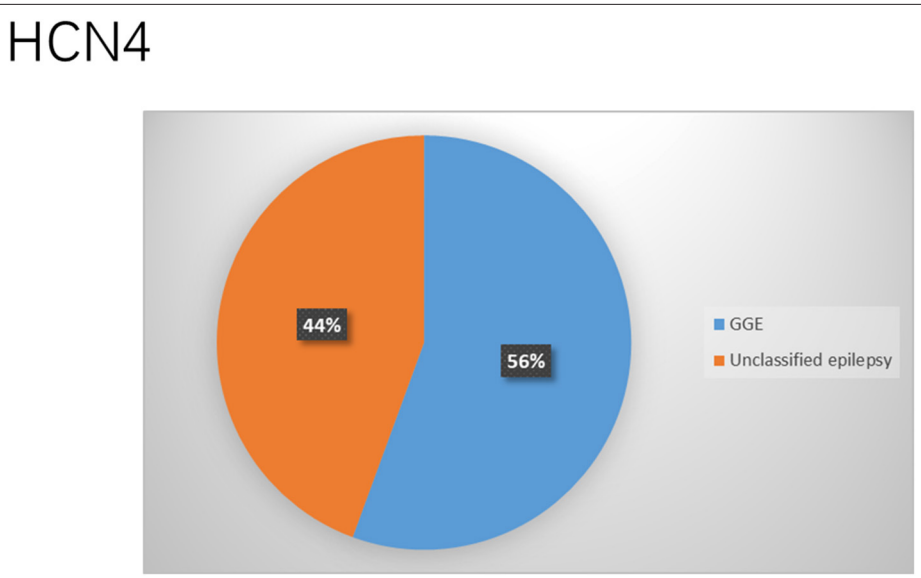

FIGURE 11 | Clinical phenotypes related to *HCN4* variants. Most of the cases were diagnosed with genetic or idiopathic generalized epilepsy (GGE) followed by those with unclassified or unknown epileptic syndrome (majority are those who died due to SUDEP).

variant can also eliminate dendritic attenuation as in pyramidal neurons (Noam et al., 2011). A total of two cases carrying the GOF variant (p.M153I) according to the electrophysiological study on CHO-K1 cells presented with two different epileptic syndromes, namely, EIEE and unclassified epilepsy of infantile-onset. Then, one of them had daily seizures and the other one had weekly seizures, which suggests that one variant can present with different phenotypes (Marini et al., 2018). A total of two cases carrying the LOF variant (p.M243R) according to the electrophysiological study on CHO-K1 cells presented with febrile seizures and febrile seizure plus, and they also manifested as rare seizures (Marini et al., 2018).

A total of two cases carrying the LOF variant (p.M305L) based on the electrophysiological studies performed on both CHO-K1 and HEK293T cells presented with two different phenotypes with different severities, which suggests that the same mutation can produce different phenotypes. A number of one case presented with unclassified infantile epilepsy and mild GDD, and the patient achieved seizure freedom. The other case presented with EIEE, severe ID, and microcephaly, and this patient also achieved

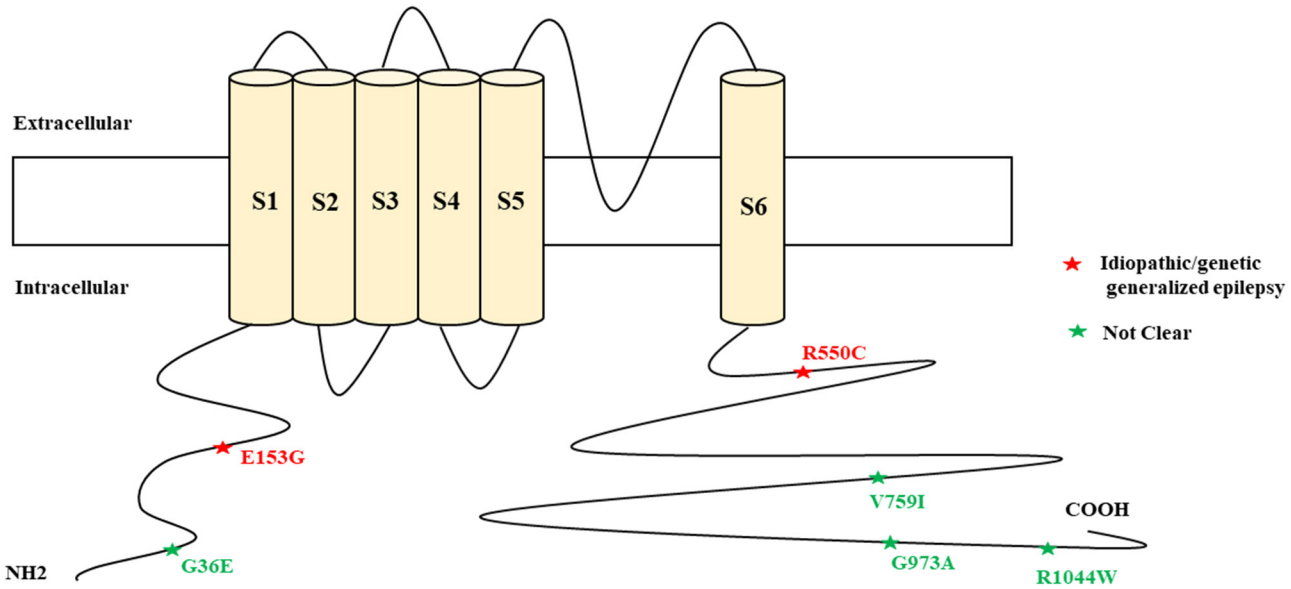

FIGURE 12 | Schematic representation of *HCN4* variants related to different clinical epileptic phenotypes.

seizure freedom (Marini et al., 2018). The exploration of the neuroanatomical localization and distribution pattern of this variant is needed. The variant of p.R590Q (LOF according to the electrophysiological study on CHO-K1 cells) was associated with childhood absence seizures in two separate case reports (Marini et al., 2018; DiFrancesco et al., 2019). This variant affects a residue of CNBD which is critical for cAMP binding. However, the two cases that were reported had mild phenotypes.

The residue G391 seems to be a hotspot and is associated with both mild and severe phenotypes. The p.G391S and p.G391C are related to milder phenotypes and are associated with GOF and LOF effects, respectively, when co-transfected with the wild-type according to the electrophysiological studies performed on both CHO-K1 and HEK293T cells. In contrast, p.G391D with LOF effect on the electrophysiological studies performed on both CHO-K1 and HEK293T cells is resulted in the most severe phenotype which was associated with 2 deaths (Marini et al., 2018). This implies that the severity of the phenotype may depend on the type of the variants rather than the location of the variants. Notably, it is difficult to understand the underlying mechanisms of these variants since functional experiments were only limited to the electrophysiological studies. Some of the reported *HCN1* pathogenic variants, such as p.M305L, p.G391D, and p.S399P, demonstrated no current on electrophysiological studies conducted on both CHO-K1 and HEK293T cells, which implies LOF effect (Marini et al., 2018). For p.M305L which is located in the S5 domain, it has been shown recently that there is a loss of voltage dependence in the activation and deactivation according to the electrophysiological study performed on Xenopus oocytes, leading to continuous excitatory cation flow at membrane potentials that would usually close the channel (Hung et al., 2021).

Two more cases died in other studies, and the postmortem results showed that one carried the non-synonymous novel p.G46V (Tu et al., 2011) and the other one carried a variant of unknown significance, p.72_74del (c.187_195delGGCGGTGGC) (Coll et al., 2016). Coll et al. (2016) performed a custom resequencing panel, including 9 genes known to be involved in SUDEP and 88 candidate genes among 14 SUDEP cases from both postmortem (2 Cases) and from alive patients (12 Cases), in which they found this variant [p.72_74del (c.187_195delGGCGGTGGC)]. Likewise, Tu et al. (2011) performed a genome-wide association study to investigate the role of pathogenic DNA variants in the *HCN1–4* genes in a large SUDEP cohort involving 48 SUDEP cases in which they identified six novels and three previously reported non-synonymous variants, including p.G46V. The former 2 cases (carrying p.G391D variant) died due to cardiopulmonary failure and the latter (carrying p.G46V and p.72_74del (c.187_195delGGCGGTGGC variants) died due to SUDEP. Two of the variants that were associated with deaths are clustered in the N-terminal part of the channel, and one variant is in the C-terminal. HCN1 channels play a role in the enhancement of long-term potentiation, synaptic plasticity, and cognitive process (Beaumont et al., 2002; Zhong and Zucker, 2004). Therefore, their dysfunction can result in neurodevelopmental disorders, such as ID, GDD, and ADHD. Noteworthy, some of the same *HCN1* variants are related to different epileptic syndromes: p.M234R is associated with both typical and atypical febrile seizures, p.C329S and p.V414M are each related to both febrile seizures and genetic or idiopathic generalized epilepsy,

TABLE 1 | General information of the HCN1-4 channelopathy in relation to epilepsy based on the available information.

Characteristics	Proportion and percentage (when applicable)/further description			
	***HCN1* (43 cases)**	***HCN2* (n = 20 cases)**	***HCN3* (2 cases)**	***HCN4* (9 cases)**
Age of onset				
Mean (range)	15.4 (0–84) months.	No enough information	No enough information	No enough information/infantile age
Sex			No enough information	
Females	25/41 (61%)	3/9 (33.3%)		1/5 (20%)
Males	16/41 (40%)	6/9 (66.7%)		4/5 (80%)
Pathogenic variants (mode of inheritance)			No enough information	
De novo	26/41 (63.4%)	-		
Inherited	15/41 (36.6%)	12/20 (60%)		
Sporadic	-	2/20 (10%)		
Unknown	2/41 (4.9%)	8/20 (40%)		
Altered protein function			No enough information	
GOF	6/26 (23%)	4/8 (50%)		-
LOF	10/26 (38.5%)	1/8 (12.5%)		2/6 (26.7%)
Unknown	10/26 (38.5%)	3/8 (37.5%)		4/6 (66.7%)
Initial seizure semiology			No enough information	
Febrile seizures	26/42 (61.9%)	3		-
Tonic seizures	10/42 (23.8%)	-		-
Clonic seizures	5/42 (11.9%)	-		-
Generalized seizures	1/42 (2.4%)	-		3/9 (33.3%)
Absence seizures	2/42 (4.8%)	2		-
The presence of status epilepticus			No enough information	No enough information
Yes	5/9 (55.6%)	-		
Epileptic syndromes	Childhood focal epilepsy, childhood absence epilepsy, early infantile epileptic encephalopathy (EIEE), febrile seizures, febrile seizure plus, fever-sensitive EIEEs, genetic generalized epilepsy, generalized epilepsy, genetic epilepsy with febrile seizure plus, generalized epilepsy with eyelid myoclonus, neonatal-onset epileptic encephalopathy (MMPSI), and unclassified epilepsy infantile.	Absence seizures, febrile seizures, generalized epilepsy, focal seizures, genetic epilepsy with febrile seizure plus, juvenile myoclonic epilepsy, idiopathic generalized epilepsy, idiopathic photosensitive occipital epilepsy, and photosensitive genetic generalized epilepsy	No enough information	Familial benign myoclonic epilepsy and genetic generalized epilepsy are the major epileptic syndromes
Additional clinical phenotypes			No enough information	No enough information
ID/GDD	22/43 (51.1%)	1/20 (5%)		
Others	Behavioral disturbances, autistic features, polyphagia, motor delay, and attention-deficit/hyperactivity disorder, truncal ataxia, language delay, and microcephaly.	Attention-deficit/hyperactivity disorder and abnormal behavior		
Seizure outcome				
Seizure free	16/41 (39%)	-	-	2/9 (22.2%)
Controlled seizures	2/41 (4.9%)	-	-	-
Drug-resistant epilepsy	5/41 (12.2%)	1/20 (5%)	-	-
Daily seizures	6/41 (14.6%)	-	-	-
Weekly seizures	1/41 (2.4%)	-	-	-
Rare seizures	3/41 (7.3%)	-	-	-
Monthly seizures,	2/41 (4.9%)	-	-	-
Yearly seizures	2/41 (4.9%)	-	-	-
Died	4/41 (9.8%)	2/20 (10%)	2/2 (100%)	4/9 (44.4%)
Unknown	2/41 (4.9%)	17/20 (85%)	-	3/9 (33.3%)

TABLE 2 | An overview of HCN channel subunits, modulators, and pharmacology.

Gene	OMIM number	Name	Modulators	Pharmacology
HCN1	602780	Hyperpolarization-activated cyclic nucleotide-gated potassium channel 1	cAMP (Kanyshkova et al., 2009), casein kinase 2 (Schulze et al., 2020), glycosylation (Zha et al., 2008), protein kinase C (Williams et al., 2015), and phosphorylation (Concepcion et al., 2021)	Blockers include Ivabradine (Bucchi et al., 2006) and MEL55A (Dini et al., 2018), MEL57A (Resta et al., 2018), lidocaine (Putrenko et al., 2017), capsazepine (Gill et al., 2004), ketamine (Zhou et al., 2013), carvedilol (Cao et al., 2018), loperamide, CP-339,818, DK-AH269, and ZD7288 (Lee et al., 2008), and dexmedetomidine (Yang et al., 2014). Nitric oxide suppresses fast Ih current (Kopp-Scheinpflug et al., 2015). CRISPRi or RNA interference (RNAi) (Deutsch et al., 2021) and L-stepholidine reduces HCN1 expression (Zhou et al., 2019a). Cyclophosphamide increased its expression (Liu et al., 2017).
HCN2	602781	Hyperpolarization-activated cyclic nucleotide-gated potassium and sodium channel 2	Intracellular chloride ions, pH, cAMP (Kanyshkova et al., 2009), Shox2 (Yu et al., 2021), glycosylation (Zha et al., 2008), phosphorylation (Concepcion et al., 2021), and SUMOylation (Parker et al., 2016)	Blockers include MEL55A (Dini et al., 2018), carvedilol (Cao et al., 2018), dexmedetomidine (Yang et al., 2014). CRISPRi or RNA interference (RNAi) (Deutsch et al., 2021) reduced HCN2 expression.
HCN3	609973	Hyperpolarization-activated cyclic nucleotide-gated potassium channel 3	Casein kinase 2 (Schulze et al., 2020)	Blockers include Cs (1+), ZD7288, and Ivabradine (Mistrík et al., 2005)
HCN4	605206	Hyperpolarization-activated cyclic nucleotide-gated potassium channel 4	Shox2 (Yu et al., 2021)	The current can be blocked by Ivabradine (Bucchi et al., 2006), EC18 (Kharouf et al., 2020b), carvedilol (Cao et al., 2018), gabapentin (Tae et al., 2017), DK-AH269 (Lee et al., 2008). CRISPRi or RNA interference (RNAi) (Deutsch et al., 2021) reduced its expression.

and p.M153I and p.M305L are each related to both EIEE and unclassified epilepsy which occurs in infants (**Figure 6**). This suggests heterogeneity of the *HCN1* phenotypes. In summary, based on the electrophysiological studies on cell models, both GOF and LOF are associated with epilepsy; but LOF is associated with more severe phenotypes, including 3 deaths due to the deletion and strong reduction in HCN1 current density. The underlying mechanisms for both GOF and LOF variants remain unclear since most of the functional studies were limited to the electrophysiological studies, and only a few were done to explore the neuroanatomical localization in different neuronal subtypes not to mention the distribution patterns.

Most rodent models of epilepsy support the fact that the loss of the HCN1 current in pyramidal, cortical, and thalamic neurons is associated with the occurrence of epilepsy, but there is limited evidence showing that the upregulation of this current can produce epilepsy. The HCN1-knockout rat model of the absence seizures reveals a reduction of Ih current in the cortical and hippocampal pyramidal neurons, pronounced hyperpolarizing shift of the resting membrane potential, and increased input resistance. Besides, this model is prone to pentylenetetrazol-induced acute convulsions and shows spontaneous spike-wave discharges and behavioral arrest (Nishitani et al., 2019). The loss of dendritic HCN1 subunits in entorhinal cortical and hippocampal pyramidal cell dendrites leads to the enhancement of cortical excitability and greater seizure susceptibility in adult HCN1-null mice (Huang et al., 2009). *In vitro* electrophysiological studies disclosed that this greater seizure susceptibility of adult HCN1-null mice occurs due to enhanced excitability of entorhinal cortical layer III neurons as a result of lack of dendritic Ih current. Therefore, the lack of dendritic Ih current in pyramidal cell results in an imbalance in excitatory and inhibitory synaptic activity which influence cortical neural network activity (Huang et al., 2009). Altogether, these studies suggest that the reduction of HCN1current in the neocortex and hippocampus can lead to the absence epilepsy. The HCN1 p.M294L heterozygous knock-in (HCN1M294L) mouse demonstrates the clinical manifestations of patients with the *HCN1* p.M305L variant, including spontaneous seizures, learning deficit, seizure exaggeration by lamotrigine, and the seizure reduction by sodium valproate (Bleakley et al., 2021). The functional analysis of HCN1M294L on Xenopus laevis oocytes and layer V somatosensory cortical pyramidal neurons in *ex vivo* tissue revealed a loss of voltage dependence that was accompanied by open channel that allowed for cation "leak" resulting in layer V somatosensory cortical pyramidal neurons and CA1 hippocampal pyramidal neuron depolarization at rest (Bleakley et al., 2021). Therefore, impaired voltage-dependent gating properties of HCN1 channels due to certain variants can allow continuous excitatory cation flow that produces epilepsy (Bleakley et al., 2021; Hung et al., 2021).

The GOF property of WAG-HCN1 (animal model of absence seizures) is caused by N-terminal deletion, change in N-terminal wild-type sequence (GNSVCF) motif, increased current, enhanced HCN1 expression, reduced cAMP sensitivity, and suppressed HCN2 and HCN4 currents according to the functional analysis performed on Xenopus oocytes and thalamus of WAG/Rij rat strain (Wemhöner et al., 2015). The Genetic

TABLE 3 | HCN subtypes directly and indirectly related to epilepsy in animal models.

Gene	Animal model for epilepsy	Phenotype	Key findings
HCN1	KO (Nishitani et al., 2019)	Absence epilepsy (Nishitani et al., 2019)	Reduction of Ih current in the cortical and hippocampal pyramidal neurons, pronounced hyperpolarizing shift of the resting membrane potential, and increased input resistance. Prone to pentylenetetrazol-induced acute convulsions. Showed spontaneous spike-wave discharges and behavioral arrest (Nishitani et al., 2019).
	KO (Saito et al., 2012)	Epileptic seizures (Saito et al., 2012)	Ablation of HCN1 in mice augmented the production of amyloid-β peptide (Aβ) (Saito et al., 2012).
	Adult *HCN1*-null mice (Huang et al., 2009)	Kainic acid-induced seizures (Huang et al., 2009)	Loss of dendritic HCN1 subunits which resulted in the enhanced cortical excitability and the development of epilepsy (Huang et al., 2009).
	GABAAγ2 (R43Q) mouse (Phillips et al., 2014)	Absence epilepsy (Phillips et al., 2014)	Diminished hippocampal HCN1 expression and function as well as spatial learning deficit (Phillips et al., 2014).
	HCN1-deficient rats (Nishitani et al., 2020)	Absence seizures, loose muscle tension, and abnormal gait (Nishitani et al., 2020).	HCN1 is involved in motor coordination and muscle strength (Boychuk and Teskey, 2017; Boychuk et al., 2017; Nishitani et al., 2020).
	HCN1 M294L heterozygous knock-in (HCN1M294L) mouse (Bleakley et al., 2021)	Severe developmental impairment and drug-resistant epilepsy (Bleakley et al., 2021)	The mechanism of epilepsy is continuous cation leak that resulted in hyperexcitability of the layer V somatosensory cortical pyramidal neurons (Bleakley et al., 2021).
HCN2	*HCN2*-null mice (Ludwig et al., 2003)	Absence seizures (105)	HCN2-deficient mice demonstrated spontaneous absence seizures. The thalamocortical relay had complete loss of the HCN current thus increased hyperexcitabilty. This was accompanied with dysrhythmia (Ludwig et al., 2003).
	HCN2 knock-in mouse model (HCN2EA) (Hammelmann et al., 2019).	Absence seizures and learning disability (Hammelmann et al., 2019).	cAMP regulates HCN2 channel (Hammelmann et al., 2019).
HCN4	Conditional *HCN4* –KO model (Kharouf et al., 2020a).	Seizures (Kharouf et al., 2020a)	EC18 and HCN4-KO reduced seizure susceptibility (Kharouf et al., 2020a).
	GSK3β [S9A] mice (Urbanska et al., 2019)	Kainic acid-induced seizures (Urbanska et al., 2019)	GSK3β regulates HCN4 level and the expression of synaptic AMPA receptors (Urbanska et al., 2019).
TRIP8b	*TRIP8b* KO (Heuermann et al., 2016)	Absence seizures (Heuermann et al., 2016)	Decreased HCN channel expression and function in thalamic-projecting cortical layer 5b neurons and thalamic relay neurons. Preserved HCN function in inhibitory neurons of the reticular thalamic nucleus (Heuermann et al., 2016).
	TRIP8b-null mice (Huang et al., 2012).	Kainic acid-induced seizures (Huang et al., 2012)	Presynaptic adult cortical HCN channel expression continually diminished following induction of seizures and not dendritic HCN channels. Modulation of the adult presynaptic cortical HCN expression is independent of TRIP8b (Huang et al., 2012).
Others	Genetic Absence Epilepsy Rats from Strasbourg (GAERS) model (Cain et al., 2015)	Absence seizures (Cain et al., 2015)	Increased HCN-1 and HCN-3 expression in ventrobasal thalamic neurons and the blockage of Ih current suppressed burst-firing (usually accompany spike-and-wave discharges) (Cain et al., 2015).
	Genetic Absence Epilepsy Rats from Strasbourg (GAERS) model (Kuisle et al., 2006)	Absence seizures (Kuisle et al., 2006)	The binding of cAMP to HCN channels was weakened in acute phase thus promoted epilepsy and the compensatory mechanisms to stabilize Ih current activity led to the cessation of spike-and-wave discharges in chronic epilepsy. Calcium ions trigger the synthesis of cAMP (Kuisle et al., 2006).
	Genetic Absence Epilepsy Rats from Strasbourg (GAERS) and acquired temporal lobe epilepsy model (Smith and Delisle, 2015)	Absence seizure and status epilepticus (Smith and Delisle, 2015)	Diminished cardiac expression of HCN2 in both models. Chronic epilepsy can induce cardiac channelopathies thus SUDEP (Smith and Delisle, 2015)
	Genetic Absence Epilepsy Rats from Strasbourg (GAERS) and acquired temporal lobe epilepsy (Powell et al., 2014)	Post–status epilepticus (Powell et al., 2014)	Secondary ion channelopathies and cardiac dysfunction can result from the chronic epilepsy (Powell et al., 2014)
	Genetic Absence Epilepsy Rats from Strasbourg (GAERS), male Wistar rats, male Stargazer mice (David et al., 2018)	Absence seizures (David et al., 2018)	Blockage of HCN channels *via* ZD7288 antagonist in ventrobasal thalamus decreases thalamocortical neuron firing and eliminates spontaneous absence seizures in GAERS, Wistar rats and male Stargazer mice (David et al., 2018).
	Wistar Albino Glaxo rats, bred in Rijswijk (Budde et al., 2005)	Absence epilepsy (Budde et al., 2005)	There is a need of the balance of HCN1 and HCN2 gene expression in thalamocortical for the modulation of burst firing in thalamic networks (spindle-like or spike-wave-like patterns). Increased expression of HCN1 and no changes for the rest of HCN channels (Budde et al., 2005).

(Continued)

TABLE 3 | Continued

Gene	Animal model for epilepsy	Phenotype	Key findings
	Rat Pilocarpine Model of Epilepsy (Jung et al., 2007)	Spontaneous induced recurrent seizures (Jung et al., 2007)	The diminished expression of the dendritic HCN channels during the acute phase of the epilepsy is accompanied by the loss of hyperpolarization of voltage-dependent activation. These phenomena progressed to the chronic phase which increases neuronal excitability and thus epileptogenesis. Phenobarbital could suppress seizures and reversed the current changes but not the expression (Jung et al., 2007).
	Rat Pilocarpine Model of Epilepsy (Jung et al., 2011)	Spontaneous induced recurrent seizures (Jung et al., 2011)	Loss Ih current and HCN1channel expression start 1 h after status epilepticus and involves several steps including dendritic HCN1 channel internalization, deferred loss of protein expression, and finally the downregulation of mRNA expression (Jung et al., 2011).
	Wistar Albino Glaxo/Rij strain (Wemhöner et al., 2015)	Absence epilepsy (Wemhöner et al., 2015)	Gain-of-function of WAG-HCN1is caused by N-terminal deletion, increase of the HCN1expression and current, suppression of HCN2 and HCN4 currents as well as reduction of cAMP sensitivity (Wemhöner et al., 2015).
	Tottering mice (Kase et al., 2012)	Absence seizures (Kase et al., 2012)	Reduction of HCN function which led to enhancement of membrane excitability in subthalamic nucleus neurons. The activation of HCN channel activity *in vitro* could rescue the situation (Kase et al., 2012).

KO, knockout.

Absence Epilepsy Rats from Strasbourg (GAERS) is a model of absence seizures. It reveals an increase of HCN-1 and HCN-3 expression in the ventrobasal thalamic neurons (subsets of thalamic relay neurons) and enhanced Ih current which suppresses neuronal burst firing (Cain et al., 2015). This model also shows a reduction of T-type calcium channel whole-cell currents in ventrobasal thalamic, CaV3.1 mRNA, and protein levels (Cain et al., 2015). The Wistar Albino Glaxo rat that is bred in Rijswijk (WAG/Rij) is an animal model of absence seizures. It shows the need for the balance of *HCN1* and *HCN2* gene expression in the thalamocortical area, to enable the modulation of burst firing in thalamic networks (Budde et al., 2005). Notably, there is an increased expression of HCN1 on mRNA and protein levels and no further changes to the other HCN channels' expression (Budde et al., 2005). The tottering mice of absence seizures is a model that demonstrates the reduction of HCN function and the resultant enhancement of membrane excitability in subthalamic nucleus neurons, although the activation of HCN channel activity *in vitro* can reverse the situation (Kase et al., 2012). Thus, based on these studies, it seems that enhanced Ih current in the thalamus can suppress neuronal burst firing in the absence epilepsy. In addition, the reduction of the T-type calcium channel currents in the ventrobasal thalamus can play a role in suppressing neuronal burst firing in the absence epilepsy.

The rat pilocarpine model of epilepsy is an animal model of spontaneous, induced, and recurrent seizures. It revealed that there is a diminished expression of the dendritic HCN channels during the acute phase of the epilepsy, and this is accompanied by the loss of channel expression and hyperpolarization of voltage-dependent activation (Jung et al., 2007). This change may progress to the chronic phase which increases neuronal excitability and thus epileptogenesis (Jung et al., 2007). Phenobarbital can suppress seizures and reverse the neuronal current changes, but not the expression of HCN channel (Jung et al., 2007). The loss of Ih current and HCN1 channel expression starts 1 h after status epilepticus: it involves several steps, including dendritic HCN1 channel internalization, deferred loss of protein expression, and the final downregulation of mRNA expression (Jung et al., 2011).

There are currently some HCN1 channel blocker drugs, but they have low efficacy. MEL55A is a potential HCN1/2 blocker, but it may also increase seizure susceptibility (Kharouf et al., 2020b). However, another study showed that MEL55A does not affect seizure susceptibility (Kharouf et al., 2020b). This ambiguity could be due to the low binding affinity of MEL55A. A recent study of HCN1 channels unveiled the hidden hydrophobic groove in the pore that may be responsible for the low binding affinity (Tanguay et al., 2019). **Table 3** summarizes this information. New HCN1-blocking drugs with high affinity may be developed in the future. Since HCN1 current is essential for the prevention of epilepsy, there is also the need to develop HCN1 channel openers.

HCN2

HCN2 encodes for the hyperpolarization-activated cyclic nucleotide-gated potassium channel 2 (HCN2). HCN2 channels are expressed in the hippocampus (Lee et al., 2019), cerebral cortex (Shah, 2014), cerebellar Purkinje cells (Han et al., 2002), thalamus (Kanyshkova et al., 2012), cholinergic interneurons of nucleus accumbens (Cheng et al., 2019), and hippocampal inhibitory interneurons (Matt et al., 2011). They are also expressed in astrocytes (Honsa et al., 2014), microglia (Vay et al., 2020), and oligodendrocytes (Notomi and Shigemoto, 2004; Swire et al., 2021). In the cerebral cortex, HCN2 channels are primarily located on pyramidal cell dendrites and at lower concentrations in the soma of pyramidal neurons where they regulate spike firing and synaptic potential integration by influencing the membrane resistance and resting membrane potential (Shah, 2014). HCN2 channels in hippocampal

inhibitory interneurons modulate synaptic plasticity by enabling the GABAergic output onto pyramidal neurons (Matt et al., 2011).

HCN2 pathogenic variants are associated with absence seizures, febrile seizures, generalized epilepsy, focal seizures, genetic epilepsy with febrile seizure plus, juvenile myoclonic epilepsy, idiopathic generalized epilepsy, idiopathic photosensitive occipital epilepsy, and photosensitive genetic generalized epilepsy (**Figure 7**). Of the 8 reported *HCN2* variant cases, 4 were GOF and 1 was LOF according to the electrophysiological studies (**Figure 2**). Then, two cases died. It is surprising that most of the variants had a GOF effect rather than LOF, which is in contrast to HCN1 variants. Similar to HCN1, some of variants are related to different epileptic syndromes; p.S632W and delPPP (p.719–721) are each related to both febrile seizures and genetic or idiopathic generalized epilepsy (**Figure 8**).

The *HCN2* cases with GOF variants according to the electrophysiological studies performed on oocytes from Xenopus laevis include the inherited p.S632W variant as observed in 2 cases with idiopathic photosensitive occipital epilepsy, 1 case with febrile seizures, and 1 case with absence seizures. It included the inherited p.V246M variant as identified in 1 case with photosensitive generalized genetic epilepsy, 1 case with juvenile myoclonic epilepsy, and 1 case with generalized or focal seizures (Li et al., 2018). The GOF effects of these variants resulted in a depolarized resting membrane potential that took neurons closer to a threshold for action potential firing (Li et al., 2018). The inherited p.S126L variant with the GOF property according to the electrophysiological study on HEK293 cells was detected in 2 cases with febrile seizures (Nakamura et al., 2013). Electrophysiological study of the *HCN2* variant p.S126L (with GOF effect) revealed substantial cAMP-independent enhanced availability of Ih currents during high temperatures, which can explain hyperthermia-induced neuronal hyperexcitability in some cases with febrile seizures (Nakamura et al., 2013). It has been shown that hyperthermia may reduce GABAA receptor-mediated synaptic inhibition in hippocampal CA1 neurons of immature rats (Qu et al., 2007). Therefore, the decrease of the GABAA receptor-mediated synaptic inhibition which is coupled with the shift in the activation kinetics of *HCN2* p.S126L during hyperthermia can accelerate the development of the febrile seizures. Thomas et al. (2019) performed a computational or simulation study on hippocampal CA1 pyramidal neuron synapse model to explore the effect of three *HCN2* variants with GOF property reported before (p.S126L, p.S632W, and p.V246M). Their study unveiled that for the GOF variants to cause neuronal hyperexcitability, the depolarizing effect of HCN2 currents must be greater than the effects of decreased input resistance (Thomas et al., 2019). The variant delPPP (p.719–721) with the GOF property according to the electrophysiological study on oocytes from Xenopus laevis was detected in the 6 cases that presented with febrile seizures and genetic epilepsy with febrile seizure plus (Dibbens et al., 2010). Similarly, the increase of the depolarizing membrane potential that takes neurons closer to the firing potential has been proposed as a possible mechanism of epilepsy for delPPP (p.719–721) (Dibbens et al., 2010). The *HCN2* knock-in mouse model (HCN2EA) in which the tie of cAMP to HCN2 was abolished by two variants (p.R591E and p. T592A) showed that cAMP gating is vital for the regulation of the transition between the burst and tonic firing in thalamic dorsal lateral geniculate and ventrobasal nuclei (Hammelmann et al., 2019). *HCN2EA* mice exhibited generalized seizures of thalamic origin (Hammelmann et al., 2019). This suggests that cAMP regulates the HCN2 channels and the abolishment of cAMP sensitivity in HCN2 channels produces generalized seizures (Hammelmann et al., 2019).

The LOF variants based on the electrophysiological studies on CHO cells and neonatal rat cortical neurons include the sporadic heterozygous p.E515K as identified in 2 cases who presented with generalized epilepsy (DiFrancesco et al., 2011, 2019). The p.E515K variant causes increased neuronal excitability in newborn rat cortical neurons. Thomas et al. (2019) performed a computational or simulation study on a hippocampal CA1 pyramidal neuron synapse model to explore the effect of *HCN2* p. E515K variant. Their study unveiled that for the LOF variants to cause neuronal hyperexcitability, the increased input resistance must be greater than the hyperpolarization in resting membrane potential due to the low levels of Ih (Thomas et al., 2019). It has been shown that HCN2 channels drive inhibitory signal from local interneurons onto distal dendrites of CA1 pyramidal neurons, and a loss of these channels on interneurons impairs inhibition of CA1 pyramidal cells in mice carrying a global deletion of the channel (HCN2–/–) (Matt et al., 2011). Two non-synonymous novel variants, F738C and P802S, were identified in two cases in postmortem (Tu et al., 2011). Notably, these variants are located in the C-terminal of the channel. The HCN2 p.R527Q variant of unknown significance has been reported in one case that presented with idiopathic generalized epilepsy (Tang et al., 2008).

The *HCN2*-null mouse demonstrates a complete loss of the Ih current in thalamocortical relay neurons, leading to increased neuronal hyperexcitability (spontaneous absence seizures) and dysrhythmia (Ludwig et al., 2003). The suggested mechanism for the occurrence of the absence seizures includes the hyperpolarizing shift in the resting potential of HCN2-deficient thalamocortical relay neurons, which eradicates inactivation from T-type Ca2+ channels and thus stimulates low-threshold burst firing in response to depolarizing inputs (Ludwig et al., 2003). This implies that the loss of inhibitory components in thalamocortical relay neurons can explain the occurrence of epilepsy. Dysrhythmia and cardiac dysfunction due to autonomic disturbances may be the possible cause of SUDEP. Compound 4e can inhibit the HCN2 channel (Chen et al., 2019). MEL55A is a potential HCN1/2 blocker but it increases seizure susceptibility (Kharouf et al., 2020b). Propofol can block HCN2 current, leading to the reduction of neuronal excitability and burst firing in thalamocortical neurons, *in vivo* and *in vitro* (Ying et al., 2006). Currently, there is no pharmacological agent that opens the HCN2 channel.

HCN3

HCN3 encodes for the hyperpolarization-activated cyclic nucleotide-gated potassium channel 3 (HCN3). HCN3 channels

are found in the cerebellum (Zúñiga et al., 2016), supraoptic nucleus of hypothalamus (Monteggia et al., 2000), thalamus (Kanyshkova et al., 2012), and Martinotti cells (somatostatin-expressing interneurons) (Wang et al., 2004). Martinotti cells are located in different neocortical layers where they provide feedback inhibition in and between neocortical layers and columns (Wang et al., 2004). HCN3 channels are also expressed in astrocytes (Honsa et al., 2014) and microglia (Vay et al., 2020). Non-synonymous variants of *HCN3* have been described in humans and are associated with epilepsy and SUDEP (**Figure 3**). Such variants (p.K69R and p.P630L) were identified in two cases in postmortem (Tu et al., 2011). However, there was inadequate information regarding their functional properties (**Figure 3**) and clinical phenotypes. Notably, p.K69R is located in the N-terminal whereas p.P630L is in the C-terminal. There is no HCN3 animal model for epilepsy. A study showed that *HCN3*-deficient mice exhibit compromised processing of contextual information, but this study only explored the role of HCN3 channel in the regulation of circadian rhythm and behavior, rather than epilepsy (Stieglitz et al., 2018). Due to the fact that HCN3 channelopathy is related to epilepsy and SUDEP, future studies can explore its association with the occurrence of epilepsy.

Ivabradine can block HCN3 current in HEK293T cells (Mistrík et al., 2005). It is an approved drug for the treatment of systolic heart failure and chronic stable angina (Koruth et al., 2017), and it has shown anticonvulsant effects in epileptic animal models. It has anticonvulsant, neuroprotective, and antioxidant effects, especially against pentylenetetrazole-induced and picrotoxin-induced seizures in mice (Cavalcante et al., 2019). It acts through GABA-A receptors (Cavalcante et al., 2019). It is more effective in models of febrile or thermogenic seizures (Kharouf et al., 2020b), electroshock-induced tonic seizures in mice (Luszczki et al., 2013), and absence seizures when administered orally (Iacone et al., 2021). Ivabradine can reduce the potency of lamotrigine in epilepsy patients, as shown in mice. However, it can be co-administered with lacosamide, pregabalin, and topiramate (Sawicka et al., 2017). Sodium valproate, gabapentin, and carbamazepine are effective in blocking epileptic activities in the hippocampus that occur among others due to magnesium or potassium ion dysfunction (Arias and Bowlby, 2005). **Table 3** summarizes this information.

HCN4

HCN4 encodes for the hyperpolarization-activated cyclic nucleotide-gated potassium channel 4. HCN4 channels are distributed in the neocortex (Battefeld et al., 2012), cerebellum (Zúñiga et al., 2016), hippocampus and spinal cord (Hughes et al., 2013; Nakagawa et al., 2020), cerebellar Purkinje fibers (Han et al., 2002), thalamus (Kanyshkova et al., 2012; Oyrer et al., 2019), corpus striatum, globus pallidus, and habenula (Oyrer et al., 2019). They can be found in neurons that regulate spontaneous rhythmic activity, such as in the thalamocortical relay, substantia nigra, cholinergic interneurons, and medial habenula (Santoro et al., 2000; Notomi and Shigemoto, 2004). Additionally, they can also be found in fast-spiking interneurons of the rat hippocampus (Hughes et al., 2013) and also in the astrocytes (Honsa et al., 2014) and microglia (Vay et al., 2020). HCN4 channels are activated with hyperpolarizing potentials: therefore, they are involved in the neuronal hyperexcitability that is observed in seizures (Sartiani et al., 2017).

The clinical features of HCN4 channelopathy manifest in infantile age, as shown in two cases (Campostrini et al., 2018). Idiopathic or genetic generalized epilepsy, including familial benign myoclonic epilepsy and genetic generalized epilepsy, are the major epileptic syndromes (**Figure 11**). Two variants are LOF (**Figure 4**), whereas 4 variants have not been characterized. The familial heterozygous variant p.R550C (LOF) was observed in 4 cases with familial benign myoclonic epilepsy (Campostrini et al., 2018; DiFrancesco et al., 2019) and inherited variant p.E153G in a case with genetic generalized epilepsy (Becker et al., 2017). The p.R550C variant increased neuronal excitability in CHO cells and pyramidal neurons according to the electrophysiological analysis findings (Campostrini et al., 2018). This implies that the loss of Ih current in pyramidal neurons can produce epilepsy.

Four non-synonymous novel variants, p.G36E, p.V759I, p.G973R, and p.R1044W, were identified in two *HCN4* cases in postmortem (Tu et al., 2011). Three of these variants are located in the C-terminal of the channel. Among the four *HCN* genes, *HCN4* has the highest mortality rate and the reason remains unclear. However, future studies can explore the possible reasons. *HCN4*-knockout mice showed that thalamic ventrobasal nuclei-specific deletion of *HCN4* cannot induce generalized seizures of the absence type (Hammelmann et al., 2019). Another study showed that brain-specific *HCN4*-knockout adult mice exhibit reduced seizure susceptibility in cortical neurons; this suggests that HCN4 channel suppression may decrease seizure susceptibility and neuronal excitability (Kharouf et al., 2020a). The study concluded that HCN4 channels are the controllers of brain excitability since their inhibition reduces thalamocortical bursting firing, and that blockers of these channels can be effective antiseizure medications (Kharouf et al., 2020a). This implies that increased HCN4 current can produce seizures. This is also supported by the evidence of the augmented HCN4 mRNA levels in the pilocarpine rodent model of temporal lobe epilepsy that relates to enlarged Ih in dentate granule cells (Surges et al., 2012). Since the reported *HCN4* cases had epilepsy and pathogenic variants with LOF effects, there is a need to investigate how LOF mutations can produce seizures. One of the possible reasons is the loss of Ih current in pyramidal neurons that can produce epilepsy; in contrast, the loss of Ih current in thalamocortical neurons is protective against epilepsy. *HCN4*-knockout mice with dorsal hippocampus dysfunction exhibit anxiety-like behavior, and this suggests heterogeneity of the phenotypes (Günther et al., 2019). EC18 is an HCN4 blocker and it is efficacious in reducing seizure susceptibility, as shown in mice (Kharouf et al., 2020b). Gabapentin reduces HCN4 current in mice (Tae et al., 2017). Glycogen synthase kinase-3β (GSK3β) inhibits seizures (Urbanska et al., 2019). The blockage of HCN channels *via* ZD7288 antagonism in the ventrobasal thalamus decreases thalamocortical neuronal firing and eliminates spontaneous absence seizures in GAERS, Wistar rats, and male Stargazer mice (David et al., 2018).

HCN Channel Auxiliary Subunits and Epilepsy

Currently, there is no known direct link between mutations of HCN auxiliary subunits and epilepsy. However, some variants of unknown significance have been reported, which indicate that existing dysfunctions may produce more information in the future (DiFrancesco et al., 2019). TRIP8b is a type of voltage-dependent cation channel that is modulated by direct cAMP binding, and it interacts with the C-terminal and CNBD of HCN channels to control channel trafficking or gating (Han et al., 2020). TRIP8b promotes HCN channel expression and enhances Ih current (Lewis et al., 2009). It hinders channel opening by shifting activation to more negative potentials (Santoro et al., 2009). TRIP8b modulates the trafficking of the HCN channel to dendrites; however, the modulation of the adult presynaptic cortical HCN expression is independent of TRIP8b (Huang et al., 2012). It enhances the distal dendritic enrichment of HCN channels in CA1 pyramidal neurons (Han et al., 2020). In addition, it is crucial for the regulation of thalamocortical oscillations since it can decrease HCN channel expression in the thalamocortical relay and cortical pyramidal neurons, with a possible mechanism that is secondary to reduced cAMP signaling, as shown in *TRIP8b*-deficient mice (TRIP8b-/-) (Budde et al., 2005; Zobeiri et al., 2018). *TRIP8b*-knockout mice serve as an animal model for absence epilepsy (Heuermann et al., 2016). TRIP8b–HCN interaction is regulated by phosphorylation: consequently, loss of TRIP8b phosphorylation may affect HCN function during the development of temporal lobe epilepsy (Foote et al., 2019). The loss of HCN1 in distal dendrites minimizes the interaction between TRIP8b and HCN1 channels in animal models of temporal lobe epilepsy, which implies that TRIP8b interaction with HCN1 is important for appropriate HCN1 channel function in CA1 pyramidal neuron dendrites (Shin et al., 2008). *TRIP8b*-knockout animal model of absence seizures demonstrates decreased HCN channel expression and function in thalamic-projecting cortical layer 5b neurons and thalamic relay neurons (Heuermann et al., 2016). However, HCN function is preserved in inhibitory neurons of the reticular thalamic nucleus (Heuermann et al., 2016). *TRIP8b*-null mice with kainic acid-induced seizures show that presynaptic adult cortical HCN channel expression continually diminishes following seizure occurrence, but there is no affection of dendritic HCN channels (Huang et al., 2012). Therefore, the modulation of adult presynaptic cortical HCN expression is independent of TRIP8b (Huang et al., 2012). Altogether, these animal model studies suggest that the function of TRIP8b in the regulation of HCN channels is neuronal-specific.

Potassium voltage-gated channel subfamily E regulatory subunit-2 (KCNE2), also known as MinK-related protein (MiRP1), belongs to the family of single-helix transmembrane proteins (5 members) that play a major role in regulating HCN channels (Brandt et al., 2009). They stand as a beta-subunit of HCN channels (Yu et al., 2001; Qu et al., 2004). KCNE2 can increase the Ih current density of the HCN channels (Brandt et al., 2009). Deletion of the *KCNE2* gene decreases the Ih current density and reduces brain expression of HCN1 and HCN2 (but not HCN4), which is associated with increased excitability in the cortico-thalamo-cortical loop neurons (Ying et al., 2012). *KCNE2* deletion also increases input resistance and temporal summation, with consequent increased intrinsic excitability and enhanced burst firing (Ying et al., 2012). It has been shown that the number of KCNE2 subunits that form the complex with HCN channels may differ according to the HCN isoform and may depend on their concentration (Lussier et al., 2019). For example, one study revealed that only the C-terminal of KCNE2, but not other KCNE subunits, can interact with HCN4 channels (Decher et al., 2003).

Hyperpolarization-activated cyclic nucleotide-gated channel 1 can interact and form a complex with F-actin-binding filamin A (Gravante et al., 2004; Ramakrishnan et al., 2012). Filamin A interacts with HCN1 by binding to the C-terminal to slow down HCN1 channel kinetics and to induce channel clustering in certain parts of the cell membrane, which decreases channel expression and whole-cell conductance (Gravante et al., 2004). Filamin A modulates internalization of HCN1 channels, which is associated with redistribution of HCN1 channels on cell membranes, accumulation of channels in endosomes, and reduction of Ih current (Noam et al., 2014). The redistribution of the HCN1 channel intensifies the efficiency of channel control *via* modulating agents (Gravante et al., 2004). The deletion of filamin A in hippocampal neurons facilitates the expression of HCN1 (Noam et al., 2014). Caveolin-3 (Cav3) is another important accessory subunit. An increase in the number of caveolae can enhance the function of HCN channels in diabetic cytopathy (Dong et al., 2016). HCN4 interacts with caveolin-3 during cardiomyocyte development (Bosman et al., 2013). The P104L mutation on caveolin-3 impairs HCN4 function and causes reduction in cardiac pacemaker activity (Ye et al., 2008).

Tamalin, also known as GRP1-associated scaffold protein (GRASP), has many separate protein regions, including PSD-95, discs large, zona occludens 1 (PDZ)—domain, glycine-rich, alanine-rich, proline-rich, leucine zipper sequence, and C-terminal PDZ-binding motif (Kitano et al., 2002). Tamalin is involved in multimolecular protein assembly in neurons, and it forms complexes with postsynaptic receptors or scaffold proteins, such as group 1 mGluRs, synaptic scaffolding molecule (S-SCAM), PSD-95, and SAP90/PSD-95-associated proteins (SAPAPs) (Kimura et al., 2004). It enhances intracellular trafficking and cell surface expression of group 1 mGluRs (Kimura et al., 2004). It has been shown that Tamalin interacts with HCN2 at both the PDZ-binding motif and C-terminal of HCN2 (Kimura et al., 2004), although its role is unknown. It remains unclear whether distorted Tamalin-HCN2 interaction can alter the Ih current or HCN2 expression. S-SCAM is a synaptic protein comprising PDZ, guanylate kinase, and two tryptophan (WW) domains. S-SCAM interacts with C-terminal of HCN2 *via* CNBD (Kimura et al., 2004). *S-SCAM*-knockout mice developed well and were born alive, although they died

within 24 h (Iida et al., 2007). Future studies should explore whether distorted Tamalin-HCN2 interaction can alter Ih current or HCN2 expression.

Mint2, also known as APBA2 (amyloid beta-precursor protein-binding family A member 2), is a synaptic adaptor protein that plays a major role in excitatory synaptic transmission. It binds to Munc-18 (a protein that is important for synaptic vesicle exocytosis) and CASK (a protein essential for targeting and localization of synaptic membrane proteins) (Butz et al., 1998). Mint2 has two PDZ domains and a phosphotyrosine domain, and it interacts with amyloid precursor and Munc-18 proteins (Lewis et al., 2010). The CNBD downstream sequence of HCN2 may interact with Munc-18-interacting domains of Mint2 (Kimura et al., 2004). The interaction between HCN2 and Mint2 is essential for Mint2-mediated escalation of the HCN2 protein cellular contents (Kimura et al., 2004). Mint1-knockout mice exhibit enhanced release probability of aminobutyric acid in hippocampal interneurons (Ho et al., 2003); however, it is unknown whether impaired Mint1-HCN interaction can affect Ih current. In Alzheimer's disease (AD), amyloid-β has been reported to have a potential link between epilepsy and dementia. Some fluctuating dementias are currently attributed to unrecognized interictal epileptiform discharges and subclinical seizures (Sen et al., 2020; Romoli et al., 2021). There is an augmented burden of Aβ pathology in the brain in AD cases with epilepsy (Romoli et al., 2021). It has been shown that targeting the amyloid precursor protein Mint2 protein–protein interaction with a peptide-based inhibitor can reduce amyloid-β formation in a neuronal model of AD (Bartling et al., 2021). In addition, the amyloid precursor protein-binding-deficient Mint2 variant demonstrates a substantial reduction of the amyloid-β levels (Bartling et al., 2021). Currently, it is recommended that antiseizure medications with mood-stabilizing functions (such as lamotrigine) be administered instead of acetylcholinesterase inhibitors for the old patients with epilepsy, including AD cases (Sen et al., 2020). Lamotrigine can activate the HCN channel (Mader et al., 2018) and increase Ih current in rat hippocampal slices, which reduces neuronal firing and dendritic excitability (Poolos et al., 2002). Based on these studies, we speculate that the heightened interaction between Mint2 and HCN channels can increase seizure susceptibility because Mint1-knockout mice exhibit enhanced release probability of aminobutyric acid which is protective against epilepsy, amyloid precursor protein-binding-deficient Mint2 variant shows a considerable reduction of the amyloid-β levels which might correlate with the reduction of the epilepsy burden in AD cases, and the fact that the enhancement of the Ih current *via* lamotrigine can reduce neuronal firing and dendritic excitability. Nevertheless, more studies are required to confirm this hypothesis.

Phosphatidylinositol 4,5-bisphosphate (PIP2) is another important regulator of the HCN channels. HCN2 can be regulated by blocking P1P2 which decelerates the hyperpolarizing shift in activation, and by antibody-induced depletion of PIP2 which causes further hyperpolarizing shift in activation (Pian et al., 2006). These shifts in activation can be partially reversed by magnesium ATP, although this may also be blocked by Wortmannin (PI kinase inhibitor) (Pian et al., 2006). There is further evidence regarding the role of P1P2 in enhancing the gating properties of HCN1 and HCN2 (Pian et al., 2007). It has been revealed that changes in pH can alter HCN2 gating properties; but are independent of cAMP concentration (Lewis et al., 2010). Orexin A is an arousal peptide that can regulate HCN channels. In layer V pyramidal neurons of mice prelimbic cortex, orexin A represses Ih currents, shifts the activation curve in the negative direction, and enhances excitability of pyramidal neurons, thereby contributing to arousal and cognition (Li et al., 2010). The effect of orexin A depends on potassium channels and non-selective cation channels (Yan et al., 2012). Orexin A (hypocretin-1) employs a postsynaptic excitatory action on prefrontal cortex neurons by inhibiting potassium currents *via* the activation of protein kinase C (PKC) and phospholipase C (PLC) signaling pathways (Xia et al., 2005). Orexin deficiency is related to narcolepsy according to the reviews (Mahoney et al., 2019; Nepovimova et al., 2019; Mignot et al., 2021). Therefore, high Ih current due to the lack of orexin can play a role in the pathogenesis of narcolepsy.

HCN Channel Regulators and Epilepsy

Cyclic AMP-mediated neurotransmitters regulate HCN channels by enhancing their opening. cAMP is the chief endogenous positive modulator of Ih current (Simeone et al., 2005). The binding of cAMP to the CNBD speeds HCN channel activation at more depolarized potentials (Wang et al., 2002; Robinson and Siegelbaum, 2003; Ulens and Siegelbaum, 2003). A study of rat thalamocortical neurons showed that rat growth or maturity is associated with increased mRNA and protein expression levels of HCN1 and HCN2, but less of HCN4 that interacts with cAMP to modulate Ih activity (Kanyshkova et al., 2009). Besides, cAMP and cGMP inhibit the HCN3 current (Mistrík et al., 2005). HCN2 and HCN4 isoforms are the most sensitive to cAMP, followed by HCN1, but HCN3 is not sensitive (Santoro and Shah, 2020). The absence seizures, impaired visual learning, and altered non-rapid eye movement sleep properties are noticed in *HCN2* knock-in mouse model (HCN2EA) in which the binding of cAMP to HCN2 is eliminated by two amino acid substitutions (R591E and T592A) (Hammelmann et al., 2019). Impaired binding of cAMP to HCN channels promotes epileptogenesis in Genetic Absence Epilepsy Rat from Strasbourg (GAERS) *via* enhancement of the T-current-mediated calcium ion signaling (Kuisle et al., 2006). The binding of cAMP to HCN channels in GAERS is weakened in the acute phase, thereby promoting seizures, and the compensatory mechanisms to stabilize Ih current activity may cause cessation of spike-wave discharges in chronic epilepsy.

P38 mitogen-activated protein kinase (p38 MAPK) is a strong modulator of HCN1 biophysical properties. The inhibition of p38 MAPK reduces Ih current in rats' hippocampal pyramidal neurons, and its activation improves Ih current (Poolos et al., 2006). The inhibition of p38 MAPK in rat's hippocampal pyramidal neurons caused 25 mV hyperpolarization of Ih activation with consequent hyperpolarization of resting potential, increased input resistance, and enhanced temporal summation of excitatory inputs (Poolos et al., 2006). In contrast, the activation of p38 MAPK by anisomycin caused 11 mV depolarizing shift of Ih activation in conjunction with depolarization of resting

potential, reduced input resistance, and decreased temporal summation (Poolos et al., 2006). The increased input resistance and temporal summation of excitatory inputs can be the possible mechanisms for epilepsy. Short Stature Homeobox 2 (Shox2) regulates HCN current in thalamocortical neurons (Yu et al., 2021). *Shox2*-knockout mice exhibit the reduced expression of HCN2, HCN4, and Cav3.1 channels, which implies that Shox2 is an important transcription factor for these channels (Yu et al., 2021). Also, *Shox2*-knockout mice are more vulnerable to pilocarpine-induced seizures (Yu et al., 2021). Casein kinase II (CK2) is an active serine or threonine protein kinase, a tetramer of two alpha- and two beta-subunits. The inhibition of CK2 by 4,5,6,7-tetrabromotriazole in acute epilepsy slice models resulted in increased expression of HCN1 channels, HCN3 channels, and voltage-independent calcium (Ca^{2+})-activated potassium (K^+) channels (KCa2.2), also known as small-conductance Ca^{2+}-activated K^+ channels (SK2), thereby producing antiepileptic effects (Schulze et al., 2020). When HCN channel blocker ZD7288 was administered, pretreatment with 4,5,6,7-tetrabromotriazole salvaged the hyperpolarizing potential and spike frequency adaptation *via* the activity of the KCa2.2 (Schulze et al., 2020).

Glycosylation is a post-translational protein modification that affects intracellular processes, such as the folding and trafficking of most glycoproteins. It can modulate and influence the total number of HCN channels in the membrane and channel heteromerization (Noam et al., 2011). It has been shown in HEK293 cells that N-linked glycosylation is required for cell surface trafficking of HCN channels (Much et al., 2003). Seizure activity increases the amount of glycosylated HCN1 but not HCN2 channel molecules, and blocking of HCN1 glycosylation abolishes seizure evoked increase of heteromerization (Zha et al., 2008). The developmental seizures stimulate the formation of hippocampal HCN1/HCN2 heteromeric channels due to the augmented amount of HCN2 channels (mRNA and protein levels), compared to HCN1 channels (Brewster et al., 2005). Heteromeric HCN channels activate hippocampal hyperexcitability, leading to the development of epilepsy (Brewster et al., 2005). In particular, seizures increase HCN1/HCN2 heteromerization in the hippocampus (Zha et al., 2008).

Protein kinase C (PKC) is a family of serine–threonine kinases located in many cell types, and they play many roles in signal transduction processes. The activation of PKC reduces Ih currents, HCN1 surface expression, and HCN1 channel phosphorylation in hippocampal principal neurons (Williams et al., 2015). However, the inhibition of PKC could reverse the situation (Williams et al., 2015), which indicates that the PKC pathway may be a good target for modulating HCN1 expression and Ih current. Phosphatase calcineurin (CaN) and p38 MAPK are the phosphorylation pathways in epilepsy that contribute to the downregulation of HCN channel gating, resulting in neuronal hyperexcitability (Jung et al., 2010). Tyrosine phosphorylation modulates HCN channels *via* tyrosine kinase Src. The receptor-like protein tyrosine phosphatase-alpha (RPTP-alpha) considerably inhibits or abolishes HCN2 channel expression in HEK293 cells, which is associated with decreased tyrosine phosphorylation in the channel protein (Huang et al., 2008). Alteration of the phosphorylation of HCN1 and HCN2 channels plays a role in chronic epileptogenesis, as shown in rats' CA1 hippocampal tissue and human brain tissue (Concepcion et al., 2021). Several phosphosites for HCN1 and HCN2 have been mapped in chronic epilepsy cases and animal models of temporal lobe epilepsy (Concepcion et al., 2021). Phosphosites for HCN1 include T41, S56, G80, T99, S116, T472, Y513, S599, T646, S770, T771, S846, S847, S871, S872, and S873 (Concepcion et al., 2021). Phosphosites for HCN2 include S80, S81, T87, S97, S110, S132, S146, S771, S779, A785, S786, S793, Y795, A801, A853, S860, S866, S868, and G873 (Concepcion et al., 2021). The HCN1 channel phosphosites S791 and S791D were implicated in the pathogenesis of chronic epilepsy in rats (Concepcion et al., 2021). Importantly, TRIP8b–HCN interaction is regulated by phosphorylation; therefore, the loss of TRIP8b phosphorylation may affect HCN function during the development of epilepsy (Foote et al., 2019).

SUMOylation was recently reported as a modulator of the Ih current (Parker et al., 2019). Post-translational SUMOylation regulates ion channel interactions; therefore, its dysregulation causes nervous system disorders, such as epilepsy (Parker et al., 2019). SUMOylation increases the surface expression of HCN2 channel, thereby augmenting Ih current in the mouse brain (Parker et al., 2016). HCN2 has several SUMOylation sites, including K464, K484, K534, and K669 (Parker et al., 2016). The K464, K534, and K484 sites are located in the C-linker which is necessary for channel trafficking and cAMP gating, whereas K669 enhances surface expression of the HCN2 channel (Parker et al., 2016). The K464 and K484 sites are in the C-linker that connects the CNBD to the transmembrane region, whereas K534 is found within the CNBD. SUMOylation in the C-linker and/or the distal fragment can promote or hinder the binding of the TRIP8b. It has been shown, in a rat model of complete Freund's adjuvant-induced hindpaw inflammation, that the increased Ih current in the early stages of inflammation is influenced by increased HCN2 protein expression and post-translational SUMOylation (Forster et al., 2020).

Acquired HCN Channelopathies and Epilepsy

Hyperpolarization-activated cyclic nucleotide-gated channels are also related to inflammation-associated epilepsy. It has been shown that the injection of lipopolysaccharide (inflammatory molecule) into rats will elicit a strong and long-lasting inflammatory response in hippocampal microglia (Frigerio et al., 2018). This is accompanied by the upregulation of Toll-like receptors (TLR4), reduction of expression and protein levels of dendritic cAMP-HCN1 channels, reduction of TRIP8b, decrease of HCN1 current, and alteration of rhythmic activities (Frigerio et al., 2018). The injured cerebral cortex can develop seizures due to changes in HCN channel expression which increases neuronal excitability (Paz et al., 2013).

Febrile infection-related epilepsy syndrome (FIRES) is a rare epileptic condition that is preceded by febrile illness about 24 h−2 weeks prior to the onset of refractory status epilepticus, and the condition is not limited by age (Kessi et al.,

2020b). This condition has high mortality rates, most cases die from cardiorespiratory failure, most cases do not respond to anticonvulsants or immunotherapies, and the underlying mechanism is unknown (Kessi et al., 2020b). In the acute phase, most cases (61%) have a normal brain scan, but 25% of cases have diffuse cerebral edema plus defects in the temporal lobes, basal ganglia, thalami, and brainstem (Culleton et al., 2019). In the chronic phase, there is brain atrophy and mesial temporal sclerosis (Culleton et al., 2019). The mice models of FIRES, which were made using low-dose lipopolysaccharide injection and hyperthermia, revealed that lipopolysaccharides cause seizure-induced proinflammatory cytokine production, microglial activation, disruption of blood–brain barrier, and sparse ischemic lesions in the cerebral cortex (Koh et al., 2020). Microglial activation leads to the production of proinflammatory cytokines, such as interleukin-1 (IL-1), interleukin-6 (IL-6), and tumor necrosis factor-alpha (TNF-α) (Smith et al., 2012). Inflammatory cytokines that include IL-1, TNF-α, and IL-6 can result in gliosis, as demonstrated in the brain biopsy of seven FIRES cases (van Baalen et al., 2010). The ketogenic diet's antiseizure and anti-inflammatory activity may provide effective therapy for the acute phase of FIRES, and cannabidiol is effective for the chronic phase of FIRES (Kessi et al., 2020b). Phenobarbital is an effective therapy in the acute and chronic phases of FIRES, despite the minimal evidence (Kessi et al., 2020b). Phenobarbital can increase the Ih current in hippocampal pyramidal neurons (Jung et al., 2007). Anakinra (human interleukin-1 receptor antagonist), a drug with anti-inflammatory activity, has been reported to be effective in the acute phase of FIRES (Kenney-Jung et al., 2016; Dilena et al., 2019; Lai et al., 2020; L'Erario et al., 2021). The cerebrospinal fluid of FIRES cases demonstrated high levels of proinflammatory cytokines before treatment, but the levels were normalized after anakinra therapy (Kenney-Jung et al., 2016).

Similar to HCN channels, the transient receptor potential vanilloid-1 (TRPV1) channel can respond to noxious heat and oxidative stress (Caterina et al., 1997). Moreover, the activation of the mitochondrial TRPV1 channel leads to microglial migration which is essential for neuroinflammation (Miyake et al., 2015). Capsazepine, a blocker of the TRPV1 channel, inhibits HCN1-mediated currents in a non-use-dependent manner (Gill et al., 2004). The proposed mechanisms of cannabidiol action include its ability to desensitize TRPV1 channels (Franco et al., 2021). Its antiseizure activity *via* TRPV1 results from its ability to modulate calcium ions release and thus neuronal excitability (Franco et al., 2021). Therefore, there may be a relationship between cannabidiol and HCN channels. We hypothesize that the efficacy of cannabidiol in the chronic phase of FIRES may be due to its ability to modulate channels, including HCN and TRPV1.

Although there is currently no direct evidence to support the involvement of HCN and TRPV1 channelopathies in the pathogenesis of FIRES, we believe or propose that they contribute to the pathogenesis. The initial febrile illness observed in FIRES can alter the expression of HCN channels in astrocytes and microglia, which may result in progressive status epilepticus, and permanent acquired channelopathy in the brain and heart. Inflammation in astrocytes and microglia can reduce HCN1 and HCN2 expression, leading to the reduction of inhibitory effect and enhanced neuronal excitability. Our previous published review on FIRES showed that most cases die from cardiorespiratory failure or SUDEP (Kessi et al., 2020b). The rat pilocarpine model of epilepsy is an animal model of spontaneous induced recurrent seizures, and it revealed that there is a diminished expression of dendritic HCN channels during the acute phase of epilepsy, which is accompanied by the loss of hyperpolarization of voltage-dependent activation (Jung et al., 2007). The phenomenon progresses to the chronic phase which increases neuronal excitability and consequent epileptogenesis (Jung et al., 2007). Phenobarbital can suppress seizures and reverse the neuronal current changes but not the protein expression changes (Jung et al., 2007). This may explain why phenobarbital is not as efficient as cannabidiol in reducing seizures during the chronic phase of FIRES. The loss of Ih current and HCN1channel expression starts 1 h after status epilepticus and involves several steps, including dendritic HCN1 channel internalization, deferred loss of protein expression, and finally the downregulation of mRNA expression (Jung et al., 2011). Consequently, we propose that FIRES may be a neuroinflammatory condition that produces acquired channelopathies. The clinical animal models of FIRES can be used to further explore whether there is acquired HCN and TRPV1 channelopathies.

Other HCN-Related Epileptic Disorders

Epilepsy can reduce the expression of HCN channels, leading to increased neuronal excitability in dorsal hippocampal CA1 neurons (Arnold et al., 2019). The disruption of Ih current disturbs hippocampal theta function in rat models of temporal lobe epilepsy (Marcelin et al., 2009), and during seizures, there is a reduced expression of HCN1 channel and upregulation of HCN2 channel (Richichi et al., 2008). According to one study, messenger RNA and protein expression of HCN1 and HCN2 were downregulated in controls compared to the cases with medial temporal lobe epilepsy and hippocampal sclerosis (Lin et al., 2020). In these cases of mesial temporal lobe epilepsy with hippocampal sclerosis, the lowered expression of HCN1 and HCN2 during chronic phases reduces Ih current density and function, thereby decreasing inhibitory effects and enhancing neuronal excitability (Lin et al., 2020). The downregulation of HCN1 expression after seizures augments dendritic excitability, resulting in the development of temporal lobe epilepsy (Powell et al., 2008). The mechanisms for HCN1 downregulation include calcium-permeable AMPA receptor-mediated calcium ion influx, followed by the activation of calcium or calmodulin-dependent protein kinase II (Richichi et al., 2008). The other proposed mechanism is the alteration of phosphorylation signaling that is facilitated by phosphatase calcineurin (CaN) or p38 MAPK (Jung et al., 2010). Another study showed that after status epilepticus, there is reduced expression of HCN channels and reduced relocalization from distal dendrites to soma, which influence CA1 excitability (Shin et al., 2008).

The animal model of Rett syndrome [Mecp2 (-/y)] CA1 exhibits heightened neuronal excitability as the pH increases from normal to high (pH 7.4–8.4) (Balakrishnan and Mironov,

2018). This alkaline pH enhances neuronal excitability *via* the loss of the Ih current and modulation of calcium channels (Balakrishnan and Mironov, 2018). HCN channels function as voltage absorbers and reduce dendritic membrane resistance in pyramidal neurons, resulting in reduced membrane excitability (Kase and Imoto, 2012). Consequently, modulation of pH and magnesium levels in Rett syndrome can modulate the expression and functions of HCN and calcium channels, which may reduce epilepsy (Balakrishnan and Mironov, 2018).

Hyperpolarization-activated cyclic nucleotide-gated channels play a role in epilepsy that is related to cortical development malformations. HCN channels modulate excitatory postsynaptic potentials in diverse classes of GABAergic interneurons *via* different ways, and this function is altered in malformed rat neocortex (Albertson et al., 2017). In rats' L5 pyramidal neurons with induced focal cortical dysplasia, there is a reduced Ih current in distal dendrites, resulting in increased intrinsic and synaptic excitability (Hablitz and Yang, 2010; Albertson et al., 2011). Induction of cortical dysplasia in rats during prenatal period reduces the expression of *HCN1* and *HCN2* genes in CA1 and CA3 pyramidal neurons, although none of the rats exhibit seizure activity (Işler et al., 2008).

A General Overview of Treatments

Based on the literature, few cases achieved seizure freedom without receiving any antiseizure medication, less than half of the cases became seizure-free after receiving one or more antiseizure medications, including sodium valproate, and some developed drug-resistant epilepsy, even after receiving sodium valproate. It was shown that HCN1 M294L heterozygous knock-in (HCN1M294L) mouse demonstrates the clinical manifestations of patients with the *HCN1* M305L variant, including spontaneous seizures, seizure exaggeration by lamotrigine, and the seizure reduction by sodium valproate (Bleakley et al., 2021). Nevertheless, we attempted to do some statistics to see whether sodium valproate has any association with seizure freedom but there was no correlation (p-value $= 0.717$). Therefore, it is difficult to tell which antiseizure medication can result in seizure freedom; however, sodium valproate can be tried for cases with epilepsy of unknown origin and genetically positive screening for HCN channelopathy.

Some antiseizure medications work through or act *via* HCN channels as shown on cell culture models, animal models, and human brain slices. Lamotrigine can activate HCN channel (Mader et al., 2018) and increase Ih current in rat hippocampal slices, which reduces neuronal firing and dendritic excitability (Poolos et al., 2002). Through the whole-cell and cell-attached recordings, it has been shown in rat hippocampal slices that lamotrigine selectively reduces action potential firing from dendritic depolarization, whereas it minimally affects firing at the soma, suggesting that lamotrigine targets dendrites specifically (Poolos et al., 2002). In addition, there is the evidence from human cortical pyramidal neurons that lamotrigine reduces input resistance and enhances Ih current in layers 2/3 in patients with drug-resistant epilepsy (Lehnhoff et al., 2019). Based on the electrophysiological studies on Xenopus oocytes, mouse spinal cord slices targeting either parvalbumin-positive or calretinin-positive inhibitory neurons, it was revealed that there is a hyperpolarizing shift in the V1/2 of Ih current measured from HCN4-expressing PV+ inhibitory neurons in the spinal dorsal horn but not calretinin-positive inhibitory neurons (Tae et al., 2017). In contrast, another study of CA1 pyramidal cells in hippocampal slices has shown that gabapentin can increase Ih current *via* cAMP-independent mechanism (Surges et al., 2003). Phenobarbital can increase Ih current in rat pilocarpine model of epilepsy but cannot reverse the loss of HCN channel expression in CA1 hippocampal pyramidal neurons (Jung et al., 2007). Acetazolamide can enhance Ih current in rat thalamic relay neurons *via* intracellular alkalinization (Munsch and Pape, 1999). Ethosuximide can suppress seizures in HCN1-knockout rats whose cortical and hippocampal pyramidal neurons exhibited a significant reduction of Ih current, although its mechanism of action is not clear (Nishitani et al., 2019). We speculate that ethosuximide can increase Ih current in cortical and hippocampal pyramidal neurons. Capsazepine, a blocker of the TRPV1 channel, inhibits HCN1-mediated currents in a non-use-dependent manner as shown in CV-1 and CHO cell lines (Gill et al., 2004).

Notably, some of the anesthetics used in status epilepticus work through HCN channels too. Propofol can inhibit HCN1 subunit mediated Ih current in mouse cortical pyramidal neurons (Chen et al., 2005). Ketamine has been shown to be effective and relatively safe for the control of multidrug-resistant refractory status epilepticus in children and adults (Fang and Wang, 2015). In cortical pyramidal neurons, ketamine was suggested to work *via* HCN1 channels (Chen et al., 2009a). Likewise, isoflurane has been reported to associate with a good effect in stopping refractory status epilepticus or super refractory status epilepticus (Stetefeld et al., 2021). Isoflurane can affect neuronal Ih current as shown in cortical pyramidal neurons of HCN1-knockout mice (Chen et al., 2009b).

CONCLUSION

Hyperpolarization-activated cyclic nucleotide-gated channels are widespread in the body especially in the brain, microglia, and astrocytes. HCN channel auxiliary subunits include TRIP8b, KCNE2, actin-binding protein filamin A, caveolin-3, Tamalin, S-SCAM, and Mint2. HCN channels can be regulated *via* cAMP system, p38 MAPK, Shox2, CK2, N-linked glycosylation, PKC, phosphorylation, and SUMOylation. HCN channelopathies are implicated in epilepsy. Pathogenic variants of *HCN1*, *HCN2*, *HCN3*, and *HCN4* have been reported to be associated with epilepsy in 74 cases, and they have diverse phenotypes. Less than half of the cases with HCN channelopathies achieve seizure-freedom. A total of twelve cases (16.2%) died due to SUDEP: *HCN1* ($n = 4$), *HCN2* ($n = 2$), *HCN3* ($n = 2$), and *HCN4* ($n = 4$).

For the *HCN1* gene, majority of the cases can present with either febrile seizures, or febrile seizure plus or genetic generalized epilepsy with febrile seizure plus or genetic/idiopathic generalized epilepsy. Some of the variants are related to different epileptic syndromes, which suggest

heterogeneity of the *HCN1* phenotypes. Besides epilepsy, intellectual disability, behavioral disturbances, autistic features, polyphagia, motor delay, ADHD, truncal ataxia, language delay, and microcephaly can be noticed in the cases with *HCN1* pathogenic variants. According to the electrophysiological studies on cell culture models, both GOF and LOF *HCN1* variants are associated with epilepsy, but LOF is associated with more severe phenotypes, including 3 deaths due to the deletion and a strong reduction in HCN1 current density. The underlying mechanisms of epilepsy for both GOF and LOF variants remain unclear since most of the functional studies were limited to the electrophysiological studies and only a few were done to explore the neuroanatomical localization in different neuronal subtypes not to mention the distribution patterns. Most rodent models of epilepsy (especially absence seizures) support the fact that the loss of the HCN1 current is associated with the occurrence of epilepsy in pyramidal, cortical, and thalamic neurons, but there is limited evidence showing that the upregulation of this current in the same or other neurons can produce epilepsy.

Most of the cases carrying *HCN2* gene pathogenic variants can present clinically with either febrile seizures, or febrile seizure plus or genetic generalized epilepsy with febrile seizure plus or genetic or idiopathic generalized epilepsy. Similar to *HCN1* gene, some of the variants are related to different epileptic syndromes which suggest heterogeneity of the *HCN2* phenotypes. Based on the electrophysiological studies on cell models, both GOF and LOF *HCN2* variants are related to epilepsy. However, GOF effect is more common in *HCN2* gene. The proposed mechanisms of epilepsy for the GOF variants include continuous cation leak, N-terminal deletion, increased HCN1 expression and current, suppression of HCN2 and HCN4 currents, reduction of cAMP sensitivity, reduction of the GABAA receptor-mediated synaptic inhibition, depolarizing shift in the resting membrane potential, impaired input resistance, and cAMP-independent enhanced availability of Ih during high temperatures, whereas the suggested mechanism of epilepsy for the LOF variants includes the loss of the voltage dependence in activation and deactivation leading to continuous excitatory cation flow. Besides, the loss of HCN2 channels on interneurons and thalamocortical relay neurons has been suggested as a possible underlying mechanism of epilepsy as shown in simulation study on a hippocampal CA1 pyramidal neuron synapse model and HCN2-null mouse. For the *HCN4* gene, most cases present with genetic or idiopathic generalized epilepsy. Most cases had LOF variants. Evidence from the animal models suggests that HCN4 channels are the controllers of brain excitability, and their inhibition reduces thalamocortical bursting firing. Nevertheless, it is unclear whether the same protective activity against epilepsy can be observed in other types of neurons. Currently, there is no direct link between mutations of HCN auxiliary and regulatory subunits with epilepsy in humans. However, there are some variants of unknown significance that have been reported, which indicate possibilities of future occurrences or research. Therefore, future studies should explore links between these unknown variants and epilepsy. HCN channels are also involved in the epileptogenesis of temporal lobe epilepsy, Rett syndrome, malformation of cortical development, and possibly FIRES. Since HCN channels are also expressed in astrocytes and microglia, future studies should explore their relation with inflammatory-related epilepsy, including FIRES.

The regulation of neuronal excitability *via* HCN channels depends on their neuroanatomical locations in the brain as well as neuronal distribution patterns: dendrites, axons, and soma of specific neurons. Although there are several rodent animal models, most of them focused to study the absence seizures. There are few animal models focused to explore the specific neuroanatomical location and distribution patterns of the reported variants, thus hampering to know more about the mechanisms of both GOF and LOF variants in causing epilepsy. Besides pharmacological targets and modulators, precise antiseizure medications are yet to be found. Currently, there are some HCN1 channel blockers with low efficiency. New HCN1-blocking drugs with high affinity should be developed. Since HCN1 current seems to be essential for the prevention of certain types of epilepsy, there is also the need to develop channel openers. There is no HCN2 channel opener, and this should be developed in the future. Due to the fact that HCN3 channelopathy is related to epilepsy and death, future studies may explore its association with the occurrence of epilepsy in living patients. HCN4 channels are the controllers of brain excitability, and blockers of these channels can be effective antiseizure medications. Since the reported HCN4 cases had epilepsy and carried pathogenic variants with LOF effects, there is a need to investigate how LOF mutations produce seizures whereas the brain-specific *HCN4*-knockout adult mice exhibit reduced seizure susceptibility.

Interestingly, the blockage of HCN1-mediated Ih current in the pyramidal, cortical, and thalamic neurons contributes to epilepsy, whereas blockers of HCN3- and HCN4-mediated currents suppress seizures. Likewise, propofol can block HCN2 current, leading to the reduction of neuronal excitability and burst firing in thalamocortical neurons. This finding suggests that HCN isoform-selective blockage might have different effects on seizure susceptibility (Kharouf et al., 2020b). This phenomenon has been hypothesized to occur due to the fact that HCN channel isoforms might have different biophysical features, anatomical expression, and functions in regulating neuronal excitability. For instance, in thalamocortical neurons, HCN4 channels are highly found in the soma; in contrast, HCN2 channels are highly expressed in dendritic spines (Abbas et al., 2006). Consequently, there is a need to develop HCN isoform-selective compounds that are based on biophysical features, anatomical expression, and functions.

RECOMMENDATIONS

The availability of few cases of HCN-related epilepsy in the literature may suggest that less attention is being paid to the affected cases. We recommend that clinicians should include *HCN* genes in epilepsy gene panels. Researchers should do further genetic screening and consider HCN channel roles in epileptic syndromes of unknown cause and/or mechanisms with clues of possible neuroinflammation (including FIRES). Future studies should try to explore the possible

underlying mechanisms for both GOF and LOF variants in the occurrence of epilepsy by focusing on exploring the specific neuronal subtypes, neuroanatomical location, and distribution patterns of each identified pathogenic variant. Future research should identify specific HCN channel openers and blockers with high binding affinity, which may help to produce targeted treatments.

DATA AVAILABILITY STATEMENT

The original contributions presented in the study are included in the article/**Supplementary Material**, further inquiries can be directed to the corresponding author.

AUTHOR CONTRIBUTIONS

MK designed the study, reviewed the articles, drafted, and wrote the manuscript. OB, HD, HH, BC, JX, and KK assisted in the literature review and preparation of tables and figures. OB, JP, YW, LY, GW, and FY revised the manuscript and supervised each step involved in the preparation of the manuscript. All authors have read and agreed to the content of the manuscript.

FUNDING

This work was supported by the National Natural Science Foundation of China (No. 81771408), the National Natural Science Foundation of China (No. 81801297), and the Hunan Key Research and Development Program (No. 2019SK2081).

SUPPLEMENTARY MATERIAL

The Supplementary Material for this article can be found online at: https://www.frontiersin.org/articles/10.3389/fnmol.2022.807202/full#supplementary-material

REFERENCES

Abbas, S. Y., Ying, S.-W., and Goldstein, P. A. (2006). Compartmental distribution of hyperpolarization-activated cyclic-nucleotide-gated channel 2 and hyperpolarization-activated cyclic-nucleotide-gated channel 4 in thalamic reticular and thalamocortical relay neurons. *Neuroscience* 141, 1811–1825. doi: 10.1016/j.neuroscience.2006.05.034

Albertson, A. J., Bohannon, A. S., and Hablitz, J. J. (2017). HCN channel modulation of synaptic integration in GABAergic interneurons in malformed rat neocortex. *Front. Cell. Neurosci.* 11, 109. doi: 10.3389/fncel.2017.00109

Albertson, A. J., Williams, S. B., and Hablitz, J. J. (2013). Regulation of epileptiform discharges in rat neocortex by HCN channels. *J. Neurophysiol.* 110, 1733–1743. doi: 10.1152/jn.00955.2012

Albertson, A. J., Yang, J., and Hablitz, J. J. (2011). Decreased hyperpolarization-activated currents in layer 5 pyramidal neurons enhances excitability in focal cortical dysplasia. *J. Neurophysiol.* 106, 2189–2200. doi: 10.1152/jn.00164.2011

Arias, R. L., and Bowlby, M. R. (2005). Pharmacological characterization of antiepileptic drugs and experimental analgesics on low magnesium-induced hyperexcitability in rat hippocampal slices. *Brain Res.* 1047, 233–244. doi: 10.1016/j.brainres.2005.04.052

Arnold, E. C., McMurray, C., Gray, R., and Johnston, D. (2019). Epilepsy-induced reduction in HCN channel expression contributes to an increased excitability in dorsal, but not ventral, hippocampal CA1 neurons. *eNeuro* 6, ENEURO.0036-19.2019. doi: 10.1523/ENEURO.0036-19.2019

Balakrishnan, S., and Mironov, S. L. (2018). Rescue of hyperexcitability in hippocampal CA1 neurons from Mecp2 (-/y) mouse through surface potential neutralization. *PLoS ONE* 13, e0195094. doi: 10.1371/journal.pone.0195094

Bartling, C. R. O., Jensen, T. M. T., Henry, S. M., Colliander, A. L., Sereikaite, V., Wenzler, M., et al. (2021). Targeting the APP-Mint2 protein-protein interaction with a peptide-based inhibitor reduces amyloid-β formation. *J. Am. Chem. Soc.* 143, 891–901. doi: 10.1021/jacs.0c10696

Battefeld, A., Rocha, N., Stadler, K., Bräuer, A. U., and Strauss, U. (2012). Distinct perinatal features of the hyperpolarization-activated non-selective cation current I(h) in the rat cortical plate. *Neural Dev.* 7, 21. doi: 10.1186/1749-8104-7-21

Beaumont, V., Zhong, N., Froemke, R. C., Ball, R. W., and Zucker, R. S. (2002). Temporal synaptic tagging by I(h) activation and actin: involvement in long-term facilitation and cAMP-induced synaptic enhancement. *Neuron* 33, 601–613. doi: 10.1016/S0896-6273(02)00581-0

Becker, F., Reid, C. A., Hallmann, K., Tae, H.-S., Phillips, A. M., Teodorescu, G., et al. (2017). Functional variants in HCN4 and CACNA1H may contribute to genetic generalized epilepsy. *Epilepsia Open* 2, 334–342. doi: 10.1002/epi4.12068

Benarroch, E. E. (2013). HCN channels: function and clinical implications. *Neurology* 80, 304–310. doi: 10.1212/WNL.0b013e31827dec42

Biel, M., Wahl-Schott, C., Michalakis, S., and Zong, X. (2009). Hyperpolarization-activated cation channels: from genes to function. *Physiol. Rev.* 89, 847–885. doi: 10.1152/physrev.00029.2008

Bleakley, L. E., McKenzie, C. E., Soh, M. S., Forster, I. C., Pinares-Garcia, P., Sedo, A., et al. (2021). Cation leak underlies neuronal excitability in an HCN1 developmental and epileptic encephalopathy. *Brain* 144, 2060–2073. doi: 10.1093/brain/awab145

Bohannon, A. S., and Hablitz, J. J. (2018). Developmental changes in HCN channel modulation of neocortical layer 1 interneurons. *Front. Cell. Neurosci.* 12, 20. doi: 10.3389/fncel.2018.00020

Bonzanni, M., DiFrancesco, J. C., Milanesi, R., Campostrini, G., Castellotti, B., Bucchi, A., et al. (2018). A novel *de novo* HCN1 loss-of-function mutation in genetic generalized epilepsy causing increased neuronal excitability. *Neurobiol. Dis.* 118, 55–63. doi: 10.1016/j.nbd.2018.06.012

Bosman, A., Sartiani, L., Spinelli, V., Del Lungo, M., Stillitano, F., Nosi, D., et al. (2013). Molecular and functional evidence of HCN4 and caveolin-3 interaction during cardiomyocyte differentiation from human embryonic stem cells. *Stem Cells Dev.* 22, 1717–1727. doi: 10.1089/scd.2012.0247

Boychuk, J. A., Farrell, J. S., Palmer, L. A., Singleton, A. C., Pittman, Q. J., and Teskey, G. C. (2017). HCN channels segregate stimulation-evoked movement responses in neocortex and allow for coordinated forelimb movements in rodents. *J. Physiol.* 595, 247–263. doi: 10.1113/JP273068

Boychuk, J. A., and Teskey, G. C. (2017). Loss of HCN channel mediated I(h) current following seizures accounts for movement dysfunction. *Channels.* 11, 176–177. doi: 10.1080/19336950.2016.1256517

Brandt, M. C., Endres-Becker, J., Zagidullin, N., Motloch, L. J., Er, F., Rottlaender, D., et al. (2009). Effects of KCNE2 on HCN isoforms: distinct modulation of membrane expression and single channel properties. *Am. J. Physiol. Heart Circ. Physiol.* 297, H355–H363. doi: 10.1152/ajpheart.00154.2009

Brenner, R., and Wilcox, K. S. (2012). "Potassium channelopathies of epilepsy," in *Jasper's Basic Mechanisms of the Epilepsies, 4th Edn*, eds J. L. Noebels, M. Avoli, M. A. Rogawski, R. W. Olsen, and A. V. Delgado-Escueta (Bethesda, MD: National Center for Biotechnology Information).

Brewster, A. L., Bernard, J. A., Gall, C. M., and Baram, T. Z. (2005). Formation of heteromeric hyperpolarization-activated cyclic nucleotide-gated (HCN) channels in the hippocampus is regulated by developmental seizures. *Neurobiol. Dis.* 19, 200–207. doi: 10.1016/j.nbd.2004.12.015

Bucchi, A., Tognati, A., Milanesi, R., Baruscotti, M., and DiFrancesco, D. (2006). Properties of ivabradine-induced block of HCN1 and HCN4 pacemaker channels. *J. Physiol.* 572, 335–346. doi: 10.1113/jphysiol.2005.100776

Budde, T., Caputi, L., Kanyshkova, T., Staak, R., Abrahamczik, C., Munsch, T., et al. (2005). Impaired regulation of thalamic pacemaker channels through an imbalance of subunit expression in absence epilepsy. *J. Neurosci.* 25, 9871–9882. doi: 10.1523/JNEUROSCI.2590-05.2005

Butz, S., Okamoto, M., and Südhof, T. C. (1998). A tripartite protein complex with the potential to couple synaptic vesicle exocytosis to cell adhesion in brain. *Cell* 94, 773–782. doi: 10.1016/S0092-8674(00)81736-5

Cain, S. M., Tyson, J. R., Jones, K. L., and Snutch, T. P. (2015). Thalamocortical neurons display suppressed burst-firing due to an enhanced Ih current in a genetic model of absence epilepsy. *Pflugers Arch.* 467, 1367–1382. doi: 10.1007/s00424-014-1549-4

Campostrini, G., DiFrancesco, J. C., Castellotti, B., Milanesi, R., Gnecchi-Ruscone, T., Bonzanni, M., et al. (2018). A loss-of-function HCN4 mutation associated with familial benign myoclonic epilepsy in infancy causes increased neuronal excitability. *Front. Mol. Neurosci.* 11, 269. doi: 10.3389/fnmol.2018.00269

Cao, Y., Chen, S., Liang, Y., Wu, T., Pang, J., Liu, S., et al. (2018). Inhibition of hyperpolarization-activated cyclic nucleotide-gated channels by β-blocker carvedilol. *Br. J. Pharmacol.* 175, 3963–3975. doi: 10.1111/bph.14469

Caterina, M. J., Schumacher, M. A., Tominaga, M., Rosen, T. A., Levine, J. D., and Julius, D. (1997). The capsaicin receptor: a heat-activated ion channel in the pain pathway. *Nature* 389, 816–824. doi: 10.1038/39807

Cavalcante, T. M. B., De Melo, J. M. A., Lopes, L. B., Bessa, M. C., Santos, J. G., et al. (2019). Ivabradine possesses anticonvulsant and neuroprotective action in mice. *Biomed. Pharmacother.* 109, 2499–2512. doi: 10.1016/j.biopha.2018.11.096

Chen, S.-J., Xu, Y., Liang, Y.-M., Cao, Y., Lv, J.-Y., Pang, J.-X., et al. (2019). Identification and characterization of a series of novel HCN channel inhibitors. *Acta Pharmacol. Sin.* 40, 746–754. doi: 10.1038/s41401-018-0162-z

Chen, X., Shu, S., and Bayliss, D. A. (2005). Suppression of ih contributes to propofol-induced inhibition of mouse cortical pyramidal neurons. *J. Neurophysiol.* 94, 3872–3883. doi: 10.1152/jn.00389.2005

Chen, X., Shu, S., and Bayliss, D. A. (2009a). HCN1 channel subunits are a molecular substrate for hypnotic actions of ketamine. *J. Neurosci.* 29, 600–609. doi: 10.1523/JNEUROSCI.3481-08.2009

Chen, X., Shu, S., Kennedy, D. P., Willcox, S. C., and Bayliss, D. A. (2009b). Subunit-specific effects of isoflurane on neuronal Ih in HCN1 knockout mice. *J. Neurophysiol.* 101, 129–140. doi: 10.1152/jn.01352.2007

Cheng, J., Umschweif, G., Leung, J., Sagi, Y., and Greengard, P. (2019). HCN2 channels in cholinergic interneurons of nucleus accumbens shell regulate depressive behaviors. *Neuron* 101, 662–672.e5. doi: 10.1016/j.neuron.2018.12.018

Coll, M., Allegue, C., Partemi, S., Mates, J., Del Olmo, B., Campuzano, O., et al. (2016). Genetic investigation of sudden unexpected death in epilepsy cohort by panel target resequencing. *Int. J. Legal Med.* 130, 331–339. doi: 10.1007/s00414-015-1269-0

Concepcion, F. A., Khan, M. N., Ju Wang, J.-D., Wei, A. D., Ojemann, J. G., Ko, A. L., et al. (2021). HCN channel phosphorylation sites mapped by mass spectrometry in human epilepsy patients and in an animal model of temporal lobe epilepsy. *Neuroscience* 460, 13–30. doi: 10.1016/j.neuroscience.2021.01.038

Culleton, S., Talenti, G., Kaliakatsos, M., Pujar, S., and D'Arco, F. (2019). The spectrum of neuroimaging findings in febrile infection-related epilepsy syndrome (FIRES): a literature review. *Epilepsia* 60, 585–592. doi: 10.1111/epi.14684

David, F., Çarçak, N., Furdan, S., Onat, F., Gould, T., Mészáros, Á., et al. (2018). Suppression of hyperpolarization-activated cyclic nucleotide-gated channel function in thalamocortical neurons prevents genetically determined and pharmacologically induced absence seizures. *J. Neurosci.* 38, 6615–6627. doi: 10.1523/JNEUROSCI.0896-17.2018

Decher, N., Bundis, F., Vajna, R., and Steinmeyer, K. (2003). KCNE2 modulates current amplitudes and activation kinetics of HCN4: influence of KCNE family members on HCN4 currents. *Pflugers Arch.* 446, 633–640. doi: 10.1007/s00424-003-1127-7

Deutsch, M., Günther, A., Lerchundi, R., Rose, C. R., Balfanz, S., and Baumann, A. (2021). AAV-mediated CRISPRi and RNAi based gene silencing in mouse hippocampal neurons. *Cells* 10, 324. doi: 10.3390/cells10020324

Dibbens, L. M., Reid, C. A., Hodgson, B., Thomas, E. A., Phillips, A. M., Gazina, E., et al. (2010). Augmented currents of an HCN2 variant in patients with febrile seizure syndromes. *Ann. Neurol.* 67, 542–546. doi: 10.1002/ana.21909

DiFrancesco, J. C., Barbuti, A., Milanesi, R., Coco, S., Bucchi, A., Bottelli, G., et al. (2011). Recessive loss-of-function mutation in the pacemaker HCN2 channel causing increased neuronal excitability in a patient with idiopathic generalized epilepsy. *J. Neurosci.* 31, 17327–17337. doi: 10.1523/JNEUROSCI.3727-11.2011

DiFrancesco, J. C., Castellotti, B., Milanesi, R., Ragona, F., Freri, E., Canafoglia, L., et al. (2019). HCN ion channels and accessory proteins in epilepsy: genetic analysis of a large cohort of patients and review of the literature. *Epilepsy Res.* 153, 49–58. doi: 10.1016/j.eplepsyres.2019.04.004

Dilena, R., Mauri, E., Aronica, E., Bernasconi, P., Bana, C., Cappelletti, C., et al. (2019). Therapeutic effect of Anakinra in the relapsing chronic phase of febrile infection-related epilepsy syndrome. *Epilepsia Open* 4, 344–350. doi: 10.1002/epi4.12317

Dini, L., Del Lungo, M., Resta, F., Melchiorre, M., Spinelli, V., Di Cesare Mannelli, L., et al. (2018). Selective blockade of HCN1/HCN2 channels as a potential pharmacological strategy against pain. *Front. Pharmacol.* 9, 1252. doi: 10.3389/fphar.2018.01252

Dong, X., Song, Q., Zhu, J., Zhao, J., Liu, Q., Zhang, T., et al. (2016). Interaction of Caveolin-3 and HCN is involved in the pathogenesis of diabetic cystopathy. *Sci. Rep.* 6, 24844. doi: 10.1038/srep24844

Fang, Y., and Wang, X. (2015). Ketamine for the treatment of refractory status epilepticus. *Seizure* 30, 14–20. doi: 10.1016/j.seizure.2015.05.010

Fiest, K. M., Sauro, K. M., Wiebe, S., Patten, S. B., Kwon, C.-S., Dykeman, J., et al. (2017). Prevalence and incidence of epilepsy: a systematic review and meta-analysis of international studies. *Neurology* 88, 296–303. doi: 10.1212/WNL.0000000000003509

Foote, K. M., Lyman, K. A., Han, Y., Michailidis, I. E., Heuermann, R. J., Mandikian, D., et al. (2019). Phosphorylation of the HCN channel auxiliary subunit TRIP8b is altered in an animal model of temporal lobe epilepsy and modulates channel function. *J. Biol. Chem.* 294, 15743–15758. doi: 10.1074/jbc.RA119.010027

Forster, L. A., Jansen, L.-A. R., Rubaharan, M., Murphy, A. Z., and Baro, D. J. (2020). Alterations in SUMOylation of the hyperpolarization-activated cyclic nucleotide-gated ion channel 2 during persistent inflammation. *Eur. J. Pain* 24, 1517–1536. doi: 10.1002/ejp.1606

Franco, V., Bialer, M., and Perucca, E. (2021). Cannabidiol in the treatment of epilepsy: current evidence and perspectives for further research. *Neuropharmacology* 185, 108442. doi: 10.1016/j.neuropharm.2020.108442

Frigerio, F., Flynn, C., Han, Y., Lyman, K., Lugo, J. N., Ravizza, T., et al. (2018). Neuroinflammation alters integrative properties of rat hippocampal pyramidal cells. *Mol. Neurobiol.* 55, 7500–7511. doi: 10.1007/s12035-018-0915-1

George, M. S., Abbott, L. F., and Siegelbaum, S. A. (2009). HCN hyperpolarization-activated cation channels inhibit EPSPs by interactions with M-type K(+) channels. *Nat. Neurosci.* 12, 577–584. doi: 10.1038/nn.2307

Gill, C. H., Randall, A., Bates, S. A., Hill, K., Owen, D., Larkman, P. M., et al. (2004). Characterization of the human HCN1 channel and its inhibition by capsazepine. *Br. J. Pharmacol.* 143, 411–421. doi: 10.1038/sj.bjp.0705945

Gravante, B., Barbuti, A., Milanesi, R., Zappi, I., Viscomi, C., and DiFrancesco, D. (2004). Interaction of the pacemaker channel HCN1 with filamin A. *J. Biol. Chem.* 279, 43847–43853. doi: 10.1074/jbc.M401598200

Günther, A., Luczak, V., Gruteser, N., Abel, T., and Baumann, A. (2019). HCN4 knockdown in dorsal hippocampus promotes anxiety-like behavior in mice. *Genes. Brain. Behav.* 18, e12550. doi: 10.1111/gbb.12550

Hablitz, J. J., and Yang, J. (2010). Abnormal pyramidal cell morphology and HCN channel expression in cortical dysplasia. *Epilepsia* 51(Suppl. 3), 52–55. doi: 10.1111/j.1528-1167.2010.02610.x

Hammelmann, V., Stieglitz, M. S., Hülle, H., Le Meur, K., Kass, J., Brümmer, M., et al. (2019). Abolishing cAMP sensitivity in HCN2 pacemaker channels induces generalized seizures. *JCI insight* 4, e126418. doi: 10.1172/jci.insight.126418

Han, W., Bao, W., Wang, Z., and Nattel, S. (2002). Comparison of ion-channel subunit expression in canine cardiac Purkinje fibers and ventricular muscle. *Circ. Res.* 91, 790–797. doi: 10.1161/01.RES.0000039534.18114.D9

Han, Y., Lyman, K. A., Foote, K. M., and Chetkovich, D. M. (2020). The structure and function of TRIP8b, an auxiliary subunit of hyperpolarization-activated cyclic-nucleotide gated channels. *Channels.* 14, 110–122. doi: 10.1080/19336950.2020.1740501

Herrmann, S., Stieber, J., and Ludwig, A. (2007). Pathophysiology of HCN channels. *Pflugers Arch.* 454, 517–522. doi: 10.1007/s00424-007-0224-4

Heuermann, R. J., Jaramillo, T. C., Ying, S.-W., Suter, B. A., Lyman, K. A., Han, Y., et al. (2016). Reduction of thalamic and cortical Ih by deletion of TRIP8b produces a mouse model of human absence epilepsy. *Neurobiol. Dis.* 85, 81–92. doi: 10.1016/j.nbd.2015.10.005

Ho, A., Morishita, W., Hammer, R. E., Malenka, R. C., and Sudhof, T. C. (2003). A role for Mints in transmitter release: mint 1 knockout mice exhibit impaired GABAergic synaptic transmission. *Proc. Natl. Acad. Sci. U. S. A.* 100, 1409–1414. doi: 10.1073/pnas.252774899

Honsa, P., Pivonkova, H., Harantova, L., Butenko, O., Kriska, J., Dzamba, D., et al. (2014). Increased expression of hyperpolarization-activated cyclic nucleotide-gated (HCN) channels in reactive astrocytes following ischemia. *Glia* 62, 2004–2021. doi: 10.1002/glia.22721

Huang, J., Huang, A., Zhang, Q., Lin, Y.-C., and Yu, H.-G. (2008). Novel mechanism for suppression of hyperpolarization-activated cyclic nucleotide-gated pacemaker channels by receptor-like tyrosine phosphatase-alpha. *J. Biol. Chem.* 283, 29912–29919. doi: 10.1074/jbc.M804205200

Huang, Z., Lujan, R., Kadurin, I., Uebele, V. N., Renger, J. J., Dolphin, A. C., et al. (2011). Presynaptic HCN1 channels regulate Cav3.2 activity and neurotransmission at select cortical synapses. *Nat. Neurosci.* 14, 478–486. doi: 10.1038/nn.2757

Huang, Z., Lujan, R., Martinez-Hernandez, J., Lewis, A. S., Chetkovich, D. M., and Shah, M. M. (2012). TRIP8b-independent trafficking and plasticity of adult cortical presynaptic HCN1 channels. *J. Neurosci.* 32, 14835–14848. doi: 10.1523/JNEUROSCI.1544-12.2012

Huang, Z., Walker, M. C., and Shah, M. M. (2009). Loss of dendritic HCN1 subunits enhances cortical excitability and epileptogenesis. *J. Neurosci.* 29, 10979–10988. doi: 10.1523/JNEUROSCI.1531-09.2009

Hughes, D. I., Boyle, K. A., Kinnon, C. M., Bilsland, C., Quayle, J. A., Callister, R. J., et al. (2013). HCN4 subunit expression in fast-spiking interneurons of the rat spinal cord and hippocampus. *Neuroscience* 237, 7–18. doi: 10.1016/j.neuroscience.2013.01.028

Hung, A., Forster, I. C., Mckenzie, C. E., Berecki, G., Petrou, S., Kathirvel, A., et al. (2021). Biophysical analysis of an HCN1 epilepsy variant suggests a critical role for S5 helix Met-305 in voltage sensor to pore domain coupling. *Prog. Biophys. Mol. Biol.* 166, 156–172. doi: 10.1016/j.pbiomolbio.2021.07.005

Iacone, Y., Morais, T. P., David, F., Delicata, F., Sandle, J., Raffai, T., et al. (2021). Systemic administration of ivabradine, a hyperpolarization-activated cyclic nucleotide-gated channel inhibitor, blocks spontaneous absence seizures. *Epilepsia* 62, 1729–1743. doi: 10.1111/epi.16926

Iida, J., Ishizaki, H., Okamoto-Tanaka, M., Kawata, A., Sumita, K., Ohgake, S., et al. (2007). Synaptic scaffolding molecule alpha is a scaffold to mediate N-methyl-D-aspartate receptor-dependent RhoA activation in dendrites. *Mol. Cell. Biol.* 27, 4388–4405. doi: 10.1128/MCB.01901-06

Işler, C., Tanriverdi, T., Kavak, E., Sanus, G. Z., Ulu, M. O., Erkanli, G., et al. (2008). Prenatal expressions of hyperpolarization-activated cyclic-nucleotide-gated channel (HCN) genes in dysplastic hippocampi in rats. *Turk. Neurosurg.* 18, 327–335.

Jung, S., Bullis, J. B., Lau, I. H., Jones, T. D., Warner, L. N., and Poolos, N. P. (2010). Downregulation of dendritic HCN channel gating in epilepsy is mediated by altered phosphorylation signaling. *J. Neurosci.* 30, 6678–6688. doi: 10.1523/JNEUROSCI.1290-10.2010

Jung, S., Jones, T. D., Lugo, J. N. J., Sheerin, A. H., Miller, J. W., D'Ambrosio, R., et al. (2007). Progressive dendritic HCN channelopathy during epileptogenesis in the rat pilocarpine model of epilepsy. *J. Neurosci.* 27, 13012–13021. doi: 10.1523/JNEUROSCI.3605-07.2007

Jung, S., Warner, L. N., Pitsch, J., Becker, A. J., and Poolos, N. P. (2011). Rapid loss of dendritic HCN channel expression in hippocampal pyramidal neurons following status epilepticus. *J. Neurosci.* 31, 14291–14295. doi: 10.1523/JNEUROSCI.1148-11.2011

Kanyshkova, T., Meuth, P., Bista, P., Liu, Z., Ehling, P., Caputi, L., et al. (2012). Differential regulation of HCN channel isoform expression in thalamic neurons of epileptic and non-epileptic rat strains. *Neurobiol. Dis.* 45, 450–461. doi: 10.1016/j.nbd.2011.08.032

Kanyshkova, T., Pawlowski, M., Meuth, P., Dubé, C., Bender, R. A., Brewster, A. L., et al. (2009). Postnatal expression pattern of HCN channel isoforms in thalamic neurons: relationship to maturation of thalamocortical oscillations. *J. Neurosci.* 29, 8847–8857. doi: 10.1523/JNEUROSCI.0689-09.2009

Kase, D., and Imoto, K. (2012). The role of HCN channels on membrane excitability in the nervous system. *J. Signal Transduct.* 2012, 619747. doi: 10.1155/2012/619747

Kase, D., Inoue, T., and Imoto, K. (2012). Roles of the subthalamic nucleus and subthalamic HCN channels in absence seizures. *J. Neurophysiol.* 107, 393–406. doi: 10.1152/jn.00937.2010

Kenney-Jung, D. L., Vezzani, A., Kahoud, R. J., LaFrance-Corey, R. G., Ho, M.-L., Muskardin, T. W., et al. (2016). Febrile infection-related epilepsy syndrome treated with anakinra. *Ann. Neurol.* 80, 939–945. doi: 10.1002/ana.24806

Kessi, M., Chen, B., Peng, J., Tang, Y., Olatoutou, E., He, F., et al. (2020a). Intellectual disability and potassium channelopathies: a systematic review. *Front. Genet.* 11, 614. doi: 10.3389/fgene.2020.00614

Kessi, M., Chen, B., Peng, J., Yan, F., Yang, L., and Yin, F. (2021). Calcium channelopathies and intellectual disability: a systematic review. *Orphanet J. Rare Dis.* 16, 219. doi: 10.1186/s13023-021-01850-0

Kessi, M., Liu, F., Zhan, Y., Tang, Y., Wu, L., Yang, L., et al. (2020b). Efficacy of different treatment modalities for acute and chronic phases of the febrile infection-related epilepsy syndrome: a systematic review. *Seizure* 79, 61–68. doi: 10.1016/j.seizure.2020.04.015

Kharouf, Q., Phillips, A. M., Bleakley, L. E., Morrisroe, E., Oyrer, J., Jia, L., et al. (2020a). The hyperpolarization-activated cyclic nucleotide-gated 4 channel as a potential anti-seizure drug target. *Br. J. Pharmacol.* 177, 3712–3729. doi: 10.1111/bph.15088

Kharouf, Q., Pinares-Garcia, P., Romanelli, M. N., and Reid, C. A. (2020b). Testing broad-spectrum and isoform-preferring HCN channel blockers for anticonvulsant properties in mice. *Epilepsy Res.* 168, 106484. doi: 10.1016/j.eplepsyres.2020.106484

Kimura, K., Kitano, J., Nakajima, Y., and Nakanishi, S. (2004). Hyperpolarization-activated, cyclic nucleotide-gated HCN2 cation channel forms a protein assembly with multiple neuronal scaffold proteins in distinct modes of protein-protein interaction. *Genes Cells* 9, 631–640. doi: 10.1111/j.1356-9597.2004.00752.x

Kitano, J., Kimura, K., Yamazaki, Y., Soda, T., Shigemoto, R., Nakajima, Y., et al. (2002). Tamalin, a PDZ domain-containing protein, links a protein complex formation of group 1 metabotropic glutamate receptors and the guanine nucleotide exchange factor cytohesins. *J. Neurosci.* 22, 1280–1289. doi: 10.1523/JNEUROSCI.22-04-01280.2002

Knoll, A. T., Halladay, L. R., Holmes, A. J., and Levitt, P. (2016). Quantitative trait loci and a novel genetic candidate for fear learning. *J. Neurosci.* 36, 6258–6268. doi: 10.1523/JNEUROSCI.0177-16.2016

Koh, S., Dupuis, N., and Auvin, S. (2020). Ketogenic diet and Neuroinflammation. *Epilepsy Res.* 167, 106454. doi: 10.1016/j.eplepsyres.2020.106454

Kopp-Scheinpflug, C., Pigott, B. M., and Forsythe, I. D. (2015). Nitric oxide selectively suppresses IH currents mediated by HCN1-containing channels. *J. Physiol.* 593, 1685–1700. doi: 10.1113/jphysiol.2014.282194

Koruth, J. S., Lala, A., Pinney, S., Reddy, V. Y., and Dukkipati, S. R. (2017). The clinical use of ivabradine. *J. Am. Coll. Cardiol.* 70, 1777–1784. doi: 10.1016/j.jacc.2017.08.038

Kuisle, M., Wanaverbecq, N., Brewster, A. L., Frère, S. G. A., Pinault, D., Baram, T. Z., et al. (2006). Functional stabilization of weakened thalamic pacemaker channel regulation in rat absence epilepsy. *J. Physiol.* 575, 83–100. doi: 10.1113/jphysiol.2006.110486

Lai, Y.-C., Muscal, E., Wells, E., Shukla, N., Eschbach, K., Hyeong Lee, K., et al. (2020). Anakinra usage in febrile infection related epilepsy syndrome: an international cohort. *Ann. Clin. Transl. Neurol.* 7, 2467–2474. doi: 10.1002/acn3.51229

Lee, C.-H., Park, J. H., and Won, M.-H. (2019). Protein expression changes of HCN1 and HCN2 in hippocampal subregions of gerbils during the normal aging process. *Iran. J. Basic Med. Sci.* 22, 1308–1313.

Lee, Y. T., Vasilyev, D. V., Shan, Q. J., Dunlop, J., Mayer, S., and Bowlby, M. R. (2008). Novel pharmacological activity of loperamide and CP-339,818 on human HCN channels characterized with an automated electrophysiology assay. *Eur. J. Pharmacol.* 581, 97–104. doi: 10.1016/j.ejphar.2007.11.058

Lehnhoff, J., Strauss, U., Wierschke, S., Grosser, S., Pollali, E., Schneider, U. C., et al. (2019). The anticonvulsant lamotrigine enhances I(h) in layer 2/3 neocortical pyramidal neurons of patients with pharmacoresistant epilepsy. *Neuropharmacology* 144, 58–69. doi: 10.1016/j.neuropharm.2018.10.004

L'Erario, M., Roperto, R. M., and Rosati, A. (2021). Sevoflurane as bridge therapy for plasma-exchange and anakinra in febrile infection-related epilepsy syndrome. *Epilepsia Open*. 6, 788–792. doi: 10.1002/epi4.12545

Lewis, A. S., Estep, C. M., and Chetkovich, D. M. (2010). The fast and slow ups and downs of HCN channel regulation. *Channels.* 4, 215–231. doi: 10.4161/chan.4.3.11630

Lewis, A. S., Schwartz, E., Chan, C. S., Noam, Y., Shin, M., Wadman, W. J., et al. (2009). Alternatively spliced isoforms of TRIP8b differentially control h channel trafficking and function. *J. Neurosci.* 29, 6250–6265. doi: 10.1523/JNEUROSCI.0856-09.2009

Li, B., Chen, F., Ye, J., Chen, X., Yan, J., Li, Y., et al. (2010). The modulation of orexin A on HCN currents of pyramidal neurons in mouse prelimbic cortex. *Cereb. Cortex* 20, 1756–1767. doi: 10.1093/cercor/bhp241

Li, M., Maljevic, S., Phillips, A. M., Petrovski, S., Hildebrand, M. S., Burgess, R., et al. (2018). Gain-of-function HCN2 variants in genetic epilepsy. *Hum. Mutat.* 39, 202–209. doi: 10.1002/humu.23357

Lin, W., Qin, J., Ni, G., Li, Y., Xie, H., Yu, J., et al. (2020). Downregulation of hyperpolarization-activated cyclic nucleotide-gated channels (HCN) in the hippocampus of patients with medial temporal lobe epilepsy and hippocampal sclerosis (MTLE-HS). *Hippocampus* 30, 1112–1126. doi: 10.1002/hipo.23219

Liu, Q., Long, Z., Dong, X., Zhang, T., Zhao, J., Sun, B., et al. (2017). Cyclophosphamide-induced HCN1 channel upregulation in interstitial Cajal-like cells leads to bladder hyperactivity in mice. *Exp. Mol. Med.* 49, e319. doi: 10.1038/emm.2017.31

Ludwig, A., Budde, T., Stieber, J., Moosmang, S., Wahl, C., Holthoff, K., et al. (2003). Absence epilepsy and sinus dysrhythmia in mice lacking the pacemaker channel HCN2. *EMBO J.* 22, 216–224. doi: 10.1093/emboj/cdg032

Luján, R., Albasanz, J. L., Shigemoto, R., and Juiz, J. M. (2005). Preferential localization of the hyperpolarization-activated cyclic nucleotide-gated cation channel subunit HCN1 in basket cell terminals of the rat cerebellum. *Eur. J. Neurosci.* 21, 2073–2082. doi: 10.1111/j.1460-9568.2005.04043.x

Lussier, Y., Fürst, O., Fortea, E., Leclerc, M., Priolo, D., Moeller, L., et al. (2019). Disease-linked mutations alter the stoichiometries of HCN-KCNE2 complexes. *Sci. Rep.* 9, 9113. doi: 10.1038/s41598-019-45592-3

Luszczki, J. J., Prystupa, A., Andres-Mach, M., Marzeda, E., and Florek-Łuszczki, M. (2013). Ivabradine (a hyperpolarization activated cyclic nucleotide-gated channel blocker) elevates the threshold for maximal electroshock-induced tonic seizures in mice. *Pharmacol. Rep.* 65, 1407–1414. doi: 10.1016/S1734-1140(13)71500-7

Mader, F., Müller, S., Krause, L., Springer, A., Kernig, K., Protzel, C., et al. (2018). Hyperpolarization-activated cyclic nucleotide-gated non-selective (HCN) ion channels regulate human and murine urinary bladder contractility. *Front. Physiol.* 9, 753. doi: 10.3389/fphys.2018.00753

Mahoney, C. E., Cogswell, A., Koralnik, I. J., and Scammell, T. E. (2019). The neurobiological basis of narcolepsy. *Nat. Rev. Neurosci.* 20, 83–93. doi: 10.1038/s41583-018-0097-x

Marcelin, B., Chauvière, L., Becker, A., Migliore, M., Esclapez, M., and Bernard, C. (2009). h channel-dependent deficit of theta oscillation resonance and phase shift in temporal lobe epilepsy. *Neurobiol. Dis.* 33, 436–447. doi: 10.1016/j.nbd.2008.11.019

Marini, C., Porro, A., Rastetter, A., Dalle, C., Rivolta, I., Bauer, D., et al. (2018). HCN1 mutation spectrum: from neonatal epileptic encephalopathy to benign generalized epilepsy and beyond. *Brain* 141, 3160–3178. doi: 10.1093/brain/awy263

Matt, L., Michalakis, S., Hofmann, F., Hammelmann, V., Ludwig, A., Biel, M., et al. (2011). HCN2 channels in local inhibitory interneurons constrain LTP in the hippocampal direct perforant path. *Cell. Mol. Life Sci.* 68, 125–137. doi: 10.1007/s00018-010-0446-z

Mignot, E., Zeitzer, J., Pizza, F., and Plazzi, G. (2021). Sleep problems in narcolepsy and the role of hypocretin/orexin deficiency. *Front. Neurol. Neurosci.* 45, 103–116. doi: 10.1159/000514959

Mistrík, P., Mader, R., Michalakis, S., Weidinger, M., Pfeifer, A., and Biel, M. (2005). The murine HCN3 gene encodes a hyperpolarization-activated cation channel with slow kinetics and unique response to cyclic nucleotides. *J. Biol. Chem.* 280, 27056–27061. doi: 10.1074/jbc.M502696200

Miyake, T., Shirakawa, H., Nakagawa, T., and Kaneko, S. (2015). Activation of mitochondrial transient receptor potential vanilloid 1 channel contributes to microglial migration. *Glia* 63, 1870–1882. doi: 10.1002/glia.22854

Moher, D., Liberati, A., Tetzlaff, J., and Altman, D. G. (2009). Preferred reporting items for systematic reviews and meta-analyses: the PRISMA statement. *PLoS Med.* 6, e1000097. doi: 10.1371/journal.pmed.1000097

Monteggia, L. M., Eisch, A. J., Tang, M. D., Kaczmarek, L. K., and Nestler, E. J. (2000). Cloning and localization of the hyperpolarization-activated cyclic nucleotide-gated channel family in rat brain. *Brain Res. Mol. Brain Res.* 81, 129–139. doi: 10.1016/S0169-328X(00)00155-8

Much, B., Wahl-Schott, C., Zong, X., Schneider, A., Baumann, L., Moosmang, S., et al. (2003). Role of subunit heteromerization and N-linked glycosylation in the formation of functional hyperpolarization-activated cyclic nucleotide-gated channels. *J. Biol. Chem.* 278, 43781–43786. doi: 10.1074/jbc.M306958200

Munsch, T., and Pape, H. C. (1999). Upregulation of the hyperpolarization-activated cation current in rat thalamic relay neurones by acetazolamide. *J. Physiol.* 519, 505–514. doi: 10.1111/j.1469-7793.1999.0505m.x

Nakagawa, T., Yasaka, T., Nakashima, N., Takeya, M., Oshita, K., Tsuda, M., et al. (2020). Expression of the pacemaker channel HCN4 in excitatory interneurons in the dorsal horn of the murine spinal cord. *Mol. Brain* 13, 127. doi: 10.1186/s13041-020-00666-6

Nakamura, Y., Shi, X., Numata, T., Mori, Y., Inoue, R., Lossin, C., et al. (2013). Novel HCN2 mutation contributes to febrile seizures by shifting the channel's kinetics in a temperature-dependent manner. *PLoS ONE* 8, e80376. doi: 10.1371/journal.pone.0080376

Nava, C., Dalle, C., Rastetter, A., Striano, P., de Kovel, C. G. F., Nabbout, R., et al. (2014). *De novo* mutations in HCN1 cause early infantile epileptic encephalopathy. *Nat. Genet.* 46, 640–645. doi: 10.1038/ng.2952

Nepovimova, E., Janockova, J., Misik, J., Kubik, S., Stuchlik, A., Vales, K., et al. (2019). Orexin supplementation in narcolepsy treatment: a review. *Med. Res. Rev.* 39, 961–975. doi: 10.1002/med.21550

Nishitani, A., Kunisawa, N., Sugimura, T., Sato, K., Yoshida, Y., Suzuki, T., et al. (2019). Loss of HCN1 subunits causes absence epilepsy in rats. *Brain Res.* 1706, 209–217. doi: 10.1016/j.brainres.2018.11.004

Nishitani, A., Yoshihara, T., Tanaka, M., Kuwamura, M., Asano, M., Tsubota, Y., et al. (2020). Muscle weakness and impaired motor coordination in hyperpolarization-activated cyclic nucleotide-gated potassium channel 1-deficient rats. *Exp. Anim.* 69, 11–17. doi: 10.1538/expanim.19-0067

Noam, Y., Bernard, C., and Baram, T. Z. (2011). Towards an integrated view of HCN channel role in epilepsy. *Curr. Opin. Neurobiol.* 21, 873–879. doi: 10.1016/j.conb.2011.06.013

Noam, Y., Ehrengruber, M. U., Koh, A., Feyen, P., Manders, E. M. M., Abbott, G. W., et al. (2014). Filamin A promotes dynamin-dependent internalization of hyperpolarization-activated cyclic nucleotide-gated type 1 (HCN1) channels and restricts Ih in hippocampal neurons. *J. Biol. Chem.* 289, 5889–5903. doi: 10.1074/jbc.M113.522060

Noebels, J. L. (2012). "The voltage-gated calcium channel and absence epilepsy," in *Jasper's Basic Mechanisms of the Epilepsies, 4th Edn, eds* J. L. Noebels, M. Avoli, M. A. Rogawski, R. W. Olsen, and A. V. Delgado-Escueta (Bethesda, MD: National Center for Biotechnology Information).

Nolan, M. F., Dudman, J. T., Dodson, P. D., and Santoro, B. (2007). HCN1 channels control resting and active integrative properties of stellate cells from layer II of the entorhinal cortex. *J. Neurosci.* 27, 12440–12451. doi: 10.1523/JNEUROSCI.2358-07.2007

Notomi, T., and Shigemoto, R. (2004). Immunohistochemical localization of Ih channel subunits, HCN1-4, in the rat brain. *J. Comp. Neurol.* 471, 241–276. doi: 10.1002/cne.11039

Oyrer, J., Bleakley, L. E., Richards, K. L., Maljevic, S., Phillips, A. M., Petrou, S., et al. (2019). Using a multiplex nucleic acid *in situ* hybridization technique to determine HCN4 mRNA expression in the adult rodent brain. *Front. Mol. Neurosci.* 12, 211. doi: 10.3389/fnmol.2019.00211

Parker, A. R., Forster, L. A., and Baro, D. J. (2019). Modulator-gated, SUMOylation-mediated, activity-dependent regulation of ionic current densities contributes to short-term activity homeostasis. *J. Neurosci.* 39, 596–611. doi: 10.1523/JNEUROSCI.1379-18.2018

Parker, A. R., Welch, M. A., Forster, L. A., Tasneem, S. M., Dubhashi, J. A., and Baro, D. J. (2016). SUMOylation of the hyperpolarization-activated cyclic nucleotide-gated channel 2 increases surface expression and the maximal conductance of the hyperpolarization-activated current. *Front. Mol. Neurosci.* 9, 168. doi: 10.3389/fnmol.2016.00168

Paz, J. T., Davidson, T. J., Frechette, E. S., Delord, B., Parada, I., Peng, K., et al. (2013). Closed-loop optogenetic control of thalamus as a tool for interrupting seizures after cortical injury. *Nat. Neurosci.* 16, 64–70. doi: 10.1038/nn.3269

Phillips, A. M., Kim, T., Vargas, E., Petrou, S., and Reid, C. A. (2014). Spike-and-wave discharge mediated reduction in hippocampal HCN1 channel function associates with learning deficits in a genetic mouse model of epilepsy. *Neurobiol. Dis.* 64, 30–35. doi: 10.1016/j.nbd.2013.12.007

Pian, P., Bucchi, A., Decostanzo, A., Robinson, R. B., and Siegelbaum, S. A. (2007). Modulation of cyclic nucleotide-regulated HCN channels by PIP(2) and receptors coupled to phospholipase C. *Pflugers Arch.* 455, 125–145. doi: 10.1007/s00424-007-0295-2

Pian, P., Bucchi, A., Robinson, R. B., and Siegelbaum, S. A. (2006). Regulation of gating and rundown of HCN hyperpolarization-activated channels by exogenous and endogenous PIP2. *J. Gen. Physiol.* 128, 593–604. doi: 10.1085/jgp.200609648

Poolos, N. P., Bullis, J. B., and Roth, M. K. (2006). Modulation of h-channels in hippocampal pyramidal neurons by p38 mitogen-activated protein kinase. *J. Neurosci.* 26, 7995–8003. doi: 10.1523/JNEUROSCI.2069-06.2006

Poolos, N. P., Migliore, M., and Johnston, D. (2002). Pharmacological upregulation of h-channels reduces the excitability of pyramidal neuron dendrites. *Nat. Neurosci.* 5, 767–774. doi: 10.1038/nn891

Powell, K. L., Jones, N. C., Kennard, J. T., Ng, C., Urmaliya, V., Lau, S., et al. (2014). HCN channelopathy and cardiac electrophysiologic dysfunction in genetic and acquired rat epilepsy models. *Epilepsia* 55, 609–620. doi: 10.1111/epi.12563

Powell, K. L., Ng, C., O'Brien, T. J., Xu, S. H., Williams, D. A., Foote, S. J., et al. (2008). Decreases in HCN mRNA expression in the hippocampus after kindling and status epilepticus in adult rats. *Epilepsia* 49, 1686–1695. doi: 10.1111/j.1528-1167.2008.01593.x

Putrenko, I., Yip, R., Schwarz, S. K. W., and Accili, E. A. (2017). Cation and voltage dependence of lidocaine inhibition of the hyperpolarization-activated cyclic nucleotide-gated HCN1 channel. *Sci. Rep.* 7, 1281. doi: 10.1038/s41598-017-01253-x

Qu, J., Kryukova, Y., Potapova, I. A., Doronin, S. V., Larsen, M., Krishnamurthy, G., et al. (2004). MiRP1 modulates HCN2 channel expression and gating in cardiac myocytes. *J. Biol. Chem.* 279, 43497–43502. doi: 10.1074/jbc.M405018200

Qu, L., Liu, X., Wu, C., and Leung, L. S. (2007). Hyperthermia decreases GABAergic synaptic transmission in hippocampal neurons of immature rats. *Neurobiol. Dis.* 27, 320–327. doi: 10.1016/j.nbd.2007.06.003

Ramakrishnan, N. A., Drescher, M. J., Khan, K. M., Hatfield, J. S., and Drescher, D. G. (2012). HCN1 and HCN2 proteins are expressed in cochlear hair cells: HCN1 can form a ternary complex with protocadherin 15 CD3 and F-actin-binding filamin A or can interact with HCN2. *J. Biol. Chem.* 287, 37628–37646. doi: 10.1074/jbc.M112.375832

Ramentol, R., Perez, M. E., and Larsson, H. P. (2020). Gating mechanism of hyperpolarization-activated HCN pacemaker channels. *Nat. Commun.* 11, 1419. doi: 10.1038/s41467-020-15233-9

Resta, F., Micheli, L., Laurino, A., Spinelli, V., Mello, T., Sartiani, L., et al. (2018). Selective HCN1 block as a strategy to control oxaliplatin-induced neuropathy. *Neuropharmacology* 131, 403–413. doi: 10.1016/j.neuropharm.2018.01.014

Richichi, C., Brewster, A. L., Bender, R. A., Simeone, T. A., Zha, Q., Yin, H. Z., et al. (2008). Mechanisms of seizure-induced "transcriptional channelopathy" of hyperpolarization-activated cyclic nucleotide gated (HCN) channels. *Neurobiol. Dis.* 29, 297–305. doi: 10.1016/j.nbd.2007.09.003

Rivolta, I., Binda, A., Masi, A., and DiFrancesco, J. C. (2020). Cardiac and neuronal HCN channelopathies. *Pflugers Arch.* 472, 931–951. doi: 10.1007/s00424-020-02384-3

Robinson, R. B., and Siegelbaum, S. A. (2003). Hyperpolarization-activated cation currents: from molecules to physiological function. *Annu. Rev. Physiol.* 65, 453–480. doi: 10.1146/annurev.physiol.65.092101.142734

Romoli, M., Sen, A., Parnetti, L., Calabresi, P., and Costa, C. (2021). Amyloid-β: a potential link between epilepsy and cognitive decline. *Nat. Rev. Neurol.* 17, 469–485. doi: 10.1038/s41582-021-00505-9

Roth, F. C., and Hu, H. (2020). An axon-specific expression of HCN channels catalyzes fast action potential signaling in GABAergic interneurons. *Nat. Commun.* 11, 2248. doi: 10.1038/s41467-020-15791-y

Saito, Y., Inoue, T., Zhu, G., Kimura, N., Okada, M., Nishimura, M., et al. (2012). Hyperpolarization-activated cyclic nucleotide gated channels: a potential molecular link between epileptic seizures and Aβ generation in Alzheimer's disease. *Mol. Neurodegener.* 7, 50. doi: 10.1186/1750-1326-7-50

Santoro, B., Chen, S., Luthi, A., Pavlidis, P., Shumyatsky, G. P., Tibbs, G. R., et al. (2000). Molecular and functional heterogeneity of hyperpolarization-activated pacemaker channels in the mouse CNS. *J. Neurosci.* 20, 5264–5275. doi: 10.1523/JNEUROSCI.20-14-05264.2000

Santoro, B., Piskorowski, R. A., Pian, P., Hu, L., Liu, H., and Siegelbaum, S. A. (2009). TRIP8b splice variants form a family of auxiliary subunits that regulate gating and trafficking of HCN channels in the brain. *Neuron* 62, 802–813. doi: 10.1016/j.neuron.2009.05.009

Santoro, B., and Shah, M. M. (2020). Hyperpolarization-activated cyclic nucleotide-gated channels as drug targets for neurological disorders. *Annu. Rev. Pharmacol. Toxicol.* 60, 109–131. doi: 10.1146/annurev-pharmtox-010919-023356

Sartiani, L., Mannaioni, G., Masi, A., Novella Romanelli, M., and Cerbai, E. (2017). The hyperpolarization-activated cyclic nucleotide-gated channels: from biophysics to pharmacology of a unique family of ion channels. *Pharmacol. Rev.* 69, 354–395. doi: 10.1124/pr.117.014035

Sawicka, K. M., Załuska, K., Wawryniuk, A., Załuska-Patel, K., Szczyrek, M., Drop, B., et al. (2017). Ivabradine attenuates the anticonvulsant potency of lamotrigine, but not that of lacosamide, pregabalin and topiramate in the tonic-clonic seizure model in mice. *Epilepsy Res.* 133, 67–70. doi: 10.1016/j.eplepsyres.2017.04.011

Schulze, F., Müller, S., Guli, X., Schumann, L., Brehme, H., Riffert, T., et al. (2020). CK2 inhibition prior to status epilepticus persistently enhances KCa2 function in CA1 which slows down disease progression. *Front. Cell. Neurosci.* 14, 33. doi: 10.3389/fncel.2020.00033

Sen, A., Jette, N., Husain, M., and Sander, J. W. (2020). Epilepsy in older people. *Lancet.* 395, 735–748. doi: 10.1016/S0140-6736(19)33064-8

Shah, M. M. (2014). Cortical HCN channels: function, trafficking and plasticity. *J. Physiol.* 592, 2711–2719. doi: 10.1113/jphysiol.2013.270058

Shankar, R., Donner, E. J., McLean, B., Nashef, L., and Tomson, T. (2017). Sudden unexpected death in epilepsy (SUDEP): what every neurologist should know. *Epileptic Disord.* 19, 1–9. doi: 10.1684/epd.2017.0891

Shin, M., Brager, D., Jaramillo, T. C., Johnston, D., and Chetkovich, D. M. (2008). Mislocalization of h channel subunits underlies h channelopathy in temporal lobe epilepsy. *Neurobiol. Dis.* 32, 26–36. doi: 10.1016/j.nbd.2008.06.013

Simeone, T. A., Rho, J. M., and Baram, T. Z. (2005). Single channel properties of hyperpolarization-activated cation currents in acutely dissociated rat hippocampal neurones. *J. Physiol.* 568, 371–380. doi: 10.1113/jphysiol.2005.093161

Singh, G., and Sander, J. W. (2020). The global burden of epilepsy report: implications for low- and middle-income countries. *Epilepsy Behav.* 105, 106949. doi: 10.1016/j.yebeh.2020.106949

Smith, B. N., and Delisle, B. P. (2015). The long and the short of it: seizures induce cardiac remodeling and arrhythmia. *Epilepsy Curr.* 15, 90–91. doi: 10.5698/1535-7597-15.2.90

Smith, J. A., Das, A., Ray, S. K., and Banik, N. L. (2012). Role of pro-inflammatory cytokines released from microglia in neurodegenerative diseases. *Brain Res. Bull.* 87, 10–20. doi: 10.1016/j.brainresbull.2011.10.004

Speigel, I. A., and Hemmings, H. C., Jr. (2022). Relevance of cortical and hippocampal interneuron functional diversity to general anesthetic mechanisms: a narrative review. *Front. Synaptic Neurosci.* 13, 812905. doi: 10.3389/fnsyn.2021.812905

Stetefeld, H. R., Schaal, A., Scheibe, F., Nichtweiß, J., Lehmann, F., Müller, M., et al. (2021). Isoflurane in (super-) refractory status epilepticus: a multicenter evaluation. *Neurocrit. Care* 35, 631–639. doi: 10.1007/s12028-021-01250-z

Stieglitz, M. S., Fenske, S., Hammelmann, V., Becirovic, E., Schöttle, V., Delorme, J. E., et al. (2018). Disturbed processing of contextual information in HCN3 channel deficient mice. *Front. Mol. Neurosci.* 10, 436. doi: 10.3389/fnmol.2017.00436

Surges, R., Freiman, T. M., and Feuerstein, T. J. (2003). Gabapentin increases the hyperpolarization-activated cation current Ih in rat CA1 pyramidal cells. *Epilepsia* 44, 150–156. doi: 10.1046/j.1528-1157.2003.36802.x

Surges, R., Kukley, M., Brewster, A., Rüschenschmidt, C., Schramm, J., Baram, T. Z., et al. (2012). Hyperpolarization-activated cation current Ih of dentate gyrus granule cells is upregulated in human and rat temporal lobe epilepsy. *Biochem. Biophys. Res. Commun.* 420, 156–160. doi: 10.1016/j.bbrc.2012.02.133

Swire, M., Assinck, P., McNaughton, P. A., Lyons, D. A., Ffrench-Constant, C., and Livesey, M. R. (2021). Oligodendrocyte HCN2 channels regulate myelin sheath length. *J. Neurosci.* 41, 7954–7964. doi: 10.1523/JNEUROSCI.2463-20.2021

Tae, H.-S., Smith, K. M., Phillips, A. M., Boyle, K. A., Li, M., Forster, I. C., et al. (2017). Gabapentin modulates HCN4 channel voltage-dependence. *Front. Pharmacol.* 8, 554. doi: 10.3389/fphar.2017.00554

Tang, B., Sander, T., Craven, K. B., Hempelmann, A., and Escayg, A. (2008). Mutation analysis of the hyperpolarization-activated cyclic nucleotide-gated channels HCN1 and HCN2 in idiopathic generalized epilepsy. *Neurobiol. Dis.* 29, 59–70. doi: 10.1016/j.nbd.2007.08.006

Tanguay, J., Callahan, K. M., and D'Avanzo, N. (2019). Characterization of drug binding within the HCN1 channel pore. *Sci. Rep.* 9, 465. doi: 10.1038/s41598-018-37116-2

Thomas, M., Ranjith, G., Radhakrishnan, A., and Arun Anirudhan, V. (2019). Effects of HCN2 mutations on dendritic excitability and synaptic plasticity: a computational study. *Neuroscience* 423, 148–161. doi: 10.1016/j.neuroscience.2019.10.019

Tsay, D., Dudman, J. T., and Siegelbaum, S. A. (2007). HCN1 channels constrain synaptically evoked Ca2+ spikes in distal dendrites of CA1 pyramidal neurons. *Neuron* 56, 1076–1089. doi: 10.1016/j.neuron.2007.11.015

Tu, E., Waterhouse, L., Duflou, J., Bagnall, R. D., and Semsarian, C. (2011). Genetic analysis of hyperpolarization-activated cyclic nucleotide-gated cation channels in sudden unexpected death in epilepsy cases. *Brain Pathol.* 21, 692–698. doi: 10.1111/j.1750-3639.2011.00500.x

Ulens, C., and Siegelbaum, S. A. (2003). Regulation of hyperpolarization-activated HCN channels by cAMP through a gating switch in binding domain symmetry. *Neuron* 40, 959–970. doi: 10.1016/S0896-6273(03)00753-0

Urbanska, M., Kazmierska-Grebowska, P., Kowalczyk, T., Caban, B., Nader, K., Pijet, B., et al. (2019). GSK3β activity alleviates epileptogenesis and limits GluA1 phosphorylation. *EBioMedicine* 39, 377–387. doi: 10.1016/j.ebiom.2018.11.040

van Baalen, A., Häusler, M., Boor, R., Rohr, A., Sperner, J., Kurlemann, G., et al. (2010). Febrile infection-related epilepsy syndrome (FIRES): a nonencephalitic encephalopathy in childhood. *Epilepsia* 51, 1323–1328. doi: 10.1111/j.1528-1167.2010.02535.x

Vay, S. U., Flitsch, L. J., Rabenstein, M., Monière, H., Jakovcevski, I., Andjus, P., et al. (2020). The impact of hyperpolarization-activated cyclic nucleotide-gated (HCN) and voltage-gated potassium KCNQ/Kv7 channels on primary microglia function. *J. Neuroinflammation* 17, 100. doi: 10.1186/s12974-020-01779-4

Wang, J., Chen, S., Nolan, M. F., and Siegelbaum, S. A. (2002). Activity-dependent regulation of HCN pacemaker channels by cyclic AMP: signaling through dynamic allosteric coupling. *Neuron* 36, 451–461. doi: 10.1016/S0896-6273(02)00968-6

Wang, Y., Toledo-Rodriguez, M., Gupta, A., Wu, C., Silberberg, G., Luo, J., et al. (2004). Anatomical, physiological and molecular properties of Martinotti cells in the somatosensory cortex of the juvenile rat. *J. Physiol.* 561, 65–90. doi: 10.1113/jphysiol.2004.073353

Wemhöner, K., Kanyshkova, T., Silbernagel, N., Fernandez-Orth, J., Bittner, S., Kiper, A. K., et al. (2015). An N-terminal deletion variant of HCN1 in the epileptic WAG/Rij strain modulates HCN current densities. *Front. Mol. Neurosci.* 8, 63. doi: 10.3389/fnmol.2015.00063

Williams, A. D., Jung, S., and Poolos, N. P. (2015). Protein kinase C bidirectionally modulates Ih and hyperpolarization-activated cyclic nucleotide-gated (HCN) channel surface expression in hippocampal pyramidal neurons. *J. Physiol.* 593, 2779–2792. doi: 10.1113/JP270453

Xia, J., Chen, X., Song, C., Ye, J., Yu, Z., and Hu, Z. (2005). Postsynaptic excitation of prefrontal cortical pyramidal neurons by hypocretin-1/orexin A through the inhibition of potassium currents. *J. Neurosci. Res.* 82, 729–736. doi: 10.1002/jnr.20667

Yan, J., He, C., Xia, J.-X., Zhang, D., and Hu, Z.-A. (2012). Orexin-A excites pyramidal neurons in layer 2/3 of the rat prefrontal cortex. *Neurosci. Lett.* 520, 92–97. doi: 10.1016/j.neulet.2012.05.038

Yang, Y., Meng, Q., Pan, X., Xia, Z., and Chen, X. (2014). Dexmedetomidine produced analgesic effect *via* inhibition of HCN currents. *Eur. J. Pharmacol.* 740, 560–564. doi: 10.1016/j.ejphar.2014.06.031

Ye, B., Balijepalli, R. C., Foell, J. D., Kroboth, S., Ye, Q., Luo, Y.-H., et al. (2008). Caveolin-3 associates with and affects the function of hyperpolarization-activated cyclic nucleotide-gated channel 4. *Biochemistry* 47, 12312–12318. doi: 10.1021/bi8009295

Ying, S.-W., Abbas, S. Y., Harrison, N. L., and Goldstein, P. A. (2006). Propofol block of I(h) contributes to the suppression of neuronal excitability and rhythmic burst firing in thalamocortical neurons. *Eur. J. Neurosci.* 23, 465–480. doi: 10.1111/j.1460-9568.2005.04587.x

Ying, S.-W., Kanda, V. A., Hu, Z., Purtell, K., King, E. C., Abbott, G. W., et al. (2012). Targeted deletion of Kcne2 impairs HCN channel function in mouse thalamocortical circuits. *PLoS ONE* 7, e42756. doi: 10.1371/journal.pone.0042756

Yu, D., Febbo, I. G., Maroteaux, M. J., Wang, H., Song, Y., Han, X., et al. (2021). The transcription factor Shox2 shapes neuron firing properties and suppresses seizures by regulation of key ion channels in thalamocortical neurons. *Cereb. Cortex* 31, 3194–3212. doi: 10.1093/cercor/bhaa414

Yu, H., Wu, J., Potapova, I., Wymore, R. T., Holmes, B., Zuckerman, J., et al. (2001). MinK-related peptide 1: a beta subunit for the HCN ion channel subunit family enhances expression and speeds activation. *Circ. Res.* 88, E84–E87. doi: 10.1161/hh1201.093511

Zha, Q., Brewster, A. L., Richichi, C., Bender, R. A., and Baram, T. Z. (2008). Activity-dependent heteromerization of the hyperpolarization-activated, cyclic-nucleotide gated (HCN) channels: role of N-linked glycosylation. *J. Neurochem.* 105, 68–77. doi: 10.1111/j.1471-4159.2007.05110.x

Zhao, Z., Zhang, K., Liu, X., Yan, H., Ma, X., Zhang, S., et al. (2016). Involvement of HCN channel in muscarinic inhibitory action on tonic firing of dorsolateral striatal cholinergic interneurons. *Front. Cell. Neurosci.* 10, 71. doi: 10.3389/fncel.2016.00071

Zhong, N., and Zucker, R. S. (2004). Roles of Ca2+, hyperpolarization and cyclic nucleotide-activated channel activation, and actin in temporal synaptic tagging. *J. Neurosci.* 24, 4205–4212. doi: 10.1523/JNEUROSCI.0111-04.2004

Zhou, C., Douglas, J. E., Kumar, N. N., Shu, S., Bayliss, D. A., and Chen, X. (2013). Forebrain HCN1 channels contribute to hypnotic actions of ketamine. *Anesthesiology* 118, 785–795. doi: 10.1097/ALN.0b013e318287b7c8

Zhou, M., Gong, X., Ru, Q., Xiong, Q., Chen, L., Si, Y., et al. (2019a). The Neuroprotective effect of L-stepholidine on methamphetamine-induced memory deficits in mice. *Neurotox. Res.* 36, 376–386. doi: 10.1007/s12640-019-00069-z

Zhou, M., Lin, K., Si, Y., Ru, Q., Chen, L., Xiao, H., et al. (2019b). Downregulation of HCN1 channels in hippocampus and prefrontal cortex in methamphetamine re-exposed mice with enhanced working memory. *Physiol. Res.* 68, 107–117. doi: 10.33549/physiolres.933873

Zobeiri, M., Chaudhary, R., Datunashvili, M., Heuermann, R. J., Lüttjohann, A., Narayanan, V., et al. (2018). Modulation of thalamocortical oscillations by TRIP8b, an auxiliary subunit for HCN channels. *Brain Struct. Funct.* 223, 1537–1564. doi: 10.1007/s00429-017-1559-z

Zúñiga, R., González, D., Valenzuela, C., Brown, N., and Zúñiga, L. (2016). Expression and cellular localization of HCN channels in rat cerebellar granule neurons. *Biochem. Biophys. Res. Commun.* 478, 1429–1435. doi: 10.1016/j.bbrc.2016.08.141

Conflict of Interest: The authors declare that the research was conducted in the absence of any commercial or financial relationships that could be construed as a potential conflict of interest.

Publisher's Note: All claims expressed in this article are solely those of the authors and do not necessarily represent those of their affiliated organizations, or those of the publisher, the editors and the reviewers. Any product that may be evaluated in this article, or claim that may be made by its manufacturer, is not guaranteed or endorsed by the publisher.

frontiers | Frontiers in Molecular Neuroscience

ORIGINAL RESEARCH
published: 19 May 2022
doi: 10.3389/fnmol.2022.826183

SCN1A-Related Epilepsy: Novel Mutations and Rare Phenotypes

Rui Ma[1,2], Yiran Duan[1,2], Liping Zhang[3], Xiaohong Qi[3], Lu Zhang[1,2], Sipei Pan[1,2], Lehong Gao[1,2†], Chaodong Wang[1*†] and Yuping Wang[1,2*†]*

[1] Department of Neurology, Xuanwu Hospital, Capital Medical University, Beijing, China, [2] Beijing Key Laboratory of Neuromodulation, Beijing, China, [3] Department of Pediatrics, Xuanwu Hospital, Capital Medical University, Beijing, China

Objectives: To expand the genotypes and phenotypes of sodium voltage-gated channel alpha subunit 1 (SCN1A)-related epilepsy.

Methods: We retrospectively collected the clinical and genetic information of 22 epilepsy patients (10 males, 12 females; mean: 9.2 ± 3.9 years; 3.9–20.3 years) carrying 22 variants of SCN1A. SCN1A mutations were identified by next-generation sequencing.

Results: Twenty-two variants were identified, among which 12 have not yet been reported. The median age at seizure onset was 6 months. Sixteen patients were diagnosed with Dravet syndrome (DS), two with genetic epilepsy with febrile seizures plus [one evolved into benign epilepsy with centrotemporal spikes (BECTS)], one with focal epilepsy, one with atypical childhood epilepsy with centrotemporal spikes (ABECTS) and two with unclassified epilepsy. Fourteen patients showed a global developmental delay/intellectual disability (GDD/ID). Slow background activities were observed in one patient and epileptiform discharges were observed in 11 patients during the interictal phase.

Significance: This study enriches the genotypes and phenotypes of SCN1A-related epilepsy. The clinical characteristics of patients with 12 previously unreported variants were described.

Keywords: epilepsy, *SCN1A* gene, novel mutation, BECTS, cohort

OPEN ACCESS

Edited by:
Weiping Liao, Second Affiliated Hospital of Guangzhou Medical University, China

Reviewed by:
Xiaorong Liu, Guangzhou Medical University, China
Edward Haig Beamer, Nottingham Trent University, United Kingdom

***Correspondence:**
Lehong Gao
gaolehong@sina.com
Chaodong Wang
cdongwang01@xwhosp.org
Yuping Wang
mdwangyp@sina.cn

[†]These authors share senior authorship

Specialty section:
This article was submitted to Brain Disease Mechanisms, a section of the journal Frontiers in Molecular Neuroscience

Received: *30 November 2021*
Accepted: *23 March 2022*
Published: *19 May 2022*

Citation:
Ma R, Duan Y, Zhang L, Qi X, Zhang L, Pan S, Gao L, Wang C and Wang Y (2022) SCN1A-Related Epilepsy: Novel Mutations and Rare Phenotypes. Front. Mol. Neurosci. 15:826183. doi: 10.3389/fnmol.2022.826183

INTRODUCTION

SCN1A is a member of the voltage-gated sodium channel (VGSC) gene family (OMIM:182389) and has been mapped to 2q24.3. *SCN1A* is the most clinically relevant gene in a wide spectrum of epilepsy phenotypes ranging from febrile seizures to Dravet syndrome (DS) (Aljaafari et al., 2017). Baulac et al. (1999) and Moulard et al. (1999) reported 2 unrelated families with generalized epilepsy with febrile seizures plus those who showed linkage to a locus on chromosome 2q21-q33. Escayg et al. (2000) identified 2 missense mutations in the *SCN1A* gene of these two families in 2000, marking *SCN1A* as a new disease gene for human inherited epilepsy. Since then, a wide variety of mutations of *SCN1A* from epilepsy patients have been identified. More than 80% of patients with DS have pathogenic variants (or mutations) in *SCN1A* (Scheffer and Nabbout, 2019). Data from a cohort of 363 Chinese DS patients in 2015 showed that 70.3% of the patients carried potentially pathogenic mutations in *SCN1A*, with a total of 223 mutations (Xu et al., 2015). As of 2015, 1727 *SCN1A* mutations had been identified in epilepsy patients. Patients with mild genotypes

have a high frequency of missense mutations, which do not result in protein truncation. For more severe phenotypes, missense mutations occur less frequently. In addition, missense mutations are found in severe phenotypes, such as DS, with a higher potential to occur in the pore region of Nav1.1 than those occurring in mild phenotypes (Meng et al., 2015). However, the genotypes and phenotypes of *SCN1A* have not been completely identified. In this study, we elaborate on the clinical manifestations of 22 mutations of *SCN1A* in 22 patients in a Chinese cohort and provide more novel genotypes and phenotypes of *SCN1A*-related epilepsy.

MATERIALS AND METHODS

Participants

Patients with epilepsy with *SCN1A* heterozygous variants were enrolled at the Neurology and Pediatric Department of Xuanwu Hospital Capital Medical University between September 2015 and November 2018. In the cohort, 367 patients with epilepsy without acquired factors were assessed by the epilepsy panel. Of these, 22 patients carried *SCN1A* variants. Clinical registrations, including name, sex, date of birth, perinatal conditions, age at the onset of seizures, clinical manifestations, family history, genetic data, video electroencephalography (EEG), magnetoencephalography (MEG), brain magnetic resonance imaging (MRI), and therapeutic regimens, were established for all patients without acquired factors. Follow-up clinical information was collected online or by telephone call.

Genetic Analysis

SCN1A mutation screening was performed using next-generation sequencing of epilepsy-associated genes or whole-exome sequencing. Variants were validated using Sanger sequencing. The *SCN1A* isoform was referenced (NM_001202435 and GRCh37/hg19). All the samples were sequenced on an Illumina Nova series platform (Illumina, San Diego, CA, United States) by Kangso (Beijing, China). We analyzed the data as follows. Synonymous changes and single nucleotide polymorphisms with a minor allele frequency greater than 5% were removed.[1] The clinical significance of the identified variants was interpreted according to the guidelines set out by the American College of Medical Genetics. The pathogenicity of the identified variants was predicted using the Mutation Taster server,[2] Polymorphism Phenotyping version 2 (Polyphen-2),[3] PROVEAN, and Sorting Intolerant From Tolerant (SIFT).[4] *SCN1A* variants identified in the patients were compared with those identified in a comparison group of approximately 150,000 individuals from the Genome Aggregation Database and *SCN1A* mutation database.[5]

[1]http://www.ncbi.nlm.nih.gov/projects/SNP

[2]http://www.mutationtaster.org/

[3]http://genetics.bwh.harvard.edu/pph2/

[4]http://sift.jcvi.org/

[5]http://scn1a.caae.org.cn/

Ethical Issues

This research was approved by the Ethics Committee of Xuanwu Hospital Capital Medical University. Written informed consent was obtained from the parents or guardians of all patients included in this study.

RESULTS

Clinical Features

The 22 patients (10 males, 12 females; mean: 9.2 ± 3.9 years; 3.9–20.3 years) were from 22 unrelated families. Demographic and clinical characteristics are summarized in **Supplementary Table 1**. The median age at seizure onset and sampling was 6 months and 9 years, respectively. The first seizure type varied among the patients with an *SCN1A* mutation: febrile seizures in sixteen patients, myoclonic seizure in one patient, simple partial seizure in one patient and secondary generalized tonic-clonic seizure (GTCS) in one patient. Status epilepticus was present in 13 patients. For seizure-precipitating factors, low-grade fever in ten patients, vaccines in two patients and hot baths in twelve patients were identified.

All 22 patients had normal perinatal period and 11 patients had a family history of febrile seizures or epilepsy. The father and brother of patient 27 shared the same *SCN1A* variant with the proband with a history of febrile seizures in childhood. The twin sister of patient 28 with DS carrying the same *SCN1A* (p.Arg1892Ter) heterozygous mutation died from a sudden unexpected death in epilepsy (SUDEP) at the age of 16. The father of patient 22 suffered febrile seizures plus and became seizure-free at 8 years of age.

No patient had a developmental delay before seizure onset. Fourteen patients showed global developmental delay/intellectual disability (GDD/ID) during the disease course. These patients showed a delay in at least two of the following domains: motor skills, speech and language, cognitive skills, and social and emotional skills (Moeschler and Shevell, 2014). Patient 5 had autistic features in addition to their intellectual disability and received special education.

Video Electroencephalography and Brain Imaging

Electroencephalography was obtained in 17 patients, and abnormalities were detected in 12 patients. Slow background activity was observed except for epileptiform discharges in one patient. All 11 patients had epileptiform discharges during the interictal phase. Generalized spike waves, polyspike-and-waves were captured in one patient. Focal or multifocal epileptic discharges were present in six patients. Both focal and generalized epileptic discharges were observed in four patients. Clinical seizures were captured in four patients. Two patients (9 and 25) exhibited focal to bilateral tonic-clonic seizures. Patient 1 experienced myoclonic seizures. Patient 7 had myoclonic seizures, eyelid myoclonic seizures and automatism seizures at different times. Typical electroencephalogram

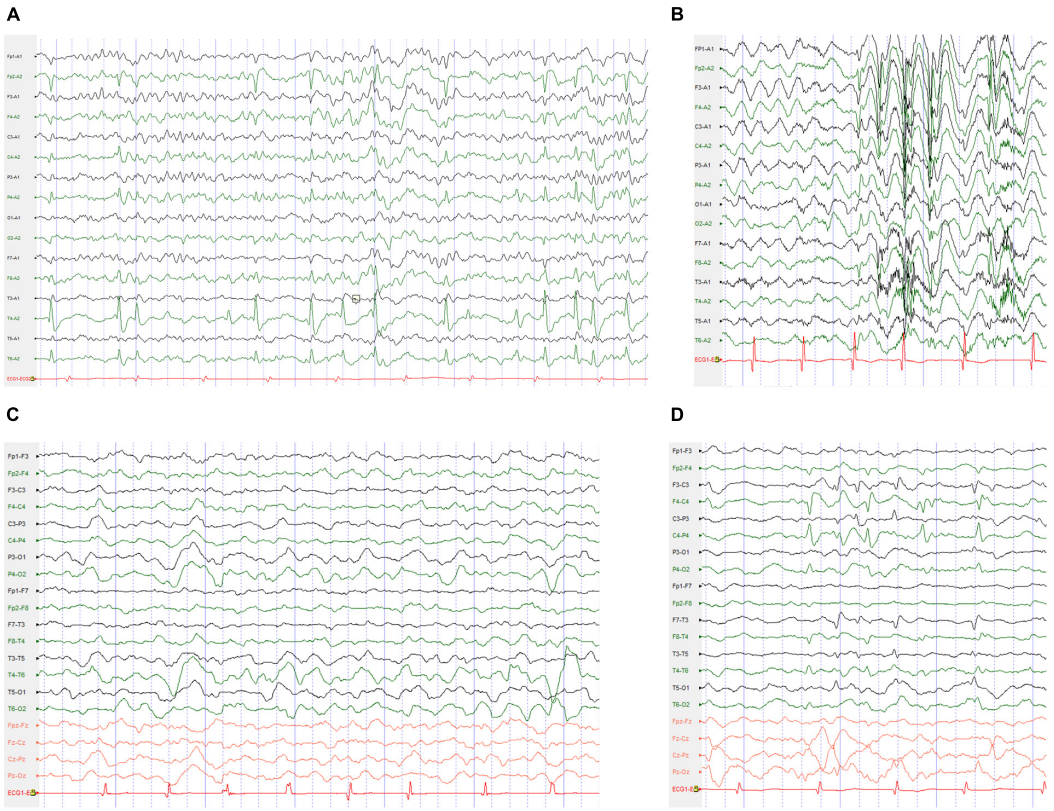

FIGURE 1 | Typical electroencephalogram (EEG) changes in the cases with *SCN1A* mutations. **(A)** The interictal EEG for the patient 29 with BECTS obtained at the age of 9 years showed right mid-temporal spikes during sleep. **(B)** Interictal EEG for the patient 7 with DS obtained at the age of 5 years showed high-voltage generalized 3–4 Hz polyspike-and-waves. **(C)** Interictal EEG for the patient 12 with DS obtained at the age of 4 years showed bilateral occipital and posterior temporal 2–3.5 Hz slow waves. **(D)** Interictal EEG for the patient 6 with ABECTS obtained at the age of 8 years showed independently bilateral central and mid-temporal spikes.

changes in four cases with *SCN1A* mutations are shown in **Figure 1**.

Among the 22 patients with brain MRI results, 17 showed a normal MRI. The MRI abnormalities included small left occipital gyrus (patient 21), left hippocampus higher signal in FLAIR (patient 18), post-operative changes of bilateral frontal and parietal lobe and corpus callosotomy (patient 8), slightly small bilateral hippocampus (patient 7) and abnormal signal in posterior horn of bilateral ventricles (patient 4).

Phenotypic Spectrum

The phenotypic spectrum of patients with *SCN1A* variants included sixteen (72.7%) with DS, two (9.1%) with genetic epilepsy with febrile seizures plus [one evolved into benign epilepsy with centrotemporal spikes (BECTS)], one (4.5%) with focal epilepsy, one (4.5%) with atypical childhood epilepsy with centrotemporal spikes (ABECTS) and two (9.1%) with unclassified epilepsy.

Genetic Analysis

All patients underwent genetic sequencing and carried *SCN1A* heterozygous mutations. Twenty-two kinds of pathogenic mutations were identified in the *SCN1A* mutations, including eleven missense, four non-sense, six frameshift and one splicing site mutation. Seventeen were confirmed to be *de novo*, four were inherited (one from his unaffected mother, three from their affected parents with febrile seizures or febrile seizures plus) (**Figure 2**) and one was unknown. The twelve novel variants (location of novel variants shown in **Figure 3**) and ten previously reported *SCN1A* variants are summarized in **Table 1** and **Supplementary Table 1**. Twenty-one identified variants were likely to cause changes in the Nav1.1 protein, eight of which were in the pore region (reentrant loop between segment 5 and segment 6, and segment 6), one in the voltage sensory (segment 4), six in the transmembrane segments, two in the linker regions of domains, three in the C-terminal domain and one in the N-terminal domain.

Variants of uncertain significance of *SCN1B* (c.566C > T, p.Thr189Met) and *SCN9A* (c.5678G > A, p.Arg1893His) were also detected in two patients (patients 4 and 16) and one patient (patient 10), respectively, all with DS.

Correlation Between Genotype and Phenotype

In our cohort, eleven patients carried *SCN1A* mutations (non-sense, frameshift and splicing mutation), which might cause more

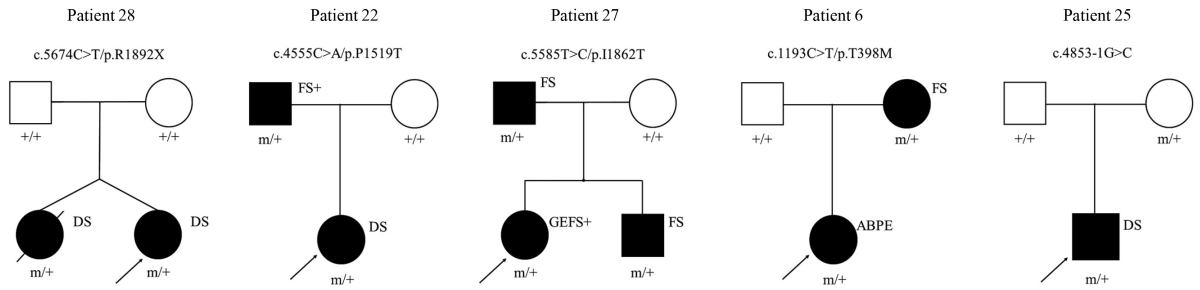

FIGURE 2 | Pedigrees of the cases with inherited *SCN1A* variants and their corresponding phenotypes. ABPE, atypical benign partial epilepsy; DS, dravet syndrome; FS, febrile seizures; FS+, febrile seizures plus; GEFS+: generalized epilepsy with febrile seizures plus. ○ represents female; □ represents male; ● and ■ represents affected individuals; arrow represents proband; m/+ represents heterozygous mutation, +/+ represents wild type.

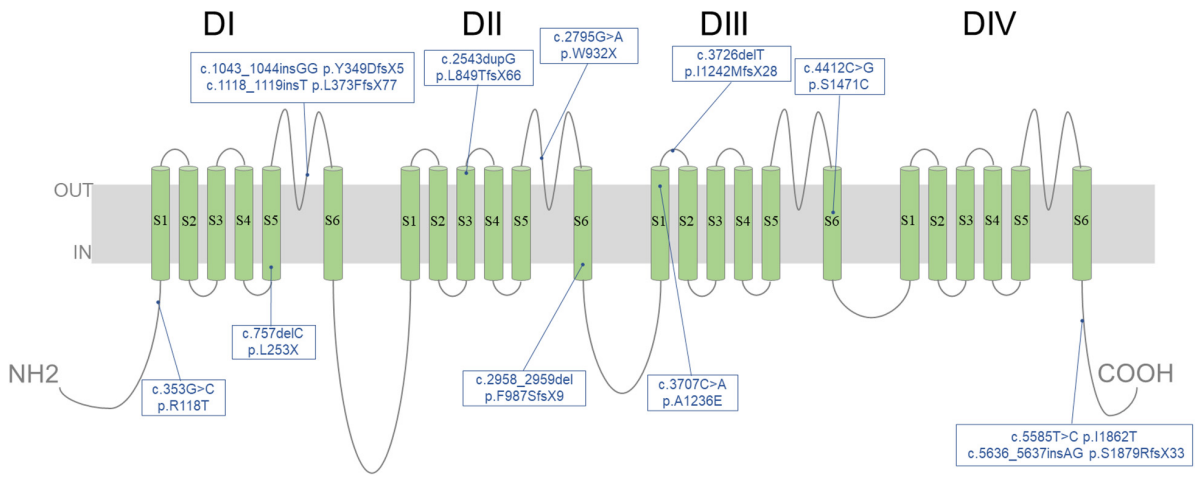

FIGURE 3 | Location of 12 novel variants identified in *SCN1A* in our cohort. Schematic diagram illustrating the transmembrane topology of a voltage-gated sodium channel and location of novel variants characterized in this study.

severe protein structural changes. Eight patients (72.7%) were diagnosed with DS, one (9.1%) with generalized epilepsy with febrile seizures plus (GEFS +) converting to BECTS and two (18.2%) with unclassified epilepsy. Three (75%) of four patients with missense mutations in the pore region of the Nav1.1 channel had DS and one (25%) had ABECTS. Five (71.4%) of seven patients with missense mutations in other regions had DS, one (14.3%) had focal epilepsy and one (14.3%) had GEFS +.

Treatment and Follow-Up

The age at which the final follow-up was taken of the 19 patients in our cohort ranged from 3 to 19 years. The mean follow-up period was 43 months. Eight patients were seizure-free for 5 months to 3 years. Patients 1 with DS had self-remission without antiepileptic medication. Seven patients were seizure-free with antiepileptic medication: two patients with DS (patients 12 and 18) and patient 29 with BECTS had valproate and levetiracetam combination therapy; patients 27 with GEFS + had levetiracetam monotherapy; two patients with DS (patients 14 and 25) were on valproate and topiramate or valproate, levetiracetam and clobazam therapy; and one patient with unclassified epilepsy accompanied by right limb dysplasia and right external auditory canal atresia (patient 13) had valproate, levetiracetam and clobazam therapy.

Eleven patients still had seizures, and their age at last follow-up ranged from 3 to 19 year 5 mo. Eight of these patients had tried at least three antiepileptic drugs. Two patients (patients 16 and 22) with DS presented increased myoclonic seizures after exposure to oxcarbazepine. Patient 8 with DS underwent epileptic lobectomy (pathological result suggested focal cortical dysplasia type I), corpus callosum resection, vagus nerve stimulation and acupuncture. She still experienced weekly GTCSs.

DISCUSSION

The spectra of phenotypes and genotypes of *SCN1A* mutations have been expanding. As Meng et al. (2015) counted in 2015, 1727 *SCN1A* mutations have been identified in epilepsy patients. In this study, 12 unreported mutations from 12 patients were identified, and the clinical features and mutations of the patients were described. BECTS and ABECTS are both parts of the spectrum of idiopathic rolandic epilepsy syndromes

TABLE 1 | Summary of 12 unreported *SCN1A* variants.

Patient number	cDNA	Protein	Type of mutation	Inheritance	ACMG-based classification	SIFT;Polyphen;Mutation taster
4	1043_1044insGG	Tyr349AspfsTer5	Frameshift	*De novo*	PAT	–; –; –
5	1118_1119insT	Leu373PhefsTer77	Frameshift	*De novo*	PAT	–; –; –
8	757delC	Leu253Ter	Non-sense	*De novo*	PAT	–; –; –
9	2543dupG	Leu849ThrfsTer66	Frameshift	*De novo*	PAT	–; –; –
11	2795G > A	Trp932Ter	Non-sense	*De novo*	PAT	–; –; –
13	2958_2959del	Phe987SerfsTer9	Frameshift	*De novo*	PAT	–; –; –
16	353G > C	Arg118Thr	Missense	*De novo*	LP	Deleterious; Probably damaging; Disease causing
18	3707C > A	Ala1236Glu	Missense	*De novo*	PAT	Damaging; Probably damaging; Disease causing
19	3726delT	Ile1242MetfsTer28	Frameshift	*De novo*	PAT	–; –; –
21	4412C > G	Ser1471Cys	Missense	*De novo*	PAT	Deleterious; Probably damaging; Disease causing
27	5585T > C	Ile1862Thr	Missense	Paternal	LP	Damaging; Probably damaging; Disease causing
29	5636_5637insAG	Ser1879ArgfsTer33	Frameshift	*De novo*	PAT	–; –; –

ACMG, American College of Medical Genetics and Genomics; LP, likely pathogenic; PAT, pathogenic.

(IRES) (Gobbi et al., 2006), which are related to several genes, such as recombinant ionotropic glutamate receptor, *N*-methyl-D-aspartate 2A (*GRIN2A*), γ-aminobutyric acid A receptor (*GABAA-R*), DEP domain-containing 5 (*DEPDC5*), and RNA binding protein fox-1 homolog 1/3 (*RBFOX1/3*) (Lal et al., 2013, 2014; Lemke et al., 2013; Reinthaler et al., 2015). One patient from a GEFS + family carried with a pathogenic heterozygous *SCN1A* (c.2624C > A) variant was diagnosed with ABECTS (Kivity et al., 2017). Patients with *SCN1A* (p.R604H, p.T1250M and p.T1174S) variants were reported to have Rolandic epilepsy (Lal et al., 2016). IRES is a rare phenotype of *SCN1A* variants compared to DS. Two patients in our cohort who presented with BECTS and ABECTS carried the *SCN1A* variants (c.5636_5637insAG, p.Ser1879ArgfsX33; c.1193C > T, p.Thr398Met), respectively, adding strong evidence that the *SCN1A* variants might be responsible for IRES.

To determine genotype-phenotype associations in *SCN1A*-related epilepsy, some investigators have attempted to make a prognosis based on *SCN1A* mutations. For instance, Cetica et al. (2017) reported that truncating mutations result in earlier onset disease and a significantly higher risk of developing DS. A study by Meng et al. (2015) indicated that missense mutations in voltage sensory and ion-pore regions are associated with the DS phenotype rather than GEFS +. The frequency of missense *SCN1A* mutations in the pore region of the Nav1.1 channel in DS patients was 54.1% (Meng et al., 2015). In our cohort, most patients with truncating mutations and missense mutations in pore regions presented with a more severe DS phenotype, which corresponded with previous reports. The mutation in patient 25 was inherited from his mother without epilepsy-related phenotype but with migraine, indicating the case of phenotypic heterogeneity of this gene mutation. A recent systematic review (Hasırcı Bayır et al., 2021) summarized six families of 33 patients with mutations in the *SCN1A* gene related to epilepsy and familial hemiplegic migraine (FHM). Recent works showed the role of hyperactivity of GABAergic interneurons in a mechanism of cortical spreading depression (CSD) initiation, which is relevant as a pathological mechanism of SCN1A mutations (Jansen et al., 2020; Chever et al., 2021). The pathogenesis of the mutations identified in our study remains to be further investigated.

The VGSC subtype Nav1.7 is encoded by *SCN9A*, which is well known to be involved in the generation, development, and maintenance of pain responses (Bang et al., 2018; Chang et al., 2018). *SCN9A* was proven to be both a cause of febrile seizure and variable epilepsy phenotypes and a partner with *SCN1A* in DS (Singh et al., 2009; Yang et al., 2018). *SCN1B* encodes the VGSCβ1 and β1B non-pore-forming subunits. Early infantile developmental and epileptic encephalopathy resulting from homozygous *SCN1B* loss-of-function variants has a more severe clinical phenotype with earlier onset than typical DS (Aeby et al., 2019). The *SCN1B* (p.Thr189Met) variant was detected in sudden unexplained nocturnal death syndrome (Liu et al., 2014) and atrial fibrillation cases (Hayashi et al., 2015). This gain-of-function variant was predicted to lower the threshold potential for cellular excitability (Hayashi et al., 2015). Three patients carried mutations in not only *SCN1A* but also *SCN1B* and *SCN9A*. Whether mutations in *SCN1B* and *SCN9A* influence

the phenotype cannot be defined unless functional studies are performed. Further investigations of these mutations should be conducted in the future as one of our future research directions.

Sudden unexpected death in epilepsy has been reported to account for approximately 2–18% of all epilepsy-related deaths (Gaitatzis and Sander, 2004) and has a higher incidence in DS (Dravet et al., 2005). SUDEP in GEFS + (Hindocha et al., 2008) and DS (Le Gal et al., 2010) patients with *SCN1A* mutations have also been reported. SUDEP was not observed in patients in our cohort but in a twin sister of patient 28 with DS carrying the same *SCN1A* heterozygous mutation at the age of 16. The specific reason for death in our patient's twin sister is unknown. The proposed mechanisms of SUDEP include (Tomson et al., 2008): effects of long-standing seizure disorder; predisposition to SUDEP, incidental or related to etiology of epilepsy; factors related to drug treatment; unknown factors that transform a seizure into a fatal event; precipitating seizure. Ultimately, apnea/hypoxia and cardiac arrhythmia with electrocerebral shutdown cause SUDEP. Patients with DS seem predisposed to SUDEP, with an imbalance of cardiac autonomic function with decreased heart rate variability and increased P wave and QT dispersion compared with other forms of epilepsy (Delogu et al., 2011; Ergul et al., 2013).

Our cohort was not large, and a significant pattern between phenotype severity and mutation location may not be concluded. Large-scale prospective studies are needed to assess the effect of treatment on development in the long term.

This study involved a cohort of 22 patients carrying *SCN1A* variants from a single center. We described the details of the clinical and genetic alterations of patients with some atypical symptoms, mainly BECTS and ABECTS. We also identified 12 novel variants of *SCN1A* in a Chinese population, extending the phenotypic and genotypic spectra. In addition, we reported the prognosis of the 19 patients with a mean follow-up period of 43 months. One case of SUDEP with variants of p.Arg1892Ter was described, reminding us that clinical methods to predict SUDEP risks need to be developed. Supervision in appropriate cases and provision of balanced information to patients and relatives are also of vital importance.

DATA AVAILABILITY STATEMENT

The datasets presented in this study can be found in online repositories. The names of the repository/repositories and accession number(s) can be found below: GenBank, OM280336–OM280357.

ETHICS STATEMENT

The studies involving human participants were reviewed and approved by the Ethics Committee of Xuanwu Hospital Capital Medical University. Written informed consent to participate in this study was provided by the participants' legal guardian/next of kin. Written informed consent was obtained from the individual(s), and minor(s)' legal guardian/next of kin, for the publication of any potentially identifiable images or data included in this article.

AUTHOR CONTRIBUTIONS

RM: writing – original draft and visualization. YD, LiZ, XQ, LuZ, and SP: resources. LG: writing – reviewing and editing and validation. CW: data curation and conceptualization. YW: supervision, project administration, and funding acquisition. All authors contributed to the article and approved the submitted version.

FUNDING

This study was supported by the National Key R&D Program (Nos. 2018YFC1314500 and 2018YFC13145040) and the Clinical Cohort Study of Epilepsy Patient (2017YFC0907702).

ACKNOWLEDGMENTS

We are grateful for the cooperation and permission to publish this information of patients and patients' family.

SUPPLEMENTARY MATERIAL

The Supplementary Material for this article can be found online at: https://www.frontiersin.org/articles/10.3389/fnmol.2022.826183/full#supplementary-material

REFERENCES

Aeby, A., Sculier, C., Bouza, A. A., Askar, B., Lederer, D., Schoonjans, A. S., et al. (2019). SCN1B-linked early infantile developmental and epileptic encephalopathy. *Ann. Clin. Transl. Neurol.* 6, 2354–2367. doi: 10.1002/acn3.50921

Aljaafari, D., Fasano, A., Nascimento, F. A., Lang, A. E., and Andrade, D. M. (2017). Adult motor phenotype differentiates dravet syndrome from lennox-gastaut syndrome and links SCN1A to early onset parkinsonian features. *Epilepsia* 58, e44–e48. doi: 10.1111/epi.13692

Bang, S., Yoo, J., Gong, X., Liu, D., Han, Q., Luo, X., et al. (2018). Differential inhibition of Nav1.7 and neuropathic Pain by hybridoma-produced and recombinant monoclonal antibodies that target nav1.7 : differential activities of nav1.7-targeting monoclonal antibodies. *Neurosci. Bull.* 34, 22–41. doi: 10.1007/s12264-018-0203-0

Baulac, S., Gourfinkel-An, I., Picard, F., Rosenberg-Bourgin, M., Prud'homme, J. F., Baulac, M., et al. (1999). A second locus for familial generalized epilepsy with febrile seizures plus maps to chromosome 2q21-q33. *Am. J. Hum. Genet.* 65, 1078–1085. doi: 10.1086/302593

Cetica, V., Chiari, S., Mei, D., Parrini, E., Grisotto, L., Marini, C., et al. (2017). Clinical and genetic factors predicting dravet syndrome in infants with SCN1A mutations. *Neurology* 88, 1037–1044. doi: 10.1212/WNL.0000000000003716

Chang, W., Berta, T., Kim, Y. H., Lee, S., Lee, S. Y., and Ji, R. R. (2018). Expression and role of voltage-gated sodium channels in human dorsal root ganglion neurons with special focus on nav1.7, species differences, and regulation by paclitaxel. *Neurosci. Bull.* 34, 4–12. doi: 10.1007/s12264-017-0132-3

Chever, O., Zerimech, S., Scalmani, P., Lemaire, L., Pizzamiglio, L., Loucif, A., et al. (2021). Initiation of migraine-related cortical spreading depolarization by hyperactivity of GABAergic neurons and NaV1.1 channels. *J. Clin. Invest* 131:e142203. doi: 10.1172/JCI142203

Delogu, A. B., Spinelli, A., Battaglia, D., Dravet, C., De Nisco, A., Saracino, A., et al. (2011). Electrical and autonomic cardiac function in patients with dravet syndrome. *Epilepsia* 52, 55–58. doi: 10.1111/j.1528-1167.2011.03003.x

Dravet, C., Bureau, M., Oguni, H., Fukuyama, Y., and Cokar, O. J. A. N. (2005). Severe myoclonic epilepsy in infancy: dravet syndrome. *Adv. Neurol.* 95, 71–102.

Ergul, Y., Ekici, B., Tatli, B., Nisli, K., and Ozmen, M. (2013). QT and P wave dispersion and heart rate variability in patients with dravet syndrome. *Acta Neurol. Belg.* 113, 161–166. doi: 10.1007/s13760-012-0140-z

Escayg, A., MacDonald, B. T., Meisler, M. H., Baulac, S., Huberfeld, G., An-Gourfinkel, I., et al. (2000). Mutations of SCN1A, encoding a neuronal sodium channel, in two families with GEFS$^+$2. *Nat. Genet.* 24, 343–345. doi: 10.1038/74159

Gaitatzis, A., and Sander, J. W. (2004). The mortality of epilepsy revisited. *Epileptic Disord.* 6, 3–13.

Gobbi, G., Boni, A., and Filippini, M. (2006). The spectrum of idiopathic Rolandic epilepsy syndromes and idiopathic occipital epilepsies: from the benign to the disabling. *Epilepsia* 47, 62–66. doi: 10.1111/j.1528-1167.2006.00693.x

Hasırcı Bayır, B. R., Tutkavul, K., Eser, M., and Baykan, B. (2021). Epilepsy in patients with familial hemiplegic migraine. *Seizure* 88, 87–94. doi: 10.1016/j.seizure.2021.03.028

Hayashi, K., Konno, T., Tada, H., Tani, S., Liu, L., Fujino, N., et al. (2015). Functional Characterization of rare variants implicated in susceptibility to lone atrial fibrillation. *Circ. Arrhythm. Electrophysiol.* 8, 1095–1104. doi: 10.1161/CIRCEP.114.002519

Hindocha, N., Nashef, L., Elmslie, F., Birch, R., Zuberi, S., Al-Chalabi, A., et al. (2008). Two cases of sudden unexpected death in epilepsy in a GEFS$^+$ family with an SCN1A mutation. *Epilepsia* 49, 360–365. doi: 10.1111/j.1528-1167.2007.01439_2.x

Jansen, N. A., Dehghani, A., Linssen, M. M. L., Breukel, C., Tolner, E. A., and van den Maagdenberg, A. (2020). First FHM3 mouse model shows spontaneous cortical spreading depolarizations. *Ann. Clin. Transl. Neurol.* 7, 132–138. doi: 10.1002/acn3.50971

Kivity, S., Oliver, K. L., Afawi, Z., Damiano, J. A., Arsov, T., Bahlo, M., et al. (2017). SCN1A clinical spectrum includes the self-limited focal epilepsies of childhood. *Epilepsy Res.* 131, 9–14. doi: 10.1016/j.eplepsyres.2017.01.012

Lal, D., Reinthaler, E. M., Altmüller, J., Toliat, M. R., Thiele, H., Nürnberg, P., et al. (2013). RBFOX1 and RBFOX3 mutations in rolandic epilepsy. *PLoS One* 8:e73323. doi: 10.1371/journal.pone.0073323

Lal, D., Reinthaler, E. M., Dejanovic, B., May, P., Thiele, H., Lehesjoki, A. E., et al. (2016). Evaluation of presumably disease causing SCN1A variants in a cohort of common epilepsy syndromes. *PLoS one.* 11:e0150426. doi: 10.1371/journal.pone.0150426

Lal, D., Reinthaler, E. M., Schubert, J., Muhle, H., Riesch, E., Kluger, G., et al. (2014). DEPDC5 mutations in genetic focal epilepsies of childhood. *Ann. Neurol.* 75, 788–792. doi: 10.1002/ana.24127

Le Gal, F., Korff, C. M., Monso-Hinard, C., Mund, M. T., Morris, M., Malafosse, A., et al. (2010). A case of sudep in a patient with dravet syndrome with SCN1A mutation. *Epilepsia* 51, 1915–1918. doi: 10.1111/j.1528-1167.2010.02691.x

Lemke, J. R., Lal, D., Reinthaler, E. M., Steiner, I., Nothnagel, M., Alber, M., et al. (2013). Mutations in GRIN2A cause idiopathic focal epilepsy with rolandic spikes. *Nat. Genet.* 45, 1067–1072. doi: 10.1038/ng.2728

Liu, C., Tester, D. J., Hou, Y., Wang, W., Lv, G., Ackerman, M. J., et al. (2014). Is sudden unexplained nocturnal death syndrome in Southern China a cardiac sodium channel dysfunction disorder? *Forensic Sci. International.* 236, 38–45. doi: 10.1016/j.forsciint.2013.12.033

Meng, H., Xu, H. Q., Yu, L., Lin, G. W., He, N., Su, T., et al. (2015). The SCN1A mutation database: updating information and analysis of the relationships among genotype, functional alteration, and phenotype. *Hum. Mutat.* 36, 573–580. doi: 10.1002/humu.22782

Moeschler, J. B., and Shevell, M. (2014). Comprehensive evaluation of the child with intellectual disability or global developmental delays. *Pediatrics* 134, e903–e918. doi: 10.1542/peds.2014-1839

Moulard, B., Guipponi, M., Chaigne, D., Mouthon, D., Buresi, C., and Malafosse, A. (1999). Identification of a new locus for generalized epilepsy with febrile seizures plus (GEFS$^+$) on chromosome 2q24-q33. *Am. J. Hum. Genet.* 65, 1396–1400. doi: 10.1086/302621

Reinthaler, E. M., Dejanovic, B., Lal, D., Semtner, M., Merkler, Y., Reinhold, A., et al. (2015). Rare variants in γ-aminobutyric acid type a receptor genes in rolandic epilepsy and related syndromes. *Ann. Neurol.* 77, 972–986. doi: 10.1002/ana.24395

Scheffer, I. E., and Nabbout, R. (2019). SCN1A-related phenotypes: epilepsy and beyond. *Epilepsia* 60, S17–S24. doi: 10.1111/epi.16386

Singh, N. A., Pappas, C., Dahle, E. J., Claes, L. R., Pruess, T. H., De Jonghe, P., et al. (2009). A role of SCN9A in human epilepsies, as a cause of febrile seizures and as a potential modifier of Dravet syndrome. *PLoS Genet.* 5:e1000649. doi: 10.1371/journal.pgen.1000649

Tomson, T., Nashef, L., and Ryvlin, P. (2008). Sudden unexpected death in epilepsy: current knowledge and future directions. *Lancet Neurol.* 7, 1021–1031. doi: 10.1016/s1474-4422(08)70202-3

Xu, X., Yang, X., Wu, Q., Liu, A., Yang, X., Ye, A. Y., et al. (2015). Amplicon resequencing identified parental mosaicism for approximately 10% of "de novo" SCN1A mutations in children with Dravet Syndrome. *Hum. Mutat.* 36, 861–872. doi: 10.1002/humu.22819

Yang, C., Hua, Y., Zhang, W., Xu, J., Xu, L., Gao, F., et al. (2018). Variable epilepsy phenotypes associated with heterozygous mutation in the SCN9A gene: report of two cases. *Neurol. sci.* 39, 1113–1115. doi: 10.1007/s10072-018-3300-y

Conflict of Interest: The authors declare that the research was conducted in the absence of any commercial or financial relationships that could be construed as a potential conflict of interest.

Publisher's Note: All claims expressed in this article are solely those of the authors and do not necessarily represent those of their affiliated organizations, or those of the publisher, the editors and the reviewers. Any product that may be evaluated in this article, or claim that may be made by its manufacturer, is not guaranteed or endorsed by the publisher.

frontiers | Frontiers in Molecular Neuroscience

ORIGINAL RESEARCH
published: 31 May 2022
doi: 10.3389/fnmol.2022.872407

Functional Characterization of *CLCN4* Variants Associated With X-Linked Intellectual Disability and Epilepsy

Raul E. Guzman, Juan Sierra-Marquez, Stefanie Bungert-Plümke, Arne Franzen and Christoph Fahlke*

Institute of Biological Information Processing, Molecular and Cellular Physiology (IBI-1), Forschungszentrum Jülich, Jülich, Germany

OPEN ACCESS

Edited by:
Tobias Stauber, Medical School Hamburg, Germany

Reviewed by:
Hyun-Ho Lim, Korea Brain Research Institute, South Korea
Giovanni Zifarelli, Institute of Biophysics (CNR), Italy

***Correspondence:**
Raul E. Guzman
r.guzman@fz-juelich.de

Specialty section:
This article was submitted to Brain Disease Mechanisms, a section of the journal Frontiers in Molecular Neuroscience

Received: *09 February 2022*
Accepted: *27 April 2022*
Published: *31 May 2022*

Citation:
Guzman RE, Sierra-Marquez J, Bungert-Plümke S, Franzen A and Fahlke C (2022) Functional Characterization of CLCN4 Variants Associated With X-Linked Intellectual Disability and Epilepsy. Front. Mol. Neurosci. 15:872407. doi: 10.3389/fnmol.2022.872407

Early/late endosomes, recycling endosomes, and lysosomes together form the endo-lysosomal recycling pathway. This system plays a crucial role in cell differentiation and survival, and dysregulation of the endo-lysosomal system appears to be important in the pathogenesis of neurodevelopmental and neurodegenerative diseases. Each endo-lysosomal compartment fulfils a specific function, which is supported by ion transporters and channels that modify ion concentrations and electrical gradients across endo-lysosomal membranes. CLC-type Cl^-/H^+ exchangers are a group of endo-lysosomal transporters that are assumed to regulate luminal acidification and chloride concentration in multiple endosomal compartments. Heterodimers of ClC-3 and ClC-4 localize to various internal membranes, from the endoplasmic reticulum and Golgi to recycling endosomes and late endosomes/lysosomes. The importance of ClC-4-mediated ion transport is illustrated by the association of naturally occurring *CLCN4* mutations with epileptic encephalopathy, intellectual disability, and behavioral disorders in human patients. However, how these mutations affect the expression, subcellular localization, and function of ClC-4 is insufficiently understood. We here studied 12 *CLCN4* variants that were identified in patients with X-linked intellectual disability and epilepsy and were already characterized to some extent in earlier work. We analyzed the consequences of these mutations on ClC-4 ion transport, subcellular trafficking, and heterodimerization with ClC-3 using heterologous expression in mammalian cells, biochemistry, confocal imaging, and whole-cell patch-clamp recordings. The mutations led to a variety of changes in ClC-4 function, ranging from gain/loss of function and impaired heterodimerization with ClC-3 to subtle impairments in transport functions. Our results suggest that even slight functional changes to the endosomal Cl^-/H^+ exchangers can cause serious neurological symptoms.

Keywords: ion channels and epilepsy, *CLCN4*, patch clamp, chloride-proton exchanger, intellectual disability

INTRODUCTION

The endo-lysosomal system degrades and recycles internalized material and damaged cell components and is involved in repairing the plasma membrane and releasing non-degradable material (Medina et al., 2011). Pronounced differences in luminal pH suggest that luminal acidification is a major determinant of the functional specificity of endo-lysosomal compartments. Acidification of endosomes and lysosomes is driven by the H^+-ATPase and regulated by a variety of ion channels and transporters. Five CLC transporters are expressed in endosomal membranes, with isoform-specific localization and functions (Stauber and Jentsch, 2010; Bose et al., 2021). The transporters utilize the stoichiometrically coupled exchange of two Cl^- ions with one H^+ ion to regulate and maintain endosomal pH and Cl^- concentration (Ishida et al., 2013; Stauber and Jentsch, 2013). ClC-3 and ClC-4 are found in various human organs, with strong expression in the brain. Alternative splicing of *CLCN3* results in the targeting of ClC-3 variants to the Golgi, recycling and late endosomes, and lysosomes (Guzman et al., 2015). ClC-4 homodimers are mainly found in the endoplasmic reticulum (ER), whereas heterodimerization with ClC-3 targets ClC-4 subunits to recycling and late endosomes/lysosomes (Guzman et al., 2017). ClC-5 is expressed in early endosomes in the kidney, where it regulates endocytic uptake in the proximal tubule (Jentsch and Pusch, 2018; Sakhi et al., 2021). ClC-6 and ClC-7 localize to late endosomes and lysosomes (Jentsch and Pusch, 2018).

Animal models lacking ClC-4 do not exhibit an apparent phenotype (van Slegtenhorst et al., 1994; Rickheit et al., 2010; Weinert et al., 2020), in contrast to the severe phenotypes caused by genetic ablation of the other CLC exchangers (Piwon et al., 2000; Kornak et al., 2001; Stobrawa et al., 2001; Dickerson et al., 2002; Yoshikawa et al., 2002; Poet et al., 2006). Sequence variations in *CLCN4* have recently been associated with X-linked intellectual disability, epilepsy, white matter abnormality, and cortical atrophy in humans (Veeramah et al., 2013; Hu et al., 2016; Palmer et al., 2018; Zhou et al., 2018; He et al., 2021; Xu et al., 2021). So far, more than 20 different *CLCN4* mutations have been identified. Several disease-associated *CLCN4* mutations were tested by electrophysiological analysis after heterologous expression in oocytes (Hu et al., 2016; Palmer et al., 2018). These experiments revealed reduced macroscopic current amplitudes, however, no attempts were done to distinguish altered trafficking from impaired transport function or to identify mechanisms underlying reduced anion transport. Although endosomal targeting of ClC-4 requires association to ClC-3 (Guzman et al., 2017; Weinert et al., 2020), only homodimers were studied and potential changes in hetero-oligomerization were ignored. Here, we studied the functional consequences of 12 disease-associated *CLCN4* mutations in a mammalian heterologous expression system using whole-cell patch clamping, confocal imaging, and denaturing and native gel electrophoresis. We report changes in transport, subcellular localization, protein stability, and oligomerization capacity of the ClC-4 variants.

MATERIALS AND METHODS

Plasmid Construction

cDNAs encoding full-length WT human ClC-4 (Alekov and Fahlke, 2009) or mouse ClC-3b (Guzman et al., 2015) were cloned into FsY1.1 G.W. or p156rrL vectors (kindly provided by Dr. Mikhail. Filippov, Nizhny Novgorod, Russia, and Dr. Dieter. Bruns, Homburg, Germany). Enhanced green or monomeric cherry fluorescent proteins (eGFP or mCherry) were fused in frame to the 5′ end of the coding sequence of each CLC transporter. Overlapping PCR strategies were used to introduce the ClC-4 mutations and to generate chimeric constructs. All constructs were verified by sequencing the complete open reading frame, and two independent recombinants from each transformation were tested for possible functional differences. To help distinguish ClC-3b and ClC-4 electrophoretically, we increased the molecular weight of ClC-3b by adding the coding sequence of maltose-binding protein (MBP) in frame to its 3′ end. We also inserted point mutations to substitute glutamine at N880 and N883 to prevent MBP -ClC-3b glycosylation.

Electrophysiological Experiments

For electrophysiological recordings, HEK293T cells were transfected with plasmids encoding WT or mutant ClC-4-eGFP fusion proteins using the calcium phosphate method (Garcia-Olivares et al., 2008). Only fluorescent cells were studied by whole-cell patch-clamp recordings with an EPC-10 amplifier controlled by PatchMaster (HEKA Elektronik, Harvard Bioscience, Reutlingen, Germany) (Guzman et al., 2013). Images were taken with an Andor's Neo 5.5 sCMOS camera and analyzed using ImageJ 1.44p software (Image J v.1.53c, Wayne Rasband, National Institutes of Health, Bethesda, Rockville, MD, United States) (Schneider et al., 2012). Borosilicate pipettes (GC150F-10, Harvard Apparatus, Holliston, MA, United States) were pulled with resistances of 1.0–2.0 MΩ; in all experiments, capacitance cancelation and 80–85% series resistance compensation were applied to ensure a voltage error of below 5 mV. Currents were elicited by applying 10 ms test pulses (–115 mV to +175 mV in 10 mV increment every 500 ms) from a holding potential of 0 mV and digitized with 100 kHz sampling rates. For all representative recordings, P/8 leak subtraction with a baseline potential of -30 mV was used to cancel linear capacitances (Bezanilla and Armstrong, 1977). We carefully tested all mutant proteins for potential alterations in the current response to negative voltages. For electrophysiological experiments, bath solutions contained (in mM) 145 NaCl, 15 HEPES, 4 K-gluconate, 2 $CaCl_2$, and 1 $MgCl_2$, pH 7.4, and internal recording solutions contained (in mM) 120 NaCl, 15 HEPES, 5 $MgCl_2$, 5 EGTA, and 5 Na-ATP, pH 7.4.

Confocal Microscopy and Image Analysis

For confocal imaging, HEK293T cells were co-transfected with the WT or mutant ClC-4-eGFP fusion construct and a plasmid encoding fluorescent calnexin or ClC-3b-mCherry (Guzman et al., 2015. We received the ER marker calnexin

as gift from Michael Davidson (Addgene plasmid # 55005[1]; RRID:Addgene_55005). Cells were plated on poly-L-lysine-coated coverslips at 24 h after transfection, and images were taken 24 h later with a Leica TCS SP5 II inverted microscope (Leica Microsystems, Wetzlar, Germany) using a 63 × /1.40 NA oil immersion objective in phosphate-buffered saline at room temperature. Images were digitalized with a resolution of 1024 × 1024 pixels, 200 Hz velocity, and 6-line average in sequential scanning mode. eGPF was excited with a 488-nm Ar-laser and mCherry with a 594-nm He-Ne laser. Emission signals were detected after filtering with a 500–550 or 600–650 nm bandpass filter. Confocal images were processed for publications using ImageJ 1.44p software (Image J v.1.53c, Wayne Rasband, National Institutes of Health, Bethesda, Rockville, MD, United States) (Schneider et al., 2012).

Biochemical Analysis

HEK293T cells were transfected with plasmids encoding WT or mutant ClC-4-eGFP fusion proteins with or without a plasmid encoding the glycosylation-defective mutant, MBP-ClC-3b-eGFP N880/883Q. Transfected HEK293T cells were washed with ice-cold phosphate-buffered saline and lysed with buffer containing 0.1 M sodium phosphate, pH 8.0, 0.5% digitonin, protease inhibitors, and 20 mM iodoacetamide, as previously described (Guzman et al., 2017). Approximately 10 μg whole-cell lysate was analyzed by reducing 10% SDS-PAGE (Laemmli, 1970) at room temperature for approximately 2 h at 18 mA. For high-resolution clear native gel electrophoresis (hrCNE), native 4–14% acrylamide gradient gels were prepared as previously described (Nicke et al., 1998; Wittig et al., 2007); the anode buffer contained 25 mM imidazole/HCl, pH 7.0, and the cathode buffer contained 50 mM tricine, 7.5 mM imidazole, pH 7.0, the anionic detergent DOC (0.05%), and the non-ionic detergent DDM (0.01%) (Wittig et al., 2007). Approximately 10 μg whole-cell lysate samples were run at 8°C for a total of 3 h (100 V for 1 h, followed by 150 V for 2 h).

Protein bands were visualized using a fluorescence gel scanner (Typhoon FLA9500, GE Healthcare, Freiburg, Germany) at 100 μm resolution. eGFP was excited at 473 nm and emissions were recorded using a 530/20 bandpass filter. Gel images were quantified using ImageJ 1.44p software (Schneider et al., 2012). Gels were analyzed in black and white and the appearance of the entire gel was adjusted using the Brightness and Contrast tool of ImageJ. For glycosylation analysis, a rectangular ROI (region of interest) was selected between apparent molecular weights of 80–140 kDa to cover bands containing non-glycosylated or glycosylated WT ClC-4-eGFP or mutant protein in the absence or presence of MBP-ClC-3b-eGFP N880/883Q. Within these ROIs, the intensity of glycosylated and non-glycosylated ClC-4-eGFP bands was determined and used to calculate the percentage of glycosylated ClC-4-eGFP molecules. The total protein was calculated as the sum of intensities of the glycosylated and non-glycosylated ClC-4-eGFP bands. To quantify the oligomerization capacity of ClC-4 mutant variants, a rectangular ROI was selected that covered all ClC-3b or ClC-4 homodimeric or heterodimeric assemblies of WT/mutant protein bands (**Supplementary Figure 1**). Total protein was calculated as the sum of intensities of all expressed proteins, and intensities of ClC-3b/ClC-4 WT/mutant heterodimeric bands divided by total fluorescence were used to quantify the percentage of heterodimers. Bands from experiments with transfections of ClC-3b or ClC-4 alone were used to appropriately assign protein bands in co-expression experiments.

For PNGaseF or EndoH treatment, 10 μg whole-cell lysate was incubated with 0.5 μl enzyme at 30°C for 30 min. The glycosylation states of ClC proteins were analyzed by reducing 10% SDS-PAGE and subsequent Typhoon scanning.

Homology Modeling Structure of ClC-4

Atomic-resolution structures of a human ClC-4 dimer (UniProt ID P51793) were generated using the neural network-based model AlphaFold-Multimer (Evans et al., 2021), a recent improvement of AlphaFold2 (Jumper et al., 2021) trained to predict multimeric protein structures. We generated 20 ClC-4 models and selected the best-ranked model according to model confidence as described (Evans et al., 2021). A local installation of AlphaFold-Multimer (version 2.1.1[2]) was used on Linux servers equipped with four Nvidia A100 GPUs.

Data Analysis

Data were analyzed using a combination of FitMaster (HEKA), Origin (OriginLab, Northampton, United States), SigmaPlot (Systat Software, Düsseldorf, Germany), and Excel (Microsoft, Redmond, WAS, United States) software. All summary data are given as mean ± s.e.m (standard error of the mean). Data are graphically presented as mean ± standard error of the mean (s.e.m) or box-whisker plots indicating the upper and the lower quartiles and whiskers the upper and lower 90%. The comparison was made using ANOVA after passing assumptions of normality (Shapiro–Wilk test) and equal variances (Levene's test) or Mann–Whitney Rank Sum test with $^{*}p < 0.05$, $^{**}p < 0.01$, $^{***}p < 0.001$ levels of significance.

RESULTS

Most Disease-Causing Mutations Do Not Affect Protein Expression or Stability

We here analyzed a total of 12 *CLCN4* variants that were associated with X-linked intellectual disability and epilepsy in previous studies, G78S, L221V, V536M, G731R (Hu et al., 2016), D15N, V212G, L221P, V275M, S534L, A551V, R718W (Palmer et al., 2018) and G544R (Veeramah et al., 2013). These naturally occurring variants result in amino acid substitutions across the whole protein, from the cytosolic amino-terminus (D15N) to the carboxy-terminal CBS domains (R718W, G731R; **Figure 1A**). To determine whether disease-causing mutations affect protein expression/stability, we quantified protein expression and glycosylation by SDS-PAGE after the transient expression of eGFP-tagged WT or mutant ClC-4 in mammalian cells

[1]http://n2t.net/addgene:55005

[2]https://github.com/deepmind/alphafold

(Janssen et al., 2009; Winter et al., 2012; Kovermann et al., 2017). Since ClC-4 can form homodimers, as well as heterodimers with ClC-3 (Guzman et al., 2017), we analyzed cells expressing WT or mutant ClC-4 either alone or together with the lysosomal ClC-3 isoform, ClC-3b (Guzman et al., 2015). **Figure 1B** shows the migration of WT and mutant ClC-4 under denaturing conditions in the presence or absence of ClC-3b. ClC-4-eGFP migrates as a main band with a molecular weight of approximately 100 kDa. Additional faint higher-molecular-weight bands were sensitive to PNGase F (**Supplementary Figure 2**), but not to EndoH, indicating that heterologously expressed ClC-4 is complex glycosylated.

There was no band corresponding to full-length L221V ClC-4 protein, but the presence of proteolytic fragments linked to eGFP was consistent with the mutation promoting ClC-4 degradation (**Supplementary Figures 1A,B**). Heterodimerization with ClC-3b did not prevent proteolysis of the mutant protein L221V (**Figure 1B**). **Figures 1C,D** provide eGFP fluorescence levels obtained from such SDS PAGE, which report on expression levels of WT and mutant ClC-4. V212G, L221P, S534L, G544R, and A555V reduce ClC-4 expression levels, whereas the remaining mutations left transporter amounts unaffected (**Figure 1C**). Relative expression levels of mutant ClC-4 were similar in the presence or absence of co-transfected ClC-3b (**Figure 1C** vs. **Figure 1D**). For many membrane proteins, exit from the ER is associated with complex glycosylation. Therefore, we measured glycosylation levels to determine the proportion of WT and mutant ClC-4 exiting the ER (**Figures 1E,F**). Most disease-associated mutations did not affect complex glycosylation. However, G78S and V275M increased the complex glycosylation of ClC-4 (**Figures 1E,F**), whereas S534L decreased the level. No differences were observed between cells expressing ClC-4 alone or ClC-4 plus ClC-3b. Therefore, heterodimerization with ClC-3b does not stimulate the exit of ClC-4 from the ER.

Disease-Causing Mutations Affect the Efficacy and the Voltage Dependence of ClC-4 Cl^-/H^+ Exchange

Although ClC-4 is predominantly localized in intracellular compartments of transfected mammalian cells, sufficient transporters are inserted into the plasma membrane to permit the analysis of ClC-4 transport by whole-cell patch-clamp recordings (Friedrich et al., 1999; Alekov and Fahlke, 2009; Guzman et al., 2017). We used whole-cell recordings from transiently transfected HEK293T cells to determine whether disease-associated variants modify ClC-4 transport (**Figure 2A**; variants associated with epilepsy are shown in red and the others in black). D15N, V275M, V536M, G544R, and R718W reduced current amplitudes only slightly. Currents in cells expressing G78S, V212G, A555V, or G731R ClC-4 resembled WT currents, but with much smaller amplitudes (**Figure 2B**). L221V, L221P, and S534L reduced ClC-4 currents to the levels measured in untransfected cells (**Figures 2A,B**). WT and mutant ClC-4 were expressed as eGFP fusion proteins, permitting quantification of transporter expression levels by measuring eGFP fluorescence intensities in individual cells and correlating expression levels and current amplitudes (Schänzler and Fahlke, 2012; Ronstedt et al., 2015; Tan et al., 2017; Kovermann et al., 2022). **Figure 2C** provides plots of steady-state current amplitudes at +175 mV versus whole-cell fluorescence intensities for HEK293T cells expressing WT or mutant cells. We observed similar expression levels for WT and all mutant ClC-4, however, lower mutant current amplitudes at comparable whole-cell intensities. To obtain averaged and expression-level independent values of the mutation-specific effects on the macroscopic current amplitudes we fitted linear regressions to these plots. The obtained slope factors (**Figure 2D**) provide macroscopic current amplitudes normalized to expression levels and follow the same order of averaged macroscopic current amplitudes shown in **Figure 2B**.

ClC-4 currents exhibit a characteristic voltage dependence, with currents close to background at negative voltages and pronounced outward rectification and voltage-dependent current activation upon depolarizing voltage steps (Friedrich et al., 1999; Alekov and Fahlke, 2009). Voltage steps from depolarizing pulses back to the holding potential of 0 mV elicit a characteristic capacitive current (Smith and Lippiat, 2010; Grieschat and Alekov, 2012; Guzman et al., 2013; Rohrbough et al., 2018). Capacitive membrane currents originate from the repositioning of charges by membrane proteins within the membrane (Armstrong and Bezanilla, 1974). In many transporters, incomplete transport cycles in the absence of transport substrates generate capacitive currents that disappear after the application of all necessary substrates (Mager et al., 1993; Wadiche et al., 1995). Grieschat and Alekov (2012) demonstrated that a transport-incompetent mutant ClC-5 transporter carrying the E268C mutation can be rescued by site-specific addition of a negative MTSES moiety. E268C ClC-5 transporters generate capacitive currents before modification, and the addition of MTSES converts transport-incompetent transporters that function as capacitors are converted into functional transporters. Capacitive currents by ClC-3, ClC-4, or ClC-5 are therefore often assumed to be generated by transporters that perform incomplete transport cycles (please see Discussing for alternative explanations). Dividing the off-gating capacitive charge (Q_{off}) by the ionic current amplitude (current) at the preceding voltage (**Figures 3A,B**) can therefore be used as relative measure of the transport efficiency (Grieschat and Alekov, 2012; Guzman et al., 2013). ClC-4 has significantly lower capacitive currents than ClC-3 and ClC-5 when expressed at the same level and, therefore, is considered the most effective transporter in this CLC branch (Guzman et al., 2013). V275W, G544R, and R718W increased the Q_{off}/current ratio (**Figures 3A,B**).

The voltage dependence of transport can be determined by plotting the integrated capacitive currents at 0 mV against the preceding voltages. Fitting Boltzmann functions to these voltage dependences provides a similar half-maximal activation voltage ($V_{0.5}$) for WT, D15N, and R718W ClC-4 (WT, +75 ± 2 mV, n = 14; D15N, +77 ± 2 mV, n = 7; and R718W, +80 ± 1 mV, n = 5) (**Figures 3C,D**). V275M shifts the activation curve by about 11 mV in the hyperpolarizing direction (+64 ± 1 mV, n = 14), demonstrating activation at less positive potentials than the WT. In contrast, V536M and G544R cause a change in voltage dependence in the opposite direction (V536M, +112 ± 3 mV,

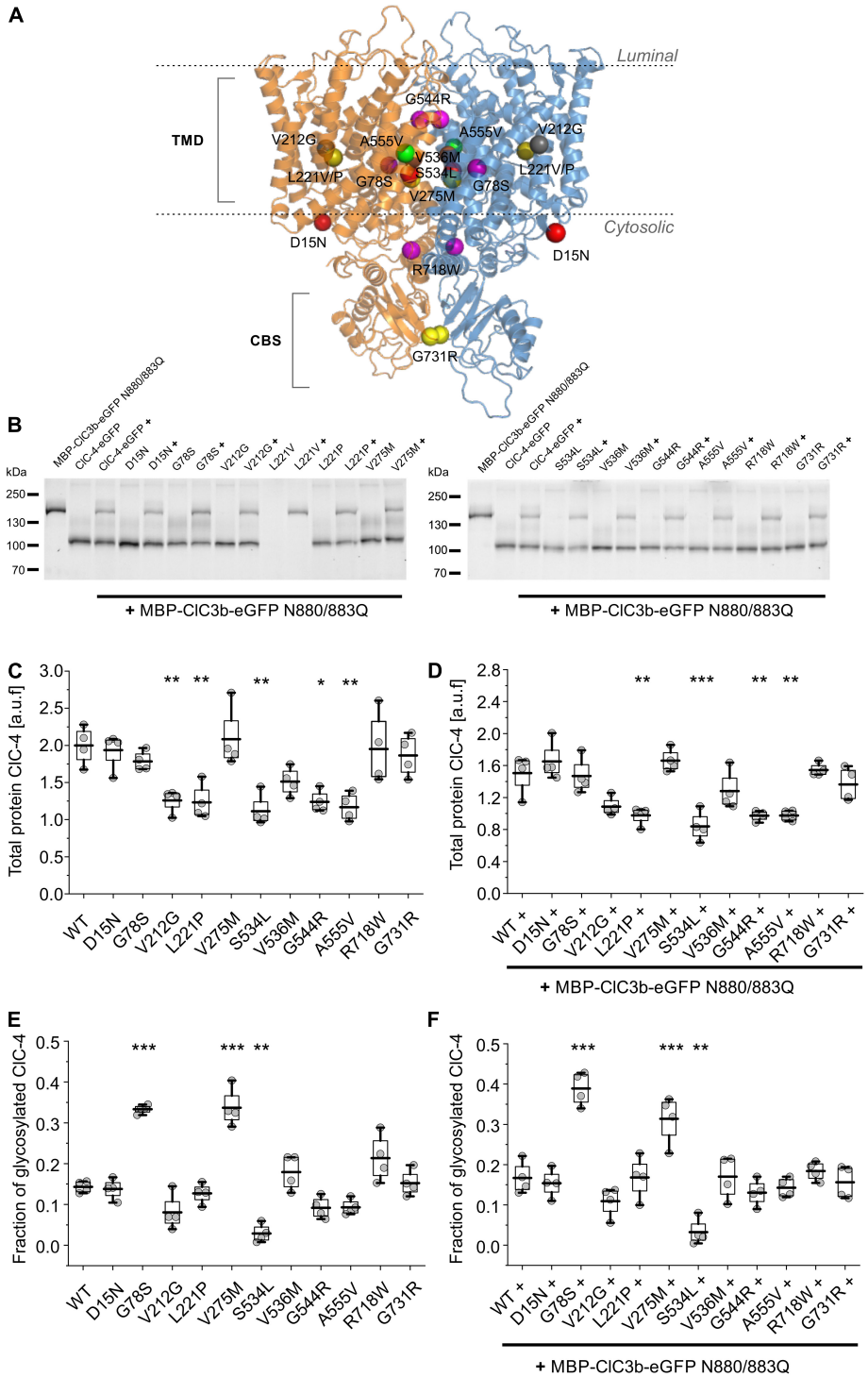

FIGURE 1 | Effects of disease-causing mutations on protein expression and stability. **(A)** Position of amino acid substitutions examined in this study mapped onto the backbone fold of an atomic-resolution model of the human ClC-4 dimer generated using AlphaFold-Multimer (Evans et al., 2021). **(B)** Representative SDS-PAGE analysis of lysates from HEK293T cells expressing WT or mutant ClC-4, alone or with ClC-3b. **(C,D)** Total WT or mutant ClC-4-eGFP protein amounts were estimated by quantifying fluorescence intensities in SDS-PAGE of lysates from HEK293T cells expressing ClC-4 **(C)** alone or **(D)** with ClC-3b (a.u. denotes arbitrary units). **(E,F)** Ratio of the intensities of complex glycosylated to total WT or mutant ClC-4-eGFP fluorescence from HEK293T cells expressing ClC-4 **(E)** alone or **(F)** with ClC-3b. ClC-4 variants were compared with WT using one-way analysis of variance (with Tukey's HSD *post hoc* testing), $^{***}p < 0.001$, $^{**}p < 0.01$, and $^{*}p < 0.05$. Data were obtained from four independent experiments and are represented as boxplot boxes indicating upper and lower quartiles and whiskers indicating upper and lower 90%.

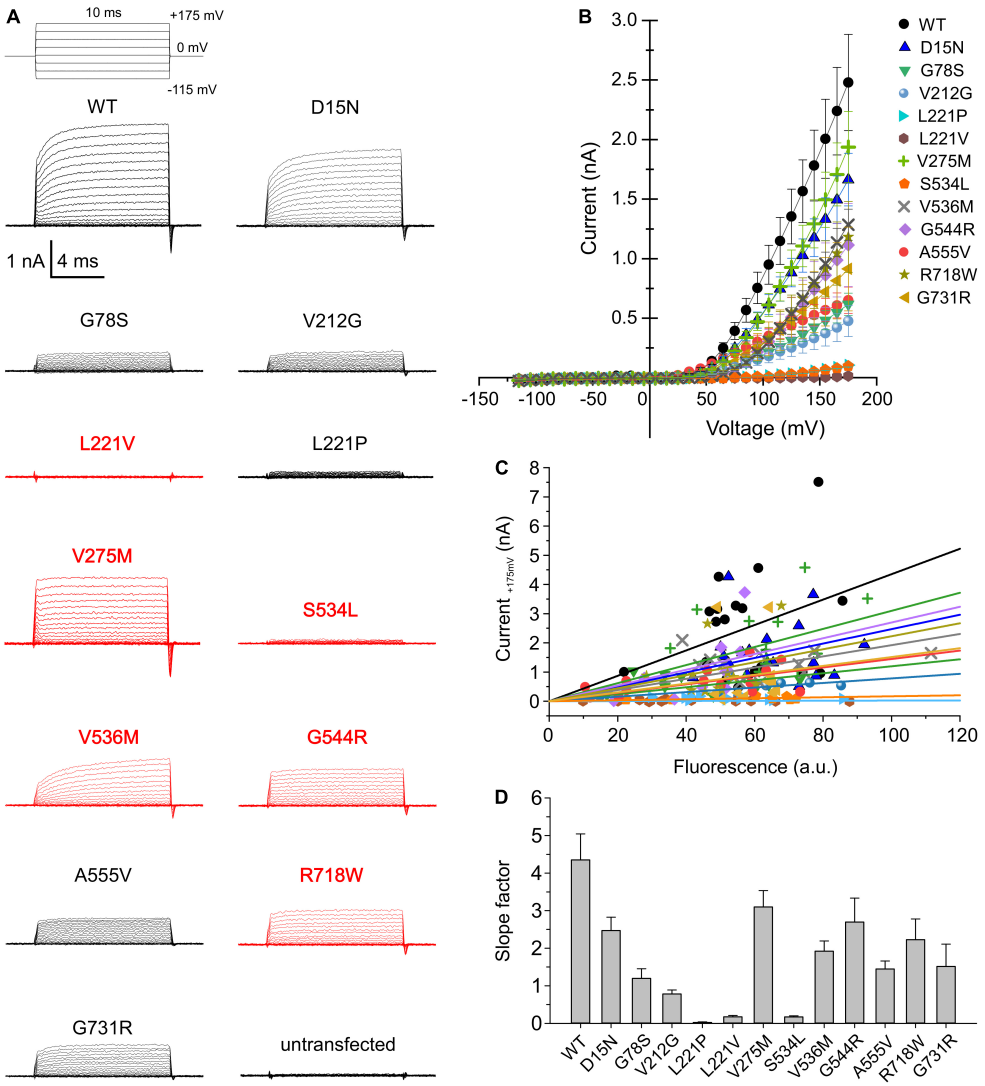

FIGURE 2 | Whole-cell patch clamp analysis of WT and mutant ClC-4 currents. **(A)** Test pulse protocol and representative whole-cell recordings from HEK293T cells expressing WT or mutant ClC-4. **(B)** Steady-state current–voltage relationships for WT and mutant ClC-4 variants, the steady-state current represent the mean value ± s.e.m. **(C)** Current-fluorescence plots for WT and mutant ClC-4. Solid lines represent linear fits (a.u. denotes arbitrary units). **(D)** Slope factors obtained from linear fits to the current-fluorescence plots shown in **(C)**, ClC-4 mutants were compared with WT using one-way analysis of variance (with Tukey's HSD *post hoc* testing). (WT, $n = 19$; D15N, $n = 19$; G78S, $n = 10$; V212G, $n = 10$; L221P, $n = 12$; L221V, $n = 12$; V275M, $n = 15$; S534L, $n = 7$; V536M, $n = 12$; G544R, $n = 10$; A555V, $n = 15$; R718W, $n = 12$; and G731R, $n = 11$). Data were obtained from four or five independent transfections.

$n = 10$; and G544R, +89 ± 2 mV, $n = 5$) (**Figures 3D,E**), indicating that V536M and G544R ClC-4 exhibit lower Cl^-/H^+ transport rates as WT when operating at the same voltage. To account for the difference in the relative transport to capacitive currents (**Figures 3A,B**), we divided the capacitive currents measured at 0 mV after different prepulse by the off gating/transport current ratio. This novel parameter – that we will call transport activity hereafter – reports on voltage-dependent changes in transport efficacy. We observed reduced transport activities for V275M, V536M, G544R, and R718W ClC-4 (**Figure 3E**).

Since ClC-4 homodimers are present only at low densities in the plasma membrane, low whole-cell current amplitudes in cells expressing G78S, V212G, L221P, S534L, or G731R ClC-4 may be caused by changes in the subcellular distribution. We increased the surface density of these mutant ClC-4 transporters by exchanging the ClC-4 linker region between the CBS domains with the corresponding ClC-3 sequence (Guzman et al., 2017) to form a chimeric ClC-$4_{LinkerClC-3}$ (**Figures 4**, **5**). **Figure 4** provides a comparison of the subcellular distribution and the transport function of WT ClC-4 and WT ClC-$4_{LinkerClC-3}$. Whereas WT ClC-4-eGFP is mainly localized to the ER, we observed predominant surface membrane insertion after expressing WT ClC-$4_{LinkerClC-3}$ (**Figure 4A**). In agreement with increased surface membrane insertion, the steady-state current (**Figures 4B,C**) and slope factors in current-fluorescence plots (**Figures 4D,E**) were about twofold increased by the interlinker

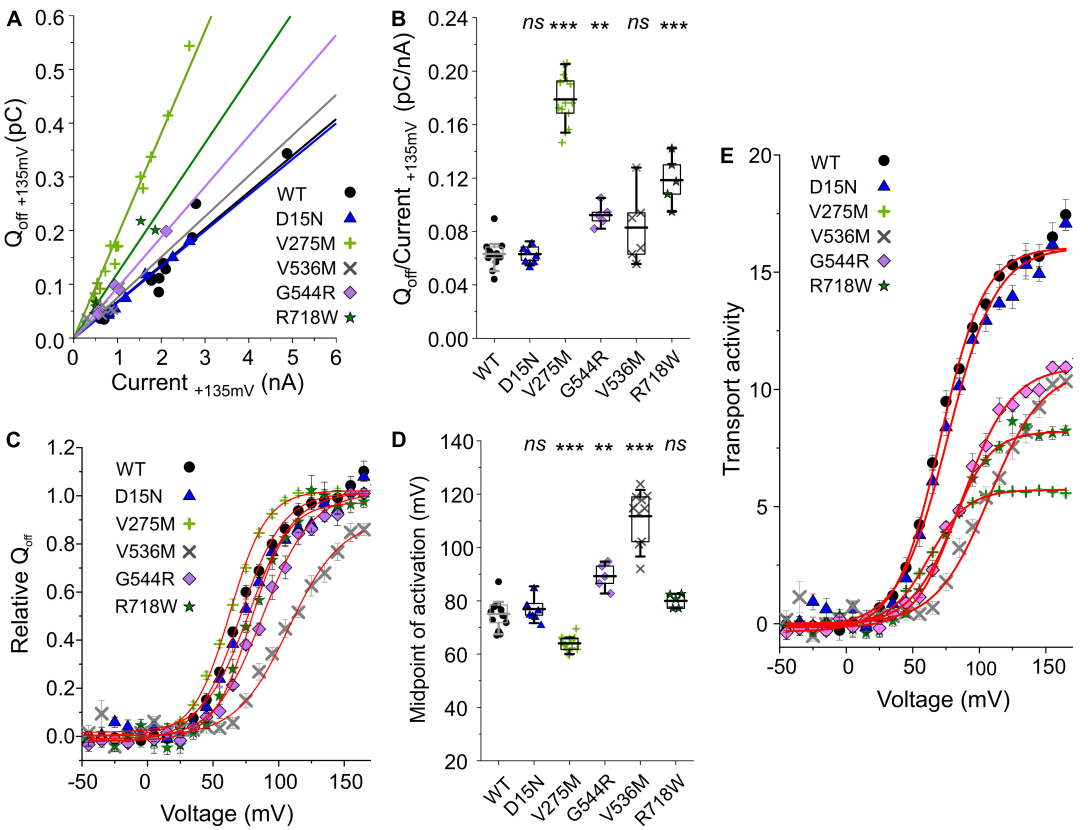

FIGURE 3 | Analysis of WT and mutant ClC-4 capacitive currents. **(A)** Plots of integrated capacitive current amplitudes at 0 mV (Q_{off}) after a prepulse to +135 mV against the transport current amplitude at +135 mV for WT and mutant ClC-4 variants. **(B)** Q_{off}/current ratios for WT and mutant ClC-4 variants (WT, n = 14; D15N, n = 7; V275M, n = 14; V536M, n = 6; and G544R, n = 5; R718W, n = 5). **(C)** ClC-4 activation curves constructed by plotting the mean value ± s.e.m. of the normalized Q_{off} against the preceding voltage. Solid lines provide fits to single Boltzmann functions. **(D)** Mean values for the midpoint of activation ($V_{0.5}$) obtained from Boltzmann fits to the Q_{off}-V relationship for WT and mutant ClC-4 variants (WT, n = 14; D15N, n = 7; V275M, n = 14; V536M, n = 10; G544R, n = 5; and R718W, n = 5). ***$p < 0.001$, **$p < 0.01$, and *ns* (not significant). **(E)** Comparison of the transport activities of WT and mutant ClC-4. Transport activities were calculated by dividing normalized Q_{off} determined after various prepulses by Q_{off}/current ratios shown in **(B)**. ClC-4 mutants were compared with WT using one-way analysis of variance (with Tukey's HSD *post hoc* testing). Data were obtained from four or five independent transfections and are presented as means ± s.e.m. and boxplot boxes indicating upper and lower quartiles; whiskers indicate upper and lower 90%.

substitution. We did not observe any differences in the ratio of capacitive by transport currents (**Supplementary Figures 3A,B**) or in the voltage dependence of the gating charge movement (**Supplementary Figures 3C,D**) between WT ClC-4 and WT ClC-4$_{LinkerClC-3}$, in agreement with earlier studies (Guzman et al., 2017). These results indicate that exchanging the ClC-4 linker region between the CBS domains with the corresponding ClC-3 sequence leaves transport unaltered, but increases the surface membrane insertion of ClC-4.

Exchanging the ClC-4 linker region promoted surface membrane insertion for G78S, V212G, and G731R, but not for L221P and S534L (**Figure 5A**). It stabilized L221V ClC-4 protein and also promote surface membrane localization for the chimeric L221V (**Figure 5A**). Moreover, it significantly increased the amplitude of the transport current for V212G, L221V and G731R ClC-4, but not for G78S ClC-4 (**Figures 2**, **5A,B**). V212G and L221V ClC-4$_{LinkerClC-3}$ exhibited larger Q_{off}/late current ratios than WT ClC-4$_{LinkerClC-3}$, but unaltered values for G731R ClC-4$_{LinkerClC-3}$ (**Figures 6A,B**). The voltage dependency of the gating charge movement shifted to more negative voltages by about 21 mV for V212G ($V_{0.5}$ = + 51 ± 1 mV, n = 12) and 44 mV for L221V ($V_{0.5}$ = 28 ± 1 mV, n = 12) (**Figures 5B** inset, 6C,D) compared to WT, but was unchanged for G731R. These results suggest a higher transport activity for V212G ClC-4 and possibly also for L221V ClC-4 (**Figure 6E**); however only under conditions, in which mutant proteins are stabilized by associated proteins. Chimeric transporters carrying G78S, L221P, or S544L and the ClC-3 linker sequence did not produce measurable transport ionic currents (**Figures 5A,B**).

Intracellular Trafficking of Mutant ClC-4

We next studied possible disease-associated alterations in subcellular targeting by confocal imaging of transfected mammalian cells. Homodimeric ClC-4 localizes to the ER, but reaches distinct endosomal compartments in heterodimeric assemblies with various ClC-3 splice variants (Guzman et al., 2017). We first determined the localization of fluorescent ClC-4 fusion proteins in HEK293T cells after

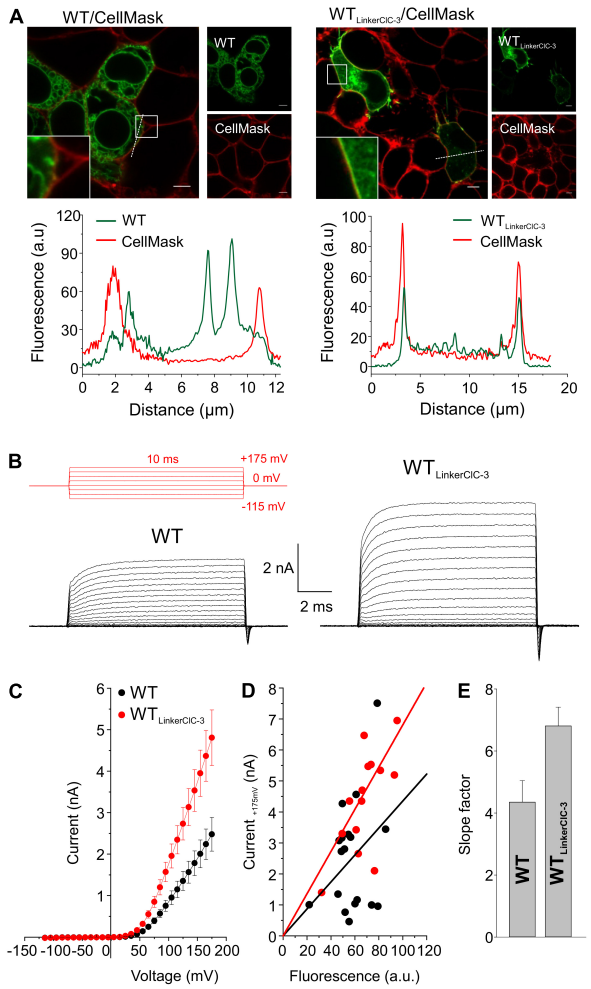

FIGURE 4 | Exchanging the ClC-4 linker region increases ClC-4 surface membrane insertion without affecting ion transport. **(A)** Representative confocal pictures of HEK293T cells co-expressing WT or WT ClC-$4_{LinkerClC-3}$ together with the plasma membrane marker CellMask and line scan analyses illustrating that subcellular distribution pattern at both channels (dashed lines). Inset shows areas outlined in the white boxes. Scale bars 5 µm. **(B)** Test pulse protocol (in red) and representative whole-cell recordings from HEK293T cells expressing WT or WT ClC-$4_{LinkerClC-3}$. **(C)** Steady-state current–voltage relationships for WT and WT ClC-$4_{LinkerClC-3}$, given as means ± s.e.m. **(D)** Current-fluorescence plots for WT and WT ClC-$4_{LinkerClC-3}$. Solid lines represent linear fits, (a.u. denotes arbitrary units). **(E)** Slope factors obtained from **(D)**. (WT, n = 18 and WT ClC-$4_{LinkerClC-3}$, n = 15) Data were obtained from four or five independent transfections.

co-expression with the ER marker calnexin (**Figure 7**). Extensive co-localization was apparent between WT ClC-4 and calnexin. All mutants, except for L221V ClC-4, were localized to the ER (**Figure 7A**). The fluorescence signal for L221V ClC-4 was rather homogenous throughout the cytoplasm, but also present in the nucleus, albeit at a lower intensity. The slight nuclear fluorescence signal may be explained by the formation of soluble fusion proteins of variable size, some of which are small enough to pass through nuclear pores (Hebeisen et al., 2004), consistent with the proteolytic degradation of L221V ClC-4 (**Figure 1B**). In cells expressing L221V ClC-$4_{LinkerClC-3}$-eGFP, a fluorescent signal was apparent in the ER (**Supplementary Figure 4**), consistent with the expression of the full-length mutant chimeric protein. The subcellular distribution of other mutants was not restricted to the ER: V275M and R718W showed a pronounced plasma membrane localization, and D15N, V536M, A555V, and S534L also localized to structures near to the nucleus (**Figure 7**).

We next evaluated the subcellular distribution of heterodimers assembled from ClC-3b and mutant ClC-4. Confocal images of HEK293T cells co-expressing WT ClC-4-eGFP and ClC-3b-mCherry showed that the proteins co-localize to enlarged endosomal compartments (**Figure 8A**; Guzman et al., 2015), with a Mander's overlap coefficient of 0.83 ± 0.03 (n = 11) (**Figure 8B**). Confocal images of cells co-expressing D15N, V275M, V536M, G544R, or R718W ClC-4 and ClC-3b resembled cells expressing WT ClC-4 and ClC-3b (**Figure 8A**). Mutant proteins carrying these mutations were detected in close proximity to ClC-3b in endo-lysosomal structures, with similar Mander's overlap coefficients to those of WT ClC-4 (**Figure 8B**). In cells expressing L221V ClC-4, we observed fluorescent signals in multiple subcellular compartments, consistent with the presence of eGFP-tagged ClC-4 fragments (**Figures 1**, **7**). The detection of ClC-3b outside lysosomes suggests that some of these ClC-4 fragments may interfere with ClC-3b targeting to the lysosome. Co-expression of ClC-3b and WT ClC-4 is typically associated with enlargement of the lysosomal compartment, which contains the highest density of heterodimers. However, this was not the case for the mutants G78S and L221P or, to a lesser extent, for S534L and G731R (**Figure 8A**). Co-expression of L221V ClC-$4_{LinkerClC-3}$-eGFP and ClC-4-mCherry led to the generation of enlarged lysosomes containing both fluorescent signals (**Supplementary Figure 4**). Heterodimers of L221P, S534L, or G731R with ClC-3b showed more pronounced residual ER expression compared with WT (**Figure 8A**).

Heterodimerization of Mutant ClC-4 With ClC-3

Since confocal microscopy can only provide indirect evidence of homo- or heterodimerization, we used hrCNE to quantify the oligomerization capacity of ClC-4 mutants (Nicke et al., 1999; Wittig et al., 2007; Detro-Dassen et al., 2008; Nothmann et al., 2011). To enable ClC-3b (91 kDa) and ClC-4 (84 kDa) to be distinguished electrophoretically, we increased the size of ClC-3b by attaching a MBP moiety (42.5 kDa) to the amino-terminus (Guzman et al., 2017). Furthermore, as the presence of multiple glycosylation moieties would make it difficult to identify the different native conformations of ClC-3b and ClC-4, we reduced ClC-3b glycosylation by exchanging Asn-880 and Asn-883 for glutamine.

Figure 9A shows a representative hrCNE of whole-cell lysates of mammalian cells expressing WT or mutant ClC-4-eGFP with or without MBP-ClC-3b-eGFP N880/883Q. For transfected ClC-3b, two distinct bands of similar intensity were seen by hrCNE (**Figure 9A**; one representing monomers, lower red triangle, and the other homodimers upper red triangles);

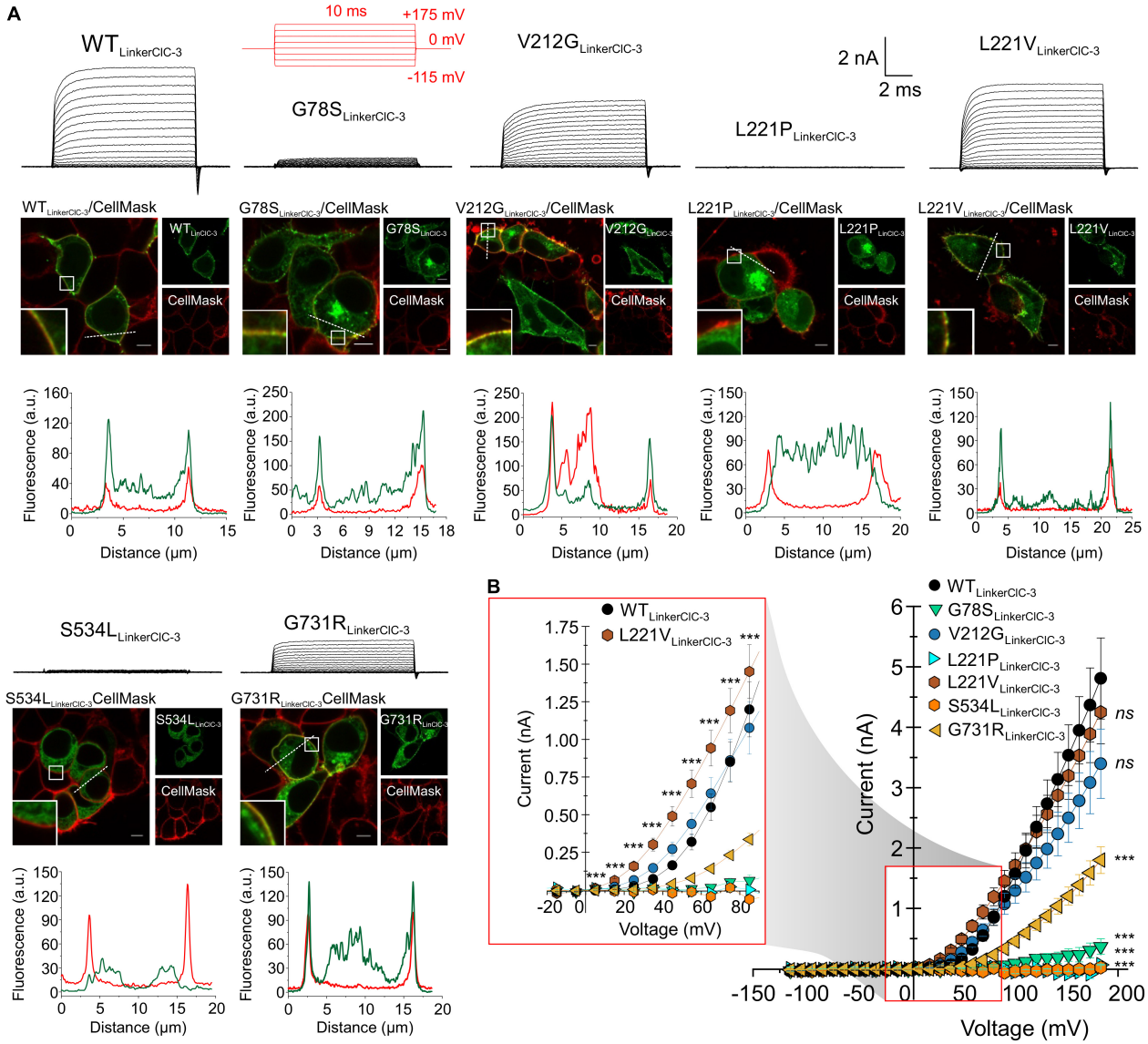

FIGURE 5 | Subcellular expression and transport functions of WT and mutant chimeric ClC-4$_{LinkerClC-3}$. **(A)** Test pulse protocol (in red) and representative transport currents (black traces) for chimeric WT, G78S, V212G, L221P, L221V, S534L, or G731R ClC-4$_{LinkerClC-3}$ expressed in HEK293T cells (upper panels). Representative confocal images of HEK293T cells co-expressing WT or mutants chimeric ClC-4$_{LinkerClC-3}$ together with the plasma membrane marker CellMask (middle panels) and line scan analyses illustrating that subcellular distribution pattern at both channels (dashed lines), (lower panels), (a.u. denotes arbitrary units). Inset shows areas outlined in the white boxes. Scale bars 5 μm. **(B)** Steady-state current-voltage relationships (mean value ± s.e.m.) for WT and mutant ClC-4 chimeric proteins. The inset gives an expanded view of the current-voltage relationship (WT, n = 14; G78S, n = 10; V212G, n = 12; L221P, n = 4; L221V, n = 12; S534L, n = 8; and G731R, n = 11). Data were obtained from four or five independent transfections.

in contrast, transfected ClC-4 was predominantly monomeric, lower green triangle, with only a faint band representing homodimers, upper green triangles (**Figure 9A**). When the proteins were co-expressed, heterodimerization resulted in two additional bands (yellow triangles in **Figure 9A**). We used the ratio of eGFP intensity for these particular bands to the sum of intensities for all fluorescent bands to quantify the heterodimerization capability of ClC-4. The capabilities of ClC-4 D15N, G78S, V212G, V275M, V536M, G544R, A555V, and R718W to heterodimerize with ClC-3b were similar to the WT. In contrast, L221P, S534L, and G731R ClC-4 had lower capabilities. If we assume that ClC-4 requires ClC-3 for export from the ER to endo-lysosomal compartments (Guzman et al., 2017), our findings suggest that L221P, S534L, and G731R ClC-4 are less likely to be inserted into endo-lysosomal membranes. V275M ClC-4 had an increased probability of heterodimerization with ClC-3b and, thus, this mutation may increase the number of ClC-4 transporters in the endo-lysosome. Since L221V impaired ClC-4 stability, we excluded this mutation from the analysis.

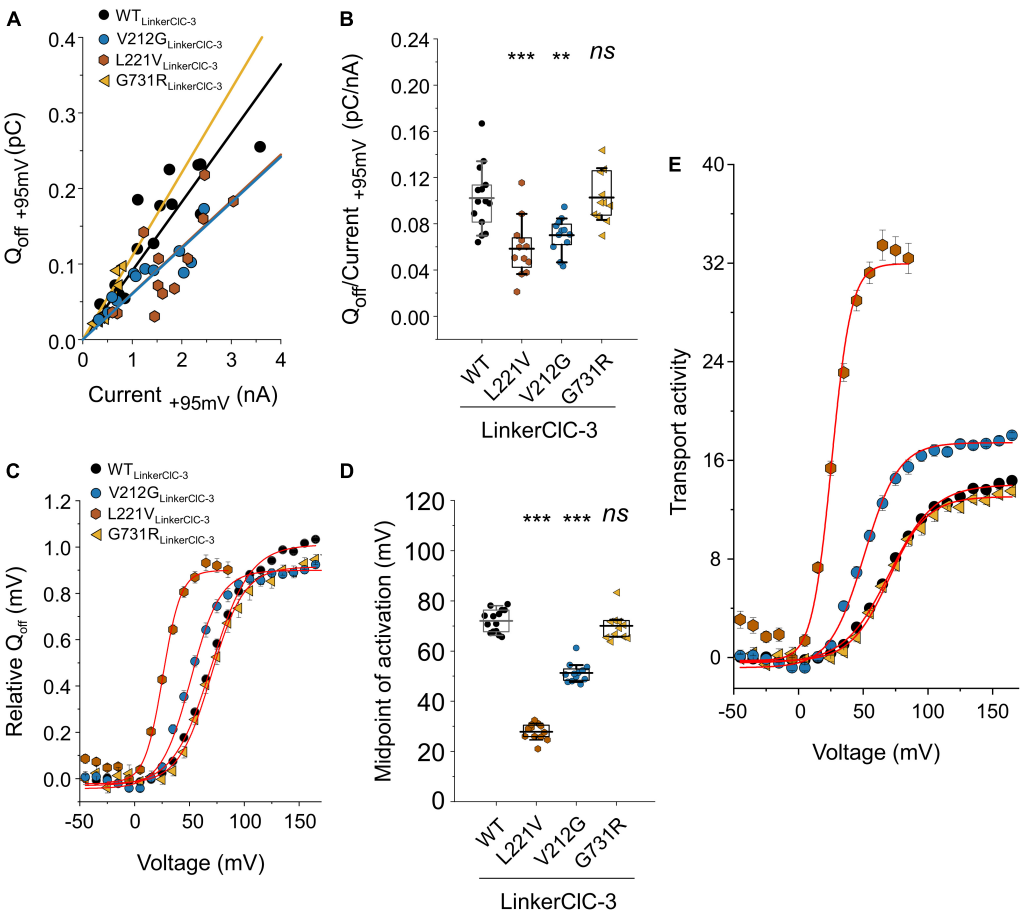

FIGURE 6 | Analysis of WT and mutant chimeric ClC-4$_{LinkerClC-3}$ capacitive currents. **(A)** Plots of integrated capacitive current amplitudes at 0 mV (Q_{off}) after a prepulse to +95 mV against transport current amplitudes at +95 mV for WT and mutant chimeric proteins. **(B)** Q_{off}/current ratios for WT and mutant ClC-4 chimeric proteins. **(C)** ClC-4 activation curves constructed by plotting mean value ± s.e.m. of the normalized Q_{off} against the preceding voltage. Solid lines show fits to single Boltzmann functions. **(D)** Mean values of activation midpoints ($V_{0.5}$) obtained from Boltzmann fits to Q_{off}-V relationship for WT and mutant chimeric transporters (WT, n = 14; V212G, n = 12; L221V, n = 12; and G731R, n = 11). (WT, n = 14; V212G, n = 12; L221V, n = 12; and G731R, n = 11). ***$p < 0.001$, **$p < 0.01$, and *ns* (not significant). **(E)** Transport activities of WT and mutant ClC-4 chimeric proteins calculated by dividing normalized Q_{off} determined after various prepulses by Q_{off}/current ratios shown in **(B)**. Mutant chimeric ClC-4$_{LinkerClC-3}$ were compared with ClC-4 WT$_{LinkerClC-3}$ using one-way analysis of variance (with Tukey's HSD *post hoc* testing). Data were obtained from four or five independent transfections and are presented as mean ± s.e.m. and boxplot boxes indicating upper and lower quartiles; whiskers indicate upper and lower 90%.

DISCUSSION

X-linked intellectual disability and epilepsy represents a group of syndromes with large variability in the severity of symptoms (Ropers and Hamel, 2005). The discovery of causative *CLCN4* mutations in several patients with distinct symptom severity (**Table 1**) provides the opportunity to link changes in endo-lysosomal Cl^-/H^+ exchange with specific neurological symptoms (Hu et al., 2016; Palmer et al., 2018). Here we examined the functional consequences of 12 disease-associated *CLCN4* mutations that result in the substitution of single amino acids (Hu et al., 2016; Palmer et al., 2018) using biochemical, microscopy, and electrophysiological approaches. Our analysis permitted classification of the tested disease-associated ClC-4 mutations into three groups: one group encompassing mutations (D15N, V275M, V536M, G544R, A555V, and R718W) with only subtle changes in transport properties and almost normal subcellular localization, a second group causing pronounced reductions in endosomal ClC-4 transport (G78S, L221P, L221V, and S534L), and a third group (V212G and G731R) mainly affecting transporter biogenesis or trafficking.

We used SDS-PAGE and confocal imaging to describe protein expression, stability, and subcellular distribution of WT and mutant ClC-4. While D15N, G78S, V275M, V536M, R718W, and G731R ClC-4 were indistinguishable from WT in these analyses, we observed reduced full-length expression levels of V212G, L221P, S534L, G544R, and A555V ClC-4. A small fraction of WT ClC-4 was complex glycosylated. G78S and V275M mutations led to increased and the S524L mutation to reduced complex glycosylation, indicating changes in intracellular trafficking of the mutant proteins. Furthermore, confocal imaging revealed increased insertion of V275M ClC-4

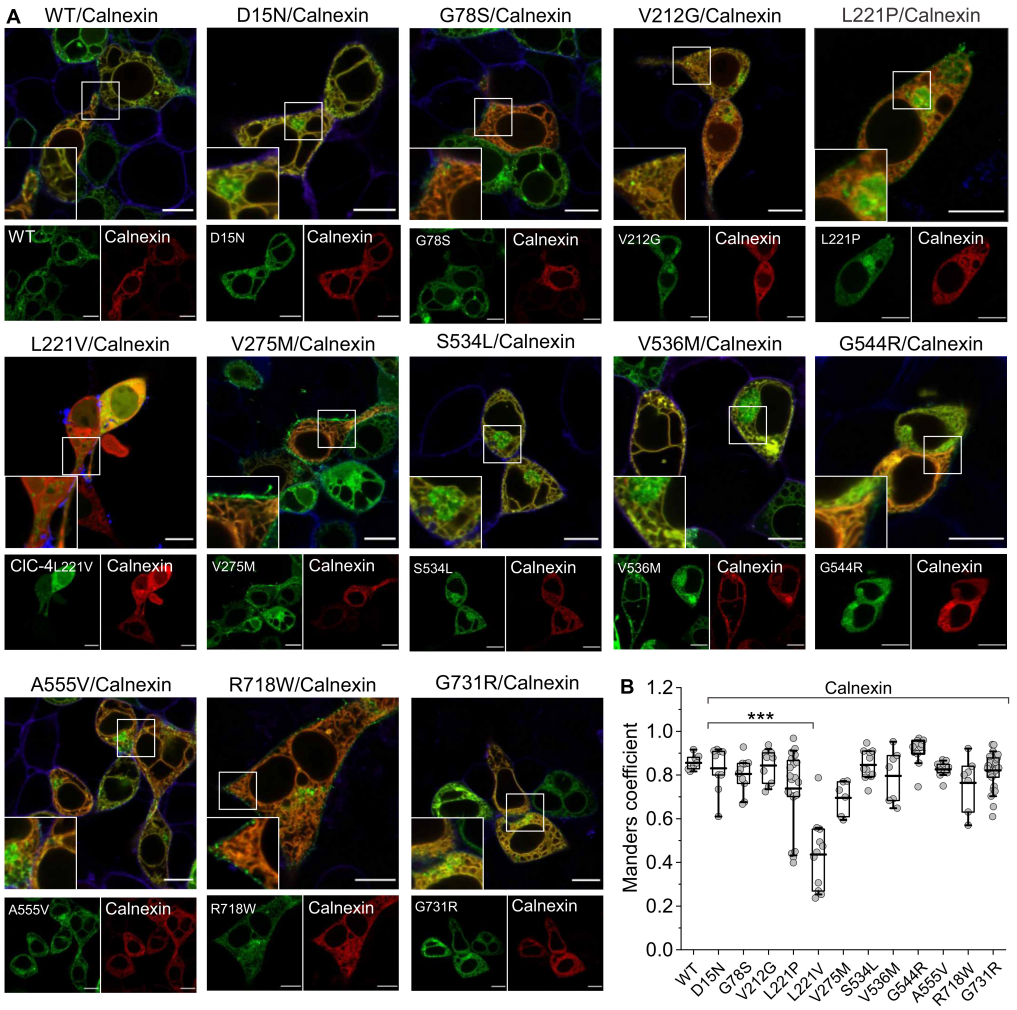

FIGURE 7 | Subcellular localization of WT and mutant ClC-4 homodimers. **(A)** Representative confocal images of HEK293T cells co-expressing WT or mutant ClC-4 together with the endoplasmic reticulum marker calnexin. Note that all mutants localize to the ER; however, the V275M and R718W variants are also present within the plasma membrane, and D15N, V536M, A555V, and S534L also localize to perinuclear structures. Inset shows areas outlined in the white boxes. **(B)** Mean values for Mander's overlapping coefficients (WT, $n = 8$; D15N, $n = 9$; G78S, $n = 11$; V212G, $n = 10$; L221P, $n = 20$; L221V, $n = 11$; V275M, $n = 6$; S534L, $n = 11$; V536M, $n = 7$; G544R, $n = 11$; A555V, $n = 11$; R718W, $n = 7$; G731R, $n = 27$). ***$p < 0.001$. ClC-4 mutants plus calnexin were compared with WT ClC-4 plus calnexin using one-way analysis of variance (with Tukey's HSD *post hoc* testing). Data were obtained from three or four independent transfections and are presented as boxplot boxes indicating upper and lower quartiles; whiskers indicate upper and lower 90%. Scale bar represents 10 μm.

into the plasma membrane (**Figure 7**). L221V was the only tested mutation with pronounced effects on expression and stability of ClC-4. In lysates from cells transfected with an L221V ClC-4 expression plasmid only protein fragments were detected, indicating decreased protein stability (**Figure 1**). Confocal imaging of cells expressing L221V ClC-4 with or without ClC-3b revealed fluorescence signals in multiple cell compartments, including the nucleus, consistent with the proteolytic generation of diffusible ClC-4 fragments (**Figures 7**, **8**). These results suggest that L221V mutation leads to complete loss of function of ClC-4; however, exchange of the carboxy-terminal inter-CBS linker stabilized and rescued the function of the mutant (**Figures 5**, **6**). Therefore, we cannot exclude the possibility that endogenous L221V ClC-4 function is retained in affected patients owing to its association with undefined chaperones. In agreement with such stabilization of L221V ClC-4, expression in oocytes resulted in measurable currents (Hu et al., 2016).

In whole-cell patch-clamp experiments, currents were only slightly reduced for five mutants, D15N, V275M, V536M, G544R, and R718W, permitting detailed analysis of disease-associated changes in ClC-4 ion transport (**Figures 2**, **3**). A distinctive feature of ClC-3, ClC-4, and ClC-5 is strong outward rectification with virtually no inward currents at negative potentials; however, none of the tested mutations affected rectification. CLC Cl^-/H^+ exchangers generate voltage and time-dependent currents in response to voltage steps. This behavior might be due to processes that switch transporters from an inactive into an

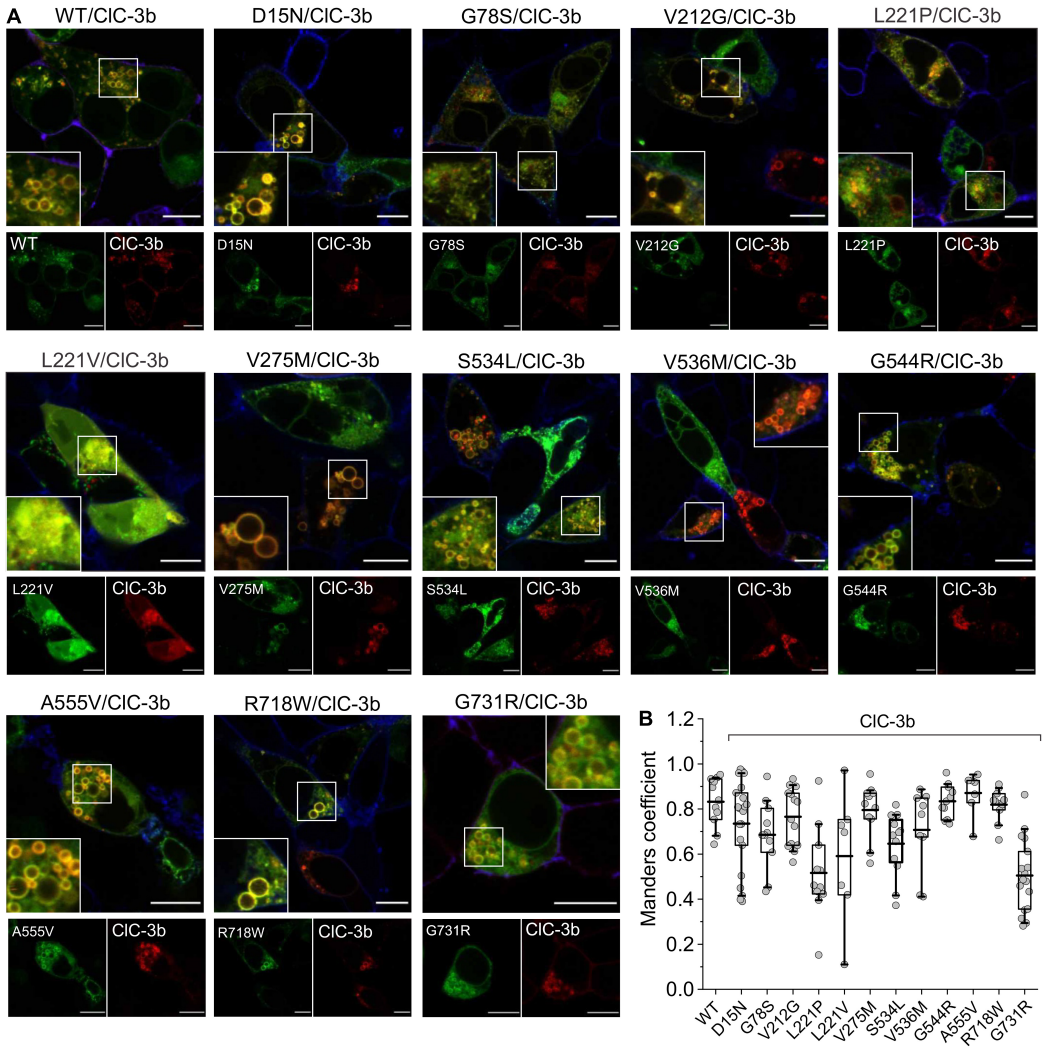

FIGURE 8 | Subcellular localization of ClC-3b/ClC-4 (WT and mutant) heterodimers. **(A)** Representative confocal images of HEK293T cells co-expressing WT or mutant ClC-4 together with ClC-3b. ClC-4 was tagged with eGFP and ClC-3b with mCherry. Inset shows areas outlined in the white boxes. **(B)** Mean values of Mander's overlapping coefficient analyses. (WT, n = 11; D15N, n = 21; G78S, n = 11; V212G, n = 14; L221P, n = 11; L221V, n = 7; V275M, n = 11; S534L, n = 12; V536M, n = 9; G544R, n = 11; A555V, n = 7; R718W, n = 11; G731R, n = 17). ClC-4 mutants plus ClC-3b were compared with WT ClC-4 plus ClC-3b using one-way analysis of variance (with Tukey's HSD *post hoc* testing). Data were obtained from three or four independent transfections and are presented as boxplot boxes indicating upper and lower quartiles; whiskers indicate upper and lower 90%. Scale bar represents 10 μm.

active form, resembling opening and closing of ion channels (Alekov and Fahlke, 2009; De Stefano et al., 2013; Pusch and Zifarelli, 2021). Alternatively, there might be voltage-dependent steps in the transport cycle that become rate-limiting under certain conditions and determine the time course of transport currents. Both mechanisms remain hypothetical, and neither of these possible explanations has been excluded so far. None of the studied mutations causes major alterations in the voltage dependence or kinetics of transport or capacitive currents.

All CLC-type Cl^-/H^+ exchangers generate capacitive currents (Smith and Lippiat, 2010; Grieschat and Alekov, 2012; Guzman et al., 2013; Rohrbough et al., 2018; Pusch and Zifarelli, 2021), whose mechanistic basis has remained unclear (Zifarelli et al., 2012; Pusch and Zifarelli, 2021). Capacitive currents generated by incomplete transport cycles have been reported for many secondary active transporters (Loo et al., 1993; Mager et al., 1993; Wadiche et al., 1995; Kovermann et al., 2017). For CLC transporters, two conserved glutamates, called gating and transport glutamate, are crucially involved in proton transport. Neutralizing the transport glutamate abolishes ClC-3, ClC-4, and ClC-5 transport (Smith and Lippiat, 2010; Guzman et al., 2013) and results in prominent capacitive currents by such mutants. Site-specific MTS modification of E268 ClC-5, in which the transport glutamate was substituted by cysteine, converts the capacitor in a transporter (Grieschat and Alekov, 2012), providing strong support for incomplete transport cycles as the basis of capacitive currents. These results support the notion that capacitive currents in CLC transporters are generated by

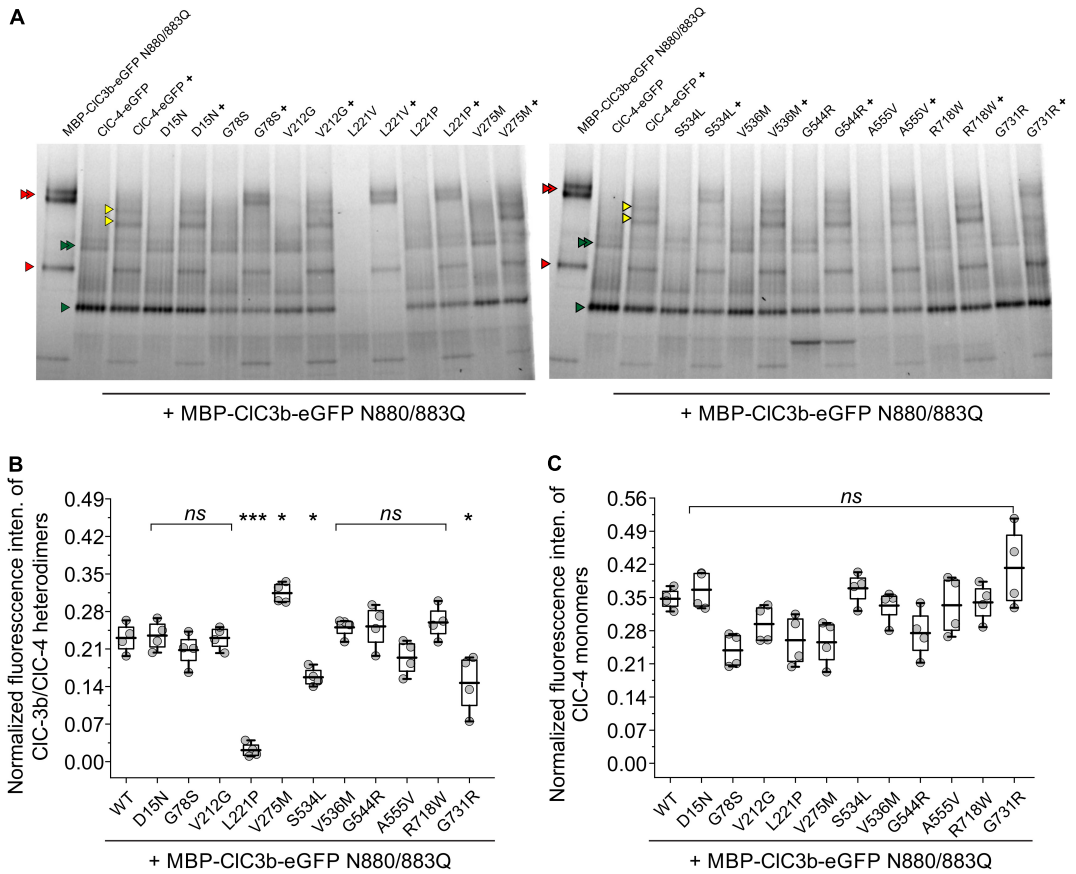

FIGURE 9 | Quantification of the oligomerization capacity of ClC-4 mutant variants. **(A)** hrCNE analysis of ClC-3b or WT/mutant ClC-4 after heterologous expression in HEK293T cells. Red triangles indicate ClC-3b monomer and ClC-3b homodimer bands, green triangles indicate ClC-4 monomer and ClC-4 homodimer bands, yellow triangles indicate heterodimer ClC- 3b/ClC-4 bands. The homodimers, as well as the heterodimer, appear as double bands in the gel due to its glycosylation status. Non-glycosylated protein, lower band and glycosylated protein, upper band. Glycosylated ClC-4 monomer bands are not indicated explicitly but run in between ClC-4 monomer and ClC-3b monomer band. **(B)** Relative fluorescence intensities of ClC-3b/ClC-4 heterodimeric bands. **(C)** Normalized fluorescence intensities of ClC-4 monomers. ***$p < 0.001$, *$p < 0.05$, and *ns* (not significant). ClC-4 variants plus ClC-3b were compared with WT plus ClC-3b using one-way analysis of variance (with Tukey's HSD *post hoc* testing). Data were obtained from four independent transfections/gels and are presented as boxplot boxes indicating upper and lower quartiles; whiskers indicate upper and lower 90%.

transporters that perform only incomplete transporters, and that ratios of transport to capacitive currents can be used as an estimate of transport efficacy (Guzman et al., 2013). We used this analysis to estimate transport efficacy for WT and mutant ClC-4 and found reduced transport efficacy at +135 mV by three of the 12 mutations, V275M, R718W, and G534R.

The alternative explanation for the capacitive currents, i.e., that capacitive currents represent gating currents associated with transport activation, predicts a similar change in mutant transport rates. Since CLC capacitive currents are linked to transitions in the transport cycle (Zifarelli et al., 2012; Pusch and Zifarelli, 2021) and since none of these mutations caused major alterations of the kinetics of the capacitive currents, the capacitive charge can be used to provide an estimate of the number of transporters. In this mechanistic framework, increased charge by current ratios also corresponds to reduced transport efficacies.

Cl^-/H^+ exchange by ClC-4 is voltage-dependent (Alekov and Fahlke, 2009), and the voltage dependence of ion transport can be assessed by plotting capacitive currents against the preceding voltages (**Figures 3C,D**; Smith and Lippiat, 2010; Grieschat and Alekov, 2012). Whereas the V275M mutation shifted voltage dependence to less positive potentials, V536M and G544R caused an opposite shift to more depolarized potentials. Moreover, hrCNE analysis showed that V275M increased the percentage of heterodimers formed with ClC-3b (**Figure 9**): the remaining mutations of this group have no obvious effects on the subcellular localization (**Figure 7**) nor the capability to interact with ClC-3 (**Figures 8**, **9**). D15N substitution did not affect the functional characteristics of ClC-4 in our assays; however, whole-cell currents were reduced with unaltered protein expression (**Figures 1**, **2**). We conclude that D15N, V275M, V536M, G544R, and R718W moderately reduce ClC-4-mediated Cl^-/H^+ transport at the ER or at other parts of the endo-lysosomal system under physiological conditions.

Most ClC-4 homodimers remain in the ER, with only a small proportion exported from the ER and inserted into the plasma

TABLE 1 | Mutation-associated changes in ClC-4 function, trafficking, oligomerization, and clinical symptoms in patients carrying these mutations.

Variant	Protein dysfunction					Functional category	Clinical phenotype in humans (Palmer et al., 2018)
	Trafficking	Dimerization with ClC-3	$V_{0.5}$	Transport efficiency	*Iss* at + 175 mV		
p.D15N	Increased ER staining Perinuclear staining	Not altered	77.0 ± 1.6 mV	Not altered	Not altered	Normal function, normal homodimer localization,	Borderline intellectual disability, delayed speech, infantile hypotonia, congenital diaphragmatic hernia, bilateral hip dysplasia, umbilical hernia, and infantile failure to thrive
p.G78S	Not altered	Not altered	ND	ND	Reduced	Loss-of-function, normal trafficking	Moderate intellectual disability and anxiety
p.V212G	Increased ER staining Perinuclear staining	Not altered	51.2 ± 1.1 mV	Increased	Reduced	Gain-of-transport function, altered trafficking	Mild to moderate intellectual disability, delayed speech, self-abusive and obsessive, compulsive behavior, anxiety, and depression.
p.L221P	Increased ER staining Perinuclear staining	Reduced	ND	ND	Reduced	Heterodimerization	Moderate intellectual disability, delayed speech, self-abusive behavior, sleep initiation disorder, infantile hypotonia, and unsteady wide-base gait
p.L221V	Impaired	Reduced	27.8 ± 0.9 mV	Increased	Not altered	Loss-of-transport function, altered trafficking as homo- and heterodimer, impaired heterodimerization	Mild to moderate intellectual disability, delayed speech, depression, bipolar and seizures disorder, epilepsy, neurological features, and gastroesophageal reflux
p.V275M	Increased ER staining Perinuclear staining	Not altered	64.0 ± 1.0 mV	Reduced	Not altered	Normal trafficking, moderate impairment of Cl^--H^+ transport	Moderate to severe intellectual disability, delayed speech, epilepsy, brisk patella reflexes
p.S534L	Increased ER staining Perinuclear staining	Slightly reduced	ND	ND	Reduced	Loss-of-function or altered trafficking	Severe intellectual disability, delayed speech, epilepsy, infantile hypotonia, cortical visual impartment and upper limb hypertonia and spasticity at the age of 3 years
p.V536M	Increased ER staining Perinuclear staining	Not altered	112.0 ± 3.1 mV	Not altered	Reduced	Altered homodimer trafficking, normal heterodimerization, moderately impaired transport	Moderate to severe intellectual disability delayed speech, aggressive behavior, hyperactivity, epilepsy, progressive spasticity, and progressive unsteady gait
p.G544R	Not altered	Not altered	89.2 ± 2.1 mV	Reduced	Reduced	Heterodimerization	Severe intellectual disability, epilepsy, infantile hypotonia, and dystonic posturing
p.A555V	Increased ER staining Perinuclear staining	Not altered	ND	ND	Reduced	Loss-of-transport function normal homodimer trafficking	Mild to moderate intellectual disability, delayed speech, exotropia, feeding difficulties, and constipation
p.R718W	Increased ER staining Perinuclear and surface membrane staining	Not altered	80.0 ± 1.2 mV	Reduced	Reduced	Moderately impaired transport function, normal trafficking	Severe intellectual disability, delayed speech, drooling and self-abusive behavior, epilepsy, infantile hypotonia, feeding difficulties in infancy and scoliosis
p.G731R	Increased ER staining Perinuclear staining	Impaired	70.0 ± 1.6 mV	Not altered	Reduced	Normal transport, change in homodimer trafficking, normal heterodimer trafficking	Severe to profound intellectual disability, delayed speech, hyperactivity, slowness and apathy, perseveration and anxiety, infantile hypotonia, and strabismus

PM, plasma membrane; PS, perinuclear structures; ND, = non-determined; Iss, steady-state anion current; $V_{0.5}$ *ClC-4 WT = 75.0 ± 1.05 mV or ClC-4*$_{linkerClC-3}$ *= 72.0 ± 1.2 mV (Palmer et al., 2018).*

membrane. Since reduced macroscopic current amplitudes of some mutant proteins might be due to changes in ER export, we removed a previously identified ER retention signal in the inter-CBS domain (Guzman et al., 2017) in mutants associated with complete loss-of-function, when inserted into the WT ClC-4 sequence (G78S, V212G, L221V, S534L, and G731R; **Figure 3**). Exchanging the ClC-4 linker region between the CBS domains with the corresponding ClC-3 sequence increases current amplitudes of chimeric V212G, L221V, and G731R ClC-4, but leaves currents by chimeric G78S, L221P, and S534L ClC-4 unaffected (**Figure 5**). Cells expressing V212G and L221V ClC-4 have large current amplitudes with slightly reduced relative capacitive currents that are activated at lower positive voltages, similar to WT (**Figures 5A,B**). Thus, both V212G and L221V variants have enhanced ClC-4 transport at physiological voltages (**Figures 5**, **6**). However, L221V, as well as V212G, reduce expression levels (**Figure 1**). We, therefore, conclude that none of the mutations results in gain-of-function mutation of ClC-4.

Co-expression of WT ClC-4 with the lysosomal ClC-3 splice variant ClC-3b (Guzman et al., 2015) result in enlarged lysosome (**Figure 8**). Currents by chimeric G78S and L221P ClC-$4_{LinkerClC-3}$ are very small (**Figure 5**), and G78S and L221P prevent enlargement of lysosome in cells expressing mutant ClC-4 with ClC-3 (**Figure 8**). The L221P and S534L mutations reduced the ability of ClC-4 to heterodimerize with ClC-3 in biochemical assays (**Figure 9**); despite this, co-expression of S534L ClC-4 and ClC-3b still led to enlarged vesicles. L221P, S534L, and A555V, but not G78S, reduce expression levels of ClC-4 (**Figures 1C,D**). Increased complex glycosylation of G78S ClC-4 indicated additional trafficking defects (**Figure 1**). The S534L mutation reduced the level of complex glycosylation (**Figure 1**), consistent with altered trafficking. Cells expressing A555V ClC-4 exhibited only very small transport currents but developed enlarged lysosomes upon ClC-3b co-expression (**Figures 2**, **8**). However, confocal imaging of A555V ClC-4 showed ER localization with additional perinuclear fluorescence signals (**Figure 7**), which might explain the reduced transport currents. We conclude that G78S, L221P, S534L, and A555V reduce ClC-4 Cl^-/H^+ exchange via a number of mechanisms, such as impaired expression, impaired maturation, altered heterodimerization or function.

Patients carrying either of the two mutations that significantly decrease endosomal Cl^-/H^+ transport, G78S, and L221P, have only moderate intellectual disability without epilepsy (**Table 1**). This finding is consistent with the moderate disease symptoms observed in patients carrying *CLCN4* nonsense mutations (Palmer et al., 2018). Patients carrying the L221V mutation suffer from epilepsy and mild-moderate intellectual disability; thus, their phenotype more closely resembles those of patients with mutations that reduce Cl^-/H^+ exchange than those with *CLCN4* loss-of-function mutations. S534L and A555V, which also cause pronounced decreases in macroscopic currents in HEK293T cells are both associated with moderate to severe intellectual disability and epilepsy. Of the mutations causing only minor effects on transport (V212G, V275M, V536M, G544R, G731R, and R718W), there was no correlation between the severity of functional changes and the neurological phenotype of affected patients. Mutations with only slight effects on ClC-4 transport are found in patients with (V275M, V536M, G544R, and R718W) or without (D15N, V212G, and G731R) epilepsy. The D15N mutation, which had little effect on ClC-4 function in our analyses, causes only very mild symptoms in patients. Patients carrying the G544R, R718W, or the G731R mutations had severely impaired intellectual performances, but the mutations caused only minor changes in Cl^-/H^+ exchange in our functional assays. The V275M mutation increases the ability of ClC-4 to form heterodimers with ClC-3b and is, thus, expected to increase endo-lysosomal ClC-4 Cl^-/H^+ transport levels; this mutation was identified in a patent with epilepsy and moderate-severe intellectual disability.

In summary, we performed a detailed functional analysis of the effects of 12 *CLCN4* mutations identified in patients with X-linked intellectual disability and epilepsy on ClC-4 transport, subcellular localization, and heterodimerization with ClC-3. Surprisingly, there are mutations associated with severe intellectual impairments and epilepsy that cause only minor biophysical changes to ClC-4 and mutations causing less severe symptoms, but pronounced alteration in biophysical properties. ClC-4 lacks endosomal targeting signals (Stauber and Jentsch, 2010) and requires association with ClC-3 for insertion into endosomal membranes (Guzman et al., 2017). However, only three of the mutations (L221P, V275M, and G731R) affected heterodimerization with ClC-3. Our results illustrate a lack of correlation between alterations that can be studied in heterologous expression systems and complex neurological phenotypes in these genetic syndromes. It appears likely that impaired ClC-4 functions are either compensated or aggravated by additional, as-yet unidentified partner proteins, compensatory processes, and other genetic factors. Alternatively, disease-associated *CLCN4* mutations might modify processes during development that require tightly regulated Cl^-/H^+ exchange and are, therefore, affected by even small changes in ClC-4 transport rates or membrane densities. More complex experimental systems, such as cell or animal models, are required to address these possibilities. However, despite its limitations, our description of multiple changes in CLC-mediated Cl^-/H^+ exchange by disease-associated mutations represents a first step toward understanding the molecular basis of X-linked intellectual disability and epilepsy.

DATA AVAILABILITY STATEMENT

The original contributions presented in the study are included in the article/**Supplementary Material**, further inquiries can be directed to the corresponding author/s.

ETHICS STATEMENT

All experiments were performed according to the German regulation for genetically modified organisms of Risk Group 1

(§§6.7 GenTG; GenTSV, Appendix 2), Aktenzeichen 53.02.01-K-1.119/15.

AUTHOR CONTRIBUTIONS

RG and CF conceived the project. RG and CF wrote the manuscript, with input from all co-authors. RG, JS-M, SB-P, and AF performed the research and analyzed the data. All authors contributed to the article and approved the submitted version.

FUNDING

This work was supported by the German Research Foundation (DFG) (GU 2042/2–1) to RG.

ACKNOWLEDGMENTS

We would like to thank Dr. Michael Pusch (Istituto di Biofisica, CNR, Genova, Italy) for helpful discussions on the origin of CLC capacitive currents. We are grateful to Dr. Jan-Philipp Machtens for generating the ClC-4 structure (**Figure 1A**) and for helpful discussion and to Petra Thelen for excellent technical assistance. We gratefully acknowledge the computing time granted through JARA on the supercomputer JURECA at Forschungszentrum Jülich.

SUPPLEMENTARY MATERIAL

The Supplementary Material for this article can be found online at: https://www.frontiersin.org/articles/10.3389/fnmol.2022.872407/full#supplementary-material

REFERENCES

Alekov, A. K., and Fahlke, C. (2009). Channel-like slippage modes in the human anion/proton exchanger ClC-4. *J. Gen. Physiol.* 133, 485–496. doi: 10.1085/jgp.200810155

Armstrong, C. M., and Bezanilla, F. (1974). Charge movement associated with the opening and closing of the activation gates of the Na channels. *J. Gen. Physiol.* 63, 533–552. doi: 10.1085/jgp.63.5.533

Bezanilla, F., and Armstrong, C. M. (1977). Inactivation of the sodium channel. I. Sodium current experiments. *J. Gen. Physiol.* 70, 549–566. doi: 10.1085/jgp.70.5.549

Bose, S., He, H., and Stauber, T. (2021). Neurodegeneration upon dysfunction of endosomal/lysosomal CLC chloride transporters. *Front. Cell. Dev. Biol.* 9:639231. doi: 10.3389/fcell.2021.639231

De Stefano, S., Pusch, M., and Zifarelli, G. (2013). A single point mutation reveals gating of the human ClC-5 Cl-/H+ antiporter. *J. Physiol.* 591, 5879–5893. doi: 10.1113/jphysiol.2013.260240

Detro-Dassen, S., Schanzler, M., Lauks, H., Martin, I., zu Berstenhorst, S. M., Nothmann, D., et al. (2008). Conserved dimeric subunit stoichiometry of SLC26 multifunctional anion exchangers. *J. Biol. Chem.* 283, 4177–4188. doi: 10.1074/jbc.M704924200

Dickerson, L. W., Bonthius, D. J., Schutte, B. C., Yang, B., Barna, T. J., Bailey, M. C., et al. (2002). Altered GABAergic function accompanies hippocampal degeneration in mice lacking ClC-3 voltage-gated chloride channels. *Brain Res.* 958, 227–250. doi: 10.1016/s0006-8993(02)03519-9

Evans, R., O'Neill, M., Pritzel, A., Antropova, N., Senior, A., Green, T., et al. (2021). Protein complex prediction with AlphaFold-Multimer. *bioRxiv [Preprint]*. Available online at: https://www.biorxiv.org/content/10.1101/2021.10.04.463034v2 (accessed on March 10, 2022).

Friedrich, T., Breiderhoff, T., and Jentsch, T. J. (1999). Mutational analysis demonstrates that ClC-4 and ClC-5 directly mediate plasma membrane currents. *J. Biol. Chem.* 274, 896–902. doi: 10.1074/jbc.274.2.896

Garcia-Olivares, J., Alekov, A., Boroumand, M. R., Begemann, B., Hidalgo, P., and Fahlke, C. (2008). Gating of human ClC-2 chloride channels and regulation by carboxy-terminal domains. *J. Physiol.* 586(Pt 22), 5325–5336. doi: 10.1113/jphysiol.2008.158097

Grieschat, M., and Alekov, A. K. (2012). Glutamate 268 regulates transport probability of the anion/proton exchanger ClC-5. *J. Biol. Chem.* 287, 8101–8109. doi: 10.1074/jbc.M111.298265

Guzman, R. E., Bungert-Plümke, S., Franzen, A., and Fahlke, C. (2017). Preferential association with ClC-3 permits sorting of ClC-4 into endosomal compartments. *J. Biol. Chem.* 292, 19055–19065. doi: 10.1074/jbc.M117.801951

Guzman, R. E., Grieschat, M., Fahlke, C., and Alekov, A. K. (2013). ClC-3 is an intracellular chloride/proton exchanger with large voltage-dependent nonlinear capacitance. *ACS Chem. Neurosci.* 4, 994–1003. doi: 10.1021/cn400032z

Guzman, R. E., Miranda-Laferte, E., Franzen, A., and Fahlke, C. (2015). Neuronal ClC-3 splice variants differ in subcellular localizations, but mediate identical transport functions. *J. Biol. Chem.* 290, 25851–25862. doi: 10.1074/jbc.M115.668186

He, H., Guzman, R. E., Cao, D., Sierra-Marquez, J., Yin, F., Fahlke, C., et al. (2021). The molecular and phenotypic spectrum of CLCN4-related epilepsy. *Epilepsia* 62, 1401–1415. doi: 10.1111/epi.16906

Hebeisen, S., Biela, A., Giese, B., Muller-Newen, G., Hidalgo, P., and Fahlke, C. (2004). The role of the carboxyl terminus in ClC chloride channel function. *J. Biol. Chem.* 279, 13140–13147. doi: 10.1074/jbc.M312649200

Hu, H., Haas, S. A., Chelly, J., Van Esch, H., Raynaud, M., de Brouwer, A. P., et al. (2016). X-exome sequencing of 405 unresolved families identifies seven novel intellectual disability genes. *Mol. Psychiatry* 21, 133–148. doi: 10.1038/mp.2014.193

Ishida, Y., Nayak, S., Mindell, J. A., and Grabe, M. (2013). A model of lysosomal pH regulation. *J. Gen. Physiol.* 141, 705–720. doi: 10.1085/jgp.201210930

Janssen, A. G., Scholl, U., Domeyer, C., Nothmann, D., Leinenweber, A., and Fahlke, C. (2009). Disease-causing dysfunctions of barttin in Bartter syndrome type IV. *J. Am. Soc. Nephrol.* 20, 145–153. doi: 10.1681/ASN.2008010102

Jentsch, T. J., and Pusch, M. (2018). CLC chloride channels and transporters: structure, function, physiology, and disease. *Physiol. Rev.* 98, 1493–1590. doi: 10.1152/physrev.00047.2017

Jumper, J., Evans, R., Pritzel, A., Green, T., Figurnov, M., Ronneberger, O., et al. (2021). Highly accurate protein structure prediction with AlphaFold. *Nature* 596, 583–589. doi: 10.1038/s41586-021-03819-2

Kornak, U., Kasper, D., Boesl, M. R., Kaiser, E., Schweizer, M., Schulz, A., et al. (2001). Loss of the ClC-7 chloride channel leads to osteopetrosis in mice and man. *Cell* 104, 205–215. doi: 10.1016/s0092-8674(01)00206-9

Kovermann, P., Hessel, M., Kortzak, D., Jen, J. C., Koch, J., Fahlke, C., et al. (2017). Impaired K+ binding to glial glutamate transporter EAAT1 in migraine. *Sci. Rep.* 7:13913. doi: 10.1038/s41598-017-14176-4

Kovermann, P., Kolobkova, Y., Franzen, A., and Fahlke, C. (2022). Mutations associated with epileptic encephalopathy modify EAAT2 anion channel function. *Epilepsia* 63, 388–401. doi: 10.1111/epi.17154

Laemmli, U. K. (1970). Cleavage of structural proteins during the assembly of the head of bacteriophage T4. *Nature* 227, 680–685. doi: 10.1038/227680a0

Loo, D. D., Hazama, A., Supplisson, S., Turk, E., and Wright, E. M. (1993). Relaxation kinetics of the Na+/glucose cotransporter. *Proc. Natl. Acad. Sci. U. S. A.* 90, 5767–5771. doi: 10.1073/pnas.90.12.5767

Mager, S., Naeve, J., Quick, M., Labarca, C., Davidson, N., and Lester, H. A. (1993). Steady states, charge movements, and rates for a cloned GABA transporter expressed in Xenopus oocytes. *Neuron* 10, 177–188. doi: 10.1016/0896-6273(93)90309-f

Medina, D. L., Fraldi, A., Bouche, V., Annunziata, F., Mansueto, G., Spampanato, C., et al. (2011). Transcriptional activation of lysosomal exocytosis promotes cellular clearance. *Dev. Cell* 21, 421–430. doi: 10.1016/j.devcel.2011.07.016

Nicke, A., Baumert, H. G., Rettinger, J., Eichele, A., Lambrecht, G., Mutschler, E., et al. (1998). P2X1 and P2X3 receptors form stable trimers: a novel structural motif of ligand-gated ion channels. *EMBO J.* 17, 3016–3028. doi: 10.1093/emboj/17.11.3016

Nicke, A., Rettinger, J., Mutschler, E., and Schmalzing, G. (1999). Blue native PAGE as a useful method for the analysis of the assembly of distinct combinations of nicotinic acetylcholine receptor subunits. *J. Recept. Signal Transduct. Res.* 19, 493–507. doi: 10.3109/10799899909036667

Nothmann, D., Leinenweber, A., Torres-Salazar, D., Kovermann, P., Hotzy, J., Gameiro, A., et al. (2011). Hetero-oligomerization of neuronal glutamate transporters. *J. Biol. Chem.* 286, 3935–3943. doi: 10.1074/jbc.M110.187492

Palmer, E. E., Stuhlmann, T., Weinert, S., Haan, E., Van Esch, H., Holvoet, M., et al. (2018). De novo and inherited mutations in the X-linked gene CLCN4 are associated with syndromic intellectual disability and behavior and seizure disorders in males and females. *Mol. Psychiatry* 23, 222–230. doi: 10.1038/mp.2016.135

Piwon, N., Günther, W., Schwake, M., Bösl, M. R., and Jentsch, T. J. (2000). ClC-5 Cl^--channel disruption impairs endocytosis in a mouse model for Dent's disease. *Nature* 408, 369–373. doi: 10.1038/35042597

Poet, M., Kornak, U., Schweizer, M., Zdebik, A. A., Scheel, O., Hoelter, S., et al. (2006). Lysosomal storage disease upon disruption of the neuronal chloride transport protein ClC-6. *Proc. Natl. Acad. Sci. U. S. A.* 103, 13854–13859. doi: 10.1073/pnas.0606137103

Pusch, M., and Zifarelli, G. (2021). Large transient capacitive currents in wild-type lysosomal Cl-/H+ antiporter ClC-7 and residual transport activity in the proton glutamate mutant E312A. *J. Gen. Physiol.* 153:e202012583. doi: 10.1085/jgp.202012583

Rickheit, G., Wartosch, L., Schaffer, S., Stobrawa, S. M., Novarino, G., Weinert, S., et al. (2010). Role of ClC-5 in renal endocytosis is unique among ClC exchangers and does not require PY-motif-dependent ubiquitylation. *J. Biol. Chem.* 285, 17595–17603. doi: 10.1074/jbc.M110.115600

Rohrbough, J., Nguyen, H. N., and Lamb, F. S. (2018). Modulation of ClC-3 gating and proton/anion exchange by internal and external protons and the anion selectivity filter. *J. Physiol.* 596, 4091–4119. doi: 10.1113/jp276332

Ronstedt, K., Sternberg, D., Detro-Dassen, S., Gramkow, T., Begemann, B., Becher, T., et al. (2015). Impaired surface membrane insertion of homo- and heterodimeric human muscle chloride channels carrying amino-terminal myotonia-causing mutations. *Sci. Rep.* 5:15382. doi: 10.1038/srep15382

Ropers, H. H., and Hamel, B. C. J. (2005). X-linked mental retardation. *Nat. Rev. Genet.* 6, 46–57. doi: 10.1038/nrg1501

Sakhi, I., Bignon, Y., Frachon, N., Hureaux, M., Arévalo, B., González, W., et al. (2021). Diversity of functional alterations of the ClC-5 exchanger in the region of the proton glutamate in patients with Dent disease 1. *Hum. Mutat.* 42, 537–550. doi: 10.1002/humu.24184

Schänzler, M., and Fahlke, C. (2012). Anion transport by the cochlear motor protein prestin. *J. Physiol.* 590, 259–272. doi: 10.1113/jphysiol.2011.209577

Schneider, C. A., Rasband, W. S., and Eliceiri, K. W. (2012). NIH Image to ImageJ: 25 years of image analysis. *Nat. Methods* 9, 671–675. doi: 10.1038/nmeth.2089

Smith, A. J., and Lippiat, J. D. (2010). Voltage-dependent charge movement associated with activation of the CLC-5 2Cl-/1H^+ exchanger. *FASEB J.* 24, 3696–3705. doi: 10.1096/fj.09-150649

Stauber, T., and Jentsch, T. J. (2010). Sorting motifs of the endosomal/lysosomal CLC chloride transporters. *J. Biol. Chem.* 285, 34537–34548. doi: 10.1074/jbc.M110.162545

Stauber, T., and Jentsch, T. J. (2013). Chloride in vesicular trafficking and function. *Annu. Rev. Physiol.* 75, 453–477. doi: 10.1146/annurev-physiol-030212-183702

Stobrawa, S. M., Breiderhoff, T., Takamori, S., Engel, D., Schweizer, M., Zdebik, A. A., et al. (2001). Disruption of ClC-3, a chloride channel expressed on synaptic vesicles, leads to a loss of the hippocampus. *Neuron* 29, 185–196. doi: 10.1016/s0896-6273(01)00189-1

Tan, H., Bungert-Plumke, S., Fahlke, C., and Stolting, G. (2017). Reduced membrane insertion of CLC-K by V33L barttin results in loss of hearing, but leaves kidney function intact. *Front. Physiol.* 8:269. doi: 10.3389/fphys.2017.00269

van Slegtenhorst, M. A., Bassi, M. T., Borsani, G., Wapenaar, M. C., Ferrero, G. B., de Conciliis, L., et al. (1994). A gene from the Xp22.3 region shares homology with voltage-gated chloride channels. *Hum. Mol. Genet.* 3, 547–552. doi: 10.1093/hmg/3.4.547

Veeramah, K. R., Johnstone, L., Karafet, T. M., Wolf, D., Sprissler, R., Salogiannis, J., et al. (2013). Exome sequencing reveals new causal mutations in children with epileptic encephalopathies. *Epilepsia* 54, 1270–1281. doi: 10.1111/epi.12201

Wadiche, J. I., Arriza, J. L., Amara, S. G., and Kavanaugh, M. P. (1995). Kinetics of a human glutamate transporter. *Neuron* 14, 1019–1027. doi: 10.1016/0896-6273(95)90340-2

Weinert, S., Gimber, N., Deuschel, D., Stuhlmann, T., Puchkov, D., Farsi, Z., et al. (2020). Uncoupling endosomal CLC chloride/proton exchange causes severe neurodegeneration. *EMBO J.* 39:e103358. doi: 10.15252/embj.2019103358

Winter, N., Kovermann, P., and Fahlke, C. (2012). A point mutation associated with episodic ataxia 6 increases glutamate transporter anion currents. *Brain* 135, 3416–3425. doi: 10.1093/brain/aws255

Wittig, I., Karas, M., and Schagger, H. (2007). High resolution clear native electrophoresis for in-gel functional assays and fluorescence studies of membrane protein complexes. *Mol. Cell Proteomics* 6, 1215–1225. doi: 10.1074/mcp.M700076-MCP200

Xu, X., Lu, F., Zhang, L., Li, H., Du, S., and Tang, J. (2021). Novel CLCN4 variant associated with syndromic X-linked intellectual disability in a Chinese girl: a case report. *BMC Pediatr.* 21:384. doi: 10.1186/s12887-021-02860-4

Yoshikawa, M., Uchida, S., Ezaki, J., Rai, T., Hayama, A., Kobayashi, K., et al. (2002). CLC-3 deficiency leads to phenotypes similar to human neuronal ceroid lipofuscinosis. *Genes Cells* 7, 597–605. doi: 10.1046/j.1365-2443.2002.00539

Zhou, P., He, N., Zhang, J. W., Lin, Z. J., Wang, J., Yan, L. M., et al. (2018). Novel mutations and phenotypes of epilepsy-associated genes in epileptic encephalopathies. *Genes Brain Behav.* 17:e12456. doi: 10.1111/gbb.12456

Zifarelli, G., De Stefano, S., Zanardi, I., and Pusch, M. (2012). On the mechanism of gating charge movement of ClC-5, a human Cl^-/H^+ antiporter. *Biophys. J.* 102, 2060–2069. doi: 10.1016/j.bpj.2012.03.067

Conflict of Interest: The authors declare that the research was conducted in the absence of any commercial or financial relationships that could be construed as a potential conflict of interest.

The handling editor TS declared a past co-authorship with several of the authors RG, JS-M, and CF.

Publisher's Note: All claims expressed in this article are solely those of the authors and do not necessarily represent those of their affiliated organizations, or those of the publisher, the editors and the reviewers. Any product that may be evaluated in this article, or claim that may be made by its manufacturer, is not guaranteed or endorsed by the publisher.

frontiers | Frontiers in Molecular Neuroscience

ORIGINAL RESEARCH
published: 27 June 2022
doi: 10.3389/fnmol.2022.919718

Nedd4-2 Haploinsufficiency in Mice Impairs the Ubiquitination of Rer1 and Increases the Susceptibility to Endoplasmic Reticulum Stress and Seizures

*Xiaoliang Liu, Lu Zhang, Hebo Zhang, Xiaoyan Liang, Bijun Zhang, Jianqiao Tu and Yanyan Zhao**

Department of Clinical Genetics, Shengjing Hospital of China Medical University, Shenyang, China

OPEN ACCESS

Edited by:
Jing Peng,
Central South University, China

Reviewed by:
Hee Jung Chung,
University of Illinois at Urbana-Champaign, United States
Ahmad Reza Dehpour,
Tehran University of Medical Sciences, Iran

***Correspondence:**
Yanyan Zhao
yyzhao@sj-hospital.org

Specialty section:
This article was submitted to Brain Disease Mechanisms, a section of the journal Frontiers in Molecular Neuroscience

Received: *13 April 2022*
Accepted: *06 June 2022*
Published: *27 June 2022*

Citation:
Liu X, Zhang L, Zhang H, Liang X, Zhang B, Tu J and Zhao Y (2022) Nedd4-2 Haploinsufficiency in Mice Impairs the Ubiquitination of Rer1 and Increases the Susceptibility to Endoplasmic Reticulum Stress and Seizures. Front. Mol. Neurosci. 15:919718. doi: 10.3389/fnmol.2022.919718

Neural precursor cell expressed developmentally downregulated gene 4-like (NEDD4-2) is an epilepsy-associated gene encoding an E3 ligase that ubiquitinates neuroactive substrates. An involvement of NEDD4-2 in endoplasmic reticulum (ER) stress has been recently found with mechanisms needing further investigations. Herein, *Nedd4-2*$^{+/-}$ mice were found intolerant to thapsigargin (Tg) to develop ER stress in the brain. Pretreatment of Tg aggravated the pentylenetetrazole (PTZ)-induced seizures. Retention in endoplasmic reticulum 1 (Rer1), an ER retrieval receptor, was upregulated through impaired ubiquitination in *Nedd4-2*$^{+/-}$ mouse brain. Nedd4-2 interacted with Rer1 more strongly in mice with Tg administration. The negative regulation and NEDD4-2-mediated ubiquitination on RER1 were evaluated in cultured neurocytes and gliacytes by NEDD4-2 knockdown and overexpression. NEDD4-2 interacted with RER1 at higher levels in the cells with Tg treatment. Disruption of the ^{36}STPY^{39} motif of RER1 attenuated the interaction with NEDD4-2, and the ubiquitinated RER1 underwent proteasomal degradation. Furthermore, the interactome of Rer1 was screened by immunoprecipitation-mass spectrometry in PTZ-induced mouse hippocampus, showing multiple potential ER retrieval cargoes that mediate neuroexcitability. The α1 subunit of the $GABA_A$ receptor was validated to interact with Rer1 and retain in ER more heavily in Nedd4-2$^{+/-}$ mouse brain by Endo-H digestion. In conclusion, Nedd4-2 deficiency in mice showed impaired ubiquitination of Rer1 and increased ER stress and seizures. These data indicate a protective effect of NEDD4-2 in ER stress and seizures possibly *via* RER1. We also provided potential ER retention cargoes of Rer1 awaiting further investigation.

Keywords: NEDD4L, epilepsy, ubiquitination, retention in endoplasmic reticulum 1, stress

INTRODUCTION

The neural precursor cell expressed developmentally downregulated gene 4-2 (*NEDD4-2*) is a seizure susceptibility gene with at least three missense mutations identified in epileptic patients (Dibbens et al., 2007; Allen et al., 2013; Vanli-Yavuz et al., 2015). Supporting evidence were also found in *Nedd4-2* knockout mouse models: deficiency of the major Nedd4-2 isoform in mouse brain caused elevated susceptibility to kainic acid-induced seizures (Zhu et al., 2017); neuronal absence of the Nedd4-2 C2-lacking isoform elevated the excitatory synaptic strength (Zhu et al., 2019); and haploinsufficiency of both isoforms increased the susceptibility to pentylenetetrazole (PTZ)-induced seizures in our previous study (Liu et al., 2021). As a highly expressed E3 ligase in the brain, NEDD4-2 could ubiquitinate ion channels and neuroexcitability regulators to elicit proteasomal/lysosomal degradation or endosomal trafficking (Ekberg et al., 2007, 2014; Zhu et al., 2017, 2019; Liu et al., 2021).

The endoplasmic reticulum (ER) is an important organelle involved in the folding and quality control of secretory and membrane proteins. Dysregulation of protein processing in ER might induce ER stress, a condition with excessive ER accumulation of unfolded or misfolded proteins that have been observed in both human epilepsy and epileptic experimental models (Fu et al., 2020). ER stress caused could upregulate hepatic Nedd4-2 to induce an autophagic response to clear unfolded proteins (Wang et al., 2016). Recently, neuronal Nedd4-2 was found to elicit ER stress-associated translational suppression through interaction with ribosomal proteins and to modulate seizure susceptibility by integrating the ER stress responses (Eagleman et al., 2021; Lodes et al., 2022). These studies indicated a protective role of Nedd4-2 in relieving ER stress and seizures besides direct ubiquitination of neuroactive substrates. Moreover, an upregulation of retention in endoplasmic reticulum 1 (Rer1), an ER retrieval receptor that might contribute to ER stress, was found in our previous hippocampal proteomic analysis on the epileptic *Nedd4-2*$^{+/-}$ mice (Liu et al., 2021). A possible protective role of Nedd4-2 against ER stress and seizures *via* Rer1 was suspected.

RER1 acts as an ER quality control receptor at the *cis*-Golgi by retention of ER-resident proteins as well as unassembled subunits of transmembrane complexes through the coat protein I (COPI)-dependent pathway (Sato et al., 1995; Boehm et al., 1997). Structurally, it contains four transmembrane domains with both N- and C-terminus facing the cytosol (Füllekrug et al., 1997). A STPY motif, with the potential PY or TP/SP sequences for NEDD4-2 binding (Sudol and Hunter, 2000), could be found in its N-terminal domain. Rer1 could be modified by ubiquitination through an ER-localized E3 ligase of synoviolin in mouse fibroblasts (Tanabe et al., 2012). RER1 could likely be ubiquitinated by NEDD4-2 in the central nervous system. In addition, being thus far the only known ER-retention receptor through transmembrane domain-based signals, RER1 has cargoes identified far less than there should be. Rer1 retrieved Nav1.1 and Nav1.6 in the cerebellar Purkinje cells (Valkova et al., 2011) and nicotinic acetylcholine receptor (nACHR) at the neuromuscular junctions in mice (Valkova et al., 2017). RER1 was implicated in Alzheimer's disease, Charcot-Marie-Tooth disease, retinitis pigmentosa, and Parkinson's disease through impaired assembly and excessive ER accumulation of substrates, including γ-secretase complex (Kaether et al., 2007; Park et al., 2012), peripheral myelin protein 22 (Hara et al., 2014), rhodopsin (Yamasaki et al., 2014), and α-synuclein (Park et al., 2017). It is not known whether RER1 is implicated in epilepsy through some transmembrane ion channels or neurotransmitter receptors.

In the present study, *Nedd4-2*$^{+/-}$ mice were found intolerant to ER stress inducers and PTZ-induced seizures. RER1 was identified as a novel ubiquitination substrate of NEDD4-2 through a STPY motif and degraded through the proteasomal pathway. The interactome of Rer1 in the mouse hippocampus was explored by immunoprecipitation-mass spectrometry (IP-MS), among which the α1 subunit of the $GABA_A$ receptor was validated.

MATERIALS AND METHODS

Animals

The *Nedd4-2* knockout mouse line was constructed as described (Liu et al., 2021). Male heterozygous *Nedd4-2*$^{+/-}$ and wildtype C57BL/6J mice at 8–10 weeks of age were used in this study. The mice were housed in standard cages on a 12-h light-dark cycle with *ad libitum* access to food and water. All animal experiments conformed to *the Guide for the Care and Use of Laboratory Animals* (NIH Publication No. 8023, revised 1978) to minimize animal numbers and animal suffering. This study was approved by the Ethics Committees of the Shengjing Hospital of China Medical University (2021PS348K).

Drug Administration and Seizures Evaluation

Nedd4-2$^{+/-}$ and wildtype mice (n = 4 in each group) were intraperitoneally injected with 2 mg/kg of thapsigargin (Tg) (Adipogen, United States, #AG-CN2-0003) or saline vehicle for 6 h, and brain tissues were isolated to evaluate the expression of C/EBP homologous protein (CHOP). In the chronic PTZ-induced seizures, *Nedd4-2*$^{+/-}$ and wildtype mice underwent daily intraperitoneal injection with 1 mg/kg of Tg (n = 8 in each group), 2 mg/kg of salubrinal (MedChemExpress, China, #HY-15486, n = 8 in each group) or saline vehicle (n = 8 in each group) for 1 h, followed by 35 mg/kg of PTZ (Sigma, United States, #54-95-5). Mice were observed for 1 h after each PTZ injection, and the seizure scores were evaluated by researchers blinded to the genotype and pretreatment drugs according to the revised seven-point Racine scale (Van Erum et al., 2019): 0, whisker trembling; 1, sudden behavioral arrest; 2, facial jerks; 3, neck jerks; 4, clonic seizure (sitting); 5, tonic-clonic seizure (lying on belly); 6, tonic-clonic seizure (lying on side) and wild jumping; and 7, tonic extension leading to death. The experiment ended when the first mouse died at a score of 7 in each pretreatment group, and all animals were anesthetized by carbon dioxide and sacrificed by cervical dislocation for further analysis. Another group of *Nedd4-2*$^{+/-}$ and wildtype mice (n = 4 in each group) were induced

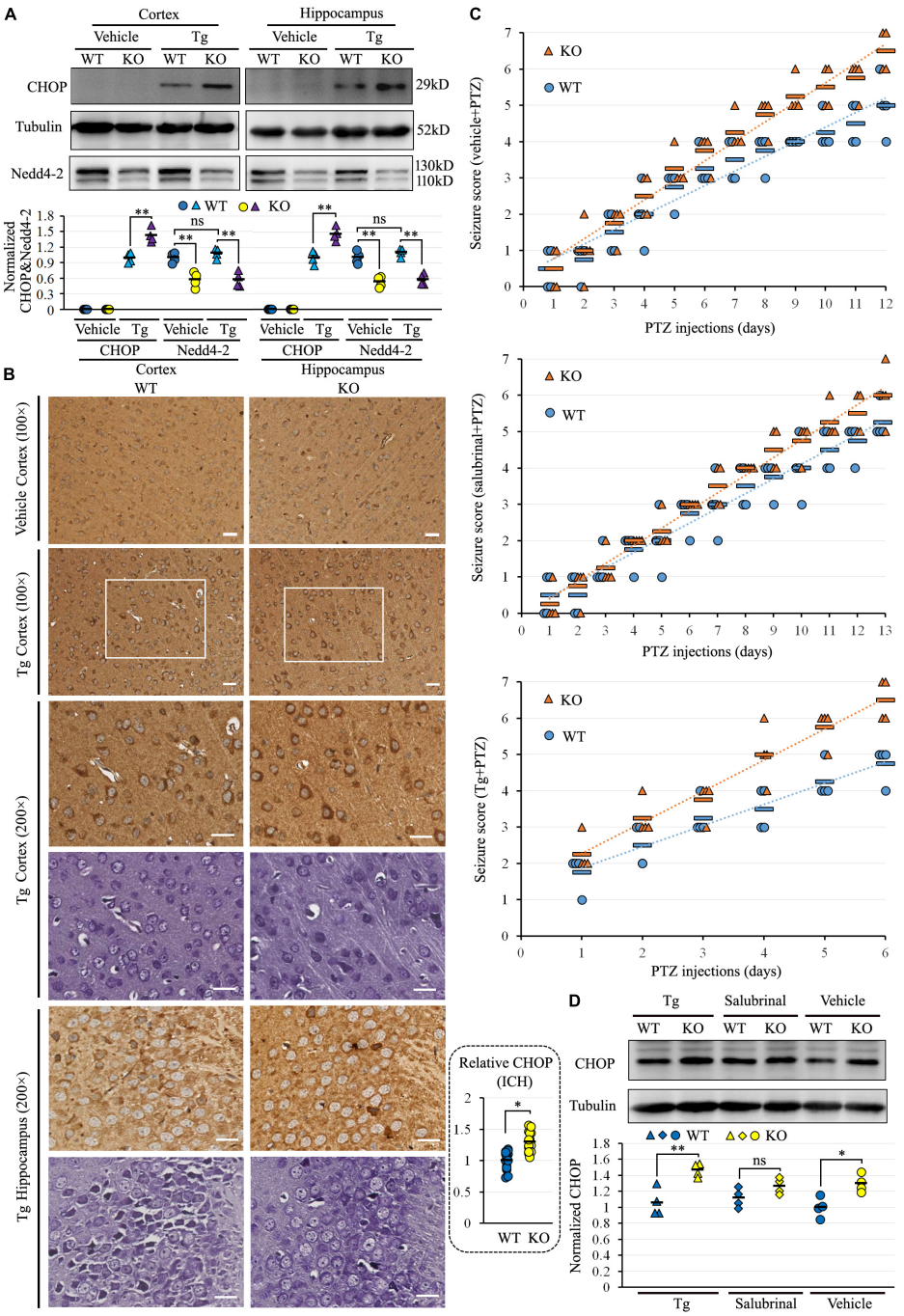

FIGURE 1 | *Nedd4-2*$^{+/-}$ (KO) mice were vulnerable to ER stress and pentylenetetrazole (PTZ)-induced seizures. **(A)** Western blot analysis of Nedd4-2 and the ER stress marker of CHOP in KO and wild-type (WT) mice (n = 4 in each group) with ER stress inducer of Tg (2 mg/kg) treatment for 6 h. The CHOP in the vehicle-treated group was undetectable and not analyzed. ns, not significant, $^{**}P < 0.01$ analyzed with 2-way ANOVA for Nedd4-2 and *post hoc* Tukey for CHOP. **(B)** Immunohistochemistry (ICH) of CHOP and Nissl staining on serial brain slices (cortex and hippocampus CA3 region) of mice with acute Tg induction. The CHOP signals (brown) were stronger in KO than WT mice, and co-localized to the Nissl staining (purple) signals. Scale bar: 20 μm. $^{*}P < 0.05$ by Student's t-test for the quantification (16 areas of 200 × 200 μm^2) by ImageJ. **(C)** Seizure scores were evaluated according to the Racine scale in mice with pretreatment of 1 mg/kg Tg, 2 mg/kg ER stress inhibitor of salubrinal, or vehicle control for 1 h, followed by PTZ (35 mg/kg) induction (n = 8 in each group). Tg treatment significantly elevated the seizure scores in 6 days of treatment (KO mice: P = 0.037 in Tg vs. Vehicle, P = 0.008 in Tg vs. salubrinal; WT mice: P = 0.045 in Tg vs. Vehicle, P = 0.020 in Tg vs. salubrinal analyzed using Kruskal–Wallis tests). Relatively higher seizure scores could be observed in KO mice over WT mice within each pre-treatment group, with no statistical significance analyzed by the Mann–Whitney U test. **(D)** Western blotting analysis of the CHOP expression in mouse brains at the end of chronic induction. The CHOP levels were higher in KO than WT mice in all three groups, with the most significant disparity in the Tg pretreatment group (n = 4 in each group). ns, not significant, $^{*}P < 0.05$, $^{**}P < 0.01$ compared with WT controls by *post hoc* Tukey analysis.

to chronic seizures by PTZ as described above for hippocampal IP-MS screening and validation.

Plasmid Construction and Cell Transfection

Human HA-tagged *NEDD4-2* (NM_015277), Flag-tagged *RER1* (NM_002241), and its TP37_38AA mutant expression vectors were constructed by GeneChem Co., Ltd., (China) Human *NEDD4-2*-targeted siRNAs were synthesized by GenePharma Co., Ltd., (China) Human neuroblastoma SH-SY5Y and glioma U251 cells were cultured with maximum passage number within 20. Cells were seeded in six-well plates for transfection with 2 μg of expression vectors, 0.5 μg of the siRNAs, or relevant vacant vectors using the Advanced DNA RNA Transfection Reagent (Zetalife, United States, #AD600150). Cells were administered with Tg (0.5 μM) or vehicle at 24 h post-transfection and incubated for an additional 24 h. The proteasomal inhibitor of MG132 (10 μM, Beyotime, China, #S1748), lysosomal inhibitor of leupeptin (10 μM, MedChemExpress, China, #HY-18234A), or solvent control were administered at 36 h post-transfection, for additional 12 h of incubation before harvesting. The protein synthesis inhibitor cycloheximide (CHX) (Sigma, #C7698) was administered at 100 μg/mL as appropriate.

Western Blotting

Total protein was extracted using RIPA lysis buffer from transfected cells or mouse brains. For the Endo-H digestion, the brain lysates were denatured with 0.5% SDS and 40 mM DTT at 100°C for 10 min and incubated with 0.5 U/ml Endo-H (New England Biolabs, United States,# P0702S) in 50 mM sodium acetate (pH 6.0) at 37°C for 1 h. Equal amounts of protein were separated by 10% SDS-PAGE electrophoresis and transferred to polyvinylidene fluoride membranes. The membranes were blocked for 2 h in TBST buffer containing 5% non-fat milk, and immunoblotted overnight at 4°C with anti-CHOP antibody (1:1,000, Proteintech, United States, #15204-1-AP), anti-NEDD4-2 antibody (1:1,000, Cell Signaling, United States, #4013), anti-RER1 (1:1,000, Novusbio, United States, #NBP1-59953), anti-Flag (1:2,000, Proteintech, #20543-1-AP), anti-GABRA1 (1:2,000, Proteintech, #12410-1-AP), anti-Ubiquitin (1:1,000, Proteintech, #10201-2-AP), anti-Tubulin (1:5,000, Proteintech, #11224-1-AP), or anti-GAPDH (1:5,000, Proteintech, #60004-1-Ig) as primary antibodies, followed by HRP-conjugated IgG (1:5,000, Proteintech, #SA00001-1 or #SA00001-2) as secondary antibodies at room temperature for 2 h. The bands were detected using SuperLumia ECL Kit (Abbkine, China, #K22020), and normalized to that of Tubulin or Gapdh as internal controls in the densitometry using Quantity One software version 5.0 (Bio-Rad Laboratories, United States). The relative density of the control group was normalized to "1."

Co-immunoprecipitation

The protein for co-immunoprecipitation (co-IP) was extracted using gentle RIPA lysis buffer from transfected cells and mouse brains and immunoprecipitated with 3 μg of anti-NEDD4-2 (Proteintech, #13690-1-AP), anti-RER1, anti-Flag, anti-HA (Proteintech, #51064-2-AP), anti-GABRA1 antibodies, or non-immune rabbit IgG (Proteintech, #B900610) in Protein A/G Magnetic beads (Bimake, United States, #B23202) by rotation at 4°C overnight. The immunoprecipitated protein was eluted from the beads using 2 × SDS sample buffer for subsequent electrophoresis on 10% SDS-PAGE gels and membrane transfer. Immunoblotting was performed using corresponding primary antibodies, followed by HRP-conjugated IgG as secondary antibodies. The IPKine HRP-conjugated IgG Light Chain Specific (Abbkine, #A25022) was applied as appropriate to avoid the interference of the antibody heavy chain.

Immunoprecipitation-Mass Spectrometry

Nedd4-2$^{+/-}$ and wild-type mice were induced into chronic seizures by PTZ as described above. The hippocampus was rapidly isolated for protein extraction using gentle RIPA lysis buffer, and immunoprecipitated using anti-RER1 antibodies as above. The eluted sample was reduced by 10 mM DTT, alkylated by 55 mM iodoacetamide, and digested in a trypsin solution (0.01 μg/μL in 25 mM ammonium bicarbonate, pH 8.9) overnight at 37°C. The resulting peptides were recovered by 50% acetonitrile and 0.5% formic acid, vacuum dried, and resuspended in 2% acetonitrile and 0.1% formic acid. The peptides were separated on a Dionex Ultimate 3000 nano liquid chromatography (LC) system through a reversed-phase C18 column (75 μm × 10 cm, 5 μm, 300 Å, Agela Technologies, China) by 400 nL/min flow rate of gradient: 0–6 min, 5%–8% solvent B (*B* = 95% acetonitrile, 0.1% formic acid); 6–40 min, 8%–30% buffer B; 40–45 min, 30%–60% buffer B; 45–48 min, 60%–80% buffer B; 48–56 min, 80% buffer B; 56–58 min, 80%–5% buffer B (decreasing to 5%); and 58–65 min, 5% Buffer B. LC was coupled with Q-Exactive mass spectrometer (Thermo Fisher, United States) setting in positive ion mode and data-dependent manner. A full MS scan from 350 to 2,000 m/z was acquired with a resolution of 70,000. In the MS/MS acquisition by higher collision energy dissociation, normalized collision energy was applied with a resolution of 17,500, a minimum signal threshold of 1e + 5, and an isolation width of 2 Da. Peptide identification was carried out using the Mascot software Version 2.3.01 (Matrix Science, United States). The proteomic data were assayed by gene ontology (GO) and Kyoto Encyclopedia of Genes and Genomes (KEGG) pathway enrichment. The software program Blast2GO was used and the annotations were retrieved from the online database([1]).

Immunohistochemistry and Nissl Staining

The Tg-induced *Nedd4-2*$^{+/-}$ and wild-type mouse brains were rapidly isolated and fixed in 10% neutral-buffered formalin at 4°C overnight. The tissues were embedded in low-temperature paraffin wax and sliced at 3 μm thick. Immunohistochemistry was performed by the avidin-biotin-peroxidase complex method using the VECTASTAIN ABC Kit (Vector Laboratories, United

[1] http://geneontology.org/

States, #PK-4000) according to the manufacturer's instructions, with anti-CHOP (1:100) as the primary antibody. Nissl staining was performed on the serial sections using Nissl Stain Solutions (Solarbio, China, #G14300). The photomicrographs were taken using an OLYMPUS IX51 inverted microscope.

Statistical Analysis

The quantitative data are presented as mean ± SEM and analyzed using SPSS version 23.0 for Windows. The Shapiro–Wilk test was used to verify the normal distribution of data. No test for outliers was conducted and no data point was excluded. The sample number was estimated from our previous study (Liu et al., 2021), and no power analysis was performed. The quantification of the IP experiment on proteins A and B was by the relative densitometry of IP:A IB:B to IP:A IB:A (both single and smeared bands were calculated for ubiquitination analysis), and *vice versa*. The quantification of the Western blot experiments was by the relative densitometry of target protein (both long and short isoform bands were calculated for Nedd4-2) to internal controls. Comparisons between quantitative variables were performed by Student's *t*-test, 2-way ANOVA, or *post hoc* Tukey analysis as appropriate. Comparisons between non-parametric data were performed by Mann–Whitney *U* test or Kruskal–Walls tests as appropriate. Fisher's exact test was employed in the GO and KEGG analyses of proteomic data. The $P < 0.05$ was considered to indicate statistical significance.

RESULTS

Nedd4-2$^{+/-}$ Mice Are Vulnerable to Endoplasmic Reticulum Stress and PTZ-Induced Seizures

We previously found the alteration of ER protein processing pathway in the proteomic analysis of *Nedd4-2*$^{+/-}$ mice (Liu et al., 2021). To address whether Nedd4-2 deficiency caused defects in maintaining ER homeostasis, *Nedd4-2*$^{+/-}$ and wild-type mice were intraperitoneally injected with the ER stress inducer of Tg for 6 h and the ER stress marker of CHOP was determined by Western blotting (**Figure 1A**). The CHOP was undetectable in both cortex and hippocampus of *Nedd4-2*$^{+/-}$ and wild-type mice at basal condition (vehicle treatment) and was arose by Tg more significantly in *Nedd4-2*$^{+/-}$ mice than wild-type controls. Immunohistochemistry (**Figure 1B**) on brain slices also showed stronger staining signals of CHOP in the cortex and hippocampus of *Nedd4-2*$^{+/-}$ mice than wild-type controls. The CHOP is mainly localized to the Nissl body-positive cells stained on serial sections. Therefore, *Nedd4-2*$^{+/-}$ mice were susceptible to ER stress in the brain.

To evaluate the role of Nedd4-2 in chronic ER stress and seizure susceptibility, *Nedd4-2*$^{+/-}$ and wild-type mice underwent daily intraperitoneal injection with Tg, ER stress inhibitor of salubrinal, or saline vehicle for 1 h, followed by subthreshold PTZ induction. The seizure scores were recorded according to the revised Racine scale after each injection until the first mouse in each pretreatment group died at score 7 (**Figure 1C**). Tg seriously aggravated the seizures by early kindling on the 2nd day and death on the 6th day compared with vehicle (kindling on the 5th day and death on the 12th day) and salubrinal (kindling on the 7th day and death on the 13th day) treatments. The seizure scores in the first 6 days were significantly higher in the Tg-pretreatment mice compared with the vehicle- and salubrinal-pretreatment mice ($P < 0.05$). Although, without statistical significance, we could observe relatively higher seizure scores in the *Nedd4-2*$^{+/-}$ mice over the wild-type controls in each pre-treatment group, with the disparities seemingly weakened by salubrinal and strengthened by Tg. The CHOP expression at the end of PTZ induction was assayed in the brain by Western blotting (**Figure 1D**), showing positive expression and relatively higher levels in *Nedd4-2*$^{+/-}$ than wild-type mice in all the three groups. The disparity of CHOP levels was also the most significant in the Tg-pretreatment group. The CHOP levels were not variable among the three groups, possibly because of the unequal injection numbers. Collectively, *Nedd4-2*$^{+/-}$ mice were vulnerable to ER stress in the brain, which might contribute to chronic PTZ-induced seizures.

Rer1 Is Upregulated Through Impaired Ubiquitination and Association With Nedd4-2 in *Nedd4-2*$^{+/-}$ Mice

There was an increase of Rer1 by 1.98-fold in *Nedd4-2*$^{+/-}$ mice over wild-type control in the previous proteomic data (Liu et al., 2021). We first validated the upregulation of Rer1 by Western blotting (**Figure 2A**). In response to approximately half decrease of Nedd4-2, Rer1 was significantly increased to about 1.7-fold in the cortex and hippocampus of PTZ-induced *Nedd4-2*$^{+/-}$ mice compared with wild-type controls. The mRNA expression of Rer1 was assayed by quantitative real-time PCR, showing almost equivalent levels between *Nedd4-2*$^{+/-}$ and wild-type mice (data not shown).

To investigate whether the post-translational upregulation of Rer1 in *Nedd4-2*$^{+/-}$ mice was through impaired ubiquitination, the Rer1-immunoprecipitated brain lysates were immunoblotted with anti-ubiquitin antibodies, showing isolated and smeared immunoblotting bands which were reduced in *Nedd4-2*$^{+/-}$ mice compared with wild-type controls (**Figure 2B**). The interaction between Nedd4-2 and Rer1 was also investigated by co-IP (**Figure 2C**), showing the Rer1-immunoprecipitated brain lysates could be immunoblotted with Nedd4-2, and *vice versa*. Comparatively, the blotting bands in *Nedd4-2*$^{+/-}$ mice were weakened to about 60% of wild-type controls. Furthermore, in mice with an intraperitoneal injection of Tg for 6 h (**Figure 2D**), the interactive bands were significantly enhanced by Tg over vehicle control in wild-type mice but were much less responsive to Tg in *Nedd4-2*$^{+/-}$ mice. Together, these data indicated impaired Nedd4-2-mediated ubiquitination of Rer1 and ER-stress responsive interaction between Nedd4-2 and Rer1 in *Nedd4-2*$^{+/-}$ mice.

NEDD4-2 Ubiquitinates RER1 Especially Under Endoplasmic Reticulum Stress *in vitro*

Human-cultured neuroblastoma SH-SY5Y and glioma U251 cells, with endogenous expression of both NEDD4-2 and RER1,

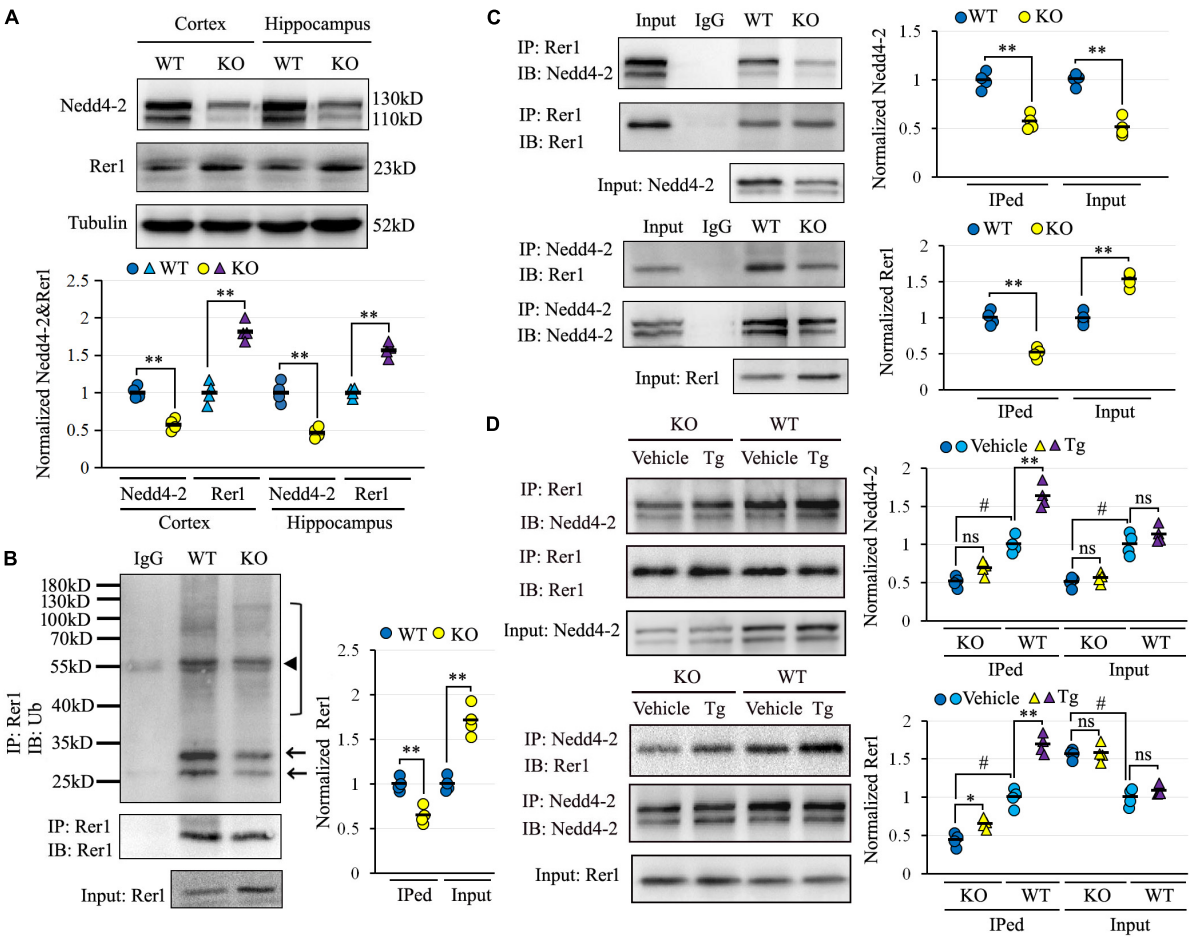

FIGURE 2 | Impaired Nedd4-2-mediated and ER stress-responsive ubiquitination of Rer1 in *Nedd4-2*$^{+/-}$ mice. **(A)** Western blot analyses of Rer1 and Nedd4-2 in brain cortex and hippocampus of *Nedd4-2*$^{+/-}$ (KO) and wild-type (WT) mice (n = 4 in each group). $^{**}P < 0.01$ compared with WT controls by Student's t-test. **(B)** Ubiquitination of Rer1 in mouse brain lysates immunoprecipitated with Rer1 antibodies and immunoblotted with ubiquitin antibodies (n = 4 in each group). The arrows and bracket indicate the ubiquitinated Rer1. The triangle indicates the heavy chain of IgG. $^{**}P < 0.01$ compared with WT controls by Student's t-test. **(C)** Co-immunoprecipitation (co-IP) analysis for the interaction of Rer1 and Nedd4-2 in mouse brain lysates (n = 4 in each group). $^{**}P < 0.01$ compared with WT controls by Student's t-test. **(D)** Co-IP analysis of Rer1 and Nedd4-2 in mice with 2 mg/kg ER stress inducer of Tg for 6 h (n = 4 in each group). ns, not significant, $^{*}P < 0.05$, $^{**}P < 0.01$ compared with vehicle group; $\#P < 0.01$ compared with WT group by *post hoc* Tukey's analysis.

were used to investigate the NEDD4-2-mediated ubiquitination of RER1 *in vitro*. The negative regulation of NEDD4-2 on RER1 was first assayed by Western blotting. Cells transfected with three siRNAs against NEDD4-2 showed varied knockdown efficiencies, and the RER1 was increased correspondingly. For example, the half decrease of NEDD4-2 by siRNA3 increased RER1 to about 1.8-fold over the controls (**Figure 3A**). On the other hand, the cells underwent co-transfection of RER1-Flag with either NEDD4-2-HA or a vacant vector. In response to the overexpression of NEDD4-2, RER1 was significantly brought down to nearly half the level of vacant control in both cells by Western blotting (**Figure 3B**).

The ubiquitination of RER1 was assayed in the RER1-Flag and NEDD4-2-HA overexpressed SH-SY5Y and U251 cells. The immunoprecipitated cell lysates with anti-Flag antibodies were immunoblotted with anti-ubiquitin antibodies, showing mainly isolated bands that were significantly increased by NEDD4-2 compared with vacant vector controls (**Figure 3C**). The interplay between NEDD4-2 and RER1 was furthermore assayed by co-IP in the overexpressed cells, with or without Tg treatment post-transfection (**Figure 3D**). The Flag-immunoprecipitated cell lysates could be immunoblotted with anti-HA antibodies, and *vice versa*. Moreover, the interactive bands were enhanced by Tg compared with vehicle controls in both cell lines. Together, we identified a negative regulation of RER1 by NEDD4-2 through ubiquitination, especially under ER stress *in vitro*.

RER1 Interacts With NEDD4-2 Through a ^{36}STPY^{39} Motif and Undergoes the Proteasomal Degradation

Since NEDD4-2 binds to substrates containing PY or TP/SP motifs, the ^{36}STPY^{39} sequence of RER1 in the N-terminal intracellular domain was disrupted by generating a TP37_38AA

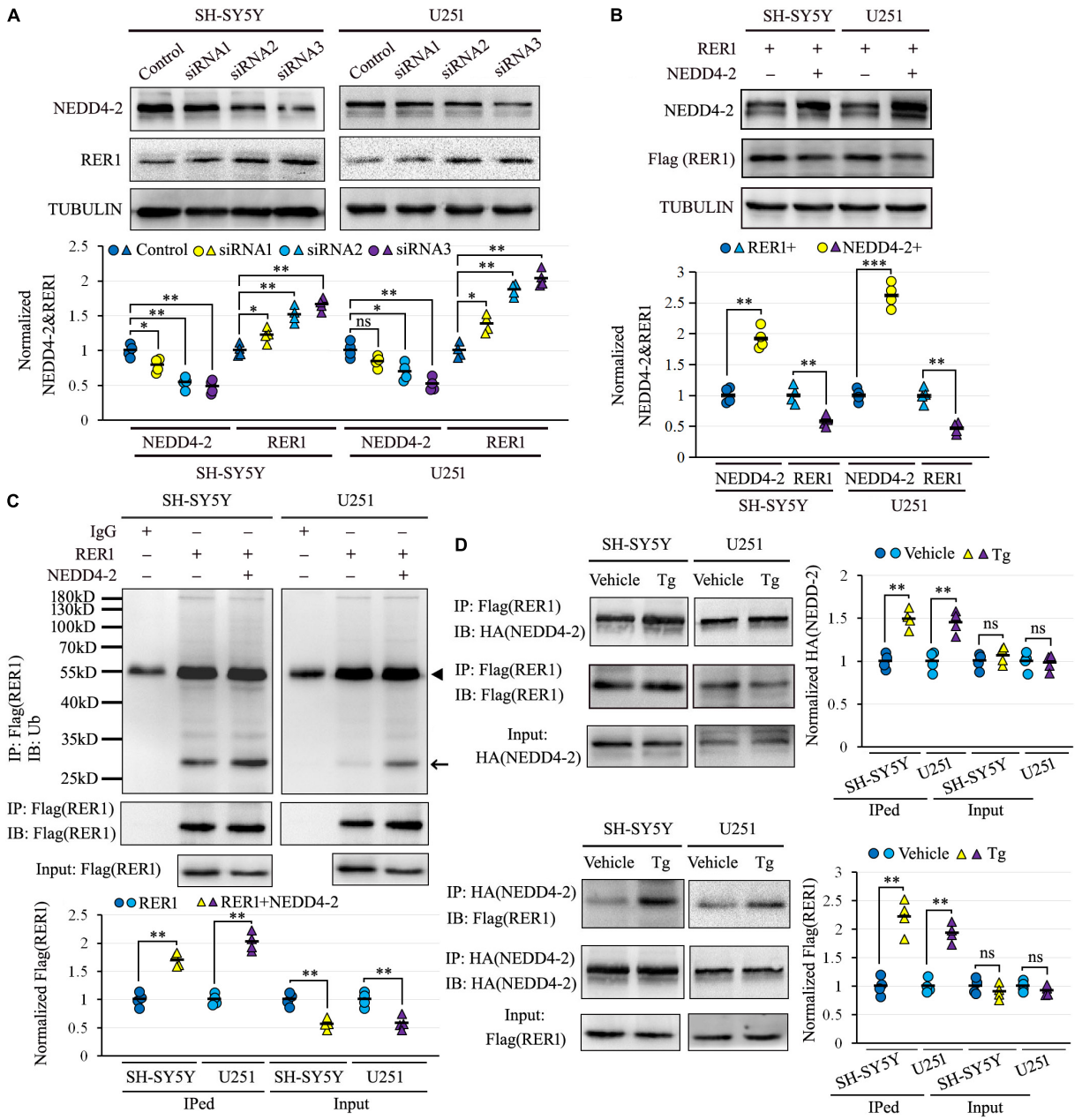

FIGURE 3 | NEDD4-2 ubiquitinated RER1, especially under ER stress *in vitro*. **(A)** Western blotting of RER1 and NEDD4-2 in SH-SY5Y and U251 cells treated with NEDD4-2 siRNAs ($n = 4$ independent cell preparations). ns, not significant, $^{*}P < 0.05$, $^{**}P < 0.01$ compared with the control cells by *post hoc* Tukey's analysis. **(B)** Western blotting of RER1 and NEDD4-2 in SH-SY5Y and U251 cells co-transfected with RER1-Flag and NEDD4-2-HA or vacant vectors ($n = 4$ independent cell preparations). $^{**}P < 0.01$, $^{***}P < 0.001$ compared with the control cells by Student's *t*-test. **(C)** Ubiquitination of RER1 in the co-transfected cells immunoprecipitated with Flag antibodies and immunoblotted with ubiquitin antibodies ($n = 4$ independent cell preparations). The ubiquitinated Flag-tagged RER1 is indicated by an arrow. The heavy chain of IgG is indicated by a triangle. $^{**}P < 0.01$ compared with the control cells by Student's *t*-test. **(D)** Co-immunoprecipitation analysis for the interaction of NEDD4-2 and RER1 using anti-Flag and anti-HA antibodies in the transfected cells with or without Tg (0.5 μM) treatment ($n = 4$ independent cell preparations). ns, not significant, $^{**}P < 0.01$ compared with vehicle group by Student's *t*-test.

mutant construct (**Figure 4A**). The Flag-tagged mutant and wild-type RER1 were co-transfected with the NEDD4-2-HA expression vector into SH-SY5Y and U251 cells. In the co-IP (**Figure 4B**), the interactions of NEDD4-2 with the mutant RER1 were attenuated to about 30–40% of wild-type controls in both cells. The protein synthesis inhibitor of CHX was furthermore applied to the cells after co-transfection of NEDD4-2 with wild-type and mutant RER1. The mutant RER1 sustained at higher levels after 3 h and 6 h of CHX treatment compared with the wild-type control by Western blotting (**Figure 4C**), indicating

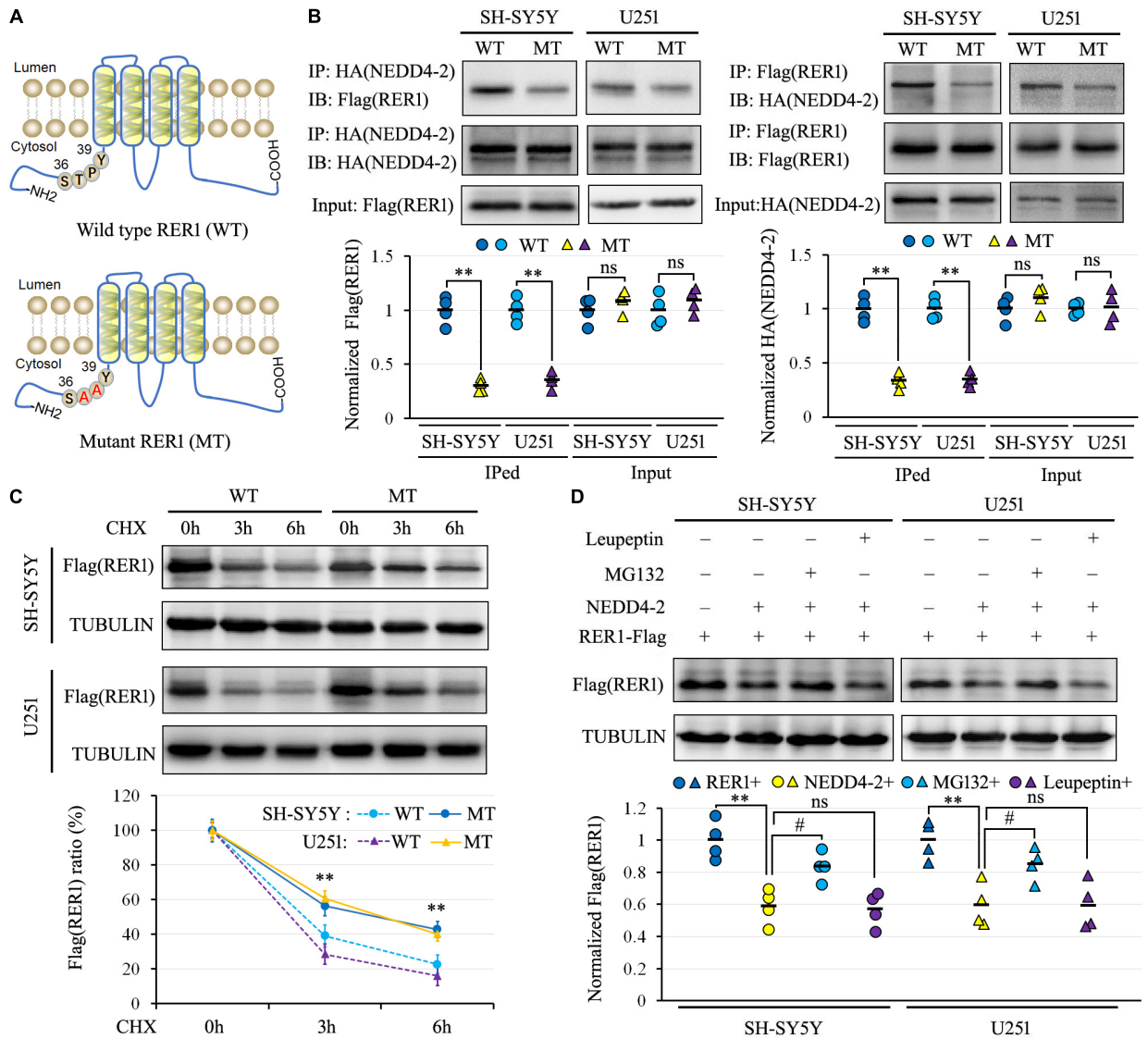

FIGURE 4 | NEDD4-2 interacted with the ^{36}STPY^{39} motif of RER1 to elicit proteasomal degradation. **(A)** The schematic depiction of the wild-type (WT) and TP37_38AA mutant (MT) RER1. **(B)** Co-immunoprecipitation analysis for the interaction of NEDD4-2 and RER1 in co-transfected SH-SY5Y and U251 cells (n = 4 independent cell preparations). $^{**}P < 0.01$ compared with WT control by Student's t-test. **(C)** The stability analysis of RER1 in co-transfected cells with 100 μg/mL CHX treatment by Western blotting (n = 4 independent cell preparations). $^{**}P < 0.01$ compared with WT control by *post hoc* Tukey's analysis. **(D)** Western blot analysis of RER1 in co-transfected cells treated with a proteasomal inhibitor of MG132 (10 μM) or lysosomal inhibitor of leupeptin (10 μM) (n = 4 independent cell preparations). $^{**}P < 0.01$ compared with vacant vector controls; ns, not significant, #, $P < 0.05$ compared with the vehicle treatment by *post hoc* Tukey's analysis.

the TP37_38AA mutation partially abolished the NEDD4-2-mediated ubiquitination and degradation.

In addition, the protein degradation pathway of RER1 was investigated in transfected SH-SY5Y and U251 cells using a proteasomal inhibitor of MG132 or a lysosomal inhibitor of leupeptin. As shown in **Figure 4D** by Western blotting, the expression levels of RER1 were decreased by NEDD4-2 to about 60% of vacant controls. The reductions of RER1 were restored to about 85% of control levels by MG132, but not by leupeptin. Thus, NEDD4-2 binds to the ^{36}STPY^{39} motif of RER1 to elicit proteasomal degradation.

Interactome of Rer1 in PTZ-Induced Mouse Hippocampus by Immunoprecipitation-Mass Spectrometry

To uncover potential Rer1-dependent cargoes that might participate in seizure susceptibility, we investigated the interactome of Rer1 by IP-MS in *Nedd4-2*$^{+/-}$ and wild-type mice with chronic PTZ-induced seizures. The hippocampus lysates were immunopurified using Rer1 antibodies and analyzed by LC-MS/MS. With the IgG immunoprecipitated proteins

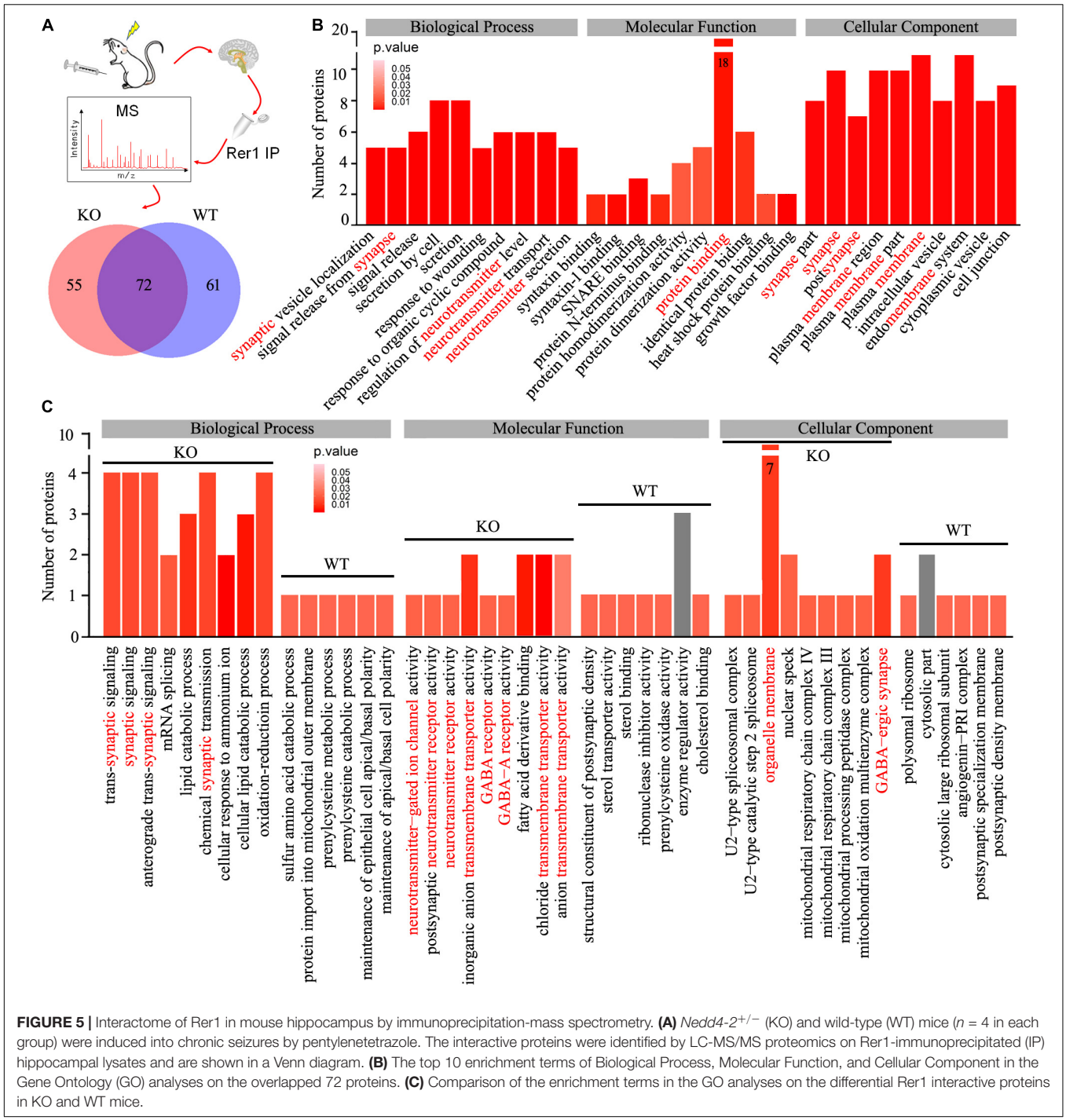

FIGURE 5 | Interactome of Rer1 in mouse hippocampus by immunoprecipitation-mass spectrometry. **(A)** *Nedd4-2*$^{+/-}$ (KO) and wild-type (WT) mice (n = 4 in each group) were induced into chronic seizures by pentylenetetrazole. The interactive proteins were identified by LC-MS/MS proteomics on Rer1-immunoprecipitated (IP) hippocampal lysates and are shown in a Venn diagram. **(B)** The top 10 enrichment terms of Biological Process, Molecular Function, and Cellular Component in the Gene Ontology (GO) analyses on the overlapped 72 proteins. **(C)** Comparison of the enrichment terms in the GO analyses on the differential Rer1 interactive proteins in KO and WT mice.

subtracted as non-specific background, the proteins consistently present in all the four biological replicates of each group were defined as positive. Overall, the Rer1-interacted proteins were 127 in *Nedd4-2*$^{+/-}$ and 133 in wild–type mice, among which 72 overlapped in both groups (**Figure 5A**). GO analyses on the overlapped proteins showed enriched terms of "protein binding" in Molecular Function, "neurotransmitter" and "synapse" in Biological Process, as well as "membrane" and "synapse" in Cellular Component (**Figure 5B**). These interactive proteins were shown in **Supplementary Table 1**, including a previously identified Rer1 cargo of Snca (α-synuclein) (Park et al., 2017), as well as some ER-resident proteins (Pdia3, Rtn3, Rtn4) and chaperones (Hspa8, Hspa9, Dnaja1, Canx).

We are interested in the 55 differential interactive proteins in *Nedd4-2*$^{+/-}$ mice with increased Rer1 expression and seizures. Compared with the wild-type group by GO analyses,

more proteins were enriched in terms containing "synaptic," "neurotransmitter receptor," and "transmembrane transporter" (**Figure 5C**). These 55 differential proteins in *Nedd4-2*$^{+/-}$ mice (**Table 1**) included multiple neurotransmitter receptors and synaptic regulators (Gabra1, Gria1, Snap47, Slc12a5, Plcb1, Phf24, Nbea, Kif1a, Syn1) as well as Copb1, a component of COPI which mediate the retrograde trafficking of Rer1 (Boehm et al., 1997). These data provided potential cargoes of Rer1 that might be involved in increased seizure susceptibility of *Nedd4-2*$^{+/-}$ mice.

The α1 Subunit of GABA$_A$ Receptor Interacts With Rer1 and Retains in Endoplasmic Reticulum in *Nedd4-2*$^{+/-}$ Mice

The α1 subunit of GABA$_A$ receptor (Gabra1), which belongs to the same Cys-loop receptor family (Hernandez and Macdonald, 2019) as a confirmed Rer1 cargo of nAChR (Valkova et al., 2011), was chosen for validation by co-IP. As shown in **Figure 6A**, Rer1-immunoprecipitated brain lysates showed positive immunoblotting bands with both Nedd4-2 and Gabra1. In contrast to the weaker interaction with Nedd4-2, the blotting band was stronger with Gabra1 in *Nedd4-2*$^{+/-}$ mice compared with wild-type controls. The reverse immunoprecipitation with Gabra1 also showed stronger immunoblotting bands with Rer1 in *Nedd4-2*$^{+/-}$ mice than wild-type controls. These data confirmed the interaction of Rer1 with the α1 subunit of the GABA$_A$ receptor, which was increased in *Nedd4-2*$^{+/-}$ mice.

We next evaluated the ER retention of the α1 subunit of the GABA$_A$ receptor by Endo-H digestion, which is known to remove the ER-modified high mannose N-linked carbohydrates (Helenius and Aebi, 2004). As shown in **Figure 6B** by Western blotting, the α1 subunit of the GABA$_A$ receptor was expressed at slightly lower levels in undigested brain lysates of *Nedd4-2*$^{+/-}$ mice than wild-type controls. On the contrary, the Endo-H digested bands, with reductions in molecular weight from the monomer as well as a possible dimer form, were significantly higher in *Nedd4-2*$^{+/-}$ mice compared with wild-type controls. Therefore, the α1 subunit of the GABA$_A$ receptor interacted with Rer1 and was retained in ER more heavily in *Nedd4-2*$^{+/-}$ mice.

TABLE 1 | Differential interactive proteins of Rer1 in the hippocampus of PTZ-induced *Nedd4-2*$^{+/-}$ mice.

Gene name	Protein description
Acad9	Acyl-CoA dehydrogenase family member 9, mitochondrial
Acadl	Long-chain specific acyl-CoA dehydrogenase, mitochondrial
Ahcyl1	Adenosylhomocysteinase
Bcan	Brevican core protein isoform X3
C1qa	Complement C1q subcomponent subunit A
Cct5	T-complex protein 1 subunit epsilon
Cct6a	T-complex protein 1 subunit zeta
Copb1	Coatomer subunit beta, also known as the coat protein complex 1
Cops2	COP9 signalosome complex subunit 2
Ctbp1	C-terminal-binding protein 1
Ctsb	Cathepsin B
Ddx6	Probable ATP-dependent RNA helicase DDX6
Echs1	Enoyl-CoA hydratase, mitochondrial isoform X2
Eps15l1	Epidermal growth factor receptor substrate 15-like 1
Ewsr1	RNA-binding protein EWS isoform X4
G3bp2	Ras GTPase-activating protein-binding protein 2 isoform X1
Gabra1	Gamma-aminobutyric acid receptor subunit alpha-1
Git1	ARF GTPase-activating protein GIT1 isoform X2
Gria1	Glutamate receptor
Hadha	Trifunctional enzyme subunit alpha, mitochondrial
Kbtbd11	Kelch repeat and BTB domain-containing protein 11
Kif1a	Kinesin-like protein KIF1A
LOC110288534	Tubulin alpha-1 chain-like
LOC110300684	ATP synthase membrane subunit f
LOC110310287	Cytochrome c1, heme protein, mitochondrial
Lta4h	Leukotriene A(4) hydrolase
Map4	Microtubule-associated protein
Myh10	Myosin-10
Nbea	Neurobeachin
Nebl	Nebulette isoform X2
Ogt	*O*-GlcNAc transferase subunit p110
Pgm2l1	Glucose 1,6-bisphosphate synthase
Phf24	PHD finger protein 24 isoform X1
Plcb1	1-phosphatidylinositol 4,5-bisphosphate phosphodiesterase beta-1
Ppp2r1a	Serine/threonine-protein phosphatase 2A 65 kDa regulatory subunit A alpha isoform
Rptor	Regulatory-associated protein of mTOR
Psmc1	26S proteasome regulatory subunit 4
Psmd5	26S proteasome non-ATPase regulatory subunit 5
Purb	Transcriptional activator protein Pur-beta
Rasal1	RasGAP-activating-like protein 1
Rgs14	Regulator of G-protein signaling 14 isoform X1
Rplp0	60S acidic ribosomal protein P0
Rptor	Regulatory-associated protein of mTOR
Sfxn3	Sideroflexin-3
Slc12a5	KCC2a-S25 variant 1
Slc24a2	Sodium/potassium/calcium exchanger 2 isoform X4
Snap47	Synaptosomal-associated protein 47
Srrm2	Serine/arginine repetitive matrix protein 2
Sucla2	Succinate-CoA ligase subunit beta (Fragment)
Syn1	Synapsin I
Trim2	Tripartite motif-containing protein 2 isoform X2
Ubqln2	Ubiquilin-2
Uqcrc2	Cytochrome b-c1 complex subunit 2, mitochondrial
Vps51	Vacuolar protein sorting-associated protein 51 homolog
Wdr37	WD repeat-containing protein 37 isoform X2

DISCUSSION

We elaborated in the present study that *Nedd4-2*$^{+/-}$ mice were vulnerable to ER stress and chronic PTZ-induced seizures. Rer1 was upregulated through impaired ubiquitination in *Nedd4-2*$^{+/-}$ mice. NEDD4-2 ubiquitinated RER1 in response to ER stress, through binding to the ^{36}STPY^{39} motif of RER1 to elicit proteasomal degradation. The interactome screening of Rer1 revealed potential cargoes that mediate neuroexcitability, among which the α1 subunit of the GABA$_A$ receptor was validated to interact with Rer1 and retained in ER more seriously in *Nedd4-2*$^{+/-}$ mice (**Figure 7**).

NEDD4-2 has been known to be epilepsy-associated through the direct ubiquitination of neuroactive substrates. A new understanding of NEDD4-2 was proposed in ER stress, a status with excessive ER accumulation of unfolded or misfolded proteins. Cells elicit the activation of unfolded protein response (UPR) involving global translational suppression and controlled

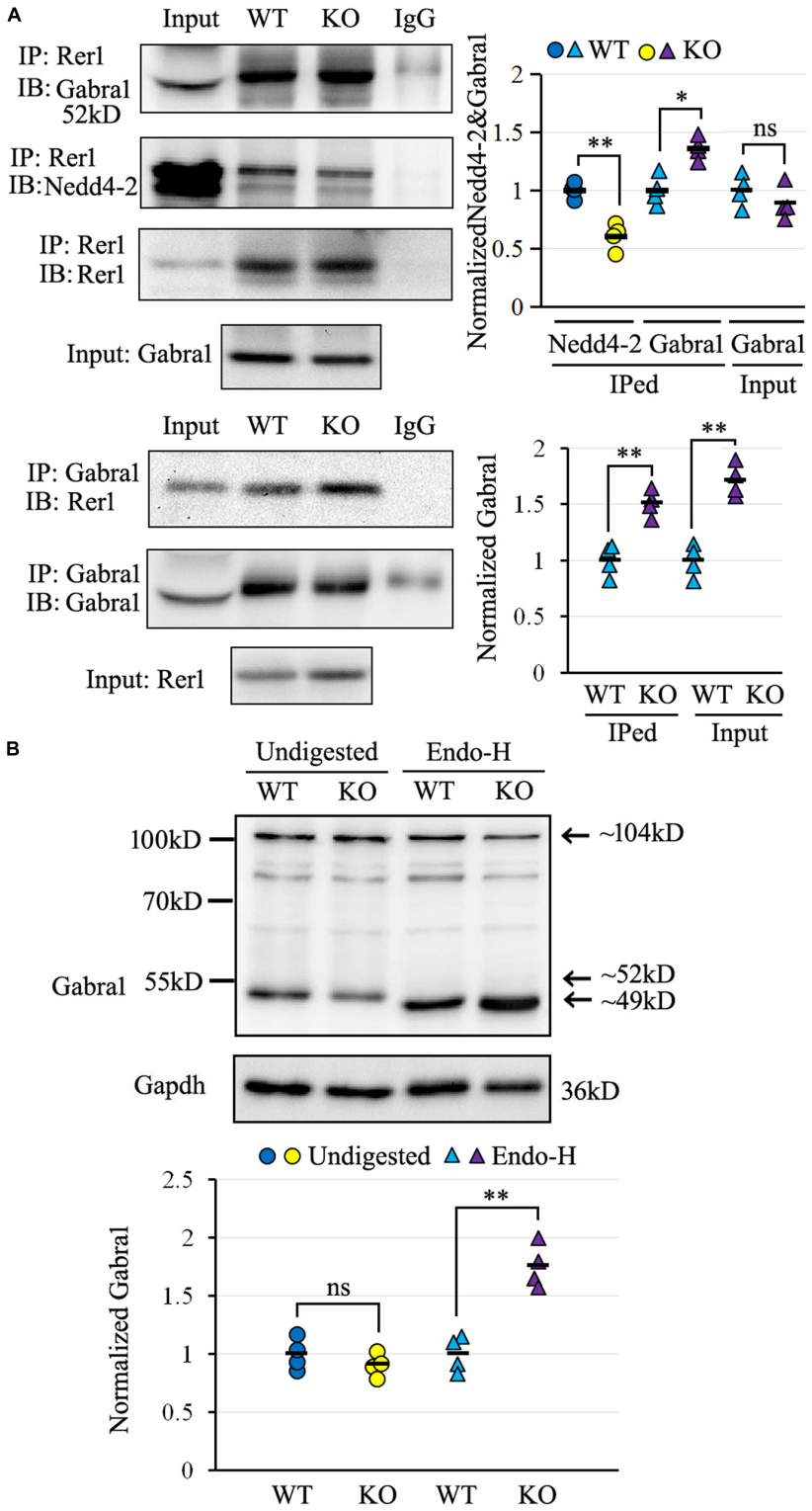

FIGURE 6 | The α1 subunit of $GABA_A$ receptor (Gabra1) interacted with Rer1 and was retained in ER more heavily in *Nedd4-2*$^{+/-}$ (KO) mice than wild-type (WT) control. **(A)** Co-immunoprecipitation analysis for the interaction of Rer1 with Gabra1 and Nedd4-2 in mouse brain lysates ($n = 4$ in each group). *$P < 0.05$, **$P < 0.01$ compared with WT controls by Student's *t*-test. **(B)** Western blotting analysis of Gabra1 in the brain lysates with or without Endo-H digestion ($n = 4$ in each group). The Endo-H digested bands represent the ER retention of Gabra1 by removing the ER-modified high mannose N-linked carbohydrates and reducing the molecular weight (around 49 kD) from the monomer (around 52 kD) as well as a possible dimer (around 104 kD). ns, not significant, **$P < 0.01$ compared with WT controls by Student's *t*-test.

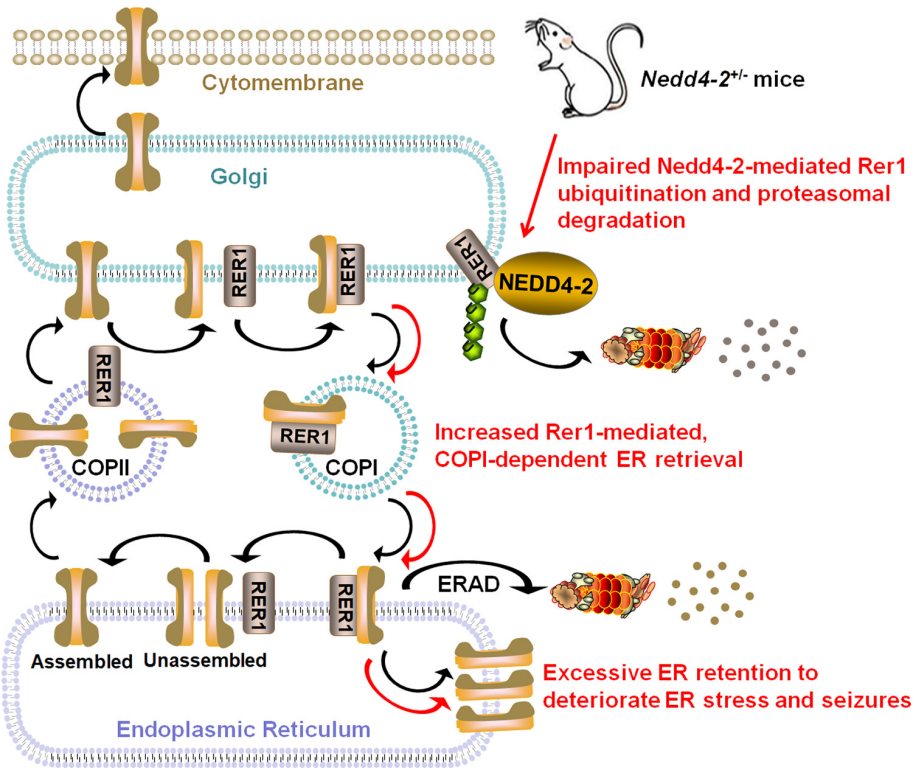

FIGURE 7 | Schematic diagram showing that Nedd4-2 deficiency in mice increases ER stress and seizure susceptibility possibly through impaired ubiquitination of Rer1. The *cis*-Golgi localized Rer1 retrieves unassembled subunits back to ER for further assembly or ER-associated degradation (ERAD) through a coat protein I (COPI)-dependent pathway. The interactome screening of Rer1 showed potential cargoes that mediate neuroexcitability, among which excessive Rer1-dependent ER retention of the α1 subunit of the $GABA_A$ receptor was found in *Nedd4-2*$^{+/-}$ mice.

degradation of misfolded proteins to counteract ER stress (Cao and Kaufman, 2014). NEDD4-2 seemed to take part in both UPR machineries: degradation of unfolded proteins through autophagy (Wang et al., 2016) and translational suppression through association with ribosomal proteins (Eagleman et al., 2021). NEDD4-2 was recently reported to integrate the ER stress response to modulate seizure susceptibility (Lodes et al., 2022). We also found the changes in ER protein processing pathway in the proteomic analysis of *Nedd4-2*$^{+/-}$ mice with increased seizure susceptibility (Liu et al., 2021). These collectively indicated the possible role of Nedd4-2 against ER stress and seizures, which deserves further investigation. Herein, *Nedd4-2*$^{+/-}$ mice showed vulnerability to ER stress in the brain induced by Tg. It is accepted that chronic ER stress and seizures mutually deteriorate, in that epileptogenic insults result in excitotoxicity which is a potential source of ER stress, and long-term ER stress promotes neuronal loss that is implicated in epileptogenesis (Fu et al., 2020). Whereas acute ER stress response played a beneficial role in repressing neural activity and seizure severity (Liu et al., 2019). In our study, the CHOP was undetectable in the brain at basal condition but positive after chronic PTZ-induction, indicating an ER stress status elicited by chronic seizures. The seizures were significantly deteriorated by Tg pretreatment, indicating a contributive role of ER stress in chronic seizures. Moreover, *Nedd4-2*$^{+/-}$ mice showed higher CHOP and seizures than the wild-type group. Although we did not obtain statistical significance possibly because of limited sample sizes, the disparities of seizures were seemingly weakened by salubrinal pretreatment and strengthened by Tg pretreatment. Our data indicate that Nedd4-2 insufficiency compromised the resistance to ER stress and chronic seizures, supporting the protective role of Nedd4-2 against ER stress and seizures.

RER1 is a guarding receptor at the early-Golgi for ER quality control, in that it recognizes misfolded/immature/unassembled subunits and retrieves them back to ER for either ER-associated degradation (ERAD) or appropriate assembly. Under some pathological conditions, however, RER1 is implicated in the excessive accumulation of wild-type or mutant substrates that triggers ER stress (Annaert and Kaether, 2020). Rer1 was found upregulated in *Nedd4-2*$^{+/-}$ mouse brain. RER1 was also negatively regulated by NEDD4-2 knockdown and overexpression in cultured neurocytes and gliacytes. The ubiquitination of RER1 by NEDD4-2 was confirmed by a series of ubiquitination and co-IP experiments *in vivo* and *in vitro*. The interaction between NEDD4-2 and RER1 was enhanced by the ER stress inducer. The disruption of the ^{36}STPY^{39} motif in the N-terminal cytosolic domain of RER1 attenuated the binding with NEDD4-2 and sustained long after the blocking of

protein synthesis. Finally, the ubiquitinated RER1 by NEDD4-2 underwent degradation through the proteasomal pathway. To our best knowledge, the above data indicated for the first time a role of NEDD4-2 against ER stress *via* ubiquitination of RER1 and clarified the detailed molecular mechanisms.

RER1 is implicated in human diseases through abnormal intracellular trafficking and excessive ER accumulation of cargo proteins. Systemic and brain-specific knockout of Rer1 in mice caused prenatal and early postnatal lethality, respectively (Valkova et al., 2017; Hara et al., 2018). Extracerebral ion channels of Nav1.1, Nav1.6 (Valkova et al., 2011), nACHR, (Valkova et al., 2017), and rhodopsin (Yamasaki et al., 2014) have been identified as cargoes of RER1. RER1 might likely be involved in epilepsy through ER retention of cerebral ion channels. We performed an IP-MS-based proteomic analysis on the PTZ-induced *Nedd4-2*$^{+/-}$ and wild-type mouse hippocampus to explore the repertoire of interactive proteins. The overlapped proteins mainly fell within the currently acknowledged functions of Rer1 in protein binding of membrane proteins. An important role of RER1 in ER quality control is to retrieve escaped ER-resident proteins (Sato et al., 1995). We identified ER-resident proteins of Pdia3, Rtn3, and Rtn4 in both groups of mice, which deserves further validation. The ER lumen is filled with ER chaperones that usually facilitate protein processing and regulate ER signaling in response to ER stress (Ni and Lee, 2007). We found ER chaperones of Hspa8, Hspa9, Dnaja1, and Canx in both groups, which might facilitate Rer1 to dissociate the retrieved cargos in ER or to cycle back to Golgi through COPII. We also reproduced the known cargo of α-synuclein (Park et al., 2017) and the interactor of the COPI component (Boehm et al., 1997). The differential proteins in *Nedd4-2*$^{+/-}$ mice with an overdose of Rer1 might be informative for seizure susceptibility. Intriguingly, these proteins were more related to "synaptic," "neurotransmitter receptor," and "transmembrane transporter" by GO analyses. In detail, Gabra1 and Gria1 are the α1 subunits of the major inhibitory $GABA_A$ and excitatory glutamate neurotransmitter receptors, respectively. Snap47 is an atypical member of the SNAP family that does not localize specifically to surface membranes, but to the cytoplasm, ER, and ERGIC, and shuttles between the cytoplasm and the nucleus (Kuster et al., 2015). It also localizes in the pre- and postsynaptic compartments of glutamatergic and GABAergic neurons and may be involved in intracellular vesicle trafficking and fusion events (Münster-Wandowski et al., 2017). Slc12a5 encodes neuron-specific K^+-Cl^- cotransporter 2 (KCC2), the main Cl^- extruder to maintain the function of the inhibitory neurotransmitters GABA and glycine (Fukuda and Watanabe, 2019). Some disease-causing mutations of KCC2 affected the surface transport, whereas the exact trafficking signals were not defined (Tang, 2016). Phf24 is expressed in the presynaptic terminals, synaptic membranes, and cytoplasmic matrix of neuronal soma of the inhibitory interneurons (Numakura et al., 2021). It acts as an inhibitory modulator in epileptogenesis through association with the $GABA_B$ receptor, the most abundant inhibitory G protein (Gi/o)-coupled receptors in the mammalian brain (Serikawa et al., 2019). Nbea encodes a multidomain scaffolding protein located at the tubulovesicular endomembranes near the *trans*-Golgi network and is involved in neuronal post-Golgi membrane trafficking (Volders et al., 2011). It regulates synaptic transmission under basal conditions by targeting glutamate and $GABA_A$ neurotransmitter receptors to synapses (Nair et al., 2013). Synapsin I is the most abundant phosphoprotein and a key regulator of synaptic vesicle dynamics in presynaptic terminals (Shupliakov et al., 2011). It synchronizes the release of GABA in distinct interneuron subpopulations (Forte et al., 2020). These potential interactive proteins of neuroexcitability regulators might be the important targets for possible involvement of Rer1 in seizures.

The pentameric $GABA_A$ receptors are the major inhibitory neurotransmitter receptors that are assembled in ER. Only the appropriate $GABA_A$ receptor complexes undergo anterograde trafficking to access the cell surface (Kittler et al., 2002). Mutations identified in epilepsy, mainly in genes encoding subunits of $GABA_A$ receptors, undermine intracellular trafficking that may lead to ER retention, ER stress, and neuronal degeneration (Hirose, 2006). We chose the α1 subunit of the $GABA_A$ receptor for validation in the present study by two reasons: ① $GABA_A$ receptors belong to the Cys-loop receptor family (Hernandez and Macdonald, 2019), among which the α subunit of nAChR has been confirmed to be a cargo of Rer1 (Valkova et al., 2011); ② The A322D mutation in *GABRA1*, which introduces a negatively charged aspartate residue into the hydrophobic M3 transmembrane domain of the α1 subunit, had been identified with reduced total and surface subunit expression and increased ER retention (Gallagher et al., 2005; Fu et al., 2018). Our validation work showed the interaction of Rer1 with the α1 subunit of the $GABA_A$ receptor, which was stronger in *Nedd4-2*$^{+/-}$ mice. Meanwhile, more Endo-H digested α1 subunit, which represents the ER-trapped fraction, was found in *Nedd4-2*$^{+/-}$ mice. More data are needed to further clarify the Rer1-mediated ER retention of α1 subunit and to evaluate the role of Rer1 in trafficking efficiency, surface expression, and current activity of $GABA_A$ receptors. In addition, other potential Rer1 interactive proteins might also be possible mediators of the Nedd4-2-regulation of ER stress and seizure susceptibility which awaits further investigation.

CONCLUSION

Our study on *Nedd4-2*$^{+/-}$ mice demonstrated a protective role of Nedd4-2 against ER stress and seizures possibly through ubiquitination of Rer1. The molecular mechanism of NEDD4-2-mediated ubiquitination of RER1 was elaborated. We also provided the interactome data of Rer1 in the epileptic mouse hippocampus, showing multiple potential cargoes with neurotransmitter receptor and synaptic regulator activities. The α1 subunit of the $GABA_A$ receptor was validated to interact with Rer1 and accumulate in ER more heavily in *Nedd4-2*$^{+/-}$ mice.

DATA AVAILABILITY STATEMENT

The original contributions presented in this study are included in the article/**Supplementary Material**, further inquiries can be directed to the corresponding author.

ETHICS STATEMENT

The animal study was reviewed and approved by Ethics Committees of Shengjing Hospital of China Medical University (2021PS348K).

AUTHOR CONTRIBUTIONS

XLL and YZ conceived the study and acquired the funding. XLL wrote the manuscript. LZ and XYL performed the experiments. HZ and BZ analyzed the experimental data. JT maintained the mice and cell lines. YZ supervised the manuscript. All authors contributed to the article and approved the submitted version.

FUNDING

This work was supported by the grants from The National Key Research and Development Program of China (2021YFC1005300, 2021YFC1005303, 2021YFC1005304) and the New Medical Technology and Project of China Medical University (112-3110210717).

SUPPLEMENTARY MATERIAL

The Supplementary Material of raw immunoblots for this article can be found online at: https://www.frontiersin.org/articles/10.3389/fnmol.2022.919718/full#supplementary-material

REFERENCES

Allen, A. S., Berkovic, S. F., Cossette, P., Delanty, N., Dlugos, D., Eichler, E. E., et al. (2013). De novo mutations in epileptic encephalopathies. *Nature* 501, 217–221. doi: 10.1038/nature12439

Annaert, W., and Kaether, C. (2020). Bring it back, bring it back, don't take it away from me - the sorting receptor RER1. *J. Cell Sci.* 133:jcs231423. doi: 10.1242/jcs.231423

Boehm, J., Letourneur, F., Ballensiefen, W., Ossipov, D., Démollière, C., and Schmitt, H. D. (1997). Sec12p requires Rer1p for sorting to coatomer (COPI)-coated vesicles and retrieval to the ER. *J. Cell Sci*. 110, 991–1003. doi: 10.1242/jcs.110.8.991

Cao, S. S., and Kaufman, R. J. (2014). Endoplasmic reticulum stress and oxidative stress in cell fate decision and human disease. *Antioxid. Redox Signal*. 21, 396–413. doi: 10.1089/ars.2014.5851

Dibbens, L. M., Ekberg, J., Taylor, I., Hodgson, B. L., Conroy, S. J., Lensink, I. L., et al. (2007). NEDD4-2 as a potential candidate susceptibility gene for epileptic photosensitivity. *Genes. Brain Behav*. 6, 750–755. doi: 10.1111/j.1601-183x.2007.00305.x

Eagleman, D. E., Zhu, J., Liu, D. C., Seimetz, J., Kalsotra, A., and Tsai, N. P. (2021). Unbiased proteomic screening identifies a novel role for the E3 ubiquitin ligase Nedd4-2 in translational suppression during ER stress. *J. Neurochem*. 157, 1809–1820. doi: 10.1111/jnc.15219

Ekberg, J., Schuetz, F., Boase, N. A., Conroy, S. J., Manning, J., Kumar, S., et al. (2007). Regulation of the voltage-gated K(+) channels KCNQ2/3 and KCNQ3/5 by ubiquitination. Novel role for Nedd4-2. *J. Biol. Chem*. 282, 12135–12142. doi: 10.1074/jbc.m609385200

Ekberg, J. A., Boase, N. A., Rychkov, G., Manning, J., Poronnik, P., and Kumar, S. (2014). Nedd4-2 (NEDD4L) controls intracellular Na(+)-mediated activity of voltage-gated sodium channels in primary cortical neurons. *Biochem. J*. 457, 27–31. doi: 10.1042/bj20131275

Forte, N., Binda, F., Contestabile, A., Benfenati, F., and Baldelli, P. (2020). Synapsin I Synchronizes GABA Release in Distinct Interneuron Subpopulations. *Cereb. Cortex* 30, 1393–1406. doi: 10.1093/cercor/bhz174

Fu, J., Tao, T., Li, Z., Chen, Y., Li, J., and Peng, L. (2020). The roles of ER stress in epilepsy: Molecular mechanisms and therapeutic implications. *Biomed. Pharmacother*. 131:110658. doi: 10.1016/j.biopha.2020.110658

Fu, Y. L., Han, D. Y., Wang, Y. J., Di, X. J., Yu, H. B., and Mu, T. W. (2018). Remodeling the endoplasmic reticulum proteostasis network restores proteostasis of pathogenic GABAA receptors. *PLoS One* 13:e0207948. doi: 10.1371/journal.pone.0207948

Fukuda, A., and Watanabe, M. (2019). Pathogenic potential of human SLC12A5 variants causing KCC2 dysfunction. *Brain Res*. 1710, 1–7. doi: 10.1016/j.brainres.2018.12.025

Füllekrug, J., Boehm, J., Röttger, S., Nilsson, T., Mieskes, G., and Schmitt, H. D. (1997). Human Rer1 is localized to the Golgi apparatus and complements the deletion of the homologous Rer1 protein of Saccharomyces cerevisiae. *Eur. J. Cell Biol*. 74, 31–40.

Gallagher, M. J., Shen, W., Song, L., and Macdonald, R. L. (2005). Endoplasmic reticulum retention and associated degradation of a GABAA receptor epilepsy mutation that inserts an aspartate in the M3 transmembrane segment of the alpha1 subunit. *J. Biol. Chem*. 280, 37995–38004. doi: 10.1074/jbc.m508305200

Hara, T., Hashimoto, Y., Akuzawa, T., Hirai, R., Kobayashi, H., and Sato, K. (2014). Rer1 and calnexin regulate endoplasmic reticulum retention of a peripheral myelin protein 22 mutant that causes type 1A Charcot-Marie-Tooth disease. *Sci. Rep*. 4:6992. doi: 10.1038/srep06992

Hara, T., Maejima, I., Akuzawa, T., Hirai, R., Kobayashi, H., Tsukamoto, S., et al. (2018). Rer1-mediated quality control system is required for neural stem cell maintenance during cerebral cortex development. *PLoS Genet.* 14:e1007647. doi: 10.1371/journal.pgen.1007647

Helenius, A., and Aebi, M. (2004). Roles of N-linked glycans in the endoplasmic reticulum. *Annu. Rev. Biochem*. 73, 1019–1049. doi: 10.1146/annurev.biochem.73.011303.073752

Hernandez, C. C., and Macdonald, R. L. (2019). A structural look at GABAA receptor mutations linked to epilepsy syndromes. *Brain Res*. 1714, 234–247. doi: 10.1016/j.brainres.2019.03.004

Hirose, S. (2006). A new paradigm of channelopathy in epilepsy syndromes: intracellular trafficking abnormality of channel molecules. *Epilepsy Res.* 70, S206–S217. doi: 10.1016/j.eplepsyres.2005.12.007

Kaether, C., Scheuermann, J., Fassler, M., Zilow, S., Shirotani, K., Valkova, C., et al. (2007). Endoplasmic reticulum retention of the gamma-secretase complex component Pen2 by Rer1. *EMBO Rep*. 8, 743–748. doi: 10.1038/sj.embor.7401027

Kittler, J. T., McAinsh, K., and Moss, S. J. (2002). Mechanisms of GABAA receptor assembly and trafficking: implications for the modulation of inhibitory neurotransmission. *Mol. Neurobiol.* 26, 251–268. doi: 10.1385/MN:26:2-3:251

Kuster, A., Nola, S., Dingli, F., Vacca, B., Gauchy, C., Beaujouan, J. C., et al. (2015). The Q-soluble N-Ethylmaleimide-sensitive Factor Attachment Protein Receptor (Q-SNARE) SNAP-47 Regulates Trafficking of Selected Vesicle-associated Membrane Proteins (VAMPs). *J. Biol. Chem.* 290, 28056–28069. doi: 10.1074/jbc.M115.666362

Liu, D. C., Eagleman, D. E., and Tsai, N. P. (2019). Novel roles of ER stress in repressing neural activity and seizures through Mdm2- and p53-dependent protein translation. *PLoS Genet*. 15:e1008364. doi: 10.1371/journal.pgen.1008364

Liu, X., Zhang, H., Zhang, B., Tu, J., Li, X., and Zhao, Y. (2021). Nedd4-2 haploinsufficiency in mice causes increased seizure susceptibility and impaired Kir4.1 ubiquitination. *Biochim. Biophys. Acta Mol. Basis Dis*. 1867:166128. doi: 10.1016/j.bbadis.2021.166128

Lodes, D. E., Zhu, J., and Tsai, N. P. (2022). E3 ubiquitin ligase Nedd4-2 exerts neuroprotective effects during endoplasmic reticulum stress. *J. Neurochem*. 160, 613–624. doi: 10.1111/jnc.15567

Münster-Wandowski, A., Heilmann, H., Bolduan, F., Trimbuch, T., Yanagawa, Y., and Vida, I. (2017). Distinct Localization of SNAP47 Protein in GABAergic and Glutamatergic Neurons in the Mouse and the Rat Hippocampus. *Front. Neuroanat*. 11:56. doi: 10.3389/fnana.2017.00056

Nair, R., Lauks, J., Jung, S., Cooke, N. E., de Wit, H., Brose, N., et al. (2013). Neurobeachin regulates neurotransmitter receptor trafficking to synapses. *J. Cell Biol.* 200, 61–80. doi: 10.1083/jcb.201207113

Ni, M., and Lee, A. S. (2007). ER chaperones in mammalian development and human diseases. *FEBS Lett*. 581, 3641–3651. doi: 10.1016/j.febslet.2007.04.045

Numakura, Y., Uemura, R., Tanaka, M., Izawa, T., Yamate, J., Kuramoto, T., et al. (2021). PHF24 is expressed in the inhibitory interneurons in rats. *Exp. Anim.* 70, 137–143. doi: 10.1538/expanim.20-0105

Park, H. J., Ryu, D., Parmar, M., Giasson, B. I., and McFarland, N. R. (2017). The ER retention protein RER1 promotes alpha-synuclein degradation via the proteasome. *PLoS One* 12:e0184262. doi: 10.1371/journal.pone.0184262

Park, H. J., Shabashvili, D., Nekorchuk, M. D., Shyqyriu, E., Jung, J. I., Ladd, T. B., et al. (2012). Retention in endoplasmic reticulum 1 (RER1) modulates amyloid-β (Aβ) production by altering trafficking of γ-secretase and amyloid precursor protein (APP). *J. Biol. Chem*. 287, 40629–40640. doi: 10.1074/jbc.m112.418442

Sato, K., Nishikawa, S., and Nakano, A. (1995). Membrane protein retrieval from the Golgi apparatus to the endoplasmic reticulum (ER): characterization of the RER1 gene product as a component involved in ER localization of Sec12p. *Mol. Biol. Cell*. 6, 1459–1477. doi: 10.1091/mbc.6.11.1459

Serikawa, T., Kunisawa, N., Shimizu, S., Kato, M., Alves Iha, H., Kinboshi, M., et al. (2019). Increased seizure sensitivity, emotional defects and cognitive impairment in PHD finger protein 24 (Phf24)-null rats. *Behav. Brain Res.* 369:111922. doi: 10.1016/j.bbr.2019.111922

Shupliakov, O., Haucke, V., and Pechstein, A. (2011). How synapsin I may cluster synaptic vesicles. *Semin. Cell Dev. Biol.* 22, 393–399. doi: 10.1016/j.semcdb.2011.07.006

Sudol, M., and Hunter, T. (2000). NeW wrinkles for an old domain. *Cell* 103, 1001–1004. doi: 10.1016/s0092-8674(00)00203-8

Tanabe, C., Maeda, T., Zou, K., Liu, J., Liu, S., Nakajima, T., et al. (2012). The ubiquitin ligase synoviolin up-regulates amyloid β production by targeting a negative regulator of γ-secretase, Rer1, for degradation. *J. Biol. Chem*. 287, 44203–44211. doi: 10.1074/jbc.m112.365296

Tang, B. L. (2016). K+-Cl- co-transporter 2 (KCC2) - a membrane trafficking perspective. *Mol. Membr. Biol.* 33, 100–110. doi: 10.1080/09687688.2017.1393566

Valkova, C., Albrizio, M., Röder, I. V., Schwake, M., Betto, R., Rudolf, R., et al. (2011). Sorting receptor Rer1 controls surface expression of muscle acetylcholine receptors by ER retention of unassembled alpha-subunits. *Proc. Natl. Acad. Sci. U.S.A*. 108, 621–625. doi: 10.1073/pnas.1001624108

Valkova, C., Liebmann, L., Krämer, A., Hübner, C. A., and Kaether, C. (2017). The sorting receptor Rer1 controls Purkinje cell function via voltage gated sodium channels. *Sci. Rep*. 7:41248. doi: 10.1038/srep41248

Van Erum, J., Van Dam, D., and De Deyn, P. P. (2019). PTZ-induced seizures in mice require a revised Racine scale. *Epilepsy Behav*. 95, 51–55. doi: 10.1016/j.yebeh.2019.02.029

Vanli-Yavuz, E. N., Ozdemir, O., Demirkan, A., Catal, S., Bebek, N., Ozbek, U., et al. (2015). Investigation of the possible association of NEDD4-2 (NEDD4L) gene with idiopathic photosensitive epilepsy. *Acta Neurol. Belg.* 115, 241–245. doi: 10.1007/s13760-014-0412-x

Volders, K., Nuytens, K., and Creemers, J. W. (2011). The autism candidate gene Neurobeachin encodes a scaffolding protein implicated in membrane trafficking and signaling. *Curr. Mol. Med.* 11, 204–217. doi: 10.2174/156652411795243432

Wang, H., Sun, R. Q., Camera, D., Zeng, X. Y., Jo, E., Chan, S. M., et al. (2016). Endoplasmic reticulum stress up-regulates Nedd4-2 to induce autophagy. *FASEB J.* 30, 2549–2556. doi: 10.1096/fj.201500119

Yamasaki, A., Hara, T., Maejima, I., Sato, M., Sato, K., and Sato, K. (2014). Rer1p regulates the ER retention of immature rhodopsin and modulates its intracellular trafficking. *Sci. Rep*. 4:5973. doi: 10.1038/srep05973

Zhu, J., Lee, K. Y., Jewett, K. A., Man, H. Y., Chung, H. J., and Tsai, N. P. (2017). Epilepsy-associated gene Nedd4-2 mediates neuronal activity and seizure susceptibility through AMPA receptors. *PLoS Genet*. 13:e1006634. doi: 10.1371/journal.pgen.1006634

Zhu, J., Lee, K. Y., Jong, T. T., and Tsai, N. P. (2019). C2-lacking isoform of Nedd4-2 regulates excitatory synaptic strength through GluA1 ubiquitination-independent mechanisms. *J. Neurochem.* 151, 289–300. doi: 10.1111/jnc.14840

Conflict of Interest: The authors declare that the research was conducted in the absence of any commercial or financial relationships that could be construed as a potential conflict of interest.

Publisher's Note: All claims expressed in this article are solely those of the authors and do not necessarily represent those of their affiliated organizations, or those of the publisher, the editors and the reviewers. Any product that may be evaluated in this article, or claim that may be made by its manufacturer, is not guaranteed or endorsed by the publisher.

frontiers | Frontiers in Molecular Neuroscience

ORIGINAL RESEARCH
published: 30 June 2022
doi: 10.3389/fnmol.2022.870182

Novel *HCN1* Mutations Associated With Epilepsy and Impacts on Neuronal Excitability

*Changning Xie[1], Fangyun Liu[1], Hailan He[1], Fang He[1], Leilei Mao[1], Xiaole Wang[1], Fei Yin[1,2] and Jing Peng[1,2]**

[1] Department of Pediatrics, Xiangya Hospital, Central South University, Changsha, China, [2] Hunan Intellectual and Development Disabilities Research Center, Changsha, China

Hyperpolarization-activated cyclic nucleotide-gated (HCN) channel plays a critical role in regulating the resting membrane potential and integrating synaptic transmission. Variants of *HCN1* have been recognized as causes of epilepsy, and mutant HCN1 channels could act with loss-of-function (LOF), loss- and gain-of-function (LOF and GOF) and gain-of-function (GOF) mechanisms. However, phenotypes and pathogenesis of HCN1-related epilepsy are still poorly understood. This study enrolled five epileptic cases carrying five different *HCN1* variants: two pathogenic variants (I380F and S710Rfs*71), two likely pathogenic variants (E240G and A395G), and a paternally inherited variant (V572A). Four variants were novel. Electrophysiological experiments revealed impaired biophysical properties of the identified mutants, including current densities and activation/deactivation kinetics. Moreover, three variants exerted effects on the biophysical properties of wild-type HCN1 channels in heterozygous conditions. Immunofluorescence experiments showed that two variants reduced the protein expression of HCN1channels in neurons. Neurons expressing E240G (GOF) variant showed increased input resistance. However, the variant of I380F (LOF) increased the neuronal firing rate, thus leading to neuronal hyperexcitability. In conclusion, the present study expands the genotypic and phenotypic spectrum of patients with *HCN1*-related epilepsy and clarifies the underlying mechanisms. We reported five new cases including four unreported likely/pathogenic variants. We provided assessments of biophysical function for each variant, which could help patients to receive individual therapy in the future. We confirmed that *HCN1* variants contributed to neuronal hyperexcitability by regulating input resistance and the action potential firing rate, and we have shown that they can affect protein expression in neurons for the first time.

Keywords: epilepsy, intellectual disorders, patch clamp, neuronal excitability, *HCN1*

OPEN ACCESS

Edited by:
Maria Teresa Fiorenza, Sapienza University of Rome, Italy

Reviewed by:
Lu-Yang Wang, University of Toronto, Canada
Ilaria Rivolta, University of Milano-Bicocca, Italy

***Correspondence:**
Jing Peng
pengjing4346@163.com

Specialty section:
This article was submitted to Brain Disease Mechanisms, a section of the journal Frontiers in Molecular Neuroscience

Received: *06 February 2022*
Accepted: *16 May 2022*
Published: *30 June 2022*

Citation:
Xie C, Liu F, He H, He F, Mao L, Wang X, Yin F and Peng J (2022) Novel HCN1 Mutations Associated With Epilepsy and Impacts on Neuronal Excitability. Front. Mol. Neurosci. 15:870182. doi: 10.3389/fnmol.2022.870182

INTRODUCTION

With the development of whole-exon sequencing, mutations in *HCN1* have been identified as causes of epilepsy (Oyrer et al., 2018). Hyperpolarization-activated cyclic nucleotide-gated ion channel 1 (HCN1), which is encoded by the *HCN1* gene, contains an amino-terminal domain, six transmembrane domains (S1–S6), and a carboxyl terminus with a cyclic nucleotide-binding domain (Lee and MacKinnon, 2017). HCN channels are enriched in the brain and play important roles in the resting membrane potential, neuronal rhythmic activity, and dendritic integration (Brewster et al., 2006; Postea and Biel, 2011) by mediating hyperpolarizing activated non-selective cation current (Ih) (Benarroch, 2013; Santoro and Shah, 2020). Initially, the clinical manifestation of *HCN1*-related epilepsy was termed Dravet syndrome (Steel et al., 2017; Mei et al., 2019). Indeed, they have some similarities, such as early onset age, fever sensitivity, and developmental regression (Nava et al., 2014; Wang et al., 2019). Over the years, more phenotypes of *HCN1*-related epilepsy have been identified, including severe epilepsy of infancy with migrating focal seizures, absence, and other neurodevelopmental diseases (Lucariello et al., 2016; Marini et al., 2018). Clinical manifestations including frequency of episodes, severity, and type of seizures vary among patients.

Previous studies have shown variants of *HCN1* have loss-of-function (LOF) and gain-of-function (GOF) effects on HCN1 channels (Nava et al., 2014; Bonzanni et al., 2018; Marini et al., 2018; Porro et al., 2021). LOF variants impact neuronal excitability, including resting membrane potential, input resistance, and firing properties (Bonzanni et al., 2018; Bleakley et al., 2021), contributing to epilepsy. However, the altered functions of the mutated channels are various, including current densities, voltage-dependent activation, and/or altered kinetics. There is no doubt that this variety brings great challenges to the description of the relationship between the function of mutated channels and clinical phenotypes, as well as neuronal mechanisms underlying epilepsy.

In the present study, we reported five new patients with *HCN1*-related epilepsy and identified four unreported variants. We found all five variants showed altered biophysical properties of HCN1 channels. Furthermore, neurons expressing mutant channels showed reduced HCN1 protein expression and impaired neuronal excitability.

MATERIALS AND METHODS

Patient Recruitment

This study was approved by the ethics committee of Xiangya Hospital of Central South University. Written informed consent was obtained from parents or guardians of all patients before any study. We retrospectively collected clinical data from patients, including seizure onset, seizure types, electroencephalogram (EEG), brain MRI, and anti-seizure therapy. All EEG recordings were obtained with a time-locked synchronized video and carefully analyzed by a certified pediatric neurologist and two Asian Epilepsy Academy certified electroencephalographers. Genetic analysis was performed by trio whole-exome sequencing, and candidate causative variants were confirmed by Sanger sequencing. We rechecked all the variants with nucleotide and amino acid numbering according to the *HCN1* reference transcript (NM_021072). The minor allele frequency of variants and pathogenicity were evaluated using Genome Aggregation Database (gnomAD)[1] and two missense prediction programs (SIFT, PROVEAN). The clinical significance of variants was determined under the American College of Medical Genetics and Genomics (ACMG) (Richards et al., 2015) standard guidelines.

Cell Culture and Transfection

Human embryonic kidney (HEK) 293 cells were cultured in Dulbecco's Modified Eagle's Medium (supplemented with 10% FBS and 1% penicillin/streptomycin). The human *HCN1* plasmids were purchased from Genscript Corporation. *HCN1* cDNA was subcloned into the pCDNA3.1 vector or pCAGGS vector for neurons, and variants were introduced into this cDNA with the KOD site-directed mutagenesis kit (Toyobo). Then, correct constructs were confirmed by sequencing and reserved for subsequent experiments. The mixtures of WT or mutant *HCN1* plasmids (1 μg) and 0.5 μg of enhanced fluorescent protein (EGFP) were transfected into HEK 293 cells by Lipofectamine (Invitrogen). For co-expression experiments, WT plasmids, mutant *HCN1* plasmids, and EGFP (at a ratio of 1:1:0.5) were mixed and added to the cultures.

Primary cortical neurons were obtained from embryonic day 17–18 (E17-18) C57BL/6 mice as previously reported (Guo et al., 2019). Briefly, the fetal cortex was digested by adding 2 mg/ml papain (Worthington Biomedical Corporation) and incubating for 30 min at 37°C. Neurons were seeded onto 12-mm diameter coverslips at a density of 10^5 cells/well in the culture medium (neurobasal medium supplemented with 2% B27, 1% glutamax, and 1% penicillin/streptomycin). One microgram of WT/mutant plasmids and 0.25 μg of enhanced GFP DNA were transfected using lipofectamine at day *in vitro* 8–9 (DIV8-9).

Electrophysiology

Electrophysiological recordings were performed as described in the previous studies (Marini et al., 2018). Briefly, experiments were performed on CHO cells 24–36 h after transfection. The pipette solution contained the following compounds (in mM): 120 potassium aspartate, 10 KCl, 10 NaCl, 10 EGTA, 1 $CaCl_2$, 10 HEPES, and 2 Mg-ATP. The bath solution contained (in mM) NaCl 130, KCl 15, $MgCl_2$ 0.5, $CaCl_2$ 1.8, glucose 10, and HEPES 5. To determine the current–voltage relationship, the peak current was measured at various hyperpolarization steps from the holding potential of –20 mV (–10 mV increment, hyperpolarized to –130 mV) and normalized to membrane capacitance. To obtain the activation curves of the HCN1 channels, tail currents were recorded at –110 mV (or –130 mV) after hyperpolarized

[1] http://gnomad.broadinstitute.org/

steps from –20 to –110 (or –130) mV in –10 mV increments and calculated by the Boltzmann function:

$$I(V) = I_{max}/(1 + exp(V - V_{1/2})/k_V)$$

where I is the recorded current amplitude at test potential, I_{max} is the maximal current, V is the voltage, $V_{1/2}$ indicates the voltage at half-maximal activation, and K_v is the slope. Activation time constants were obtained by fitting current traces acquired from the activation protocol using a double-exponential function after an initial delay, and deactivation time constants were obtained by fitting current traces recorded (at + 10 mV) after a fully activating step at –120 mV.

All data were acquired using a 700 B amplifier (Molecular Devices) and analyzed using Clampfit 10.6 software (Axon Instruments). The series resistance was < 10 MΩ.

For neurons, current-clamp experiments were performed at DIV 4–5 after transfection. Cells were held at –70 mV, and resting membrane potentials were recorded within 2 min after the membrane breaking ($I_{holding}$ = 0 pA). The intracellular solution is composed of the following compounds (in mM): 123 K-gluconate, 10 KCl, 1 $MgCl_2$, 1 EGTA, 0.1 $CaCl_2$, 0.2 Na-GTP, 1.5 Mg-ATP, 4 D-glucose, and 10 Hepes (pH = 7.3, 290 mOsm). The extracellular solution contains the following compounds (in mM): 140 NaCl, 3 KCl, 2 $CaCl_2$, 1 $MgCl_2$, 10 D-glucose, and 10 Hepes. To block excitatory and inhibitory synaptic inputs, APV (20 μM), CNQX (10 μM), and bicuculline (10 μM) were added. The spikes were elicited by current injection ranging from 0 to 180 pA with 20 pA increment, lasting for 500 ms. Input resistance was calculated when cells received a current stimulus (–100 pA). Spike threshold was defined as the first current injection being able to elicit action potentials. Sag ratio was calculated using the equation: Sag ratio = $(V_{peak} - V_{ss})/V_{peak}$, where V_{peak} represents the maximum voltage and Vss indicates the steady-state voltage at the late phase of the hyperpolarizing current step.

Immunocytochemistry

Cells were fixed with 4% paraformaldehyde in PBS for 10 min. Next, they were blocked with 5% BSA with or without (for surface expression) 0.3% Triton after washing in PBS. They were next incubated with anti-HCN1 antibody (Alomone, 1:500, overnight, 4°C) followed by secondary antibodies (anti-rabbit Cy3, Jackson lab, 6 h, room temperature). Subsequently, the coverslips were washed with PBS for three times and mounted on glass slides. Fluorescent images were acquired using a confocal microscope (Zeiss, LSM800).

Statistics

Data are represented as mean ± SEM. Statistical analyses were performed using SPSS software, version 17.0 (SPSS Inc., Chicago, IL). Shapiro–Wilk's test and Levene's test were used to verify the normality and homogeneity of variance, respectively. Two-group comparisons were carried out using an independent two-sample *t*-test. Comparison of multiple groups was assessed by one-way ANOVA, followed by the Bonferroni *post hoc* test or Dunnett's T3 test. The Mann–Whitney test was used to evaluate the statistical significance where data were not conformed to normal distribution. In all cases, the significance level was set at $P < 0.05$.

RESULTS

Identification of Hyperpolarization-Activated Cyclic Nucleotide-Gated Ion Channel 1 Variants in Five New Cases

We identified four novel *HCN1* variants (E240G, A395G, S710Rfs*71, and V572A) and one previously reported variant (I380F) in five patients. All the five variants were classified as likely pathogenic or pathogenic under the ACMG variant classification guidelines (**Supplementary Table 1**). Clinical and genetic features are presented in **Table 1**, **Figures 1**, **2**, **Supplementary Tables 1, 2**, and **Supplementary Figure 1**.

Patient #1 is an 11-month-old girl, born at term with a birth weight of 3,250 g. Her parents were healthy and did not have a consanguineous relationship. She presented with febrile seizures at the age of 8 months. Generalized seizures occurred once a week and lasted for 2–3 min. The EEG displayed bursts of high-amplitude spikes and sharp waves in the bifrontal and temporal regions. The brain MRI was normal. Seizures were relieved following treatment with sodium valproate (VPA) for 2 months. Her cognitive and motor developments were not affected at the last follow-up. She carried a *de novo* variant (c.719A > G, p. E240G) of *HCN1,* and this variant was absent from gnomAD, and the amino acid is evolutionarily conserved among different species. It is predicted to be tolerant and deleterious in SIFT and PROVEAN, respectively. The variant meets ACMG/AMP guidelines (PS2 + PM1 + PM2 + PP3) to be considered likely pathogenic.

Patient #2 is a 1-year-old girl who had seizures within 2 days after birth. She was born at term with a birth weight of 3,000 g. Her parents were healthy and non-consanguineous. Her growth parameters were normal. At the age of 2 months, seizures became more frequent and severe. Seizures evolved into tonic asymmetric seizures with prolonged cyanosis and occurred two to four times a day. At 3 months, she developed more frequent seizures that occurred 20–30 times/day triggered by fever. At 4 months, she suffered from dozens of episodes per day and uncontrollable recurrent status epilepticus. Her overall development was regressed. Seizures could be slightly relieved by nitrazepam (NZP) but were resistant to levetiracetam (LEV) and VPA. Her brain MRI was normal, but her cardiac color ultrasound displayed a ventricular septal defect. EEG showed abnormal background activity including diffuse 1.5–5 Hz mixed slow waves with low-medium amplitude and a small number of fast waves with low amplitude in the awake state. Interictal EEG showed a large number of sharp waves, with sharp slow waves appearing suddenly or continuously. During the 15-h video EEG recording, 11 seizures were monitored, of which 6 partial seizures started with a paroxysmal ictal discharge in the left temporal region, 2 partial seizures started in the Rolandic region, and

TABLE 1 | Phenotypic features of patients with different type of variants according to channel properties.

***N* = 33**	**LOF (*n* = 18)**	**GOF(*n* = 13)**	**GOF/LOF (*n* = 2)**
Variants	p.Met243Arg (2); p.Ser272Pro (1); p.Arg297Thr (1); p.Met305Leu (2); p.Cys329Ser (5); p.Ile380Phe (1); p.Gly391Asp (2); p.Gly391Cys (1); p.Ala395Gly (1); p.Ser399Pro (1); p.Arg590Gln (1)	p. Ser100Phe (1); p. Met153Ile (2); p. Glu240Gly (1); p. His279Tyr (1); p. Gly391Ser (2); p. Ile397Leu (1); p. Asp401His (1); p.Val414Met (3); p.Val572Ala (1)	p. Leu157Val; p. S710Rfs*71
Domain	S3–S4 (1/11); S4 (1/11) S5 (2/11); S5–S6 (1/11); S6 (3/11); C (3/11)	N (1/9); S1 (1/9); S3–S4 (1/9); S4 (1/9); S6 (1/9); C (4/9)	S1 (1); C (1)
Epilepsy onset age	< 1 Year (13/18); > 1 year (5/18)	<1 Year (8/13); > 1 year (5/13)	< 1 Year (1/2); > 1 year (1/2)
Seizure types	Focal (4/15)	Focal (7/11)	Focal (1/2)
	Generalized (14/15)	Generalized (11/11)	Generalized (1/2)
	Both (3/15)	Both (7/11)	Both (0/2)
Sensitivity to fever	(12/17)	(12/13)	(1/2)
Status epilepticus	(5/18)	(1/13)	(0/2)
Seizure outcome	Seizure-free without therapy (0/18); seizure-free with monotherapy (6/18); seizure-free with combined therapy (2/18)	Seizure-free without therapy (2/13); seizure-free with monotherapy (4/13); seizure-free with combined therapy (1/13)	Seizure-free without therapy (0/2); seizure-free with monotherapy (2/2); seizure-free with combined therapy (0/2)
	Uncontrolled (10/18)	Uncontrolled (6/13)	Uncontrolled (0/2)
Intellectual disability	Normal (6/18)	Normal (6/13)	Normal (2/2)
	Mild (2/18)	Mild (4/13)	Mild (0/2)
	Moderate/severe (10/18)	Moderate/severe (3/13)	Moderate/severe (0/2)
Language or movement disorders	(7/7)	(5/6)	(0/1)
EEG	Normal (6/15); abnormal (9/15)	Normal (1/12); abnormal (11/12)	Normal (0/2); abnormal (2/2)
MRI	Normal (11/14); abnormal (3/14)	Normal (11/11); abnormal (0/11)	Normal (2/2); abnormal (0/2)
Additional findings	Microcephaly (3/18)	Microcephaly (0/2)	Microcephaly (0/1)

3 seizures started in the right temporal region (**Figure 2A**). Unfortunately, at the age of 1 year, she died of uncontrollable seizures. Her trio-based exome analysis identified a *de novo* variant in *HCN1* (c.1138A > T, p. I380F). The variant is absent from gnomAD, and the amino acid is evolutionarily conserved among different species. The pathogenic evaluations in SIFT and PROVEAN were damaging and deleterious, respectively. It is considered pathogenic under ACMG/AMP guidelines (PS1 + PS2 + PM1 + PM2 + PP3).

Patient #3 was a 2-year-old girl, born at term. Her parents were non-consanguineous without a family history. At the age of 3 months, she had her first generalized tonic seizure after a fever. Status epilepticus appeared twice a month and lasted for 20 min. Her development milestone has been delayed since the first seizure. Her brain MRI was normal. The EEG showed multifocal spike waves in the right temporal and occipital and the left posterior regions (**Figure 2B**). No seizures were monitored during a 15-h video EEG recording. At first, she was treated with VPA, which improved her daily seizures. However, focal seizures and status epilepticus still appeared approximately twice a month. At the age of 17 months, she was absent of language and could not sit alone. Accordingly, oxcarbazepine (OXC) and lamotrigine (LTG) were added to the treatment but were ineffective. At the age of 20 months, clobazam (CLB) was added to her treatment. At the last follow-up, she had been seizure-free for 6 months and acquired slight improvements in language and motor development. Her trio-based exome analysis identified a *de novo* variant in *HCN1* (c.1184C > G, p. A395G). The variant is absent from gnomAD, and the amino acid is evolutionarily conserved among different species. The pathogenic evaluations in SIFT and PROVEAN were damaging and deleterious, respectively. The variant meets ACMG/AMP guidelines to be considered likely pathogenic (PS2 + PM1 + PM2 + PP3).

Patient #4 was a 2-year-old girl, who was born at term. Her parents were healthy and did not have a consanguineous relationship. She suffered from episodic paralysis, and could not walk at the age of 7 months. Three months later, she had seizures 2–3 times/day in addition to the paralysis. She did not show any prominent delay in motor and cognition development. Her brain MRI was normal. Four-hour video EEG showed a slow background, and diffusive fast waves in the occipital regions (**Figure 2C**). Fortunately, she became seizure-free with OXC treatment and got recovered from paralysis. Also, the 4-h video EEG was normal after

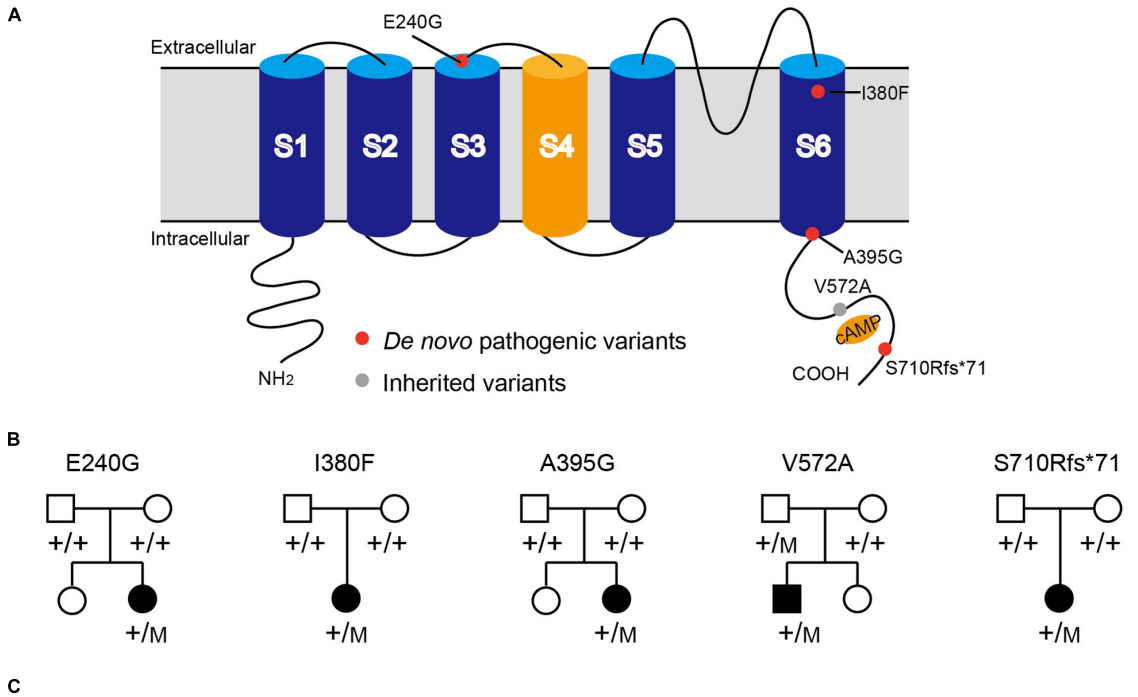

FIGURE 1 | Mutations in *HCN1* channels. **(A)** Structure of HCN1 channels with S1-S6 segments and N/C-terminal region. **(B)** Pedigrees of patients with HCN1 variants. **(C)** All variants are highly conserved among different species.

the 6-month treatment of OXC. Exome sequencing analysis identified a *de novo* frame-shift variant in *HCN1* (c.2128-2129dup, p. S710Rfs*71). The variant is absent from gnomAD, and the amino acid is evolutionarily conserved among different species. Combined with the functional experiment in this study, it is considered a variant of pathogenic under ACMG/AMP guidelines (PVS1 + PS2 + PM2).

Patient #5 was a 7-year-old boy, who was born at term to a non-consanguineous family. His parents were healthy without a family history. He underwent normal development until the appearance of seizures at the age of 16 months. At first, he presented with febrile generalized tonic-clonic seizures. At the age of 3 years, he exhibited tonic-clonic seizures once a month with or without fever. His seizures were not well controlled with a combination therapy of VPA and OXC. LEV was added to the therapy at the age of 4 years, and he became seizure-free. However, he still presented with ataxia, tremor, slight language disorders, and motor disorders. There was a malformation in the right tragus. His brain MRI was normal. The EEG background displayed 4 Hz activity in the occipital region. No ictal discharge was monitored in the interictal EEG. EEG showed 3.5–4 Hz spike-wave discharges lasting for 90 s, while the patient was having a tonic-clonic seizure in sleep (**Figure 2D**). Exome sequencing analysis identified a variant in *HCN1* (c.1715T > C, p. V572A) inherited from his asymptomatic father. The variant is absent from gnomAD, and the amino acid is evolutionarily conserved among different species. No other pathogenic or likely pathogenic variants were detected accounting for his phenotypes. It was predicted to be damaging and deleterious both in SIFT and PROVEAN. It is considered a variant of uncertain significance under ACMG/AMP criteria (PVS1 + PS2 + PM2), while the subsequent functional experiment proved to be likely pathogenic.

Biophysical Properties of Mutant Hyperpolarization-Activated Cyclic Nucleotide-Gated Ion Channel 1 Channels Expressed in HEK293 Cells

To verify the effects of variants on functional properties of HCN1 channels, we transfected WT, mutant, and WT/mutant

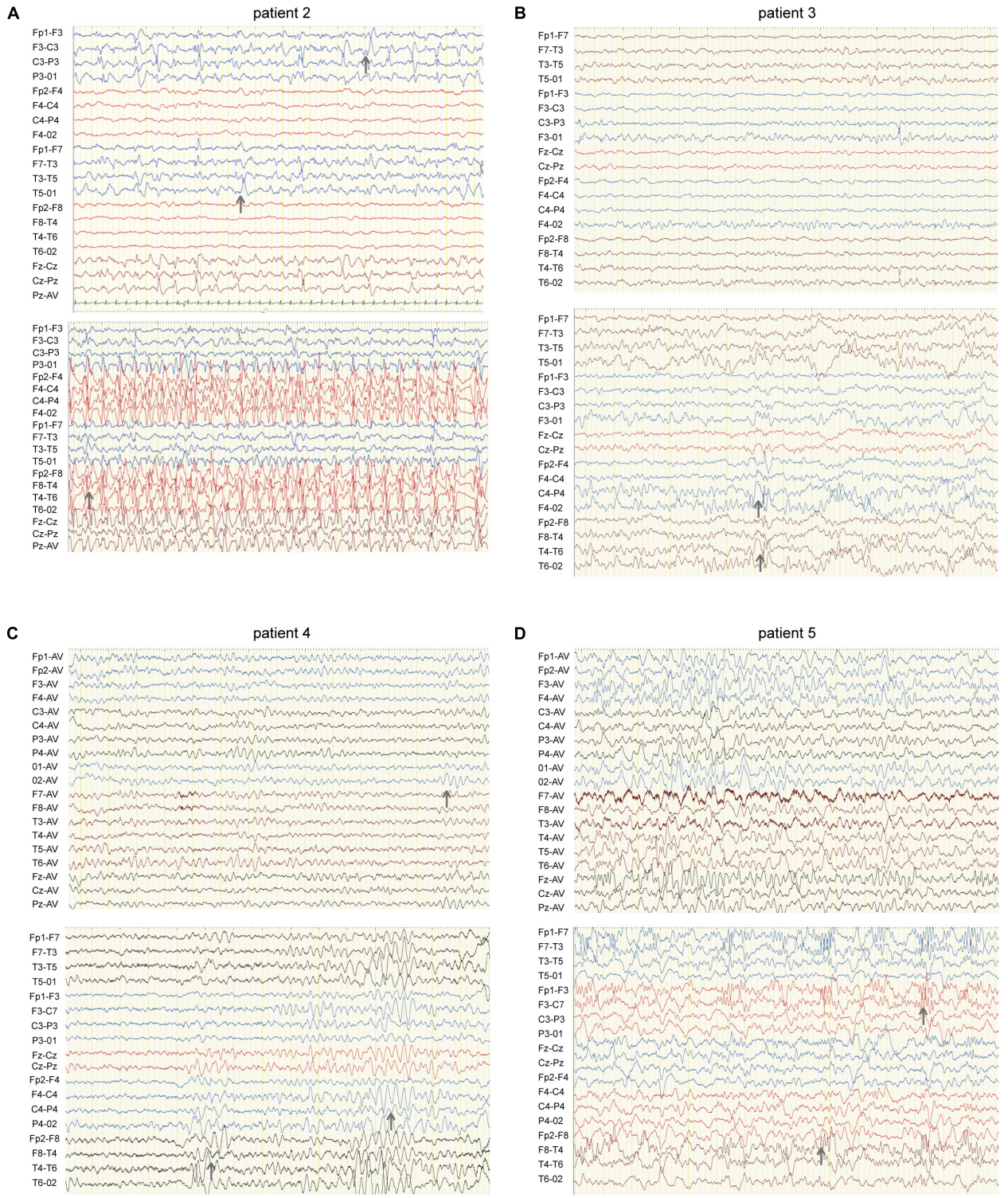

FIGURE 2 | EEG of four patients carrying *HCN1* variants. **(A)** EEG of patient 2 (I380F) shows sharp waves in the left hemisphere during sleep (top) and spike waves during status epilepticus (bottom). Gray arrows indicate abnormal EEG waves. **(B)** EEG of patient 3 (A395G) shows sharp and sharp slow waves in the right occipital region during sleep (bottom). **(C)** EEG of patient 4 (S710Rfs*71) features a slow rhythm of background in the occipital region (top) and a paroxysm of diffused 4–5 Hz slow waves (bottom). **(D)** EEG of patient 5 (V572A) shows θ rhythm mixed δ waves in the background (top) and diffused 3.5–4 Hz multifocal spike-slow waves during a tonic-clonic seizure, while the patient was having a tonic-clonic seizure in sleep (**Figure 2D**) (bottom).

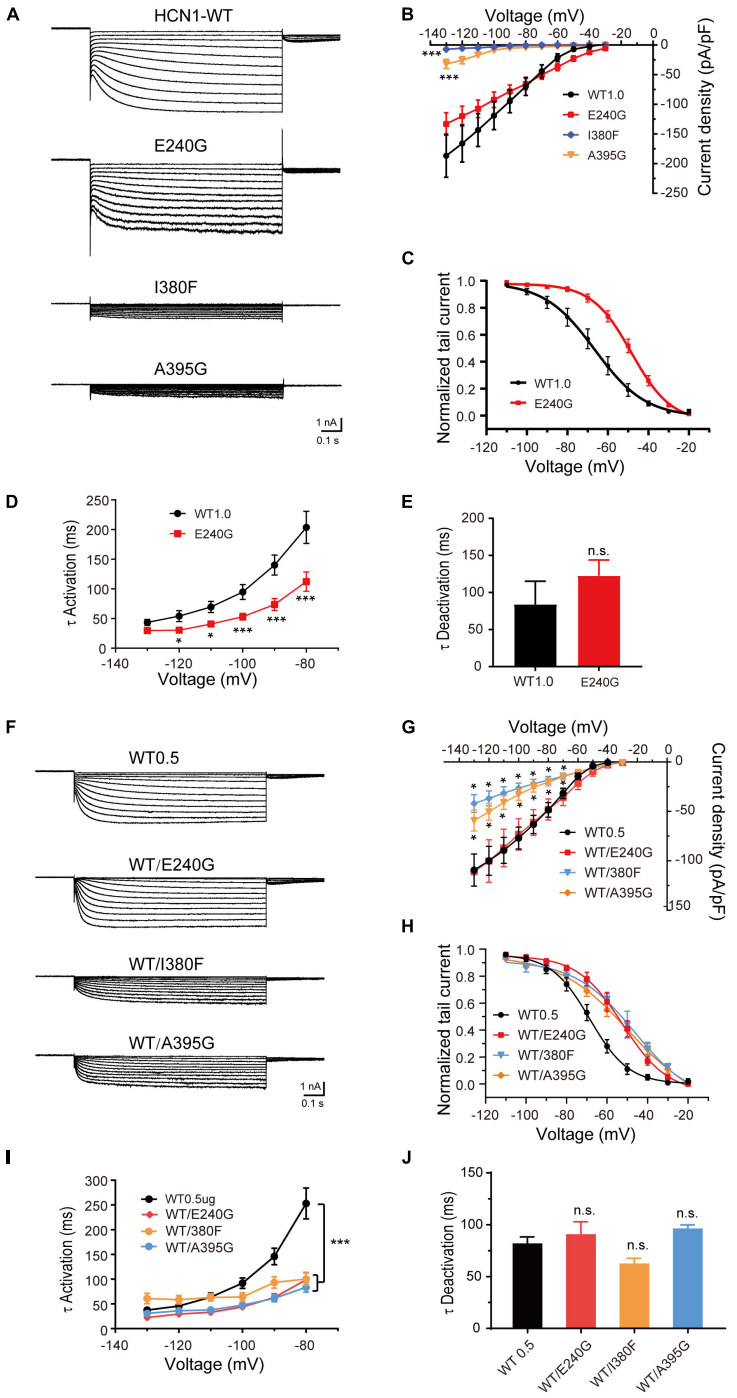

FIGURE 3 | Electrophysiological properties of novel and *de novo* variants in *HCN1* located in or close to transmembrane regions. **(A)** Representative recordings of currents mediated by mutant HCN1 channels. **(B)** Current densities of E240G (n = 16), I380F (n = 9), and A395G channels (n = 8) (WT1.0: n = 9). Dunnett's T3 *post hoc* test. **(C)** Activation curves of WT and E240G channels (WT: n = 12; E240G: n = 11), and lines represent Boltzmann functions fit to the data points. **(D)** Mean time constants of activation obtained for HCN-WT (black) and E240G channels (red). (WT: n = 8; E240G: n = 15). Dunnett's T3 *post hoc* test. **(E)** Bar graph shows mean deactivation time constants of WT and E240G channels recorded at + 10 mV (WT: n = 8; E240G: n = 12). Two-sample t-test. **(F)** Representative traces of heterozygous channels. **(G)** Plot of mean current densities of WT/E240G (n = 13), WT/I380F (n = 13), WT/A395G (n = 12), and WT channels (n = 18). Dunnett's T3 *post hoc* test. **(H)** Activation curves of WT channels (n = 6, black), WT/I380F channels (n = 6, blue), WT/E240G (n = 11, red), and WT/A395G channels (n = 12, orange). Bonferroni *post hoc* test. **(I,J)** Graphs show the effects of the activation (WT/E240G: n = 17; WT/I380F: n = 12; WT/A395G: n = 19; WT0.5: n = 12) and deactivation time constants (WT/I380F: n = 12; WT/E240G: n = 17; WT/A395G n = 17; WT0.5 n = 14) induced by mutant heterozygous channels. Bonferroni *post hoc* test. All data are presented as mean ± S.E.M. values (n.s. = not significant, $^*P < 0.05$, $^{***}P < 0.005$, in this and other figures).

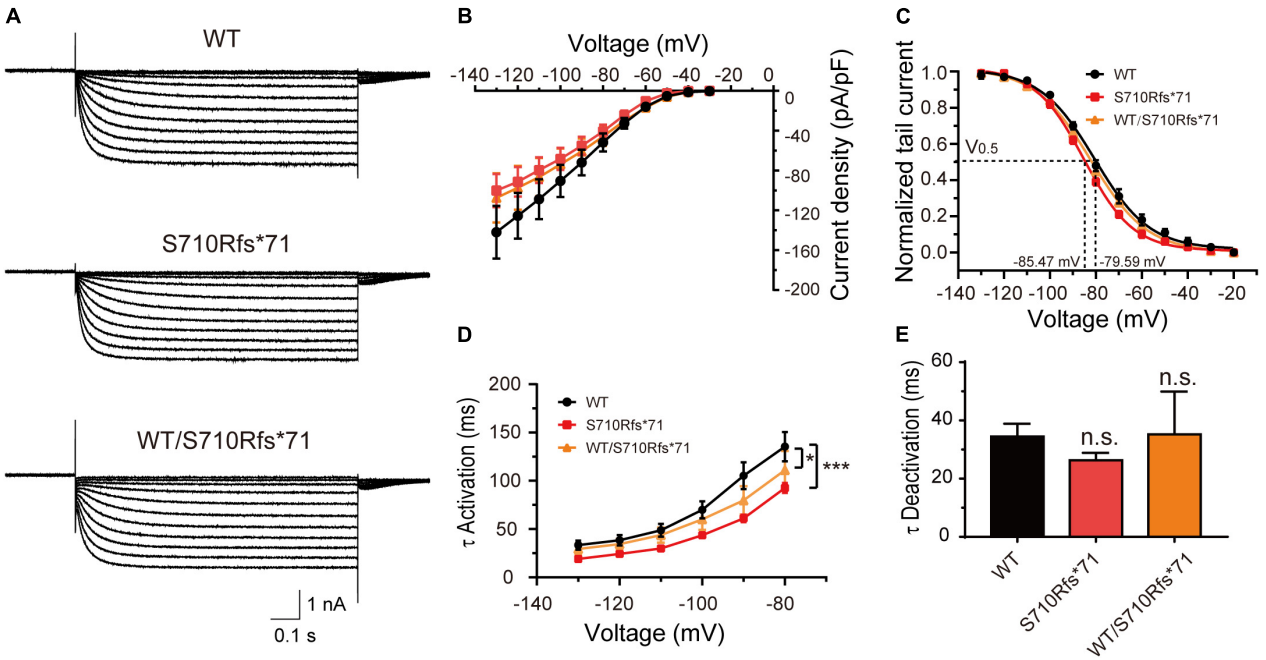

FIGURE 4 | Functional changes of the S710Rfs*71 variant. **(A)** Representative recordings of currents mediated by HCN1 channels. **(B)** Plot of mean current densities (pA/pF) of WT, S710Rfs*71, and WT/S710Rf*71 channels (WT: n = 14; S710Rfs*71: n = 20; WT/S710Rfs*71: n = 16). **(C)** Activation curves obtained by normalizing the tail currents of WT, S710Rfs*71, and WT/S710Rf*71 channels (WT: n = 11; S710Rfs*71: n = 13; WT/S710Rf*71: n = 7). **(D)** Plot of mean activation time constants obtained for HCN1-WT, S710Rfs*71, and WT/S710Rf*71 channels (WT: n = 16; S710Rfs*71: n = 16; WT/S710Rf*71: n = 6). **(E)** Bar graph shows mean deactivation time constants obtained for HCN1-WT, S710Rfs*71, and WT/S710Rf*71 channels (WT: n = 12; S710Rfs*71: n = 16; WT/S710Rfs*71: n = 6). All the statistical analyses in this figure were performed by one-way ANOVA and Bonferroni *post hoc* test. *P < 0.05, ***P < 0.005.

constructs into HEK cells. Representative traces of currents mediated by HCN1 channels were recorded from HEK cells expressing different mutant channels (**Figures 3A,F**). The E240G mutant did not affect current densities (WT: –186.7 ± 36.28 pA/pF; E240G: –144 ± 19.46 pA/pF; Dunnett's T3 test, $P > 0.05$), but induced a rightward shift in the activation curve of 19 mV (**Figures 3A–C**). So, we recognized this variant produced a gain-of-function effect, and the activation time constant (τ) was significantly shorter than that of WT channels within the range of –80 mV to –130 mV (Dunnett's T3 test, $P < 0.05$; **Figure 3D**) with deactivation time constants not affected (Two-sample t-test; $P > 0.05$; **Figure 3E**). The current densities of I380F and A395G were much smaller than WT channels at –130 mV (I380F: –7.14 ± 2.20 pA/pF; A395G: –31.95 ± 7.84 pA/pF) (**Figures 3A,B**), which indicated that these two variants likely exerted severe loss-of-function effects on HCN1 channels.

To investigate the function of heterozygous HCN1 channels formed by WT and mutant subunits, we performed co-expression experiments. WT/E240G channels produced a depolarizing shift in the activation curve of 15.9 mV (Bonferroni *post hoc* test, $P < 0.05$; **Figures 3F,H**), and the activation time constants were faster than the WT channels (Bonferroni *post hoc* test, $P < 0.05$; **Figures 3I,J**), which was similar to the homozygous state. Both heterozygous I380F channels and A395G channels presented with smaller current densities (Dunnet T3 test, $P < 0.05$; **Figures 3F,G**) and depolarized the activation curves by 24.4 and 18.1 mV, respectively (Bonferroni *post hoc* test, $P < 0.05$; **Figure 3H**). The activation time constants (–80 mV) were reduced by heterozygous WT/A395G channels (WT = 253.10 ± 31.37 ms; WT/A395G = 83.70 ± 9.84 ms; Bonferroni *post hoc* test, $P < 0.05$) and WT/I380F (Bonferroni *post hoc* test, WT/I380F = 100.03 ± 12.71 ms; Bonferroni *post hoc* test, $P < 0.05$) (**Figure 3I**). The deactivation time constants of heterozygous variant channels did not show any significant changes (WT1.0: 83.97 ± 31.24 ms; WT/I380F: 61.86 ± 5.70 ms; WT/A395G: 95.65 ± 4.25 ms; Bonferroni *post hoc* test, $P > 0.05$) (**Figure 3J**). These results indicate variants produced negative effects on the function of HCN1 channels in the heterozygous conditions.

Given that the C-terminal region is important to the activation kinetics, we investigated whether S710Rfs*71 or V572A affected channel function in order to assess the pathogenicity of these variants. The half-activation voltage of S710Rfs*71 was shifted to the left by 5.88 mV (Bonferroni *post hoc* test, $P < 0.05$), and the activation time constants were faster than those of WT channels (–130 mV: WT, 33.41 ± 4.60 ms; S710Rfs*71, 19.10 ± 1.06 ms; $P < 0.05$). The other properties of HCN1 channels including current density, activation curve, and the deactivation time constants were not affected. Co-expression experiments indicated that the activation time constants of WT/S710Rfs*71 were slightly faster than the WT channels (–130 mV: S710Rfs*71, 29.41 ± 5.42 ms; $P < 0.01$). However, current

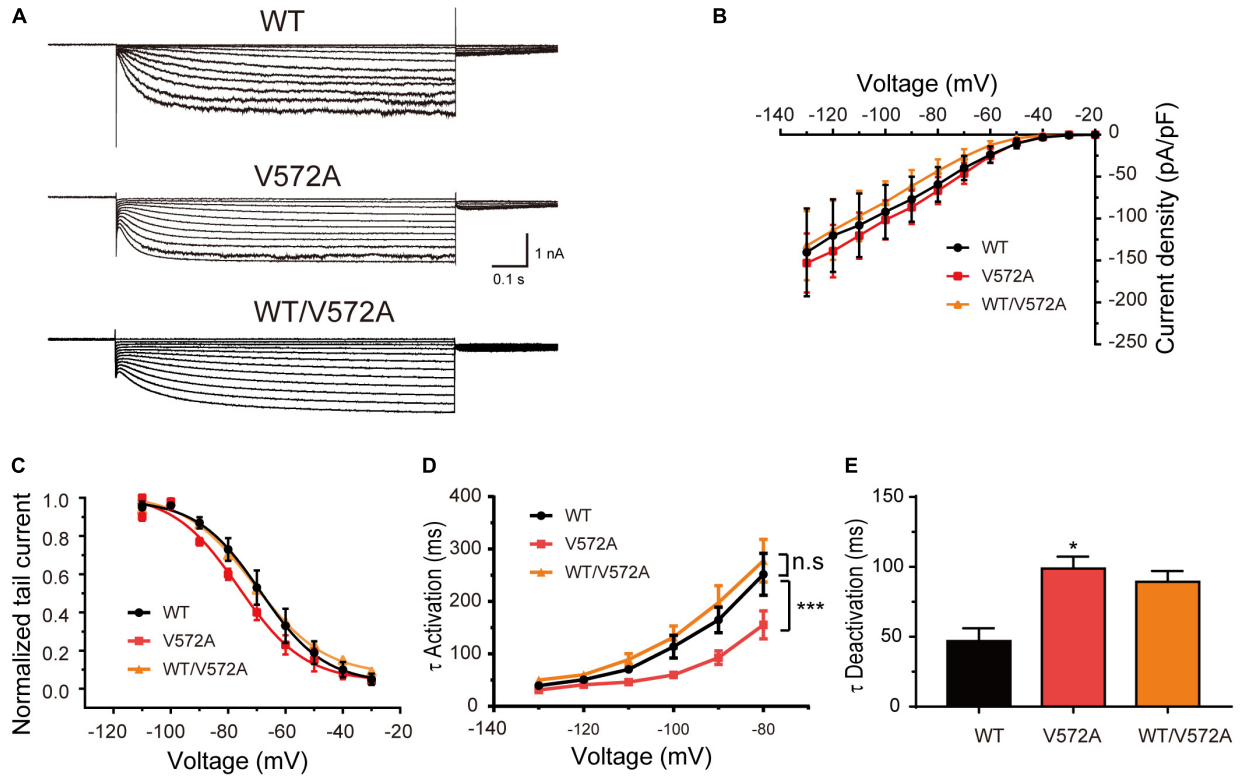

FIGURE 5 | Functional changes of the V572A variant. **(A)** Representative traces of WT, V572A, and WT/V572A channels. **(B)** Plot of mean current densities of WT (n = 11), V572A (n = 10), and WT/572A channels (n = 14). Two-sample t-test. **(C)** Voltage-dependent activation curves of WT channels (n = 9), V572A (n = 11), and WT/572A channels (n = 8). Analysis was done by two-sample t-test. **(D,E)** Summaries of mean activation time constants (WT: n = 16; V572A: n = 8; WT/V572A n = 11) and deactivation constants (WT: n = 10; V572A: n = 9; WT/V572A n = 12) for WT, V572A, and WT/572A. Analysis was done by two-sample t-test. $^*P < 0.05$, $^{***}P < 0.005$.

densities, activation curve, and deactivation time constants of WT/S710Rfs*71 were not affected (**Figure 4**).

In addition, the current densities and activation curves of V572A channels were unaffected in comparison with WT channels (Two-sample t-test, $P > 0.05$). However, V572A channels exhibited faster activation (at −110 mV: WT, 70.50 ± 6.98 ms; V572A, 46.19 ± 3.82 ms; two-sample t-test, $P < 0.05$) and slower deactivation (WT: 46.89 ± 9.18 ms; V572A: 98.76 ± 6.06 ms; two-sample t-test, $P < 0.05$) (**Figure 5**). The biophysical properties of WT/V572A channels were not changed compared to those of WT channels. These data demonstrated that variants affecting the C-terminal region also impaired channel function, including activation and deactivation kinetics.

The Expression of Hyperpolarization-Activated Cyclic Nucleotide-Gated Ion Channel 1 Channels in Neurons Was Impaired by Hyperpolarization-Activated Cyclic Nucleotide-Gated Ion Channel 1 Variants

To estimate the expression levels of HCN1 protein, we transfected WT and mutant plasmids into cortical neurons. In accordance with previous studies (Noam et al., 2010), immunoreactive HCN1 channels were detected in cortical neurons transfected with WT plasmids. The expressing patterns of A395G and S710Rfs71 channels were similar to that of WT channels. However, we observed that neurons expressing E240G and I380F channels showed weak immunoreactive HCN1 channels (**Figure 6**). These observations indicated that variants could reduce HCN1 protein expression in neurons.

Impact of Hyperpolarization-Activated Cyclic Nucleotide-Gated Ion Channel 1 Variants on Neuronal Excitability

Given that HCN1 channels mediate non-selective cation currents which play critical roles in neuronal excitability, we further studied the effects of *HCN1* variants on neurons. We chose two *HCN1* variants (E240 and I380F) with different biophysical properties in HEK293 cells. We observed neurons expressing WT, and E240G channels displayed voltage sags in response to a hyperpolarizing step (**Figure 7**). As the I380F channels lost the ability to mediate currents, the voltage sag was absent in neurons expressing the I380F channel (**Figure 7**).

As expected from the biophysical properties of HCN channels, neurons transfected with all types of HCN1 channels resulted in

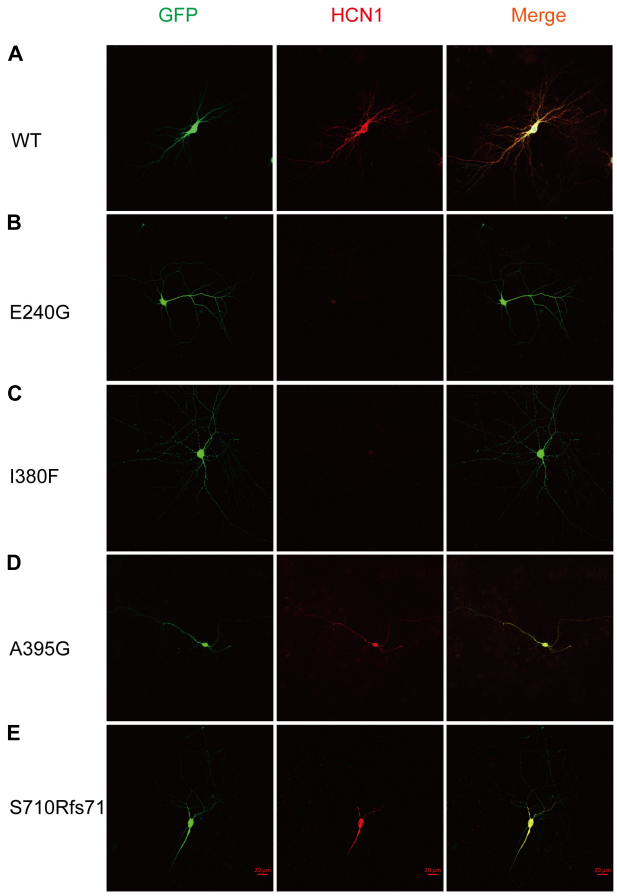

FIGURE 6 | Mutant HCN1 channels distributed differently in cortical neurons. **(A–E)** The expression of WT (n = 13), E240G (n = 7), I380F (n = 9), A395G (n = 9), and S710Rfs*71 (n = 9) channels in cortical neurons, respectively.

a depolarization of the membrane potential of neurons compared to the neurons transfected with plasmid vectors (**Figure 8B**) (Control: −51.7 ± 1.75 mV; WT: −40 ± 1.9 mV; E240G: −36.3 ± 1.46 mV; I380F: −42.80 ± 3.20 mV). Neurons transfected with all types of channels showed decreased input resistance (Control: 443.5 ± 30.87 MΩ; WT: 164.1 ± 17.12 MΩ; E240G: 284.7 ± 43 MΩ; I380F: 299.5 ± 26.3 MΩ). Both WT/E240G and WT/I380F caused a right shift in the activation curves, which indicated HCN1 channels were more likely to open at more depolarized potential, thus affecting resting membrane potential as well as input membrane resistance (**Figure 8C**). However, E240G and I380F channels might affect neuronal activity differently, since the two channels differ in biophysical properties. Considering this issue, we compared the excitability of neurons expressing WT or mutant channels under depolarizing current injection. Spike thresholds of neurons were not affected by either WT or mutant channels (**Figure 8D**). Neurons expressing WT and E240G channels showed a reduction in the number of action potentials fired in response to depolarizing current steps compared to those expressing empty channels, while neurons transfected with *HCN1* I380F showed a higher firing rate compared to the neurons expressing WT channels (**Figures 8A,E**). These data indicated mutant channels with different biophysical properties might exert different effects on neuronal excitability.

DISCUSSION

In the present study, we identified four novel variants causing *HCN1*-related epilepsy and investigated functional changes of the five variants in five new cases. According to our study and a previous study (Marini et al., 2018), the clinical phenotypes caused by different mutations overlap in many aspects, including the early age of onset, febrile sensitivity, seizure types, and developmental delay. The electrophysiological experiments verified functional changes of the five variants. In addition, two variants (E240G and I380F) showed reduced protein expression in the cortical neurons of mice and affected neuronal excitability.

The dysfunctions of the mutant HCN1 channels, including changes in current densities and activation/deactivation kinetics, played essential roles in neuronal excitability. The E240G mutation produced a gain-of-function effect due to the right-shift activation curve and faster activation time constants. The I380F and A395G mutations significantly reduced current densities, suggesting a loss-of-function effect. The S710Rfs*71 mutation showed a loss- and gain-of-function effect since the activation curve shifted to the left and the activation time constants were reduced. The V572 mutation displayed a faster activation, suggesting a GOF effect. Besides, all the three *HCN1* mutations (E240G, I380F, and A395G) produced dominant-negative effects in heterozygous conditions. Notably, some variants might cause some confusing effects in heterozygous conditions. For example, two LOF mutations (I380F and A395G) displayed a significant rightward shift in the activation curve in heterozygous conditions implying a GOF effect, which is similar to the previously reported mutation (M305L).

Also, when the variants were expressed in neurons, they exerted dominate-negative effects, since a mutant subunit could be assembled into heteromeric channels with WT subunits. Epilepsy has been recognized as a brain disorder resulting from neuronal hyperexcitability and hypersynchronous firing. In addition to the findings that LOF and GOF *HCN1* mutants could cause epilepsy, we unveiled that the *HCN1* mutants could exert effects on neurons in different manners. First, we found that the protein expression of HCN1 channels in neurons could also be affected. The surface expression of HCN1 depends on many factors, including protein synthesis and trafficking. Interestingly, we noted that these two variants caused more severe clinical phenotypes than other mutants, as patients presented with more frequent seizures, longer seizure duration, and even sudden death. Although altered protein expression might not be sufficient to clarify the phenotypes, it is advisable to pay more attention to the protein expression in different neurons when evaluating the pathogenicity of the mutants. Second, LOF and GOF variants may impose effects on neural excitability differently. The present study showed that

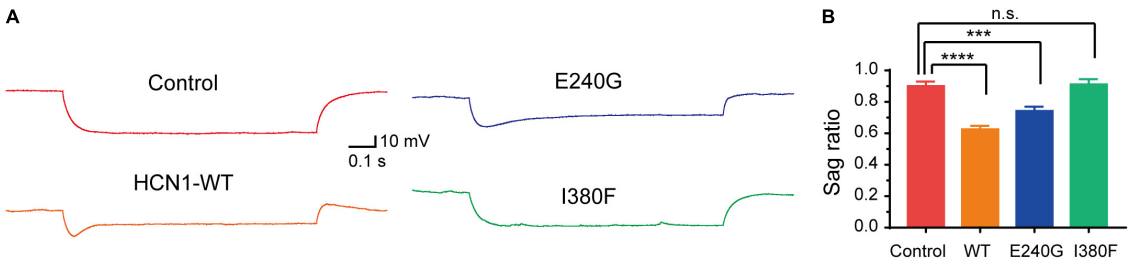

FIGURE 7 | Hyperpolarizing voltage sag in cortical neurons expressing WT and mutant channels. **(A)** Representative recordings of voltage sag in response to a −100 pA hyperpolarizing current injection in WT and mutant *HCN1*-transfected neurons. **(B)** Bar graph shows mean voltage sag ratios for different types of HCN1 channels. ***$P < 0.005$, ****$P < 0.001$.

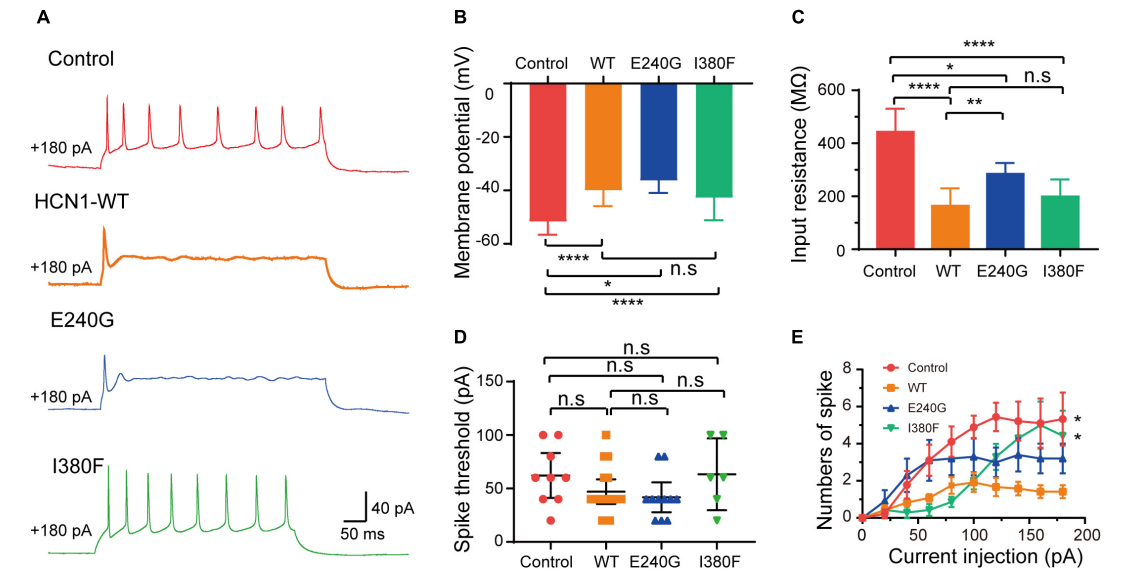

FIGURE 8 | Neuronal excitability was affected by HCN1 variants. **(A)** Representative recordings of action potential firing patterns in response to current injection (180 pA). **(B)** Bar graph summarizes the mean membrane potential in neurons expressing different HCN1 channel types. Analysis was done by Bonferroni *post hoc* test. **(C)** Bar graph shows mean input resistance in neurons expressing different HCN1 channel types. Dunnett's T3 *post hoc* test. **(D)** Bar graph shows spike thresholds elicited by current injection were not affected. Analysis was done by Mann–Whitney test. **(E)** Plot of the mean firing rates of neurons in response to current injections. *$P < 0.05$, **$P < 0.01$, ****$P < 0.001$.

neurons transfected with *HCN1* E240G might contribute to neuronal hyperexcitability by depolarizing membrane potential and impairing the ability to fire action potentials. Since the reversal potential of HCN1 channels is higher than the threshold for action potential generation, HCN1 channel currents depolarize the membrane potential when it reaches the resting membrane potential (Robinson and Siegelbaum, 2003). Besides, firing deficits of excitatory neurons might impair information transmission among neurons. Accordingly, this epileptic activity caused by GOF mutants could be reduced by HCN1 channel inhibitors (Inaba et al., 2006).

It is worth noting that the *HCN1* I380F variant increased firing rate, which suggests LOF variants could cause hyperexcitability of excitatory neurons. Previous studies have shown that two LOF variants (L157V and M294L) depolarized membrane potential, decreased input resistance, and increased firing rate (Bonzanni et al., 2018; Bleakley et al., 2021), thus contributing to neuronal hyperexcitability. *HCN1* null mice showed higher susceptibility to seizures and higher mortality rates (Santoro et al., 2010). Additionally, dendrites could become more excitable due to the enhancement of excitatory synaptic inputs that impair the excitatory/inhibitory balance in neuronal circuits following a reduction in input resistance (Huang et al., 2009; Yi et al., 2016). It is notable that seizures, particularly for status epilepticus, decrease the expression and suppress the function of HCN1 channels (Shin et al., 2008), which may imply worse endings of epilepsy caused by LOF variants.

Previous studies have shown that the biophysical properties of channelopathy-causing variants, such as *SCN1A* (Berecki et al., 2019), *KCNA2* (Syrbe et al., 2015), *KCNQ2* (Miceli et al., 2015), and *GluN2B* (Platzer et al., 2017) may correlate with phenotypes. By analyzing the results of functional experiments of 17 variants in previous studies and five variants in our study, we found that LOF variants caused more severe and

complicated phenotypes (**Table 1** and **Supplementary Table 2**). We observed that LOF variants displayed a higher rate of epilepsy onset within the first year of life (13/18), death (3/18), status epilepticus (5/18), uncontrolled seizures (10/18), and moderate/severe intellectual disabilities (12/18). We also observed that LOF variants might be more likely to cause microencephaly (3/18) and abnormalities in brain structure (3/14), while no patient carrying GOF variants presented with microencephaly or abnormal neuroimaging. However, it is difficult to distinguish the types of variants according to phenotypes, because phenotypes of patients with LOF variants or GOF variants overlap in some aspects, such as the age of seizure onset, seizure types, intellectual disorders, and EEG. Additionally, we noted six out of seven variants located in the S5 through S6 domains showed LOF actions by reducing the current densities of the channels, and four out of seven variants located in the C-terminal domain displayed GOF actions by shifting the voltage-dependent activation curves to the right. Coincidentally, a previous study (Marini et al., 2018) showed that variants located in transmembrane or the domains of pore structure (from S5 to S6) caused more severe phenotypes compared to those located in the C-terminal region. It is known that a loop between the S5 and S6 domains, forming an ion selectivity filter and a C-terminal domain, affects the voltage dependence of activation (Postea and Biel, 2011; Lee and MacKinnon, 2017). Despite the fact that both biophysical properties and the location of variants may correlate with the severity of phenotypes, and the location of mutant residue determines the channel function to some extent, we are unable to determine which factor plays a decisive role. In the future, more functional studies are necessary to verify this.

CONCLUSION

In conclusion, the present study expands the genotypic and phenotypic spectrum of patients with HCN1-related epilepsy and clarifies the underlying mechanisms. We reported five new cases, including four unreported pathogenic/likely pathogenic variants. We provided an assessment of biophysical function for each variant, which could help patients to receive individual therapy in the future. We confirmed that *HCN1* variants contributed to neural hyperexcitability by regulating input resistance and firing rate of action potentials, and we have shown that they can affect protein expression in neurons for the first time.

DATA AVAILABILITY STATEMENT

The datasets presented in this study can be found in online repositories. The names of the repository/repositories and accession number(s) can be found in the article/**Supplementary Material**.

ETHICS STATEMENT

The studies involving human participants were reviewed and approved by the ethics committee of Xiangya Hospital of Central South University. Written informed consent to participate in this study was provided by the participants' legal guardian/next of kin. The animal study was reviewed and approved by the ethics committee of Xiangya Hospital of Central South University. Written informed consent was obtained from the individual(s), and minor(s)' legal guardian/next of kin, for the publication of any potentially identifiable images or data included in this article.

AUTHOR CONTRIBUTIONS

CX and JP conceived the experiments and wrote the article. CX and FL performed functional experiments and analyses. FH, XW, LM, HH, and FY carried out genetic analyses of patients. JP analyzed seizure types of patients and carried out clinical characterization. All authors contributed to the article and approved the submitted version.

FUNDING

This work was supported by the National Natural Science Foundation of China (Nos. 81771409 and 82071462) and the Fundamental Research Funds for the Central Universities of Central South University (No. 2019zzts340).

ACKNOWLEDGMENTS

We thank patients as well as other participants for their contribution to this study.

SUPPLEMENTARY MATERIAL

The Supplementary Material for this article can be found online at: https://www.frontiersin.org/articles/10.3389/fnmol.2022.870182/full#supplementary-material

REFERENCES

Benarroch, E. E. (2013). HCN channels: function and clinical implications. *Neurology* 80, 304–310. doi: 10.1212/WNL.0b013e31827dec42

Berecki, G., Bryson, A., Terhag, J., Maljevic, S., Gazina, E. V., Hill, S. L., et al. (2019). SCN1A gain of function in early infantile encephalopathy. *Ann. Neurol.* 85, 514–525. doi: 10.1002/ana.25438

Bleakley, L. E., McKenzie, C. E., Soh, M. S., Forster, I. C., Pinares-Garcia, P., Sedo, A., et al. (2021). Cation leak underlies neuronal excitability in an HCN1 developmental and epileptic encephalopathy. *Brain* 144, 2060–2073. doi: 10.1093/brain/awab145

Bonzanni, M., DiFrancesco, J. C., Milanesi, R., Campostrini, G., Castellotti, B., Bucchi, A., et al. (2018). A novel de novo HCN1 loss-of-function mutation in genetic generalized epilepsy causing increased neuronal

excitability. *Neurobiol. Dis.* 118, 55–63. doi: 10.1016/j.nbd.2018.06.012

Brewster, A. L., Chen, Y., Bender, R. A., Yeh, A., Shigemoto, R., and Baram, T. Z. (2006). Quantitative Analysis and Subcellular Distribution of mRNA and Protein Expression of the Hyperpolarization-Activated Cyclic Nucleotide-Gated Channels throughout Development in Rat Hippocampus. *Cereb. Cortex* 17, 702–712. doi: 10.1093/cercor/bhk021

Guo, H., Li, Y., Shen, L., Wang, T., Jia, X., Liu, L., et al. (2019). Disruptive variants of CSDE1 associate with autism and interfere with neuronal development and synaptic transmission. *Sci. Adv.* 5:eaax2166. doi: 10.1126/sciadv.aax2166

Huang, Z., Walker, M. C., and Shah, M. M. (2009). Loss of dendritic HCN1 subunits enhances cortical excitability and epileptogenesis. *J. Neurosci.* 29, 10979–10988. doi: 10.1523/JNEUROSCI.1531-09.2009

Inaba, Y., Biagini, G., and Avoli, M. (2006). The H current blocker ZD7288 decreases epileptiform hyperexcitability in the rat neocortex by depressing synaptic transmission. *Neuropharmacology* 51, 681–691. doi: 10.1016/j.neuropharm.2006.05.017

Lee, C. H., and MacKinnon, R. (2017). Structures of the Human HCN1 Hyperpolarization-Activated Channel. *Cell* 168, 111–120.e11. doi: 10.1016/j.cell.2016.12.023

Lucariello, M., Vidal, E., Vidal, S., Saez, M., Roa, L., Huertas, D., et al. (2016). Whole exome sequencing of Rett syndrome-like patients reveals the mutational diversity of the clinical phenotype. *Hum. Genet.* 135, 1343–1354. doi: 10.1007/s00439-016-1721-3

Marini, C., Porro, A., Rastetter, A., Dalle, C., Rivolta, I., Bauer, D., et al. (2018). HCN1 mutation spectrum: from neonatal epileptic encephalopathy to benign generalized epilepsy and beyond. *Brain* 141, 3160–3178. doi: 10.1093/brain/awy263

Mei, D., Cetica, V., Marini, C., and Guerrini, R. (2019). Dravet syndrome as part of the clinical and genetic spectrum of sodium channel epilepsies and encephalopathies. *Epilepsia* 60, S2–S7. doi: 10.1111/epi.16054

Miceli, F., Soldovieri, M. V., Ambrosino, P., De Maria, M., Migliore, M., Migliore, R., et al. (2015). Early-onset epileptic encephalopathy caused by gain-of-function mutations in the voltage sensor of Kv7.2 and Kv7.3 potassium channel subunits. *J. Neurosci.* 35, 3782–3793. doi: 10.1523/JNEUROSCI.4423-14.2015

Nava, C., Dalle, C., Rastetter, A., Striano, P., de Kovel, C. G., Nabbout, R., et al. (2014). De novo mutations in HCN1 cause early infantile epileptic encephalopathy. *Nat. Genet.* 46, 640–645. doi: 10.1038/ng.2952

Noam, Y., Zha, Q., Phan, L., Wu, R. L., Chetkovich, D. M., Wadman, W. J., et al. (2010). Trafficking and surface expression of hyperpolarization-activated cyclic nucleotide-gated channels in hippocampal neurons. *J. Biol. Chem.* 285, 14724–14736. doi: 10.1074/jbc.M109.070391

Oyrer, J., Maljevic, S., Scheffer, I. E., Berkovic, S. F., Petrou, S., and Reid, C. A. (2018). Ion Channels in Genetic Epilepsy: from Genes and Mechanisms to Disease-Targeted Therapies. *Pharmacol. Rev.* 70, 142–173. doi: 10.1124/pr.117.014456

Platzer, K., Yuan, H., Schütz, H., Winschel, A., Chen, W., Hu, C., et al. (2017). GRIN2Bencephalopathy: novel findings on phenotype, variant clustering, functional consequences and treatment aspects. *J. Med. Genet.* 54, 460–470. doi: 10.1136/jmedgenet-2016-104509

Porro, A., Abbandonato, G., Veronesi, V., Russo, A., Binda, A., Antolini, L., et al. (2021). Do the functional properties of HCN1 mutants correlate with the clinical features in epileptic patients? *Prog. Biophys. Mol. Biol.* 166, 147–155. doi: 10.1016/j.pbiomolbio.2021.07.008

Postea, O., and Biel, M. (2011). Exploring HCN channels as novel drug targets. *Nat. Rev. Drug Discov.* 10, 903–914. doi: 10.1038/nrd3576

Richards, S., Aziz, N., Bale, S., Bick, D., Das, S., Gastier-Foster, J., et al. (2015). Standards and guidelines for the interpretation of sequence variants: a joint consensus recommendation of the American College of Medical Genetics and Genomics and the Association for Molecular Pathology. *Genet. Med.* 17, 405–424. doi: 10.1038/gim.2015.30

Robinson, R. B., and Siegelbaum, S. A. (2003). Hyperpolarization-activated cation currents: from molecules to physiological function. *Annu. Rev. Physiol.* 65, 453–480. doi: 10.1146/annurev.physiol.65.092101.142734

Santoro, B., and Shah, M. M. (2020). Hyperpolarization-Activated Cyclic Nucleotide-Gated Channels as Drug Targets for Neurological Disorders. *Annu. Rev. Pharmacol. Toxicol.* 60, 109–131. doi: 10.1146/annurev-pharmtox-010919-023356

Santoro, B., Lee, J. Y., Englot, D. J., Gildersleeve, S., Piskorowski, R. A., Siegelbaum, S. A., et al. (2010). Increased seizure severity and seizure-related death in mice lacking HCN1 channels. *Epilepsia* 51, 1624–1627. doi: 10.1111/j.1528-1167.2010.02554.x

Shin, M., Brager, D., Jaramillo, T. C., Johnston, D., and Chetkovich, D. M. (2008). Mislocalization of h channel subunits underlies h channelopathy in temporal lobe epilepsy. *Neurobiol. Dis.* 32, 26–36. doi: 10.1016/j.nbd.2008.06.013

Steel, D., Symonds, J. D., Zuberi, S. M., and Brunklaus, A. (2017). Dravet syndrome and its mimics: beyond SCN1A. *Epilepsia* 58, 1807–1816. doi: 10.1111/epi.13889

Syrbe, S., Hedrich, U. B. S., Riesch, E., Djemie, T., Muller, S., Moller, R. S., et al. (2015). De novo loss- or gain-of-function mutations in KCNA2 cause epileptic encephalopathy. *Nat. Genet.* 47, 393–399. doi: 10.1038/ng.3239

Wang, J., Wen, Y., Zhang, Q., Yu, S., Chen, Y., Wu, X., et al. (2019). Gene mutational analysis in a cohort of Chinese children with unexplained epilepsy: identification of a new KCND3 phenotype and novel genes causing Dravet syndrome. *Seizure* 66, 26–30. doi: 10.1016/j.seizure.2019.01.025

Yi, F., Danko, T., Botelho, S. C., Patzke, C., Pak, C., Wernig, M., et al. (2016). Autism-associated SHANK3 haploinsufficiency causes Ih channelopathy in human neurons. *Science* 352:aaf2669. doi: 10.1126/science.aaf2669

Conflict of Interest: The authors declare that the research was conducted in the absence of any commercial or financial relationships that could be construed as a potential conflict of interest.

Publisher's Note: All claims expressed in this article are solely those of the authors and do not necessarily represent those of their affiliated organizations, or those of the publisher, the editors and the reviewers. Any product that may be evaluated in this article, or claim that may be made by its manufacturer, is not guaranteed or endorsed by the publisher.

frontiers | Frontiers in Molecular Neuroscience

ORIGINAL RESEARCH
published: 22 July 2022
doi: 10.3389/fnmol.2022.807671

Beclin1 Deficiency Suppresses Epileptic Seizures

Min Yang[1†], Peijia Lin[1†], Wei Jing[1], Haokun Guo[1], Hongnian Chen[1], Yuanyuan Chen[1], Yi Guo[1], Yixue Gu[1], Miaoqing He[1], Junhong Wu[1], Xuejun Jiang[2,4], Zhen Zou[3,4], Xin Xu[1], Chengzhi Chen[4,5], Fei Xiao[1]*, Xuefeng Wang[1]* and Xin Tian[1]**

[1] Chongqing Key Laboratory of Neurology, Department of Neurology, The First Affiliated Hospital of Chongqing Medical University, Chongqing, China, [2] Center of Experimental Teaching for Public Health, Experimental Teaching and Management Center, Chongqing Medical University, Chongqing, China, [3] Molecular Biology Laboratory of Respiratory Diseases, Institute of Life Sciences, Chongqing Medical University, Chongqing, China, [4] Research Center for Environment and Human Health, School of Public Health, Chongqing Medical University, Chongqing, China, [5] Department of Occupational and Environmental Health, School of Public Health and Management, Chongqing Medical University, Chongqing, China

OPEN ACCESS

Edited by:
Yuwu Jiang,
Peking University, China

Reviewed by:
Anna Fassio,
University of Genoa, Italy
Rochelle Marie Hines,
University of Nevada, Las Vegas, United States

***Correspondence:**
Chengzhi Chen
chengzhichen@cqmu.edu.cn
Fei Xiao
feixiao_81@126.com
Xuefeng Wang
xfyp@163.com
Xin Tian
xintian@cqmu.edu.cn

[†]These authors have contributed equally to this work and share first authorship

Specialty section:
This article was submitted to Brain Disease Mechanisms, a section of the journal Frontiers in Molecular Neuroscience

Received: 02 November 2021
Accepted: 17 June 2022
Published: 22 July 2022

Citation:
Yang M, Lin P, Jing W, Guo H, Chen H, Chen Y, Guo Y, Gu Y, He M, Wu J, Jiang X, Zou Z, Xu X, Chen C, Xiao F, Wang X and Tian X (2022) Beclin1 Deficiency Suppresses Epileptic Seizures. Front. Mol. Neurosci. 15:807671. doi: 10.3389/fnmol.2022.807671

Epilepsy is a common disease of the nervous system. Autophagy is a degradation process involved in epilepsy, and in turn, seizures can activate autophagy. Beclin1 plays a critical role in autophagy and participates in numerous physiological and pathological processes. However, the mechanism underlying the effect of Beclin1 on epilepsy remains unclear. In this study, we detected increased expression of Beclin1 in brain tissues from patients with temporal lobe epilepsy (TLE). Heterozygous disruption of *beclin1* decreased susceptibility to epilepsy and suppressed seizure activity in two mouse epilepsy models. We further illustrated for the first time that heterozygous disruption of *beclin1* suppresses excitatory synaptic transmission, which may be caused by a decreased dendritic spine density. These findings suggest for the first time that the regulation of Beclin1 may serve as a strategy for antiepileptic therapy. In addition, Beclin1 participates in synaptic transmission, and the development of dendritic spines may be a biological function of Beclin1 independent of its role in autophagy.

Keywords: epilepsy, Beclin1, transgenic mice, excitatory synaptic transmission, dendritic spines

INTRODUCTION

Epilepsy is a common disease of the nervous system that is caused by the abnormal discharge of highly synchronized neurons; it is characterized by recurrent seizures (Fisher et al., 2014) and affects approximately 65 million people worldwide. Although more than 20 antiepileptic drugs (AEDs) have been developed and are used to treat epilepsy, approximately one-third of patients fail to achieve seizure control or soon become resistant to their effects (Pitkänen and Lukasiuk, 2011). Therefore, the identification of novel therapeutic targets and development of effective drugs that prevent or reverse the molecular mechanisms underlying epilepsy progression are urgently needed.

Based on accumulating evidence, autophagy may be involved in epilepsy (Egan et al., 2011). Autophagy is a process for degrading intracellular substances that is highly conserved among species and involves the transport of abnormal proteins, damaged organelles and other macromolecules to lysosomes for degradation (Levine and Kroemer, 2019). Some researchers have found that knockout of the autophagy gene ATG7 in mice leads to spontaneous epilepsy (Wong, 2013). Lafora disease, an autosomal recessive epilepsy syndrome, is caused mainly by deficiency

of the phosphatase laforin or the ubiquitin ligase malin, and knockout of either enzyme results in the same clinical phenotype as defective autophagy (Criado et al., 2012). Hence, researchers have proposed that impaired autophagy might trigger the occurrence of epilepsy and conversely epilepsy might likewise result in the dysregulation of autophagy, which would further exacerbate epilepsy and create a vicious cycle (Li et al., 2018). However, the mechanism of autophagy in epilepsy has not been completely elucidated (McDaniel et al., 2011). Therefore, a deeper understanding of the mechanisms may be needed.

Beclin1 is a key molecule involved in the autophagy process that was first identified as a novel protein in 1998 (Liang et al., 1998). Subsequently, Beclin1 was confirmed to be a homolog of the yeast autophagy gene Apg6/Vps30, which compensates for the autophagy disorder caused by *apg6* gene defects. Therefore, *beclin1* was considered the first identified autophagy-related gene in humans (Liang et al., 1999). Beclin1 participates in many physiological and pathological processes by forming a complex with PI3K along with VPS34 and other proteins (Liang et al., 2006). Beclin1 is expressed in the nervous system and participates in a variety of neurodegenerative diseases, such as Alzheimer's disease and Huntington's disease (Ashkenazi et al., 2017). However, the potential role of Beclin1 in regulating epilepsy remains unclear. Therefore, in the present study, we aimed to investigate whether Beclin1 modulates epilepsy. We further observed whether the heterozygous disruption of *beclin1* affects neuronal synaptic transmission by performing whole-cell patch clamp recordings. We observed changes in the development of dendritic spines and autophagy in *beclin1*$^{\pm}$ mice to elucidate the underlying mechanisms. These findings indicate that modulating Beclin1 may represent a new approach for preventing epilepsy and may provide new insights into the biological functions of Beclin1.

MATERIALS AND METHODS

Human Brain Tissues

We obtained cerebral temporal lobe cortical tissues from patients with drug-refractory temporal lobe epilepsy (TLE) or patients with brain trauma who underwent surgery at The First Affiliated Hospital of Chongqing Medical University. According to the classification of epileptic seizures proposed by the International League Against Epilepsy (ILAE) in 2001 (Engel, 2001), patients diagnosed with TLE had typical epilepsy symptoms and electroencephalographic features and recurrent seizures despite having taken 3 or more different AEDs for more than 2 years. Age- and sex-matched patients who were treated for increased intracranial pressure secondary to traumatic brain injury and had no history of epilepsy, no exposure to AEDs, or no other history of neurological and psychiatric disorders were considered the control group. The surgery was performed using the anterior temporal lobe resection procedure (Falconer and Taylor, 1968), and the resected epileptic temporal lesion was localized using high-resolution magnetic resonance imaging, prolonged video-EEG monitoring, and/or positron-emission tomography (PET). The clinical features of the patients included in this study are summarized in **Table 1**.

Animals

All experiments were conducted in accordance with the guidelines of the Guide for the Care and Use of Laboratory Animals. Healthy, specific pathogen-free (SPF) adult wild-type (WT) male C57BL/6J mice (weight 25 ± 2 g, age 8–10 weeks) were provided by the Experimental Animal Center of Chongqing Medical University. *beclin1*$^{\pm}$ mice on a C57BL/6J background were obtained from the laboratory of Beth Levin as previously described (Liu and Wang, 2019). All mice were housed in groups of 5 mice per cage under standard conditions, including a 12-h light/dark cycle, temperature of 23 ± 1°C, relative humidity of 50 ± 10%, and an SPF environment with sufficient standard feed and water.

Epileptic brain tissues were obtained from mice with kainic acid (KA)-induced epilepsy presenting spontaneous recurrent seizures (SRSs) or mice that were fully kindled after pentylenetetrazol (PTZ) treatment. Correspondingly, control brain tissues were obtained from mice injected with saline under the same conditions.

Pentylenetetrazol - Kindled Epilepsy Model

Mice received intraperitoneal injections of 35 mg/kg PTZ every other day for 30 days to establish the PTZ-kindled chronic epilepsy model. After each injection, the seizures experienced the mice in each group were graded for 30 min according to the Racine scale (Racine, 1972): grade I, clustered whisker and facial movements with chewing motions; grade II, facial spasm with

TABLE 1 | Clinical characteristics of patients with intractable TLE and control patients.

Number	Sex (M/F)	Age (Years)	Course (Years)	AEDs taken before surgery
T1	F	26	7	CBZ, VPA, OXC, TPM
T2	M	22	5	CBZ, TPM, CZP
T3	F	25	10	CBZ, PB, LTG, LEV
T4	M	24	8	VPA, CBZ, TPM, PB
T5	M	18	7	PHT, PB, CBZ, VPA
T6	F	35	10	CBZ, VPA, TPM, OCX
T7	F	22	9	CBZ, TPM, CZP
T8	M	29	14	CBZ, LTG, LEV, PB
C1	M	11	0	None
C2	F	38	0	None
C3	M	40	0	None
C4	F	34	0	None
C5	M	30	0	None
C6	F	17	0	None
C7	M	11	0	None
C8	M	25	0	None

T, TLE temporal lobe epilepsy; C, control; M, male; F, female; CBZ, carbamazepine; LTG, lamotrigine; LEV, levetiracetam; OXC, oxcarbazepine; PHT, phenytoin; PB, phenobarbital; TPM, topiramate; VPA, valproic acid.

rhythmic nodding; grade III, unilateral forelimb clonus or tonus; grade IV, bilateral forelimb tonic–clonic seizures with rearing; and grade V, loss of posture or generalized tonic–clonic seizures (GTCSs) with a fall or death.

Establishment of the Kainic Acid -Induced Chronic Epilepsy Model and Local Field Potential Recording

To establish the KA-induced chronic epilepsy model, mice were anesthetized and fixed on a stereotaxic apparatus. Then, 1.0 nmol of KA (Sigma–Aldrich) in 50 ml of saline was injected into the hippocampi [anteroposterior (AP), −1.6 mm; mediolateral (ML), −1.5 mm; dorsoventral (DV), −1.5 mm] of the mice. Diazepam (10 mg/kg) was administered to terminate non-convulsive status epilepticus (SE) 2 h after the injection. The mice were continuously recorded with a digital video camera for 1 month. The observers counted the number of grade IV or V SRSs in each group. The latency and total number of SRSs were analyzed.

After video monitoring of KA-induced chronic seizures, intracranial local field potential (LFP) recordings were performed as previously described (Yang et al., 2018). Two stainless steel screws were implanted in the anterior cranium, and a platinum-iridium alloy microwire (25 μm in diameter; Plexon, Hong Kong, SAR, China) was implanted into the right dorsal hippocampus (AP, 1.6 mm; ML, 1.6 mm; DV, 1.5 mm). The guide cannula, the microwire, and a U-shaped frame were cemented to the skull to hold the head. Each mouse was continuously recorded for 30 min using a MAP data acquisition system (Plexon, Dallas, TX, United States). The LFP data were analyzed using NeuroExplorer (Nex Technologies, Littleton, MA, United States). Each mouse was continuously recorded for 30 min to assess LFP signals. A cluster of paroxysmal discharges with amplitudes two times greater than those at baseline that occurred spontaneously with a frequency greater than 1 Hz and a duration greater than 5 was recorded as a seizure-like event (SLE). The total number of SLEs, the duration of each SLE and the spectrograms obtained during the 30-min recording were analyzed using NeuroExplorer VR software (Version 4, Plexon, Hong Kong SAR, China).

Protein Extraction and Western Blot Analysis

For protein extraction, mice were anesthetized with 1% sodium pentobarbital, and the cortex and hippocampus were isolated from the brain of each mouse and placed on ice. A RIPA protein extraction kit (P0013B, Beyotime Biotechnology, China) containing phenylmethylsulfonyl fluoride (PMSF) was used to extract total protein. An enhanced bicinchoninic acid (BCA) protein assay kit (P0012S, Beyotime Biotechnology, China) was used to determine the protein concentrations.

Western blotting was completed using published protocols (Li et al., 2016). SDS–PAGE Sample Loading Buffer-5 × (P0012A, Beyotime Biotechnology, China) was used to denature the proteins. Extracts were resolved on SDS–PAGE gels (5% spacer gel and 10% separating gel) and then subjected to western blot analysis. The following antibodies were used in the present study: rabbit anti-Beclin1 antibody (11306-1-AP, Proteintech, China, RRID:AB_2259061), rabbit anti-LC3 antibody (14600-1-AP, Proteintech, China, RRID:AB_2137737), rabbit anti-p62/sequestosome-1 (SQSTM1) antibody (18420-1-AP, Proteintech, China, RRID:AB_10694431), rabbit anti-GAPDH antibody (10494-1-AP, Proteintech, China, RRID:AB_2263076), and goat anti-rabbit IgG antibody (SA00001-2, Proteintech, China, RRID:AB_2722564). The bands were visualized using Western Bright ECL reagent (Advansta, United States) and a Fusion FX5 image analysis system (Vilber Lourmat, France).

Primary Hippocampal Neuron Culture, Plasmid Transfection and Drug Intervention

Primary neuronal cultures were established as previously described (Guo et al., 2020). Postnatal brain tissue was dissected from early postnatal mice, and the tissues were digested with trypsin and mechanical dissociation to obtain neurons. The cell suspension was diluted with DMEM supplemented with 20% FBS (Gibco, Thermo Fisher Scientific). Neurons were plated at a density of 100,000 cells on poly-L-lysine–coated 35-mm dishes or glass coverslips in 6-well plates and incubated in a cell culture incubator at 37°C for 4 h. Four hours after plating, the cells were maintained in Neurobasal medium supplemented with B27, 2 mM L-glutamine, 100 U/ml penicillin, and 100 μg/ml streptomycin (Invitrogen). Neurons were transfected with a plasmid encoding green fluorescent protein (GFP) using the calcium phosphate transfection method at 7 days (DIV7) *in vitro* to visualize their spines. Certain cells were treated with 10 μM 3-methyladenine (3-MA) or 100 nM rapamycin (RAPA) (Selleck, United States) to assess the effects of drug interventions.

Immunofluorescence Staining and Semiquantitative Analysis

For the preparation of brain tissue sections, male C57BL/6 mice (7–8 weeks old) were anesthetized with 1% sodium pentobarbital and successively subjected to ischemia–reperfusion with 40 ml of saline and 40 ml of 4% paraformaldehyde. Brain tissues were removed, soaked in 4% paraformaldehyde for 12 h and then soaked in a 30% sucrose solution for 48 h. The tissues were embedded in optimum cutting temperature (OCT) compound (Sakura, 4583) and cut into 15 μm sections with a cryotome (Leica CM1950).

For IF staining, the tissue sections were permeabilized with 0.4% Triton X-100 at 37°C for 30 min, soaked in a sodium citrate solution (P0086, Beyotime, China), heated in a microwave oven for 3 min at high temperature and 10 min at low temperature, and then blocked with the working dilution of goat serum (C0265, Beyotime, China) for 1 h at 37°C. The sections were then incubated overnight with a mixture of primary antibodies at 4°C followed by washing and incubated with secondary antibodies in the dark at room temperature (RT) for 1 h for surface staining. For immunostaining of cultured neurons, neurons were fixed with 4% paraformaldehyde/4% sucrose in PBS for 30 min at RT, permeabilized with 0.3% Triton X-100 for 15 min and blocked with 10% goat serum for 30 min at RT. Neurons were incubated

with the primary antibody at 4°C for 6 h and incubated with the secondary antibody at RT for 1 h. Images were acquired with a confocal microscope (ZEISS, Wetzlar, Germany).

The primary antibodies applied included a rabbit anti-Beclin1 antibody (11306-1-AP; Proteintech, China, RRID:AB_2259061), mouse anti-PSD-95 antibody (MAB1596, Millipore Sigma, United States, RRID:AB_2092365), and guinea pig anti-vGluT1 antibody (135304, Synaptic Systems, Germany, RRID:AB_887878). The fluorophore-conjugated secondary antibodies used were goat anti-guinea pig Alexa Fluor 647 (ab150187; Abcam, Britain, RRID:AB_2827756), goat anti-rabbit Alexa Fluor 488 (A-11008; Invitrogen, United States, RRID:AB_143165), goat anti-mouse Alexa Fluor 549 antibodies (A-11005, Invitrogen, United States, RRID:AB_141372), goat anti-rabbit Alexa Fluor 594 antibodies (A23420, Abbkine, United States), and goat anti-mouse Alexa Fluor 488 antibodies (A23210, Abbkine, United States).

For the semiquantitative analysis, staining was performed under the same experimental conditions, and the images were captured with the same laser confocal excitation light intensity. Analyses of the fluorescence intensity of Beclin1 puncta and colocalization were performed using Image-Pro Plus 6.0 software. The dendritic spine density was analyzed using ImageJ software. Puncta positive for pre- and postsynaptic terminals were counted in 10 μm segments along the length of the dendrite.

Cell Viability Assay

Cell viability was measured by MTT Kit (Meilunbio, China) according to the manufacturer's protocol. Neurons were seeded onto 96-well plates at a density of 2×10^3 cells/well and cultured for 24 h. Then, the cells were treated with MTT reagent for 4 h. Formazan solution was incubated with the cells for 4 h at 37°C. A multifunction enzyme-linked analyzer (Varioskan LUX, Thermo Fisher Scientific, United States) was used to detect the absorbance value (OD) at 570 nm.

Nissl Staining

Frozen tissue sections were prepared for staining. Sections from mice in each group were washed with water, immersed in Nissl staining solution (Beyotime, China) for 30 min, and washed with water 2 times. Then, the tissue was dehydrated with ethanol and washed with xylene. Sections were analyzed using a brightfield microscope (Germany, ZEISS).

Golgi–Cox Staining

An FD Rapid Golgi-Stain Kit (FD Neuro-technologies, Ellicott City, MD, United States) was used to perform Golgi–Cox staining according to the manufacturer's instructions. Mice were anesthetized with 1% sodium pentobarbital, and their brain tissues were removed quickly. The tissues were immersed in Golgi–Cox solutions A and B for 2 weeks in the dark at RT, transferred to solution C and then incubated for 72 h at RT. Slices (150 μm thick) were cut using a vibratome. For Golgi–Cox staining, the sections were mounted on 3% gelatin-coated glass slides, air-dried, stained with solutions D and E, dehydrated in alcohol, cleared with xylene and mounted using resinous medium. Dendritic spines were imaged using a 20× or 40× objective and captured with a ZEISS digital camera (Wetzlar, Germany). For the quantification of the dendritic spine density, dendritic segments in layer III of the cortex were randomly selected, and counting was performed by an experimenter who was blinded to the group of each sample.

Whole-Cell Patch-Clamp Recordings

Whole-cell patch-clamp recordings were performed as previously described (Zhang et al., 2019). Mice were anesthetized, and 300-μm brain slices were prepared (Leica, Germany, VP1200S Vibratome). The slices were prepared in an ice-cold solution containing 60 mM NaCl, 100 mM sucrose, 2.5 mM KCl, 1.25 mM $NaH_2PO_4 \bullet 2H_2O$, 20 mM D-glucose, 26 mM $NaHCO_3$, 1 mM $CaCl_2$, and 5 mM $MgCl_2 \bullet 6H_2O$ saturated with 95% O_2 and 5% CO_2. A storage chamber containing Mg^{2+}-free artificial cerebrospinal fluid [ACSF; 125 mM NaCl, 2.5 mM KCl, 2 mM $CaCl_2$, 26 mM $NaHCO_3$, 1.25 mM KH_2PO_4, and 25 mM glucose (pH 7.4) bubbled with 95% O_2/5% CO_2] was used for slice recovery. The slices were fully submerged in the same flowing Mg^{2+}-free ACSF (4 ml/min) at RT for recording.

A depolarizing current of 500 ms in the current clamp mode starting from −50 pA and increasing at increments of 20 pA was used to induce action potentials (APs) to explore the intrinsic excitability of neurons. The first current step that was able to induce AP firing in a neuron was regarded as the rheobase. The internal solution contained the following components: 60 mM K_2SO_4, 60 mM *N*-methyl-D-glucamine, 40 mM HEPES, 4 mM $MgCl_2 \bullet 6H_2O$, 0.5 mM BAPTA, 12 mM phosphocreatine, 2 mM Na_2ATP, and 0.2 mM Na_3GTP.

Glass pipette electrodes were filled with the following internal solution to measure the miniature inhibitory postsynaptic currents (mIPSCs): 100 mM CsCl, 10 mM HEPES, 1 mM $MgCl_2$, 1 mM EGTA, 5 mM MgATP, 0.5 mM Na_3GTP, 12 mM phosphocreatine, and 30 mM *N*-methyl-D-glucamine (NMG) (pH 7.4, 280 to 290 mOsm). The membrane potential was held at −70 mV in voltage-clamp mode, and mIPSCs were recorded in the presence of 20 μM 6,7-dinitroquinoxaline-2,3 (1H,4H)-dione (DNQX), 50 μM dl-2-amino-5-phosphonovaleric acid (D-APV), and 1 μM tetrodotoxin (TTX). In addition, glass pipette electrodes were filled with an internal solution containing 130 mM $CsMeSO_4$, 10 mM $CsCl_2$, 10 mM HEPES, 4 mM NaCl, 1 mM $MgCl_2$, 1 mM EGTA, 5 mM MgATP, 0.5 mM Na_3GTP, 12 mM phosphocreatine, and 5 mM NMG (pH 7.4, 280 to 290 mOsm) to record mEPSCs. mEPSCs were recorded at a holding potential of −70 mV in the presence of 1 μM TTX and 100 μM picrotoxin (PTX).

Evoked currents were recorded to evaluate NMDAR- and AMPAR-mediated EPSCs. The glass microelectrodes were filled with the same solution used to record the mEPSCs. A bipolar stimulation electrode located approximately 50 μm rostral to the recording electrode in the same layer was used to evoke AMPAR- and NMDAR-mediated synaptic responses. In the presence of 100 μM PTX, at −70 mV, the peak amplitude of the evoked EPSCs was identified as the AMPAR-mediated current; at + 40 mV, the amplitude of the evoked EPSCs at 50 ms post-stimulus was identified as the NMDAR-mediated current.

For the analysis of the paired-pulse ratio (PPR), the holding potential was −70 mV in the presence of 100 μM PTX. The interval for paired stimulations was set at 50 ms. The PPRs were calculated as the ratio of the second peak amplitude to the first peak amplitude.

The signals were acquired with a MultiClamp 700B amplifier (Axon, United States), followed by recording using pClamp 9.2 software (Molecular Devices, Sunnyvale, CA, United States). Synaptic activity was analyzed using the Mini Analysis Program (Synaptosoft, Leonia, NJ, United States) and pClamp 9.2 software (Molecular Devices, Sunnyvale, CA, United States).

Statistical Analysis

Statistical analyses were performed using Prism 6.0 software (GraphPad, San Diego, CA, United States). Unpaired two-tailed Student's *t*-test or one-way analysis of variance (ANOVA) was used for analyses. Group differences in the mean seizure score were evaluated with repeated-measures ANOVA. For the electrophysiological tests, the n values represent the numbers of neurons and slices. All the results are presented as the means ± SEMs, and $p < 0.05$ was considered to indicate statistical significance.

RESULTS

Beclin1 Expression Was Increased in Patients With Temporal Lobe Epilepsy and Epileptic Mice

Beclin1 has been shown to reflect change in autophagy under conditions of epilepsy (Li et al., 2018). We measured Beclin1 protein levels in temporal cortical tissues obtained from patients with TLE and non-epileptic patients using western blot analysis to verify the relationship between Beclin1 and epilepsy. Beclin1 expression in the temporal cortex was higher in patients with TLE than in non-epileptic patients (**Figures 1A,B**), and a similar result was observed in the cortical tissues obtained from the KA-induced (**Figures 1C,D**) and PTZ-kindled model mice (**Figures 1E,F**). The hippocampus is an area of important epileptic pathological changes and plays a key role in the occurrence and development of epilepsy. We next measured the Beclin1 protein level in hippocampal tissues from KA- and PTA-induced epileptic animal models. Compared with control tissues, Beclin1 expression was also increased in the epileptic tissue (**Figures 1D,F**). IF staining and a semiquantitative analysis were also performed (**Figure 1G**). The fluorescence density of Beclin1 puncta was higher in both the cortex and hippocampus of the epilepsy group than in the control group (**Figure 1H**), that was consistent with the results of the western blot analysis.

Knockdown of *beclin1* Altered Autophagy

The dynamic process of autophagy consists of two aspects: the formation and degradation of autophagosomes. Microtubule-associated protein light chain 3 (LC3) is a marker of autophagy, and the LC3-II/LC3-I ratio correlates with the number of autophagosomes (Mizushima and Yoshimori, 2007). In the present study, we measured the protein levels of LC3 (**Figure 2A**) and adaptor protein p62 (SQSTM1), a substrate protein of autophagy (**Figure 2C**). Among epileptic mice, the LC3-II/LC3-I ratio was increased (**Figure 2B**), and the SQSTM1/p62 level was decreased compared with those in the WT mice (**Figure 2D**). In addition, we also detected the expression of LC3 and p62 in cultured neurons (**Figure 2E**). As a result, the decreased LC3 level observed in *beclin1*$^{\pm}$ mice was increased by the autophagy inducer RAPA, but the autophagy blocker 3-MA did not further reduce the expression of LC3 (**Figure 2F**). However, increased p62 levels were decreased by RAPA and further increased by 3-MA (**Figure 2G**). Because the autophagy impairment in *beclin1*$^{\pm}$ mice might result in tumorigenesis and/or neuronal loss, Nissl bodies in nerve cells were identified using Nissl staining. In the WT mouse, hippocampal structures were clear, nerve cells were arranged neatly, and the cytoplasm was rich in Nissl bodies. In *beclin1*$^{\pm}$ mice, hippocampal structures were chaotic, nerve cells were sparsely arranged, and Nissl bodies were decreased (**Figure 2H**). In addition, we determined cell viability using MTT assays. The viability of cultured cortical and hippocampal neurons from *beclin1*$^{\pm}$ mice was decreased compared to that in neurons from WT mice (**Figure 2I**).

Knockdown of *beclin1* Decreased Epileptic Activity in the Kainic Acid -Induced Epilepsy Model

Altered Beclin1 expression may be an epiphenomenon or indicate that Beclin1 plays a causal role in epilepsy. We subsequently performed behavioral experiments to investigate whether incomplete knockout of *beclin1* affected seizure activities and epileptiform discharges in two epilepsy models.

In mice with KA-induced epilepsy, we counted only grade IV and V seizures, since grade I-III seizures were easily overlooked or were ambiguous. The first SRSs in the *beclin1*$^{\pm}$ group appeared at approximately 8 days on average, but appeared on day 5 in the WT group (**Figure 3A**). In addition, the average total number of SRSs within 30 days was 18 in the *beclin1*$^{\pm}$ group and approximately 32 in the WT group (**Figure 3B**). Thus, the heterozygous disruption of *beclin1* prolonged the latency of SRSs and decreased the total number of SRSs in the KA-induced epilepsy model.

Knockdown of *beclin1* Decreased Seizure Susceptibility in the Pentylenetetrazol - Kindled Epilepsy Model

We selected another chronic epilepsy model with different mechanisms to avoid limiting our study to a single model. In the PTZ-kindled mouse model, the mice in the WT group exhibited grade III seizures after the administration of subthreshold doses of PTZ, and grade V seizures began to appear after the administration of the 8th–9th doses (**Figures 3C,D**). In contrast, in the *beclin1*$^{\pm}$ group, grade III seizures began to appear at the 8th–9th PTZ injection, but no grade V seizures

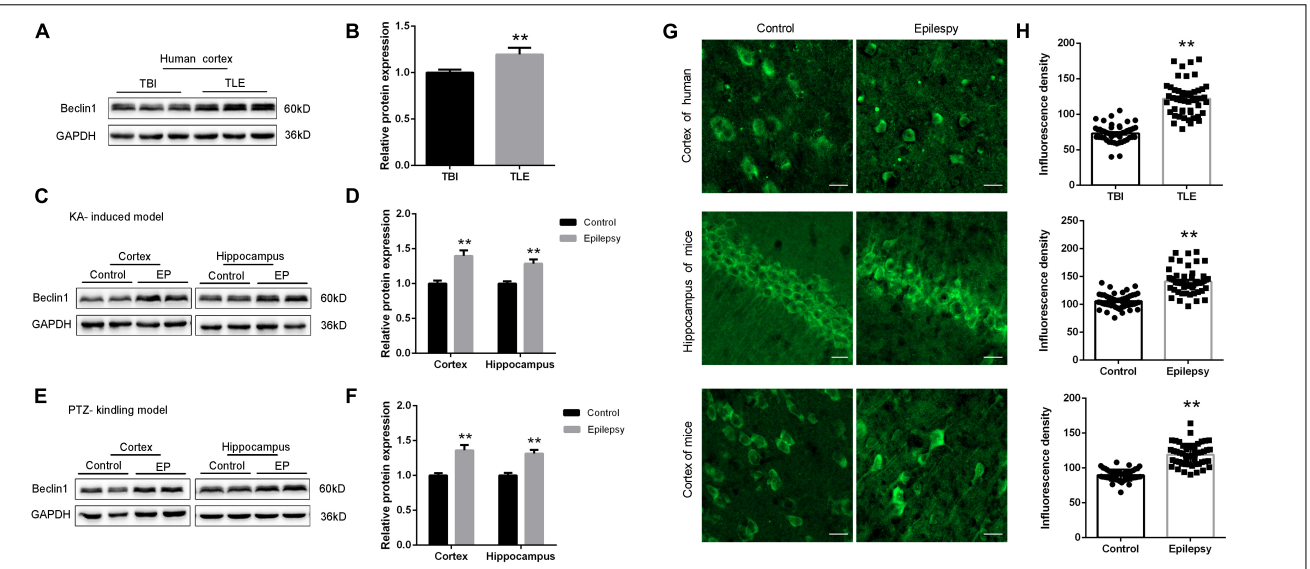

FIGURE 1 | Beclin1 expression was increased in patients with TLE and epileptic mice. **(A,B)** Beclin1 protein levels in patients with traumatic brain injury (TBI) and patients with epilepsy (n = 8 patients per group). **(C,D)** The Beclin1 protein levels in cortex and hippocampus from wild-type (WT) mice and kainic acid (KA)-treated mice (n = 8 mice per group). **(E,F)** The Beclin1 protein levels in cortex and hippocampus from WT mice and pentylenetetrazol (PTZ)-treated mice (n = 8 mice per group). **(G,H)** IF staining and semi-quantitative analysis of Beclin1 puncta fluorescence intensity in cortical and hippocampal tissues from patients with temporal lobe epilepsy (TLE) and two epileptic mouse models (n = 50 samples per group). Scale bars: 50 μm. Data are presented as the means ± SEM, $^{**}p < 0.01$. Student's t-tests were performed.

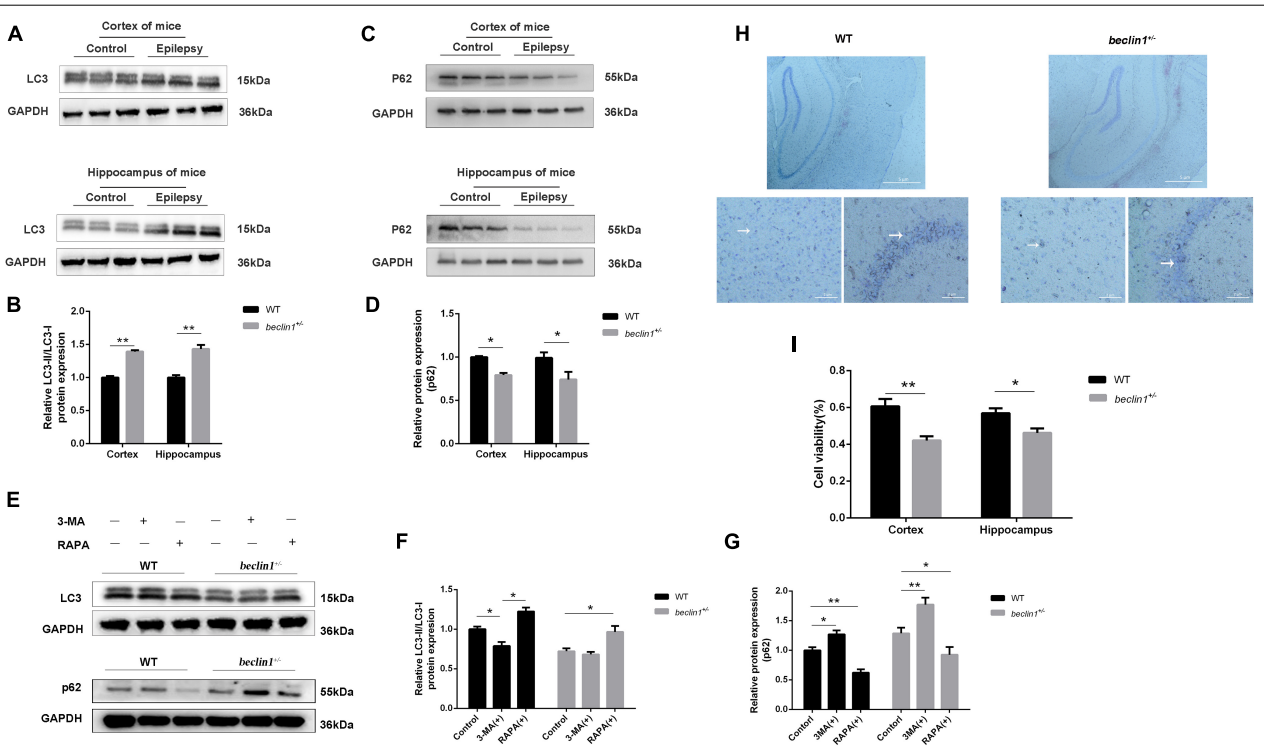

FIGURE 2 | Autophagy was activated in epilepsy but suppressed in *beclin1*$^{\pm}$ mice. **(A,B)** LC3-II/LC3-I protein levels in the cortex and hippocampus of brain tissues from wild-type (WT) and epilepsy model mice (n = 3 mice per group). **(C,D)** p62 protein levels in the cortex and hippocampus of brain tissues from WT and epilepsy model mice (n = 3 mice per group). **(E,G)** LC3-II/LC3-I and p62 protein level in cultured primary neurons from WT and *beclin1*$^{\pm}$ mice under basal conditions and upon autophagy induction (RAPA)/blockade (3-MA) (n = 3 samples per group). **(H)** Nissl staining of WT and *beclin1*$^{\pm}$ mouse brain slices. Scale bars: 52 μm. **(I)** The viability of cultured neurons dissected from WT and *beclin1*$^{\pm}$ mice was detected using the MTT assay (n = 6 samples per group). Data are presented as the means ± SEM. $^{*}p < 0.05$ and $^{**}p < 0.01$. Student's t-tests and one-way ANOVA were performed.

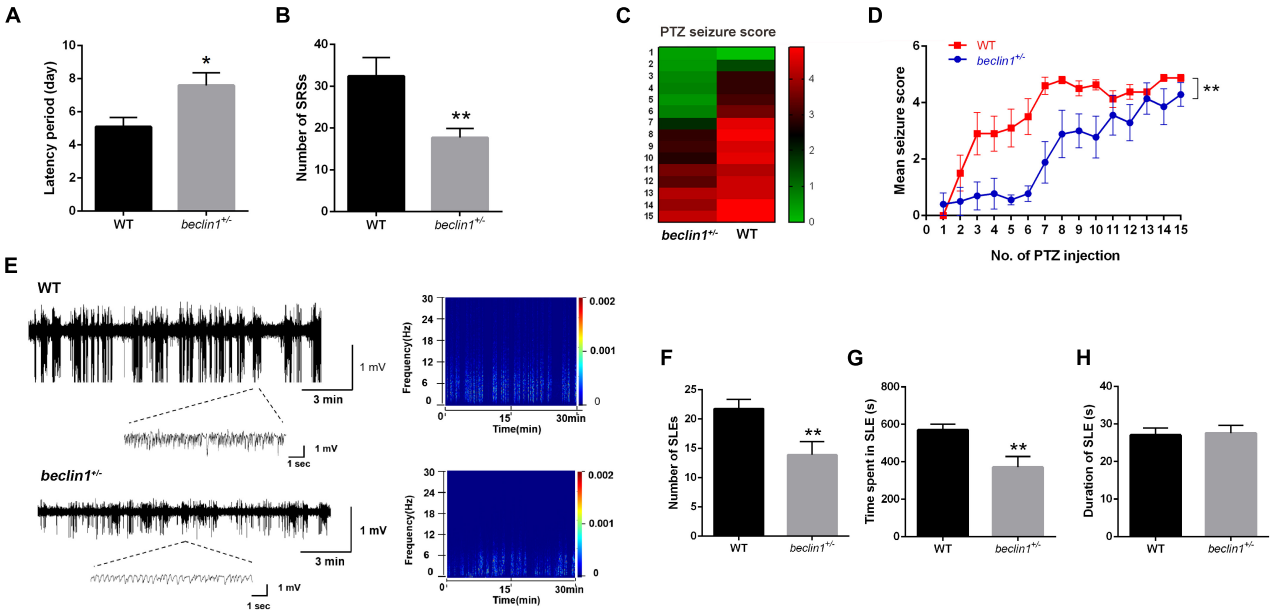

FIGURE 3 | Knockdown of *beclin1* decreased seizure susceptibility and epileptic activity. **(A,B)** Quantitative analysis of the spontaneous recurrent seizure (SRS) latency and total number of SRSs in the kainic acid (KA)-induced epilepsy model in the two groups (n = 10 mice per group). **(C,D)** Mean seizure scores recorded after the injection of pentylenetetrazol (PTZ) in the two groups on alternate days (n = 10 mice per group). **(E)** Representative traces of local field potentials (LFPs) from the wild-type (WT) and *beclin1*$^{\pm}$ groups. **(F–H)** Quantitative analysis of the number, time spent, and duration of seizure-like event (SLE) of the LFPs from two groups (n = 8 mice per group). Data are presented as the means ± SEM. *$p < 0.05$ and **$p < 0.01$. Group differences in the mean seizure score during PTZ kindling were evaluated with repeated-measures ANOVA. Student's t-tests were performed.

were observed after 15 injections (**Figures 3C,D**). Based on these results, the mice in the *beclin1*$^{\pm}$ group had lower seizure scores and decreased seizure susceptibility than those in the WT group.

Beclin1 Affected Local Field Potentials in the Hippocampi of Epileptic Mice

The judgment of epileptic seizures based on behavior has some limitations, since some subclinical epileptic discharges may be characterized only by abnormal EEGs. A more convincing judgment might be obtained by recording abnormal electrophysiological epileptiform discharges and SLEs during seizure intervals than by observing behavior. Therefore, after the behavioral analysis in the KA model, we obtained stable LFPs from each mouse continuously for 30 min, and SLEs were recorded in the two groups (**Figure 3E**). The total number of SLEs, the duration of each SLE, and the time spent in all SLEs were analyzed within the recorded 30 min. The total number of SLEs in the *beclin1*$^{\pm}$ group was significantly lower than that in the WT group (**Figure 3F**). Interestingly, the total time spent in SLEs was significantly reduced in *beclin1*$^{\pm}$ group (**Figure 3G**), but the duration of a single SLE of two groups was not significantly different (**Figure 3H**). These results suggest that the heterozygous disruption of *beclin1* affected SLEs in the interictal phase in the KA-induced epilepsy model by decreasing the number of SLEs and reducing the total time spent of SLEs but not by affecting the duration of a single SLE.

Beclin1 Altered Excitatory Synaptic Transmission in Brain Slices

Intrinsic excitability or altered synaptic transmission may increase neuronal firing. We subsequently performed whole-cell patch-clamp recordings of hippocampal CA1 pyramidal neurons in mouse brain slices. First, the intrinsic excitability of the neurons was assessed, and no difference was observed between the WT and *beclin1*$^{\pm}$ groups (**Supplementary Figures 1C–G**); therefore, we speculated that *beclin1*$^{\pm}$ might affect synaptic transmission.

Then, we recorded mEPSCs and mIPSCs in neurons of the brain slices (**Figure 4A**). Compared with those of the WT group, both the amplitude and frequency of mEPSCs were decreased in the *beclin1*$^{\pm}$ group (**Figures 4B,C**), but significant differences in mIPSCs were not observed between the two groups (**Figures 4D,E**). Thus, *beclin1* knockdown mainly affected excitatory synaptic transmission. We also identified the subcellular location of Beclin1 in mouse brain tissues to investigate this hypothesis. We immunostained neurons with antibodies against Beclin1 combined with antibodies against the excitatory postsynaptic membrane protein PSD-95 and the excitatory presynaptic membrane protein vGluT1 (**Figure 5A**) and vGluT1 (**Figure 5C**). The colocalization analysis suggested that Beclin1 was significantly correlated with PSD95 (**Figure 5B**) and vGluT1 (**Figure 5D**).

We then measured evoked EPSCs to investigate whether the altered excitatory synaptic transmission was caused by AMPAR-mediated or NMDAR-mediated currents (**Figure 4F**). We

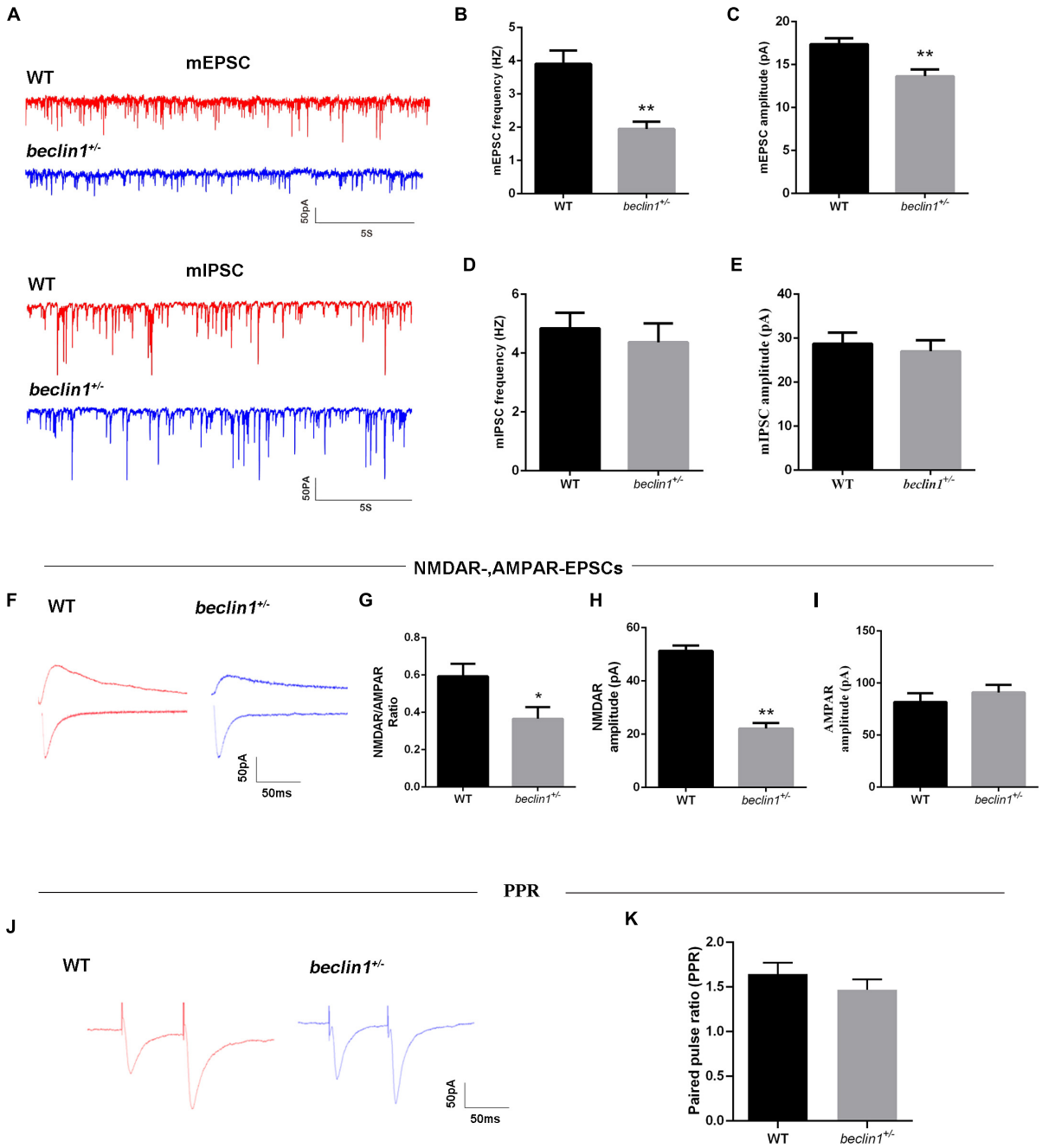

FIGURE 4 | Knockdown of *beclin1* affected excitatory synaptic transmission. **(A)** Representative traces of mEPSCs and miniature inhibitory postsynaptic currents (mIPSCs) from the two groups. **(B,C)** Quantitative analysis of the frequency and amplitude of the mEPSCs [wild-type (WT) group: $n = 10$, *beclin1*$^{\pm}$ group: $n = 8$]. **(D,E)** Quantitative analysis of the frequency and amplitude of the mIPSCs ($n = 12$ per group). **(F)** Representative traces of NMDAR-mediated and AMPAR-mediated EPSCs from the two groups. **(G–I)** Summary of the EPSC amplitude from the two groups ($n = 6$ per group). **(J)** Representative traces of the paired-pulse ratios (PPRs) for AMPA-mediated EPSCs at three different interstimulus intervals. **(K)** Summary of the PPRs between the two groups ($n = 6$ per group). Data are presented as the means ± SEM. $^{*}p < 0.05$ and $^{**}p < 0.01$. Student's *t*-tests were performed.

observed decreases in the NMDAR/AMPAR ratio (**Figure 4G**) and in the average amplitude of the NMDAR-mediated EPSCs (**Figure 4H**) from the *beclin1*$^{\pm}$ mice. However, AMPAR-mediated EPSCs were unchanged between the groups (**Figure 4I**). Alterations in NMDAR-mediated synaptic responses may occur presynaptically or postsynaptically. Therefore, the paired pulse ratios (PPRs) were recorded (**Figure 4J**), and no significant difference was observed between the two groups (**Figure 4K**). Taken together, these results indicate that *beclin1* may modulate glutamatergic

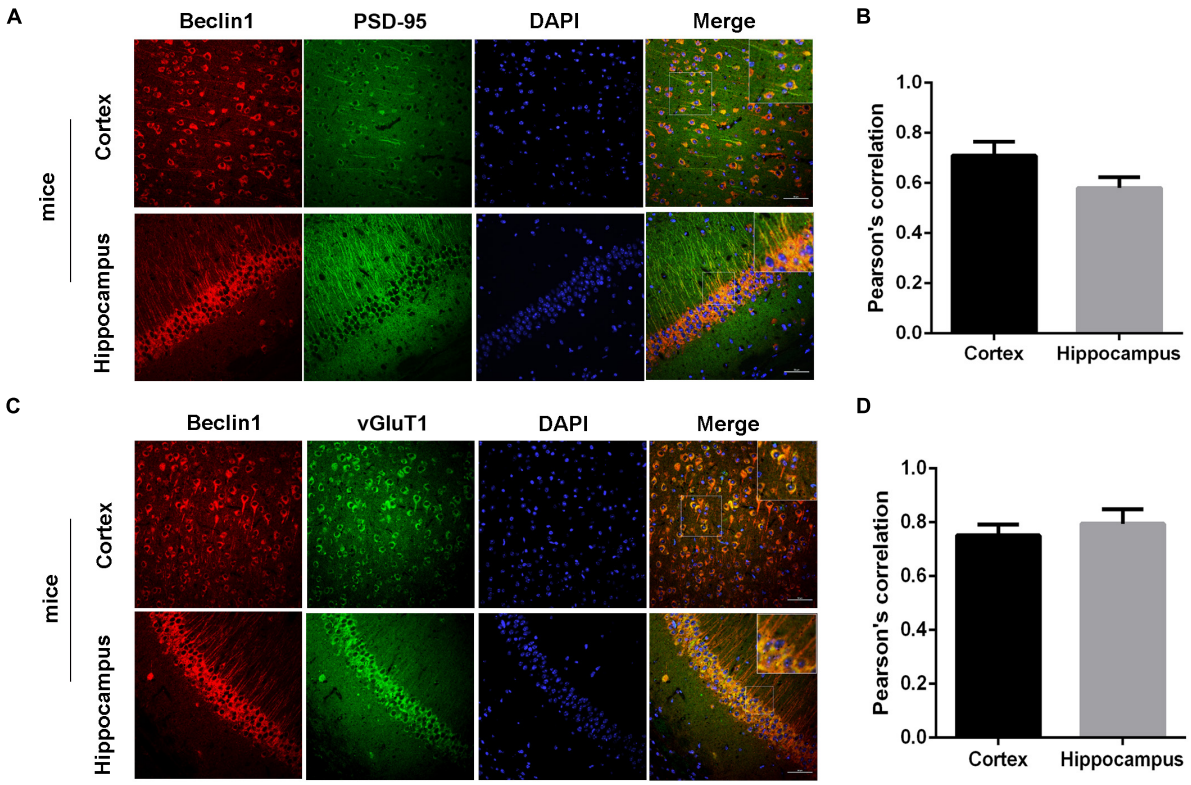

FIGURE 5 | Beclin1 was colocalized with an excitatory synaptic protein. **(A)** Representative image showing the distributions of Beclin1 and the excitatory postsynaptic protein PSD-95 in mouse brain sections. **(B)** The extent of the colocalization was quantified using Image-Pro Plus software. **(C)** Representative image showing the distributions of Beclin1 and the excitatory presynaptic protein vGluT1 in mouse brain sections. **(D)** The extent of colocalization was quantified [wild-type (WT) group: $n = 11$, *beclin1*$^{\pm}$ group: $n = 9$]. Data are presented as the means ± SEM. Scale bars: 50 μm. Student's *t*-tests were performed.

transmission through a postsynaptic mechanism rather than a presynaptic mechanism.

The Dendritic Spine Density Was Decreased in *beclin1*$^{\pm}$ Mice

Postsynaptic activity is closely related to the morphology of dendritic spines. We then examined whether Beclin1 was involved in dendritic morphogenesis in brain slices stained with a Golgi kit (**Figure 6A**). As a result, both apical and basal dendritic spine densities of cortical pyramidal neurons were lower in the *beclin1*$^{\pm}$ group than in the WT group (**Figures 6B,C**). A similar trend was observed in cultured hippocampal neurons (**Figures 6E,H**). In addition, the presynaptic and postsynaptic regions were labeled with antibodies against PSD-95 (**Figure 6D**) and vGluT1, respectively (**Figure 6E**), to quantify whether changes in synaptic contacts accompanied the decreased dendritic spine density, and the results suggested that the densities of vGluT1 and PSD-95 puncta were both decreased in the *beclin1*$^{\pm}$ group (**Figure 6F**).

As *beclin1* knockdown caused autophagy defects, we treated cultured neurons from *beclin1*$^{\pm}$ mice with the autophagy inducer RAPA to further investigate whether the changes in the dendritic spines were caused by impaired autophagy (**Figure 6G**). However, no significant difference was observed in the dendritic spine density between the two groups (**Figure 6H**).

Prior to using the primary cultured neurons in this experiment, Beclin1 expression was confirmed by western blotting (**Supplementary Figure 1A**). Next, *beclin1*$^{\pm}$ mice and WT mice were identified, and the expression of the Beclin1 protein in the *beclin1*$^{\pm}$ group was significantly lower than that in the WT group (**Supplementary Figure 1B**). This finding indicated that Beclin1 protein expression was reduced, as expected, in the cortex and hippocampus of *beclin1*$^{\pm}$ mice.

DISCUSSION

Numerous studies have focused on the underlying pathophysiological mechanisms of epilepsy, and the proposed mechanisms involve proteins, channels, receptors, signaling pathways and enzymes (Zavala-Tecuapetla et al., 2020). The role of autophagy in the development of epilepsy has received increasing attention, as defective autophagy has been shown to induce epilepsy (Wong, 2013). Thus, we investigated the role of Beclin1, a core molecule in autophagosome formation, in the occurrence and development of epilepsy.

Epileptogenesis is the process by which abnormal electrical activity develops into chronic epilepsy after functional changes

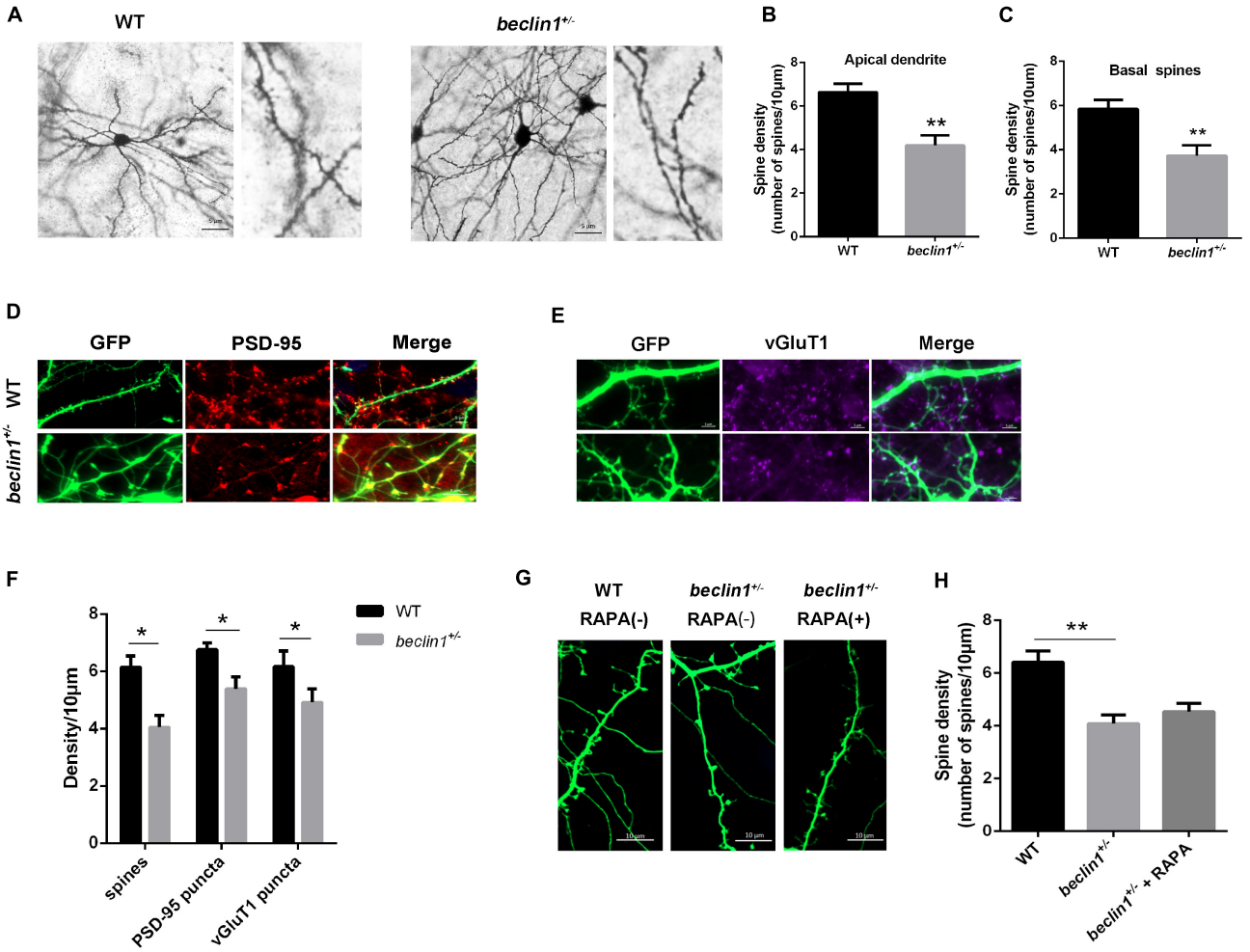

FIGURE 6 | Knockdown of *beclin1* altered the dendritic spine density. **(A)** Representative image of the apical dendritic spine morphology of pyramidal neurons in brain slices from wild-type (WT) and *beclin1*$^{\pm}$ mice detected using Golgi staining. Scale bars: 5 μm. **(B,C)** Quantification of the apical and basal dendritic spine density in the two groups (n = 5 mice/genotype, 21 cells from WT mice and 16 cells from *beclin1*$^{\pm}$). **(D,E)** Representative image of dendrites and PSD-95/vGluT1 staining in cultured neurons from the two groups. **(F)** Quantification of the dendritic spine density and PSD-95/vGluT1 puncta density in the two groups (n = 12 cells). **(G,H)** Representative image and quantification of the dendritic spine density in cultured neurons from WT and *beclin1*$^{\pm}$ mice under basal conditions and upon autophagy induction (RAPA) (n = 3 mice/genotype, 15 neurons per group). Spines on apical dendrites in the stratum radiatum (SR) located within 20 μm from the soma were counted. Data are presented as the means ± SEM. $^{*}p < 0.05$ and $^{**}p < 0.01$. Student's t-tests and one-way ANOVA were performed.

occur in normal brain tissue. During this period, neurons and non-neuronal cells in brain tissue change at different levels, including the genetic, epigenetic, molecular and structural levels (Devinsky et al., 2018). These changes result in abnormal network formation, changes in cell excitability, and ultimately spontaneous seizures. To date, numerous changes in protein expression levels, expression sites, molecular structure and function have been identified during the process of epilepsy and even after epilepsy development (Pitkänen and Lukasiuk, 2009). Previous studies have reported significantly increased Beclin1 expression in PTZ-treated epileptic rats (Zhu et al., 2016) and KA-induced epilepsy models (Cao et al., 2020). Consistent with these results, we also detected increased Beclin1 levels in both KA-induced and PTZ-kindled epileptic mice. Notably, we first confirmed elevated Beclin1 protein levels in the cortices of patients with TLE.

Autophagy is characterized by the engulfment of cellular components into double-membrane or multiple-membrane cytoplasmic vesicles called autophagosomes that form from a membranous structure called the phagophore. Autophagosomes ultimately fuse with lysosomes, forming autolysosomes, which ultimately degrade the engulfed proteins or organelles. This whole process is called autophagy flux (Ge et al., 2022). An increase in the level of the LC3-II isoform potentially indicates reduced autophagy flux (Klionsky et al., 2021). Considering that Beclin1 is a key molecule involved in autophagy, we further evaluated autophagy flux in epilepsy and observed that the ratio of LC3-II to LC3-I was decreased, while p62 accumulated in epileptic mice, these findings

are consistent with previous research (Li et al., 2018) suggesting an activation in autophagy flux rather than the impairment of autophagy.

We next investigated whether the elevated level of Beclin1 correlated with epileptic seizures in mice with a heterozygous disruption of *beclin1*. Previous studies have observed that autophagy is inhibited in mice with incomplete knockout of *beclin1* (*beclin1*$^{\pm}$ mice) (Sun et al., 2018). Several investigations have reported that inhibiting autophagy reduces the susceptibility to epilepsy in KA-induced or pilocarpine-induced epileptic mice (Jeong et al., 2015; Ying et al., 2020), implying that the suppression of autophagy is sufficient to inhibit epilepsy. We measured autophagy flux to determine the level of autophagy in *beclin1*$^{\pm}$ mice. In *beclin1*$^{\pm}$ mice, autophagy flux was lower than that in WT mice, indicating that incomplete knockout of *beclin1* inhibited autophagy. An autophagy inducer (rapamycin) and inhibitor (3-MA) were used to observe the corresponding changes in autophagy flux. Our results revealed that rapamycin altered autophagy flux in *beclin1*$^{\pm}$ mice, while 3-MA had little effect.

Imbalances between excitatory and inhibitory signals have been suggested to cause epilepsy. AEDs that are currently used to stop epileptic seizures act mainly by inhibiting neuronal excitability, blocking ion channels and inhibiting synaptic neurotransmitter release (Kwon et al., 2019). Studies have provided insights into the genes involved in synaptic transmission or the regulation of synaptic transmission (Pitkänen and Lukasiuk, 2011). We next focused on the effects of Beclin1 on synaptic transmission. Our results first revealed that both the frequency and amplitude of mEPSCs were decreased in *beclin1*$^{\pm}$ mice. As epileptic activity is caused by an imbalance in excitatory and inhibitory transmission (Rubenstein and Merzenich, 2003), the unaffected mIPSCs in the *beclin1*$^{\pm}$ group in our study suggest that Beclin1 leads to a hypoexcitable state by decreasing excitatory transmission.

In a patch-clamp experiment, incomplete knockout of *beclin1* was shown to affect the NMDAR-mediated current but not the AMPAR-mediated current. According to previous studies, autophagy exerts a protective effect on the process of NMDAR-mediated excitotoxicity (Pérez-Carrión et al., 2012; Pérez-Carrión and Ceña, 2013). We assessed neuronal PPRs to further explore whether the NMDAR-mediated current was affected by presynaptic or postsynaptic changes. The results of PPR and colocalization analyses indicated that incomplete knockout of *beclin1* affected synaptic transmission mainly *via* postsynaptic effects. An experiment on long-term social isolation found that, long-term social isolation can reduce the protein level of Beclin1, inhibit autophagy, and lead to postsynaptic dysfunction, impairment of spatial memory and cognitive function (Wang et al., 2019). Therefore, in our study, the current changes may be related to the inhibition of autophagy, which is in turn related to Beclin1. Overall, our study suggests that Beclin1 may alter excitatory synaptic transmission at the postsynaptic site, eventually resulting in epilepsy.

Dendritic spines are small, thin, specialized protrusions from neuronal dendrites that are primarily localized in excitatory synapses (Chidambaram et al., 2019) and usually receive and integrate most excitatory synaptic inputs from the mammalian cortex and hippocampus and directly affect neuronal excitability and seizures under pathological conditions (Wong and Guo, 2013). Since dendritic spines constitute the most important parts of excitatory synapses, their morphology and density play crucial roles in synaptic plasticity (Chidambaram et al., 2019). We found that the dendritic spine density was decreased in the neurons of *beclin1*$^{\pm}$ mice, indicating that incomplete deletion of *beclin1* alters synaptic transmission by inhibiting synapse formation. However, we observed that this defect was not significantly reversed by the autophagy inducer rapamycin *in vitro*. More *in vivo* studies are needed to further verify this finding.

Autophagy is a catabolic process that liberates free amino acids through protein degradation. Impaired autophagy might disturb the homeostasis of neurotransmitters that are implicated in brain physiology and pathophysiology (Bejarano and Rodríguez-Navarro, 2015). Based on this justification, the altered excitatory synaptic transmission in *beclin1*$^{\pm}$ mice in this study may be explained by the alterations in autophagy caused by Beclin1 deficiency. However, further exploration is needed to confirm this conjecture in the future.

CONCLUSION

In summary, we report a previously unrecognized but important role of Beclin1 in epilepsy. Our results reveal that Beclin1 expression is increased in brain tissues from patients with TLE. Additionally, heterozygous disruption of *beclin1* significantly decreases seizure activity and may be involved in altered excitatory synaptic transmission caused by abnormal dendritic spine formation. These findings contribute to our understanding of the biological roles of Beclin1 at synapses. Moreover, this study provides insights into the development of an alternative approach for epilepsy treatment by identifying a novel therapeutic target, Beclin1.

DATA AVAILABILITY STATEMENT

The original contributions presented in this study are included in the article/**Supplementary Material**, further inquiries can be directed to the corresponding authors.

ETHICS STATEMENT

The studies involving human participants were reviewed and approved by the Ethics Committee of the First Affiliated Hospital of Chongqing Medical University. The patients/participants were informed to participate in this study. The animal study was

reviewed and approved by the Ethics Committee of Chongqing Medical University.

AUTHOR CONTRIBUTIONS

MY, PL, XT, CC, XW, and FX conceived the project and designed the experiments. MY, PL, WJ, HG, HC, YC, YG, YxG, MH, JW, XJ, ZZ, and XX performed the experiments. MY, PL, XT, CC, and FX analyzed the data. MY, XT, and XW wrote the manuscript. All the authors revised and approved the final version of the manuscript.

FUNDING

This work was supported by grants from the National Natural Science Foundation of China (82001378, 81922023, 81873788, and 82171440) and CQMU Program for Youth Innovation in Future Medicine (W0043).

ACKNOWLEDGMENTS

We thank all the patients and their families for their participation in this study.

SUPPLEMENTARY MATERIAL

The Supplementary Material for this article can be found online at: https://www.frontiersin.org/articles/10.3389/fnmol.2022.807671/full#supplementary-material

Supplementary Figure 1 | Knockdown of *beclin1* altered the intrinsic excitability of neurons. **(A,B)** Beclin1 protein levels in the cortex and hippocampus of brain tissues from wild-type (WT) and *beclin1*$^{\pm}$ mice (cortex: $n = 5$ mice per group; hippocampus: $n = 4$ mice per group). **(C)** Paradigm used to record passive excitability in the excitatory neurons. **(D)** Representative traces of sAPs. **(E)** Resting membrane potential of the examined neurons from the two groups ($n = 6$ per group). **(F)** Injected currents used to induce the first spikes ($n = 6$ per group). **(G)** Summary of the number of APs induced by the injected currents ($n = 6$ per group). Data are presented as the means ± SEM. $^{**}p < 0.01$. Student's *t*-tests were performed.

REFERENCES

Ashkenazi, A., Bento, C. F., Ricketts, T., Vicinanza, M., Siddiqi, F., Pavel, M., et al. (2017). Polyglutamine tracts regulate beclin 1-dependent autophagy. *Nature* 545, 108–111. doi: 10.1038/nature22078

Bejarano, E., and Rodríguez-Navarro, J. A. (2015). Autophagy and amino acid metabolism in the brain: implications for epilepsy. *Amino Acids* 47, 2113–2126. doi: 10.1007/s00726-014-1822-z

Cao, J., Tang, C., Gao, M., Rui, Y., Zhang, J., Wang, L., et al. (2020). Hyperoside alleviates epilepsy-induced neuronal damage by enhancing antioxidant levels and reducing autophagy. *J. Ethnopharmacol.* 257:112884. doi: 10.1016/j.jep.2020.112884

Chidambaram, S. B., Rathipriya, A. G., Bolla, S. R., Bhat, A., Ray, B., Mahalakshmi, A. M., et al. (2019). Dendritic spines: revisiting the physiological role. *Prog. Neuropsychopharmacol. Biol. Psychiatry* 92, 161–193. doi: 10.1016/j.pnpbp.2019.01.005

Criado, O., Aguado, C., Gayarre, J., Duran-Trio, L., Garcia-Cabrero, A. M., Vernia, S., et al. (2012). Lafora bodies and neurological defects in malin-deficient mice correlate with impaired autophagy. *Hum. Mol. Genet.* 21, 1521–1533. doi: 10.1093/hmg/ddr590

Devinsky, O., Vezzani, A., O'Brien, T. J., Jette, N., Scheffer, I. E., de Curtis, M., et al. (2018). Epilepsy. *Nat. Rev. Dis. Primers* 4:18024. doi: 10.1038/nrdp.2018.24

Egan, D., Kim, J., Shaw, R. J., and Guan, K. L. (2011). The autophagy initiating kinase ULK1 is regulated *via* opposing phosphorylation by AMPK and mTOR. *Autophagy* 7, 643–644. doi: 10.4161/auto.7.6.15123

Engel, J. Jr. (2001). A proposed diagnostic scheme for people with epileptic seizures and with epilepsy: report of the ILAE task force on classification and terminology. *Epilepsia* 42, 796–803. doi: 10.1046/j.1528-1157.2001.10401.x

Falconer, M. A., and Taylor, D. C. (1968). Surgical treatment of drug-resistant epilepsy due to mesial temporal sclerosis. Etiology and significance. *Arch. Neurol.* 19, 353–361. doi: 10.1001/archneur.1968.00480040019001

Fisher, R. S., Acevedo, C., Arzimanoglou, A., Bogacz, A., Cross, J. H., Elger, C. E., et al. (2014). ILAE official report: a practical clinical definition of epilepsy. *Epilepsia* 55, 475–482. doi: 10.1111/epi.12550

Ge, P., Lei, Z., Yu, Y., Lu, Z., Qiang, L., Chai, Q., et al. (2022). *M. tuberculosis* PknG manipulates host autophagy flux to promote pathogen intracellular survival. *Autophagy* 18, 576–594. doi: 10.1080/15548627.2021.1938912

Guo, Y., Chen, Y., Yang, M., Xu, X., Lin, Z., Ma, J., et al. (2020). A rare KIF1A missense mutation enhances synaptic function and increases seizure activity. *Front. Genet.* 11:61. doi: 10.3389/fgene.2020.00061

Jeong, K. H., Jung, U. J., and Kim, S. R. (2015). Naringin attenuates autophagic stress and neuroinflammation in kainic acid-treated hippocampus *in vivo*. *Evid. Based Complement. Alternat. Med.* 2015:354326. doi: 10.1155/2015/354326

Klionsky, D. J., Abdel-Aziz, A. K., Abdelfatah, S., Abdellatif, M., Abdoli, A., Abel, S., et al. (2021). Guidelines for the use and interpretation of assays for monitoring autophagy (4th edition)(1). *Autophagy* 17, 1–382. doi: 10.1080/15548627.2020.1797280

Kwon, J. Y., Jeon, M. T., Jung, U. J., Kim, D. W., Moon, G. J., and Kim, S. R. (2019). Perspective: therapeutic potential of flavonoids as alternative medicines in epilepsy. *Adv. Nutr.* 10, 778–790. doi: 10.1093/advances/nmz047

Levine, B., and Kroemer, G. (2019). Biological functions of autophagy genes: a disease perspective. *Cell* 176, 11–42. doi: 10.1016/j.cell.2018.09.048

Li, J., Mi, X., Chen, L., Jiang, G., Wang, N., Zhang, Y., et al. (2016). Dock3 participate in epileptogenesis through rac1 pathway in animal models. *Mol. Neurobiol.* 53, 2715–2725. doi: 10.1007/s12035-015-9406-9

Li, Q., Han, Y., Du, J., Jin, H., Zhang, J., Niu, M., et al. (2018). Alterations of apoptosis and autophagy in developing brain of rats with epilepsy: changes in LC3, P62, Beclin-1 and Bcl-2 levels. *Neurosci. Res.* 130, 47–55. doi: 10.1016/j.neures.2017.08.004

Liang, C., Feng, P., Ku, B., Dotan, I., Canaani, D., Oh, B. H., et al. (2006). Autophagic and tumour suppressor activity of a novel Beclin1-binding protein UVRAG. *Nat. Cell Biol.* 8, 688–699.

Liang, X. H., Jackson, S., Seaman, M., Brown, K., Kempkes, B., Hibshoosh, H., et al. (1999). Induction of autophagy and inhibition of tumorigenesis by beclin 1. *Nature* 402, 672–676. doi: 10.1038/45257

Liang, X. H., Kleeman, L. K., Jiang, H. H., Gordon, G., Goldman, J. E., Berry, G., et al. (1998). Protection against fatal Sindbis virus encephalitis by beclin, a novel Bcl-2-interacting protein. *J. Virol.* 72, 8586–8596.

Liu, X., and Wang, B. (2019). Heterozygous disruption of beclin 1 alleviates zinc oxide nanoparticles-induced disturbance of cholesterol biosynthesis in mouse liver. *Int. J. Nanomed.* 14, 9865–9875. doi: 10.2147/ijn.s224179

McDaniel, S. S., Rensing, N. R., Thio, L. L., Yamada, K. A., and Wong, M. (2011). The ketogenic diet inhibits the mammalian target of rapamycin (mTOR) pathway. *Epilepsia* 52, e7–e11. doi: 10.1111/j.1528-1167.2011.02981.x

Mizushima, N., and Yoshimori, T. (2007). How to interpret LC3 immunoblotting. *Autophagy* 3, 542–545. doi: 10.4161/auto.4600

Pérez-Carrión, M. D., and Ceña, V. (2013). Knocking down HMGB1 using dendrimer-delivered siRNA unveils its key role in NMDA-induced autophagy in rat cortical neurons. *Pharm. Res.* 30, 2584–2595. doi: 10.1007/s11095-013-1049-9

Pérez-Carrión, M. D., Pérez-Martínez, F. C., Merino, S., Sánchez-Verdú, P., Martínez-Hernández, J., Luján, R., et al. (2012). Dendrimer-mediated siRNA delivery knocks down Beclin 1 and potentiates NMDA-mediated toxicity in rat cortical neurons. *J. Neurochem.* 120, 259–268. doi: 10.1111/j.1471-4159.2011.07556.x

Pitkänen, A., and Lukasiuk, K. (2009). Molecular and cellular basis of epileptogenesis in symptomatic epilepsy. *Epilepsy Behav.* 14(Suppl. 1), 16–25. doi: 10.1016/j.yebeh.2008.09.023

Pitkänen, A., and Lukasiuk, K. (2011). Mechanisms of epileptogenesis and potential treatment targets. *Lancet Neurol.* 10, 173–186. doi: 10.1016/s1474-4422(10)70310-0

Racine, R. J. (1972). Modification of seizure activity by electrical stimulation. II. Motor seizure. *Electroencephalogr. Clin. Neurophysiol.* 32, 281–294. doi: 10.1016/0013-4694(72)90177-0

Rubenstein, J. L., and Merzenich, M. M. (2003). Model of autism: increased ratio of excitation/inhibition in key neural systems. *Genes Brain Behav.* 2, 255–267. doi: 10.1034/j.1601-183x.2003.00037.x

Sun, Y., Yao, X., Zhang, Q. J., Zhu, M., Liu, Z. P., Ci, B., et al. (2018). Beclin-1-dependent autophagy protects the heart during sepsis. *Circulation* 138, 2247–2262. doi: 10.1161/circulationaha.117.032821

Wang, B., Wu, Q., Lei, L., Sun, H., Michael, N., Zhang, X., et al. (2019). Long-term social isolation inhibits autophagy activation, induces postsynaptic dysfunctions and impairs spatial memory. *Exp. Neurol.* 311, 213–224. doi: 10.1016/j.expneurol.2018.09.009

Wong, M. (2013). Cleaning up epilepsy and neurodegeneration: the role of autophagy in epileptogenesis. *Epilepsy Curr.* 13, 177–178. doi: 10.5698/1535-7597-13.4.177

Wong, M., and Guo, D. (2013). Dendritic spine pathology in epilepsy: cause or consequence? *Neuroscience* 251, 141–150. doi: 10.1016/j.neuroscience.2012.03.048

Yang, Y., Tian, X., Xu, D., Zheng, F., Lu, X., Zhang, Y., et al. (2018). GPR40 modulates epileptic seizure and NMDA receptor function. *Sci. Adv.* 4:eaau2357. doi: 10.1126/sciadv.aau2357

Ying, C., Ying, L., Yanxia, L., Le, W., and Lili, C. (2020). High mobility group box 1 antibody represses autophagy and alleviates hippocampus damage in pilocarpine-induced mouse epilepsy model. *Acta Histochem.* 122:151485. doi: 10.1016/j.acthis.2019.151485

Zavala-Tecuapetla, C., Cuellar-Herrera, M., and Luna-Munguia, H. (2020). Insights into potential targets for therapeutic intervention in epilepsy. *Int. J. Mol. Sci.* 21:8573. doi: 10.3390/ijms21228573

Zhang, H., Tian, X., Lu, X., Xu, D., Guo, Y., Dong, Z., et al. (2019). TMEM25 modulates neuronal excitability and NMDA receptor subunit NR2B degradation. *J. Clin. Invest.* 129, 3864–3876. doi: 10.1172/jci122599

Zhu, X., Shen, K., Bai, Y., Zhang, A., Xia, Z., Chao, J., et al. (2016). NADPH oxidase activation is required for pentylenetetrazole kindling-induced hippocampal autophagy. *Free Radic. Biol. Med.* 94, 230–242. doi: 10.1016/j.freeradbiomed.2016.03.004

Conflict of Interest: The authors declare that the research was conducted in the absence of any commercial or financial relationships that could be construed as a potential conflict of interest.

The handling editor YJ declared a past co-authorship with the author XW.

Publisher's Note: All claims expressed in this article are solely those of the authors and do not necessarily represent those of their affiliated organizations, or those of the publisher, the editors and the reviewers. Any product that may be evaluated in this article, or claim that may be made by its manufacturer, is not guaranteed or endorsed by the publisher.

Advantages of publishing in Frontiers

OPEN ACCESS
Articles are free to read for greatest visibility and readership

FAST PUBLICATION
Around 90 days from submission to decision

HIGH QUALITY PEER-REVIEW
Rigorous, collaborative, and constructive peer-review

TRANSPARENT PEER-REVIEW
Editors and reviewers acknowledged by name on published articles

Frontiers
Avenue du Tribunal-Fédéral 34
1005 Lausanne | Switzerland

Visit us: www.frontiersin.org
Contact us: frontiersin.org/about/contact

REPRODUCIBILITY OF RESEARCH
Support open data and methods to enhance research reproducibility

DIGITAL PUBLISHING
Articles designed for optimal readership across devices

FOLLOW US
@frontiersin

IMPACT METRICS
Advanced article metrics track visibility across digital media

EXTENSIVE PROMOTION
Marketing and promotion of impactful research

LOOP RESEARCH NETWORK
Our network increases your article's readership